DOC.20070730.0003

QA: QA

ANL-EBS-MD-000003 REV 03

July 2007

General Corrosion and Localized Corrosion of Waste Package Outer Barrier

NOTICE OF OPEN CHANGE DOCUMENTS - THIS DOCUMENT IS IMPACTED BY THE LISTED CHANGE DOCUMENTS AND CANNOT BE USED WITHOUT THEM.

----

1) ACN-001, DATED 08/03/2007

THIS DOCUMENT IS IMPACTED BY THE FOLLOWING "ERROR RESOLUTION DOCUMENTS", WHICH SHOULD BE REVIEWED PRIOR TO USING THIS DOCUMENT:

----

1) ANL-EBS-MD-000003 ERD 01 - ACCESSION NO. LLR.20080414.0018

Prepared for:
U.S. Department of Energy
Office of Civilian Radioactive Waste Management
Office of Repository Development
1551 Hillshire Drive
Las Vegas, Nevada 89134-6321

Prepared by:
Sandia National Laboratories
OCRWM Lead Laboratory for Repository Systems
1180 Town Center Drive
Las Vegas, Nevada 89144

Under Contract Number
DE-AC04-94AL85000

DISCLAIMER

This report was prepared as an account of work sponsored by an agency of the United States Government. Neither the United States Government nor any agency thereof, nor any of their employees, nor any of their contractors, subcontractors or their employees, makes any warranty, express or implied, or assumes any legal liability or responsibility for the accuracy, completeness, or any third party's use or the results of such use of any information, apparatus, product, or process disclosed, or represents that its use would not infringe privately owned rights. Reference herein to any specific commercial product, process, or service by trade name, trademark, manufacturer, or otherwise, does not necessarily constitute or imply its endorsement, recommendation, or favoring by the United States Government or any agency thereof or its contractors or subcontractors. The views and opinions of authors expressed herein do not necessarily state or reflect those of the United States Government or any agency thereof.

QA: QA

General Corrosion and Localized Corrosion of Waste Package Outer Barrier

ANL-EBS-MD-000003 REV 03

July 2007

ACKNOWLEDGEMENTS

The document authors acknowledge the contributions of the following Yucca Mountain Project personnel involved in document development:

Bryan Bullard, Areva. Provided data analysis and model development.

INTENTIONALLY LEFT BLANK

Model Signature Page/Change History

Page ~~iii~~ v

Complete only applicable items.

1. Total Pages: ~~348~~ 344

2. Type of Mathematical Model

☒ Process Model ☐ Abstraction Model ☐ System Model

Describe Intended Use of Model

To provide input to License Application activities, such as the development of Integrated Waste Package Degradation Analysis (ANL-EBS-PA-000001), to provide technical bases for assessing waste package general and localized corrosion under exposure conditions anticipated in the repository.

3. Title

General Corrosion and Localized Corrosion of Waste Package Outer Barrier

4. DI (including Revision No. and Addendum No.):

ANL-EBS-MD-000003 REV 03

	Printed Name	Signature	Date
5. Originator	Gopal C. De and Kevin G. Mon	Gopal De Kevin Mon	07/24/2007
6. Independent Technical Reviewer for	Jean Younker	Ming Zhu	7/24/07
7. Checker for	Frederick D. Wall	David G. Enos	7/24/07
8. QCS/Lead Lab QA Reviewer	Sounia Kassabian-Darnell	Sounia K. Darnell	7/25/2007
9. Responsible Manager/Lead	Neil R. Brown	Neil R. Brown	7/25/2007
10. Responsible Manager	Cliff Howard	Cliff Howard	7/25/2007

11. Remarks

Editorial Changes made to block 13 for Rev 03 Change History

Change History

12. Revision No. and Addendum No.	13. Description of Change
00	Initial Issue
01	The purpose of this revision is to include new information, data, and results pertinent to general corrosion and localized corrosion of the waste package outer barrier. Most of the sections in this model report have been rewritten with new information, and as a result, the changes were too extensive to use Revision Bars per Section 5.9d)1) of AP-SIII.10Q.
02	Complete revision is to address issues raised during a recent technical evaluation by the NRC and comments resulting from the Repository Integration Team review. Changes were too extensive to include change bars. This revision also addresses issues identified in several CRs. CR79B: DIRS 131202 and DIRS 159836 revised to "direct input, established fact" and "direct input, qualified," respectively); CR1226B (see Section 7); CR1821B: errata 37951 and 37956 reviewed and incorporated as appropriate; CR2491B (no action taken; incorrect AMR cited); CR1019D (FEPs recommendations dispositioned appropriately).

03	This report is revised: (1) to evaluate and incorporate new data sets related to general and localized corrosion of Alloy 22; (2) to ensure consistency between the localized corrosion implementation rules presented in this report with those discussed in other reports; and (3) to address issues identified by audit comments, self-assessments, TBVs, and condition reports relevant to this report. • Include uncertainty distribution for failed area due to localized corrosion. • Reevaluate the microbially influenced corrosion enhancement factor. • Delete any discussion of localized corrosion initiation under dust deliquescent conditions (e.g., for exposure temperatures above ~120°C). • TBV 6168 – Figure not used in this revision. • TBV 6198 – Updated Figure 6-2 to be consistent with current version of source report. • CR 5600, Direct Inputs for FEPs AMRs - The DIRS report of ANL-EBS-MD-000003 was modified for proper documentation of the direct inputs. • CR 5143, Localized corrosion model pH values unqualified – The calculated pH values used by the Near-Field Environment department were used in the current localized corrosion model and results documented in Section 6.4.4. • CR 5447, ANL-EBS-MD-000003 - two figures not updated to reflect editorial changes in metadata – Figures 6-10 and 6-11 updated. • CR 6481, Documentation Errors in ANL-EBS-MD-000003, REV 02 – Equations corrected in Section 6.4.2. Old Figure 6-31 Replaced by new Figure 6-28. RKM 7/26/07 • CR 6484, Improve Description of Critical Potential Measurement in ANL-EBS-MD-000003, REV 02 – Description improved and text clarified in Section 6.4.4. JCR 7/26/07 • CR 6485, Clarify Decision Tree for Localized Corrosion in ANL-EBS-MD-000003, REV 02 – Decision tree updated for clarification in Sections 1.2, 6.4.4.6, and 8.3.1 • CR 6664 Transparency of Engineered Barrier Degradation Parameters in Process-Level AMRs and TSPA – Text updated in Section 6.4.4 and footnote revised (now in Appendix IX). • CR 6656, Parameter values in the WAPDEG AMR could not be fully traced to their source AMRs and DTNs – Appendix IX (was Table VIII) now consistent with relevant DTNs used (which differ from those mentioned in the CR). Uniform rounding rule used throughout Appendices VIII and IX. • CR 6693, Defensibility of the Engineered Barrier Degradation AMRs – Regression approach to fitting critical potential data revised in REV 03 and documented in Section 6.4.4.3. • CR 7336, Use Of Unqualified Software or Untraceable Process in Analyzing Electrochemical Experiments – Echem Analyst software no longer used to process raw data for this report see source DTN: LL0609008122 51.180 [DIRS 178409]. • CR 7786, Potential Errors in Tables about Corrosion Test Solutions Repeated in various Documents – Typographic errors mentioned in CR were not in the previous revision and are not in the current revision. • CR 8508, Acid-gas devolatilization of calcium chloride - water does not appear to be supported by the open literature – No acid-gas devolatilization of calcium chloride related data or discussion appears in this report. • CR 8666, Traceability of General Corrosion Rates - Traceable Weibull distribution parameters produced in Section 6.4.3.2.1 and Appendix IV. • Address Audit BQAP-BSC-05-07 Issue 21. ~~This editorial correction was made in the current revision in that the figure is not used.~~ See CR 6481 Discussion Above. RKM 7/26/07 • Incorporate relevant information from ANL-WIS-MD-000023. JCR 7/26/07 CRs related to use of out-of-calibration relative humidity probes (e.g., CR 5430 and CR 7418) and the use of thermogravimetric analyses (e.g., CR 8508) are not applicable to this report because these data are not used in the current revision.

CONTENTS

Page

CONTENTS (Continued)

Page

CONTENTS (Continued)

Page

INTENTIONALLY LEFT BLANK

FIGURES

Page

FIGURES (Continued)

Page

FIGURES (Continued)

Page

FIGURES (Continued)

Page

FIGURES (Continued)

Page

INTENTIONALLY LEFT BLANK

TABLES

Page

TABLES (Continued)

Page

ACRONYMS AND ABBREVIATIONS

ACM	alternative conceptual model
ASTM	American Society for Testing and Materials
BSW	basic saturated water
CDF	cumulative distribution function
CNWRA	Center for Nuclear Waste Regulatory Analyses
CPP	cyclic potentiodynamic polarization
DIRS	Document Input Reference System
DTN	data tracking number
EBS	Engineered Barrier System
ECDFs	empirical cumulative distribution functions
EPRI	Electric Power Research Institute
FEPs	features, events, and processes
GTAW	gas tungsten arc welding
LME	linear mixed-effects
LPB	low-plasticity burnishing
LSP	laser-shock peening
LTCTF	Long-Term Corrosion Test Facility
m	molal (moles/kg water)
M	molar (moles/liter of solution)
MCA	multiple crevice assembly
MIC	microbially influenced corrosion
MLE	maximum likelihood estimators
NRC	U.S. Nuclear Regulatory Commission
OLS	ordinary least squares
PCA	prism crevice assembly
PDM	point defect model
PSP	potentiostatic polarization
SAW	simulated acidified water
SCE	saturated calomel electrode
SCW	simulated concentrated water
SDW	simulated dilute water
SEM	scanning electron microscope
SHE	standard hydrogen reference electrode scale
SSC	saturated silver chloride electrode

ACRONYMS AND ABBREVIATIONS (Continued)

TCP	topologically close-packed
TEM	transmission electron microscopy
THE	Tsujikawa-Hisamatsu electrochemical (technique)
TSPA	total system performance assessment
WPOB	waste package outer barrier
XPS	x-ray photoelectron spectroscopy
YMP	Yucca Mountain Project
YMRP	*Yucca Mountain Review Plan, Final Report*

1. PURPOSE

The purpose and scope of this model report is to document models for general and localized corrosion of the waste package outer barrier (WPOB) to be used in evaluating long-term waste package performance in the total system performance assessment (TSPA). The waste package design for the license application is a double-wall waste package placed underneath a protective drip shield (SNL 2007 [DIRS 179394]; SNL 2007 [DIRS 179354]). The WPOB will be constructed of Alloy 22 (UNS N06022) (SNL 2007 [DIRS 179567], Section 4.1.1.6), a highly corrosion-resistant nickel-based alloy. The inner vessel of the waste package is constructed of Stainless Steel Type 316 (UNS S31600) (SNL 2007 [DIRS 179567], Section 4.1.1.6). The Alloy 22 WPOB prevents or substantially delays the time at which water contacts and begins to degrade the Stainless Steel Type 316 inner vessel, which provides additional structural stability to the thinner Alloy 22 WPOB. No corrosion performance credit is taken for the waste package inner vessel. This is a conservative treatment because, before it breaches, the waste package inner vessel would provide some performance for waste containment and potentially decrease the rate of radionuclide transport after it breaches. However, the performance of the inner vessel is expected to be less than that of the more corrosion-resistant Alloy 22 WPOB.

Treatment of seismic and igneous events and their consequences on WPOB performance are not specifically discussed because they are outside of the scope of this report, although the general and localized corrosion models developed in this report are suitable for use in these scenarios. The localized corrosion processes considered in this report include pitting corrosion and crevice corrosion. However, the latter process is treated as the most important form of localized corrosion under repository conditions. Stress corrosion cracking of the Alloy 22 WPOB is discussed in *Stress Corrosion Cracking of Waste Package Outer Barrier and Drip Shield Materials* (SNL 2007 [DIRS 177417]).

It should be noted that the Yucca Mountain Project (YMP) has defined three barriers for the repository system in accordance with the requirements of 10 CFR 63.113(a) [DIRS 180319]. The three barrier systems to provide compliance to the regulation are: The unsaturated natural system above the repository horizon, the Engineered Barrier System (EBS), and the unsaturated and saturated natural system below the repository. The various components of the three barriers are defined as “features.” In this regard, the waste package is a “feature” of the EBS. The waste package is a principal “feature” that contributes to the performance of the EBS. In this report, and elsewhere, the YMP has referred to the performance-related “features” of the waste package as “corrosion barrier” or “outer barrier.” When the word “barrier” is prefaced by an adjective, the combined representation can appropriately describe a “feature” without changing the overall implication to the three defined system “barriers.”

The WPOB general corrosion model (developed in this report) is to be used by downstream waste package degradation analyses to evaluate the extent of WPOB degradation by general corrosion under repository environmental conditions over the regulatory performance period. The WPOB general corrosion analyses documented in this report evaluate several possible processes that may affect general corrosion of the WPOB (e.g., dry oxidation, aqueous general corrosion, the effects of aging and phase instability, and microbially influenced corrosion (MIC)). Of these, only aqueous general corrosion and MIC are determined to have significant impact and are implemented in TSPA.

The WPOB localized corrosion model is to be used by downstream waste package degradation analyses to evaluate the extent of WPOB degradation by localized corrosion under the expected repository environmental conditions over the regulatory performance period. The components of the WPOB localized corrosion model are the crevice repassivation potential, long-term corrosion potential, and crevice corrosion propagation components.

The analyses and models developed in this report are used by the waste package degradation analyses for TSPA and are prepared in accordance with *Technical Work Plan for Postclosure Engineered Barrier Degradation Modeling* (SNL 2007 [DIRS 178849]).

Lists of data tracking numbers (DTNs) and their Q-status are included in the Document Input Reference System (DIRS) database report.

1.1 BACKGROUND ON ALLOY 22

The Alloy 22 WPOB will be manufactured according to American Society for Testing and Materials (ASTM) standards (ASTM B575-99a 1999 [DIRS 147465]) with additional elemental and chemical composition restrictions (SNL 2007 [DIRS 179567], Table 4-1). Other impurity elements, for example, include phosphorus, silicon, sulfur, manganese, vanadium, and carbon. The outstanding resistance of Alloy 22 to localized corrosion is mainly due to additions of molybdenum and chromium. Addition of these alloying elements to nickel alloys significantly improves the resistance of nickel alloys to localized corrosion (ASM International 1987 [DIRS 133378], pp. 641 to 657). The Alloy 22 passive film is very stable at low pH values, making Alloy 22 highly resistant to localized corrosion. High repassivation potentials, an indication of high resistance to localized corrosion, have been experimentally observed for Alloy 22 (Gruss et al. 1998 [DIRS 100893]; Rebak et al. 2002 [DIRS 162237]). Previous researchers also observed very low corrosion rates of Alloy 22 in crevice corrosion susceptibility tests conducted using acidic solutions containing 10 wt % $FeCl_3$ (Haynes International 1997 [DIRS 100896]). These solutions are more aggressive than those the WPOB is likely to encounter in the repository. More importantly, no localized corrosion attack on Alloy 22 has been observed in crevices exposed to concentrated solutions under normal atmospheric pressure in the YMP Long-Term Corrosion Test Facility (LTCTF) (Wong et al. 2004 [DIRS 174800]; Estill 1998 [DIRS 117697]). Test media used in this facility included simulated acidified water (SAW), simulated dilute water (SDW), and simulated concentrated water (SCW). The compositions of these solutions are discussed in Section 6.

1.2 RANGES OF MODEL APPLICATION

The general and localized corrosion models developed in this report are considered to be applicable to the evaluation of the performance of structures fabricated from Alloy 22 materials, which are covered by the compositional range defined by *Standard Specification for Low-Carbon Nickel-Molybdenum-Chromium, Low-Carbon Nickel-Chromium-Molybdenum, Low-Carbon Nickel-Chromium-Molybdenum-Copper, Low-Carbon Nickel-Chromium-Molybdenum-Tantalum, and Low-Carbon Nickel-Chromium-Molybdenum-Tungsten Alloy Plate, Sheet, and Strip* (ASTM B575-99a 1999 [DIRS 147465]). Corrosion studies on welded Alloy 22 specimens, which spanned the ASTM compositional range for Alloy 22, showed that the

corrosion behavior of one heat of Alloy 22 was indistinguishable from another (Fix et al. 2005 [DIRS 179983]).

This model is applicable for all environmental conditions the waste package is subject to except for magma intrusion. Possible damage to the WPOB due to igneous events is discussed in *Dike/Drift Interactions* (SNL 2007 [DIRS 177430]). Localized corrosion due to dust deliquescence is considered in another report (SNL 2007 [DIRS 181267]). The logic diagram shown in Figure 6-1 indicates conditions under which general corrosion and localized corrosion of the WPOB could possibly occur. Dry oxidation of the WPOB has an insignificant impact on the waste package performance (Section 6.4.2). Therefore, this degradation mode is not included in the waste package degradation analysis. The effects of thermal aging and phase instability are not included in the waste package degradation analysis because thermal aging and phase instability processes are not relevant under the thermal conditions in the repository for Alloy 22 meeting the chemical composition restrictions cited in *Aging and Phase Stability of Waste Package Outer Barrier* (BSC 2004 [DIRS 171924], Section 8).

The general corrosion model is applied to all environmental conditions in the repository and is based on corrosion measurements in the presence of an aqueous electrolyte (Section 6.4.3.4). The general corrosion model (Section 6.4.3.4) is developed in this report using data in both mixed ionic solutions and data from simple salt solutions including highly concentrated chloride brines and chloride brines containing nitrate ions. In Section 7.2, the general corrosion model is validated against data obtained at temperatures as high as 180°C. At an elevated temperature, a thin-film aqueous environment to support general corrosion may not be sustainable under atmospheric pressures relevant to the repository. Therefore, application of any general corrosion rate at elevated temperature conservatively overestimates the rate of material degradation. The need to use this approach stems from the difficulty in defining a clear cut-off temperature where general corrosion would no longer be considered. As shown in Figure 6-2 and Figure 6-3, not all waste package exposure environments attain temperatures in excess of 180°C, and those that do exceed 180°C do so for short time periods relative to the simulation period. Therefore, the general corrosion model is applied to all repository exposure environments, including those with exposure temperatures in excess of 180°C. MIC effects are applied when the relative humidity at the waste package surface is greater than a threshold relative humidity sampled from a uniform distribution between 75% and 90% (Section 6.4.5).

Localized corrosion is modeled because the waste package surface may experience a wide range of exposure conditions during its service life. Crevices, which are sites at which localized corrosion may initiate, may be formed on the waste package surface at occluded regions such as in between the waste package and its supports and potentially beneath mineral scales, corrosion products, dust, rocks, and biofilms. The chemical environment in a creviced region may be more severe than the near-field environment due to hydrolysis of dissolved metals. Metal ion hydrolysis can lead to the accumulation of hydrogen ions and a corresponding decrease in pH. Electromigration of chloride ions (and other anions) into the crevice must occur to balance the charge within the creviced region (Jones 1992 [DIRS 169906], Chapter 7). In this report, the dominant form of localized corrosion that is assumed possible for all surfaces of the WPOB is crevice corrosion, rather than pitting corrosion (Assumption 5.3). This is a conservative approach because the initiation threshold for crevice corrosion is lower than that for pitting

corrosion, and the majority of the WPOB lacks the geometrically occluded surfaces required to support crevice corrosion.

The empirical correlations used in the WPOB localized corrosion initiation model for the long-term corrosion potential (E_{corr}) and crevice repassivation potential (E_{rcrev}) are expressed as functions of temperature, pH (for E_{corr} only), chloride-ion concentration, and nitrate-ion concentration (Sections 6.4.4.3 and 6.4.4.5). Based on the range of environmental conditions in which the input data were obtained (Appendices VIII and IX) and the model validation activities (Sections 7.2.2 and 7.2.3), implementation of the WPOB localized corrosion initiation model can be summarized as described in the following paragraphs.

The WPOB crevice corrosion initiation model is used to evaluate the crevice corrosion initiation behavior of the Alloy 22 WPOB. The Alloy 22 WPOB contains base metal and welded material that is solution-heat-treated with the heat-treatment oxide film removed. In addition, the WPOB contains a final closure weld that is not solution-annealed but is low-plasticity burnished for the purposes of stress-mitigation (SNL 2007 [DIRS 179394], Section 4.1.2). The area of the Alloy 22 WPOB that is contacted by seepage is potentially subject to localized corrosion. Localized corrosion of the WPOB is considered to initiate when the open-circuit corrosion potential (E_{corr}) is equal to or greater than a critical potential (the crevice repassivation potential (E_{rcrev}) in the current model), that is, ΔE ($=E_{rcrev} - E_{corr}$) ≤ 0. If the exposure temperature is greater than or equal to 20°C and less than or equal to 120°C then the WPOB crevice corrosion initiation model is implemented by evaluating the long-term corrosion potential (E_{corr}) and crevice repassivation potential (E_{rcrev}) (Sections 6.4.4.3 and 6.4.4.5) in accordance with the following implementation rules:

a) If the nitrate ion-to-chloride ion ra tio in the environment exceeds 1, then evaluate E_{rcrev} and E_{corr} at a nitrate ion-to-chloride ion ratio of 1. If the molality of chloride ion is less than 0.0005 molal (m, moles/kg water), the nitrate ion-to-chloride ion ratio should be evaluated with a chloride-ion concentration of 0.0005 m.

b) If the molality of chloride ion in the environment exceeds 20 m, then evaluate E_{rcrev} and E_{corr} at a molality of chloride ion of 20 m. If the molality of chloride ion is less than 0.0005 m, then evaluate E_{rcrev} and E_{corr} at a chloride-ion molality of 0.0005 m.

c) If the pH in the environment exceeds 10, then evaluate E_{corr} at a pH of 10. If the pH in the environment is less than 1.9, then initiate localized corrosion.

If crevice corrosion initiates, then it propagates at a constant rate throughout the simulation period regardless of changes in the bulk chemical exposure environment. This is a conservative modeling assumption, because the crevice corrosion model does not account for the possibility of crevice corrosion repassivation or stifling. Nitrate ions inhibit localized corrosion initiation (Section 6.4.4.3). Carbonate and sulfate ions have an inhibitive effect on localized corrosion. Because the model only accounts for nitrate ions, model results for solutions with significant amounts of other potentially inhibitive ions in addition to nitrate ions are conservative.

It should be noted that the chemical exposure conditions on the waste package surface can be affected by the process of salt separation (SNL 2007 [DIRS 177412], Section 6.15.1.3). If the

relative humidity on a waste package undergoing seepage falls below a threshold relative humidity value (determined by lookup tables supplied to TSPA by *Engineered Barrier System: Physical and Chemical Environment* (SNL 2007 [DIRS 177412], Section 6.15.1.3)), chloride salts (halite or sylvite) will precipitate. Once a chloride salt has precipitated, the remaining brine, or some fraction of it, can advect off of the waste package, or at least away from the precipitated salts, and hence be physically separated from the precipitated salts. Because the brine is chemically different from the bulk brine-salt geochemical system, brine-salt separation changes the bulk composition of the system represented by the precipitated salts and whatever brine is retained by them. In general, because the removed brine is nitrate-rich relative to the bulk system (chloride salts have precipitated), the remaining salt-brine system is more chloride-rich. As the relative humidity in the drift begins to rise (i.e., as the temperature decreases), the chloride-rich brine residue absorbs water, and TSPA must assume a chloride-rich brine will form. This chloride-rich brine may be aggressive enough to initiate localized corrosion. The effects of salt separation on localized corrosion are not outputs of this report. Salt separation is analyzed in *Engineered Barrier System: Physical and Chemical Environment* (SNL 2007 [DIRS 177412], Section 6.15.1.3).

1.3 BARRIER CAPABILITIES

In 10 CFR 63.2 [DIRS 180319], a barrier is defined as any material, structure, or feature that, for a period to be determined by U.S. Nuclear Regulatory Commission (NRC), prevents or substantially reduces the rate of movement of water or radionuclides from the Yucca Mountain repository to the accessible environment, or prevents the release or substantially reduces the release rate of radionuclides from the waste. In 10 CFR 63.102 (h) and 10 CFR 63.113 (a) [DIRS 180319], the repository system is required to include multiple barriers, natural and engineered. The capability of a barrier is defined by its ability to achieve one or more of the functions described above (i.e., by the extent to which it can prevent or delay the movement of water or radionuclides, or prevent or reduce the radionuclide release rate from the waste package).

In this document, the barrier considered is the EBS with particular emphasis on the performance of the WPOB. The waste package, as a feature of the EBS, contributes to waste isolation by keeping water away from the waste for its lifetime and, when breached, by reducing the contact of water with the waste and the radionuclide release rate from the waste.

INTENTIONALLY LEFT BLANK

2. QUALITY ASSURANCE

The Yucca Mountain Quality Assurance Program applies to the development of this technical product. *Technical Work Plan for Postclosure Engineered Barrier Degradation Modeling* (SNL 2007 [DIRS 178849]) determined this activity to be subject to *Quality Assurance Requirements and Description* (DOE 2007 [DIRS 182051]) requirements. All waste package configurations have been determined to be important for waste isolation as documented in *Q-List* (BSC 2005 [DIRS 175539], Table A-1).

This report is prepared in accordance with SCI-PRO-006, *Models,* and *Technical Work Plan for Postclosure Engineered Barrier Degradation Modeling* (SNL 2007 [DIRS 178849]). This model report was reviewed in accordance with SCI-PRO-003, *Document Review*.

The inputs to this report were documented according to SCI-PRO-004, *Managing Technical Product Inputs*. The methods used to control the electronic management of data as required by IM-PRO-002, *Control of the Electronic Management of Information*, were accomplished in accordance with the technical work plan (SNL 2007 [DIRS 178849]). The process for control of the electronic management of information on evaluation of work activities, processes, or process functions outlined in IM-PRO-002 was followed to ensure accuracy, completeness, and security of information and data used in preparation of this report. Examples of process controls mentioned in IM-PRO-002 are: (a) access to the information contained on personal computer is password protected; (b) secured backup copies are appropriately labeled and stored before changes are made and kept until the changes are confirmed and correct; (c) physical electronic media (tape, diskette, CD-ROM, etc.) are appropriately labeled; and (d) for nonphysical electronic media, transport mechanisms can be e-mail, TCP/IP, NetBios, etc., and methods of receipt verification may include visual inspection, transmission verification settings, check sums, application information integrity check, etc.

INTENTIONALLY LEFT BLANK

3. USE OF SOFTWARE

Microsoft Excel 97 SR-2, bundled with Microsoft Office 1997, is a commercial off-the-shelf software program used in this report. The Excel computations performed in this report use only standard built-in functions and are documented in sufficient detail to allow an independent technical reviewer to reproduce or verify the results by visual inspection or hand calculation without recourse to the originator (Sections 6.4.3 to 6.4.6, and the Excel files included in output DTNs: MO0703PAGENCOR.001 and MO0612WPOUTERB.000). Therefore, use of this software is not subject to IM-PRO-003, *Software Management*. Microsoft Excel 97 SR-2 is appropriate for this application as it offers the mathematical and graphical functionality necessary to perform and document the numerical manipulations used in this report. Microsoft Excel 97 SR-2 was executed on a computer (SNL tag S884914, located in the Summerlin offices, Las Vegas, Nevada) equipped with the Windows 2000 operating system.

Mathcad Version 13.0 is a commercial off-the-shelf software program used in this model report. The Mathcad computations performed in this report use only standard functions and are documented in sufficient detail to allow an independent technical reviewer to reproduce or verify the results by visual inspection or hand calculation without recourse to the originator (Sections 6.4.3 and 6.4.4, and the Mathcad worksheet files included in the output DTNs: MO0703PAGENCOR.001 and MO0612WPOUTERB.000). Therefore, use of this software is not subject to IM-PRO-003. This software is appropriate for this application as it offers the mathematical and graphical functionality necessary to perform and document the numerical manipulations used in this report. Mathcad Version 13.0 was executed on a computer (SNL tag S884914, located in the Summerlin offices, Las Vegas, Nevada) equipped with the Windows 2000 operating system.

S-PLUS 2000 Professional Release 2 is a commercial off-the-shelf software program used in this model report. The S-PLUS computations performed in this report use only standard functions and are documented in sufficient detail to allow an independent technical reviewer to reproduce or verify the results by visual inspection or hand calculation without recourse to the originator (Section 6.4.3 and output DTN: MO0612WPOUTERB.000). Therefore, use of this software is not subject to IM-PRO-003. This software is appropriate for this application as it offers the mathematical and graphical functionality necessary to perform and document the numerical manipulations used in this report. S-PLUS 2000 Professional Release 2 was executed on a computer (SNL tag S884301, located in the Summerlin offices, Las Vegas, Nevada) equipped with the Windows XP operating system.

INTENTIONALLY LEFT BLANK

4. INPUTS

This section documents input data and parameters used in the models and analyses in this report. This section also documents inputs from other models or analyses used in this report. Criteria directly applicable to the analyses or models in this report are identified, and a list of the applicable codes and standards used in the analyses or models in this report is provided.

4.1 DIRECT INPUT

Inputs to this report are tracked in accordance with SCI-PRO-006, *Models*, and SCI-PRO-004, *Managing Technical Product Inputs*. The data used to develop the models in this report are not used to validate the models developed in this report.

4.1.1 Data

Table 4-1 lists the input data used in the analyses or models documented in this report, and identifies the DTNs and specific sections where the data were used. Additional details of the input data are described in the following sections. The test procedures for the various electrochemical corrosion tests that were employed to generate the input data documented in this section are summarized in Appendix I, along with a summary for the test conditions and parameters. The electrochemical corrosion tests summarized in Appendix I include polarization resistance and cyclic potentiodynamic polarization (CPP) tests. The long-term open-circuit potential tests are summarized in Section 6.4.4.4. A summary of the test procedures for the weight-loss measurements of the specimens exposed for five years in the LTCTF is given in Section 6.4.3.1. The treatment of input data uncertainty is addressed in the data analysis and model development throughout Section 6.4.

Table 4-1. Summary of All Input Data Used in the Analyses and Models

Data Name	DTN/Data Source	Data Use in This Report
Oxide Layer on Alloy 22 Formed in Air	LL030406412251.045 [DIRS 163469], file: *TDMS_TS444Q_data.doc*	Section 6.4.2
Oxide Layer on Alloy 22 Formed in Mixed-Salt Environment	Andresen et al. 2003 [DIRS 170360], Section 3	Section 6.4.1
Calculated Pitzer pH and Molalities of Solutions Used in Various Electrochemical Tests	LL060904312251.186 [DIRS 178283], files: *AtmCO2GetEQData.xls* and *NoCO2GetEQData.xls*	Sections 7.2.3, 7.2.4, Appendices VIII and IX
Alloy 22 Weight-Loss Data of Crevice and Weight-Loss Specimens After Five-Year Exposure in the LTCTF	LL030412512251.057 [DIRS 163712], file: *C22 5 Year Coupon Corrosion Rates 4-14-03.xls*	Section 6.4.3, Appendices II and III
Polarization Resistance Data for Temperature Dependence	LL060900812251.180 [DIRS 178409], files*: 175 PRFitv2.xls*, *176PRFit.xls*, *179PRFit.xls*, and *187PRFit.xls*	Sections 6.4.3 and 6.4.6, Appendix VII

Table 4 1. Summary of All Input Data Used in the Analyses and Models (Continued)

Data Name	DTN/Data Source	Data Use in This Report
Long-Term Open-Circuit Potential Measurement Data in Various Solutions at Different Temperatures	LL060900512251.177 [DIRS 178271] file: *Summary Ecorr Cells 1-36 29Sep06.xls* LL060901312251.181 [DIRS 178299] files: *Cell-1-partI.xls*, *Cell-1-partII.xls*, *Cell-2-partI.xls*, *Cell-2-partII.xls*, *Cell-3-partI.xls*, *Cell-3-partII.xls*, *Cell-5-partI.xls*, *Cell-5-partII.xls*, *Cell-6-partI.xls*, *Cell-6-partII.xls*, *Cell-7-2nd.xls*, *Cell-9.xls*, and *Cell-10.xls*. LL060901412251.182 [DIRS 178300], files: *Cell-13.xls*, *Cell-14.xls*, *Cell-15.xls*, and *Cell-28.xls*	Section 6.4.4; Appendix VIII
Alteration of Corrosion Rates Associated with Microbial Activity	LL991203505924.094 [DIRS 138343], SEP table "S99502_001"	Section 6.4.5
Relative Humidity Threshold for MIC	BSC 2004 [DIRS 169991], Section 7.1	Section 6.4.5
Crevice Repassivation Potentials for Alloy 22	LL040902712251.119 [DIRS 173720], file: *Reduced Data Ahmet Yilmaz WBL 11Feb05.xls* LL050302312251.129 [DIRS 173921], file: *Mockup Developed RBR 21May05.xls* LL060603812251.164 [DIRS 178269], file: *Rep Pot N06022 vs Temp NaCl + KNO3 60-100C RBR 07Aug06.xls* LL060700312251.166 [DIRS 179385], file: *Rep Pot N06022 vs Temp 5M CaCl2 RBR 19Dec06.xls* LL060801812251.168 [DIRS 179386], file: *Rep Pot N06022 High Temp High NO3 RBR.xls* LL060803712251.170 [DIRS 179387], file: *Rep Pot N06022 vs Temp NaCl RBR 07Oct06.xls*	Section 6.4.4; Appendix IX
Density of Alloy 22	Haynes International 1997 [DIRS 100896], p. 13	Section 6.4.3; Appendices I and VII
Equivalent Weight of Alloy 22 and K_I parameter	ASTM G 102-89 1989 [DIRS 163908]	Appendix I
Universal Gas Constant	Lide 1991 [DIRS 131202], inside rear cover	Sections 6.4.2, 6.4.3; Appendix VII
Weibull Shape-Estimator Unbiasing Factor	ASTM C 1239-06A. 2006 [DIRS 178286], Table 1	Appendices IV and V
Alloy 22 Corrosion Rate in 10% Ferric Chloride Solution	Haynes International 1997 [DIRS 100897], p. 8	Section 6.4.4
Alloy 22 Corrosion Rates in Concentrated Hydrochloric Acid	Haynes International 1997 [DIRS 100896], p. 12	Section 6.4.4

4.1.1.1 Passive Film Characterization

Characterization of the passive film formed on Alloy 22 in various exposure environments is used to provide a technical basis for constructing the conceptual model of the structure and composition of the film. This information is also used as an aid in interpreting corrosion data and their implications on corrosion behavior. Table 4-2 lists the sources of the passive film characterization data and the associated DTNs (if applicable). Because these input data are used in a qualitative manner, no quantitative analysis for data uncertainty will be performed. Data from Andresen et al. (2003 [DIRS 170360]) are considered qualified data because these data are information received from a vendor or supplier such as analyses or characteristics and properties of materials that are acquired data collected under a YMP-approved quality assurance program that meets the requirements of 10 CFR Part 63 Subpart G [DIRS 180319].

Table 4-2. Alloy 22 Passive Film Characterization Data

Data Name	DTN/Data Source	Data Use in This Report
Oxide Layer on Alloy 22 Formed in Air	LL030406412251.045 [DIRS 163469], file: *TDMS_TS444Q_data.doc*	Section 6.4.2
Oxide Layer on Alloy 22 Formed in Mixed-Salt Environment	Andresen et al. 2003 [DIRS 170360], Section 3.0	Section 6.4.1

4.1.1.2 Calculated Pitzer pH and Molalities of Solutions Used in Various Electrochemical Tests

Exposure condition parameters important to corrosion are temperature and composition of the solution contacting the metal. The species that significantly affect metal corrosion are hydrogen ions (e.g., pH), halide ions (e.g., chloride ions), corrosion-inhibiting ions (e.g., nitrate and sulfate ions), and dissolved oxygen. The compositions of the solutions employed in various corrosion tests for Alloy 22 are input to the Alloy 22 corrosion analyses and models. Table 4-3 lists the source of the corrosion test solution compositions and the associated DTNs. The majority of the solutions considered are simple salt solutions (e.g., pure solutions or mixtures of NaCl, KCl, $NaNO_3$, KNO_3, $CaCl_2$, $Ca(NO_3)_2$) with well-defined compositions. Therefore, the primary source of uncertainty for these solutions would be an error in measuring the weights of the reagents added to form the solution. It is reasonable to expect such errors would be small, given that the solutions are generally concentrated (i.e., a large amount of reagents are added) and errors in the measured weight of the reagents added are expected to be small relative to the total amount of reagent added. As to uncertainty in the calculated Pitzer pH values, uncertainty (largely due to uncertainty in seepage composition) is included in the expected repository chemical exposure environment as given by lookup tables developed in *Engineered Barrier System: Physical and Chemical Environment* (SNL 2007 [DIRS 177412], Section 6.12.3). These lookup tables are used to evaluate the uncertain chemical variables (e.g., pH, $[Cl^-]$, and $[NO_3^-]$), which are then used to evaluate whether localized corrosion initiates. On this basis, inclusion of uncertainty in the calculated Pitzer pH values used to develop the E_{rcrev} and E_{corr} regression relations would result in "double-counting" the uncertainty when implementing these models. Therefore, the approach adopted in this analysis is to consider the input calculated Pitzer pH values and molalities to have no uncertainty.

Table 4-3. Compositions of Solutions Employed in Various Corrosion Tests of Alloy 22

Data Name	DTN/Data Source	Data Use in This Report
Calculated Pitzer pH and Molalities of Solutions Used in Various Electrochemical Tests	LL060904312251.186 [DIRS 178283], files: *AtmCO2GetEQData.xls* and *NoCO2GetEQData.xls*	Sections 7.2.3, 7.2.4; Appendices VIII and IX

4.1.1.3 Long-Term Corrosion Weight-Loss Data

Alloy 22 specimens with differing configurations and material conditions have been tested in the LTCTF at Lawrence Livermore National Laboratory. Five-year weight-loss data are used to calculate the general corrosion rates for the WPOB general corrosion model documented in this report (DTN: LL030412512251.057 [DIRS 163712], file: *C22 5 Year Coupon Corrosion Rates 4-14-03.xls*). The solution chemistries used in the LTCTF are listed in Table 6-3. The five-year weight-loss data and the calculated rates are listed in Appendices II and III. The calculated general corrosion rates slightly differ from those in the input DTN due to differences in the number of significant digits used. Uncertainty in these data is analyzed, quantified, and propagated into the general corrosion model (Section 6.4.3.3). Table 4-4 lists the data source and associated DTNs for the five-year Alloy 22 weight-loss data.

Table 4-4. Long-Term Corrosion Weight-Loss Data for Alloy 22

Data Name	DTN/Data Source	Data Use in This Report
Alloy 22 Weight-Loss Data of Crevice and Weight-Loss Specimens After Five-Year Exposure in the LTCTF	LL030412512251.057 [DIRS 163712] file: *C22 5 Year Coupon Corrosion Rates 4-14-03.xls*	Section 6.4.3; Appendices II and III

4.1.1.4 Polarization Resistance Data

The polarization resistance technique was used to measure the corrosion rate of Alloy 22 under various testing conditions. The corrosion rates measured by the technique are used for comparative analysis of the corrosion behavior under a wide range of test conditions. They are not used to obtain the absolute values of the corrosion rates used to model general corrosion of Alloy 22 in the repository. The polarization resistance data were used to determine the temperature-dependence of the general corrosion rate (Section 6.4.3) and to evaluate the effect of welding and thermal aging on Alloy 22 corrosion rates (Section 6.4.6). The variables in the tests are exposure condition (e.g., temperature and water chemistry), sample configuration (e.g., crevice, rod, prism, and disc), and metallurgical condition (e.g., mill-annealed, as-welded, and as-welded plus thermally aged). The range of the test conditions for the polarization resistance data includes temperatures from 30°C to 150°C, pH from 2.6 to 6.5, chloride-ion concentration from 1 *m* to 24 *m*, nitrate-ion concentration from zero to 12 *m*, and a limited number of sulphate-ion-containing solutions (up to 0.4 molar (*M*, moles/liter of solution)).

Table 4-5 lists the sources of the polarization resistance data of Alloy 22 that were used to analyze the effect of the exposure and metallurgical condition on the WPOB corrosion

performance in the repository. Details of the electrochemical testing techniques to measure the above corrosion properties of Alloy 22 are described in Appendix I. Uncertainty in the data was analyzed, quantified, and propagated into the model (Section 6.4.3.4).

The polarization resistance data for the electrolytes containing NaF and oxalic acid were not included in the quantitative model analysis because these chemical environments are not relevant to the repository as noted in DTN: LL060900512251.177 [DIRS 178271], file: *Summary Ecorr Cells 1-36 29Sep06.xls*.

Table 4-5. Polarization Resistance Measurement Data for Alloy 22

Data Name	DTN/Data Source	Data Use in This Report
Polarization Resistance Data for Temperature Effect	LL060900812251.180 [DIRS 178409], files: *175 PRFitv2.xls*, *176PRFit.xls*, *179PRFit.xls*, and *187PRFit.xls*	Sections 6.4.3, 6.4.6, Appendix VII

4.1.1.5 Long-Term Open-Circuit Corrosion Potential Data

The long-term open-circuit corrosion potential (also referred to as long-term corrosion potential, E_{corr}) is an important corrosion property of a metal/alloy. The corrosion potential of a metal or alloy may be affected by the sample configuration (e.g., boldly exposed or creviced), metallurgical condition (e.g., mill-annealed, as-welded, and aged), and exposure environment. For a given exposure environment, the corrosion potential can change over time depending mostly on the kinetics of electrochemical reactions involved. In this report, the long-term corrosion potentials, along with the critical potentials for localized corrosion initiation discussed in Section 6.4.4.3, were used for the localized corrosion initiation model. Section 6.4.4.3 provides details of the localized corrosion initiation model.

As stated above, the corrosion potential may change over time, eventually approaching a steady-state value (Section 6.4.4.4). The initial changes can be significant, depending on the exposure environment and the sample surface conditions. Therefore, the long-term steady-state corrosion potentials were used for the corrosion potential model of Alloy 22. The test conditions varied in the long-term corrosion potential measurements are exposure environment (temperature and water chemistry), sample geometry (U-bend, rod, and creviced), and metallurgical conditions (mill-annealed and as-welded). Table 4-6 lists the data sources for the long-term open-circuit corrosion potential data of Alloy 22 for a range of exposure environments and metallurgical conditions. The range of the test conditions for the long-term open-circuit corrosion potential data include temperatures from 25°C to 120°C, Pitzer pH values from 1.9 to 10, chloride concentration from very dilute to about 12.6 *m*, and nitrate concentration from zero to 10 *m*.

Because of measurement noise in the long-term corrosion potentials, the average of the measured readings for the final 30 days of exposure was used in the model. The developed E_{corr} data is contained in DTN: LL060900512251.177 [DIRS 178271], file: *Summary Ecorr Cells 1-36 29Sep06.xls*. Only the final E_{corr} data contained in DTN: LL060900512251.177 [DIRS 178271], file: *Summary Ecorr Cells 1-36 29Sep06.xls*, corresponding to test durations of 250 days and

longer, were used for the development of the model in Section 6.4.4.5. Analyses in Section 6.4.4.4 indicate E_{corr} values are reasonably stable for use in the model after 250 days. The data are listed in Appendix V. Uncertainty in the data was analyzed, quantified, and propagated into the long-term corrosion potential model. Details of the uncertainty analysis are documented in Section 6.4.4.5. A subset of the data contained in DTNs: LL060901312251.181 [DIRS 178299] and LL060901412251.182 [DIRS 178300] are graphed in Section 6.4.4.4 to give the reader an understanding of the variation of the corrosion potential as a function of time.

The long-term corrosion potential data acquired in NaF and oxalic acid (refers to cells 11 and 12 in DTN: LL060900512251.177 [DIRS 178271], file: *Summary Ecorr Cells 1-36 29Sep06.xls*) were not included in the quantitative model analysis because these chemical environments are not relevant to the repository conditions as noted in DTN: LL060900512251.177 [DIRS 178271] (file: *Summary Ecorr Cells 1-36 29Sep06.xls*). However, the test solutions used in long-term corrosion potential measurements at 60°C and 90°C include SCW, (Table 6-3), which contains about 1,400 mg/L fluoride ions and 6,700 mg/L chloride ions. Specimens immersed in SCW were included in the development of the long-term corrosion potential model and were not found to be outliers.

Table 4-6. Long-Term Open-Circuit Corrosion Potential Measurement Data for Alloy 22

Data Name	DTN/Data Source	Data Use in This Report
Long-Term Open-Circuit Potential Measurement Data	LL060900512251.177 [DIRS 178271], file: *Summary Ecorr Cells 1-36 29Sep06.xls* LL060901312251.181 [DIRS 178299], files: *Cell-1-partI.xls*, *Cell-1-partII.xls*, *Cell-2-partI.xls*, *Cell-2-partII.xls*, *Cell-3-partI.xls*, *Cell-3-partII.xls*, *Cell-5-partI.xls*, *Cell-5-partII.xls*, *Cell-6-partI.xls*, *Cell-6-partII.xls*, *Cell-7-2nd.xls*, *Cell-9.xls*, and *Cell-10.xls*. LL060901412251.182 [DIRS 178300], files: *Cell-13.xls*, *Cell-14.xls*, *Cell-15.xls*, and *Cell-28.xls*	Section 6.4.4, Appendix VIII

4.1.1.6 Alloy 22 Crevice Repassivation Potential Data

The localized corrosion conceptual model assumes that crevices form on the waste package surface in the repository (Section 5, Assumption 5.3; and Section 6.4.4). Thus, crevice corrosion was conservatively taken as the representative form of localized corrosion on the WPOB (Section 5, Assumption 5.3). The crevice repassivation potential (E_{rcrev}) from the cyclic potentiodynamic polarization curves was selected as the critical potential for localized corrosion initiation. Appendix I describes details of the electrochemical testing techniques used to measure the crevice repassivation potential of Alloy 22. As discussed in Section 6.4.4.1, the crevice repassivation potential is a conservative measure of the critical potential for localized corrosion initiation. The input DTNs in which the crevice repassivation potentials are reported are listed in Table 4-7.

The variables in the tests are exposure condition (e.g., temperature and water chemistry), sample configuration (e.g., prism crevice assemblies (PCA) and multiple crevice assemblies (MCA)), and metallurgical condition (e.g., mill-annealed, as-welded, and as-welded plus thermally aged). The range of the test conditions for the polarization resistance data includes temperatures from 30°C to 120°C, pH from 3.1 to 6.5, chloride-ion concentration from 0.0005 *m* to 20 *m*, and nitrate-ion concentration from zero to 10 *m*.

Only crevice repassivation potential data gathered in solutions with nitrate ion–to-chloride ion ratios less than or equal to 1 were used. In addition, the crevice repassivation potential data that did not show occurrence of localized corrosion were conservatively excluded from the analysis. Section 6.4.4.2 provides details on the crevice repassivation potential data analysis. The crevice repassivation potential data used in the analyses are listed in Appendix IX. Uncertainty in the data was analyzed, quantified, and propagated into the crevice repassivation potential model. Details of the uncertainty analysis are documented in Section 6.4.4.3.

The crevice repassivation potentials for two specimens, DEA3130 (from DTN: LL060803712251.170 [DIRS 179387], file: *Rep Pot N06022 vs Temp NaCl RBR 07Oct06.xls*) and KE0416 (from DTN: LL060603812251.164 [DIRS 178269], file: *Rep Pot N06022 vs Temp NaCl + KNO3 60-100C RBR 07Aug06.xls*) will be used for model validation in Section 7.2.3 and were not used for model development.

CPP data for the electrolytes containing NaF and oxalic acid were not included in the quantitative model analysis because these chemical environments are not relevant to the repository as noted in DTN: LL060900512251.177 [DIRS 178271] (file: *Summary Ecorr Cells 1-36 29Sep06.xls*).

Table 4-7. Cyclic Potentiodynamic Polarization Measurement Data for Alloy 22

Data Name	DTN/Data Source	Data Use in This Report
Crevice Repassivation Potentials for Alloy 22	LL040902712251.119 [DIRS 173720], file: *Reduced Data Ahmet Yilmaz WBL 11Feb05.xls* LL050302312251.129 [DIRS 173921], file: *Mockup Developed RBR 21May05.xls* LL060603812251.164 [DIRS 178269], file: *Rep Pot N06022 vs Temp NaCl + KNO3 60-100C RBR 07Aug06.xls* LL060700312251.166 [DIRS 179385], file: *Rep Pot N06022 vs Temp 5M CaCl2 RBR 19Dec06.xls* LL060801812251.168 [DIRS 179386], file: *Rep Pot N06022 High Temp High NO3 RBR.xls* LL060803712251.170 [DIRS 179387], file: *Rep Pot N06022 vs Temp NaCl RBR 07Oct06.xls*	Section 6.4.4, Appendix IX

4.1.1.7 Microbially Influenced Corrosion

MIC is the contribution to the corrosion of a metal or alloy due to the presence or activity, or both, of microorganisms. Nickel-based alloys such as Alloy 22 are highly resistant to MIC (Lian et al. 1999 [DIRS 110238]).

In *Evaluation of the Impact of Microbial Activities on Drift Chemistry* (BSC 2004 [DIRS 169991], Section 7.1), it is recommended that the effect of MIC on the WPOB corrosion be considered when the exposure relative humidity is greater than or equal 90% and no uncertainty for this parameter is supplied. *Evaluation of the Impact of Microbial Activities on Drift Chemistry* (BSC 2004 [DIRS 169991], Section 7.1) acknowledges that microbes can be active at a relative humidity as low as 75%. In Section 6.4.5 of this report, an uncertainty distribution is applied for this parameter allowing for the affects of MIC down to an exposure relative humidity of 75%. Table 4-8 lists the source of the input data used to evaluate the MIC effect on the WPOB general corrosion rate. DTN: LL991203505924.094 [DIRS 138343], SEP table "S99502_001," contains measurements for the corrosion potentials and corrosion rates of several engineering alloys, including Alloy 22, in the presence and absence of microbes relevant to the repository. The corrosion rates were obtained from the short-term polarization resistance tests. The MIC enhancement factor was determined from the comparative analysis of the corrosion rates of Alloy 22 samples in abiotic and biotic conditions. Uncertainty associated with the MIC enhancement factor is discussed in Section 6.4.5.

Table 4-8. Input Data for Microbially Influenced Corrosion of Alloy 22

Data Name	DTN/Data Source	Data Use in This Report
Alteration of Corrosion Rates Associated with Microbial Activity	LL991203505924.094 [DIRS 138343], SEP table "S99502_001"	Section 6.4.5
Relative Humidity Threshold for MIC	BSC 2004 [DIRS 169991], Section 7.1	Section 6.4.5

4.1.1.8 Physical Constants

The density of Alloy 22 (8.69 g/cm^3) was used to calculate the general corrosion rates of Alloy 22 from the weight-loss measurements of the specimens exposed for five years in the LTCTF (Section 6.4.3) and for determination of corrosion rates from polarization resistance tests in Appendix I. This datum (from Haynes International 1997 [DIRS 100896]) is considered established fact according to SCI-PRO-004, *Managing Technical Product Inputs*, as it is numerical data from a primary source for this specific type of data.

The equivalent weight for Alloy 22 (UNS N06022) is calculated considering that the alloy dissolves stoichiometrically and depends on the valence of the dissolved elements. The equivalent weight of Alloy 22 is used in determining general corrosion rates from the polarization resistance data in Appendix I. Table 1 of ASTM G 102-89 (1989 [DIRS 163908]) presents several choices for the Alloy 22 equivalent weight. The actual choice of which equivalent weight to use has no impact on the analysis results presented in this report because only relative corrosion rates (e.g., between welded and nonwelded samples) are used, not their

absolute values. The value of the equivalent weight used (23.28) was from Table 1 (column labeled "Third") in ASTM G 102-89 (1989 [DIRS 163908], Table 1).

The K_I parameter value of 3.272×10^{-3} mm g/μA cm yr is used for the calculation of general corrosion rates in Appendices I and VII. This value was generated from the value of 327.2 mm kg/A m yr given in ASTM G 102-89 (1989 [DIRS 163908], Table 2).

Data from ASTM G 102-89 (1989 [DIRS 163908]), ASTM C 1239-06A (2006 [DIRS 178286]), and Lide (1991 [DIRS 131202]) are considered established fact because they are sources scientists would use in their standard work practices.

Table 4-9 lists these data and their sources.

Table 4-9. Density and Equivalent Weight of Alloy 22

Data Name	DTN/Data Source	Data Use in This Report
Density of Alloy 22	Haynes International 1997 [DIRS 100896], p. 13	Section 6.4.3; Appendix I
Equivalent Weight of Alloy 22 K_I Parameter	ASTM G 102-89 (1989 [DIRS 163908]), Table 1 ASTM G 102-89 (1989 [DIRS 163908]), Table 2	Appendix I
Universal Gas Constant	Lide 1991 [DIRS 131202], inside rear cover	Sections 6.4.2, 6.4.3; Appendix VII

4.1.1.9 Weibull Shape-Estimator Unbiasing Factor

When fitting data to a Weibull distribution, it is recommended that the distribution parameters be corrected for bias resulting from the fitting procedure. Weibull shape-estimator unbiasing factors are provided in ASTM C 1239-06A (2006 [DIRS 178286], Table 1). As the datum used comes from an accepted engineering standard, it is considered established fact. Table 4-10 lists the source of the Weibull shape-estimator unbiasing factor. Data from ASTM C 1239-06A (2006 [DIRS 178286], Table 1) are considered established fact because ASTM C 1239-06A (2006 [DIRS 178286], Table 1) is a source scientists would use in their standard work practices.

Table 4-10. Weibull Shape-Estimator Unbiasing Factor

Data Name	DTN/Data Source	Data Use in This Report
Weibull Shape-Estimator Unbiasing Factor	ASTM C 1239-06A 2006 [DIRS 178286], Table 1	Appendices IV and V

4.1.1.10 Data Use for Determination of Localized Penetration Rates of Alloy 22

Corrosion rates of Alloy 22 in aggressive solutions are used to represent the localized corrosion penetration rates of Alloy 22 in Section 6.4.4. These data are bounding, represent extreme Alloy 22 penetration rates found in the literature, and are a highly conservative representation of localized corrosion rates of Alloy 22 for the exposure conditions expected in the repository.

Table 4-11 lists the source of these corrosion rates of Alloy 22. The localized corrosion penetration rate values used are listed in Table 6-15. Data from Haynes International (1997 [DIRS 100896] and 1997 [DIRS 100897]) are considered established fact according to SCI-PRO-004, as they are numerical data from a primary source for the specific type of data.

Table 4-11. Localized Corrosion Penetration Rates of Alloy 22

Data Name	DTN/Data Source	Data Use in This Report
Alloy 22 Corrosion Rates in 10% Ferric Chloride Solution	Haynes International 1997 [DIRS 100897], p. 8	Section 6.4.4
Alloy 22 Corrosion Rates in Concentrated Hydrochloric Acid	Haynes International 1997 [DIRS 100896], p. 12	Section 6.4.4

4.2 CRITERIA

Technical Work Plan for Postclosure Engineered Barrier Degradation Modeling (SNL 2007 [DIRS 178849], Table 3-1) identified the following acceptance criteria based on the requirements mentioned in *Yucca Mountain Review Plan, Final Report* (YMRP) (NRC 2003 [DIRS 163274]):

1. System Description and Demonstration of Multiple Barriers (NRC 2003 [DIRS 163274], Section 2.2.1.1.3)

   Specific requirements involve identification of multiple barriers (natural and engineered), describing the capabilities of these barriers to isolate waste, and providing technical bases for capabilities descriptions consistent with the postclosure performance objectives. To comply with these requirements, the following acceptance criteria are identified:

   - AC1: Identification of Barriers is Adequate
   - AC2: Description of the Capability of Identified Barriers is Acceptable
   - AC3: Technical Basis for Barrier Capability is Adequately Presented.

2. Degradation of Engineered Barriers (NRC 2003 [DIRS 163274], Section 2.2.1.3.1.3)

   Specific requirements include describing deterioration or degradation of engineered barriers and modeling degradation processes using data for performance assessment, including TSPA. Consideration of uncertainties and variabilities in model parameters and alternative conceptual models are also required. To fulfill these requirements, the following acceptance criteria are identified:

   - AC1: System Description and Model Integration are Adequate
   - AC2: Data are Sufficient for Model Justification
   - AC3: Data Uncertainty is Characterized and Propagated Through the Model Abstraction

- AC4: Model Uncertainty is Characterized and Propagated Through the Model Abstraction

- AC5: Model Abstraction Output is Supported by Objective Comparisons.

The YMRP (NRC 2003 [DIRS 163274]) criteria are addressed in Section 8.4.

4.3 CODES AND STANDARDS

This section lists the codes and standards used in the model analyses documented in this report.

4.3.1 Corrosion Degradation Analyses and Models

- *Standard Practice for Prediction of the Long-Term Behavior of Materials, Including Waste Forms, Used in Engineered Barrier Systems (EBS) for Geological Disposal of High-Level Radioactive Waste* (ASTM C 1174-97 2002 [DIRS 105725]).

4.3.2 Corrosion Measurements

- *Standard Reference Test Method for Making Potentiostatic and Potentiodynamic Anodic Polarization Measurements* (ASTM G 5-94 1994 [DIRS 117479])

- *Standard Test Method for Conducting Cyclic Potentiodynamic Polarization Measurements for Localized Corrosion Susceptibility of Iron-, Nickel-, or Cobalt-Based Alloys* (ASTM G 61-86 1987 [DIRS 127897])

- *Standard Practice for Making and Using U-Bend Stress-Corrosion Test Specimens* (ASTM G 30-94 1994 [DIRS 137688])

- *Standard Practice for Preparing, Cleaning, and Evaluating Corrosion Test Specimens* (ASTM G 1-90 1999 [DIRS 103515])

- *Standard Test Method for Conducting Potentiodynamic Polarization Resistance Measurements* (ASTM G 59-97 1998 [DIRS 163907])

- *Standard Practice for Conventions Applicable to Electrochemical Measurements in Corrosion Testing* (ASTM G 3-89 1989 [DIRS 138911])

- *Standard Practice for Calculation of Corrosion Rates and Related Information from Electrochemical Measurements* (ASTM G 102-89 1989 [DIRS 163908])

- *Standard Test Methods of Detecting Susceptibility to Intergranular Corrosion in Wrought, Nickel-Rich, Chromium-Bearing Alloys* (ASTM G 28-97. 1997 [DIRS 154712]).

4.3.3 Composition of Alloy 22

- *Standard Specification for Low-Carbon Nickel-Molybdenum-Chromium and Low-Carbon Nickel-Chromium-Molybdenum Steel Alloy Plate, Sheet, and Strip* (ASTM B 575-99a 1999 [DIRS 147465]).

4.3.4 Standard Related to Data Analysis

- *Standard Practice for Dealing with Outlying Observations* (ASTM E 178-02 2002 [DIRS 169968])

- *Standard Practice for Reporting Uniaxial Strength Data and Estimating Weibull Distribution Parameters for Advanced Ceramics* (ASTM C 1239-06A. 2006 [DIRS 178286]).

5. ASSUMPTIONS

This section documents the assumptions used to perform analyses and model development and, if necessary, their abstractions for general corrosion and localized corrosion of the WPOB for the environmental exposure conditions expected in the postclosure repository. Where necessary, additional details of the assumptions are described in the section(s) in which the analyses and models are documented.

5.1 Assumption: Aqueous corrosion, including "humid-air" corrosion, general corrosion, and localized corrosion, will occur only if the relative humidity exceeds a threshold relative humidity ($RH_{threshold}$). As discussed in Section 6.4.2, dry oxidation can occur at relative humidities below the threshold relative humidity. Conservatively, it is assumed that there is no threshold relative humidity for initiation of general or localized corrosion of the Alloy 22 WPOB.

Rationale: The critical relative humidity is the relative humidity below which water will not form on a clean metal surface and electrochemical processes will not occur (ASM International 1987 [DIRS 133378], p. 82). For clean metal surfaces, the relative humidity must exceed a threshold relative humidity before a thin film of moisture will form on the metal surface, providing an electrolyte for ionic current transfer. For metallic nickel, the threshold relative humidity value is 50% to 70% (ASM International 1987 [DIRS 133378], p. 82). However, lack of surface cleanliness due to such factors as corrosion product build-up or the presence of hygroscopic salts or contaminants can cause water absorption at lower relative humidities (ASM International 1987 [DIRS 133378], p. 80). On this basis, the existence of a threshold relative humidity for initiation of corrosion processes is a reasonable assumption and consistent with data presented in corrosion handbooks. However, as the surface state of the metals considered here is unknown (in terms of the presence of contamination), the relative humidity threshold is conservatively assumed to be zero.

Confirmation Status: This is a conservative assumption and does not require further confirmation.

Use in Model: This assumption is used throughout this report. In particular, this assumption is called out in Sections 6.3.1, 6.3.3, and 6.4.3.

5.2 Assumption: The general corrosion rate of Alloy 22, at a given temperature, is assumed constant (i.e., time-independent).

Rationale: This assumption is considered conservative because the general corrosion rate of metals and alloys tends to decrease with time. This behavior is discussed for Alloy 22 in Section 7.2.1, which shows that the general corrosion rates of Alloy 22 at 90°C for exposure times of up to five years decrease with increasing exposure time.

Confirmation Status: This is a conservative assumption because the general corrosion rate of metals and alloys tends to decrease with time; therefore, no additional confirmation of this assumption is necessary.

Use in Model: This assumption is used throughout this report. In particular, this assumption is called out in Sections 6.3.3, 6.4.3, 7.2.1, and 8.4.2.

5.3 Assumption: Although both pitting and crevice corrosion of Alloy 22 may occur in the repository, the localized corrosion initiation thresholds used in this report are based on the initiation of crevice corrosion, i.e., the crevice repassivation potential (obtained from creviced specimens) is conservatively assumed to be the critical potential for the initiation of localized corrosion and not the pit repassivation potential obtained from uncreviced specimens.

Rationale: This is a conservative and bounding assumption because initiation thresholds for crevice corrosion, in terms of exposure parameters such as chemistry and temperature, are lower than those required for pitting corrosion (Gdowski 1991 [DIRS 100859], Section 3.7; Agarwal 2000 [DIRS 163034], pp. 845 to 847) and most of the WPOB surface will not be creviced. Additionally, crevice corrosion may be applied to the entire wetted area of the waste package surface, though it is unlikely that crevice attack would occur over the entire wetted surface area due to the need for some cathodic area to support the anodic crevice corrosion reaction.

Confirmation Status: This is a conservative and bounding assumption; therefore, no additional confirmation of this assumption is necessary.

Use in Model: This assumption is called out in Sections 6.3.3, 6.4.4, 7.2.1, and 8.4.2.

5.4 Assumption: When localized corrosion occurs, the localized corrosion of the WPOB is assumed to propagate at a (time-independent) constant rate.

Rationale: This assumption is conservative because it is known that localized corrosion rates decrease with time (CRWMS M&O 1998 [DIRS 100349], Table 3-2; Hunkeler and Boehni 1983 [DIRS 162221]; McGuire et al. 1998 [DIRS 152193], Section 5.2.8; EPRI 2002 [DIRS 158069], Section 5.3.1; Frankel 1998 [DIRS 162216]; Newman and Franz 1984 [DIRS 162250]). Additionally, as discussed further in Section 6.4.4.8.2, localized corrosion may be stifled due to the accumulation of corrosion product deposits or slow cathodic kinetics.

Confirmation Status: This assumption is conservative because it is known that localized corrosion rates decrease with time; therefore, no additional confirmation of this assumption is necessary.

Use in Model: This assumption is called out in Sections 6.3.3, 6.4.4, 7.2.5, 8.3.2, and 8.4.2.

5.5 Assumption: The localized corrosion data of the WPOB material (Alloy 22) that were generated in fully immersed conditions are assumed to be applicable to the localized corrosion processes of the waste package in contact with thin water films resulting from seepage that have the same water chemistry as the fully immersed condition.

Rationale: Thin water films may form on the WPOB surface due to seepage or due to deliquescence of salts settled upon the WPOB in the nominal-case postclosure repository. The localized corrosion data of the WPOB material (Alloy 22) generated in fully immersed conditions are applicable to the thin film case, because a similar stagnant boundary layer is formed in the creviced region in both cases. Moreover, under inundated conditions, the metal is in contact with a practically unlimited reservoir of corrosive solution. As a result, the crevice corrosion behavior under inundated condition will not be reactant-limited. In contrast, the crevice corrosion behavior under thin film conditions will be reactant-limited because the metal will be in direct contact with a very limited volume of the corrosive solution. Therefore, crevice corrosion on Alloy 22 specimens under fully immersed conditions provides a conservative assessment of Alloy 22 crevice corrosion behavior under thin film conditions. In addition, without a bulk environment, the cathodic area outside the crevice will be limited, leading to a decrease in the ability to sustain the crevice corrosion processes. Corrosion potentials measured in short-term immersed experiments could be lower than those measured under thin film conditions due to short-term decreases in the oxygen content near the sample surface. Short-term oxygen depletion would be replenished at a faster rate under thin water film conditions than in fully immersed conditions. Short-term oxygen depletion is not expected to be a viable process during the experiments performed to obtain the corrosion potentials used in model development because these experiments were long-term experiments in which the oxygen concentration would have reached steady-state levels and the corrosion rates of Alloy 22 are so low that little oxygen would be consumed during the course of measurement.

Confirmation Status: This is a reasonable assumption and does not require further confirmation.

Use in Model: This assumption is used throughout this report.

5.6 **Assumption**: The corrosion behavior of the stress-mitigated (low-plasticity burnished or laser-peened) outer lid closure weld region does not significantly differ from the corrosion behavior of a closure lid weld region that has not undergone stress-mitigation.

Rationale: Low-plasticity burnishing (LPB) can be used to mitigate residual stresses from the waste package outer lid closure weld region. LPB is a process by which a smooth, hard ball is rolled over the surface of the metal to be burnished, resulting in compressive deformation of the metal surface. The effectiveness of LPB and laser-shock peening (LSP), which is discussed below, as surface stress-mitigation techniques have been evaluated by Fix et al. (2005 [DIRS 173721]) in a series of experiments in which surface stress-mitigated (i.e., either LPB or LSP treated) as-welded Alloy 22 specimens and their unmitigated counterparts were subjected to immersion tests in boiling ferric sulfate/sulfuric acid solution per ASTM G 28A (ASTM G 28-97 1997 [DIRS 154712]), to electrochemical polarization tests in chloride and chloride-plus-nitrate solutions (e.g., polarization resistance tests per ASTM G 59-97 (1998 [DIRS 163907])), and CPP tests per ASTM G 61-86 (1987 [DIRS 127897]) at temperatures ranging from 80°C to 100°C. According to the results of these tests, both general corrosion and localized corrosion susceptibilities of these three kinds of specimens were similar in each aqueous environment tested (i.e., ferric

sulfate/sulfuric acid solution, acidic chloride solution, and acidic chloride-plus-nitrate brine).

LSP, also known as laser peening, involves the use of a laser pulse that induces a shock wave within the material being peened, resulting in the formation of a compressive surface layer. Comparisons of the corrosion rates (measured by the polarization resistance technique in SAW at 90°C and potentiodynamic polarization curves) of unmitigated and laser-peened Alloy 22 samples have shown that laser-peened samples exhibited lower corrosion rates than unmitigated samples (Chen et al. 2002 [DIRS 165441], Figure 9). Also laser-peened samples exhibited lower passive current densities (in potentiodynamic polarization tests) than unmitigated samples (Chen et al. 2002 [DIRS 165441], Figure 10). The potentiodynamic polarization curves did not show the initiation of localized corrosion before the transpassive potential was reached. No credit is taken in this report for the possible increase in corrosion resistance imparted by stress mitigation process.

Confirmation Status: This is a reasonable assumption and does not require further confirmation.

Use in Model: This assumption is used throughout this report.

6. MODEL DISCUSSION

6.1 ANALYSIS AND MODELING OBJECTIVES

The purpose and scope of this report are to document the analyses and models for general and localized corrosion of the waste package outer barrier (WPOB). The purpose of the general corrosion model is to analyze degradation of the Alloy 22 outer barrier by general corrosion under the range of expected repository exposure conditions over the repository performance period. The purpose of the localized corrosion model is to analyze degradation of the Alloy 22 outer barrier by crevice corrosion under the range of expected repository exposure conditions over the repository performance period. The Alloy 22 corrosion modeling and analyses documented in this report include an analysis of dry oxidation, general corrosion modeling, crevice corrosion initiation modeling, crevice corrosion growth modeling, an analysis of MIC, and an analysis of the effect of aging and phase instability. Treatment of seismic and igneous events and their consequences on WPOB performance are not discussed because they are outside of the scope of this report, although the general and localized corrosion models developed in this report are suitable for use in these scenarios. This report is used as a source of information in downstream analyses of waste package degradation.

6.2 FEATURES, EVENTS, AND PROCESSES RELEVANT TO THIS REPORT

The development of a comprehensive list of features, events, and processes (FEPs) potentially relevant to postclosure performance of the Yucca Mountain repository is an iterative process based on site-specific information, design, and regulations. Table 6-1 provides a list of FEPs included in this report and provides specific references to where the included FEPs are discussed within this report. Table 6-2 provides a list of excluded FEPs discussed in this report and provides specific references to sections within this report where the excluded FEPs are discussed. MO0706SPAFEPLA.001 [DIRS 181613], file: *FEPs_be.mdb* provides a list of all FEPs related to waste package and drip shield degradation.

Table 6-1. Included Features, Events, and Processes Addressed in This Report

FEP Number	FEP Name	Section(s) Where Described
2.1.03.01.0A	General corrosion of waste packages[a]	6.4.3, 6.4.5
2.1.03.03.0A	Localized corrosion of waste packages[b]	6.4.4
2.1.03.05.0A	Microbially influenced corrosion (MIC) of waste packages	6.4.5

[a] Aqueous corrosion processes are included.
[b] Localized corrosion due to dust deliquescence is discussed in SNL 2007 [DIRS 181267].

Table 6-2. Excluded Features, Events, and Processes Addressed in this Report

FEP Number	FEP Name	Section(s) Where Described
2.1.03.01.0A	General corrosion of waste packages[a]	6.4.2
2.1.11.06.0A	Thermal sensitization of waste packages	6.4.6

[a] Dry oxidation processes are treated as aqueous corrosion processes.

6.3 CONCEPTUAL MODEL

This section summarizes the expected exposure conditions and their relationship to the test solutions used. The conceptual model that was developed for the analyses and models of the general corrosion and localized corrosion of the WPOB under the expected exposure conditions for the repository is also described. ASTM C 1174-97 (1998 [DIRS 105725]) was followed for development of the models for general and localized corrosion of the WPOB documented in this report. Semiempirical modeling approaches were adopted by incorporating mechanistic understanding of the degradation processes into the modeling process.

A schematic representation of the conceptual model is shown in Figure 6-1. Additional details are described in the sections in which the analyses and models are documented.

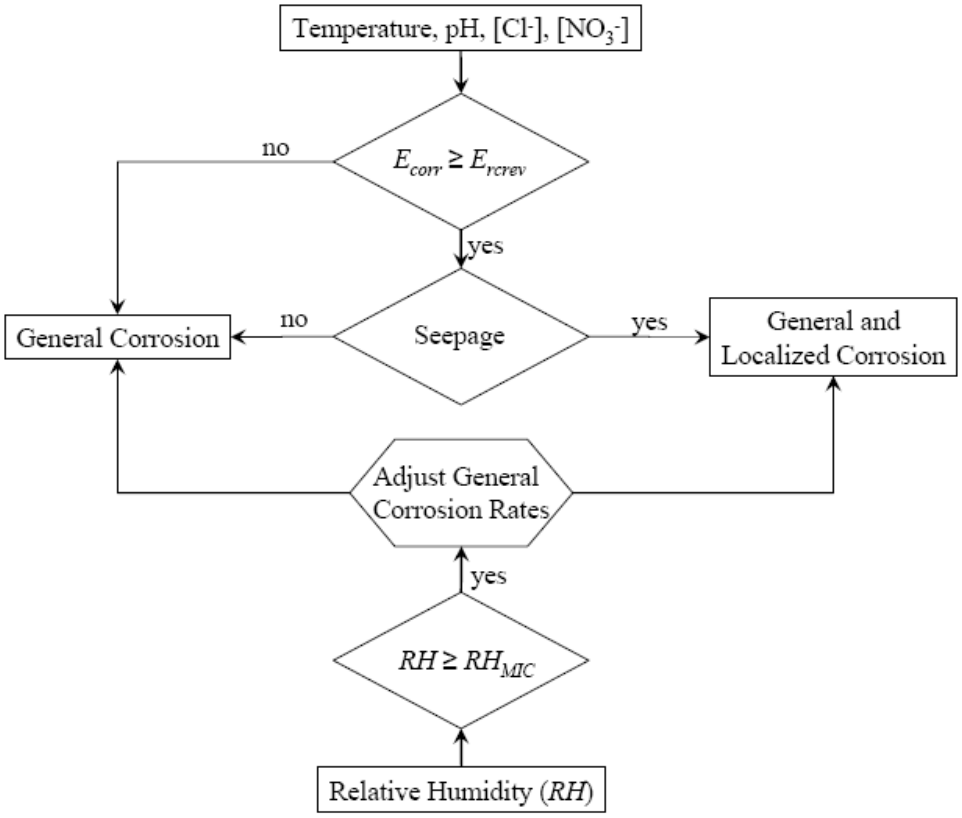

Figure 6-1. Schematic Representation of the Conceptual Model for the General and Localized Corrosion Model of the Waste Package Outer Barrier

6.3.1 Expected In-Drift Temperature and Relative Humidity

Figure 6-2 shows a summary of the range of waste package and drift wall temperature and relative humidity histories for the repository (SNL 2007 [DIRS 181383], Figures 6.3-74[a] and 6.3-79[a]). The influence of the low-probability seismic collapsed-drift scenario on in-drift thermalhydrologic conditions is shown in Figure 6-3 (SNL 2007 [DIRS 181383], Figure 6.3-80[a]).

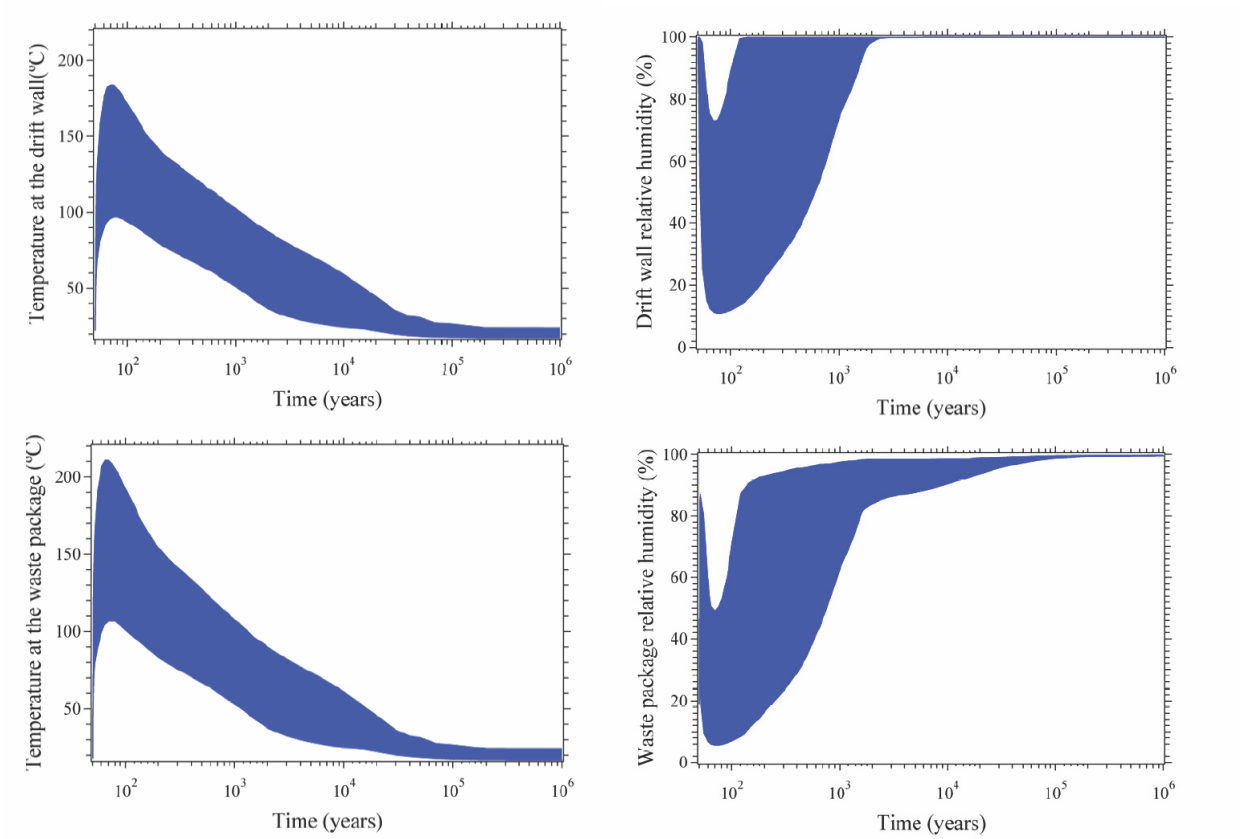

Source: SNL 2007 [DIRS 181383], Figures 6.3-74[a] and 6.3-79[a].

Figure 6-2. Waste Package and Drift Wall Temperature and Relative Humidity Ranges

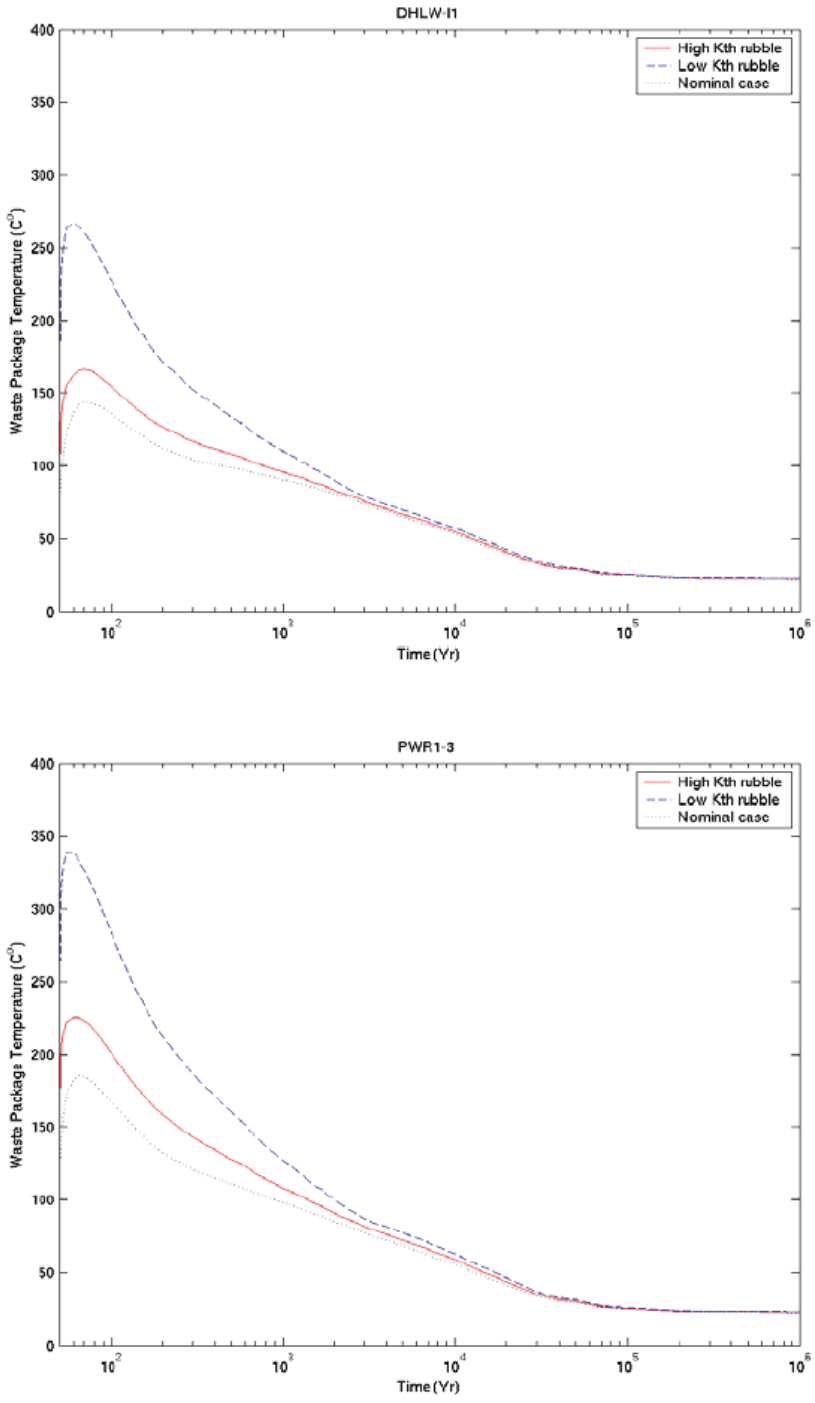

Source: SNL 2007 [DIRS 181383], Figure 6.3-80[a].

NOTE: Low and high K_{th} indicate low and high thermal conductivity, respectively, of the rubble formed in a collapsed drift.

Figure 6-3. Waste-Package Temperature Histories for the Defense High-Level Waste/Department of Energy Spent Nuclear Fuel-Long (DHLW-I1) Waste Package and 21-Pressurized Water Reactor Absorber Plate Commercial Spent Nuclear Fuel (PWR1-3) Waste Package for the Nominal (intact drift) Case and Low and High Rubble Thermal-Conductivity Collapsed-Drift Cases

Conceptually, the repository exposure conditions can be divided into three temperature regimes based on Figures 6-2 and 6-3. The attributes of each regime relative to corrosion processes can be summarized as follows:

Dryout—Drift walls will dry out quickly once waste packages are emplaced and ventilation starts during the preclosure period. Upon closure and the cessation of ventilation, the drift walls will generally increase in temperature to a temperature above the boiling point of water. No seepage should occur under these conditions, and no aqueous-phase localized corrosion would be sustainable. Localized corrosion effects due to dust and its potential deliquescence are discussed in *Analysis of Dust Deliquescence for FEP Screening* (SNL 2007 [DIRS 181267]). General corrosion is assumed to occur during this time period (Assumption 5.1).

Transition—Seepage into the drifts becomes possible as the waste package cools allowing the temperature of the drift wall to drop below the boiling point of water. If seepage happens to occur on a waste package while it is near or above the boiling point of water, the seepage will undergo evaporative concentration and form a concentrated brine solution. Hot concentrated brines have the greatest potential to cause localized corrosion. However, it is likely that the drip shields will all be intact at this time.

Low Temperature—As the waste package cools to temperatures well below the boiling point of water, the in-drift relative humidity will increase and result in less-concentrated brines potentially residing on the waste package surfaces. With further cooling of the waste package surface, solutions contacting the waste package will become even less concentrated, eventually approaching the seepage composition. Only general corrosion is expected to occur during this regime.

6.3.2 Relation of In-Drift Chemical Model Results to Corrosion Testing Environment

The project has developed an understanding of the in-drift chemical environment for the three temperature regimes described in Section 6.3.1. The understanding is based on geochemical models and supporting data and analysis appropriate for the repository conditions. A description of the evolution of the chemical environment is provided in *Engineered Barrier System: Physical and Chemical Environment* (SNL 2007 [DIRS 177412], Section 6.13.5), which includes discussions of the relationship between the geochemical process model results, the range of expected in drift environments, and the chemical environments used in corrosion related testing. A brief summary of the chemical environment applicable to corrosion related testing follows.

To assess the susceptibility of the WPOB to various corrosion processes, testing has been carried out in environmental conditions relevant to those predicted by in-drift chemical modeling. Corrosion-testing environments were designed based on the composition and other characteristics of the three types of brines found to exist in nature (SNL 2007 [DIRS 177412], Section 6.13.5): (1) calcium chloride, (2) carbonate, and (3) sulfate. Initial studies focused on the carbonate-type brine, based on reasoning that carbonate-type waters, typified by J-13 well water from the saturated zone near Yucca Mountain, are the expected types of waters at the Yucca Mountain repository (Harrar et al. 1990 [DIRS 100814]). The standardized solutions developed as repository-relevant environments are presented in Table 6-3. These solutions

include simulated dilute water (SDW), simulated concentrated water (SCW), simulated acidified water (SAW), and basic saturated water (BSW) aqueous test solutions.

Table 6-3. Target Chemical Compositions of the Electrolyte Solutions (mg/L) Employed in the Long-Term Weight-Loss Measurements

Concentration (mg/L)				
Ion	**SDW 60°C and 90°C**	**SCW 60°C and 90°C**	**SAW 60°C and 90°C**	**BSW-SC**
K	34	3,400	3,400	90,800
Na	409	40,900	37,690	231,000
Mg	1	<1	1,000	0
Ca	0.5	<1	1,000	0
F	14	1,400	0	1,620
Cl	67	6,700	24,250	178,000
NO_3	64	6,400	23,000	177,000
SO_4	167	16,700	38,600	16,900
HCO_3	947	70,000	0	107,000
Si	27 (60°C) 49 (90°C)	27 (60°C) 49 (90°C)	27 (60°C) 49 (90°C)	7060
Nominal pH	9.8 to 10.2	9.8 to 10.2	2.7	>12

Source: DTN: LL040803112251.117 [DIRS 171362].

NOTES: DTN: LL040803112251.117 [DIRS 171362] lists several different BSW solution compositions. BSW-SC is representative of these and is most relevant to the analyses in this report.

BSW-SC = basic saturated water containing silica and carbonate (with concentration values rounded to three significant digits), SAW = simulated acidic water, SCW = simulated concentrated water, SDW = simulated dilute water.

The following discussion on the relevance of the test media to the in-drift chemical environment is a summary of *Engineered Barrier System: Physical and Chemical Environment* (SNL 2007 [DIRS 177412], Section 6.13.5) and is used in this report as background information only.

Calcium Chloride Brines—The calcium chloride brines have acidic to near-neutral pH and no significant bicarbonate/carbonate, fluoride, or sulfate content. These brines also contain other cations, such as sodium, potassium, and magnesium, and other anions such as nitrate. The endpoint of the evaporative concentration of this type of brine contains Ca-Cl/NO_3 or a mixture of Ca/Mg-Cl/NO_3. The quantity of magnesium and calcium is limited due to the precipitation of calcium carbonates, sulfates, and magnesium silicates. Nitrate will be present; an endpoint brine of this type is dominated by calcium chloride and calcium nitrate. Formation of calcium-chloride brines is also expected to be limited in the repository (SNL 2007 [DIRS 177412], Section 6.13.5).

Corrosion test solutions corresponding to the calcium chloride type of brine include calcium chloride, calcium chloride plus calcium nitrate, and sodium chloride aqueous solutions. The sodium chloride test solutions simulate the moderate relative humidity scenario where calcium is a minor component in the aqueous solution.

Carbonate Brines—As mentioned in *Engineered Barrier System: Physical and Chemical Environment Model* (SNL 2007 [DIRS 177412], Section 6.13.5), carbonate brines are alkaline and do not contain significant calcium or magnesium content. In the early stages of the evaporative concentration, calcium precipitates predominately as carbonate mineral (calcite or aragonite) under equilibrium conditions. Magnesium precipitates as a minor component in the calcium carbonate species and as magnesium silicate. Potassium may be significant in some of these brines. Nitrate is expected to be an important component, and a brine of this type may evolve through a high extent of evaporation into one in which nitrate is actually the dominant anion. The carbonate brine is likely to be represented as alkali metal (sodium, potassium) carbonate brine. The relative humidity dependence of carbonate brine composition is as follows. At low relative humidity, the aqueous solutions are dominated by nitrate and chloride anions with nitrate ions dominating at the lowest relative humidity. At moderate relative humidity (greater than 70% relative humidity), chloride ions could dominate the solution composition. The nitrate-chloride solutions will have slightly elevated pH due to residual carbonate in solution. Significant amounts of carbonate and sulfate ion are not expected until the relative humidity is greater than 85%.

Corrosion test solutions corresponding to the carbonate type of brine include the SDW, SCW, BSW, and under certain circumstances, SAW aqueous test solutions (Table 6-3). The BSW test solution is a highly concentrated alkaline solution with a boiling point of about 110°C. The SCW test solution is a moderately concentrated alkaline solution and solutions in this concentration range form at relative humidity in the range of 90% to 95% (SNL 2007 [DIRS 177412], Section 6.13.5). The SDW test solution is a dilute alkaline solution, and solutions in this concentration range form at high relative humidity (greater than 99%) (SNL 2007 [DIRS 177412], Section 6.13.5). These may have characteristics of solutions at the drift wall (i.e., typical of in-drift seepage).

Under conditions of extreme evaporative concentration (i.e., low relative humidity), this type of brine containing high nitrate and chloride content would evolve into nitrate-chloride brine with low carbonate content. The SAW test solution has characteristics of low carbonate brine and of solutions in equilibrium with relative humidity of nominally 90% (SNL 2007 [DIRS 177412], Section 6.13.5). The calcium and magnesium addition to this test solution makes it more able to sustain lower pH values due to hydrolysis of these cations.

Sulfate Brines—As discussed in *Engineered Barrier System: Physical and Chemical Environment* (SNL 2007 [DIRS 177412], Section 6.13.5), the sulfate brines have near-neutral pH and no significant carbonate or calcium content. Calcium precipitates out as carbonates and possibly as sulfates. In addition, sulfate brines typically have only a small amount of magnesium, though some surface brines have been observed to have high magnesium (Drever 1997 [DIRS 140067], Table 15-1, Brines 1 to 3). The dominant cation is typically sodium. In the repository brines, potassium ion concentration may be more significant than sodium ion concentration, and magnesium ion concentration is expected to be insignificant. The relative humidity dependence of the sulfate brine is discussed below.

At low relative humidity, the aqueous solutions are dominated by nitrate and chloride anions with nitrate ions dominating at the lowest relative humidity. At moderate relative humidity (greater than 70% relative humidity) (SNL 2007 [DIRS 177412], Section 6.13.5), chloride ions

dominate the solution composition. However, unlike the carbonate brines, these brines have near-neutral to slightly acidic pH because of the lack of a carbonate component. Significant amounts of carbonate and sulfate ion do not exist until the relative humidity is greater than 85% because of the increase in solubility of sulfate minerals (sodium and potassium sulfates) (SNL 2007 [DIRS 177412], Section 6.13.5). Magnesium sulfate is present in insignificant quantities in these brines.

BSW has a boiling point near 110°C. The total concentration of dissolved salts in the starting liquid is greater than that in the standard SCW solution. After evaporation of approximately 90% of the water from the starting solution, the residual solution reaches a maximum chloride concentration and has a boiling point of approximately 110°C, with a pH of about 11. The synthetic BSW solution composition can be slightly modified (mainly by adding sodium hydroxide) to cover a range of pH values, yielding solutions referred to as BSW-11, -12, and -13 in DTN: LL040803112251.117 [DIRS 171362].

The corrosion test solution corresponding to the sulfate type of brine is SAW (Table 6-3). The SAW test solution has characteristics of solutions in equilibrium with nominally 90% relative humidity (SNL 2007 [DIRS 177412], Section 6.13.5).

6.3.3 Waste Package Outer Barrier Degradation Conceptual Model

A schematic representation of the waste package degradation conceptual model is shown in Figure 6-1. The design functions of the drip shield are to prevent the water seeping into the emplacement drifts from dripping directly onto the waste package and to provide protection from rockfall damage to the waste package. Before the drip shield breaches, the chemistry of aqueous solutions contacting the waste package would be determined by the chemistry of leachate from dust that settles on the waste package surface. As the thermal heat output from the radioactive waste decays with time, thermal-hydrologic conditions in the emplacement drift dynamically change. Concentrated brines could form on the waste package surface from the deliquescence of multi-salt assemblages present within the dust. The chemical evolution of the brines would be dependent on the humidity and temperature conditions. When the drip shield breaches and, therefore, no longer performs its seepage-diversion design function, the waste package underneath the breached drip shield could be directly contacted by seepage. In this case, the water chemistry contacting the waste package would be determined primarily by the chemistry of the seepage. In either case, hygroscopic salts may be deposited on the waste package surface due to evaporative concentration of the leachate from the dust and aerosols in contact with humid air or, after drip shield breach, due to the evaporative concentration of the seepage that contacts the waste package surface. Such hygroscopic salts enable aqueous solutions to exist as thin water films at relative humidity below 100%. The threshold relative humidity ($RH_{threshold}$) at a given temperature, at which an aqueous solution can exist, is defined as the deliquescence point at that temperature. This threshold relative humidity defines the lowest humidity condition necessary for aqueous electrochemical corrosion processes of a metal to occur at a given temperature. As stated in Assumption 5.1 (Section 5), general corrosion of the WPOB is conservatively assumed to occur at any relative humidity (above or below the threshold relative humidity, $RH_{threshold}$). Localized corrosion of the WPOB is conservatively assumed to be able to initiate regardless of the exposure relative humidity (although localized corrosion can only initiate under certain exposure conditions (Section 6.4.4)).

In postclosure repository environments, crevices could form between the waste package surfaces and the structural components, other materials in the emplacement drift, and mineral deposits from evaporative concentration of the solutions in contact with the waste package surface. The localized corrosion models for the WPOB developed in this report are based on data from crevice geometry samples. This treatment is conservative because creviced geometries will not be formed over the entire waste package surface.

Dry oxidation of the WPOB occurs at any relative humidity below the threshold relative humidity, $RH_{threshold}$. This process results in the formation of an adherent, protective oxide film of uniform thickness. The rate of dry oxidation is generally limited by mass transport through the growing oxide film. As is discussed in Section 6.4.2, dry oxidation (FEP 2.1.03.01.0A) is not a performance-limiting process of the WPOB under thermal conditions in the repository. Therefore, dry oxidation is not implemented in total system performance assessment (TSPA).

General corrosion (or passive corrosion) is the uniform thinning of the WPOB at its open-circuit corrosion potential (E_{corr}). As stated in Assumption 5.1 (Section 5), it is assumed that there is no threshold relative humidity for initiation of general corrosion of the Alloy 22 WPOB. The general corrosion rate is generally time and temperature dependent. In this modeling work, the corrosion rate is assumed constant for a given temperature, (i.e., time-independent). Therefore, at a given temperature, the depth of penetration or thinning of the WPOB due to general corrosion is equal to the general corrosion rate at that temperature multiplied by the time duration when the waste package surface is at that temperature. This assumption is considered conservative because the general corrosion rate of metals and alloys tends to decrease with time (Assumption 5.2 and Section 6.4.3.5).

The general corrosion model developed in this report uses a general corrosion rate distribution determined from weight-loss measurements of Alloy 22 crevice specimens that were exposed for over five years in a wide range of multi-ionic solutions at the LTCTF (Section 6.4.3.2). As discussed in Section 6.4.3.2, the sample configuration (crevice, disk, or rod), metallurgical condition (mill-annealed or as-welded), and water chemistry within the expected range do not have a significant effect on the general corrosion behavior of Alloy 22. Non-thermal stress-mitigation processes, used to introduce a compressive stress layer in the outer lid closure weld region in order to delay the initiation of stress corrosion cracking, may introduce cold work into the material. Angeliu (2001 [DIRS 165442]) observed that unmitigated Stainless Steel Type 316NG weldments could contain up to 20% cold work due to weld shrinkage and differential thermal expansion. Therefore, it is reasonable to consider that welded Alloy 22 specimens also have up to 20% cold work. Since it has been determined in this report that the general corrosion behavior of welded specimens does not significantly differ from that of unwelded specimens (e.g., Figure 6-14 and Figure 6-19), it is reasonable to conclude that the presence of moderate cold work has no significant effect on the general corrosion behavior of Alloy 22.

The temperature dependence of the general corrosion rate is represented with an Arrhenius relationship. The activation energy used in the Arrhenius relationship was determined from corrosion rates calculated from short-term polarization resistance measurements of Alloy 22 specimens with varying sample configurations and metallurgical conditions. The specimens were tested over a range of exposure conditions (temperature and water chemistry). As with the general corrosion rate from the long-term weight-loss measurements discussed above, the sample

configuration (crevice, disk or rod), metallurgical conditions (mill-annealed or as-welded), and water chemistry within the expected range do not have a significant effect on the temperature-dependence of the general corrosion rate of the alloy (Section 6.4.3.4). The Electric Power Research Institute (EPRI 2002 [DIRS 158069], Section 5.3.2) presented a similar conceptual description by using literature data for similar corrosion-resistant nickel-chromium-molybdenum (Ni-Cr-Mo) alloys.

Localized corrosion is a corrosion process in which the attack progresses at discrete sites or in a nonuniform manner. The rate of localized corrosion is generally much higher than the rate of general corrosion. As stated in Assumption 5.3 (Section 5), the current analysis assumes crevice corrosion is representative of localized corrosion of the WPOB under the exposure conditions expected in the postclosure repository. This is a conservative and bounding assumption because initiation thresholds for crevice corrosion of Alloy 22 in terms of water chemistry and temperature are lower than for pitting corrosion (Gdowski 1991 [DIRS 100859], Section 3.0; Haynes International 1997 [DIRS 100896]; Haynes International 1997 [DIRS 100897]).

Crevice corrosion of the WPOB is modeled with two model components: an initiation model and a propagation model. Crevice corrosion of the WPOB occurs when the open-circuit corrosion potential (E_{corr}) is equal to or greater than a critical potential ($E_{critical}$) (i.e., ΔE (= $E_{critical}$ - E_{corr}) ≤ 0. This conceptual model of crevice corrosion initiation is recognized by the corrosion research community (e.g., Dunn et al. 2005 [DIRS 178451] and Beavers et al. 2002 [DIRS 158781], Section 8.3). The ΔE criterion was developed based on information found throughout the corrosion science literature (Böhni 2000 [DIRS 164137], Section B; Dunn et al. 2000 [DIRS 164495]; Dunn et al. 2003 [DIRS 164138]; Frankel 1998 [DIRS 162216]; Frankel 2002 [DIRS 164140]; and Frankel and Kelly 2002 [DIRS 164141]). The crevice corrosion initiation model components (i.e., E_{corr} and $E_{critical}$) are represented as a function of temperature, pH (for E_{corr} *only)*, chloride-ion concentration, and nitrate-ion concentration.

When it occurs, crevice corrosion of the WPOB is assumed to propagate at a constant (time-independent) rate (Assumption 5.4). This assumption is highly conservative because it is known that the localized corrosion rate (e.g., crevice corrosion rate) decreases with time, and this is particularly more likely under discontinuous and tortuous thin water films expected to form on the waste package surface in the postclosure repository. Section 6.4.4.8 provides a more detailed discussion.

The WPOB is subject to MIC when the relative humidity at the WPOB surface is above a relative humidity threshold that is uniformly distributed between 75% and 90%. The MIC initiation threshold relative humidity is based on the analysis documented in *Evaluation of the Impact of Microbial Activities on Drift Chemistry* (BSC 2004 [DIRS 169991], Section 7.1). The effect of MIC on general corrosion of the WPOB is represented by a general corrosion enhancement factor. The enhancement factor was determined from the comparative analysis of the corrosion rates measured from the short-term polarization resistance measurements of Alloy 22 specimens tested in abiotic and biotic conditions (DTN: LL991203505924.094 [DIRS 138343], SEP table "S99502_001").

The waste package design and fabrication specification specifies that the WPOB base metal and all fabrication welds (except the closure lid welds) be fully annealed before the waste packages are loaded with waste (SNL 2007 [DIRS 179394], Section 4.1.2).

According to the analysis documented in *Aging and Phase Stability of Waste Package Outer Barrier* (BSC 2004 [DIRS 171924], Section 8), phase instabilities are not expected in Alloy 22 base-metal and welded material due to the thermal hydrologic exposure profiles in the repository. In addition, YMP data (Section 6.4.6) show that the corrosion properties of aged welds are comparable to those of unaged welds. Phase instabilities are not expected to occur, and, even if they do, they are not expected to have a significant effect on the corrosion properties; therefore, the effects of aging and phase instability of the WPOB are not modeled in TSPA.

Effects of oxidants, such as hydrogen peroxide generated from gamma radiolysis, on corrosion may be accounted for through the open-circuit corrosion potential (E_{corr}). However, radiolysis-enhanced corrosion has been screened out in DTN: MO0706SPAFEPLA.001 [DIRS 181613], file: *FEPs_be.mdb*. Therefore, radiolysis-enhanced corrosion of the WPOB is not considered in this waste package corrosion analysis.

The waste package is a double-walled container with an outer barrier constructed of the highly corrosion-resistant Alloy 22 (UNS 06022) and an inner vessel made of Stainless Steel Type 316 (UNS S31600). The inner vessel will provide structural support to the thinner outer barrier, while the outer barrier will protect the inner vessel from significant corrosion degradation until failure of the outer barrier. Although the inner vessel could provide some delay of radionuclide release before it fails and could also retard the release rate of radionuclides from the waste package, no performance credit is taken for the corrosion resistance of the inner vessel (i.e., all corrosion performance is allocated to the WPOB). This model approach is used throughout the analysis and is conservative for the reasons noted above.

After penetration of the WPOB, a crevice can form in the interfacial region between the Alloy 22 outer cylinder and Stainless Steel Type 316 inner vessel. The formation of a low-pH crevice environment in this interfacial region is possible. A local acidic water chemistry could be developed through hydrolysis of dissolved metal ions in the crevice regions between the two barriers. Moreover, due to the limited availability of oxygen (dominant oxidizer for this condition) to such an occluded area, polarization of the creviced region due to differential aeration (between the creviced region and adjacent uncreviced region(s)) may occur. However, tests conducted in the LTCTF show that Alloy 22 is highly resistant to crevice corrosion in repository-relevant solutions (e.g., SCW, SAW, and SDW). Alloy 22 will likely act as the cathode relative to the Stainless Steel Type 316 inner vessel under these exposure conditions, leading to enhanced corrosion of the inner vessel and decreased corrosion of the WPOB.

6.4 MODEL FORMULATION

This section documents the analyses and models developed for general and localized corrosion of the WPOB under repository exposure conditions. The analyses and models also consider effects of microbiological processes (Section 6.4.5) and aging and phase instability (Section 6.4.6) of the WPOB for the repository conditions.

6.4.1 Stability of the Passive Film in Repository Relevant Environments

Corrosion performance of the WPOB depends on the integrity of the thin and adherent passive film formed on the alloy surface. This section discusses the conceptual understanding of passivity and passive film stability of Ni-Cr-Mo alloys in general by summarizing the data and information from the literature. Also discussed in this section is a summary of the experimental results of characterization for passive film on Alloy 22 tested in environments relevant to the conditions expected in the repository.

6.4.1.1 Conceptual Description of Passivity and Passive Film Stability

Passivity can be defined as the formation of a thin and adherent oxide or oxyhydroxide film that protects a metal or alloy from corrosive degradation. Corrosion performance of highly corrosion-resistant alloys such as Alloy 22 depends on the integrity of the passive film formed on the alloy surface in contact with the corrosive environment. Long-term stability of the passive film on the surface of the Alloy 22 WPOB is one of the key issues that determine the long-term performance of the waste packages in the repository. Use of corrosion rates based on five-year weight-loss experiments to model Alloy 22 general corrosion in the repository is conservative because the general corrosion rates are expected to decrease with time. As shown in Figure 7-1, the corrosion rates for Alloy 22 decrease with time over a five-year period. Use of these general corrosion rates would be conservative even if the corrosion rate observed during the first five-year exposure was reproduced for every subsequent five-year period. This section provides a brief description of the conceptual understanding of passivity and the passive film formation and stability of highly corrosion-resistant alloys such as Alloy 22.

6.4.1.1.1 Passive Films Formed on Metals

The passive film formed under aqueous condition is not a single layer but rather has a stratified structure of at least two layers (Macdonald 1992 [DIRS 154720]; Macdonald 1999 [DIRS 154721]; Marcus and Maurice 2000 [DIRS 154738], p. 138). According to this bilayer model, the passive film consists of an inner layer of oxide and an outer layer of hydroxide or oxyhydroxide. The inner oxide layer plays the role of a barrier layer against corrosion, and the outer layer plays the role of an exchange layer (Marcus and Maurice 2000 [DIRS 154738], p. 138) as discussed further in Section 6.4.1.1.2. In general, the chemical composition and thickness of passive films depend on the nature of the metal, the pH of the electrolyte in which the metal is passivated, and the electrochemical potential (Macdonald 1992 [DIRS 154720]; Macdonald 1999 [DIRS 154721]; Marcus and Maurice 2000 [DIRS 154738], p. 138). For nickel, which can passivate in solutions over a wide range of pH, the passive film is generally composed of nickel (II) cations with an inner layer of NiO and an outer layer of $Ni(OH)_2$ (Marcus and Maurice 2000 [DIRS 154738], p. 140).

Passive films formed on metal surfaces are generally not electronic conductors but rather semiconductors or insulators. The electronic structures of passive films can be determined by photoelectrochemical measurements. However, structural analyses are rather difficult, due to the nanometer thickness of passive films and the roughness of the surfaces because of dissolution. The passive film formed on nickel (in 0.05 *M* H_2SO_4) displays crystallites, the sizes of which are reduced with increasing potential (Marcus and Maurice 2000 [DIRS 154738], p. 146). The

shape of these crystallites also changes with potential (Marcus and Maurice 2000 [DIRS 154738], Table 3-1). Another factor that must be considered is active dissolution, which occurs as long as the surface is not completely passivated. The dissolution rate increases with increasing potential. Dissolution processes may create new sites for oxide nucleation and, thus, can favor a higher density of oxide nuclei (Marcus and Maurice 2000 [DIRS 154738], p. 147). The passive film formed on nickel can be crystalline, with the surface exhibiting terraces and steps. The passive oxide film formed on chromium can have a nanocrystalline structure with oxide nanocrystals cemented together by the chromium hydroxide outer layer, making the passive film extremely protective against corrosion-induced damage (Marcus and Maurice 2000 [DIRS 154738], p. 149).

6.4.1.1.2 Passive Film Growth Mechanisms

As summarized in the literature (Macdonald 1992 [DIRS 154720]; Macdonald 1999 [DIRS 154721]; Marcus and Maurice 2000 [DIRS 154738], Section 3.6), the barrier oxide layer (inner layer of the passive film) forms by generation of oxygen vacancies at the metal–film interface, balanced in the steady state by dissolution of the barrier layer at the barrier layer–outer layer interface. The outer layer forms via the hydrolysis and precipitation of cations transmitted through the barrier layer or by hydrolytic restructuring of the barrier layer–outer layer interface. The distinctly different origins of the barrier and outer layers are amply demonstrated by the fact that both layers may incorporate alloying elements from the alloy substrate, but only the outer layer incorporates species from the solution. Furthermore, with respect to a fixed external frame of reference, the barrier layer grows into the substrate metal, whereas the outer layer grows outwards into the solution (Macdonald 1992 [DIRS 154720]; Macdonald 1999 [DIRS 154721]; Marcus and Maurice 2000 [DIRS 154738], Section 3.6). Thus, while the growth of the barrier layer is due to the generation of oxygen vacancies at the metal–barrier layer interface, the growth of the outer layer is commonly (but not exclusively) due to the transmission of cations through the barrier layer, either through cation vacancies or as cation interstitials, and their eventual emission at the barrier layer–outer layer interface. The origin of the outer layer is not exclusively due to cation transmission, because it may also form via hydrolytic restructuring of the barrier layer at the barrier layer–outer layer interface (Macdonald 1992 [DIRS 154720]; Macdonald 1999 [DIRS 154721]; Marcus and Maurice 2000 [DIRS 154738], Section 3.6).

Electric current is carried by all charged species in the barrier layer, including cation vacancies, cation interstitials, and oxygen vacancies, which are generated and annihilated at the interfaces and by dissolution of the barrier layer, depending on whether a change in oxidation state occurs (Macdonald 1992 [DIRS 154720]; Macdonald 1999 [DIRS 154721]). The principal mode of transport of defects is migration under the influence of a strong electric field, the magnitude of which is postulated to be established by the potential differences across the film and interfaces and by buffering due to Esaki (band-to-band) tunneling within the barrier layer (Macdonald 1992 [DIRS 154720]; Macdonald 1999 [DIRS 154721]). Because a barrier layer exists on all passive metals, all barrier layers are oxygen vacancy conductors to an extent that, in the steady state, is determined by the dissolution rate of the film. However, other defects may dominate the structural and electronic defect structures of the barrier layer. For example, the defect structure of the barrier layer on nickel is dominated by cation vacancies, while that on zinc is dominated by cation interstitials, although oxygen vacancies exist in both cases.

6.4.1.1.3 Surface-Enrichment of Chromium on Passivated Nickel-Base Alloys

Lloyd et al. (2003 [DIRS 167921]) found that passive films formed on Alloy 22 (both in air and after potentiostatic polarization (PSP)) have a distinct layer structure with an inner layer rich in chromium and nickel and an outer layer enriched in molybdenum. On this basis, the bilayer model developed in the studies of other passive alloys (Macdonald 1992 [DIRS 154720]; Macdonald 1999 [DIRS 154721]; Marcus and Maurice 2000 [DIRS 154738], Section 3.6) can be applied to Alloy 22. The concentration of Cr^{3+} in the inner oxide layer is higher than the nominal chromium content of the alloy (Marcus and Maurice 2000 [DIRS 154738], p. 153; Lorang et al. 1990 [DIRS 154718], Figures 1 and 2). The enrichment of chromium in the barrier layer of nickel-based alloys has been studied using the point defect model (PDM) (Zhang and Macdonald 1998 [DIRS 154743]; Zhang and Macdonald 1998 [DIRS 154742]). The PDM is based on the selective oxidation of the elements at the alloy–barrier layer interface, differences in transport properties of the species in the barrier layer, and selective oxidation of the elements at the barrier layer–outer layer interface. In the specific case of the passive film on iron-chromium alloys, the enrichment of chromium in the barrier layer appears to entail the dissolution of iron and the oxidative segregation of chromium (Marcus and Maurice 2000 [DIRS 154738], p. 153). Iron atoms are detached from the surface and dissolve into solution as ions, whereas chromium atoms are rapidly oxidized. The passive film forms by the nucleation and growth of a chromium oxide (Cr_2O_3)-like phase (Marcus and Maurice 2000 [DIRS 154738], p. 153). However, the barrier layers on iron-chromium and nickel-chromium alloys are not pure Cr_2O_3 but contain significant amounts of other metal species, such as nickel, ferrous, and ferric ions (Lorang et al. 1990 [DIRS 154718]).

6.4.1.1.4 Role of Molybdenum

There is a consensus that molybdenum reduces the rate of anodic dissolution in the active state (Marcus and Maurice 2000 [DIRS 154738], pp. 155 to 158). However, the mechanism by which molybdenum additions benefit the corrosion resistance of Ni-Cr-Mo alloys is not fully understood. Molybdenum tends to be located preferentially at local defects on the surface, which normally act as dissolution sites. The slowing down of the dissolution rate could be due to the strengthened metal–metal bonds when molybdenum is present (Marcus and Maurice 2000 [DIRS 154738], pp. 155 to 158). Further, the presence of molybdenum counteracts the deleterious effect of certain species such as sulfur, which can cause grain-boundary attack, in that it enriches on the surface, forms bonds to adsorbed sulfur, and then dissolves, thus mitigating the detrimental effects of adsorbed sulfur (Marcus and Maurice 2000 [DIRS 154738], p. 158). However, it should be noted that molybdenum sulfide is not readily soluble in water. It must be oxidized to a soluble form before its dissolution can occur. The expected aqueous environment at Yucca Mountain repository being oxic (Section 6.4.5) should be conducive to the oxidation of insoluble molybdenum sulfide to a soluble form. The removal of anodically segregated sulfur in this manner would pave the way for regeneration of the chromium oxide passive film on Alloy 22.

The role played by molybdenum (or any alloying element) in inhibiting passivity breakdown on alloys is discussed in terms of the PDM (Urquidi and Macdonald 1985 [DIRS 154741]). The PDM accounts quantitatively (within the accuracy of the experimental data) for the impact of molybdenum on the pitting resistance of 18 Cr-8 Ni stainless steels (e.g., Stainless Steel

Type 316, which contains molybdenum, versus Stainless Steel Type 304, which contains no molybdenum). In this case, the highly oxidized molybdenum ions present substitutionally in the barrier layer lattice form immobile, positively charged centers. For example, recognizing that the barrier layer on chromium-containing stainless steels and nickel-based alloys is essentially Cr_2O_3, substitution of Mo^{6+} into a chromium cation vacancy would produce the immobile trivalent molybdenum species at chromium vacancy sites (i.e., $Mo_{Cr}^{3\bullet}$). These immobile species can interact electrostatically with the mobile, negatively charged trivalent cation (e.g., chromium) vacancies (i.e., $V_{Cr}^{3'}$), the condensation of which at the metal–film interface is responsible for passivity breakdown (Macdonald 1992 [DIRS 154720]; Macdonald 1999 [DIRS 154721]). Thus, the solute-vacancy interaction reduces the free cation vacancy concentration and diffusivity, which results in a positive shift in the breakdown voltage and a lengthening of the induction time (i.e., the alloy becomes more resistant to passivity breakdown). The electrostatic interaction is described rigorously in terms of the ion-pairing theory that is commonly employed to describe ionic interaction in solutions. This solute-vacancy interaction model (Urquidi and Macdonald 1985 [DIRS 154741]) successfully accounts for the positive shift in the breakdown voltage upon adding molybdenum to the alloy without the need for arbitrary, adjustable parameters. Most importantly, the solute-vacancy interaction model accounts for why molybdenum must be present in the barrier layer at concentrations greater than about 2% for significant protection to be achieved.

Finally, complexing between $Mo_{Cr}^{3\bullet}$ and a defect will only occur if the defect is negatively charged (i.e., if the defect is a cation vacancy) (Urquidi and Macdonald 1985 [DIRS 154741]). However, the Cr_2O_3 passive film on chromium-containing alloys is normally n-type in electronic character because the dominant defect in the film is either a cation interstitial (i.e., M_i^{x+}) or an oxygen vacancy (i.e., $V_O^{\bullet\bullet}$), both of which are formally positively charged (Urquidi and Macdonald 1985 [DIRS 154741]). Consequently, there should be little solute ($Mo_{Cr}^{3\bullet}$)–vacancy ($V_O^{\bullet\bullet}$ or M_i^{x+}) interaction and pairing, and molybdenum should have little consistent impact on the passive current density.

6.4.1.2 Characterization of Alloy 22 Passive Film

The passive film on Alloy 22 has been studied at 95°C in a high-pH salt environment characteristic of concentrated Yucca Mountain groundwater (Andresen et al. 2003 [DIRS 170360], Section 3). Measurements of corrosion potential versus time, PSP, and cyclic potentiodynamic polarization (CPP) behavior were conducted to evaluate the passivity of these alloys. The passive films were also analyzed by x-ray photoelectron spectroscopy (XPS) and transmission electron microscopy (TEM) to obtain the chemical composition and cross-sectional view of the metal, oxide layers, and interfaces.

6.4.1.2.1 Summary of Experimental Procedures

As mentioned by Andresen et al. (2003 [DIRS 170360], Section 3), all materials were tested in the as-received condition. Specimens (cylinders 3 mm in diameter by 60 mm in length for corrosion potential, PSP, and CPP measurements, and coupons with dimensions of 10 mm × 10 mm × 0.8 mm for oxide analysis) were cut by electrodischarge machining and then wet-

ground using a 600-grit SiC paper before testing. Specimens for electrochemical measurements were spot-welded to a polytetrafluoroethylene-insulated Alloy 600 wire and mounted in an insulated fitting. The testing solution used was BSW-SC (BSW containing silica and carbonate and diluted by a factor of about 18×) (Table 6-3) at 95°C. The chemical composition of the diluted BSW-SC solution (referred to as "Dilute Y-M mixed salt solution" or "Dilute Y-M solution" in Figure 6-4, Figure 6-7, and Figure 6-8) was 10.6 g Na_2CO_3 (anhydrous), 9.7 g KCl, 8.8 g NaCl, 0.2 g NaF, 13.6 g $NaNO_3$, 1.4 g Na_2SO_4 (anhydrous), 4.1 g $Na_2SiO_3 \cdot 9H_2O$, and 1000 g H_2O (Andresen et al. 2003 [DIRS 170360], Table 3-1).

The chemicals were mixed with water that had been heated to the boiling point in an autoclave. All testing was performed in either a Hastelloy C-276 autoclave body or a commercial-purity titanium autoclave. Stainless steel components were present in all the autoclaves used. No signs of corrosion were observed on these stainless steel components, suggesting that the testing solution was not extremely aggressive. Solution was sampled from the autoclaves during the test.

To prevent evaporative loss of water, a four-foot-long tube-in-tube heat exchanger was used, with cooling water on the outside. The solution level in the test autoclave was monitored periodically by checking for continuity between the autoclave and an insulated stainless steel feed-through bar. No water addition was needed.

All potentials were measured with respect to the reference electrode, a saturated calomel electrode (SCE). A Luggin probe with a porous zirconia membrane filled with the test solution was used to maintain the reference electrode at room temperature. A flag-shaped platinum sheet was employed as a counter electrode. All tests were performed at 95°C ± 1°C. CPP scans at 0.17 mV/s were started at 50 mV below the corrosion potential (obtained one hour after immersion in solution), then continued toward the more noble potential direction. The scans were reversed when a current density of 5 mA/cm^2 was reached. After the completion of each test, specimens were cleaned ultrasonically in deionized water and dried, and the specimen surface was examined with a scanning electron microscope (SEM). In addition, PSP tests were conducted by applying various anodic potentials for 24 hours to measure the passive current and to characterize the oxide properties. The oxide composition and thickness were analyzed by XPS. The XPS data are quantitative for film composition, but the thickness of the oxide film is considered qualitative because precise calibrations of sputtering rate on an oxide of this composition were not performed (although very good estimates exist). No visual evidence of localized corrosion attack was observed after CPP or PSP measurements.

The cross-sectional TEM sample was prepared using a focused-ion-beam system. The bulk sample was placed into the focused-ion-beam system, and the region of interest was coated with a 1-μm-thick platinum layer using the in-situ metal deposition facilities of the focused-ion-beam system. The platinum layer was used to protect the underlying material. Staircase-shaped cuts were milled on either side of the region of interest using a gallium-ion source. The ion current was reduced as the thickness of the section approached the desired dimension. The dimensions of the final TEM cross section were 10-μm long, 4-μm deep, and 150-nm thick. The sample was then removed from the focused-ion-beam chamber, and the TEM cross section was removed from the bulk sample and placed on a porous carbon grid using a micromanipulator.

6.4.1.2.2 Characterization of Passive Films Formed Under Potentiostatic Polarization

The passive current transition behavior and oxide thickness formed on Alloy 22 at various anodic potentials is shown in Figure 6-4. The passive current density increases with the applied potential, and the oxide film becomes slightly thicker. Figure 6-5 shows the elemental distribution on the outermost oxide layer (not the very thin protective inner barrier layer responsible for passive behavior) formed on Alloy 22 at various anodic potentials. Applied anodic potentials in Figure 6-4 and Figure 6-5 were chosen from CPP curves (Andresen et al. 2003 [DIRS 170360], Figure 3-4). Steady-state currents were normally achieved within a 5- to 10-hour period of polarization at applied potentials. In addition to anodic dissolution, there may be contributions to the measured current due to redox reactions occurring in the mixed-salt environment. No evidence of localized corrosion attack was observed on test specimens after polarization.

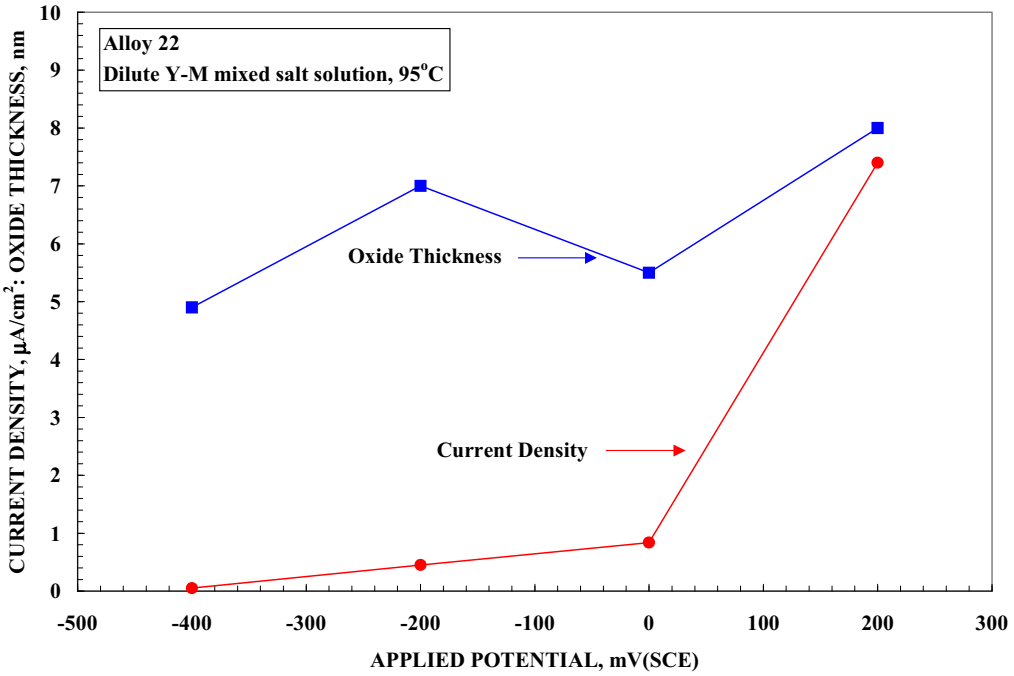

Source: Andresen et al. 2003 [DIRS 170360], Figure 3-8.

Figure 6-4. Passive Current Densities and Oxide Thickness as a Function of Applied Potential for Alloy 22

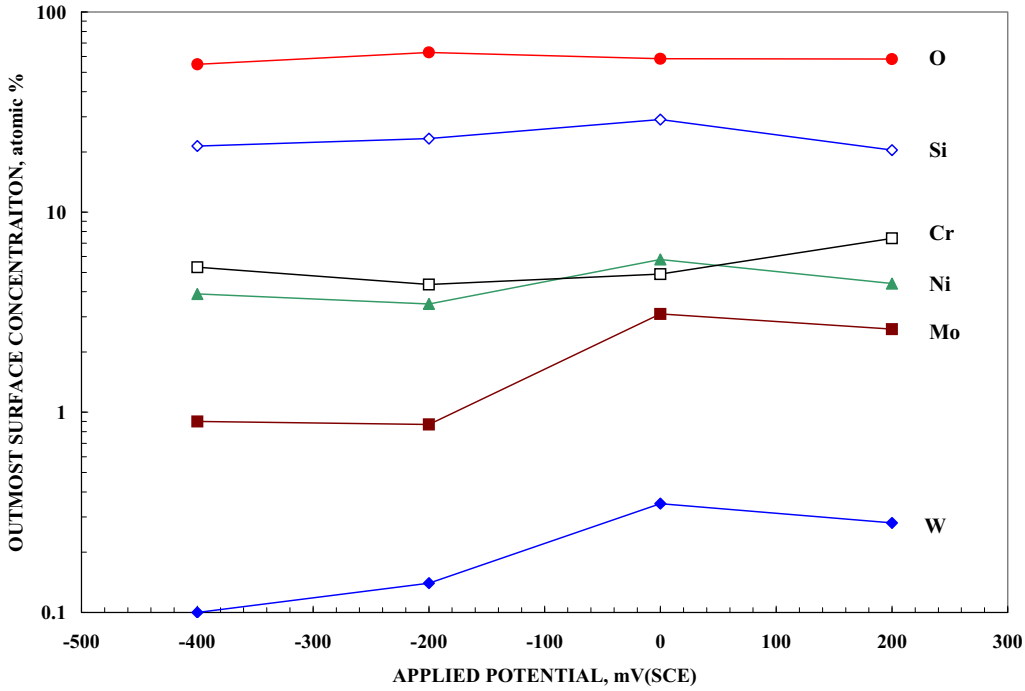

Source: Andresen et al. 2003 [DIRS 170360], Figure 3-9.

Figure 6-5. Elemental Concentration on the Outermost Oxide Layer as a Function of Applied Potential for Alloy 22

Note that the current density increased after the applied anodic potential was increased to 200 $mV_{(SCE)}$, and a slight increase in oxide thickness was observed. However, no evidence was observed to conclude the current increase and slightly thicker oxide at high anodic potentials were due to localized passive film breakdown. Andresen et al. (2003 [DIRS 170360], Section 3.3) reported that the primary cause of the high current density could be due to changes in the surface chemistry and oxidation states of molybdenum and tungsten (to MoO_4^{2-} or WO_4^{2-}) in the passive film.

6.4.1.2.3 Oxide Film Analysis

The chemical composition and structure of the oxide film plays a very important role in the corrosion protection process. The mechanism and kinetics of corrosion processes can be altered by the chemical and physical properties of oxide films. Figure 6-6 shows the TEM cross-sectional micrograph and energy-dispersive X-ray spectroscopy spectra of the oxide film formed on Alloy 22 after a two-month immersion at open-circuit potential in mixed-salt solution at 95°C. An oxide approximately 5 to 8 nm thick, enriched with chromium, was formed. Electron diffraction patterns showed a thermodynamically stable Cr_2O_3-rich oxide film containing NiO. These results are similar to the results of short-term potentiostatic experiments by Lloyd et al. (2003 [DIRS 167921], Table II).

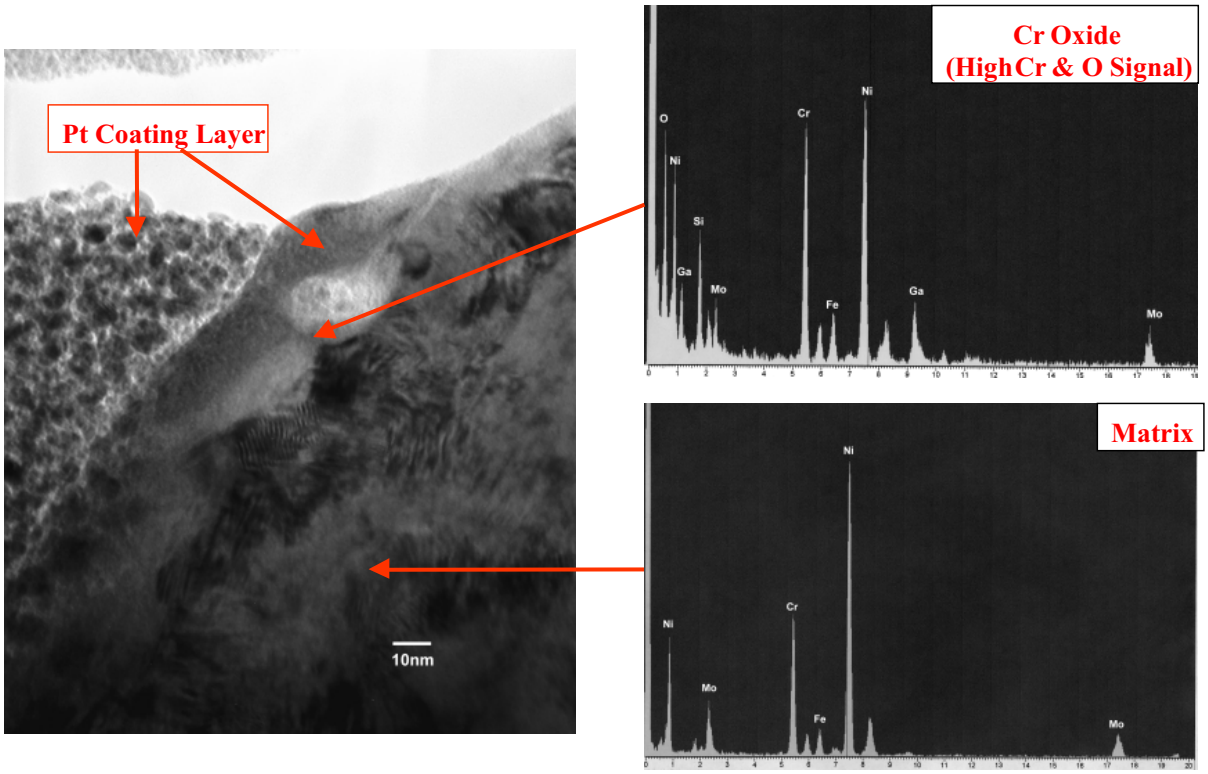

Source: Andresen et al. 2003 [DIRS 170360], Figure 3-10.

Figure 6-6. Transmission Electron Microscopy Micrograph Showing the Cross-Sectional Views and Energy-Dispersive X-Ray Spectroscopy Spectra Showing the Oxide Chemistry Formed on Alloy 22 after a Two-Month Immersion in a Mixed-Salt Environment at 95°C

XPS analysis was performed to obtain a quantitative chemical composition profile regarding the oxide thickness and elemental distribution through the oxide film. Figure 6-7 shows the elemental concentrations of the outermost oxide layer formed on Alloy 22 in a mixed-salt solution at 95°C as a function of immersion time. The oxide film on Alloy 22 was enriched with chromium and nickel, relative to the base metal, since no significant amounts of molybdenum and tungsten were measured in the oxide film. This is consistent with the findings by other investigators for nickel-based alloys (Lorang et al. 1990 [DIRS 154718]; Macdonald 1999 [DIRS 154721]; Marcus and Maurice 2000 [DIRS 154738], p. 153). Figure 6-7 shows that after two months the elemental concentrations change little with increasing exposure time. A large amount of SiO_2 (see the silicon curve in Figure 6-7) and small amounts of other salts on the outer oxide film were detected, but no evidence of penetration of SiO_2 to the underlying substrate was observed. If these elements were adjusted for (e.g., removed from consideration) in the atomic percent calculations, the amounts of the primary alloy elements (e.g., nickel, chromium, molybdenum, and tungsten) would be higher than those shown in Figure 6-7. Figure 6-8 shows the oxide thickness formed on Alloy 22 as a function of immersion time. After two months, the oxide film thickness on Alloy 22 is approximately 7 nm thick and, after eight months, the oxide film is about 13 nm thick.

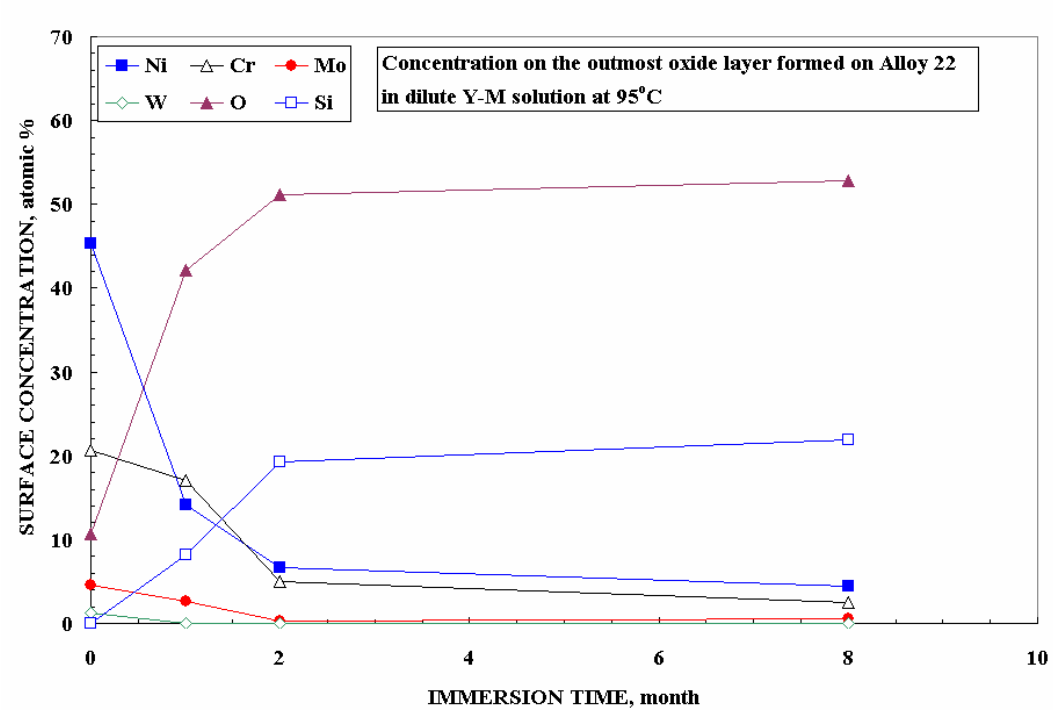

Source: Andresen et al. 2003 [DIRS 170360], Figure 3-11.

Figure 6-7. Elemental Concentration on the Outermost Oxide Layer Formed on Alloy 22 in a Mixed-Salt Environment at 95°C as a Function of Immersion Time

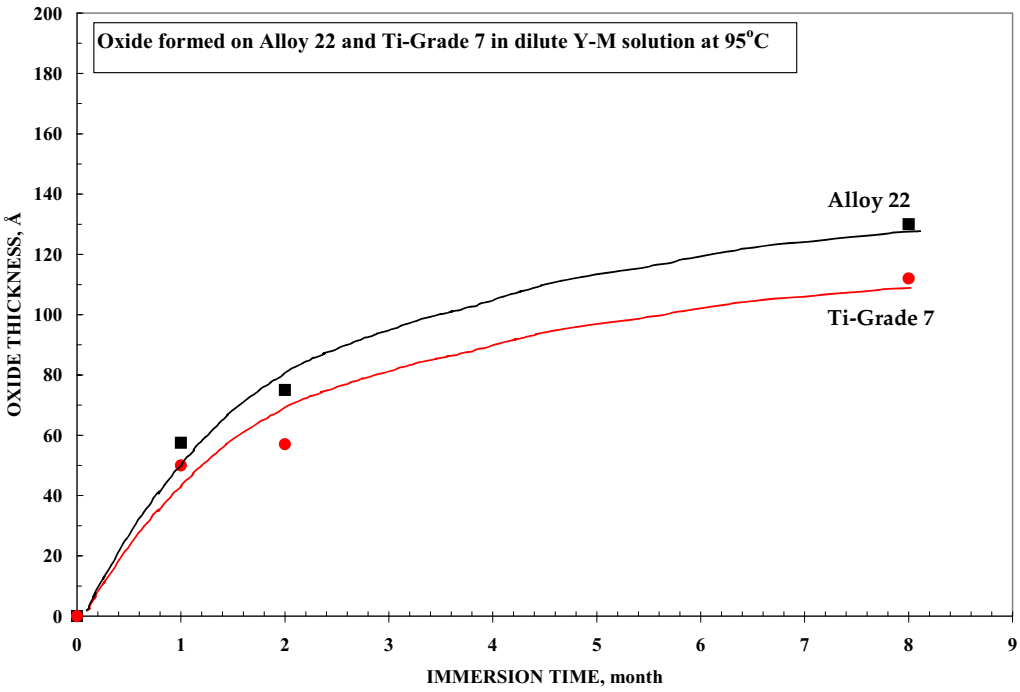

Source: Andresen et al. 2003 [DIRS 170360], Figure 3-13.

Figure 6-8. Oxide Thickness Formed on Alloy 22 and Titanium Grade 7 as a Function of Immersion Time at 95°C in a Mixed-Salt Environment

6.4.1.3 Summary

The conceptual understanding of the growth and stability of the passive film on Alloy 22 was described based on summarized data and information from the literature. The passivity of Alloy 22 was examined by measuring the corrosion potential and polarization behavior in a mixed-salt environment at 95°C with a pH of about 12.4. Steady-state corrosion potentials of Alloy 22 were measured. The surface analysis data indicated that the oxide layers responsible for passivity of Alloy 22 consist of chromium oxide (Cr_2O_3) containing NiO. After eight months of exposure to the mixed-salt solution at 95°C, 12- to 13-nm-thick oxide films were formed on Alloy 22 specimen surfaces. In addition, the passive films formed on Alloy 22 at high anodic potentials (greater than 0 mV versus SCE) contained more molybdenum and tungsten than the ones formed at lower anodic potentials (less than 0 mV versus SCE) (Andresen et al. 2003 [DIRS 170360], Section 3). No evidence of localized corrosion on Alloy 22 after PSP measurements was observed. No significant change in the open-circuit potential (or corrosion potential) of the test electrodes was observed. These data indicate that with increased time (1) the passive films become very protective and stable, (2) contributions from metal corrosion become extremely small, and (3) the redox potential of the solution is stable (Andresen et al. 2003 [DIRS 170360], Section 3). Overall, the passive films formed on Alloy 22 can be concluded to be very stable over long periods.

6.4.2 Dry Oxidation

Dry oxidation of Alloy 22 occurs at any relative humidity less than $RH_{threshold}$, thereby forming an adherent, protective oxide film of uniform thickness. The dry oxidation model presented here considers uniform oxidation of the WPOB surface. The protective oxide film is primarily Cr_2O_3, as discussed in the previous section. The oxidation reaction for the formation of this oxide is given in Equation 6-1 (Welsch et al. 1996 [DIRS 114895]):

$$4/3\ Cr + O_2 \rightarrow 2/3\ Cr_2O_3 \qquad \text{(Eq. 6-1)}$$

The rate of dry oxidation is considered limited by mass transport through this growing metal oxide film. Fick's first law (Jones 1992 [DIRS 169906], Section 12.3.1) is applied, considering a linear concentration gradient across the oxide film of thickness x, giving Equation 6-2:

$$J_{oxide} = -D_{oxide}\frac{\partial C}{\partial x} \approx -D_{oxide}\frac{\Delta C}{x} \qquad \text{(Eq. 6-2)}$$

where J_{oxide} is the molar flux of the reacting species in the oxide, D_{oxide} is the diffusivity of the reacting species in the oxide, and ΔC is the corresponding differential molar concentration. One can describe the oxide growth with a parabolic rate law as shown in Equation 6-3 (Jones 1992 [DIRS 169906], Section 12.3.1):

$$\frac{dx}{dt} = \frac{k_p'}{x} \qquad \text{(Eq. 6-3)}$$

where x is the oxide thickness, $k_p^{'}$ is the thickness-based parabolic rate constant, and t is the time. Integration of Equation 6-3 leads to Equation 6-4:

$$x = \sqrt{x_0^2 + k_p \times t} \qquad \text{(Eq. 6-4)}$$

where x_0 is the initial oxide thickness, x is the oxide thickness at time t, and k_p (= $2\,k_p^{'}$) is a temperature-dependent parabolic rate constant. Dry oxidation of metal is a thermally activated process. Therefore, the rate constant, k_p obeys the Arrhenius equation (Jones 1992 [DIRS 169906], Section 12.3.1), giving Equation 6-5:

$$k_p = k_{p0} e^{-E_a / RT} \qquad \text{(Eq. 6-5)}$$

where k_{p0} is a constant, E_a is the activation energy, and R is the universal gas constant (8.314 J/mol K) (Lide 1991 [DIRS 131202], inside rear cover).

To facilitate an approximate calculation, published values of k_p can be used (Welsch et al. 1996 [DIRS 114895]). Figure 18 of this reference shows parabolic rate constants for oxidation of chromia scale-forming alloys. It was found that all observed values of k_p fall below a line defined by Equation 6-6:

$$\log\left[k_p \left(\frac{\mathrm{m}^2}{\mathrm{sec}}\right)\right] = -3.5 - \left(\frac{12500}{T}\right) \qquad \text{(Eq. 6-6)}$$

where T is defined as the absolute temperature in Kelvin. Recent measurements of the thickness of the Alloy 22 oxide film exposed to air at 550°C showed that the oxide film approaches a limiting thickness of about 0.025 to 0.050 μm (25 to 50 nm) after about 333 days of exposure (DTN: LL030406412251.045 [DIRS 163469]). If this oxide film thickness is considered the depth of metal penetration (this is very conservative, as the oxide–metal volume (Pilling-Bedworth) ratio for chromia is about 2.02 (ASM International 1987 [DIRS 133378], p. 64)), then a penetration rate of 0.027 to 0.055 μm/yr (27 to 55 nm/yr) is obtained (output DTN: MO0612WPOUTERB.000, file: *DOX_WPOB.xmcd*). For that temperature, the value of k_p corresponding to the upper limit from Equation 6-6 is 2.06×10^{-19} m^2/s (6.51 $\mu\mathrm{m}^2/\mathrm{yr}$). Ignoring the initial oxide thickness in Equation 6-4, after one year, this corresponds to a growth of 2.55 μm (about 2.55 μm/yr). This shows that the model estimates are about 100 times greater than the measured thickness, and the above expression represents a very conservative upper bound.

Logarithmic growth laws may be more appropriate at lower temperatures than parabolic laws. However, the logarithmic law predicts that the oxide thickness (penetration) asymptotically approaches a small maximum value. In contrast, the parabolic law predicts continuous growth of the oxide, which is more conservative. As conservative estimates of the rate of dry oxidation based on parabolic growth kinetics are not life-limiting and reliable data for determining the maximum oxide thickness for Alloy 22 are not available, the parabolic growth law was used for the WPOB.

For a temperature of 350°C, a reasonably high bounding value, the value of k_p from Equation 6-6 is 2.76×10^{-24} m^2/s (8.70×10^{-5} $\mu m^2/yr$) (output DTN: MO0612WPOUTERB.000, file: *DOX_WPOB.xmcd*). After one year, this corresponds to a growth of 0.0093 μm (about 9.3 nm/yr). Assuming a constant oxide penetration rate of 0.0093 μm/yr (i.e., exposure to a constant temperature of 350°C and ignoring the parabolic dependence of oxide thickness on time given by Equation 6-4), the total penetration depth in the WPOB by dry oxidation in 10,000 years after permanent closure is only 93 μm, which is negligibly small (less than 0.5% of the total thickness of the WPOB (about 25 mm)).

Based on the above analysis, dry oxidation is not expected to be a performance-limiting process of the WPOB under the exposure conditions expected in the repository. Therefore, dry oxidation is not included in the waste package performance analysis. In Assumption 5.1 (Section 5), it is conservatively assumed that there is no threshold relative humidity for initiation of general corrosion of the Alloy 22 WPOB.

6.4.3 General Corrosion

General corrosion (or passive corrosion) is the uniform thinning of the WPOB at its open-circuit corrosion potential (E_{corr}). General corrosion can occur under immersed conditions or when a liquid film exists on the surface. At a given surface temperature, the existence of aqueous solutions on the waste package surface depends upon the hygroscopic nature of salts, minerals, or both, deposited on the surface. In the presence of such a deposit, a liquid phase can be established at a higher temperature and lower relative humidity than is otherwise possible. In Assumption 5.1 (Section 5), it is conservatively assumed that there is no threshold relative humidity for initiation of general corrosion of the Alloy 22 WPOB. The general corrosion rate is temperature-dependent. For a given temperature, the general corrosion rate is assumed constant (i.e., time-independent) (Assumption 5.2, Section 5). Therefore, for a given temperature, the depth of penetration or thinning of the WPOB by general corrosion is equal to the general corrosion rate at that temperature, multiplied by the time duration that the waste package surface is at that temperature. This assumption is considered conservative because the general corrosion rate of metals and alloys is known to decrease with time (Section 6.4.3.5).

As is discussed in the following sections, general corrosion rates of the WPOB have been estimated from the weight-loss data of Alloy 22 samples after five-year exposure in the LTCTF (Estill 1998 [DIRS 117697], Section 2.2). The LTCTF provided a comprehensive source of corrosion data for Alloy 22 in environments relevant to the repository. The LTCTF is described in detail in a previous publication by Estill (1998 [DIRS 117697], Section 2.2) and relevant experimental details are summarized in the next section. The five-year weight-loss measurement data is documented in DTN: LL030412512251.057 [DIRS 163712], file: *C22 5 Year Coupon Corrosion Rates 4-14-03.xls*.

6.4.3.1 Long-Term Weight-Loss Measurements

For long-term weight-loss measurements on Alloy 22 specimens, the LTCTF was equipped with a large number of nonmetallic tanks. Each tank had a total volume of approximately 2,000 L and was filled with approximately 1,000 L of aqueous test solution. A discussion of the LTCTF is

presented by Estill (1998 [DIRS 117697], Section 2.2). Details of the conditions under which the weight-loss testing was conducted follow in this section.

6.4.3.1.1 Test Temperatures and Aeration

The temperature of the solution in each of the LTCTF tanks was controlled at either 60°C or 90°C. The test solution in each tank was covered with a blanket of air flowing at approximately 150 cm^3/min, and agitated. It is not anticipated that oxygen depletion occurred at the interface between the specimens and the electrolytes in the LTCTF. The LTCTF tests were long-term in nature, and it is expected that dissolved oxygen reached its solubility limit in the electrolytes used at the testing temperature over the long term. Also, as the corrosion rate of the alloys in the tanks under the tested conditions was low, oxygen consumption can be reasonably expected to have been negligible. Oxygen concentrations in the solutions are given by Estill (1998 [DIRS 117697], Section 2.2.4 and Table 2.2-6).

6.4.3.1.2 Test Specimens

Samples used for determination of weight-loss during the long term were mounted on insulating racks and placed in the tanks. Approximately half of the samples were submersed, half were in the saturated vapor above the aqueous phase, and a limited number were at the water line. Condensed water was present on specimens located in the saturated vapor.

Two coupon types were used for weight-loss measurements. These are identified as weight-loss coupons and crevice coupons. The nominal dimensions were 2 in × 1 in × 1/8 in (approximately 50 mm × 25 mm × 3 mm) and 2 in × 2 in × 1/8 in (50 mm × 50 mm × 3 mm), respectively (Wong et al. 2004 [DIRS 174800]). The coupons had a 0.312-in-diameter (7.9-mm) hole in the center for sample mounting. Figure 6-9 shows schematic representations of the coupons used. The coupons were tested in the as-received conditions from the coupon manufacturer. The surface roughness of the weight-loss coupons was specified as RMS32 (approximately 150 grit). The surface roughness of the back side of the crevice coupons was also specified as RMS32, but the front side roughness was specified as RMS16 (approximately 240 grit) (Wong et al. 2004 [DIRS 174800]).

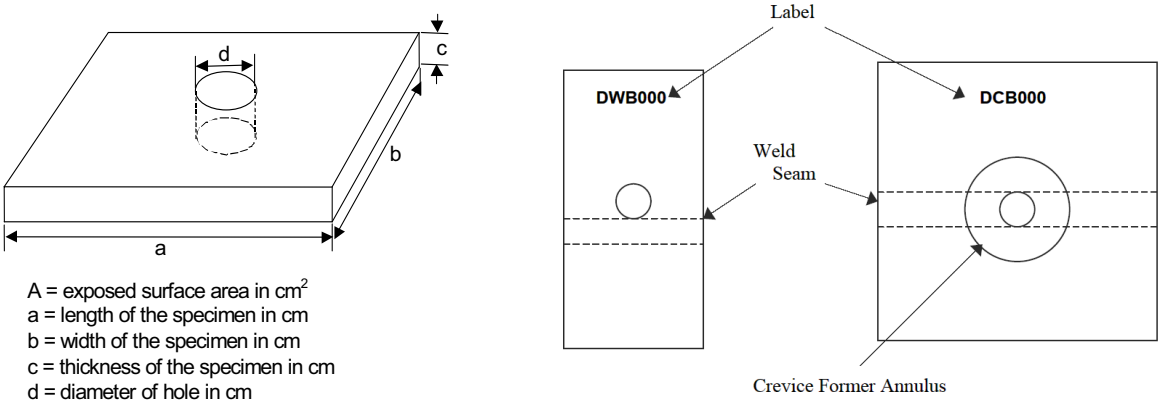

Figure 6-9. Schematics of Specimens Used in the Weight-Loss Measurements of Alloy 22 in Long-Term Corrosion Test Facility

For both coupon types (weight-loss and crevice), two metallurgical conditions were used (i.e., about half of the samples were wrought material (only base metal) and half had a gas-metal arc weld seam Figure 6-9). The coupons were fabricated from Alloy 22 plate stock. All weight-loss coupons were affixed using an insulating 0.5-in-diameter (12.7-mm) sample spacer (either a polytetrafluoroethylene or ceramic washer), while all crevice coupons were affixed using a 0.75-in-diameter (19.1-mm) polytetrafluoroethylene or ceramic crevice former. About 8% of the crevice coupon surface area was covered by the crevice former, and about 5% of the weight-loss coupon surface area was covered by the sample spacer. The purpose of the crevice former was to create an environment that might induce corrosion at the contact interface or under occluded conditions. Further details of the sample configuration are provided elsewhere (Estill 1998 [DIRS 117697], Section 2.2.5; Wong et al. 2004 [DIRS 174800]; DTN: LL030412512251.057 [DIRS 163712]).

6.4.3.1.3 Test Solutions

Weight-loss measurements were performed on samples exposed to repository-relevant test solutions, including SDW, SCW, and SAW. The compositions of three of these solutions are summarized in Table 6-3. BSW solutions could not be used in long-term weight-loss testing because no BSW solution-containing tanks were installed when LTCTF started due to lack of formulation of BSW solutions. Later, BSW solutions were formulated for use in other testing activities discussed in this report. The SCW test solution is three orders of magnitude (1,000×) more concentrated than J-13 well water and is slightly alkaline (pH approximately 10). The SAW test solution is also three orders of magnitude (1,000×) more concentrated than J-13 well water and is acidic (pH approximately 2.7). Concentrated solutions are intended to mimic the evaporative concentration of the electrolytes on the hot waste package surface (Estill 1998 [DIRS 117697], Section 2.2). The volume of the solution in the vessels was kept constant by the regular addition of de-ionized water. No other chemical adjustment was made.

6.4.3.1.4 Test Matrix

The welded and nonwelded (wrought) coupons were tested under 12 different conditions (three electrolytes × two temperatures × two exposure conditions). The exposure time for each sample was approximately five years. By using as-welded samples in the LTCTF, the results would represent the behavior of the final closure weld and also represent the least corrosion-resistant conditions for the rest of the waste package, since it is generally affirmed that annealing would reduce the corrosion susceptibility of the alloy in a given environment. It is conservative to use as-welded specimens for corrosion testing. The specimen label and vessel numbers are shown in Table 6-4. Each sample was designated with three letters and three characteristic numbers. The letter D represents Alloy 22, the letter C indicates a crevice coupon, the letter W indicates a weight-loss coupon, the letter A indicates that the coupon does not contain a weld seam, and the letter B indicates that the coupon contains a weld seam along the middle of the specimen. Table 6-4 shows that a total of 134 test specimens were examined. Twelve welded crevice samples, representing each of the different test conditions, were used for surface analyses (designated (SA) in Table 6-4) and the remaining 122 samples were used for weight-loss determination. The weight-loss samples tested at the water line were included in the model analysis as samples tested in the liquid phase because there were no noticeable differences in the measured weight-

losses between the water-line and liquid-phase samples for the same exposure conditions (i.e., water chemistry and temperature).

Table 6-4. List of Examined Weight-Loss and Crevice Alloy 22 Coupons

	SAW 60°C	SAW 90°C	SCW 60°C	SCW 90°C	SDW 60°C	SDW 90°C
Sample – Exposure	**Vessel 25**	**Vessel 26**	**Vessel 27**	**Vessel 28**	**Vessel 29**	**Vessel 30**
Weight-Loss – Vapor Phase	DWA019 DWA020 DWA021	DWA059 DWA060 DWA061	DWA089 DWA090 DWA091	DWA129 DWA130 DWA131	DWA147	DWA174
Crevice – Vapor Phase	DCA019 DCA020 DCA021	DCA049 DCA050 DCA051	DCA079 DCA080 DCA081	DCA109 DCA110 DCA111	DCA139 DCA140 DCA141	DCA175 DCA176 DCA177
Weight-Loss – Liquid Phase	DWA022 DWA023 DWA024	DWA062 DWA063 DWA064	DWA092 DWA093 DWA094	DWA132 DWA133 DWA134	DWA148	DWA175
Crevice – Liquid Phase	DCA022 DCA023 DCA024	DCA052 DCA053 DCA054	DCA082 DCA083 DCA084	DCA112 DCA113 DCA114	DCA142 DCA143 DCA144	DCA178 DCA179 DCA180
Weight-Loss – Waterline	DWA034	DWA039	DWA104	DWA109	DWA154	DWA167
Welded Weight-Loss – Vapor Phase	DWB019 DWB020 DWB021	DWB059 DWB060 DWB061	DWB089 DWB090 DWB091	DWB129 DWB130 DWB131	DWB147	DWB174
Welded Crevice – Vapor Phase	DCB019 DCB020 DCB021 (SA)	DCB049 DCB050 DCB051 (SA)	DCB079 DCB080 DCB081 (SA)	DCB109 DCB110 DCB111 (SA)	DCB139 DCB140 DCB141 (SA)	DCB175 DCB176 DCB177 (SA)
Welded Weight-Loss – Liquid Phase	DWB022 DWB023 DWB024	DWB062 DWB063 DWB064	DWB092 DWB093 DWB094	DWB132 DWB133 DWB134	DWB148	DWB175
Welded Crevice – Liquid Phase	DCB022 DCB023 DCB024 (SA)	DCB052 DCB053 DCB054 (SA)	DCB082 DCB083 DCB084 (SA)	DCB112 DCB113 DCB114 (SA)	DCB142 DCB143 DCB144 (SA)	DCB178 DCB179 DCB180 (SA)

Source: DTN: LL030412512251.057 [DIRS 163712] (for all but surface analysis (SA) designated samples).

NOTE: SA = Reserved for surface analyses (not subject to cleaning for weight-loss measurement nor included in DTN: LL030412512251.057 [DIRS 163712]).

All tests were carried out under ambient pressure. After approximately five years of exposure to each solution, the specimens were removed from their respective test vessels to determine their weight-loss. In all of the tested conditions, the coupons were covered with deposits. Therefore, the coupons were cleaned prior to final weighing. Cleaning was carried out according to a test method based upon ASTM G 1-90 (1999 [DIRS 103515]). For specimens exposed to SCW and SDW, the posttest specimens were descaled for two minutes in a cleaning solution prepared by diluting 150 mL of concentrated HCl acid (37% HCl of specific gravity of 1.19) with deionized water to make 1,000 mL of solution (TIP-CM-51 [DIRS 169585], Section 7.2.1). The cleaning temperature was ambient. For specimens exposed to SAW, the posttest specimens were first exposed for two minutes to the same HCl solution used for descaling samples exposed to SCW and SDW (TIP-CM-51 [DIRS 169585], Section 7.2.2). The samples were then immersed at

95°C for two minutes in a solution prepared by dissolving 200 g of NaOH and 30 g of $KMnO_4$ in deionized water to make 1,000 mL of solution. Finally, the specimens were immersed for three minutes in a solution prepared by dissolving 100 g of diammonium citrate in deionized water to make 1,000 mL of solution. Due to heavy surface deposits, some samples were cleaned multiple times before SEM photomicrographs indicated no significant amount of deposits remained. The only modifications to ASTM G 1-90 (1999 [DIRS 103515]) methods were an increased immersion time (found to be necessary for complete cleaning) and the use of a drying oven and desiccator to minimize air exposure (decreasing the amount of post-cleaning film formation and increasing the measured weight-loss resulting in higher determined corrosion rates). ASTM G 1-90 (1999 [DIRS 103515], Section 7.1.1) specifies that

> An ideal [cleaning] procedure should remove only corrosion products and not result in removal of any base metal. To determine the mass loss of the base metal when removing corrosion products, replicate uncorroded control specimens should be cleaned by the same procedure being used on the test specimen. By weighing the control specimen before and after cleaning, the extent of metal loss resulting from cleaning can be utilized to correct the corrosion mass loss.

Weight-loss measurements and SEM analysis showed that the cleaning methods used removed the scale from tested samples, yet did not significantly affect untested foil specimens (TIP-CM-51 [DIRS 169585], Appendix A). For this reason, the "corrosion mass loss" of the tested specimens was not corrected for the extent of metal loss resulting from the cleaning process (since it was not significant). Furthermore, not correcting for mass loss due to the cleaning process is conservative in that subtraction of the weight-loss (if there were any significant amount) of the untested foil specimens from the weight-loss of the test specimens would result in determination of a lower overall weight-loss for the test specimens and therefore a lower corrosion rate.

6.4.3.2 Weight-Loss Data Analysis

The general corrosion rate measurements are based upon ASTM G 1-90 (1999 [DIRS 103515]). The formula used to calculate the general corrosion rate from weight-loss data of the tested materials is shown in Equation 6-7:

$$Corrosion\ Rate = \frac{87.6 \times 10^9 \cdot \Delta w}{\rho \cdot A \cdot t} \qquad \text{(Eq. 6-7)}$$

where 87.6×10^9 is the proportionality constant (nm × cm^{-1} × hr × yr^{-1}), Δw is the weight-loss in grams after more than five years, ρ is the density of Alloy 22 (8.69 g/cm^3) (Haynes International 1997 [DIRS 100896], p. 13), A is the exposed surface area of each coupon (cm^2), and t is the exposure time (hours). The exposed surface area A is calculated using Equation 6-8:

$$A = 2ab + 2bc + 2ac - \left(\frac{\pi d^2}{2}\right) + \pi dc \qquad \text{(Eq. 6-8)}$$

where *a* is the length of the specimen in cm, *b* is the width of the specimen in cm, *c* is the thickness of the specimen in cm, and *d* is the diameter of the hole in cm (see Section 6.4.3.1.2 for sample dimensions). Figure 6-9 provides a schematic of the sample coupons.

Calculation of the exposed surface area of the weight-loss and crevice samples using Equation 6-8 included the area directly under the 0.75-in-diameter crevice former for the crevice samples and the area directly under the 0.5-in-diameter sample spacer for the weight-loss samples. These areas were included because the test solutions penetrated and wet the areas under the crevice former or sample spacer. About 8% of the crevice coupon surface area was covered by the crevice former and about 5% of the weight-loss coupon surface area was covered by the sample spacer. The inputs from DTN: LL030412512251.057 [DIRS 163712], file: *C22 5 Year Coupon Corrosion Rates 4-14-03.xls*, used in the model analysis were the weight-loss measurements and characteristics of the sample and exposure conditions. The calculated corrosion rates of the weight-loss and crevice coupons are listed in Appendices II and III, respectively. The calculated corrosion rates may differ slightly from those in the input DTN due to differences in the number of significant digits used in the calculations.

As noted in Appendix II, crevice specimen DCA177 is an outlier and was not included in the crevice specimen weight-loss data analysis and the WPOB general corrosion model analysis. The mean and standard deviation of all the five-year crevice sample data including sample DCA177 are 7.89 nm/yr and 7.09 nm/yr, respectively (output DTN: MO0612WPOUTERB.000, file: *Alloy22_5yr_CreviceAnalysis.xls*). Applying the Grubbs test for outliers as specified in *Standard Practice for Dealing with Outlying Observations* (ASTM E 178-02 2002 [DIRS 169968]) the computed value for T_{60} (there are $n = 60$ general corrosion measurements of crevice samples listed in Appendix II) for the measured general corrosion rate of sample DCA177 (46.67 nm/yr) is 5.469 nm/yr. From Table 1 in ASTM E 178-02 (2002 [DIRS 169968]), and using $n = 60$, a T_{60} value as large as 5.469 would occur by chance with probability less than 0.001. Thus, the evidence is against the suspect value (the measured general corrosion rate of sample DCA177) having come from the same population as the others (assuming the population is normally distributed). The measured corrosion rate (46.67 nm/yr) of sample DCA177 is beyond five standard deviations from the mean. In addition, the sample was tested in the vapor phase over the SDW solution, which is the least corrosive condition among the test conditions of the long-term weight-loss tests (see Figure 6-10 and Figure 6-11). The above arguments provide sufficient justification for exclusion of the outlier.

Also, weight-loss sample DWA089 yielded a negative corrosion rate and was conservatively excluded in the weight-loss analysis. Crevice specimen DCB139 and weight-loss specimens DWA090, DWA109, DWA147, DWA175, DWB020, DWB021, DWB059, and DWB091 yielded a zero corrosion rates and were conservatively excluded in the analysis.

Figure 6-10 and Figure 6-11 summarize the calculated corrosion rates for the Alloy 22 weight-loss coupons and crevice coupons, respectively, exposed to the SAW, SCW, and SDW solutions at 60°C and 90°C for over five years. Because there were no significant differences between mill-annealed and as-welded general corrosion rates, (e.g., Figure 6-14 and Figure 6-19) these samples were combined for these analyses. The average corrosion rates and 1.96 standard deviation ranges were calculated based on the use of a normal distribution and are presented in both figures. The 1.96 standard deviation range represents a 95% confidence level. Although

the appearance and amount of deposits on the coupons exposed to different solutions prior to cleaning were different (Wong et al. 2004 [DIRS 174800]), corrosion features of the specimens were indistinguishable after cleaning. Moreover, the calculated corrosion rates were not significantly different. The individual corrosion rates for the weight-loss coupons ranged from about 0.7 to 12 nm/yr (Figure 6-16) with the lowest mean rates observed for the coupons in the SDW solution. The individual corrosion rates for the crevice coupons ranged from about 0.4 to 23 nm/yr (Figure 6-21) with the highest mean rates usually (with the exception of 60°C vapor) observed in the SCW solution and, again, the lowest mean rates observed in the SDW solution.

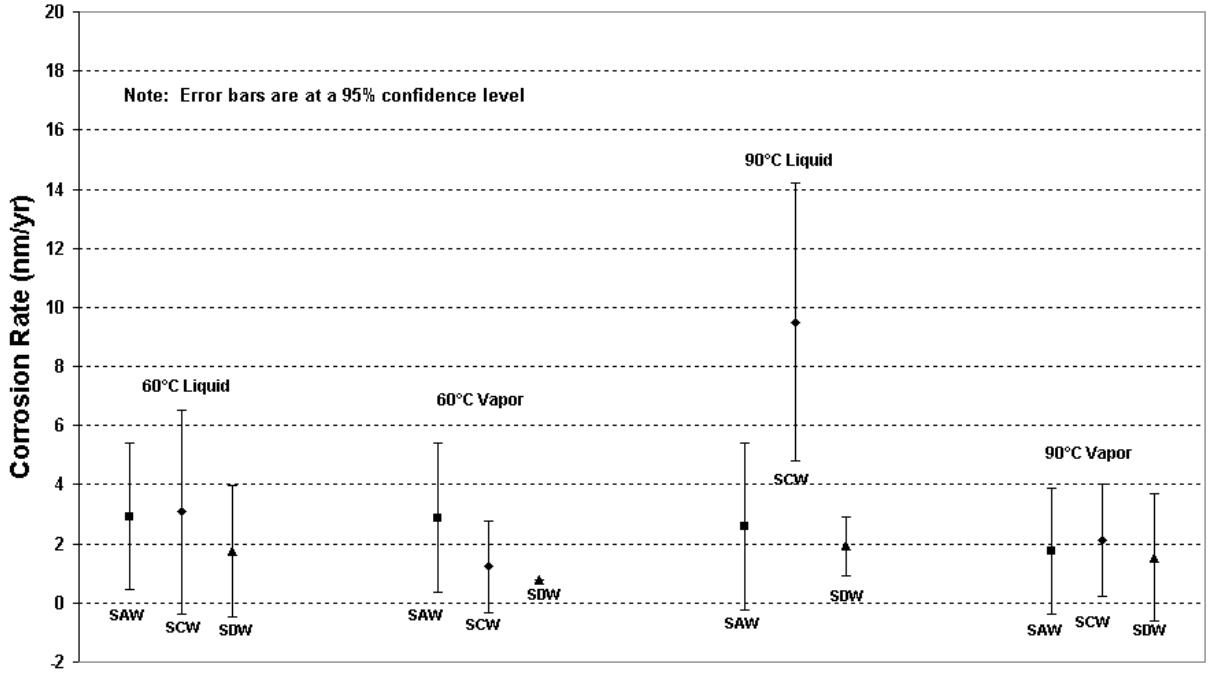

Source: DTN: LL030412512251.057 [DIRS 163712], file: *C22 5 Year Coupon Corrosion Rates 4-14-03.xls*.

Output DTN: MO0612WPOUTERB.000, file: *Error Bar Plots.xls*.

Figure 6-10. Corrosion Rates for Alloy 22 Weight-Loss Coupons in Simulated Acidified Water, Simulated Concentrated Water, and Simulated Dilute Water

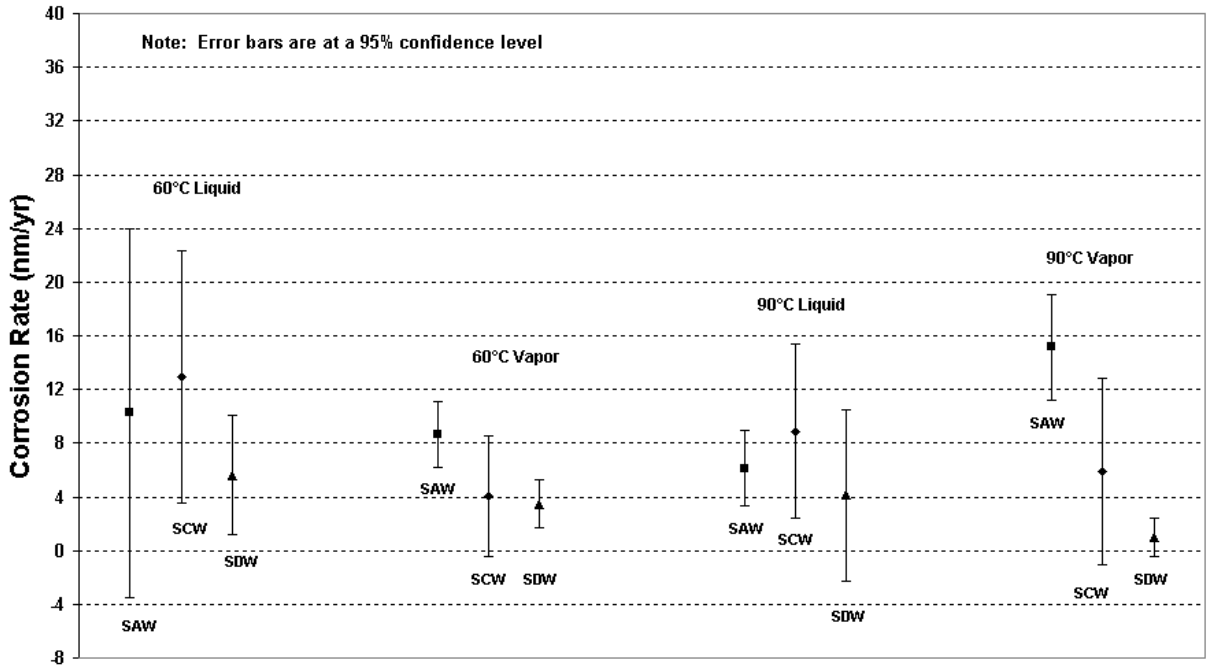

Source: DTN: LL030412512251.057 [DIRS 163712], file: *C22 5 Year Coupon Corrosion Rates 4-14-03.xls*.

Output DTN: MO0612WPOUTERB.000, file: *Error Bar Plots.xls*.

Figure 6-11. Corrosion Rates for Alloy 22 Crevice Coupons in Simulated Acidified Water, Simulated Concentrated Water, and Simulated Dilute Water

In most cases, the crevice coupons exhibited corrosion rates two to five times higher than the weight-loss coupons in the same solutions. Stereomicroscopic and SEM observations of weight-loss and crevice specimens indicated little or no sign of corrosion. The machining grooves remained uniform and sharp throughout each coupon. No crevice corrosion was observed on any of the tested coupons (Wong et al. 2004 [DIRS 174800]). As discussed later in this section, it is possible that a different surface finish treatment used for the crevice samples may have led to measurement of different corrosion rates. However, it is noteworthy that among all test specimens, a maximum corrosion rate of only about 23 nm/yr was observed. For the weight-loss and crevice coupons, the corrosion rates were generally lower for specimens exposed to vapor than those immersed in liquid, regardless of the test temperature or electrolyte solution. Overall, the test coupons in the SAW solution at 90°C exhibited slightly lower corrosion rates than at 60°C.

For the crevice coupons, the corrosion rates for the immersed samples were lower at 90°C than at 60°C. Conversely, for the crevice coupons exposed to the vapor phase, the corrosion rates were generally higher at 90°C than at 60°C. In general, for corrosion processes, the corrosion rate increases with temperature. However, in this study, since the determined corrosion rates were very low and the temperature range studied (60°C to 90°C) was narrow, a clear dependence on the temperature could not be established for these data with the exception of the results from weight-loss coupons immersed in the SCW solution. The temperature-dependence of Alloy 22 general corrosion rates of weight-loss coupons immersed in the SCW solution is evaluated in Section 6.4.3.4. Also, it may be noted that the use of a more sensitive technique than weight-loss

measurements, such as polarization resistance measurements, may lead to the observation of a temperature-dependence of corrosion rates (Section 6.4.3.4).

For the Alloy 22 weight-loss coupons, there was no detrimental effect of welds on the corrosion rate (Figure 6-14). However, the nonwelded Alloy 22 crevice coupons exhibited slightly higher corrosion rates than their welded counterparts (Figure 6-19). For most alloys, the corrosion rates of welded specimens are expected to be greater than those of the nonwelded ones; however, this is not observed in the Alloy 22 test results. The excellent corrosion resistance of Alloy 22 in repository-relevant solutions as well as the narrow temperature range used in these experiments (60°C to 90°C) could be reasons for not observing any detrimental effect of welding in these experiments.

The general corrosion rates of the coupons were analyzed with "empirical" cumulative distribution functions (ECDFs) of the calculated general corrosion rates. The ECDFs present the data trends and comparative analysis of different sets of data corresponding to various sample geometries and exposure conditions. In constructing the ECDFs, the cumulative probability values of the general corrosion rate (except the upper and lower bounds) were calculated by the plotting positions in Equation 6-9 (Stedinger et al. 1993 [DIRS 105941], Section 18.3.2):

$$q_i = \frac{i - 0.5}{n} \qquad \text{(Eq. 6-9)}$$

where q_i is the cumulative probability of the i^{th} smallest event (e.g., general corrosion rate) and n is the total number of events. The plotting position formula in Equation 6-9 is a traditional choice for probability plotting (Stedinger et al. 1993 [DIRS 105941], Section 18.3.2).

The ECDFs for the general corrosion rates of the weight-loss specimens are shown in Figure 6-12 to Figure 6-16 for comparative analyses of the effect of various experimental conditions, such as solution chemistry, temperature, and metallurgical condition, on the general corrosion rate. The ECDFs for the general corrosion rates of the crevice coupons are shown in Figure 6-17 to Figure 6-21 for comparative analyses of the effect of various experimental conditions on the general corrosion rate.

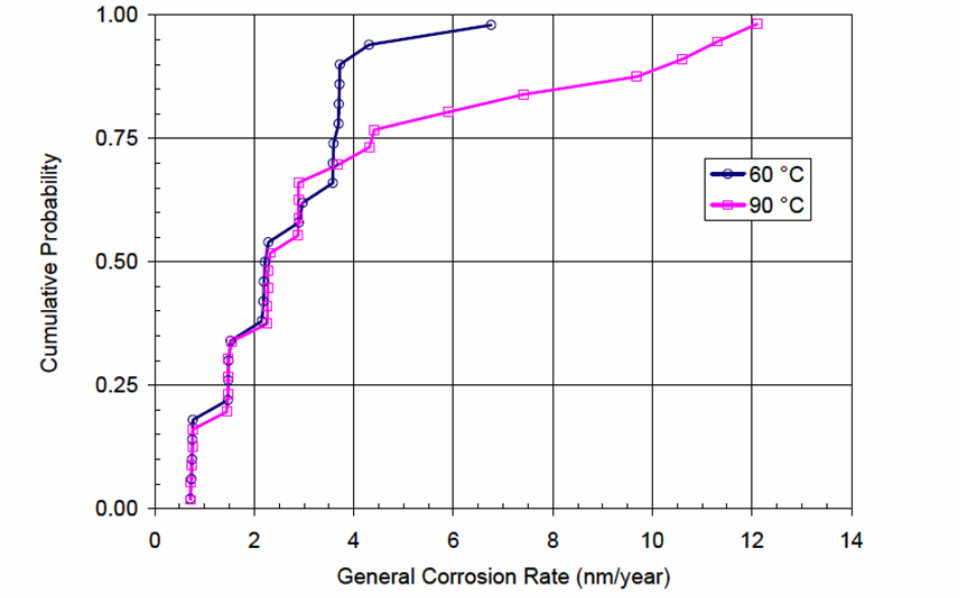

Source: DTN: LL030412512251.057 [DIRS 163712], file: *C22 5 Year Coupon Corrosion Rates 4-14-03.xls*.

Output DTN: MO0612WPOUTERB.000, file: *Alloy22_5yr_WLAnalysis.xls*.

Figure 6-12. Empirical Cumulative Distributions for General Corrosion Rate of Alloy 22 Weight-Loss Samples at 60°C and 90°C after Five-Year Exposure in the Aqueous and Vapor Phases of Simulated Acidified Water, Simulated Concentrated Water, and Simulated Dilute Water in the Long-Term Corrosion Test Facility

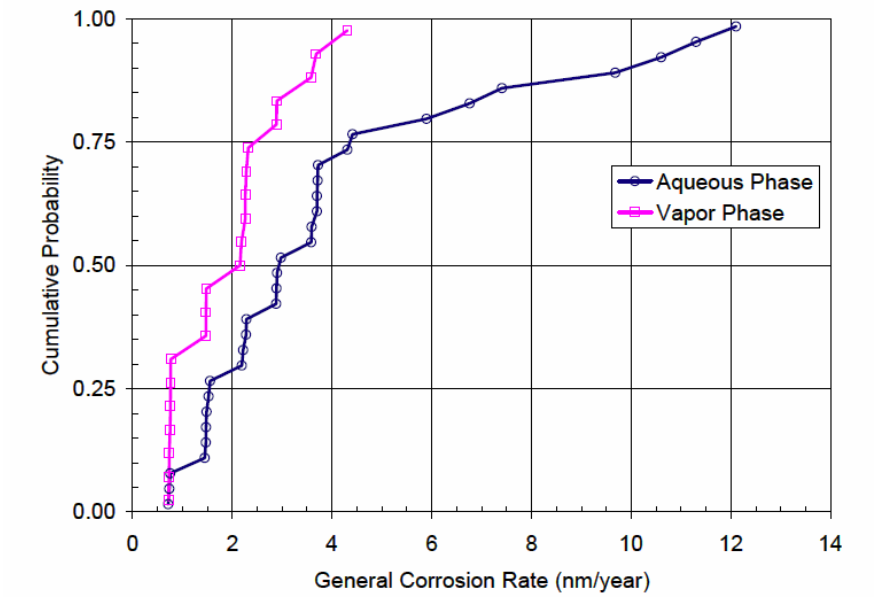

Source: DTN: LL030412512251.057 [DIRS 163712], file: *C22 5 Year Coupon Corrosion Rates 4-14-03.xls.*

Output DTN: MO0612WPOUTERB.000, file: *Alloy22_5yr_WLAnalysis.xls.*

Figure 6-13. Empirical Cumulative Distributions for General Corrosion Rate of Alloy 22 Weight-Loss Samples at 60°C and 90°C after Five-Year Exposure in the Aqueous and Vapor Phases of Simulated Acidified Water, Simulated Concentrated Water, and Simulated Dilute Water in the Long-Term Corrosion Test Facility

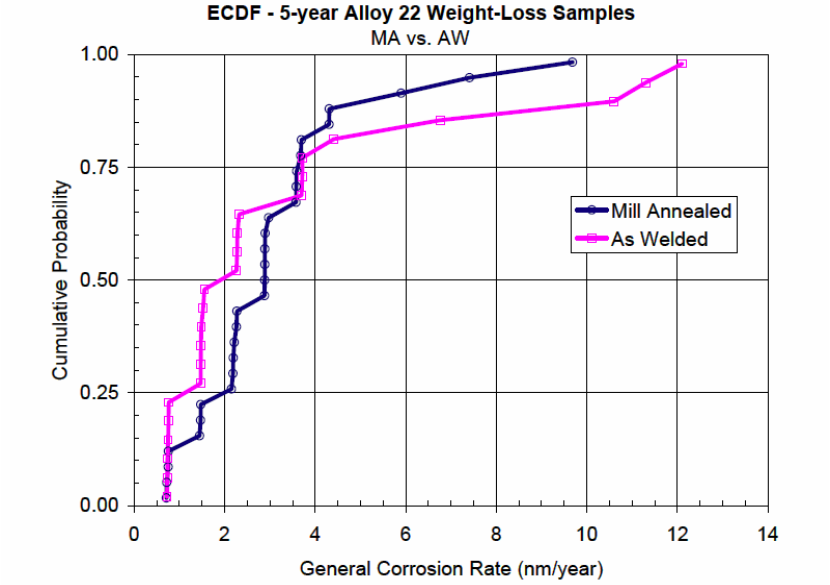

Source: DTN: LL030412512251.057 [DIRS 163712], file: *C22 5 Year Coupon Corrosion Rates 4-14-03.xls*.

Output DTN: MO0612WPOUTERB.000, file: *Alloy22_5yr_WLAnalysis.xls*.

Figure 6-14. Empirical Cumulative Distributions for General Corrosion Rate of Mill-Annealed and As-Welded Alloy 22 Weight-Loss Samples after Five-Year Exposure in the Aqueous and Vapor Phases of Simulated Acidified Water, Simulated Concentrated Water, and Simulated Dilute Water in the Long-Term Corrosion Test Facility

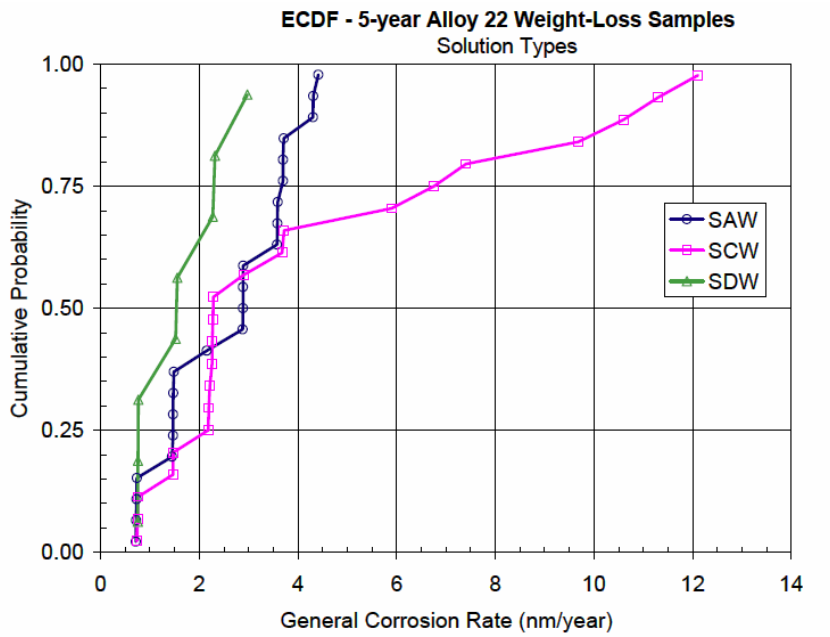

Source: DTN: LL030412512251.057 [DIRS 163712], file: *C22 5 Year Coupon Corrosion Rates 4-14-03.xls*.

Output DTN: MO0612WPOUTERB.000, file: *Alloy22_5yr_WLAnalysis.xls*.

Figure 6-15. Empirical Cumulative Distributions for General Corrosion Rate of Alloy 22 Weight-Loss Samples Tested in Three Different Solution Types at 60°C and 90°C after Five-Year Exposure in the Long-Term Corrosion Test Facility

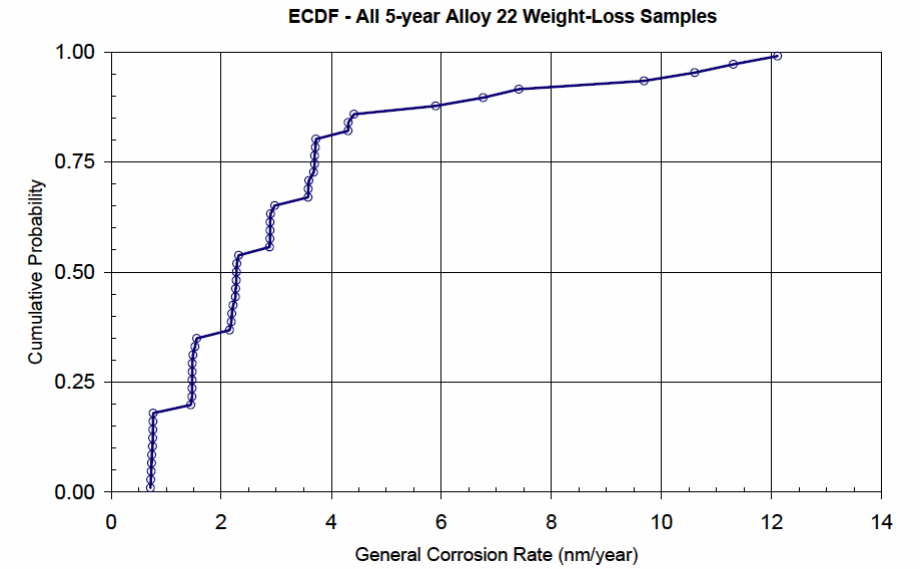

Source: DTN: LL030412512251.057 [DIRS 163712], file: *C22 5 Year Coupon Corrosion Rates 4-14-03.xls*.

Output DTN: MO0612WPOUTERB.000, file: *Alloy22_5yr_WLAnalysis.xls*.

Figure 6-16. Empirical Cumulative Distributions for General Corrosion Rate of All Alloy 22 Weight-Loss Samples at 60°C and 90°C after Five-Year Exposure in the Aqueous and Vapor Phases of Simulated Acidified Water, Simulated Concentrated Water, and Simulated Dilute Water in the Long-Term Corrosion Test Facility

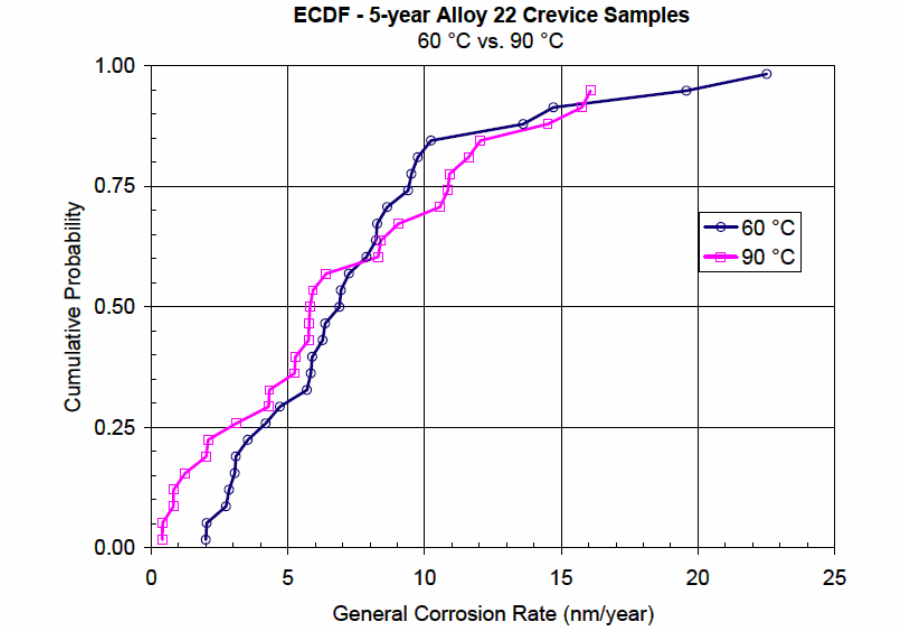

Source: DTN: LL030412512251.057 [DIRS 163712], file: *C22 5 Year Coupon Corrosion Rates 4-14-03.xls*.

Output DTN: MO0612WPOUTERB.000, file: *Alloy22_5yr_CreviceAnalysis.xls*.

Figure 6-17. Empirical Cumulative Distributions for General Corrosion Rate of Alloy 22 Crevice Samples at 60°C and 90°C after Five-Year Exposure in the Aqueous and Vapor Phases of Simulated Acidified Water, Simulated Concentrated Water, and Simulated Dilute Water in the Long-Term Corrosion Test Facility

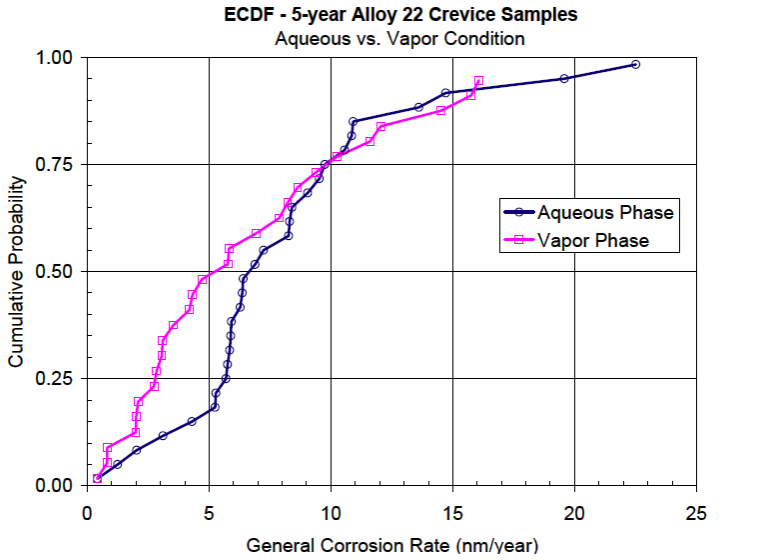

Source: DTN: LL030412512251.057 [DIRS 163712], file: *C22 5 Year Coupon Corrosion Rates 4-14-03.xls*.

Output DTN: MO0612WPOUTERB.000, file: *Alloy22_5yr_CreviceAnalysis.xls*.

Figure 6-18. Empirical Cumulative Distributions for General Corrosion Rate of Alloy 22 Crevice Samples at 60°C and 90°C after Five-Year Exposure in the Vapor Phase and Aqueous Phases of Simulated Acidified Water, Simulated Concentrated Water, and Simulated Dilute Water after Five-Year Exposure in the Long-Term Corrosion Test Facility

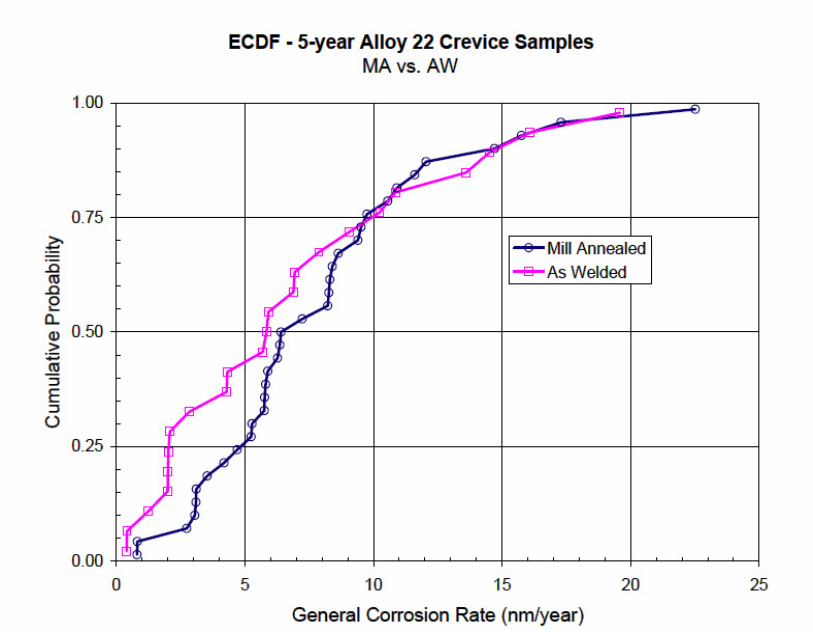

Source: DTN: LL030412512251.057 [DIRS 163712], file: *C22 5 Year Coupon Corrosion Rates 4-14-03.xls*.

Output DTN: MO0612WPOUTERB.000, file: *Alloy22_5yr_CreviceAnalysis.xls*.

Figure 6-19. Empirical Cumulative Distributions for General Corrosion Rate of Mill-Annealed and As-Welded Alloy 22 Crevice Samples at 60°C and 90°C after Five-Year Exposure in the Aqueous and Vapor Phases of Simulated Acidified Water, Simulated Concentrated Water, and Simulated Dilute Water in the Long-Term Corrosion Test Facility

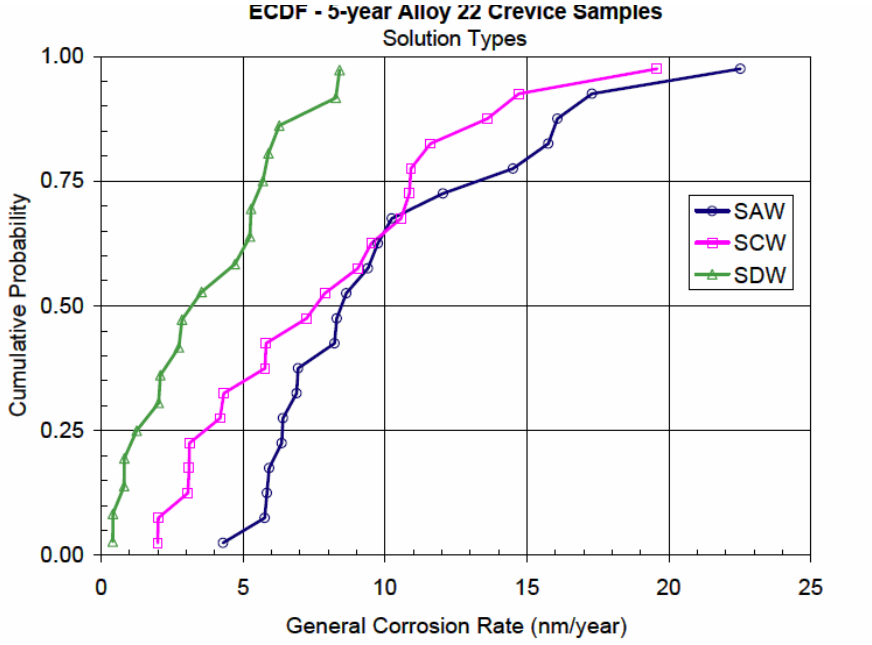

Source: DTN: LL030412512251.057 [DIRS 163712], file: *C22 5 Year Coupon Corrosion Rates 4-14-03.xls*.

Output DTN: MO0612WPOUTERB.000, file: *Alloy22_5yr_CreviceAnalysis.xls*.

Figure 6-20. Empirical Cumulative Distributions for General Corrosion Rate of Alloy 22 Crevice Samples Tested in Three Different Solution Types at 60°C and 90°C after Five-Year Exposure in the Long-Term Corrosion Test Facility

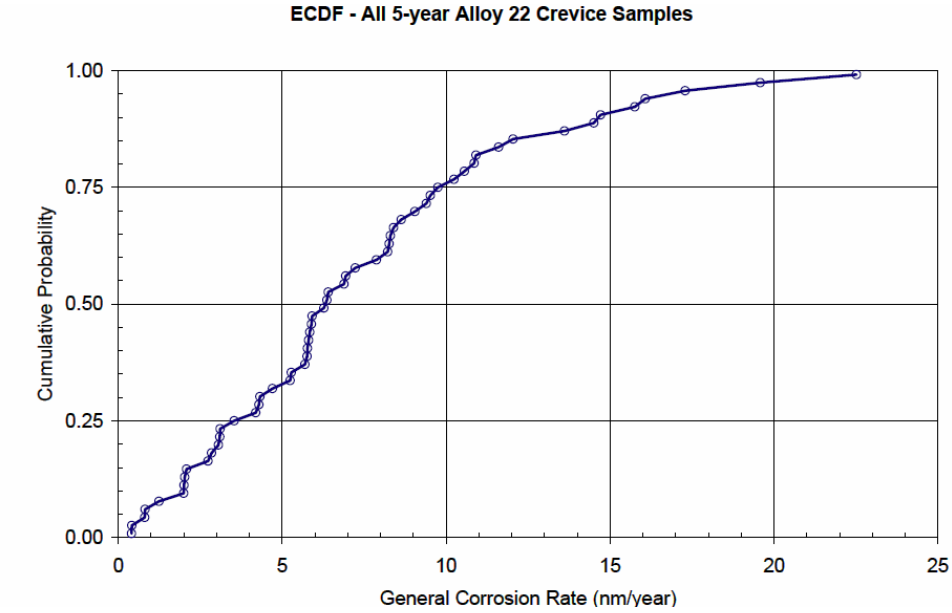

Source: DTN: LL030412512251.057 [DIRS 163712], file: *C22 5 Year Coupon Corrosion Rates 4-14-03.xls*.

Output DTN: MO0612WPOUTERB.000, file: *Alloy22_5yr_CreviceAnalysis.xls*.

Figure 6-21. Empirical Cumulative Distributions for General Corrosion Rate of All Alloy 22 Crevice Samples after Five-Year Exposure in Aqueous and Vapor Phases of Simulated Acidified Water, Simulated Concentrated Water, and Simulated Dilute Water in the Long-Term Corrosion Test Facility

The ECDFs for the general corrosion rates of all the weight-loss and crevice samples, regardless of the test medium or temperature, are shown in Figure 6-22. For the crevice samples the mean corrosion rate is 7.36 nm/yr, and the standard deviation is 4.93 nm/yr. For the weight-loss samples, the mean corrosion rate is 3.15 nm/yr and the standard deviation is 2.71 nm/yr. These are discussed in Section 6.4.3.3 and summarized in Table 6-6. The corrosion rate distribution for the crevice coupons was used as the general corrosion rate of the WPOB. Section 6.4.3.4 provides details of the general corrosion model.

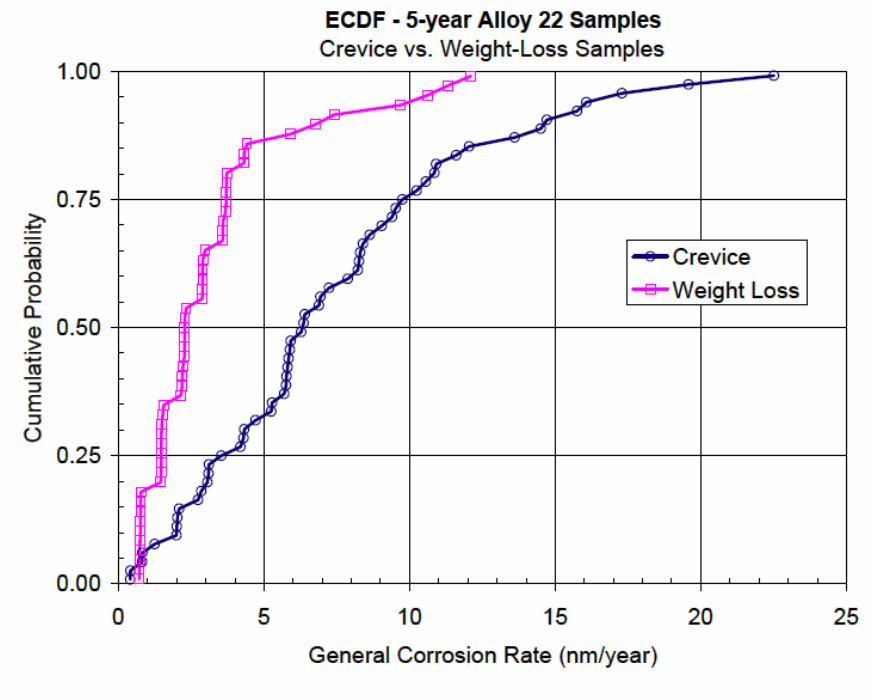

Source: DTN: LL030412512251.057 [DIRS 163712], file: *C22 5 Year Coupon Corrosion Rates 4-14-03.xls*.

Output DTN: MO0612WPOUTERB.000, file: *Alloy22_5yr_CreviceAnalysis.xls*.

Figure 6-22. Empirical Cumulative Distributions for General Corrosion Rate of Alloy 22 Weight-Loss and Crevice Samples after Five-Year Exposure in Aqueous and Vapor Phases of Simulated Acidified Water, Simulated Concentrated Water, and Simulated Dilute Water in the Long-Term Corrosion Test Facility

As shown in Figure 6-22, the observed general corrosion rates of the crevice specimens are higher than those of the "plain" weight-loss specimens. This may have been caused the difference in surface-polishing treatments between these two groups of test specimens (Wong et al. 2004 [DIRS 174800]). The weight-loss specimens were polished on both sides while the crevice specimens were polished only on one side. Thus, the unpolished surface of the crevice specimens retained the finishing given at the mill (by the primary metal producer) at the time of their immersion into the test electrolytes in the LTCTF (i.e., the crevice specimens were tested without removing the mill-annealed oxide coating from their surface). It is possible that the removal of this mill-annealed oxide film from the unpolished side of the crevice specimens during posttest specimen cleaning caused a greater amount of weight-loss for these specimens. This, in turn, could have resulted in higher general corrosion rates for the crevice specimens.

As shown in Figure 6-11 and Figure 6-18, the weight-loss-based general corrosion rates of the creviced specimens exposed in the vapor phase do not significantly differ from the weight-loss-based general corrosion rates of the creviced specimens exposed to the aqueous phase. This similarity may be due to the weight-loss measurement being dominated by the unpolished surface of the crevice specimens (i.e., the weight-loss due to removal of this unpolished surface during cleaning exceeds any real weight-loss due to corrosion). As shown in Figure 6-10 and Figure 6-13, there is a slightly greater difference between the weight-loss-based general corrosion rates of the weight-loss geometry specimens exposed in the vapor phase and the aqueous phase than for the creviced specimens, particularly for the SCW environment at 90°C. Due to the similarity between the two data sets, it is justified to use the weight-losses from crevice specimens exposed to both the vapor and aqueous phases for development of the general corrosion model for Alloy 22.

6.4.3.2.1 Fitting of Crevice Sample Data to a Distribution

For ease of implementation and analysis, as well as to represent extreme values, it is desirable to fit the empirical distribution of general corrosion rates derived from the crevice samples to a distribution. As shown in Appendix IV, several distributions were evaluated including the uniform distribution, the normal distribution, the log-normal distribution, and the gamma distribution. It was concluded based on analysis of quantile plots that the uniform distribution, the normal distribution, and the log-normal distribution did not fit the data very well. The gamma distribution resulted in a fairly good fit to the data; however, the gamma distribution resulted in a lower R-squared value (i.e., not as good a fit to the data) than did a fit using the Weibull distribution including maximum likelihood estimators. On that basis, it was determined that the Weibull distribution was the best fit to the data and is sufficient for use in further analyses. The Weibull distribution is characterized by a scale parameter, b, and a shape parameter, c (Evans et al. 1993 [DIRS 112115], Section 41). The b and c parameters that best fit the five-year exposed crevice samples were determined using maximum likelihood estimators of 8.141 nm/yr and 1.476 (after bias correction, see Appendix IV), respectively. This distribution will be discussed in more detail in Section 6.4.3.3.2 when uncertainty due to the fitting process is considered.

6.4.3.3 Uncertainty Analysis of General Corrosion Rate Data

Two sources of uncertainty are considered in this section. Uncertainty due to measurement of weight-loss is discussed in Section 6.4.3.3.1, and uncertainty due to fitting the distribution of the corrosion rates determined from these weight-loss measurements is discussed in Section 6.4.3.3.2.

6.4.3.3.1 Evaluation of Uncertainty Due to Weight-Loss Measurements

As discussed in Section 6.4.3.4, the five-year data were used for the general corrosion model for the WPOB. Therefore, it is important to adequately quantify the uncertainty associated with the data and propagate it into the general corrosion model. This section documents the analyses performed to quantify the uncertainty in the general corrosion rates of Alloy 22 calculated from the LTCTF five-year weight-loss measurements.

Length measurements of the individual coupons were performed using digital calipers. The values of length, width, and thickness of each coupon are listed in Appendix II. Only one measurement per coupon was reported. The smallest length increment is 0.5 mils (12.7 μm).

Weight measurement was the main source of uncertainty. Most of the uncertainty results from insufficient resolution of the weight-loss measurements of the samples due to the extremely low corrosion rates of the alloy in the test media. The method used in weight measurement uncertainty analysis is presented in this section. The method enables sound interpretation of the general corrosion data shown in Figure 6-22 (also in Appendices II and III) and its application in the waste package degradation analysis.

Consider a measurand *Y*, which is not measured directly but is determined from *N* other quantities $X_1, X_2, ..., X_N$ through a functional relationship *f* defined in Equation 6-10:

$$Y = f(X_1, X_2, \cdots, X_N) \quad \text{(Eq. 6-10)}$$

An estimate of the measurand *Y*, denoted by *y*, is obtained using input estimates $x_1, x_2, ..., x_N$ for the values of *N* input quantities $X_1, X_2, \cdots, X_N$. The output estimate *y*, is given by Equation 6-11:

$$y = f(x_1, x_2, \cdots, x_N) \quad \text{(Eq. 6-11)}$$

The combined uncertainty of the measurement result *y*, designated by Δy, is given by Equation 6-12, the law of propagation of uncertainty (Taylor et al. 1994 [DIRS 162260], Appendix A):

$$\Delta y = \sqrt{\sum_{i=1}^{N}\left(\frac{\partial f}{\partial x_i}\right)^2 \Delta x_i^2 + 2\sum_{i=1}^{N-1}\sum_{j=i+1}^{N}\frac{\partial f}{\partial x_i}\frac{\partial f}{\partial x_j}\Delta x_i x_j} \quad \text{(Eq. 6-12)}$$

In Equation 6-12, the partial derivatives $\frac{\partial f}{\partial x_i}$ are the sensitivity coefficients, Δx_i is the standard uncertainty associated with the input estimate x_i, and $\Delta x_i x_j$ is the estimated covariance associated with x_i and x_j.

Referring to Figure 6-9, the schematic of the Alloy 22 sample used in the weight-loss measurement in LTCTF, the exposed surface area of the sample is expressed by Equation 6-13:

$$A = 2ab + 2bc + 2ac - \left(\frac{\pi d^2}{2}\right) + \pi dc \quad \text{(Eq. 6-13)}$$

Referring to Equation 6-7 and letting the dependent variable *y* be the five-year general corrosion rate measured in the LTCTF, the equation for the general corrosion rate is expressed by Equation 6-14:

$$y = \frac{dp}{dt} = \frac{w}{\rho \times t\left(2ab + 2bc + 2ac - \left(\frac{\pi d^2}{2}\right) + \pi dc\right)} \quad \text{(Eq. 6-14)}$$

where y is the corrosion rate in cm per hour, t is the time of exposure in hours, w is the total weight-loss during the time, t, in grams, and ρ is the density in grams per cubic centimeter. The combined uncertainty of the measurement result, y, the corrosion rate, is calculated by Equation 6-15, using the law of propagation of uncertainty (Taylor et al. 1994 [DIRS 162260], Appendix A):

$$\Delta y = \sqrt{\left(\frac{\partial y}{\partial w}\right)^2 \Delta w^2 + \left(\frac{\partial y}{\partial \rho}\right)^2 \Delta \rho^2 + \left(\frac{\partial y}{\partial t}\right)^2 \Delta t^2 + \left(\frac{\partial y}{\partial a}\right)^2 \Delta a^2 + \left(\frac{\partial y}{\partial b}\right)^2 \Delta b^2 + \left(\frac{\partial y}{\partial c}\right)^2 \Delta c^2 + \left(\frac{\partial y}{\partial d}\right)^2 \Delta d^2} \quad \text{(Eq. 6-15)}$$

where w, ρ, t, a, b, c, and d were considered independent; hence, the covariance terms disappear.

The partial derivatives are given in Equations 6-16 through 6-22:

$$\frac{\partial y}{\partial w} = \frac{1}{\rho \times t\left(2ab + 2bc + 2ac - \left(\frac{\pi d^2}{2}\right) + \pi dc\right)} \quad \text{(Eq. 6-16)}$$

$$\frac{\partial y}{\partial \rho} = -\frac{w}{\rho^2 \times t\left(2ab + 2bc + 2ac - \left(\frac{\pi d^2}{2}\right) + \pi dc\right)} \quad \text{(Eq. 6-17)}$$

$$\frac{\partial y}{\partial t} = -\frac{w}{\rho \times t^2\left(2ab + 2bc + 2ac - \left(\frac{\pi d^2}{2}\right) + \pi dc\right)} \quad \text{(Eq. 6-18)}$$

$$\frac{\partial y}{\partial a} = -\frac{2w(b + c)}{\rho \times t\left(2ab + 2bc + 2ac - \left(\frac{\pi d^2}{2}\right) + \pi dc\right)^2} \quad \text{(Eq. 6-19)}$$

$$\frac{\partial y}{\partial b} = -\frac{2w(a + c)}{\rho \times t\left(2ab + 2bc + 2ac - \left(\frac{\pi d^2}{2}\right) + \pi dc\right)^2} \quad \text{(Eq. 6-20)}$$

$$\frac{\partial y}{\partial c} = -\frac{w[2(a+b)+\pi d]}{\rho \times t\left(2ab+2bc+2ac-\left(\frac{\pi d^2}{2}\right)+\pi dc\right)^2} \quad \text{(Eq. 6-21)}$$

$$\frac{\partial y}{\partial d} = -\frac{w\pi(c-d)}{\rho \times t\left(2ab+2bc+2ac-\left(\frac{\pi d^2}{2}\right)+\pi dc\right)^2} \quad \text{(Eq. 6-22)}$$

The maximum error in the corrosion rate is estimated by calculating numeric values of the partial derivatives from expected values of the independent variables, multiplying each partial derivative by the corresponding error (i.e., standard uncertainty) associated in the independent variables (Δw, $\Delta \rho$, Δt, Δa, Δb, Δc, and Δd), and summing the resulting products.

The combined standard uncertainty in the corrosion rate was estimated with Equation 6-15 by calculating numeric values of the partial derivatives from expected values of the input variables and their estimated standard uncertainties. Those values and intermediate calculation steps are summarized in Table 6-5.

Upon examining the sensitivity coefficients in Equation 6-15, it was found that Δy was most sensitive to the estimate of Δw. Because Δw was most influential on Δy, a detailed description of how Δw was calculated is given below. A Mettler AT200 balance was used to measure the weight of the specimens. The balance displays mass measurements to four decimal places. For instance, a four-digit readout might indicate a mass of 60.2675 grams for the weight of a specimen. Considering that the balance employs standard round-off practice, the displayed number is a value that lies between 60.26745 grams and 60.26755 grams. Therefore, the measured mass has an equal probability of lying between these two numbers. This, in turn, would indicate that the error term has a uniform distribution. If w_1 = original weight of specimen and w_2 = final weight of specimen, then $w_1 = \mu_1 + 10^{-4}\varepsilon_1$ and $w_2 = \mu_2 + 10^{-4}\varepsilon_2$, where $\varepsilon_1 \sim U(-0.5, 0.5)$, and $\varepsilon_2 \sim U(-0.5, 0.5)$. That is, the mass = true mass + error term. Equation 6-23 gives the weight-loss due to corrosion:

$$w = w_1 - w_2 = (\mu_1 - \mu_2) + 10^{-4}(\varepsilon_1 - \varepsilon_2) \quad \text{(Eq. 6-23)}$$

where $(\mu_1 - \mu_2)$ is the true difference in mass and $10^{-4}(\varepsilon_1 - \varepsilon_2)$ is the error term. The error term $(\varepsilon_1 - \varepsilon_2)$ has a triangular distribution (Papoulis 1965 [DIRS 162236], pp. 189 to 192) between −1 and 1 (i.e., $(\varepsilon_1 - \varepsilon_2)$ approximately triangular (−1, 1, 0)). For this distribution the standard deviation is given by Equation 6-24:

$$s = \frac{1}{\sqrt{6}} = 0.41 \quad \text{(Eq. 6-24)}$$

Therefore, $\Delta w = 0.41 \times 10^{-4}$ g. The summary of the measurement uncertainty analysis for the five-year data based upon this method is shown in Table 6-6.

Table 6-5. Summary of Measurement Uncertainty Analysis for Corrosion Rates Based Upon Weight-Loss Measurements after Five-Year Exposure in the Long-Term Corrosion Testing Facility

Uncertainty Analysis of Five-Year Weight-Loss Measurement Data			
Parameters	**Units**	**Crevice Samples**	**Weight-Loss Samples**
w	g	0.0019	0.00042
ρ	g/cm^3	8.69	8.69
t	hour	43800	43800
a	cm	5.08	5.08
b	cm	5.08	2.54
c	cm	0.3175	0.3175
d	cm	0.7925	0.7925
Δw	g	4.100×10^{-05}	4.100×10^{-05}
$\Delta\rho$	g/cm^3	0.1	0.1
Δt	hour	24	24
Δa	cm	0.00254	0.00254
Δb	cm	0.00254	0.00254
Δc	cm	0.00254	0.00254
Δd	cm	0.00254	0.00254
Surface Area	cm^2	57.5787	30.2239
$\partial y/\partial w$		4.540×10^{-08}	8.628×10^{-08}
$\partial y/\partial \rho$		-9.927×10^{-12}	-4.170×10^{-12}
$\partial y/\partial t$		-1.969×10^{-15}	-8.274×10^{-12}
$\partial y/\partial a$		-1.609×10^{-11}	-6.802×10^{-12}
$\partial y/\partial b$		-1.609×10^{-11}	-1.285×10^{-11}
$\partial y/\partial c$		-3.029×10^{-11}	-1.814×10^{-11}
$\partial y/\partial d$		2.224×10^{-12}	1.776×10^{-12}
$(\partial y/\partial w)^2 \Delta w^2$		3.465×10^{-24}	1.252×10^{-23}
$(\partial y/\partial \rho)^2 \Delta \rho^2$		9.854×10^{-25}	1.739×10^{-25}
$(\partial y/\partial t)^2 \Delta t^2$		2.234×10^{-27}	3.943×10^{-28}
$(\partial y/\partial a)^2 \Delta a^2$		1.671×10^{-27}	2.985×10^{-28}
$(\partial y/\partial b)^2 \Delta b^2$		1.671×10^{-27}	1.065×10^{-27}
$(\partial y/\partial c)^2 \Delta c^2$		5.919×10^{-27}	2.123×10^{-27}
$(\partial y/\partial d)^2 \Delta d^2$		3.192×10^{-29}	2.035×10^{-29}
Δy	cm/hr	2.112×10^{-12}	3.563×10^{-12}
Δy	µm/yr	1.850×10^{-04}	3.121×10^{-04}
Δy	nm/yr	**0.185**	**0.312**

Output DTN: MO0612WPOUTERB.000, file: *Alloy22_WtLoss_UncAnalysis.xls*.

Table 6-6. Summary of Measurement Uncertainty Analysis for Corrosion Rates Based on Weight-Loss Measurements after Five-Year Exposure in the Long-Term Corrosion Testing Facility

Sample Configuration	Average Weight-Loss (g)	Δy (nm/yr)	Mean Corrosion Rate (nm/yr)	Standard Deviation (nm/yr)
Weight-Loss	0.00042	0.312	3.15	2.71
Crevice	0.0019	0.185	7.36	4.93

Output DTN: MO0612WPOUTERB.000, file: *Alloy22_WtLoss_UncAnalysis.xls*.

The combined standard uncertainty is estimated to be approximately 0.185 nm/yr for crevice samples and 0.312 nm/yr for weight-loss samples. These estimates correspond to one standard deviation (1σ). Therefore, for the crevice samples, about 2.5% of the variation in the measured general corrosion rate is due to the measurement uncertainty, and 97.5% of the variation is from the variations of the general corrosion rate among the specimens. For the weight-loss samples, most of the variation (about 90%) in the measured corrosion rate is due to variations among the specimens, and the rest is from measurement uncertainty.

The corrosion rate distribution determined from the creviced geometry samples was used for the general corrosion rate of the WPOB (a conservative approach). Furthermore, because only a small amount (about 2.5%) of the total variation in the measured general corrosion rate of the crevice samples is due to the measurement uncertainty, all (100%) of the measured variation is considered due to the variability in the general corrosion processes for modeling purposes. This variability should be modeled on individual waste packages and among individual areas on the waste package.

It is important to note that the step change in the corrosion rates shown in Figure 6-12 to Figure 6-23 corresponds to the resolution of the balance used to determine the weight change of the coupons. Each step corresponds to the resolution limit of the balance (0.1 mg), that is, a change in the corrosion rate smaller than each step in these figures cannot be resolved.

6.4.3.3.2 Evaluation of Uncertainty Due to Fitting to a Weibull Distribution

The general corrosion rates determined from five-year exposed crevice samples were fit to a Weibull distribution in Section 6.4.3.2.1. A total of 58 general corrosion rates were used to accomplish this fitting. Uncertainty in the fitting process was evaluated by the use of Monte Carlo analysis (see Appendix V and output DTN: MO0612WPOUTERB.000, file: *Weibull_Partition.xmcd*). The first step in this process was to sample 100,000 sets of 58 general corrosion rate values from the Weibull distribution (b = 8.141 nm/yr and c = 1.476) determined in Section 6.4.3.2.1. The next step was to determine 100,000 pairs of b and c values resulting from fitting each sampled set of 58 general corrosion rate values to the Weibull distribution using maximum likelihood estimators. As with the fitting done in Section 6.4.3.2.1, the shape parameters are corrected for bias. From the covariance matrix of the 100,000 pairs of b and c values, the eigenvectors of the pairs of b and c values were determined, allowing for partitioning along the major principal component. The lowest 5% of these values and their corresponding b and c pairs were averaged resulting in a mean b and c pair to be used to represent a low level of uncertainty. The highest 5% of the major principal components were averaged and their corresponding b and c pairs result in a mean b and c pair to be used to

represent a high level of uncertainty. The remaining 90% of the major principal components were averaged resulting in the corresponding mean b and c values to be used to represent a medium level of uncertainty. The results of this analysis are presented numerically in Table 6-7. The three Weibull distributions corresponding to the low, medium, and high uncertainty levels, as well as the experimentally measured crevice sample data, are shown in Figure 6-23. As discussed in Section 6.4.3.4, these three sets of Weibull distribution parameters are used to represent the Alloy 22 general corrosion rate, R_o, at an exposure temperature of 60°C. R_o is given by an inverse Weibull distribution as shown in Equation 6-33.

Table 6-7. Results of Uncertainty Analysis of Weibull Fitting

Uncertainty Level	Scale Parameter, *b* (nm/yr)	Shape Parameter, *c* (no units)
Low	6.628	1.380
Medium	8.134	1.476
High	9.774	1.578

Output DTN: MO0703PAGENCOR.001, file: *BaseCase GC CDFs.xls*.

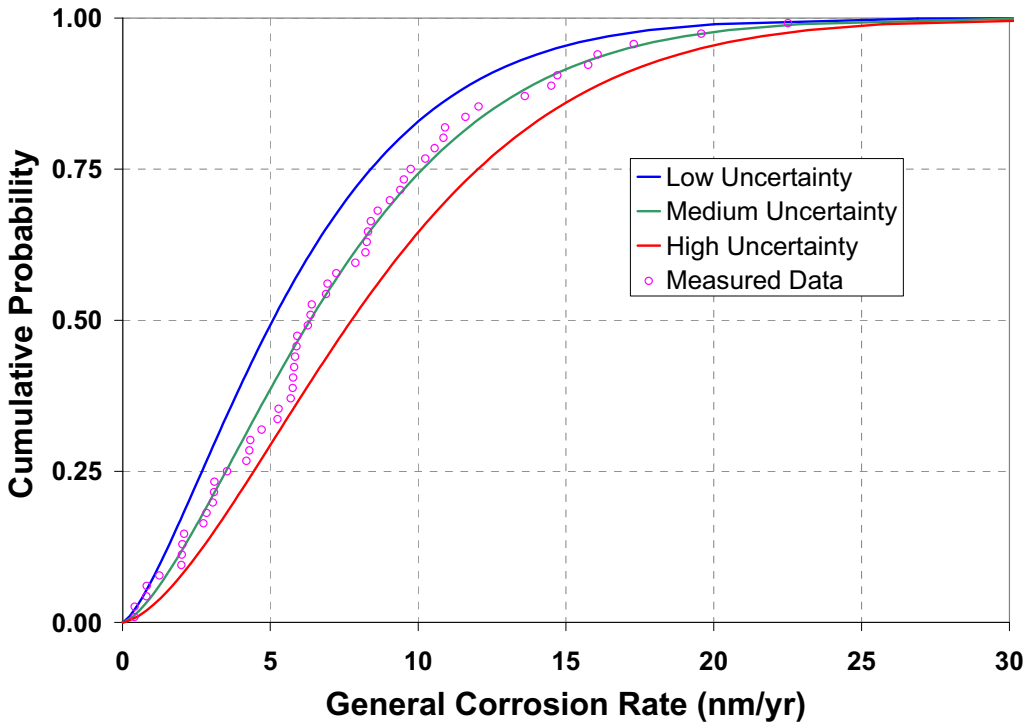

Source: DTN: LL030412512251.057 [DIRS 163712], file: *C22 5 Year Coupon Corrosion Rates 4-14-03.xls*.

Output DTN: MO0612WPOUTERB.000, file: *BaseCase GC CDFs2.xls*.

Figure 6-23. Low, Medium, and High Uncertainty Levels for General Corrosion Rate Distributions Resulting from Fitting of Five-Year Exposed Creviced Sample Data

In TSPA, the low, medium, and high general corrosion rate distributions should be randomly selected in such a way that the low and high general corrosion rate distributions are each used for 5% of realizations and the medium general corrosion rate distribution is used for the remaining 90% of realizations. This weighting is appropriate because it corresponds to partitioning areas in the analysis. It also preserves the expected mean value of each parameter. The 5%-90%-5% uncertainty partitioning should result in general corrosion rate distributions which are separated from each other and yet sampled enough times to determine if uncertainty in this parameter has a significant effect. Other choices (e.g., 1%-98%-1%) might result in the low and high general corrosion rate distributions being sampled too few times for meaningful statistics to be gathered, while choices such as 30%-40%-30% might not result in general corrosion rate distributions that are distinguishable from each other.

6.4.3.4 Temperature-Dependent General Corrosion Model

Temperature-Dependent General Corrosion Model Development

The creviced geometry specimens exposed for five years at both 60°C and 90°C in the LTCTF were used to develop a distribution for the general corrosion rate of Alloy 22 to be used at 60°C. In Section 6.4.3.2, it was noted that no temperature dependence was readily apparent from the creviced geometry specimen data. As discussed in this section, the general corrosion rate of Alloy 22 is expected to depend on temperature. For this reason, a temperature dependence for Alloy 22 was developed based on short-term polarization resistance measurements. It is probable that the polarization resistance specimens did not achieve steady-state before the measurements were conducted. As noted by other researchers (e.g., EPRI 2002 [DIRS 158069], Section 5.3.2 and Dunn et al. 2005 [DIRS 178104], Section 3.2), it may be more appropriate to determine the temperature-dependence of Alloy 22 general corrosion rates based on general corrosion rates obtained from samples which are at steady-state. For this reason, the temperature-dependence of Alloy 22 general corrosion rates of weight-loss coupons immersed in the SCW solution for five-years is also evaluated in this section, and the results compared to the aforementioned short-term polarization resistance data.

As mentioned in Section 6.4.1.2, the kinetics and mechanism of corrosion processes of a metal depends on the physicochemical properties of oxide films formed on the metal surface. For instance, the general corrosion (passive dissolution) of highly corrosion-resistant alloys such as Alloy 22 is governed by the transport properties of reacting species in the passive film and the rate of activation-controlled ion transfer at the film-solution interface. The reacting species include metal ions, oxygen ions, vacancies and interstitials. These processes are influenced by the characteristics of the passive film, electrochemical potential across the film, and the chemistry of solution contacting the film. Chromium and nickel oxides, which are the major constituents of the passive film of Ni-Cr-Mo alloys like Alloy 22 (Lorang et al. 1990 [DIRS 154718]), are stable and exhibit extremely low dissolution rates over a wide range of solution chemistry. The transport properties of the reacting species and the rates of ion transfer across the passive film-solution interface are considered thermally activated processes. Consequently, the general corrosion rate of the Alloy 22 WPOB is expected to have a certain level of temperature dependence. The literature data summarized in a report by EPRI (2002 [DIRS 158069], Section 5.3.2) show such a temperature-dependence of Alloy 22 general corrosion rates in a wide range of test solution chemistries.

The general corrosion rate at a given temperature is represented in Equation 6-25 by an Arrhenius relation in logarithmic form, i.e.:

$$\ln(R_T) = C_o - \frac{C_1}{T} \quad \text{(Eq. 6-25)}$$

where R_T is temperature-dependent general corrosion rate in nm/yr, T is the absolute temperature in Kelvin, and C_o and C_1 (in Kelvin) are constants. The higher the value of C_1, the greater the dependence of general corrosion rate on temperature. The Arrhenius relationship is used to describe the temperature dependence of activation-controlled metal corrosion processes (ASM International 1987 [DIRS 133378], p. 39). Accordingly, the Arrhenius relationship has been used in the corrosion science literature to describe the temperature dependence of Alloy 22 general corrosion rates (Pensado et al. 2002 [DIRS 166944], Section 4.3; Dunn et al. 2005 [DIRS 178104], Section 3.2; Dunn et al. 2004 [DIRS 171452]; Lloyd et al. 2003 [DIRS 167921]; and Hua and Gordon 2004 [DIRS 171013]).

Rearranging Equation 6-25 to the form of the Arrhenius relation (i.e., $R_T = A \exp(-E_a/RT)$), C_1 can be expressed as E_a/R, where E_a is the apparent activation energy (J/mol), and R is the universal gas constant (8.314 J/mol K) (Lide 1991 [DIRS 131202], inside rear cover).

The general corrosion rate distributions calculated from the weight-loss data of the five-year crevice specimens measured at 60°C and 90°C (Figure 6-23) are used to represent the distribution of long-term general corrosion rates of the WPOB at 60°C for the purposes of this model. This approach is reasonably bounding because the general corrosion rates for crevice specimens are generally higher than those of noncreviced weight-loss specimens. The intercept term, C_o, can be determined from the temperature-dependence term, C_1, as shown in Equations 6-26 and 6-27:

$$\ln(R_o) = C_o - \frac{C_1}{T_0} \quad \text{(Eq. 6-26)}$$

$$C_o = \ln(R_o) + \frac{C_1}{T_0} \quad \text{(Eq. 6-27)}$$

where R_o is the general corrosion rate distribution from the weight-loss of the five-year exposed crevice samples (Figure 6-23) in nm/yr at T_0 = 333.15 K (60°C). Substituting for C_o in Equation 6-25, results in Equation 6-28:

$$\ln(R_T) = \ln(R_o) + C_1\left(\frac{1}{T_0} - \frac{1}{T}\right) \quad \text{(Eq. 6-28)}$$

Or, in terms of the apparent activation energy, Equation 6-29 gives:

$$\ln(R_T) = \ln(R_o) + E_a\left[\frac{1}{R \cdot T_0} - \frac{1}{R \cdot T}\right] \quad \text{(Eq. 6-29)}$$

This linearized form of the exponential relationship was used to estimate the apparent activation energy. In a plot of logarithmic reaction rates versus adjusted inverse temperature, x (see below), the slope is thus expected to be E_a. The transformed variables y and x were used in the model fitting such that, as Equation 6-30 shows:

$$y = \ln(R_T) = \beta_0 + \beta_1 x$$
$$x = \left[\frac{1}{R \cdot T_0} - \frac{1}{R \cdot T} \right] \qquad \text{(Eq. 6-30)}$$
$$\beta_0 = \ln(R_o), \quad \beta_1 = E_a$$

where x is the adjusted inverse temperature. The data set used for this exercise (Table 6-8) (DTN: LL060900812251.180 [DIRS 178409], file: *175 PRFitv2.xls*) is the result of an experimental design in which corrosion rates were measured in several solutions composed of a mixture of sodium chloride and potassium nitrate at three temperature levels (60°C, 80°C, and 100°C). The solution groups are described below.

Table 6-8. Solutions Used to Determine Temperature-Dependence of General Corrosion

Solution	Solution Description	Number of Measurements	Nitrate Molality	Chloride Molality
F1	1 *m* NaCl + 0.05 *m* KNO_3	46	0.05	1
F2	1 *m* NaCl + 0.15 *m* KNO_3	33	0.15	1
F3	1 *m* NaCl + 0.5 *m* KNO_3	28	0.5	1
F4	3.5 *m* NaCl + 0.175 *m* KNO_3	33	0.175	3.5
F5	3.5 *m* NaCl + 0.525 *m* KNO_3	43	0.525	3.5
F6	3.5 *m* NaCl + 1.75 *m* KNO_3	22	1.75	3.5
F7	6 *m* NaCl + 0.3 *m* KNO_3	73	0.3	6
F8	6 *m* NaCl + 0.9 *m* KNO_3	69	0.9	6
F9	6 *m* NaCl + 3 *m* KNO_3	33	3.0	6

Source: DTN: LL060900812251.180 [DIRS 178409], file: *175 PRFitv2.xls*.

The rationale for using the exposure environments documented in Table 6-8 is that sodium chloride test solutions simulate the moderate relative humidity scenario where calcium is a minor component in the aqueous environment expected in the repository (Section 6.3.2). These brines also contain other cations such as sodium, and potassium, and anions such as nitrate.

An analysis of the data was performed graphically (Figure 6-24). The data in each solution were plotted, along with a smooth-line estimate (LOESS-fit), an ordinary-least-squares (OLS) fit within each group, and the OLS-fit to all the data (population OLS). In Figure 6-24, the OLS-fit to all the data (the black line) is the same for all the data. For temperatures of 60°C, 80°C, and 100°C, the respective x-variable values are 0 mol/kJ, 0.020 mol/kJ, and 0.039 mol/kJ.

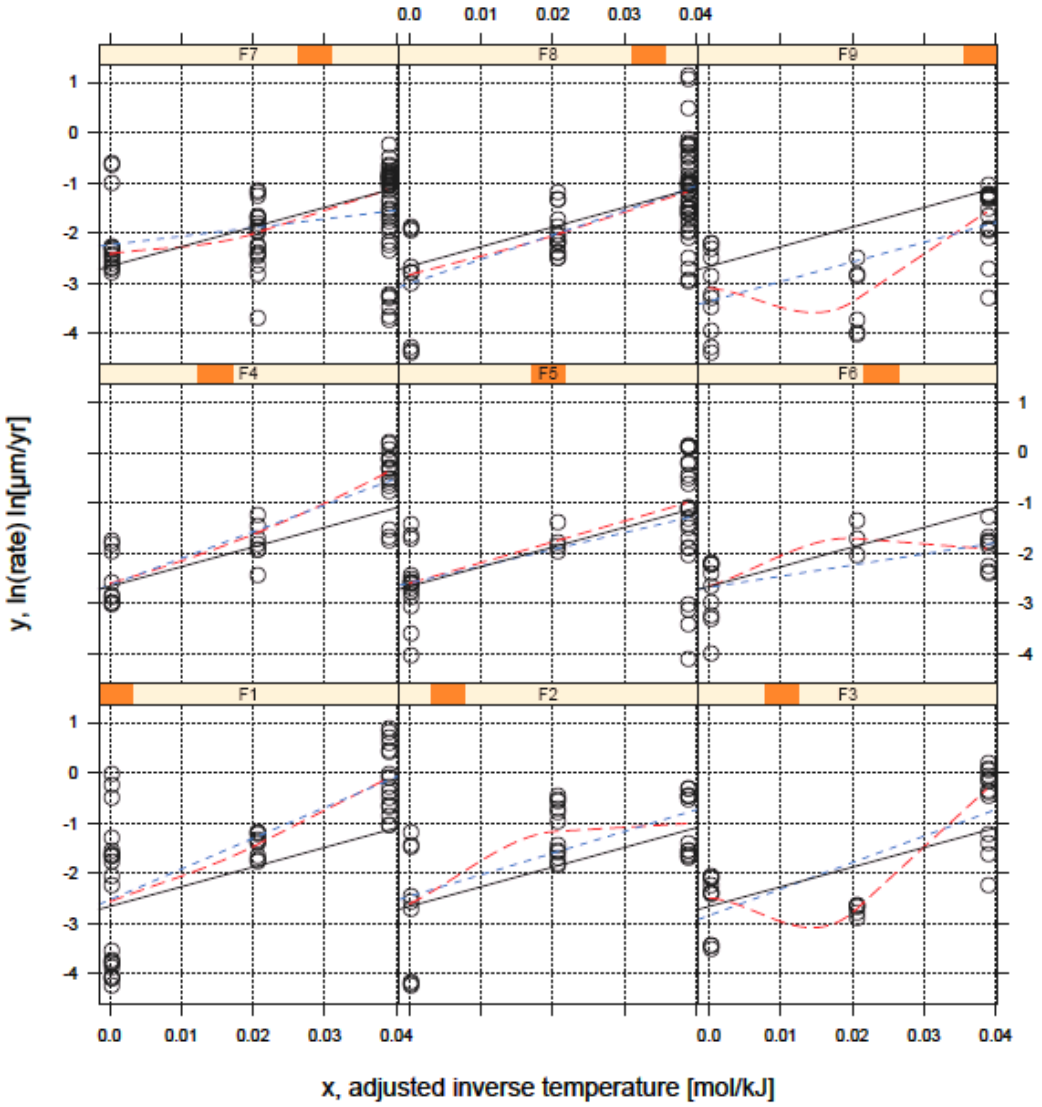

Source: DTN: LL060900812251.180 [DIRS 178409], file: *175 PRFitv2.xls*.

Output DTN: MO0612WPOUTERB.000, file: *GSD2.pdf*.

NOTE: LOESS fit = dashed red line; OLS fit = dashed blue line; population OLS = black line.

Figure 6-24. Graphic Analysis of Corrosion Rates in Each Solution

The OLS model corresponding to the simple linear regression of the estimated logarithmic corrosion rates (y) on the adjusted inverse temperature (x) is given by Equation 6-31:

$$y_{ij} = (\beta_0) + (\beta_1) x_{ij} + \varepsilon_{ij}, \quad \varepsilon_{ij} \sim N(0, \sigma^2) \qquad \text{(Eq. 6-31)}$$

where β_0 and β_1 are, respectively, the fixed effects for the intercept and the slope, and the ε_{ij} are the independent and identically distributed random error effects.

The individual slope and intercept estimates within each group indicate a degree of heterogeneity in the population that the OLS-fit cannot describe. To account for the heterogeneity in the intercepts and slopes, a linear mixed-effects (LME) model was used to fit the data (Venables and Ripley 2001 [DIRS 159088], Section 6.11). The LME model corresponding to the simple linear regression of the estimated logarithmic corrosion rates (y) for the jth sample within the ith solution group on the adjusted inverse temperature (x) is given as Equation 6-32:

$$y_{ij} = (\beta_0 + b_{0i}) + (\beta_1 + b_{1i})x_{ij} + \varepsilon_{ij},$$
$$b_i = \begin{bmatrix} b_{0i} \\ b_{1i} \end{bmatrix} \sim N\left(0, \Sigma = \begin{bmatrix} \tau_0^2 & \tau_{01} \\ \tau_{01} & \tau_1^2 \end{bmatrix}\right), \quad \varepsilon_{ij} \sim N(0, \sigma^2) \qquad \text{(Eq. 6-32)}$$

where β_0 and β_1 are, respectively, the fixed effects for the intercept and the slope; b_i is a random-effects vector, assumed to be independent for different solutions; and ε_{ij} is the independent and identically distributed within-group random error effect, considered independent of the other random effects. From Equation 6-32, it can be seen that the value of β_1 will be the mean apparent activation energy and the value of τ_1 will be the standard deviation of the apparent activation energy.

The LME model mentioned above was fit in S-PLUS 2000 Professional Release 2 using the built-in LME function. Below, the statements following the S-PLUS command line prompt, >, are user entries entered at the command line during an S-PLUS session. The lines not preceded by the > prompt are S-PLUS outputs.

```
> # fit mixed-effects model
> model2 <- lme(Y~1+X, random=~1+X|Soln, data=dataF.df, method="ML",
na.action = na.exclude)
> summary(model2)
Linear mixed-effects model fit by maximum likelihood
 Data: dataF.df
       AIC      BIC    logLik
  981.1853 1004.826 -484.5926

Random effects:
 Formula:  ~ 1 + X | Soln
 Structure: General positive-definite
                StdDev   Corr
(Intercept)  0.2181264 (Inter
          X 11.7504430 -0.011
   Residual  0.8384550

Fixed effects: Y ~ 1 + X
                Value Std.Error  DF   t-value p-value
(Intercept)  -2.68760  0.105784 370 -25.40645  <.0001
          X  40.77755  4.777778 370   8.53483  <.0001
 Correlation:
  (Intr)
X -0.334

Standardized Within-Group Residuals:
      Min         Q1        Med        Q3      Max
```

```
 -3.37215 -0.5257155 0.09103175 0.6721034 2.964984

Number of Observations: 380
Number of Groups: 9
```

The output from the summary method for the LME fitting function consists of several panels:

- The `Data` panel gives the value for `AIC` (the Akaike information criterion) and for `BIC` (the Bayesian information criterion) (Venables et al. 2001 [DIRS 159088], Section 6.11), which can be used for model selection, along with the log of the maximized likelihood.

- The `Random effects` panel displays estimates of the standard deviations and correlation for the random effects. The term labelled `Residual` is the estimate of σ, the standard deviation of ε_{ij} from Equation 6-32. Thus, $\hat{\tau}_0 = 0.22$, $\hat{\tau}_1 = 11.75$, and $\hat{\sigma} = 0.84$, where the "^" symbol denotes that the value is an estimate. Therefore, the standard deviation of the apparent activation energy is 11.75 kJ/mol.

- The `Fixed effects` panel displays the estimates for the intercept and slope fixed effects. The intercept represents an estimate of the average logarithmic corrosion rate at the reference temperature (i.e., $T_0 = 333.15$ K (60°C)). The slope coefficient is the mean value of the apparent activation energy, and is estimated as $\hat{\beta}_1 = 40.78$ kJ/mol.

- The panel labelled `Correlation` gives the estimated sampling correlation between the fixed-effect slope and intercept, which are not of direct interest unless the correlation is large (which it is not).

- The `Standardized Within-Group Residuals` panel contains information about the standardized residuals, the number of observations (380), and the number of groups (9 solution groups).

Figure 6-25 shows the corrosion rates in each solution with the population fixed-effects model (corresponding to β_0 and β_1 in Equation 6-32) and a local representation of the population fixed effects model adjusted by the random effects in each solution (corresponding to the b_i random-effects vector in Equation 6-32). The population fixed-effects model line (the red line in Figure 6-25 labeled "model2-population") is the same in every panel in the figure.

The apparent activation energy for the nine environments in Table 6-8 is 40.78 ± 11.75 kJ/mol (±1 standard deviation), as discussed in the preceding bullets. An apparent activation energy of 40.78 ± 11.75 kJ/mol translates to $C_1 = 4{,}905$ K with a standard deviation of 1,413 K. A normal distribution is selected for this parameter based on the observation of a linear quantile-normal plot (Appendix VII). In addition, the Shapiro-Wilk goodness-of-fit test calculated a p-value, which is consistent with a normal distribution.

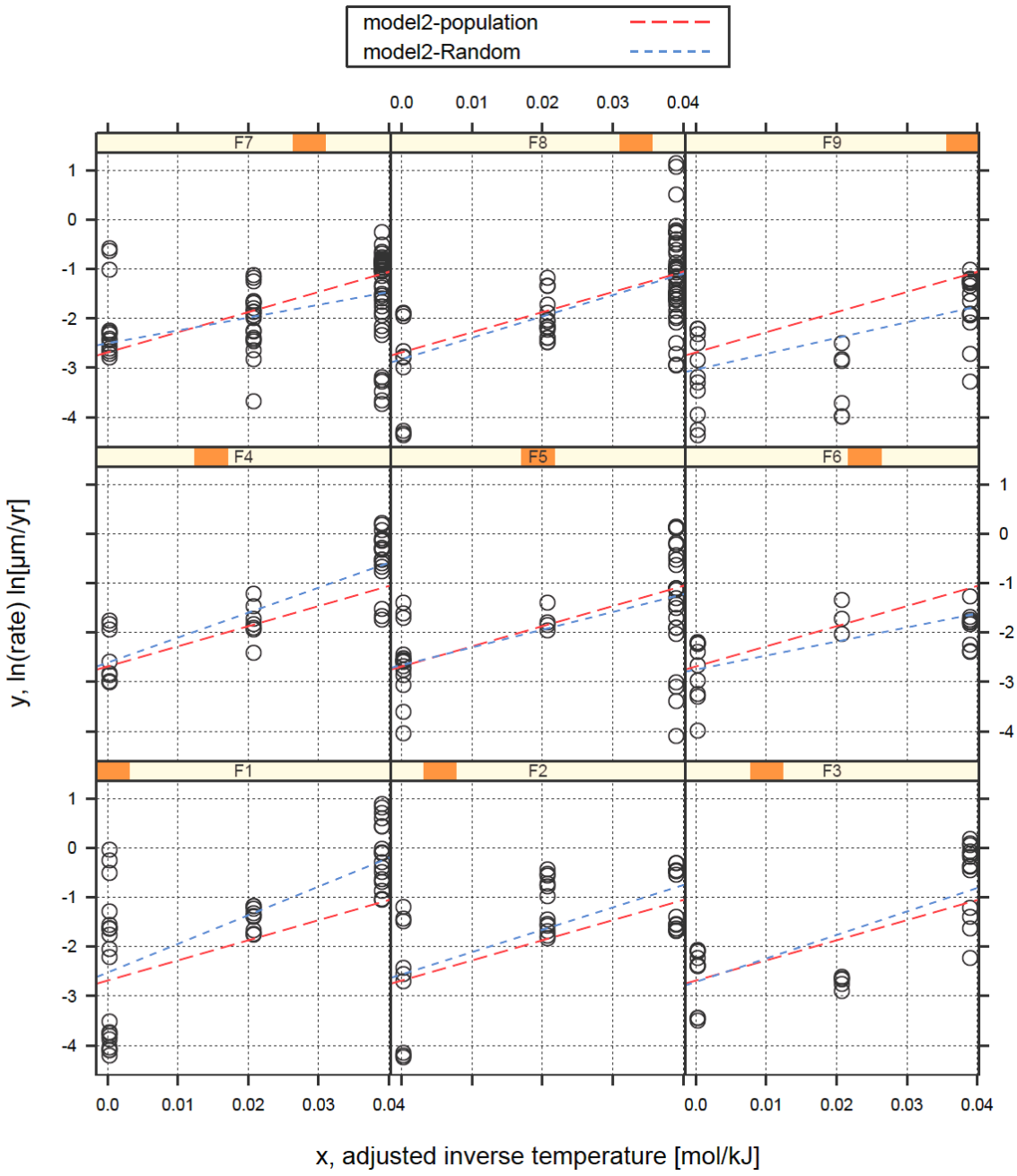

Source: DTN: LL060900812251.180 [DIRS 178409], file: *175 PRFitv2.xls*.

Output DTN: MO0612WPOUTERB.000, file: *GSD3.pdf*.

NOTES: This corresponds to β_0 and β_1 in Equation 6-32; results have been adjusted by the random effects in each solution (corresponding to the b_i random-effects vector in Equation 6-32). Red dashed line labeled "model2-population," representing the population fixed-effect model results, is the same in every panel.

Figure 6-25. Corrosion Rates in Each So lution with the Population Fixed-Effects Model and a Local Representation of the Population Fixed-Effects Model

As noted by other researchers (e.g., EPRI 2002 [DIRS 158069], Section 5.3.2 and Dunn et al. 2005 [DIRS 178104], Section 3.2), it may be more appropriate to determine the temperature-dependence of Alloy 22 general corrosion rates based on general corrosion rates obtained from

samples which are at steady-state. As can be seen from the analysis of long-term corrosion potentials in Section 6.4.4.4, achievement of steady-state conditions may require long exposure times (e.g., 250 days). Therefore, the calculated general corrosion rates of weight-loss coupons immersed in the SCW solution at 60°C and 90°C after five-years of exposure were analyzed. As discussed below, the results of this analysis corroborate the Alloy 22 general corrosion temperature-dependence model chosen to evaluate waste package performance (i.e., a normally-distributed apparent activation energy of 40.78 ± 11.75 kJ/mol (C_1 = 4,905 K with a standard deviation of 1,413 K) developed from analysis of polarization resistance data). The analysis of the immersed SCW data also provides a technical basis for truncation of the normal distribution used to represent the temperature-dependence of Alloy 22 general corrosion.

As discussed in Section 6.4.3.2, no temperature-dependence was observed in the Alloy 22 general corrosion rates calculated based on weight-loss measurements after five-years of exposure in the LTCTF with the exception of the results from weight-loss coupons immersed in the SCW solution. For coupons immersed in SCW at 60°C (note that one coupon was at the water-line and is considered to be immersed for this analysis), seven Alloy 22 general corrosion rates were calculated (output DTN: MO0612WPOUTERB.000, file: *Alloy22_5yr_WLAnalysis.xls*). Let this group of values be called b60. For coupons immersed in SCW at 90°C six Alloy 22 general corrosion rates were calculated (output DTN: MO0612WPOUTERB.000, file: *Alloy22_5yr_WLAnalysis.xls*). Let this group of values be called b90. The temperature-dependence of these general corrosion rates was calculated (to determine C_1) by a regression fit of these data to Equation 6-25 and uncertainty in this estimator was determined utilizing the bootstrap technique (Efron and Gong 1983 [DIRS 103967]) as documented in Appendix VII.

One-hundred thousand bootstrap estimates of the temperature-dependence of Alloy 22 general corrosion rates were generated. The first step in the analysis was to sample 100,000 sets of seven values (general corrosion rates) from b60 and 100,000 sets of six values from b90. b60 and b90 were treated as discrete populations (i.e., no interpolation between values occurred) from which the sampling was done with replacement (i.e., the same corrosion rate value could be sampled more than once). The first bootstrap estimate of the Alloy 22 general corrosion temperature-dependence was generated by fitting Equation 6-25 by linear regression to the first set of seven values sampled from b60 with the first set of six values sampled from b90. The second bootstrap estimate of the Alloy 22 general corrosion temperature-dependence was generated by fitting Equation 6-25 by linear regression to the second set of seven values sampled from b60 with the second set of six values sampled from b90, and so on until all 100,000 estimates of the Alloy 22 general corrosion temperature-dependence were obtained. The 100,000 bootstrap estimates of C_1 define an empirical distribution for the uncertainty in this parameter.

The minimum C_1 estimate from this empirical distribution was 682 K (corresponding to an apparent activation energy of 5.67 kJ/mol) and the maximum C_1 estimate was 7,811 K (corresponding to an apparent activation energy of 64.94 kJ/mol). The mean C_1 estimate was 4,872 K (corresponding to an apparent activation energy of 40.51 kJ/mol) and the median estimate was 4,901 K (corresponding to an apparent activation energy of 40.75 kJ/mol). These values compare well with the normally-distributed apparent activation energy of 40.78 ± 11.75 kJ/mol (C_1 = 4,905 K with a standard deviation of 1,413 K) developed from analysis of

polarization resistance data. As can be seen in Appendix VII, the apparent activation energy distribution developed from analysis of polarization resistance data is "broader" (i.e., higher and lower values of the apparent activation energy can be sampled) than the bootstrap empirical distribution developed based on analysis of weight-loss samples immersed in the SCW solution at 60°C and 90°C. For this reason, it is recommended the apparent activation energy distribution developed from analysis of polarization resistance data be truncated between −3 standard deviations (666 K corresponding to an apparent activation energy of 5.54 kJ/mol and consistent with the minimum C_1 estimate from the empirical distribution) and +2 standard deviations (7,731 K corresponding to an apparent activation energy of 64.28 kJ/mol and consistent with the maximum C_1 estimate from the empirical distribution).

The entire variance of the temperature-dependence term, C_1, is attributed to uncertainty. C_1 is represented as a normal distribution with a mean of 4,905 K and a standard deviation of 1,413 K truncated at −3 and +2 standard deviations. This treatment appropriately reflects the lack of knowledge in the exact value for the temperature-dependence term and spans apparent activation energy values from about 5.54 to 64.28 kJ/mol.

DTN: LL060900812251.180 [DIRS 178409], files: *176PRFit.xls*, *179PRFit.xls*, and *187PRFit.xls),* also contains six other data sets in addition to the data (summarized in Table 6-8) used to develop the temperature dependence for Alloy 22 general corrosion. These data sets are also candidates for use in evaluating the temperature-dependence of Alloy 22 general corrosion (i.e., data sets obtained for at least three different temperatures). The OLS-determined apparent activation energies for these data sets are shown in Table 6-9, and the mixed effects-determined apparent activation energies for the solutions in solution group F are shown in Table 6-10. The solution groups in Table 6-9 (labeled G, K, and L) were not used to develop the temperature-dependence. Note that none of the solution groups in Table 6-9 has as large a number of solutions as does solution group F in Table 6-8, nor are any of them as well-designed from a statistical analysis perspective.

Solution group F contained solutions with three specific nitrate-ion-to-chloride-ion ratios, and as discussed above, resulted in the determination of an apparent activation energy of 40.78 kJ/mol with a standard deviation of 11.75 kJ/mol. With the exception of solution L2, all of the remaining solution groups presented in Table 6-9 produced apparent activation energies which are within that distribution. In the case of solution L2, a negative apparent activation energy was determined. This observation is contrary to literature observations of the behavior of Alloy 22 (e.g., Dunn et al. 2004 [DIRS 171452] and Lloyd et al. 2003 [DIRS 167921] discussed later in this section), and has conservatively been excluded from this evaluation. Since the range of observed activation energies for a wide range of solutions is consistent with that determined by the analysis of solution group F, the use of solution group F is sufficient to evaluate the temperature dependence of the general corrosion rate of Alloy 22.

Table 6-9. Apparent Activation Energies for Solutions Not Used to Determine the Temperature-Dependence of Alloy 22 General Corrosion

Solution	Solution Description	Temperature Range °C	Activation Energy kJ/mol
G1	4 *M* NaCl	45 to 105	7.69
G2	4 *M* NaCl + 0.04 *M* Na_2SO_4	45 to 105	51.03
G3	4 *M* NaCl + 0.4 *M* Na_2SO_4	45 to 105	45.84
K1	12 *m* $CaCl_2$ + 6 *m* $Ca(NO_3)_2$	100 to 150	35.61
L1	5 *M* $CaCl_2$	30 to 120	28.07
L2	5 *M* $CaCl_2$ + 0.5 *M* $Ca(NO_3)_2$	60 to 120	−15.13

Output DTN: MO0612WPOUTERB.000, file: *Output_data2-fit.txt*.

Table 6-10. Apparent Activation Energies for Solutions Used to Determine the Temperature-Dependence of Alloy 22 General Corrosion

Solution	Solution Description	Activation Energy kJ/mol
F1	1 *m* NaCl + 0.05 *m* KNO_3	58.06
F2	1 *m* NaCl + 0.15 *m* KNO_3	45.22
F3	1 *m* NaCl + 0.5 *m* KNO_3	47.58
F4	3.5 *m* NaCl + 0.175 *m* KNO_3	50.63
F5	3.5 *m* NaCl + 0.525 *m* KNO_3	35.86
F6	3.5 *m* NaCl + 1.75 *m* KNO_3	28.46
F7	6 *m* NaCl + 0.3 *m* KNO_3	26.00
F8	6 *m* NaCl + 0.9 *m* KNO_3	43.24
F9	6 *m* NaCl + 3 *m* KNO_3	31.96

Output DTN: MO0612WPOUTERB.000, file: *Output_dataF-fit.txt*.

The temperature-dependence term (C_1) in Equation 6-28 represents the effect of temperature on corrosion rates of Alloy 22 based on polarization resistance measurements using a wide variety of specimen configurations, metallurgical conditions, and exposure environments (i.e., water chemistries). The polarization resistance of the samples was measured after 24-hour exposure of the samples in open-circuit potential in the test environments (Section 4.1.1.4, Appendix I). Polarization resistance technique is often used for obtaining the temperature dependence of corrosion reactions, because it is rapid, simple, and relatively inexpensive (Revie 2000 [DIRS 159370], Chapter 68). The technique is well-established for routine use and is described in ASTM G 59-97 (1998 [DIRS 163907]). The details of the polarization resistance measurements used in this report are discussed in Appendix I. The relative change in, rather than the absolute values of, the corrosion rates with temperature is used in this report to determine the temperature dependence used in the model. In this way, any systematic error in the measured corrosion rates has a lesser impact on the model results.

Although some investigators have observed an effect of scan rate on polarization resistance measurements on Alloy 22 (Pensado et al. 2002 [DIRS 166944], Section 4.2) and recommended the use of a slower scan rate, the Yucca Mountain Project (YMP) experiments were conducted following ASTM G 59-97 (1998 [DIRS 163907]), which recommends the use of a potential scan rate of 0.6 V/hr (0.167 mV/s). Pensado et al. (2002 [DIRS 166944], Section 4.2) found that

measured general corrosion rates increased with increasing scan rate (for scan rates above about 0.01 mV/s). The corrosion rates from the polarization resistance measurements were for a comparative analysis to extract the temperature dependence of the general corrosion rates (i.e., to obtain a relative measure of how corrosion rates change with temperature). The polarization resistance measurements are not used in this analysis to obtain the absolute values for modeling the general corrosion rate of Alloy 22 in the repository. The method for obtaining absolute values of the general corrosion rates of Alloy 22 is discussed later in this section.

Temperature-Dependent General Corrosion Model Extrapolation

Equation 6-28 is used to extrapolate corrosion rates below 60°C and above 100°C, although the experimental data used to develop the temperature-dependence of general corrosion of Alloy 22 was obtained at temperatures of 60°C, 80°C, and 100°C. It was shown earlier that other experimental data not used for development of the model, and collected at temperatures ranging from 30°C to 150°C (Table 6-9), produced apparent activation energies which were consistent with the developed model (with the exception of solution group L2, as discussed above). As shown in Appendix VII, the measured corrosion rates at low temperatures are consistent with the trend predicted by OLS regression, indicating that the general corrosion mechanism does not change as the temperature decreases. Therefore, the extrapolation of the temperature dependence relationship is justified.

It is expected that the anodic dissolution rate of the passive film on Alloy 22 will decrease with a decrease in exposure temperature. Several possible mechanisms could account for the decreased corrosion rate at lower temperatures, including decreased mass transfer rates through the passive film and cathodic limitations in the anodic dissolution rate. The primary component of the passive film formed on chromium-containing alloys such as Alloy 22 is a chromium oxide film, which is an n-type semiconductor, as discussed in Section 6.4.1.1.4. For chromium oxide, the lower the temperature, the smaller will be the number of electrons in the conduction band. Due to a reduction in the availability of electrons in the conduction band at lower temperatures, the rate of cathodic reduction reaction (e.g., reduction of dissolved oxygen in an oxidizing aqueous solution) will be correspondingly reduced. This, in turn, could proportionately reduce the anodic dissolution rate of Alloy 22 due to cathodic limitations. The general corrosion rates of Alloy 22 have been observed by other investigators to decrease with exposure temperature (Dunn et al. 2005 [DIRS 178104], Sections 3.1 and 3.2; Dunn et al. 2004 [DIRS 171452]; and Lloyd et al. 2003 [DIRS 167921]). Dunn et al. (2004 [DIRS 171452]) studied the effect of temperature on the general corrosion rate of Alloy 22 in 0.028 *M* NaCl at a pH of 5.5, as reported in *Passive and Localized Corrosion of Alloy 22 - Modeling and Experiments* (Dunn et al. 2005 [DIRS 178104], Section 3.1), and observed a temperature dependence, which was linear over a temperature range of 25°C to 95°C. They obtained general corrosion rates of Alloy 22 by measuring polarization resistance using electrochemical impedance spectroscopy and reported an apparent activation energy value of 46.3 kJ/mol, which is consistent with that documented in this report (i.e., 40.78 kJ/mol obtained by the polarization resistance method).

Dunn et al. (2005 [DIRS 178104], Section 3.2) also analyzed a set of polarization resistance results obtained in 0.028 *M* NaCl (from 25°C to 95°C) and 4 *M* NaCl (from 40°C to 175°C) solutions, where each polarization resistance measurement was performed after a minimum exposure time of 10 days. The apparent activation energy obtained in the 0.028 *M* NaCl solution

was 41.8 kJ/mol and that in 4 *M* NaCl solution was 33.6 kJ/mol. It may be noted that these same investigators had previously reported observing no temperature dependence in 4 *M* NaCl solution (Dunn et al. 1999 [DIRS 154481], Section 3.1). Of the two temperature dependence values (e.g., approximately 0 and 33.6 kJ/mol) reported by investigators at the Center for Nuclear Waste Regulatory Analyses (CNWRA) for the general corrosion rate of Alloy 22 in 4 *M* NaCl solution, the higher apparent activation energy value of 33.6kJ/mol is more reasonable, because it better represents the activation controlled ion transfer reaction that is expected to occur across the Alloy 22-solution interface during general corrosion of Alloy 22. The observed decrease in apparent activation energy from 46.3 to 41.8 kJ/mol in 0.028 *M* NaCl with longer exposure time is probably within the experimental error of the polarization resistance measurements made. The apparent activation energy for the 4 *M* NaCl solution over a temperature range from 40°C to 175°C (33.6 kJ/mol) compares well with the Alloy 22 general corrosion temperature-dependence distribution developed in this report (i.e., 40.78 ± 11.75 kJ/mol (±1 standard deviation) obtained by the polarization resistance method) indicating that extrapolation of the temperature dependence relationship to temperatures higher than 100°C is justified.

In another study, funded by the YMP, Hua and Gordon (2004 [DIRS 171013]) conducted weight-loss experiments on mill-annealed and as-welded Alloy 22 specimens at exposure temperatures from 60°C to 105°C for a total of eight weeks in a BSW solution having a room temperature pH of about 12. No significant difference was observed between the apparent activation energies of the as-welded and mill-annealed Alloy 22 specimens in this study. After four weeks of exposure, the apparent activation energy for the combined data set was 19.3 kJ/mol; this value increased to 25.3 kJ/mol after eight weeks of exposure. This indicates that the apparent activation energy for Alloy 22 general corrosion increased slightly with exposure time in this experiment. The apparent activation energies obtained by Hua and Gordon (2004 [DIRS 171013]) are on the low end of the apparent activation energy distribution documented in this report (i.e., 40.78 ± 11.75 kJ/mol (±1 standard deviation) obtained by the polarization resistance method).

Lloyd et al. (2003 [DIRS 167921]) studied the effect of temperature on the general corrosion rate of Alloy 22 in chloride-containing acidic environments relevant to the Yucca Mountain repository in the range of temperature from 25°C to 85°C. They reported apparent activation energies of 32 kJ/mol (for specimens potentiostatically polarized at 350 mV versus a silver/silver chloride reference electrode using 0.1 *M* KCl (i.e., 288 mV versus the normal hydrogen electrode)), and 46 kJ/mol (for specimens potentiostatically polarized at 500 mV relative to the same electrode) in chloride- and sulfate-containing acidic solution (pH about 1). Although Lloyd et al. (2003 [DIRS 167921]) acknowledged that steady-state conditions may not have been attained and metastable localized corrosion events were observed during some experiments, the Alloy 22 specimens maintained passivity. The apparent activation energy values reported corroborate well with those reported in this model report.

On the basis of the above discussion and observations, it is concluded that the Alloy 22 general corrosion temperature-dependence distribution developed in this report (i.e., 40.78 ± 11.75 kJ/mol (±1 standard deviation) obtained by the polarization resistance method) is consistent with values reported in the literature and can be extrapolated to ambient repository temperatures. Additionally, the apparent activation energy reported by Dunn et al. (2005 [DIRS 178104], Section 3.2) for a 4 *M* NaCl solution over a temperature range from 40°C

to 175°C, also indicates that extrapolation of the temperature dependence relationship to temperatures higher than 100°C is justified. Validation of the Alloy 22 general corrosion temperature-dependence distribution developed in this report is discussed in Section 7.2.1.

Temperature-Dependent General Corrosion Model Results

In Section 6.4.3.2.1, the five-year corrosion rate data for creviced Alloy 22 samples were fit to a Weibull distribution. Uncertainty due to measurement of weight-loss was discussed in Section 6.4.3.3.1, where it was concluded that the variation in the general corrosion rates was due to specimen-to-specimen variability in the general corrosion process itself. Uncertainty due to fitting a Weibull distribution to the corrosion rates was discussed in Section 6.4.3.3.2, where three Weibull distributions were developed that represent low, medium, and high uncertainty levels (Figure 6-23). It is these distributions that are used to represent R_o. In TSPA, the low, medium, and high general corrosion rate distributions should be randomly selected in such a way that the low and high general corrosion rate distributions are each used for 5% of realizations and the medium general corrosion rate distribution is used for the remaining 90% of realizations.

R_o is expressed as an inverse Weibull cumulative distribution function (CDF) as given in Equation 6-33 (Evans et al. 1993 [DIRS 112115], Section 41):

$$R_o = b\left[\ln\left(\frac{1}{1-p}\right)\right]^{1/c} \quad \text{(Eq. 6-33)}$$

where p is the cumulative probability, and the values of b and c are given in Table 6-7. The cumulative distribution functions for R_o are given in Figure 6-23 along with the crevice sample data (Figure 6-22).

The model outputs (R_T) (see Equation 6-28 at temperatures of 25°C, 60°C, 100°C, 150°C, and 200°C are shown in Figure 6-26 using the medium uncertainty R_o Weibull distribution (Figure 6-23) and the median value of C_1 for the temperature dependence. The medium uncertainty R_o distribution would be used in 90% of repository realizations. Figure 6-27 shows the span of the predicted general corrosion rates at both 25°C and 200°C. At 25°C, the low values are generated using the low level of uncertainty of the R_o Weibull distribution (Figure 6-23) and the high value of C_1 for the temperature dependence; the middle values are generated using the medium level of R_o uncertainty and the median value of C_1; the high values are generated using the high level of R_o uncertainty and the low value of C_1. The median general corrosion rates vary from approximately 0.33 to 6.2 nm/yr at 25°C. At 200°C, the minimum values are generated using the low level of uncertainty of the R_o Weibull distribution (Figure 6-23) and the low value of C_1 for the temperature dependence; the middle values are generated using the medium level of R_o uncertainty and the median value of C_1; the highest values are generated using the high level of R_o uncertainty and the high value of C_1. Median general corrosion rates vary from approximately 9.2 to 7,430 nm/yr at 200°C. The larger span in median values at 200°C relative to 25°C is not surprising, given that the difference between the reference temperature of 60°C and 200°C is much larger than that between 60°C and 25°C.

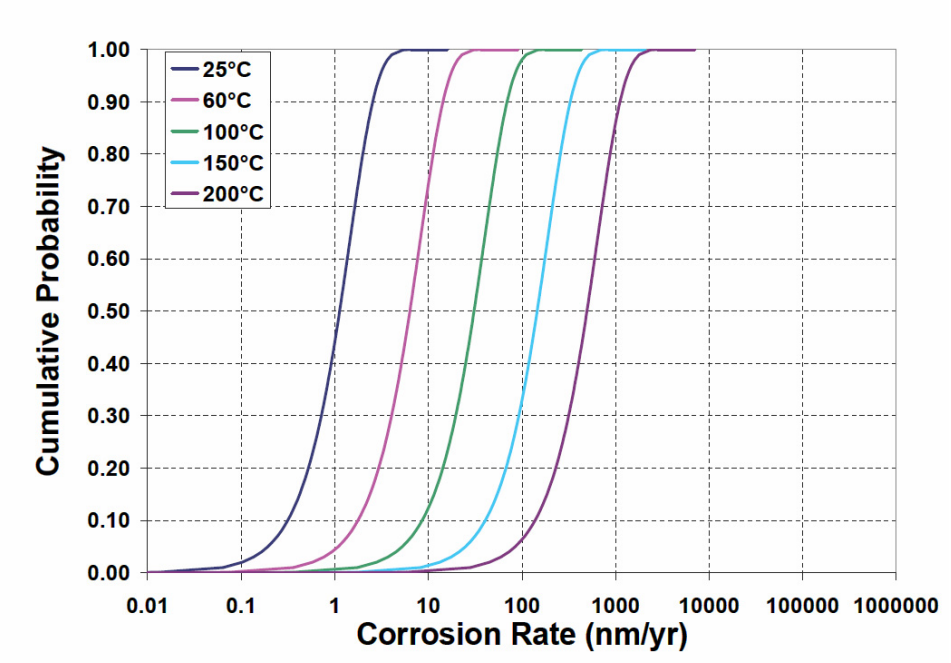

Output DTN: MO0612WPOUTERB.000, file: *BaseCase GC CDFs2.xls*.

Figure 6-26. Calculated Model Outputs of the Base-Case Temperature-Dependent General Corrosion Model with the Medium Uncertainty Level for R_o and the Mean Apparent Activation Energy of 40.78 kJ/mol at 25°C, 60°C, 100°C, 150°C, and 200°C

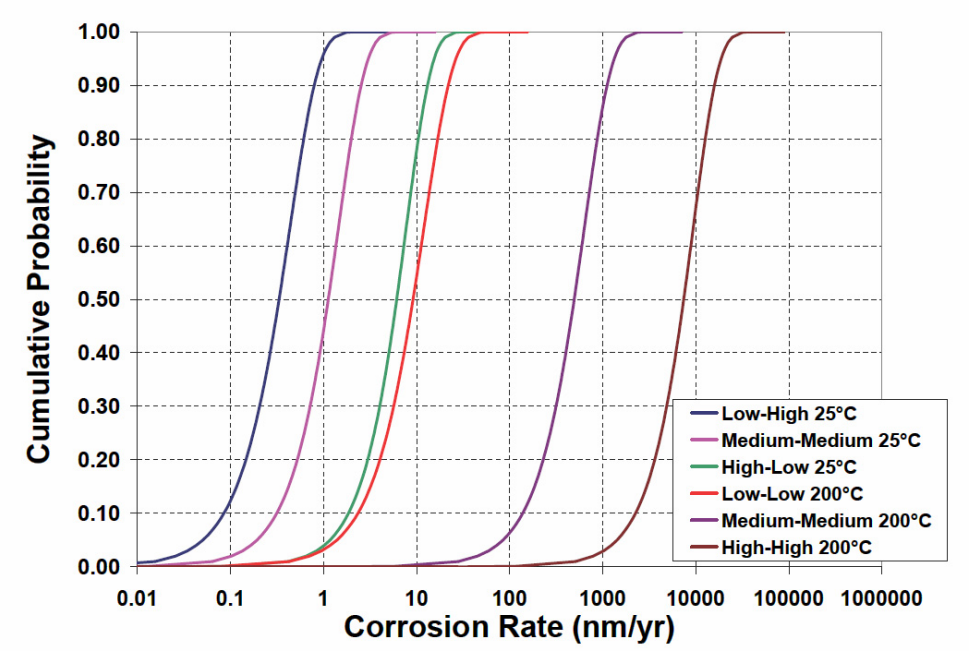

Output DTN: MO0612WPOUTERB.000, file: *BaseCase GC CDFs2.xls*.

Figure 6-27. Calculated Model Outputs of the Base-Case Temperature-Dependent General Corrosion Model with Uncertainty Levels and Apparent Activation Energies Designed to Span the Range of Possible Values at 25°C and 200°C

6.4.3.5 Alternative Conceptual Model for General Corrosion

Alternative conceptual models (ACMs) are based on modeling assumptions and simplifications different from those employed in the model. An important reason for considering ACMs is to help build confidence that changes in modeling assumptions or simplifications will not change conclusions regarding subsystem and total system performance. Conceptual model uncertainty results from having limited amounts of experimental data and a lack of available information to corroborate or refute plausible alternative interpretations of the subsystem and the processes occurring within the subsystem. This section discusses the ACMs for the general corrosion models of the WPOB. None of the general corrosion ACMs discussed in this section is output from this report.

6.4.3.5.1 Time-Dependent General Corrosion Behavior of the Waste Package Outer Barrier

As discussed in detail in Section 6.4.3.4, the general corrosion model for the WPOB is based on the five-year weight-loss measurements of Alloy 22 crevice samples from the LTCTF. The general corrosion rate is temperature-dependent, and, for a given temperature, it is assumed to be constant (time-independent) (Assumption 5.2). Therefore, for a given temperature, the depth of penetration or thinning of the WPOB by general corrosion is equal to the general corrosion rate at that temperature, multiplied by the time duration that the waste package surface is at that temperature. However, general corrosion rates of metals and alloys tend to decrease with time. Section 7.2.1 presents general corrosion rates determined from potentiostatic polarization, polarization resistance, and weight-loss measurements and shows a marked decrease in corrosion rate over time from 1 day to 2.3 years (the five-year data point is excluded from this discussion for model validation purposes). Even if the five-year data point is excluded from the calculations, general corrosion rates for Alloy 22 decrease with time. The discussion in Section 7.2 indicates that the trend of decreasing general corrosion rate with time is consistent with the expected corrosion behavior of passive alloys such as Alloy 22 under repository-type aqueous conditions.

The time-dependent general corrosion behavior of the WPOB was not included in the Alloy 22 general corrosion model because the constant (time-independent) rate model (for a given temperature) is more conservative and will bound the general corrosion behavior of the WPOB over the repository time period.

6.4.3.5.2 Alternative Approaches Using the Long-Term General Corrosion Rates of Weight-Loss Samples

As shown in Figure 6-22, the observed general corrosion rates of the crevice specimens are higher than those of the "plain" weight-loss specimens. This may have been caused by different surface-polishing treatments between these two groups of test specimens (Wong et al. 2004 [DIRS 174800]). The weight-loss specimens were polished on both sides while the crevice specimens were polished only on one side. Thus, the unpolished surface of the crevice specimens retained the finishing given at the mill (by the primary metal producer) at the time of their immersion into the test electrolytes in the LTCTF (i.e., the crevice specimens were tested without removing the mill-annealed oxide coating from their surface). It is possible that the

removal of this mill-annealed oxide film from the unpolished side of the crevice specimens during posttest specimen cleaning caused a greater amount of weight-loss for these specimens. This, in turn, could have resulted in higher general corrosion rates for the crevice specimens. Therefore, a realistic ACM would use the corrosion rates of weight-loss samples to derive the R_o distribution for use in the general corrosion model of WPOB (Equation 6-28). This ACM does not involve the use of a conceptual model that differs from that used in the WPOB general corrosion model but does make use of a different distribution for R_o.

Given that the discussion in this section involves an ACM, the level of detail applied to the analysis of the fitting of the crevice samples is not warranted. No evaluation of which distribution best fits the weight-loss data is undertaken. Instead, the weight-loss data is fit to a Weibull distribution using maximum likelihood estimators (i.e., using the same methods applied to the crevice sample data). The results of this fitting procedure are shown in Appendix VI, where it is found that the scale parameter, b, and a shape parameter, c, are 3.447 nm/yr and 1.318, respectively. Conservatively, no bias correction is applied to the shape parameter. This is conservative because application of the bias correction would decrease the value of the shape parameter resulting in lower values in the resulting Weibull distribution. A plot of the general corrosion rate distribution resulting from fitting the five-year exposed weight-loss sample data and the data themselves is shown in Figure 6-28. A comparison of Figure 6-28 to Figure 6-23 (showing the Weibull distributions based on the crevice sample data) shows that this conceptual model is less conservative relative to the general corrosion model. This is also clear from a comparison of the shape and scale factors for the distributions.

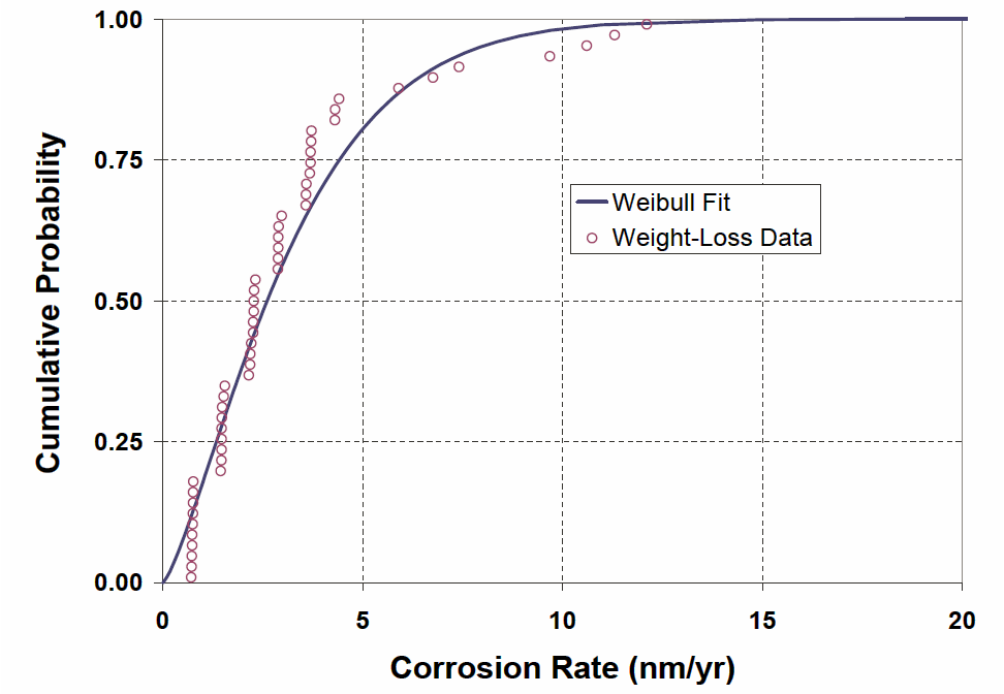

Source: DTN: LL030412512251.057 [DIRS 163712], file: *C22 5 Year Coupon Corrosion Rates 4-14-03.xls*.

Output DTN: MO0612WPOUTERB.000, file: *ACM GC Rate CDF.xls*.

Figure 6-28. General Corrosion Rate Distribution Resulting from Fitting of Five-Year Exposed Weight-Loss Sample Data

As noted by other researchers (e.g., EPRI 2002 [DIRS 158069], Section 5.3.2, and Dunn et al. 2005 [DIRS 178104], Section 3.2), it may be more appropriate to determine the temperature-dependence of Alloy 22 general corrosion based on general corrosion rates obtained from samples which are at steady-state as opposed to the use of short-term polarization resistance data as was done in Section 6.4.3.4. An ACM for the temperature-dependence of Alloy 22 general corrosion can be developed based on the calculated corrosion rates of weight-loss specimens exposed for five-years in SCW solution at 60°C and 90°C. This ACM is discussed in Section 6.4.3.4 and Appendix VII. This ACM does not involve the use of a conceptual model that differs from that used in the WPOB general corrosion model but does make use of a different distribution for C_1. The ACM analysis used a bootstrap technique (Efron and Gong 1983 [DIRS 103967]) to produce an empirical cumulative distribution function (output DTN: MO0612WPOUTERB.000, file: *WDC1GC.cdf*) which could be used as an ACM for the temperature-dependence term, C_1, in Equation 6-25. The minimum C_1 estimate from this empirical distribution was 682 K (corresponding to an apparent activation energy of 5.67 kJ/mol) and the maximum C_1 estimate was 7,811 K (corresponding to an apparent activation energy of 64.94 kJ/mol). The mean C_1 estimate was 4,872 K (corresponding to an apparent activation energy of 40.51 kJ/mol) and the median estimate was 4,901 K (corresponding to an apparent activation energy of 40.75 kJ/mol).

6.4.4 Localized Corrosion

Localized corrosion is a phenomenon in which corrosion progresses at discrete sites or in a nonuniform manner. The rate of localized corrosion penetration is generally higher than the rate of general corrosion penetration. The current analysis assumes that crevice corrosion is representative of localized corrosion of the WPOB under the exposure conditions expected in the postclosure repository (Assumption 5.3, Section 5). This is a conservative and bounding assumption because the initiation thresholds for crevice corrosion in terms of water chemistry and temperature are lower than those for pitting corrosion (Gdowski 1991 [DIRS 100859], Section 3.0; Haynes International 1997 [DIRS 100896]; Haynes International 1997 [DIRS 100897]), which is another form of localized corrosion.

Localized corrosion of the WPOB is analyzed in this report with two model components: an initiation model and a propagation model. In the localized corrosion initiation model, localized corrosion of the WPOB occurs when the open-circuit potential, or corrosion potential (E_{corr}), is equal to or greater than a critical threshold potential ($E_{critical}$), that is, ΔE (= $E_{critical}$ - E_{corr}) ≤ 0. The magnitude of ΔE is an index of the localized corrosion resistance; that is, the larger the difference, the greater the localized corrosion resistance. This conceptual model of localized corrosion initiation is recognized by the corrosion community (e.g., Dunn et al. 2005 [DIRS 178451] and Beavers et al. 2002 [DIRS 158781], Section 8.3). The ΔE criterion was developed on the basis of information found throughout the corrosion science literature (Böhni 2000 [DIRS 164137], Section B; Dunn et al. 2000 [DIRS 164495]; Dunn et al. 2003 [DIRS 164138]; Frankel 1998 [DIRS 162216]; Frankel 2002 [DIRS 164140]; Frankel and Kelly 2002 [DIRS 164141]). The localized corrosion initiation model components (i.e., E_{corr} and $E_{critical}$) could be affected by the sample configuration (crevice, disk, or rod), metallurgical condition (mill-annealed or as-welded), and exposure conditions (temperature, pH, chloride-ion concentration, or nitrate-ion concentration).

A series of the electrochemical corrosion tests were conducted to generate the data for the localized corrosion initiation model. The typical sequence for electrochemical testing is summarized in Appendix I. As discussed in Section 6.4.4.4, a set of long-term open-circuit potential measurements was used to measure the long-term corrosion potentials (E_{corr}) of Alloy 22 in a wide range of exposure environments. A series of CPP tests was also performed to measure the critical potentials ($E_{critical}$) of Alloy 22 for differing sample configurations and metallurgical conditions in a wide range of exposure environments.

Crevice corrosion initiation and propagation can be affected by the initial condition of the specimen surface prior to testing. Handbook data (Kain 1987 [DIRS 155193], p. 306) show, for a variety of alloys, that fewer crevices initiate on as-received (mill-condition) specimens than on specimens that have been wet-ground to a 120-grit surface finish. This behavior results from the ability to form a tighter crevice on ground surfaces promoting breakdown of the passive film (Kain 1987 [DIRS 155193], p. 303). In this report, as discussed in Appendix I, the samples used for analysis of crevice corrosion initiation had a 600-grit equivalent surface finish. If the as-emplaced waste packages have a rougher surface finish, the localized corrosion initiation model developed in this report will be conservative relative to the expected behavior of the waste packages in the repository.

In this report, localized corrosion of the WPOB is assumed to propagate at a (time-independent) constant rate (Assumption 5.4, Section 5). This assumption is conservative because it is known that the localized corrosion rate decreases with time (Hunkeler and Boehni 1983 [DIRS 162221]; McGuire et al. 1998 [DIRS 152193], Section 5.2.8). Section 6.4.4.7 provides additional discussion on this issue.

6.4.4.1 Overview of Approaches for Selection of Critical Potential for Localized Corrosion Initiation

The critical potential (E_{crit}) for the initiation of localized corrosion can be defined in many ways. Several possible definitions for this parameter are reviewed in this section. The critical potential for localized corrosion initiation used in this report is the crevice repassivation potential (E_{rcrev}) which is based on the potential at which the reverse scan of a CPP curve using a creviced sample crosses the forward scan.

Localized corrosion of the WPOB occurs when the long-term corrosion potential, E_{corr}, is equal to or greater than a certain critical potential, $E_{critical}$ (Figure 6-29), that is when $\Delta E = E_{critical} - E_{corr} \leq 0$. As mentioned above, E_{corr} and $E_{critical}$ could be affected by the sample configuration (crevice, disk, or rod), metallurgical condition (e.g., mill-annealed, as-welded, or as-welded plus thermally aged), and exposure condition (e.g., temperature, pH, chloride-ion concentration, or nitrate-ion concentration).

$E_{critical}$ can be defined as a potential above which the current density or corrosion rate of a material increases significantly and irreversibly above the general corrosion rate of the passive metal (ASTM G 61-86 1987 [DIRS 127897]; Jones 1992 [DIRS 169906], Chapter 7). Above this potential, local breakdown of the passive film can occur. This choice of $E_{critical}$ is also referred to as the breakdown potential (Figure 6-29). In addition, several other current-based definitions of $E_{critical}$ can be found in the scientific literature. For example, in CPP tests, the

potential at which the current density permanently exceeds 1 μA/cm^2 in the forward scan can be selected as a threshold potential to define crevice corrosion initiation (or crevice stabilization) (Kehler et al. 1999 [DIRS 162230]; Scully et al. 1999 [DIRS 110246]; Kehler et al. 2001 [DIRS 162231]). The potential at which the current density permanently exceeds 1 μA/cm^2 in the forward scan can be referred to as E_{f1}, where *f* indicates it is derived from the forward scan and *1* refers to the 1 μA/cm^2. In CPP tests, where the reverse scan intersects the forward scan, repassivation is considered complete (i.e., the passive film has been repaired). The potential at the intersection is called the repassivation potential (E_{rp}) or, more specifically, the pit repassivation potential for a boldly exposed specimen or the crevice repassivation potential for a creviced specimen (E_{rcrev}). These repassivation potentials are sometimes referred to as cross-over potentials. Other criteria have also been used to define the critical potential for initiation of localized corrosion. Two current density thresholds in the reverse scan, 10 μA/cm^2 and 1 μA/cm^2, have been used to define crevice repassivation potentials (Kehler et al. 1999 [DIRS 162230]; Scully et al. 1999 [DIRS 110246], Section 1.3; Kehler et al. 2001 [DIRS 162231]). These two potentials are referred to as E_{r10} and E_{r1}, respectively, where *r* denotes these potentials are derived from the reverse scan. As discussed in the following section, the repassivation potential, E_{rcrev} (or cross-over potential), of crevice samples will be used for localized corrosion initiation analysis in this model report.

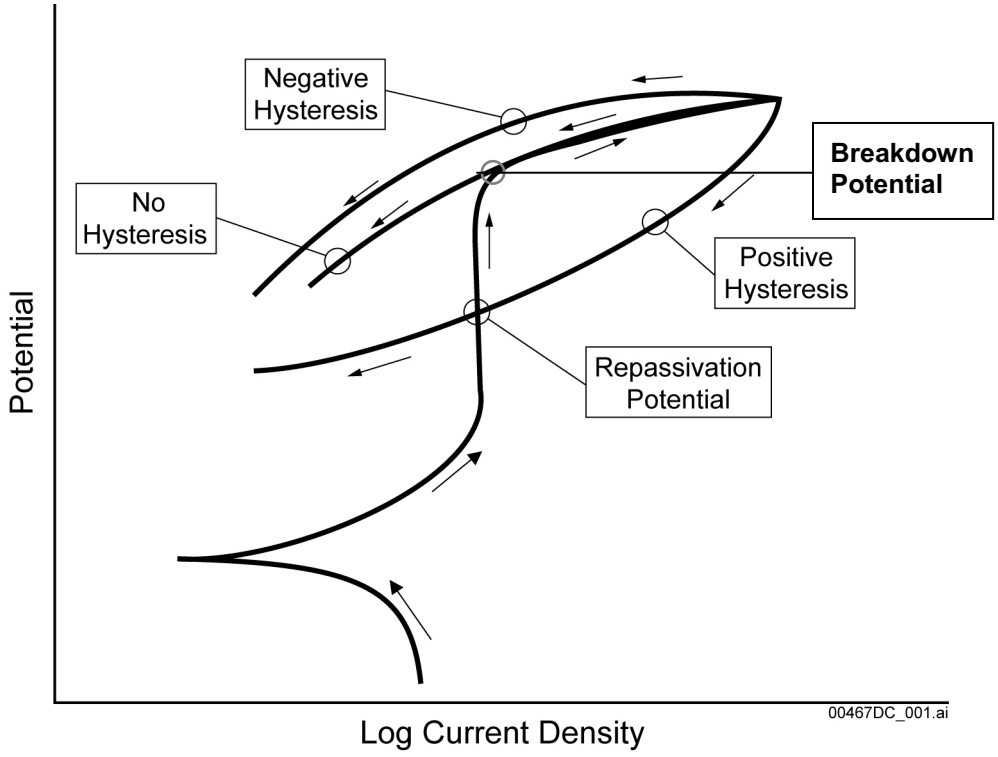

NOTE: For illustration purposes only.

Figure 6-29. Schematic Potentiodynamic Polarization Curve Showing Likely Behaviors of the Curves during Potentiodynamic Scanning of an Alloy with High Resistance to Localized Corrosion

The "true" value of $E_{critical}$ of a metal or alloy for a given set of conditions (including sample configuration, metallurgical condition, and exposure condition) would be the lowest potential at which the corrosion current (except for initial transients) does not decay with time and is

significantly higher than the passive current density, when held potentiostatically. Therefore, one approach to defining $E_{critical}$ is to conduct a series of PSP tests at predetermined potentials near the critical potentials initially measured by shorter-term CPP tests. However, CPP tests are widely used to obtain the critical potential (Jain et al. 2003 [DIRS 164087]; Dunn and Brossia 2002 [DIRS 162213]; Brossia et al. 2001 [DIRS 159836], Section 3.2.2) due to the much shorter test times required than for a series of PSP tests.

In using the CPP technique to identify critical parameters for the initiation of localized corrosion, the potential–current curves are examined to look for values of the potential where there is a significant, often abrupt, change in current. The advantage of this approach is that the current change can be related to physical and/or chemical events occurring on the metal surface over the course of the polarization cycle. Because the potential is scanned initially in the oxidizing or anodic direction, and then in the reducing or cathodic direction, hysteresis of the curve is indicative of changes that have occurred on the metal surface during polarization, and this hysteresis is related to localized corrosion susceptibility (Jones 1992 [DIRS 169906], Chapter 7). Figure 6-29 presents a schematic of CPP curves showing different polarization behaviors for an alloy with a high resistance to localized corrosion.

To produce CPP curves, the electrochemical potential is continuously scanned from slightly below the open-circuit or corrosion potential following a period of exposure of the metal specimen to the environment. If the metal is passive (as in the case of Alloy 22), the anodic current tends to have a low and nearly constant value for a wide range of potential; but eventually a potential is reached where there is a sharp increase in current. This change may be the beginning of oxygen evolution from water (if the applied potential is sufficient to electrolyze water). If this potential corresponds to oxygen evolution alone, then passive film breakdown or localized corrosion would not initiate. On the other hand, this change in current may indicate the breakdown of the passive film, which could result from a number of electrochemical reactions. After the potential scan is reversed, in cases where film breakdown due to localized corrosion has occurred, the metal surface is altered from its initial state (the passive film has broken down in some places), and the current shows, on reverse scan, a "positive" hysteresis. That is, compared to the forward scan, the current at a given potential is higher on the reverse scan. However, eventually the reverse-scan curve crosses over the curve generated during the forward scan. Where the reverse scan intersects the forward scan, repassivation is considered complete (the passive film has been repaired). The potential at the intersection is called the repassivation potential in this report (e.g., the pit repassivation potential (E_{rp}) for a boldly exposed sample or the crevice repassivation potential (E_{rcrev}) for a creviced sample geometry). As Figure 6-29 shows, in some cases there is no hysteresis or only slightly positive or slightly negative hysteresis, meaning the reactions are reversible, and the current retraces the values from the forward scan, often crossing the forward scan more than once at potentials above the passive region. In some cases, a slightly positive hysteresis is observed with no traces of localized corrosion on the specimen surface and in other cases, crevice corrosion may be observed on a specimen that produced no hysteresis.

Rebak (2005 [DIRS 174186]) identified two types of crevice attack that may occur during cyclic polarization. Type I crevice attack produces shiny crystalline area(s) rendering crystal planes visible under an optical microscope. When Type I attack is observed, the CPP data usually have a positive hysteresis loop. Type II crevice attack on Alloy 22 is generally observed when

potentials above transpassivity are applied to Alloy 22 specimens exposed to a relatively nonaggressive solution. For Type II attack on Alloy 22, no hysteresis loop is observed in the CPP curve. In general, Type II crevice attack on an Alloy 22 specimen is indicated by a spotty dull gray appearance. Rebak (2005 [DIRS 174186]) observed that Type II crevice attack on Alloy 22 produces shallow etched pits of only 5 μm or less in diameter and Type I crevice attack could produce relatively deep pits, which may appear as if they are arising from intergranular corrosion.

The current on the reverse scan usually passes through zero, as it does at E_{corr} during the anodic scan. Almost always, this new apparent corrosion potential is much more positive than the initial corrosion potential. If oxygen evolution has occurred, the solution has higher oxygen content, which would make the new corrosion potential more noble. If some additional oxidation of the alloy has occurred, this would also make the corrosion potential more noble on the reverse scan. If only transpassive dissolution has occurred, the reverse scan does not cross the forward scan; it traces down the forward scan. In the transpassive region, the entire metal surface has been depassivated (i.e., the passive film is absent). In these cases, the passive film has broken down, but not only in localized areas, so active general corrosion occurs. As the potential is scanned further in the reverse direction, this base material becomes repassivated (i.e., a new passive film forms).

Many cyclic polarization curves obtained in concentrated solutions at elevated temperatures do not exhibit the same shapes as those observed in ideal curves, such as those illustrated in ASTM G 61-86 (1987 [DIRS 127897]) (i.e., Stainless Steel Type 304 and nickel-based Alloy C-276 in 3.5% NaCl at room temperature). In some of the solutions, polarization curves of Alloy 22 did not show a well-defined passive region. These observations may indicate that the alloy is undergoing general corrosion, not localized corrosion.

Another complicating factor observed in many of the polarization curves was the appearance of one or more peaks in the passive region of the forward scan. These are due to changes in oxidation state of one or more of the metallic components in the passive film, and in some cases they indicate changes in the morphology and structure of the film, with possible implications on localized corrosion susceptibility. Usually, peaks were not observed during the reverse scan. For some test conditions in which no peak was present in the forward scan, peaks were observed in the reverse scan.

As mentioned above, researchers define the repassivation potential from CPP tests in different ways. Unlike potentials based on a certain current density such as E_{r10} and E_{r1} (Kehler et al. 1999 [DIRS 162230]; Scully et al. 1999 [DIRS 110246], Section 5.0; Kehler et al. 2001 [DIRS 162231]), the repassivation potential can be defined as the potential at which the reverse scan intersects the passive region of the forward scan (or the potential at which the forward current density equals reverse current density). The potential at the intersection is called the crevice repassivation potential (E_{rcrev}) or cross-over potential (Rebak 2005 [DIRS 174186]). As mentioned above, this potential is used for crevice repassivation potential model development in this report. A critical potential is not measured for the conditions where there is no positive hysteresis, because no localized corrosion has occurred. However, for conditions where the passive region in the forward scan is not clearly defined, the reverse scan never intersects the forward scan, or the reverse scan crosses the forward scan more than once, the repassivation

potential can be subject to the judgment of an individual investigator. This, in turn, can lead to inconsistent selection of the repassivation potential value. However, this approach has been shown to produce overly conservative repassivation potential values for Stainless Steel Type 304 materials in chloride solutions (Akashi et al. 1998 [DIRS 163903]).

Reportedly, the use of the Tsujikawa-Hisamatsu electrochemical (THE) technique (Akashi et al. 1998 [DIRS 163903]) and its variation, the potential-step technique (Jain et al. 2003 [DIRS 164087]), results in more reasonable values for the crevice repassivation potential than the CPP technique. Gruss et al. (1998 [DIRS 100893]) used the potential-step technique to obtain the crevice repassivation potential of Alloy 22. A comparison of the repassivation potential of Alloy 22 obtained using different testing methods reveals that, when an appropriate criterion was employed in selecting the critical potential value, the repassivation potential obtained with the CPP method was similar to that obtained using the more time-consuming PSP method, the THE method, or other similar methods (Jain et al. 2003 [DIRS 164087]).

In many instances, the reported crevice corrosion initiation potentials are associated with transpassive dissolution and not with actual crevice corrosion initiation. According to previous researchers (Kehler et al. 2001 [DIRS 162231]), the crevice repassivation potential E_{r1} (i.e., potential corresponding to a current of 1 $\mu A/cm^2$ in the reverse scan) can be associated with the deactivation of crevice corrosion resulting from net cathodic electrochemical reaction(s) in the crevice, and not necessarily associated with the crevice repassivation. The crevice repassivation potential E_{r10} obtained at slow scan rate has been reported to be more representative of crevice repassivation by previous researchers (Kehler et al. 1999 [DIRS 162230]).

In most CPP scans of highly corrosion-resistant alloys, the passive current is on the order of 1 to 10 $\mu A/cm^2$. The passive current density on the reverse scan is usually greater than in the initial (or forward) scan. This is because the newly formed (during the reverse scan) oxides over the crevice site are thin, defective, and can support charge transmission at higher rates than the typically thicker and less-defective oxides present during the forward scan. Moreover, the solution inside the crevice is acidified from hydrolysis of cations released into the crevice solution during the forward scan (Kehler et al. 1999 [DIRS 162230]; Kehler et al. 2001 [DIRS 162231]).

In summary, after review of the different approaches to obtaining the critical potential (E_{crit}) for localized corrosion initiation, the crevice repassivation potential (E_{rcrev}) based on the potential at which the reverse scan of a CPP curve crosses the forward scan using creviced samples was chosen. As is clear from the schematic in Figure 6-29, use of the crevice repassivation potential (E_{rcrev}) for the critical potential is conservative relative to the use of the breakdown potential.

6.4.4.2 Cyclic Potentiodynamic Polarization Data Analysis for Crevice Repassivation Potential

A series of CPP tests was performed for Alloy 22 samples over a wide range of exposure environments. Included in the tests were a variety of electrolyte solution chemistries, exposure temperatures, sample geometries and configurations (i.e., multiple crevice assembly (MCA), prism crevice assembly (PCA), rod, and disc), and metallurgical conditions (i.e., mill-annealed, as-welded, and as-welded plus thermally aged). As discussed in Section 6.4.6.1, data from as-

welded plus thermally aged specimens is not relevant for predicting repository performance, as the aging treatment (700°C for 173 hours) is not representative.

The CPP tests included simple salt solutions such as NaCl and $CaCl_2$, as well as mixed $CaCl_2$ and $Ca(NO_3)_2$ solutions and mixed NaCl and KNO_3 solutions. A wide range of concentrations up to near saturation was used. Descriptions of the electrochemical corrosion test procedures used to generate data for this report are provided in Appendix I. The CPP measurements were based on ASTM G 5-94 1994 [DIRS 117479]). Necessary deviations from the standard have been noted in the scientific notebooks corresponding to the DTNs used. Analyses of the CPP test data were performed to obtain repassivation potentials. Only data obtained at exposure temperatures of 120°C or less were used, as seepage is not expected at exposure temperatures higher than 120°C.

The localized corrosion model developed in this report is intended for use in evaluation of localized corrosion initiation due to seepage contact. For intact or moderately degraded drifts, there is no seepage contacting the waste package surface if the drift wall exposure temperature is above the boiling point of water in the drift (BSC 2004 [DIRS 169131], Sections 6.5.2 and 8.1). The threshold temperature to define boiling is 100°C at the drift wall (BSC 2004 [DIRS 169131], Section 6.5.2). The waste package surface temperature is 120°C or below when the drift wall exposure temperature is 100°C or below (e.g., SNL 2007 [DIRS 181383], Figures 6.3-67 and 6.3-69).

As discussed in Section 6.3, contact points between the waste package and structural components in the drift as well as with mineral deposits formed by evaporative concentration of solutions contacting the waste package could form crevices on the waste package surface. Therefore, only the crevice (MCA or PCA) sample data were considered for the repassivation potential model analysis.

Also, data which did not show the occurrence of localized corrosion (i.e., any "repassivation potential" reported would not represent actual repassivation of a sample undergoing localized corrosion) were not included in the model development. This approach is conservative since environments in which localized corrosion was not observed (even under polarization) will not contribute to the model results.

Table 6-11 summarizes the sources for the crevice repassivation potential (E_{rcrev}) data used to develop the crevice repassivation potential model. Appendix IX contains a detailed listing of the crevice repassivation data used to develop the new crevice repassivation potential model. Each DTN referenced in Appendix IX contains listings of measured crevice repassivation potentials as well as post-test observations of the occurrence or absence of crevice corrosion or pitting corrosion.

Table 6-11. Summary of All Input Data for Modeling the Crevice Repassivation Potential for the Waste Package Outer Barrier

Data Name	Data Source	DTN
Crevice Repassivation Potentials for Alloy 22	Waste Package Materials Testing	LL040902712251.119 [DIRS 173720], file: *Reduced Data Ahmet Yilmaz WBL 11Feb05.xls* LL050302312251.129 [DIRS 173921], file: *Mockup Developed RBR 21May05.xls* LL060603812251.164 [DIRS 178269], file: *Rep Pot N06022 vs Temp NaCl + KNO3 60-100C RBR 07Aug06.xls* LL060700312251.166 [DIRS 179385], file: *Rep Pot N06022 vs Temp 5M CaCl2 RBR 19Dec06.xls* LL060801812251.168 [DIRS 179386], file: *Rep Pot N06022 High Temp High NO3 RBR.xls* LL060803712251.170 [DIRS 179387], file: *Rep Pot N06022 vs Temp NaCl RBR 07Oct06.xls*

NOTE: See Appendix IX for a detailed list of these data.

Only crevice repassivation potential data measured at exposure temperatures of 120°C or less and for which crevice corrosion or pitting corrosion was observed were used to develop the crevice repassivation potential model. Crevice repassivation potential data from specimens that had undergone high-temperature aging treatments (e.g., 700°C for 173 hours) do not represent a repository-relevant material condition and were not used for model development. The crevice repassivation potentials for two specimens, DEA3130 (from DTN: LL060803712251.170 [DIRS 179387], file: *Rep Pot N06022 vs Temp NaCl RBR 07Oct06.xls*) and KE0416 (from DTN: LL060603812251.164 [DIRS 178269], file: *Rep Pot N06022 vs Temp NaCl + KNO3 60-100C RBR 07Aug06.xls*) will be used for model validation.

A number of measured crevice repassivation potentials were very high (greater than 550 mV versus SSC) and were not used in model development. These data are summarized in Table 6-12. Cyclic polarization curves for these samples typically showed either very little hysteresis or negative hysteresis followed by a crossover (crevice repassivation potential) at a very high value (e.g., Figure 6-30). Not using these high crevice repassivation potential values is conservative in that the mean crevice repassivation potential predicted by a model developed using these data would be higher than the mean crevice repassivation potential predicted by a model developed without the use of these data. However, use of these high crevice repassivation potential values would result in a larger variance in predicted values, i.e., the possibility of prediction of lower crevice repassivation potentials at the extremes of the uncertainty band. Nonetheless, the crevice repassivation potential measurements that are considered for exclusion from model development are not representative of the crevice repassivation potentials for Alloy 22 in the environments considered and, therefore, should not be used for model development.

Table 6-12. Summary of Crevice Repassivation Potential Data Not Used for Modeling (very high values)

DTN	Specimen ID	Specimen Type	Material Condition	Electrolyte	Type of LC	T °C	E_{rcrev} mV versus SSC
LL050302312251.129 [DIRS 173921], file: *Mockup Developed RBR 21May05.xls*	AY001	PCA	ASW - Mockup	6 *m* NaCl + 0.3 *m* KNO_3	CC	80	714
LL050302312251.129 [DIRS 173921], file: *Mockup Developed RBR 21May05.xls*	AY002	PCA	ASW - Mockup	6 *m* NaCl + 0.3 *m* KNO_3	CC	80	682
LL060803712251.170 [DIRS 179387], file: *Rep Pot N06022 vs Temp NaCl RBR 07Oct06.xls*	KE0622	PCA	ASW	0.0005 *M* NaCl	CC	60	867
LL060801812251.168 [DIRS 179386], file: *Rep Pot N06022 High Temp High NO3 RBR.xls*	KE0592	PCA	ASW	4 *m* KCl + 4 *m* NaCl + 0.4 *m* KNO_3+ 0.4 *m* $NaNO_3$	CC	90	570
LL060700312251.166 [DIRS 179385], file: *Rep Pot N06022 vs Temp 5M CaCl2 RBR 19Dec06.xls*	DEA3230	MCA	MA	5 *M* $CaCl_2$	CC-II	45	568
LL060700312251.166 [DIRS 179385], file: *Rep Pot N06022 vs Temp 5M CaCl2 RBR 19Dec06.xls*	JE0115	MCA	ASW	5 *M* $CaCl_2$	CC-II	45	570

NOTE: ASW = as-welded; MA = mill-annealed; MCA = multiple crevice assembly; PCA = prism crevice assembly; CC = crevice corrosion; CC-II = crevice corrosion type II; SSC = saturated silver chloride electrode; LC = localized corrosion.

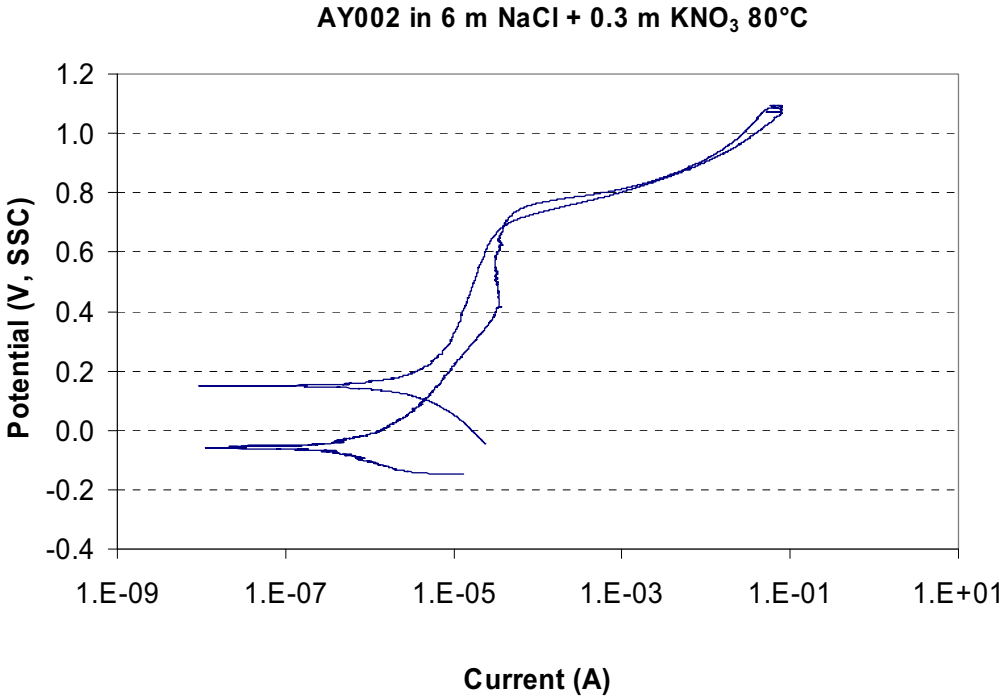

Source: DTN: LL050302312251.129 [DIRS 173921], file: *CPP AY002.xls*.

Output DTN: MO0703PAGENCOR.001, file: *CPP AY002.xls*.

Figure 6-30. Cyclic Polarization Curve for Specimen AY002 Obtained in 6 *m* NaCl + 0.3 *m* KNO_3 at 80°C Showing Very Little Hysteresis Followed by a Crossover (crevice repassivation potential) at a Very High Value (not used for model development)

In reference to the crevice repassivation potentials for specimens AY001 and AY002 (714 and 682 mV versus SSC, respectively), crevice repassivation potentials for specimens JE3313, JE3314, JE3217, and JE3228 in the same 6 *m* NaCl + 0.3 *m* KNO_3 solution at 80°C average about −103 mV versus SSC with a standard deviation of about 9 mV. Clearly the repassivation potentials for specimens AY001 and AY002 are significantly higher than similar crevice repassivation potential measurements under the same exposure conditions. Although specimens AY001 and AY002 are from a waste package mockup study, it is not expected that this is the source of their high crevice repassivation potentials, because other specimens from the mockup study do not show this behavior (i.e., specimens AY005, AY006, AY007, AY008, AY009, and AY010 in Appendix IX). On these bases, the crevice repassivation potential values of specimens AY001 and AY002 are not used for development of the crevice repassivation potential model.

In reference to specimen KE0622 exposed to 0.0005 *M* NaCl at 60°C with a crevice repassivation potential of 867 mV versus SSC, a second specimen KE0614 was also exposed to identical conditions and had a much lower crevice repassivation potential of 339 mV versus SSC. Furthermore, in DTN: LL060803712251.170 [DIRS 179387], file: *Rep Pot N06022 vs Temp NaCl RBR 07Oct06.xls*, a crevice repassivation potential of 312 mV versus SSC for specimen KE0601 was obtained in 0.0005 *M* NaCl at 60°C using a modified THE technique (see below). As discussed below, the THE method is believed to provide a more accurate measurement of the crevice repassivation potential than cyclic polarization. The very high

crevice repassivation potential reported for specimen KE0622 may be due to transpassive dissolution or oxygen evolution and not repassivation. If this is true, the crevice repassivation potential reported for KE0622 may not be relevant to a repassivation process, and it would be inappropriate to include this value in the crevice repassivation potential model. Any crevice corrosion observed for this sample is likely due to an initiation phenomenon that occurred under exposure conditions not relevant to the repository (e.g., a high potential was applied during the potentiodynamic experiment). On these bases, the crevice repassivation potential of specimen KE0622 is not used for development of the crevice repassivation potential model.

The THE method (DTN: LL040806212251.118 [DIRS 173722], file: *LL040806212251.118 ReadMe.pdf*) consists of ramping the potential at a scan rate of 0.167 mV/s until a peak current density is reached, typically on the order of 2 $\mu A/cm^2$. Once this peak current value is achieved, it is maintained for a set period (usually two hours) to allow crevice corrosion to propagate in a controlled manner. After the designated galvanostatic period elapses, the potential is stepped downward (cathodically) in 10-mV increments. Each potential is held for two hours before transitioning to the next potentiostatic step. The most anodic potential at which no increase in current is observed is taken as the crevice repassivation potential. Since this is a stepped potential method, the crevice repassivation potential obtained using this method is expected to be free from the influence of scan rates. Therefore, the crevice repassivation potential obtained using this technique should more accurately represent the crevice repassivation potential than does the crevice repassivation potential obtained using cyclic polarization technique. However, the repassivation potential data obtained using this technique was not used for model development because of the limited amount of data available.

In reference to specimen KE0592, a crevice repassivation potential of 570 mV versus SSC was measured in 4 *m* KCl + 4 *m* NaCl + 0.4 *m* KNO_3 + 0.4 *m* $NaNO_3$ at 90°C. Two other specimens, KE0688B and KE0579, were also exposed to the same solution and temperature. Crevice repassivation potential values of –82 mV and –80 mV versus SSC were obtained for KE0688B and KE0579, respectively. Clearly, the crevice repassivation potential value for specimen KE0592 is much higher than those of the specimens KE0688B and KE0579. Because the KE0592 sample had a potential well outside the replicated range of the other samples, it was excluded from the data set used for developing the crevice repassivation model.

Specimens DEA3230 and JE0115, which have crevice repassivation potential values of 568 mV and 570 mV versus SSC, respectively, were tested in 5 *M* $CaCl_2$ at 45°C. These crevice repassivation potential values are much higher than the crevice repassivation potential of 24 mV versus SSC measured under the same exposure conditions for specimen JE0114. In addition, the high crevice repassivation potential values for specimens DEA3230 and JE0115 are not consistent with the trend with temperature observed for the crevice repassivation potentials measured in 5 *M* $CaCl_2$ (Figure 6-31). On this basis, the crevice repassivation potentials of specimens DEA3230 and JE0115 are not used for development of the crevice repassivation potential model.

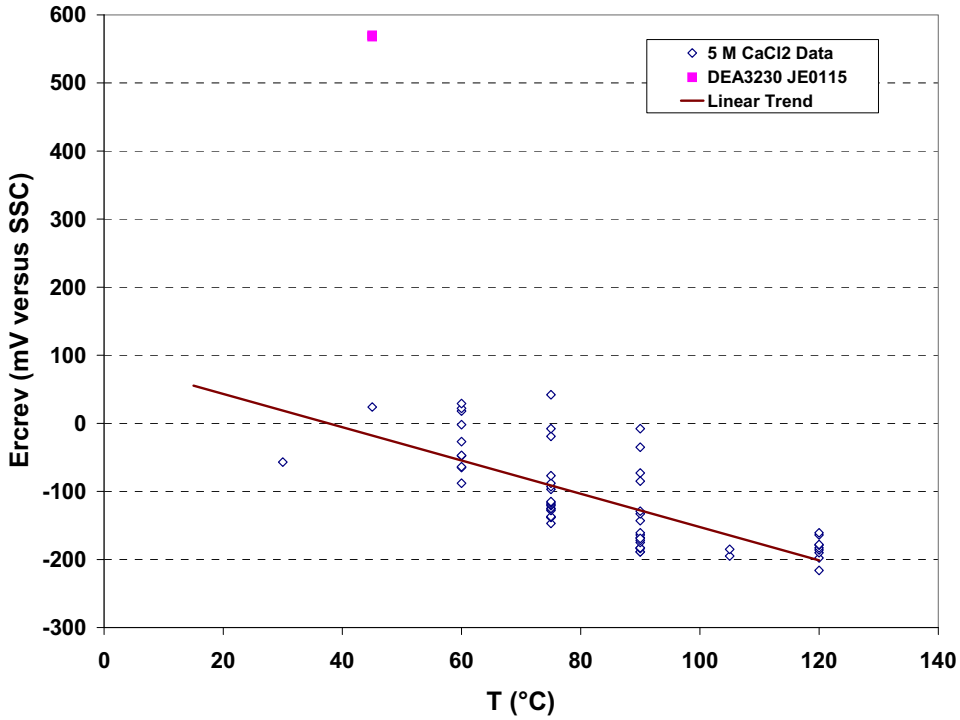

Source: DTN: LL060700312251.166 [DIRS 179385], file: *Rep Pot N06022 vs Temp 5M CaCl2 RBR 19Dec06.xls*.

Output DTN: MO0703PAGENCOR.001, file: *ErcrevRawData3.xls*.

Figure 6-31. Crevice Repassivation Potentials Measured in 5 *M* $CaCl_2$ at Various Temperatures

In addition to the data listed in Table 6-12, five other measured crevice repassivation potential values were considered outliers and, therefore, not used for developing the crevice repassivation model. These data are listed in Table 6-13.

Table 6-13. Summary of Crevice Repassivation Potential Data Not Used for Modeling (outliers)

DTN	Specimen ID	Specimen Type	Material Condition	Electrolyte	Type of LC	T °C	E_{rcrev} mV versus SSC
LL060803712251.170 [DIRS 179387] file: *Rep Pot N06022 vs Temp NaCl RBR 07Oct06.xls*	DEA3147	MCA	MA	1.25 *M* NaCl	LC	60	182
LL060803712251.170 [DIRS 179387] file: *Rep Pot N06022 vs Temp NaCl RBR 07Oct06.xls*	DEA3310	MCA	MA	4 *M* NaCl	CC	45	91
LL060603812251.164 [DIRS 178269] file: *Rep Pot N06022 vs Temp NaCl + KNO3 60-100C RBR 07Aug06.xls*	JE3213	MCA	ASW	1 *m* NaCl + 0.15 *m* KNO_3	CC-II	80	290

Table 6 13. Summary of Crevice Repassivation Potential Data Not Used for Modeling (outliers) (Continued)

DTN	Specimen ID	Specimen Type	Material Condition	Electrolyte	Type of LC	T °C	E_{rcrev} mV versus SSC
LL060603812251.164 [DIRS 178269] file: *Rep Pot N06022 vs Temp NaCl + KNO3 60-100C RBR 07Aug06.xls*	DEA3386	MCA	MA	3.5 *m* NaCl + 0.525 *m* KNO_3	CC	100	110
LL060603812251.164 [DIRS 178269] file: *Rep Pot N06022 vs Temp NaCl + KNO3 60-100C RBR 07Aug06.xls*	JE3211	MCA	ASW	3.5 *m* NaCl + 0.525 *m* KNO_3	CC	60	268

NOTE: ASW = as-welded; MA = mill-annealed; MCA = multiple crevice assembly; LC = pitting corrosion or other localized attack; CC = crevice corrosion; CC-II = crevice corrosion type II; SSC = saturated silver chloride electrode.

In reference to specimen DEA3147, exposed to 1.25 *M* NaCl at 60°C, a crevice repassivation potential value of 182 mV versus SSC was observed. Two other specimens DEA3267 and DEA3268 were also exposed to identical conditions and had much lower crevice repassivation potentials of 48 mV and 23 mV versus SSC, respectively. The observed crevice repassivation potential for specimen DEA3147 is about 150 mV higher than those for the specimens DEA3267 and DEA3268. It is concluded that the observed crevice repassivation potential for specimen DEA3147 is not representative of the crevice repassivation potential of Alloy 22 under these exposure conditions. Therefore, the crevice repassivation potential of specimen DEA3147 was not used for development of the crevice repassivation potential model.

In reference to the specimen DEA3310, exposed to 4 *M* NaCl at 45°C, the observed crevice repassivation potential value is not consistent with the temperature trend observed for crevice repassivation potentials of other specimens measured in 4 *M* NaCl (Figure 6-32). The measured crevice repassivation potential of DEA3310 is about 150 mV greater than that expected from the trend. The observed crevice repassivation potential for specimen DEA3310 is not representative of the crevice repassivation potential of Alloy 22 under these exposure conditions. Therefore, the crevice repassivation potential of specimen DEA3310 is not used for development of the crevice repassivation potential model.

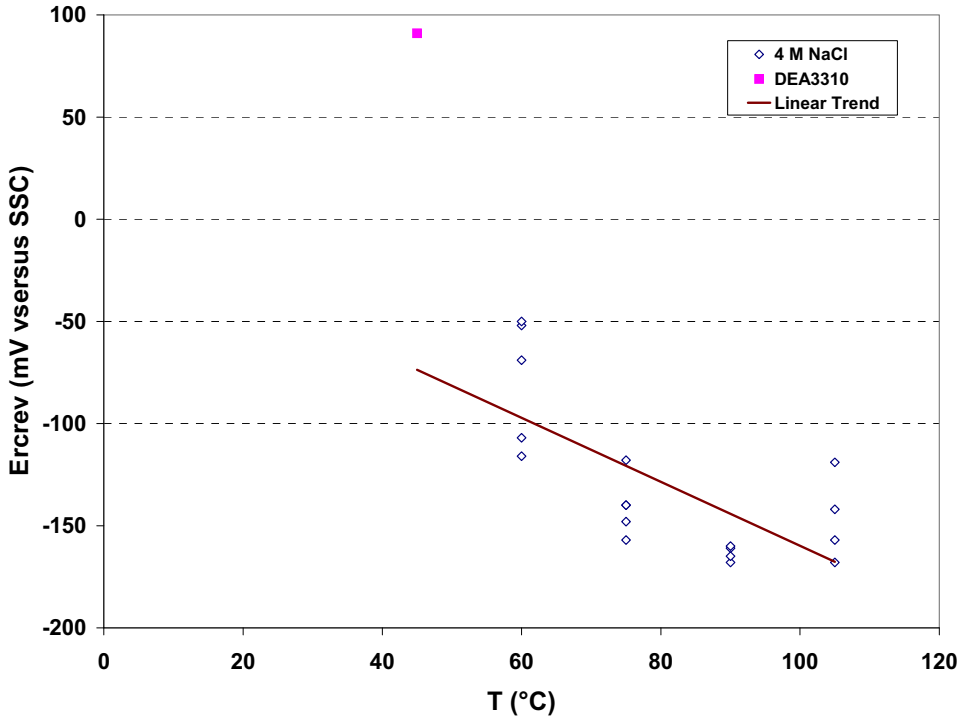

Source: DTN: LL060803712251.170 [DIRS 179387], file: *Rep Pot N06022 vs Temp NaCl RBR 07Oct06.xls*.

Output DTN: MO0703PAGENCOR.001, file: *ErcrevRawData3.xls*.

Figure 6-32. Crevice Repassivation Potentials Measured in 4 *M* NaCl at Various Temperatures

It may be that the higher crevice repassivation potential obtained for specimen DEA3310 is related to the existence of a critical temperature for crevice corrosion initiation in 4 *M* NaCl solution. If this were the case, it would be expected that decreasing the temperature would result in a large increase in measured crevice repassivation potential. The model conservatively predicts behavior at the lower temperatures by extrapolating behavior from the higher temperatures.

In reference to the specimen JE3213, exposed to 1 *m* NaCl + 0.15 *m* KNO_3 at 80°C, a crevice repassivation potential of 290 mV versus SSC was observed using CPP. The specimen KE0627, also exposed to an identical condition, had a much lower crevice repassivation potential of 68 mV versus SSC based on CPP measurement (Appendix IX). Based on CPP data, the repassivation potential value of specimen JE3213 is 222 mV higher than that of specimen KE0627. Another specimen, KE0624, was exposed in 1 *m* NaCl + 0.15 *m* KNO_3 at 80°C and its crevice repassivation potential was determined to be 19 mV versus SSC using the modified THE technique (DTN: LL060603812251.164 [DIRS 178269], file: *Rep Pot N06022 vs Temp NaCl + KNO3 60-100C RBR 07Aug06.xls*). As mentioned above, the THE method is expected to provide a more accurate measurement of the crevice repassivation potential than does cyclic polarization technique. A comparison of this value with two other values obtained under identical exposure condition using the CPP technique suggests that the crevice repassivation potential value of 290 mV for the specimen JE3213 is not representative of the crevice repassivation potential of Alloy 22 under these exposure conditions. Therefore, the crevice

repassivation potential value of the specimen JE3213 was excluded from the dataset used for development of the crevice repassivation potential model.

In reference to specimen DEA3386 exposed to 3.5 *m* NaCl + 0.525 *m* KNO_3 at 100°C, a crevice repassivation potential of 110 mV versus SSC was obtained. Four additional specimens (JE1773, DEA3385, DEA3390, and JE3242) were also exposed to an identical set of exposure conditions and a negative repassivation potential value was observed for each specimen, as shown in Table 6-14. The average repassivation potential value for these four specimens is about –68 mV versus SSC with a standard deviation of about 44 mV. Clearly, the crevice repassivation potential of 110 mV versus SSC is significantly greater than would be expected based on the measured crevice repassivation potentials of these four samples. Furthermore, as seen in DTN: LL060603812251.164 [DIRS 178269], file: *Rep Pot N06022 vs Temp NaCl + KNO3 60-100C RBR 07Aug06.xls*, a crevice repassivation potential of −55 mV versus SSC for specimen KE0181, obtained in 3.5 *m* NaCl + 0.525 *m* KNO_3 at 100°C using the modified THE technique, is expected to provide a more accurate measurement of the crevice repassivation potential than cyclic polarization. On this basis, the observed crevice repassivation potential value of 110 mV for specimen DEA3386 is not representative of that of Alloy 22 under these exposure conditions. Therefore, the crevice repassivation potential of specimen DEA3386 was not used for development of the crevice repassivation potential model.

Table 6-14. Summary of Crevice Repassivation Potential Data Used for Modeling in 3.5 *m* NaCl + 0.525 *m* KNO_3 at 100°C

DTN	Specimen ID	Specimen Type	Material Condition	Electrolyte	Type of LC	T °C	E_{rcrev} mV versus SSC
LL060603812251.164 [DIRS 178269], file: *Rep Pot N06022 vs Temp NaCl + KNO3 60-100C RBR 07Aug06.xls*	JE1773	MCA	ASW	3.5 *m* NaCl + 0.525 *m* KNO_3	CC	100	-85
LL060603812251.164 [DIRS 178269], file: *Rep Pot N06022 vs Temp NaCl + KNO3 60-100C RBR 07Aug06.xls*	DEA3385	MCA	MA	3.5 *m* NaCl + 0.525 *m* KNO_3	CC	100	-88
LL060603812251.164 [DIRS 178269], file: *Rep Pot N06022 vs Temp NaCl + KNO3 60-100C RBR 07Aug06.xls*	DEA3390	MCA	MA	3.5 *m* NaCl + 0.525 *m* KNO_3	CC	100	-3
LL060603812251.164 [DIRS 178269], file: *Rep Pot N06022 vs Temp NaCl + KNO3 60-100C RBR 07Aug06.xls*	JE3242	MCA	ASW	3.5 *m* NaCl + 0.525 *m* KNO_3	CC-II	100	-96

NOTE: ASW = as-welded, MA = mill-annealed, MCA = multiple crevice assembly, CC = crevice corrosion, CC-II = crevice corrosion type II, SSC = saturated silver chloride electrode, LC = localized corrosion.

In reference to specimen JE3211, exposed to 3.5 *m* NaCl + 0.525 *m* KNO_3 at 60°C, a crevice repassivation potential of 268 mV versus SSC was obtained. It is seen from Table 6-14 that the minimum crevice repassivation potential measured in 3.5 *m* NaCl + 0.525 *m* KNO_3 at 100°C by cyclic polarization is –96 mV versus SSC. For specimen KE0629, exposed in 3.5 *m* NaCl + 0.525 *m* KNO_3 at 80°C, a crevice repassivation potential value of 3 mV versus SSC was obtained using the modified THE technique (DTN: LL060603812251.164 [DIRS 178269], file: *Rep Pot N06022 vs Temp NaCl + KNO3 60-100C RBR 07Aug06.xls*). This indicates that a reasonable value of the crevice repassivation potential for a specimen such as JE3211, exposed to 3.5 *m* NaCl + 0.525 *m* KNO_3 at 60°C, would be about 100 mV versus SSC, i.e., an increase of about 100 mV for every 20°C decrease temperature. However, specimen JE3211 had a crevice repassivation potential of 268 mV versus SSC, which is much higher than expected. On this basis, the measured crevice repassivation potential value of 268 mV for specimen JE3211 was considered not representative of the crevice repassivation potential of Alloy 22 under these exposure conditions and, therefore, was not used for developing the crevice repassivation potential model.

6.4.4.3 Crevice Repassivation Potential Model for the Waste Package Outer Barrier

As described in Section 6.4.4.1, the WPOB is considered subject to localized corrosion when the corrosion potential (E_{corr}) exceeds or is equal to the crevice repassivation potential (E_{rcrev}), as shown in Equation 6-34:

$$E_{corr} \geq E_{rcrev} \qquad \text{(Eq. 6-34)}$$

Development of the crevice repassivation potential model for the WPOB was performed considering a set of multiple regression models as a function of the major exposure environment variables such as temperature, Pitzer pH (see Section 4.1.1.2), chloride-ion concentration and nitrate-ion concentration. The molal concentration unit (*m*, moles solute per kg water) was employed for the chloride- and nitrate-ion concentrations in the model development. This was done to ensure an internal consistency with the TSPA, which also employs the molal concentration unit for the dissolved species. An advantage of using the molal concentrations is that the base of the concentration unit (i.e., mass of solvent, in this case water) and, thus, the concentration value, does not change with temperature.

The crevice repassivation potential data for Alloy 22 used in development of the crevice repassivation potential model are listed in Appendix IX.

6.4.4.3.1 Alloy 22 Crevice Repassivation Potential Model Development

Among the functional forms that were considered, the empirical functional form shown in Equation 6-35 was found to adequately describe the relationship between the crevice repassivation potential of Alloy 22 and the test environment parameters:

$$E_{rcrev} = a_o + a_1 T + a_2 \ln\left[Cl^-\right] + a_3 \frac{\left[NO_3^-\right]}{\left[Cl^-\right]} + a_4 T \cdot \left[Cl^-\right] + \varepsilon_{rcrev} \qquad \text{(Eq. 6-35)}$$

where a_o, a_1, a_2, a_3, and a_4 are coefficients of the model parameters, T is the temperature (°C), $[Cl^-]$ is the molal chloride-ion concentration, $[NO_3^-]$ is the molal nitrate-ion concentration, and ε_{rcrev}, is the error term representing data variance not explained by the other terms in the model.

Dependence of the critical potential on a logarithmic form of chloride concentration and a linear form of temperature has also been used by other investigators to model the critical potential (Brossia et al. 2001 [DIRS 159836], Section 3.2.2; Frankel 2002 [DIRS 164140]; Kehler et al. 2001 [DIRS 162231]). The pH was neither included in the functional forms used by these investigators, nor in the functional form in Equation 6-35, because of a weak dependence of the crevice repassivation potential on bulk solution pH. The maximum pH value used in development of the crevice repassivation potential model was about 6.5 and no strong dependence of E_{rcrev} on pH was found. If the chloride-ion concentration of the exposure environment is greater than 20 *m*, the model is evaluated with a chloride-ion concentration of 20 *m*. Similarly, because the maximum nitrate ion-to-chloride ion concentration ratio in the data used for construction of the model was 1.0, this upper limit is imposed (i.e., if the exposure nitrate-to-chloride-ion concentration ratio exceeds 1.0, the value 1.0 is used in evaluating the model). Also, if only a negligible amount of chloride ions is present (i.e., when the chloride concentration is less than 0.0005 *m*, the lowest value for any data point used for model construction), the chloride-ion concentration is set to 0.0005 *m* to avoid evaluation of the natural logarithm of zero. Implementation rules for evaluating the crevice repassivation potential model and rationale for them are discussed further in Section 6.4.4.6.6.

Using the method of least squares (Draper and Smith 1981 [DIRS 118716], Chapter 2), the above functional form was fit to the crevice repassivation potential data in Appendix IX. The model fitting was performed using Mathcad version 13.0, and the Mathcad worksheet for the model fitting is given in the output DTN: MO0703PAGENCOR.001, file: *Ercrev_Ecorr3.xmcd*. The mean values of the coefficients of the model parameters and their ±1 standard deviation values from the fitting were determined to be: $a_0 = 183.686 \pm 21.587$, $a_1 = -2.919 \pm 0.265$, $a_2 = -46.109 \pm 3.675$, $a_3 = 580.849 \pm 29.974$, and $a_4 = 0.057 \pm 0.012$. The units of the coefficients are such that the units of E_{rcrev} are mV versus SSC. The variance of the model coefficients is calculated via a covariance matrix:

$$\Sigma = \begin{pmatrix} 4.660\text{E+002} & -5.394\text{E+000} & -1.278\text{E+001} & 1.207\text{E+002} & 4.865\text{E-002} \\ -5.394\text{E+000} & 7.005\text{E-002} & 1.268\text{E-001} & -1.756\text{E+000} & -1.141\text{E-003} \\ -1.278\text{E+001} & 1.268\text{E-001} & 1.350\text{E+001} & 1.955\text{E+000} & -2.827\text{E-002} \\ 1.207\text{E+002} & -1.756\text{E+000} & 1.955\text{E+000} & 8.984\text{E+002} & -3.456\text{E-002} \\ 4.865\text{E-002} & -1.141\text{E-003} & -2.827\text{E-002} & -3.456\text{E-002} & 1.395\text{E-004} \end{pmatrix} \quad \text{(Eq. 6-36)}$$

The error term, ε_{rcrev}, has a normal distribution with a mean of zero mV versus SSC and a standard deviation of 52.993 mV versus SSC.

Figure 6-33 shows model predictions versus experimental data for the crevice repassivation potential of the WPOB. The horizontal axis is the crevice repassivation potential predicted by the model while the vertical axis is either the measured repassivation potential for the measured data points represented by circles, or the ±2 standard deviation prediction intervals represented

by plus signs, or the mean model prediction represented by the solid line. As can be seen from the figure, one measured crevice repassivation potential lies substantially above the +2 standard deviation prediction interval; that is, the crevice repassivation potential model predicts a substantially less positive crevice repassivation potential for this specimen. The specimen is KE0572, from DTN: LL060801812251.168 [DIRS 179386], file: *Rep Pot N06022 High Temp High NO3 RBR.xls*, with a measured crevice repassivation potential of 446 mV versus SSC obtained in a 4 *m* KCl + 4 *m* NaCl + 2 *m* KNO_3 + 2 *m* $NaNO_3$ solution with 0.0001 *m* HCl added. The mean predicted crevice repassivation potential value from the crevice repassivation potential model is 108 mV versus SSC, and the +2 standard deviation prediction interval for this solution composition is 217 mV versus SSC. The crevice repassivation potential for specimen KE0572 is clearly an outlier and was removed from the data set used to model the crevice repassivation potential. Two other data points lie just outside of the +2 standard deviation prediction bound and are conservatively under-predicted (i.e., predicted crevice repassivation values are lower than these measured values). These two under-predicted data points are not removed from the data set and are used, along with the rest of the data set to develop the crevice repassivation potential model.

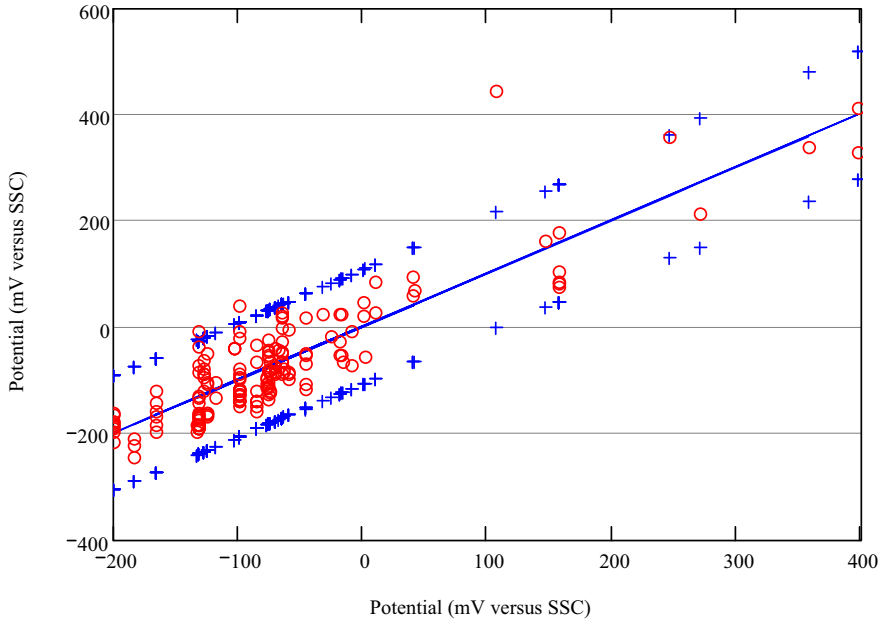

Sources: DTNs: LL040902712251.119 [DIRS 173720], file: *Reduced Data Ahmet Yilmaz WBL 11Feb05.xls*; LL050302312251.129 [DIRS 173921], file: *Mockup Developed RBR 21May05.xls*; LL060603812251.164 [DIRS 178269], file: *Rep Pot N06022 vs Temp NaCl + KNO3 60-100C RBR 07Aug06.xls*; LL060700312251.166 [DIRS 179385], file: *Rep Pot N06022 vs Temp 5M CaCl2 RBR 19Dec06.xls*; LL060801812251.168 [DIRS 179386], file: *Rep Pot N06022 High Temp High NO3 RBR.xls*; LL060803712251.170 [DIRS 179387], file: *Rep Pot N06022 vs Temp NaCl RBR 07Oct06.xls*.

Output DTN: MO0703PAGENCOR.001, file: *Ercrev_Ecorr3.xmcd*.

NOTE: The horizontal axis is the crevice repassivation potential predicted by the model while the vertical axis is either the measured repassivation potential for the measured data points represented by circles, or the ±2 standard deviation prediction intervals represented by plus signs, or the mean model prediction represented by the solid line.

Figure 6-33. Model Predictions and Experimental Data for the Crevice Repassivation Potential of the Waste Package Outer Barrier

The remaining crevice repassivation potential data, excluding the crevice repassivation potential measured for specimen KE0572, were refit to the functional form in Equation 6-35. The mean values of the coefficients of the model parameters and their ±1 standard deviation values from the fitting were determined to be: $a_0 = 190.242 \pm 18.373$, $a_1 = -3.008 \pm 0.225$, $a_2 = -46.800 \pm 3.126$, $a_3 = 535.625 \pm 26.140$, and $a_4 = 0.061 \pm 0.010$. The units of the coefficients are such that the units of E_{rcrev} are mV versus SSC. The variance of the model coefficients is calculated via a covariance matrix (Equation 6-37), and the entire variance is due to uncertainty. The model coefficients are sampled from a multivariate normal distribution with the above-mentioned mean values consistent with the covariance matrix given in Equation 6-37.

$$r\Sigma = \begin{pmatrix} 3.376\text{E+002} & -3.909\text{E+000} & -9.310\text{E+000} & 8.236\text{E+001} & 3.559\text{E-002} \\ -3.909\text{E+000} & 5.077\text{E-002} & 9.271\text{E-002} & -1.202\text{E+000} & -8.308\text{E-004} \\ -9.310\text{E+000} & 9.271\text{E-002} & 9.770\text{E+000} & 1.930\text{E+000} & -2.048\text{E-002} \\ 8.236\text{E+001} & -1.202\text{E+000} & 1.930\text{E+000} & 6.833\text{E+002} & -2.790\text{E-002} \\ 3.559\text{E-002} & -8.308\text{E-004} & -2.048\text{E-002} & -2.790\text{E-002} & 1.011\text{E-004} \end{pmatrix} \quad \text{(Eq. 6-37)}$$

The error term, ε_{rcrev}, represents data variance not explained by the fitting procedure and has a normal distribution with a mean of zero mV versus SSC and a standard deviation (referred to as s_{rcrev}) of 45.055 mV versus SSC. Variance in the error term, ε_{rcrev}, is attributed to uncertainty (output DTN: MO0703PAGENCOR.001, file: *LC_Initiation.pdf*).

The coefficient of determination, R^2, is 0.829. R^2 is the ratio of the measures of variation explained by the regression model to the total variation present in the output variable under consideration. Values of R^2 vary between 0 (no variation explained and a very poor regression model) to 1 (perfect explanation of the model variation by the regression model). With the measure of an R^2 value of 0.829, the regression model fits the experimental data well.

From the value of the temperature coefficient, $a_1 = -3.008 \pm 0.225$, the crevice repassivation potential has a strong dependence on temperature (i.e., it decreases by about 3 mV for each 1°C increase in temperature). A strong dependence of the crevice repassivation potential of Alloy 22 on temperature was also reported by others (Brossia et al. 2001 [DIRS 159836], Section 3.2.2; Kehler et al. 2001 [DIRS 162231]).

Figure 6-34 shows model predictions versus experimental data for the crevice repassivation potential of the WPOB. The horizontal axis is the crevice repassivation potential predicted by the model while the vertical axis is either the measured repassivation potential for the measured data points (circles) or the ±2 standard deviation prediction intervals represented by plus signs, or the mean model prediction represented by the solid line. As can be seen from the figure, all measured crevice repassivation data used to develop the crevice repassivation potential model lie within the ±2 standard deviation prediction intervals of the crevice repassivation potential model or are conservatively under-predicted by the crevice repassivation potential model. Where the crevice repassivation potential model underestimates the measured crevice repassivation potentials, the model is conservative.

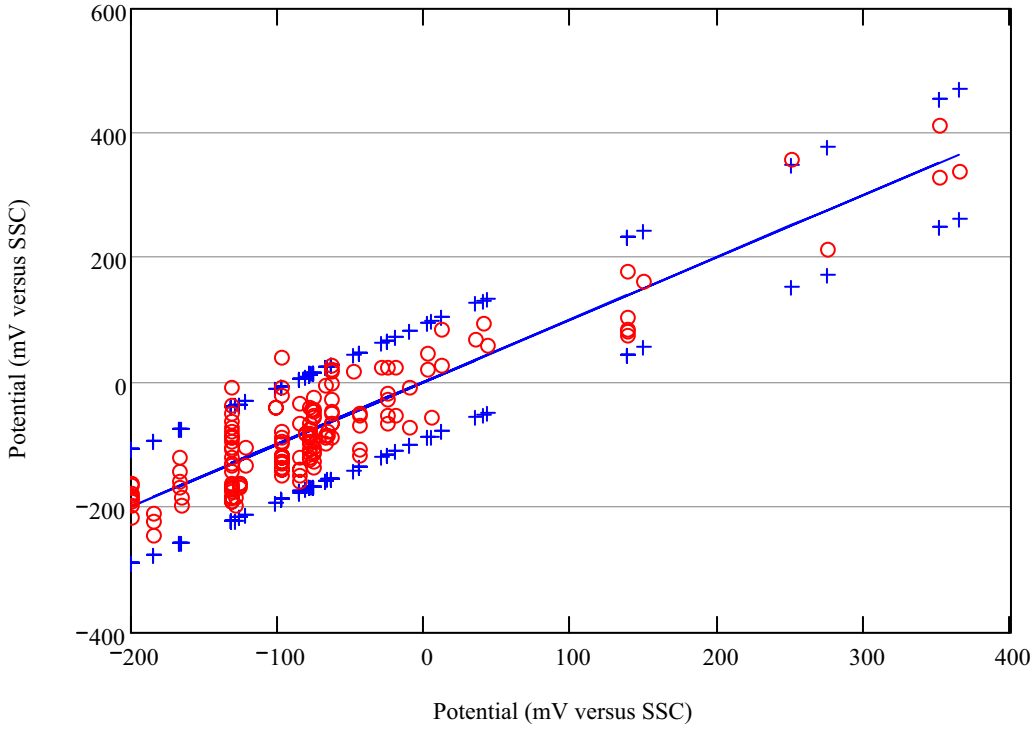

Sources: DTNs: LL040902712251.119 [DIRS 173720], file: *Reduced Data Ahmet Yilmaz WBL 11Feb05.xls*; LL050302312251.129 [DIRS 173921], file: *Mockup Developed RBR 21May05.xls;* LL060603812251.164 [DIRS 178269], file: *Rep Pot N06022 vs Temp NaCl + KNO3 60-100C RBR 07Aug06.xls*; LL060700312251.166 [DIRS 179385], file: *Rep Pot N06022 vs Temp 5M CaCl2 RBR 19Dec06.xls*; LL060801812251.168 [DIRS 179386], file: *Rep Pot N06022 High Temp High NO3 RBR.xls*; LL060803712251.170 [DIRS 179387], file: *Rep Pot N06022 vs Temp NaCl RBR 07Oct06.xls*.

Output DTN: MO0703PAGENCOR.001, file: *Ercrev_Ecorr3.xmcd*.

NOTE: The horizontal axis is the crevice repassivation potential predicted by the model while the vertical axis is either the measured repassivation potential for the measured data points represented by circles, or the ±2 standard deviation prediction intervals represented by plus signs, or the mean model prediction represented by the solid line.

Figure 6-34. Model Predictions and Experimental Data for the Crevice Repassivation Potential of the Waste Package Outer Barrier

The prediction intervals for the *unconstrained* crevice repassivation potential model are calculated by adding to the median estimate (i.e., the expected value of E_{rcrev} obtained by using the mean values of the model coefficients from Equation 6-35) an adjustment based on the standard deviation of the error term (s_{rcrev}), the covariance matrix of the model coefficients (Equation 6-37), and the values of the exposure parameters for the data point being evaluated. The adjustment factor is written in matrix form as Equation 6-38:

$$\pm z\sqrt{\left[1 \quad T \quad \ln[Cl^-] \quad \frac{[NO_3^-]}{[Cl^-]} \quad T\cdot\ln[Cl^-]\right] r\Sigma \left[1 \quad T \quad \ln[Cl^-] \quad \frac{[NO_3^-]}{[Cl^-]} \quad T\cdot\ln[Cl^-]\right]^T + s_{rcrev}^2} \qquad \text{(Eq. 6-38)}$$

where z would be the number of standard deviations at which the adjustment factor is to be evaluated.

The values of the crevice repassivation potential are *constrained* to be within the range defined by the ±2 standard deviation (i.e., $z = \pm 2$) prediction interval of the *unconstrained* crevice repassivation potential model. That is, the ±2 standard deviation prediction intervals of the *unconstrained* crevice repassivation potential relationship (Equation 6-35 adjusted by Equation 6-38) are used as bounds on the value that the crevice repassivation potential may have. That is, if the calculated *unconstrained* crevice repassivation potential exceeds the +2 standard deviation prediction bound of the *unconstrained* crevice repassivation potential model, the crevice repassivation potential value of the +2 standard deviation prediction bound of the *unconstrained* crevice repassivation potential model should be used as the value of the crevice repassivation potential for the given exposure conditions. Similarly, if the calculated *unconstrained* crevice repassivation potential does not exceed the −2 standard deviation prediction bound of the *unconstrained* crevice repassivation potential model, the crevice repassivation potential value of the −2 standard deviation prediction bound of the *unconstrained* crevice repassivation potential model should be used as the value of the crevice repassivation potential for the given exposure conditions.

It is evident from Figure 6-34 that the crevice repassivation potential data has considerable scatter. Variations in the crevice repassivation potential data for a given test condition are mostly due to the uncertainties associated with the test procedures and crevice repassivation potential selection criteria, in addition to some randomness in the crevice corrosion initiation process. Therefore, the entire variance of the model is due to uncertainty. For the waste package degradation analysis, variability in the crevice repassivation potential among waste packages is represented by the temporally and spatially varying waste package temperature and water chemistry contacting the waste package. ASTM G 61-86 (1987 [DIRS 127897]) states, "when the standard procedure for the CPP measurements is followed, an investigator's data should fall within the range of ±2 standard deviations of the mean because this includes 95% of all data provided random variations are the only source of error." While this criterion was specified for replicate CPP measurements obtained under the same exposure conditions, it is reasonable to apply this criterion to a model based on fitting these measurements to a regression surface. Therefore, it is reasonable to constrain the values of the crevice repassivation potential to be within the range defined by the ±2 standard deviation prediction interval of the *unconstrained* crevice repassivation potential model.

6.4.4.4 Long-Term Open-Circuit Corrosion Potential Data Analysis

Because the corrosion potential of Alloy 22 may change over time, it is important to know the most probable value of long-term corrosion potential (E_{corr}) for Alloy 22 under different environmental conditions to evaluate the localized corrosion susceptibility of the WPOB in the repository. As discussed above, localized corrosion will only occur when E_{corr} is equal to or greater than a critical potential (the crevice repassivation potential (E_{rcrev}) in the current model).

The specimens used to evaluate E_{corr} of Alloy 22 as a function of immersion time were machined from sheet and bar stock. No long-term corrosion potential data obtained above 120°C or for exposure times less than 250 days were used for analysis. Further discussion of the rationale for the 250-day criterion is provided in Section 6.4.4.5. The localized corrosion model developed in this report is intended for use in evaluation of localized corrosion initiation due to seepage contact. For intact or moderately degraded drifts, there is no seepage contacting the waste

package surface if the drift wall exposure temperature is above the boiling point of water in the drift (BSC 2004 [DIRS 169131], Sections 6.5.2 and 8.1). The threshold temperature to define boiling is 100°C at the drift wall (BSC 2004 [DIRS 169131], Section 6.5.2). The waste package surface temperature is 120°C or below when the drift wall exposure temperature is 100°C or below (e.g., SNL 2007 [DIRS 177405], Figures 6.3-67 and 6.3-69).

Only samples that did not show signs of localized corrosion initiation were used. The corrosion potential of samples that are undergoing localized corrosion can be much lower than samples not undergoing localized corrosion (He and Dunn 2006 [DIRS 176645]). Therefore, the use of corrosion potentials from samples undergoing localized corrosion would not be conservative for use in predicting localized corrosion initiation (i.e., evaluating whether the corrosion potential exceeds the critical potential for localized corrosion initiation).

Welded-plus-aged samples in DTN: LL060900512251.177 [DIRS 178271], file: *Summary Ecorr Cells 1-36 29Sep06.xls*, were not considered in this analysis because the aging treatment was more severe (700°C for 173 hours) than could reasonably be expected in the repository environment (Figure 6-2). Long-term corrosion potentials from solution-heat-treated specimens were not used because the solution-heat-treatment oxide film was left on the specimens (DTN: LL060900512251.177 [DIRS 178271], file: *Summary Ecorr Cells 1-36 29Sep06.xls*). These films will be removed from the waste package surface before emplacement in the repository (e.g., SNL 2007 [DIRS 179394], Section 4.1.2), making this specimen condition not relevant to the repository configuration. Some specimens were reported to have uneven general corrosion (DTN: LL060900512251.177 [DIRS 178271], file: *Summary Ecorr Cells 1-36 29Sep06.xls*). It is not expected that this uneven general corrosion had any significant impact on the long-term corrosion potentials obtained. The data and test details reported in DTN: LL060900512251.177 [DIRS 178271], file: *Summary Ecorr Cells 1-36 29Sep06.xls*, are summarized in Appendix VIII.

The samples are identified by a combination of letters and numbers. In earlier cells, these were either DUB or DEA, followed by three or four digits. The letter D stands for Alloy 22, the second letter stands for the type of sample, that is, U for U-bend specimen and E for electrochemical (or rod) specimen. The third letter could be either an A (signifying the sample is mill-annealed or not welded) or B (the sample contains weld material). In other cells, some rod specimens were designated starting with the letters JE (for John Estill) or KE (for Kenneth Evans) followed by four digits. One specimen tested in BSW solution (Cell 4) was a double U-bend specimen consisting of two strips of material and had a two-part designation (ARC22 U20A and ARC22 U20B), identifying both strips of material.

Many different electrolyte solutions were used in the tests (Appendix VIII provides the type of solutions tested). These included multi-ionic solutions and other simpler salt solutions. Solutions from the LTCTF tanks (i.e., SDW, SAW, and SCW), which were approximately 4.5 years old at the time the tests started, as well as multi-ionic solutions that were freshly prepared, were used for testing. For some solution compositions, more than one temperature was used for testing (Appendix VIII).

The volume of the electrolyte solution in each cell was two liters. The electrolyte solutions were naturally aerated; that is, a stream of air was circulated above the level of the solution. This

stream of air exited the vessel through a condenser to avoid evaporation of the electrolyte. The electrochemical potentials in Appendix VIII are reported in the SSC scale. At ambient temperature, the SSC scale with the reference electrode in a saturated KCl solution is 199 mV more positive than the standard hydrogen electrode (SHE) (Sawyer and Roberts 1974 [DIRS 162259], pp. 39 to 45, Table 2-4). The values of the corrosion potentials for each specimen (electrode) were acquired using a commercial data acquisition unit that had the input resistance set at 1×10^{10} ohm. Typically, the measurements were acquired every minute for the first week of testing and every hour after the first week. The data was logged into the internal memory of the data acquisition unit and simultaneously entered into a spreadsheet in an interfaced personal computer. Data backup was performed monthly.

The long-term corrosion potential behavior of some Alloy 22 samples in SDW, SAW, and SCW solutions from the LTCTF is shown in Figure 6-35. The data plotted in Figure 6-35 through Figure 6-37 was taken each day for the first week of exposure and then every week thereafter from the raw E_{corr} versus time data contained in DTNs: LL060901312251.181 [DIRS 178299] and LL060901412251.182 [DIRS 178300]. Step-function discontinuities shown in the graphs indicate periodic changes of reference electrodes. Figure 6-35 shows that, after an initial period of 300 to 400 days, the E_{corr} did not change substantially with time. This figure also shows that the results of the welded U-bend samples (samples DUB052 and DUB159) and (nonwelded) rod samples (samples DEA2850, DEA2851, and DEA2852) in aged SAW at 90°C show no significant differences in their long-term open-circuit corrosion potential behaviors. Figure 6-35 shows two sets of E_{corr} versus time curves for Alloy 22. In the acidic multi-ionic SAW solution the potentials tended to be in the +200 to +400 mV versus SSC range while in the alkaline multi-ionic solutions SDW and SCW, the potentials tended to be in the –100 to +100 mV versus SSC range. In the SAW solution, the potential was higher at 60°C and 90°C than at 25°C.

Figure 6-36 compares the evolution of long-term corrosion potential of freshly polished Alloy 22 rods in freshly prepared SAW at 90°C (Cell 9) with that of the welded U-bend and rod samples in aged SAW at 90°C (Cells 2 and 10, Figure 6-35) for the first 150 days of testing. Initially the Alloy 22 rods in the fresh SAW solution had corrosion potential on the order of about –150 mV versus SSC. Over approximately 50 days of testing, the corrosion potential increased rapidly to a more noble potential value of approximately 330 mV versus SSC. Figure 6-35 shows that, for the remainder of the testing time, the corrosion potential slowly reached a maximum value near 400 mV versus SSC. This high value of E_{corr} is probably due to the formation of a more-protective chromium-rich oxide film on the Alloy 22 electrodes. The test results show that, regardless of the initial condition of the metal surface or the age of the electrolyte solution, eventually Alloy 22 undergoes ennoblement in SAW. This ennoblement is probably promoted by both the pH value and the presence of nitrate in the solution (Estill et al. 2003 [DIRS 163849]). Such an ennoblement of Alloy 22 with time has also been reported elsewhere (Jayaweera et al. 2003 [DIRS 162225], Figures 9.12 and 9.13; Dunn et al. 2003 [DIRS 164138], Figures 8 and 9). According to Dunn et al. (2003 [DIRS 164138], Figures 8 and 9), the ennoblement was more significant in acidic solutions than alkaline solutions.

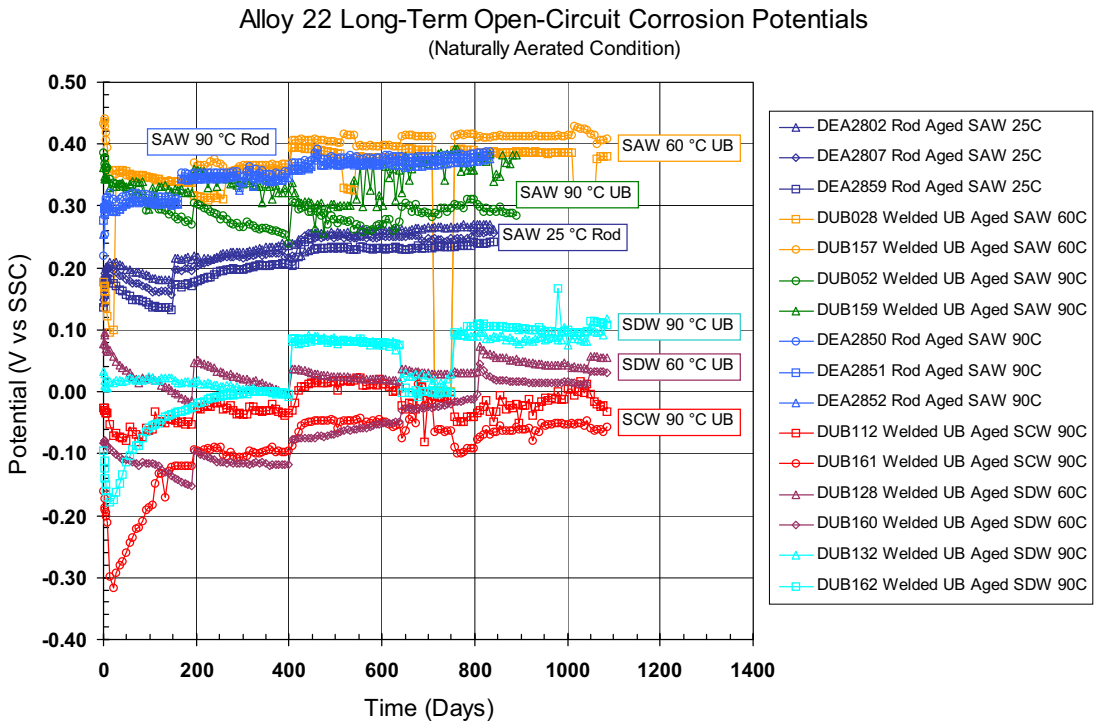

Source: DTN:LL060901312251.181 [DIRS 178299], cells 1, 2, 3, 5, 6, 7-2, and 10.

Output DTN: MO0612WPOUTERB.000, file: *LTEcorrVSTime_Graph.xls*.

Figure 6-35. Open-Circuit Corrosion Potential of Alloy 22 Samples as a Function of Time in Different Types of Long-Term Corrosion Test Facility Solutions

Figure 6-37 shows the E_{corr} of Alloy 22 in pure $CaCl_2$ solutions and in $CaCl_2$ + $Ca(NO_3)_2$ solutions as a function of testing time. A few observations can be made regarding the influence of nitrate ions on the long-term corrosion potential. In the pure $CaCl_2$ solution, the corrosion potential reached steady state at approximately –20 mV versus SSC in less than 100 days, and then the potential remained more or less stable for the next two years. For the pure chloride solution the corrosion potential was steady (i.e., had little noise or perturbations). In the solution in which the nitrate ion-to-chloride ion ratio was 1 (1 *M* $CaCl_2$ + 1 *M* $Ca(NO_3)_2$), the corrosion potential of Alloy 22 rose rapidly in the first 100 days of testing and then more slowly for the next 500 days, attaining an E_{corr} value of approximately +320 mV versus SSC. The value of the corrosion potential was practically free of noise. In the solution with a nitrate ion-to-chloride ion ratio of 0.1, the corrosion potential rose less rapidly than in the one-to-one ratio solution and at the end the corrosion potential attained a value of approximately +200 mV versus SSC (Figure 6-37). In general, the corrosion potential rose as time increased, but it had large fluctuations of almost 200 mV, and it was the least reproducible of the four systems represented. In the cell that contained the solution with a nitrate ion-to-chloride ion ratio of 0.01 (5 *M* $CaCl_2$ + 0.05 *M* $Ca(NO_3)_2$), the corrosion potential of Alloy 22 reached about +100 mV versus SSC after about two years.

Jayaweera et al. (2003 [DIRS 162225], Section 9.3.2) observed potential fluctuations during long-term (approximately 200 days) corrosion potential measurements in both aerated and deaerated saturated NaCl solutions at 80°C. Very small potential fluctuations were observed throughout the exposure time; however, larger potential fluctuations were observed after about four months of exposure. These current fluctuations were stated to have been caused by some type of surface reactivity, most likely pit initiation, as a limited amount of pitting was observed in these experiments. Variation of atmospheric conditions had no impact on the fluctuations, because these measurements were conducted in a closed system.

Dunn et al. (2003 [DIRS 164138], Figure 7) monitored the long-term open circuit potential of a creviced Alloy 22 specimen in an air-saturated 4 *M* NaCl solution at 95°C for about 750 days. They observed potential fluctuations similar to those shown in Figure 6-35 through Figure 6-37. The investigators periodically removed and disassembled the creviced specimen in order to evaluate whether localized corrosion had initiated. No evidence of localized corrosion initiation was found during the 750 days of exposure.

As discussed in Section 6.4.4.5, only long-term open circuit potential data for specimens which did not undergo crevice corrosion or pitting corrosion was used to develop the long-term corrosion potential model for this report. As shown in Figure 6-37 and in the experiment conducted by Dunn et al. (2003 [DIRS 164138], Figure 7), potential fluctuations can be observed in long-term corrosion potential measurements without localized corrosion initiation.

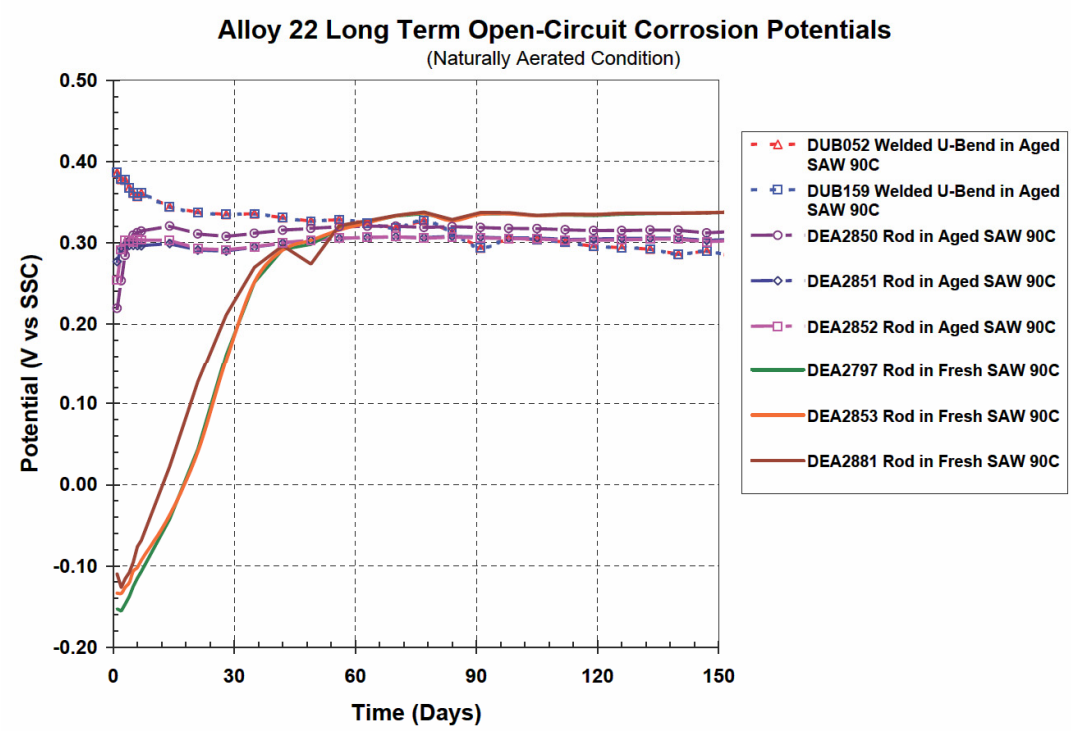

Source: DTN: LL060901312251.181 [DIRS 178299], cells 2, 9, and 10.

Output DTN: MO0612WPOUTERB.000, file: *LTEcorrVSTime_Graph.xls*.

Figure 6-36. Open-Circuit Corrosion Potential of Alloy 22 Samples as a Function of Time in Differing Conditions of Simulated Acidified Water Solutions

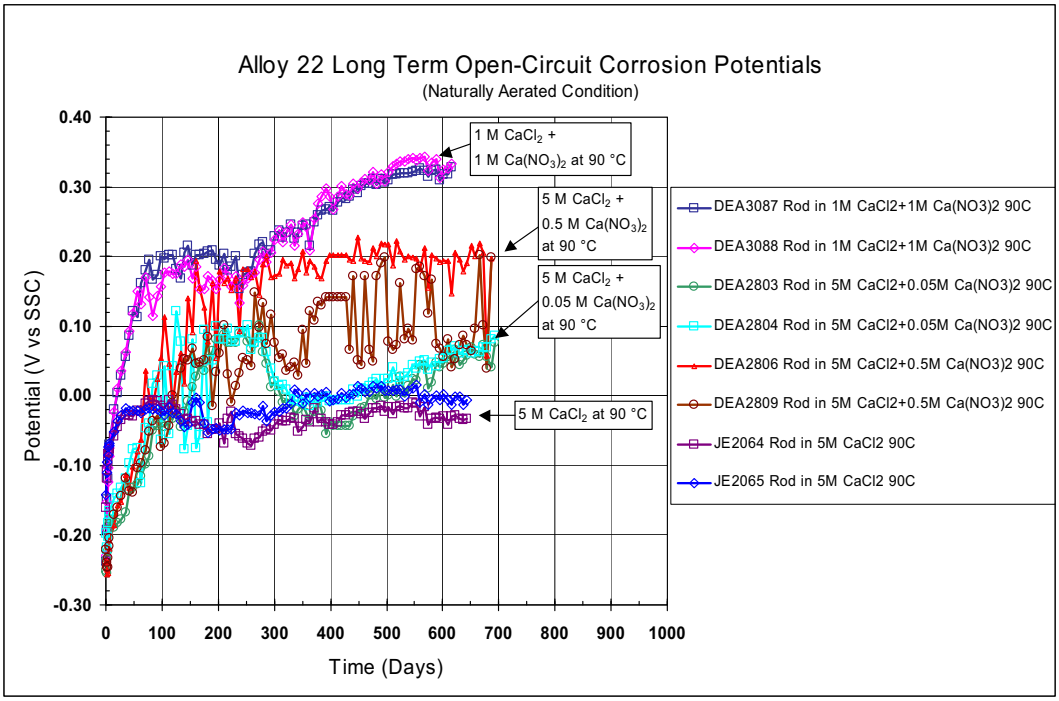

Source: DTN: LL060901412251.182 [DIRS 178300], cells 13, 14, 15, and 28.

Output DTN: MO0612WPOUTERB.000, file: *LTEcorrVSTime_Graph.xls*.

Figure 6-37. Open-Circuit Corrosion Potential of Alloy 22 Samples as a Function of Time in Differing Concentrations of $CaCl_2$ Solutions

The steady-state open-circuit potentials (or long-term corrosion potentials) of the Alloy 22 specimens from Appendix VIII (DTN: LL060900512251.177 [DIRS 178271], file: *Summary Ecorr Cells 1-36 29Sep06.xls*) used for the model and analysis are shown in Figure 6-38 and Figure 6-39 as a function of chloride-ion and nitrate-ion concentration, respectively. Figure 6-40 shows the long-term corrosion potentials versus the calculated Pitzer pH. As can be seen from Figures 6-38 through 6-40 and the long-term corrosion potential data listed in Appendix VIII, metallurgical condition (e.g., mill-annealed versus as-welded) does not have a strong effect on the long-term corrosion potential of Alloy 22. Figure 6-40 shows that the long-term corrosion potential is a function of pH, generally decreasing as the pH of the test solution increases. Although not shown in the figure, the corrosion potential of Alloy 22 would be expected to drop sharply for very low pH values because the passive film on the alloy would become unstable in such extreme acidic conditions and the alloy would become more active. Figure 6-38 and Figure 6-39 show that the long-term corrosion potentials are less strongly dependent on solution composition, although it is clear from consideration of Figures 6-38 through 6-40 that the corrosion potential is a simultaneous function of all of the various exposure variables. Likely, complex chemical processes such as the "salting-out effect" (i.e., dissolved oxygen content decreasing with increasing salt concentration) (Langmuir 1997 [DIRS 100051], Chapter 4) are tending to decrease the long-term corrosion potential as increases in nitrate-ion concentration are tending to increase the long-term corrosion potential. Overall, these processes make determination of the chemical dependencies difficult from the two-dimensional graphs (long-term corrosion potential versus one chemical variable) presented. The regression fitting presented in the next section makes the chemical dependencies more clear.

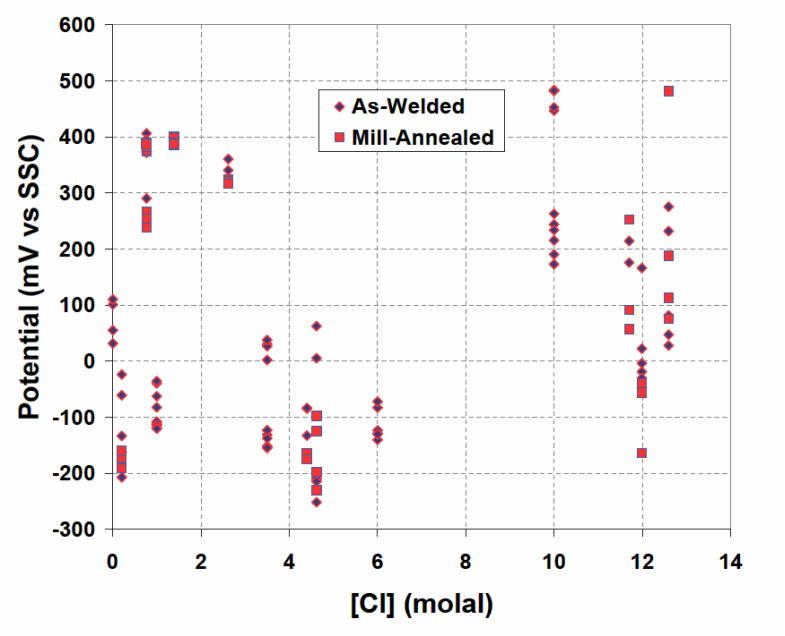

Source: DTN: LL060900512251.177 [DIRS 178271], file: *Summary Ecorr Cells 1-36 29Sep06.xls*.

Output DTN: MO0612WPOUTERB.000, file *LTEcorrData_Graph.xls*.

Figure 6-38. Long-Term Open-Circuit Corrosion Potential versus Chloride-Ion Concentration of Alloy 22 Samples with Differing Sample Configurations and Metallurgical Conditions

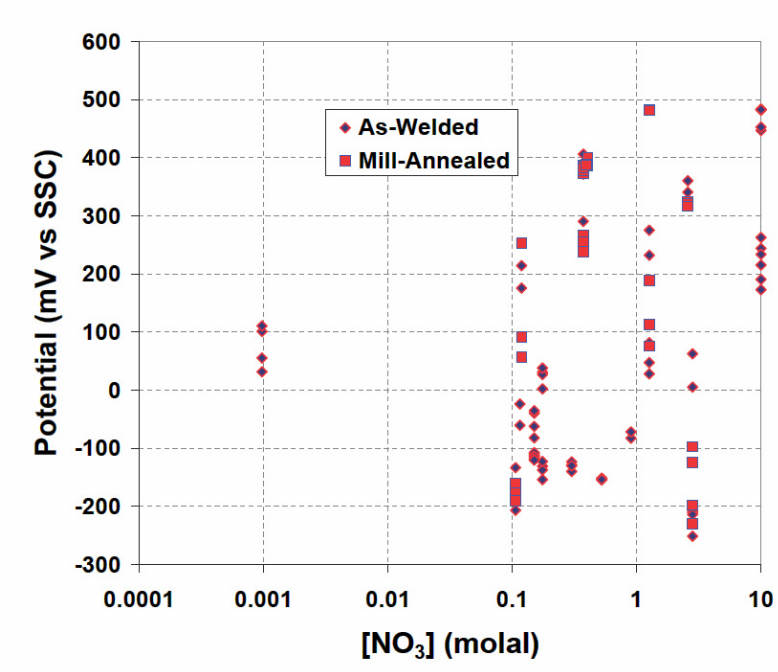

Source: DTN: LL060900512251.177 [DIRS 178271], file: *Summary Ecorr Cells 1-36 29Sep06.xls*.

Output DTN: MO0612WPOUTERB.000, file *LTEcorrData_Graph.xls*.

Figure 6-39. Long-Term Open-Circuit Corrosion Potential versus Nitrate-Ion Concentration of Alloy 22 Samples with Differing Sample Configurations and Metallurgical Conditions

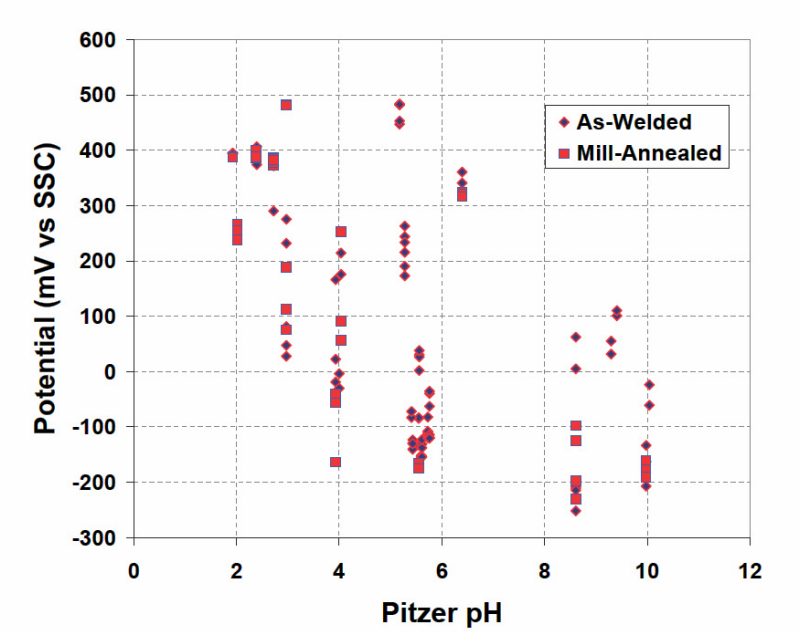

Source: DTN: LL060900512251.177 [DIRS 178271], file: *Summary Ecorr Cells 1-36 29Sep06.xls*.

Output DTN: MO0612WPOUTERB.000, file *LTEcorrData_Graph.xls*.

Figure 6-40. Long-Term Open-Circuit Corrosion Pote ntial versus pH of Alloy 22 Samples with Differing Sample Configurations and Metallurgical Conditions

6.4.4.5 Long-Term Corrosion Potential Model for the Waste Package Outer Barrier

The data reported in Appendix VIII were used to build a model for the long-term corrosion potential of the WPOB. For the long-term corrosion potential model, only the E_{corr} data after an immersion time of 250 days and higher were used. In some systems (e.g., 5 *M* $CaCl_2$ in Figure 6-37) the long-term corrosion potential seemed to stabilize in the first 50 days of exposure; however, in other systems (e.g., 5 *M* $CaCl_2$ + 0.5 *M* $Ca(NO_3)_2$ in Figure 6-37) the long-term corrosion potential shows signs of instability even after two years of exposure. That is, it is considered appropriate to use corrosion potential data after immersion times greater than 250 days to be reasonably assured that the corrosion potentials have stabilized as much as possible.

Because of measurement noise in the long-term corrosion potentials, an average of the readings for the final 30 days of exposure for each sample was used as the steady-state value for the model analysis. This approach filters out any transient (i.e., short-lived) high or low potential readings to a reasonable degree. Experimental observations of, for example, the occurrence or absence of localized corrosion initiation from long-term corrosion potential cells with exposure times less than 250 days (i.e., cells 7-1, 26, and 27) are used for validation in Section 7.2.4. In Section 7.2.4 it is found that the experimental observations as to the occurrence or absence of localized corrosion initiation are consistent with predictions made based on comparisons of the predicted long-term corrosion potential with the predicted crevice repassivation potential for these cells. As discussed in Section 6.4.4, only long-term corrosion potential data with exposure temperatures less than or equal to 120°C were used for analysis. The data that were used for model development are listed in Appendix VIII.

Development of the long-term corrosion potential model for the WPOB was performed using multiple linear regression techniques (Draper and Smith 1981 [DIRS 118716], Chapter 2) in which the long-term corrosion potential was represented as a function of test exposure environment parameters such as temperature, pH, chloride-ion concentration and nitrate-ion concentration. Regression models using various combinations of the exposure environment parameters were fit to the long-term corrosion potential data (E_{corr}) listed in Appendix VIII and evaluated for the goodness of their model fit using various statistical analysis techniques including the value of R^2. Among the models that were considered, Equation 6-39 was found to adequately describe the relationship between E_{corr} and the test environment variables above.

$$E_{corr} = c_o + c_1 T + c_2 pH + c_3 \frac{[NO_3^-]}{[Cl^-]} + c_4 T \frac{[NO_3^-]}{[Cl^-]} + c_5 pH \frac{[NO_3^-]}{[Cl^-]} + c_6 pH \ln[Cl^-] + \varepsilon_{corr} \quad \text{(Eq. 6-39)}$$

where E_{corr} is the long-term corrosion potential in mV versus SSC, T is the temperature (°C), $[Cl^-]$ is the chloride-ion concentration in molality, $[NO_3^-]$ is the molal nitrate-ion concentration, and c_o, c_1, c_2, c_3, c_4, c_5, and c_6 are coefficients of the model parameters. The error term, ε_{corr}, represents data variance not explained by the fitting procedure. Using the method of least squares, the above model was fit to the data in Appendix VIII. The model fitting was performed using Mathcad V. 13.0, and the Mathcad worksheet for the model fitting is found in the output DTN: MO0703PAGENCOR.001, file: *Ercrev_Ecorr3.xmcd*, and in Appendix X.

The estimated regression coefficients and their uncertainty (±1 standard deviation) are: c_0 = 1051.219 ± 119.774, c_1 = −3.024 ± 0.977, c_2 = −155.976 ± 11.495, c_3 = −1,352.040 ± 252.224, c_4 = 10.875 ± 1.890, c_5 = 137.856 ± 23.158, and c_6 = −8.498 ± 0.801. The units of the coefficients are such that the units of E_{corr} are mV versus SSC. The covariance matrix resulting from the fitting procedure was determined to be:

$$r\Sigma 2 = \begin{pmatrix} 1.435E{+}004 & -1.031E{+}002 & -9.152E{+}002 & -2.762E{+}004 & 1.802E{+}002 & 1.884E{+}003 & -1.660E{+}001 \\ -1.031E{+}002 & 9.539E{-}001 & 2.770E{+}000 & 1.846E{+}002 & -1.519E{+}000 & -6.817E{+}000 & -7.543E{-}002 \\ -9.152E{+}002 & 2.770E{+}000 & 1.321E{+}002 & 1.971E{+}003 & -6.909E{+}000 & -2.515E{+}002 & 4.409E{+}000 \\ -2.762E{+}004 & 1.846E{+}002 & 1.971E{+}003 & 6.362E{+}004 & -4.223E{+}002 & -4.107E{+}003 & 5.959E{+}001 \\ 1.802E{+}002 & -1.519E{+}000 & -6.909E{+}000 & -4.223E{+}002 & 3.573E{+}000 & 1.337E{+}001 & -2.622E{-}001 \\ 1.884E{+}003 & -6.817E{+}000 & -2.515E{+}002 & -4.107E{+}003 & 1.337E{+}001 & 5.363E{+}002 & -6.697E{+}000 \\ -1.660E{+}001 & -7.543E{-}002 & 4.409E{+}000 & 5.959E{+}001 & -2.622E{-}001 & -6.697E{+}000 & 6.418E{-}001 \end{pmatrix} \quad \text{(Eq. 6-40)}$$

The error term, ε_{corr}, represents data variance not explained by the fitting procedure and has a normal distribution with a mean of zero mV saturated SSC and a standard deviation (referred to as s_{corr}) of 85.265 mV versus SSC. The coefficient of determination R^2 is 0.872. An R^2 value of 0.872 indicates that the regression model fits the experimental data well.

The value of the pH coefficient, c_2 = −155.976 ± 11.495, and the presence of two pH cross terms (with the nitrate ion-to-chloride ion ratio and the natural logarithm of chloride-ion concentration) indicates that the long-term corrosion potential has a strong dependence on pH. As shown later (Section 6.4.4.6.4), the long-term corrosion potential can increase with decreasing pH. This model behavior represents the effect of ennoblement in E_{corr} of the alloy in

acidic conditions, as seen in the SAW solutions (Figure 6-36). Other investigators also reported such an ennoblement of Alloy 22 in acidic conditions (Dunn et al. 2003 [DIRS 164138], Figures 8 and 9; Jayaweera et al. 2003 [DIRS 162225], Section 9.3.2, Figure 9.13). At very low pH values, the long-term corrosion potential of Alloy 22 is expected to drop to lower values due to loss of passivity (i.e., active behavior). However, the pH values that could result in active behavior are expected to be lower than 1.9, as shown by the lack of any observation of localized corrosion after five years of exposure of Alloy 22 specimens to acidic SAW solutions (e.g., Cells 9, 10, and 17 in Appendix VIII). Oldfield and Sutton (1980 [DIRS 167863], Table III) also estimated that the pH of the "critical crevice solution" was sufficiently aggressive to break down the passive film of several alloys. For Alloy 625, a Ni-Cr-Mo alloy of similar composition to Alloy 22, they estimated a critical crevice solution pH of zero.

As shown later (Sections 6.4.4.6.1 and 6.4.4.6.2), the long-term corrosion potential can increase with temperature. This may be due to passive film becoming more defect-free at higher temperatures (Lloyd et al. 2003 [DIRS 167921]), because the defect-repair processes in the passive film could accelerate as temperature increases. To be consistent with the evaluation method for E_{rcrev} in Section 6.4.4.3.1, the chloride-ion concentration should be constrained to be between 0.0005 *m* and 20 *m*. If the exposure nitrate ion-to-chloride ion concentration ratio exceeds 1.0, the value 1.0 is used in evaluating the model. The maximum pH value used in development of the long-term corrosion potential model was about 10. Therefore, if the exposure pH exceeds 10, the value 10 should be used to evaluate the model. Implementation rules for evaluating the long-term corrosion potential model are discussed further in Section 6.4.4.6.6.

The model results and the steady-state corrosion potential data are shown in Figure 6-41. The horizontal axis is the long-term corrosion potential predicted by the model while the vertical axis is either the measured long-term corrosion potential for the measured data points (circles) or the ±2 standard deviation prediction intervals represented by plus signs, or the mean model prediction represented by the solid line.

The prediction intervals are calculated by adding to the median estimate (E_{corr} from Equation 6-39) an adjustment based on the standard deviation of the error term (s_{corr}), the covariance matrix (Equation 6-40) and the values of the exposure parameters for the data point being evaluated. The adjustment factor is written in matrix form as Equation 6-41:

$$\pm z\sqrt{\left[1 \quad T \quad pH \quad \frac{[NO_3^-]}{[Cl^-]} \quad T\cdot\frac{[NO_3^-]}{[Cl^-]} \quad pH\frac{[NO_3^-]}{[Cl^-]} \quad pH\ln[Cl^-]\right] r \Sigma 2 \left[1 \quad T \quad pH \quad \frac{[NO_3^-]}{[Cl^-]} \quad T\cdot\frac{[NO_3^-]}{[Cl^-]} \quad pH\frac{[NO_3^-]}{[Cl^-]} \quad pH\ln[Cl^-]\right]^T + s_{corr}^2} \quad \text{(Eq. 6-41)}$$

where z would be the number of standard deviations at which the adjustment factor is to be evaluated. The values of the long-term corrosion potential are *constrained* to be within the range defined by the ±2 standard deviation (i.e., $z = \pm 2$) prediction interval of the *unconstrained* long-term corrosion potential model. That is, the ±2 standard deviation prediction interval of the *unconstrained* long-term corrosion potential relationship (Equation 6-39 adjusted by Equation 6-41) is used as bounds on the value that the long-term corrosion potential may have. This means that, if the calculated *unconstrained* long-term corrosion potential exceeds the +2 standard deviation prediction bound of the *unconstrained* long-term corrosion potential model, the long-term corrosion potential value of the +2 standard deviation prediction bound of the

unconstrained long-term corrosion potential model should be used as the value of the long-term corrosion potential for the given exposure conditions. Similarly, if the calculated *unconstrained* long-term corrosion potential does not exceed the −2 standard deviation prediction bound of the *unconstrained* long-term corrosion potential model, the long-term corrosion potential value of the −2 standard deviation prediction bound of the *unconstrained* long-term corrosion potential should be used as the value of the long-term corrosion potential for the given exposure conditions.

It is evident from Figure 6-41 that the experimental data has considerable scatter. Replicated measurements of the long-term corrosion potential in the same chemical system at the same temperature are not very reproducible. Where the model predictions overestimate the measured long-term corrosion potentials, the model is conservative. As can be seen from Figure 6-41, the majority of the measured long-term corrosion potential data used to develop the long-term corrosion potential model lie within the 2 standard deviation prediction intervals of the long-term corrosion potential model (121 out of 129 data points). Eight measured long-term corrosion potentials lie outside the bounds of the long-term corrosion potential model; five of these are more positive than the upper bound of the long-term corrosion potential model for the exposure conditions under which they were measured (i.e., they are positive outliers).

Three of the measured long-term corrosion potentials that are positive outliers are from cell 21, which contained 5 *M* $CaCl_2$ + 0.5 *M* $Ca(NO_3)_2$ at 90°C (specimens DEA2827, DEA2828, and DEA2829). The long-term corrosion potentials of specimens DEA2827, DEA2828, and DEA2829 are all about 52 mV above the upper bound of the long-term corrosion potential model for the exposure conditions under which they were measured. Six specimens were used from cell 21 in developing the long-term corrosion potential model. Two of the measured long-term corrosion potentials from cell 21 are below the lower bound of the long-term corrosion potential model. The average measured long-term corrosion potential in cell 21 was 267 mV versus SSC, and the standard deviation of the measured long-term corrosion potentials in cell 21 was 236 mV versus SSC (the highest of any cell used in model development), indicating that the measured long-term corrosion potentials from cell 21 are not very reproducible.

Cell 15 contained nominally the same 5 *M* $CaCl_2$ + 0.5 *M* $Ca(NO_3)_2$ at 90°C as cell 21; the average measured long-term corrosion potential in cell 15 was 177 mV versus SSC, and the standard deviation of the measured long-term corrosion potentials in cell 15 was 83 mV versus SSC, indicating that the measured long-term corrosion potentials from cell 15 were more reproducible than those measured in cell 21. The mean value of the long-term corrosion potential model calculated under the exposure conditions relevant to cells 15 and 21 is higher than three of the six measurements in cell 21 and higher than five of the six measurements in cell 15. That is, the long-term corrosion potential model tends to overestimate the long-term corrosion potential relative to the measured values for the exposure conditions for cells 15 and 21. Furthermore, comparison of the long-term corrosion potential model results with the crevice repassivation model results for the exposure conditions for cells 15 and 21 (Section 7.2.4) indicates that crevice corrosion would be predicted to initiate with 100% probability.

One of the measured long-term corrosion potentials that is a positive outlier is from cell 14, which contained 5 *M* $CaCl_2$ + 0.05 *M* $Ca(NO_3)_2$ at 90°C (specimen DEA2801). The measured long-term corrosion potential of specimen DEA2801 was 253 mV versus SSC and is slightly

(about 12 mV) more positive than the upper bound of the long-term corrosion potential model for the exposure conditions for cell 14. The fifth positive outlier is from cell 4, which contained BSW solution at 105°C (specimen ARC22 U-20A and ARC22 U-20B, a double U-bend). The measured long-term corrosion potential of specimens ARC22 U-20A and ARC22 U-20B was 62 mV versus SSC and is slightly (about 13 mV) more positive than the upper bound of the long-term corrosion potential model for the exposure conditions for cell 4. Given the large amount of spread evident in Figure 6-41 for the long-term corrosion potential measurements, deviations on the order of 12 or 13 mV are not significant.

In summary, the long-term corrosion potential model upper bound underestimates five long-term corrosion potential measurements by small amounts (between 12 and 52 mV). Inclusion of these data points in the dataset used to develop the long-term corrosion potential model is conservative, since their inclusion increases the values predicted by the model. The long-term corrosion potential model lower bound overestimates three measured long-term corrosion potential values by small amounts (between 6 and 53 mV). The model predictions are conservative relative to these measurements, and their inclusion in the data set used to develop the long-term corrosion potential model is nonconservative, since their inclusion decreases the values predicted by the model. Overall, because these measured values are over- or under-predicted by small amounts and no bases for their exclusion was evident, these data points were included in the development of the long-term corrosion potential model.

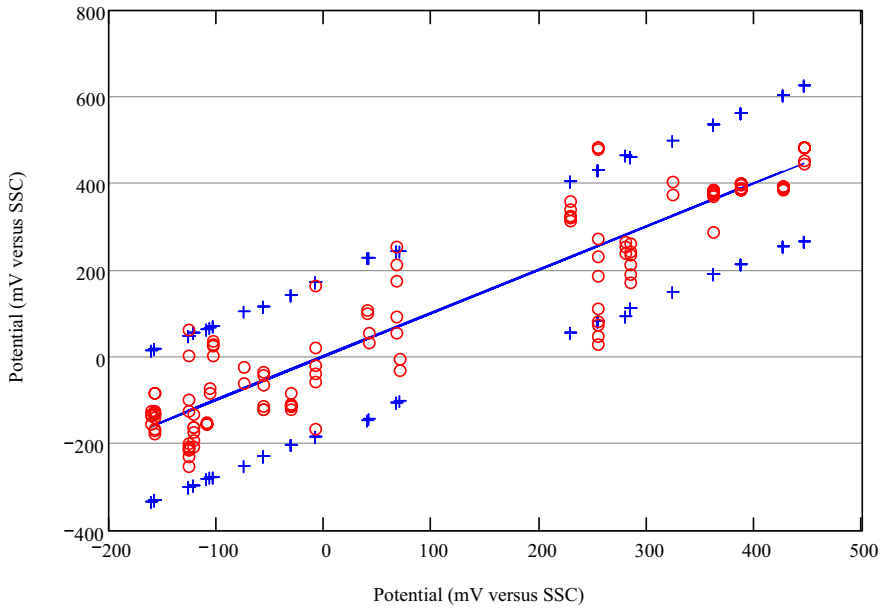

Source: DTN: LL060900512251.177 [DIRS 178271], file: *Summary Ecorr Cells 1-36 29Sep06.xls*.

Output DTN: MO0703PAGENCOR.001, file: *Ercrev_Ecorr3.xmcd*.

NOTE: The horizontal axis is the long-term corrosion potential predicted by the model while the vertical axis is either the measured long-term corrosion potential for the measured data points (circles) or the ±2 standard deviation prediction intervals represented by plus signs, or the mean model prediction represented by the solid line.

Figure 6-41. Model Prediction and Experimental Data for Long-Term E_{corr} of the Waste Package Outer Barrier

The purpose of this long-term corrosion potential model is to estimate the long-term steady-state open-circuit corrosion potential of Alloy 22 for a range of exposure conditions related to the repository. The model is not intended for evaluation of the corrosion potential during short-term transient conditions. The entire variance of the long-term corrosion potential model is due to uncertainty. For the waste package degradation analysis, variability in the long-term corrosion potential among waste packages is represented by the temporally and spatially varying waste package temperature and water chemistry contacting the waste package. As shown by the analyses in this section, it is reasonable to constrain the values of the long-term corrosion potential to be within the range defined by the ±2 standard deviation prediction interval of the *unconstrained* long-term corrosion potential model.

6.4.4.6 Analysis of Localized Corrosion Initiation Model

In the localized corrosion initiation model, localized corrosion of the WPOB occurs when the open-circuit corrosion potential (E_{corr}) is equal to or greater than a critical potential (the crevice repassivation potential (E_{rcrev}) in the current model), that is, ΔE ($=E_{rcrev} - E_{corr}$) ≤ 0. This conceptual model of localized corrosion initiation is recognized by the corrosion community (e.g., Dunn et al. 2005 [DIRS 178451] and Beavers et al. 2002 [DIRS 158781], Section 8.3). The ΔE criterion was developed based on information found throughout the corrosion science literature (Böhni 2000 [DIRS 164137], Section B; Dunn et al. 2000 [DIRS 164495]; Dunn et al. 2003 [DIRS 164138]; Frankel 1998 [DIRS 162216]; Frankel 2002 [DIRS 164140]; Frankel and Kelly 2002 [DIRS 164141]). For the current localized corrosion initiation model, a conservative measure, the crevice repassivation potential (E_{rcrev}), was used for the critical potential. The localized corrosion initiation model components (i.e., E_{corr} and E_{rcrev}) could be affected by the exposure conditions (temperature, pH, chloride-ion concentration, nitrate-ion concentration).

This section documents the analysis of the localized corrosion initiation model for long-term localized corrosion susceptibility of the WPOB for a range of environmental conditions of interest. The analyses were performed by comparing the crevice repassivation potential model results with the long-term corrosion potential model results, as described above. The analyses were conducted with Mathcad V. 13.0; the Mathcad worksheet files are included in output DTN: MO0703PAGENCOR.001, file: *Ercrev_Ecorr3.xmcd*. The localized corrosion initiation model is intended to be used to analyze the long-term localized corrosion susceptibility of the WPOB, and not for analysis of short-term transient behavior because the model makes use of long-term corrosion potentials.

6.4.4.6.1 Localized Corrosion Susceptibility versus Temperature and pH

This section illustrates the effect of temperature and pH on the localized corrosion susceptibility of Alloy 22 in a 6 *m* chloride-based brine containing 1.8 *m* nitrate ions (NO_3/Cl ratio = 0.30). Figure 6-42 shows the model results at a pH of 7. Shown in the figure are the mean estimates of the long-term corrosion potential (E_{corr}) and the crevice repassivation potential (E_{rcrev}), as well as the ±1 and ±2 standard deviation prediction intervals for their corresponding *unconstrained* models. The ±2 standard deviation prediction intervals for the *unconstrained* crevice repassivation potential model are the bounding values for the crevice repassivation potential model used to evaluate repository performance. Similarly, the ±2 standard deviation prediction intervals for the *unconstrained* long-term corrosion potential model are the bounding values for

the long-term corrosion potential model used to evaluate repository performance. The prediction intervals for the *unconstrained* crevice repassivation potential and long-term corrosion potential models are shown in the graphs presented in this and the following sections.

Given that there is very little overlap of the prediction intervals in Figure 6-42, crevice corrosion initiation is expected to be a very rare event under these exposure conditions. The mean crevice repassivation potential curve does not cross the mean long-term corrosion potential curve at any exposure temperature below 120°C. The +2 standard deviation long-term corrosion potential prediction interval crosses the –2 standard deviation crevice repassivation potential prediction interval at about 90°C. The +2 standard deviation long-term corrosion potential prediction interval crosses the –1 standard deviation crevice repassivation potential prediction interval at about 105°C. The greater the amount of overlap of the prediction intervals, the more probable is the initiation of crevice corrosion, meaning that at 110°C, crevice corrosion initiation is more probable than at 100°C. Crevice corrosion will not initiate at temperatures below about 90°C under these exposure conditions according to this model.

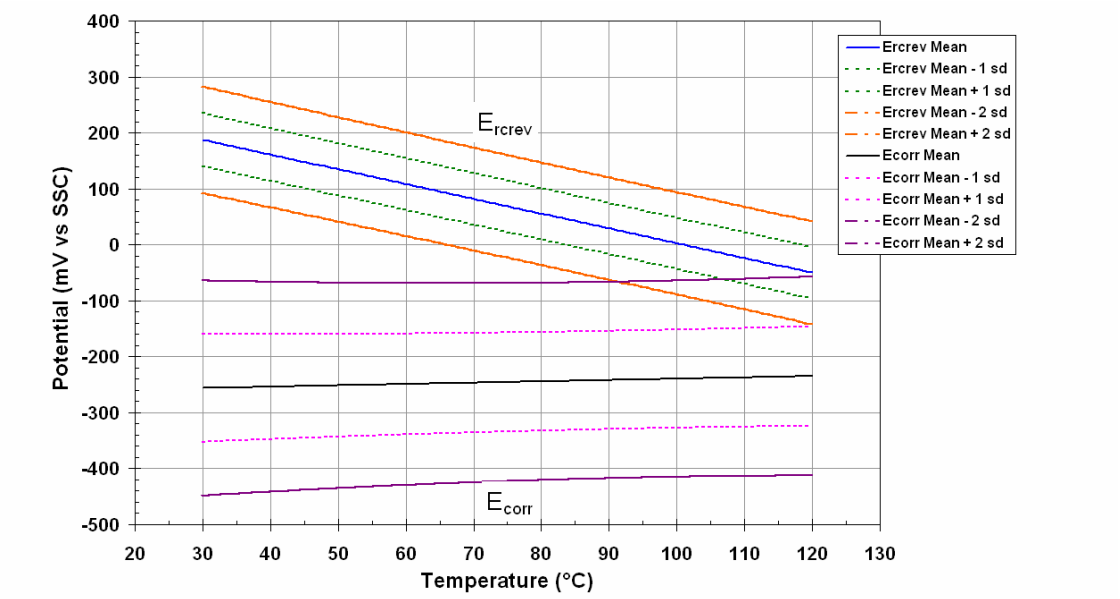

Output DTN: MO0612WPOUTERB.000, file: *dEvsT_pH7Cl6N1p8.xls*.

NOTE: Figure shows E_{rcrev} and E_{corr} versus temperature for 6 *m* chloride, with a pH of 7, and 1.8 *m* nitrate (with a NO_3/Cl ratio of 0.30).

Figure 6-42. Model Results for Crevice Corrosion Susceptibility of the Waste Package Outer Barrier as a Function of Temperature with a pH of 7

As shown in Figure 6-43, with a decrease in pH to 5, the long-term open circuit potential at each temperature increases. The mean long-term corrosion potential crosses the mean crevice repassivation potential curve at about 95°C, and crevice corrosion initiation becomes more probable as temperature increases. With a further decrease of pH to a value of 4 (Figure 6-44), the mean long-term corrosion potential crosses the mean crevice repassivation potential curve at about 50°C and the initiation of crevice corrosion is probable over the entire temperature range from 30°C to 120°C. Therefore, the model predicts that the initiation of crevice corrosion is highly dependent on the exposure pH.

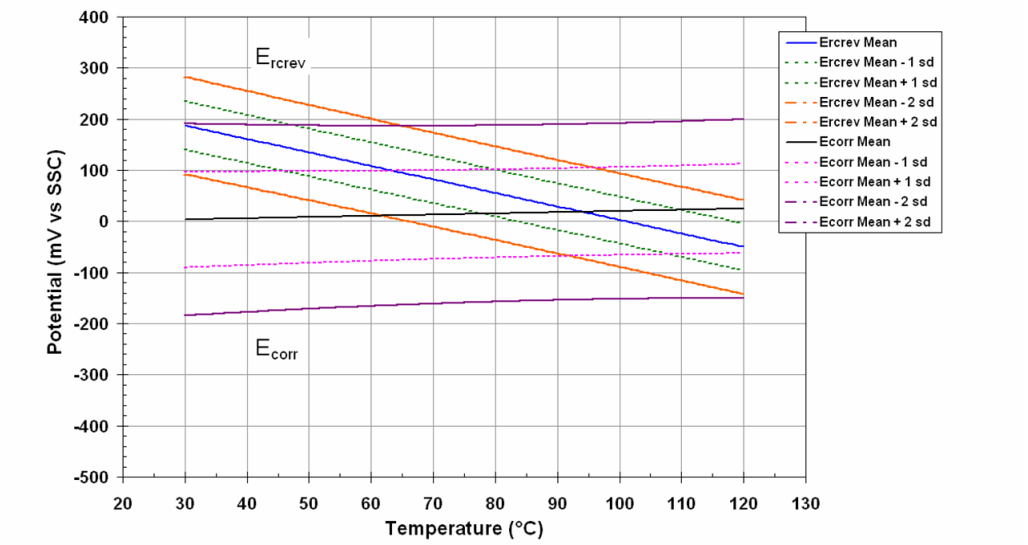

Output DTN: MO0612WPOUTERB.000, file: *dEvsT_pH5Cl6N1p8.xls*.

NOTE: Figure shows E_{rcrev} and E_{corr} versus temperature for 6 *m* chloride, with pH decreased to 5, and 1.8 *m* nitrate (with a NO_3/Cl ratio of 0.30).

Figure 6-43. Model Results for Crevice Corrosion Susceptibility of the Waste Package Outer Barrier as a Function of Temperature with a pH of 5

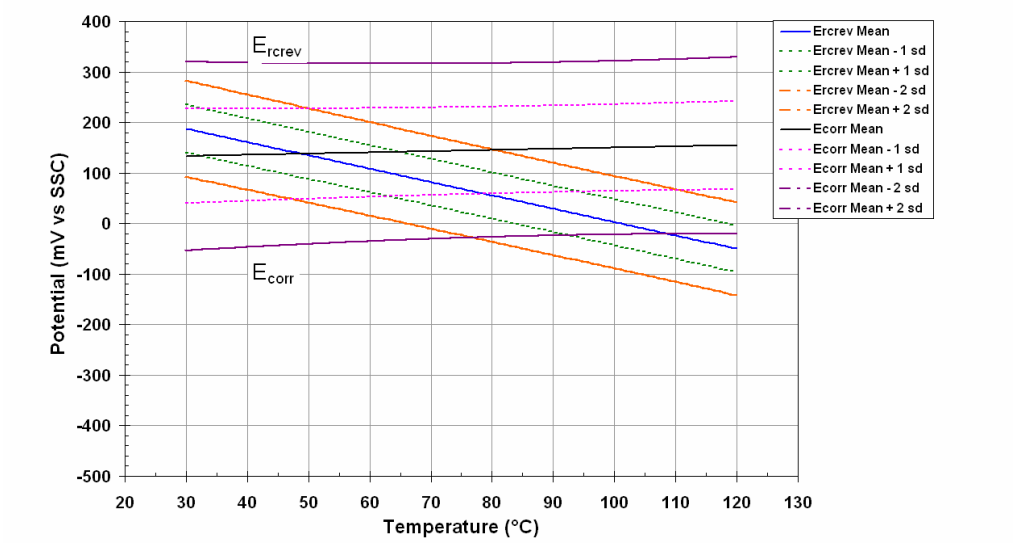

Output DTN: MO0612WPOUTERB.000, file: *dEvsT_pH4Cl6N1p8.xls*.

NOTE: Figure shows E_{rcrev} and E_{corr} versus temperature for 6 *m* chloride, with pH further decreased to 4, and 1.8 *m* nitrate (with a NO_3/Cl ratio of 0.30).

Figure 6-44. Model Results for Crevice Corrosion Susceptibility of the Waste Package Outer Barrier as a Function of Temperature with a pH of 4

6.4.4.6.2 Localized Corrosion Susceptibility versus Temperature and Nitrate-Ion Concentration

This section illustrates the effect of temperature and nitrate-ion concentration on the crevice corrosion susceptibility of Alloy 22 in a 6 *m* chloride-based brine at a pH of 4. Figure 6-45 shows the model results as a function of temperature, for an acidic chloride brine (6 *m* chloride) with a nitrate concentration of 3 *m* (NO_3/Cl ratio of 0.50). The mean long-term corrosion potential and crevice repassivation potential curves cross at about 80°C. The +1 standard deviation prediction interval long-term corrosion potential curve crosses the –1 standard deviation crevice repassivation potential prediction interval curve at about 53°C. An increase of nitrate concentration to 6 *m* (NO_3/Cl ratio of 1.0) indicates that crevice corrosion initiation is not expected below about 75°C and the mean long-term open circuit potential and crevice repassivation potential curves cross at about 102°C (Figure 6-46).

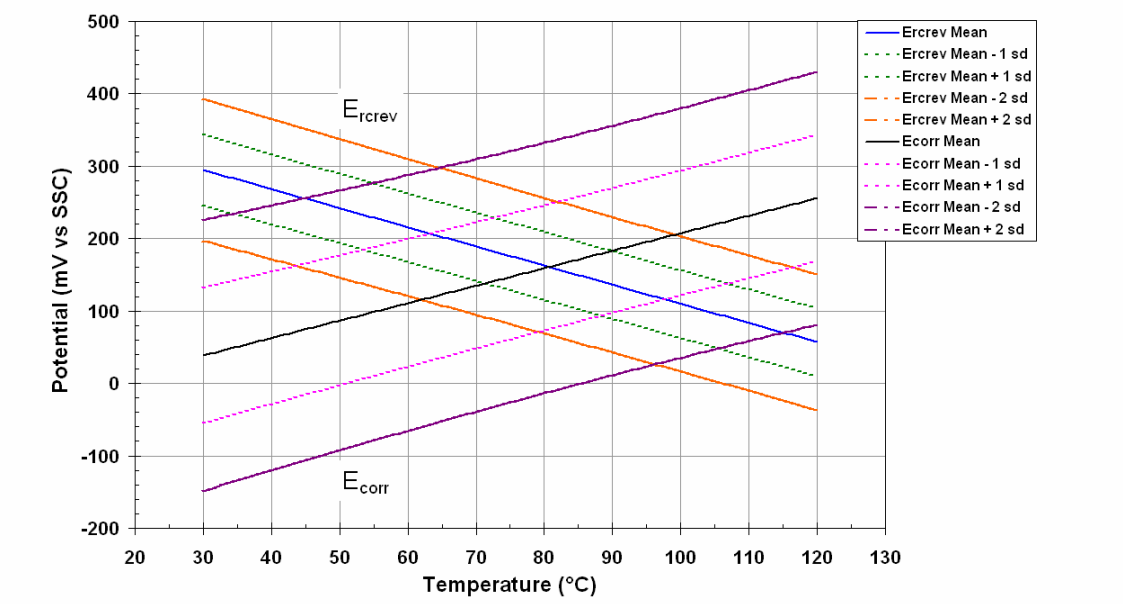

Output DTN: MO0612WPOUTERB.000, file: *dEvsT_pH4Cl6N3.xls*.

NOTE: Figure shows E_{rcrev} and E_{corr} versus temperature for 6 *m* chloride, with a pH of 4, and 3 *m* nitrate (with a NO_3/Cl ratio of 0.50).

Figure 6-45. Model Results for Crevice Corrosion Susceptibility of the Waste Package Outer Barrier as a Function of Temperature for 3 *m* Nitrate

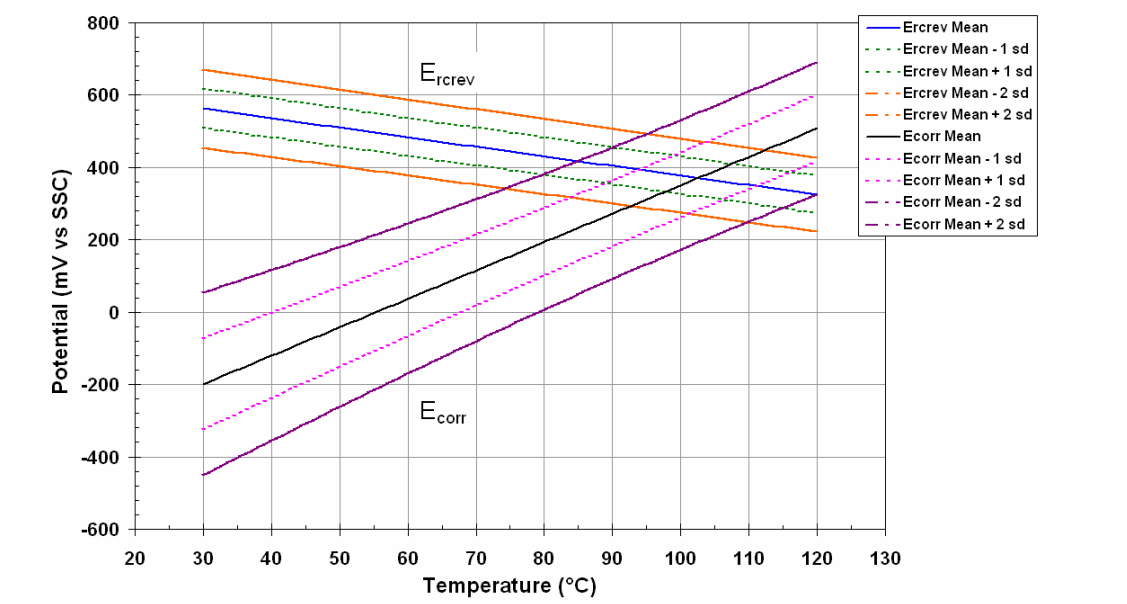

Output DTN: MO0612WPOUTERB.000, file: *dEvsT_pH4Cl6N6.xls*.

NOTE: Figure shows E_{rcrev} and E_{corr} versus temperature for 6 *m* chloride, with a pH of 4, and 6 *m* nitrate (with a NO_3/Cl ratio of 1.00).

Figure 6-46. Model Results for Crevice Corrosion Susceptibility of the Waste Package Outer Barrier as a Function of Temperature for 6 *m* Nitrate

6.4.4.6.3 Localized Corrosion Susceptibility versus Chloride-Ion Concentration and pH

This section illustrates the effect of chloride-ion concentration and pH on the localized corrosion susceptibility of Alloy 22 in a chloride-based brine with a nitrate-ion concentration of 3 *m* at a temperature of 90°C. Figure 6-47 shows the model results versus chloride-ion concentration for a solution with a pH of 7. Above a chloride concentration of about 7.5 *m*, the prediction intervals do not overlap, indicating that crevice corrosion initiation is not predicted to occur under these exposure conditions. The mean long-term corrosion potential and crevice repassivation potential curves cross at a chloride-ion concentration of about 1 *m*. The discontinuous change in slope at 3 *m* chloride is a consequence of constraining the nitrate ion-to-chloride-ion ratio to values at or below 1 in evaluating the models. There is also a change in slope at 20 *m* chloride, which is a consequence of constraining the chloride-ion concentration to values below 20 *m* in evaluating the models. At pH 4 and 90°C (Figure 6-48), the model predicts that the mean long-term corrosion potential and crevice repassivation potential curves cross at a chloride-ion concentration just below 5 *m*. A comparison between Figures 6-47 and 6-48 indicates that increases in chloride concentration appear to decrease the likelihood of crevice corrosion initiation at pH 7 and increase the likelihood of crevice corrosion initiation at pH 4 (i.e., E_{corr} decreases with increasing chloride-ion concentration more rapidly at pH 7 than it does at pH 4).

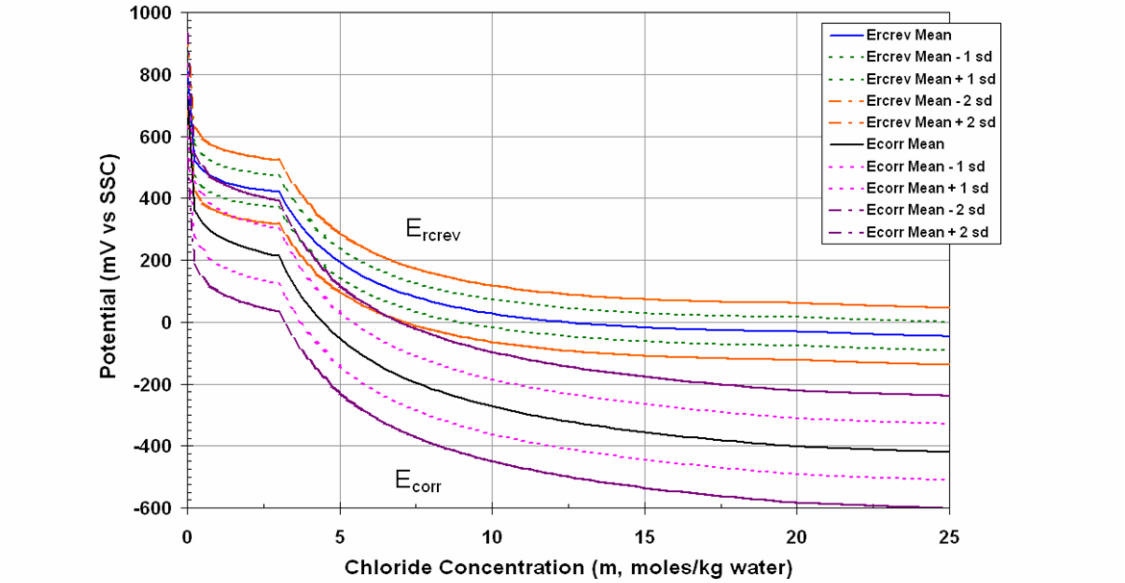

Output DTN: MO0612WPOUTERB.000, file: *dEvsCl_T90pH7N3.xls*.

NOTE: Figure shows E_{rcrev} and E_{corr} versus chloride ion concentration for 3 *m* nitrate, with a pH of 7, at 90°C.

Figure 6-47. Model Results for Crevice Corrosion Susceptibility of the Waste Package Outer Barrier as a Function of Chloride Concentration for 90°C, pH 7, and 3 *m* Nitrate

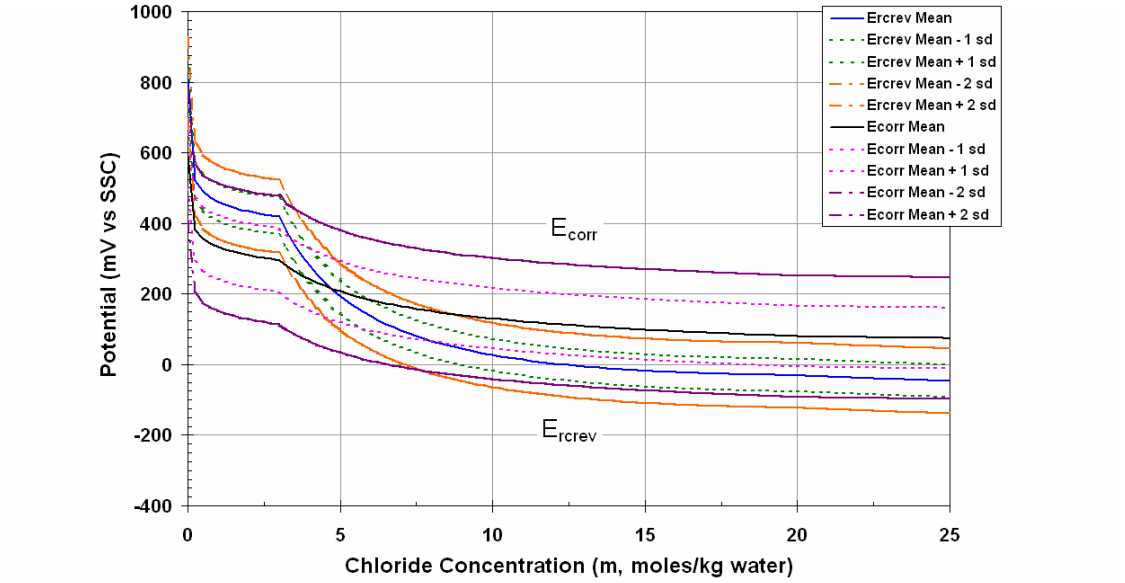

Output DTN: MO0612WPOUTERB.000, file: *dEvsCl_T90pH4N3.xls*.

NOTE: Figure shows E_{rcrev} and E_{corr} versus chloride ion concentration for 3 *m* nitrate, with a pH of 4, at 90°C.

Figure 6-48. Model Results for Crevice Corrosion Susceptibility of the Waste Package Outer Barrier as a Function of Chloride Concentration for 90°C, pH 4, and 3 *m* Nitrate

6.4.4.6.4 Localized Corrosion Susceptibility versus pH and Nitrate-Ion Concentration

This section illustrates the effect of pH and nitrate-ion concentration on the localized corrosion susceptibility of Alloy 22 in a 6 *m* chloride-based brine at 90°C. Figure 6-49 shows the model results for the localized corrosion susceptibility as a function of pH for a chloride-ion concentration of 6 *m* and a nitrate-ion concentration of 3 *m*. The model predicts that crevice corrosion initiation will not occur above a pH of about 7. The mean long-term corrosion potential and crevice repassivation potential curves cross at a pH of about 4.5. Increasing the nitrate concentration to 6 *m* (NO_3/Cl ratio = 1.0) (Figure 6-50) decreases the overall likelihood of crevice corrosion initiation because the predicted crevice repassivation potential increases relative to the predicted long-term corrosion potential. The mean long-term corrosion potential and crevice repassivation potential curves appear to cross at a pH below 2. The mean long-term corrosion potential crosses the –2 standard deviation crevice repassivation potential at a pH of about 3.2.

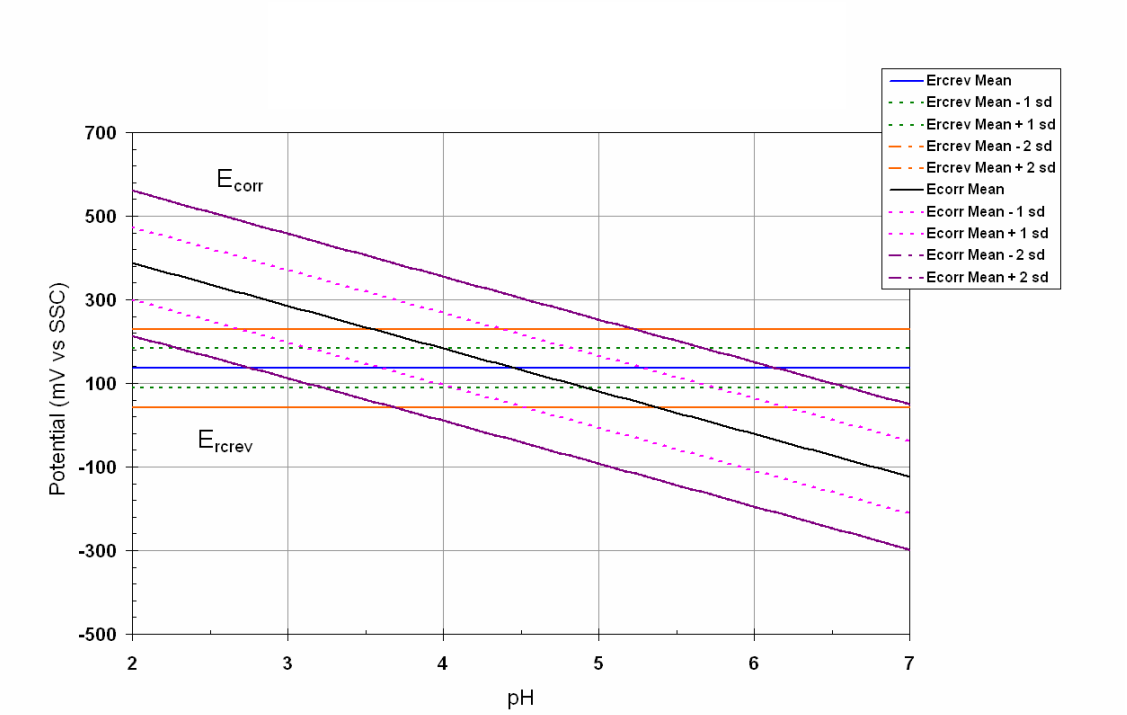

Output DTN: MO0612WPOUTERB.000, file: *dEvspH_T90Cl6N3.xls*.

NOTE: Figure shows E_{rcrev} and E_{corr} versus pH for 6 *m* chloride, with a temperature of 90°C, and 3 *m* nitrate (with a NO_3/Cl ratio of 0.50).

Figure 6-49. Model Results for Crevice Corrosion Susceptibility of the Waste Package Outer Barrier as a Function of pH for 3 *m* Nitrate

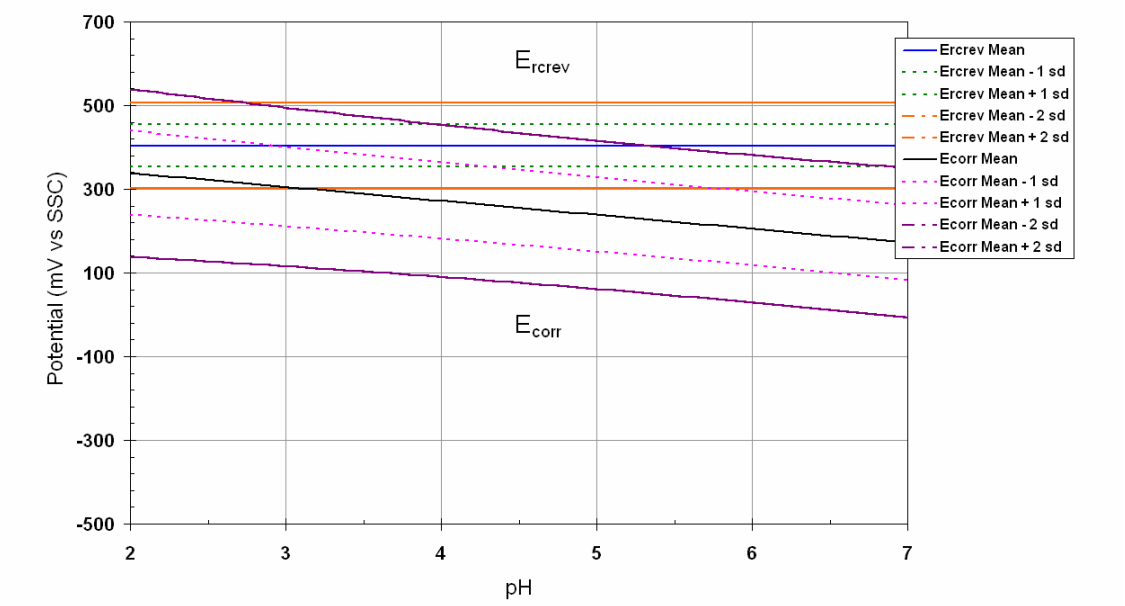

Output DTN: MO0612WPOUTERB.000, file: *dEvspH_T90Cl6N6.xls*.

NOTE: Figure shows E_{rcrev} and E_{corr} versus pH for 6 *m* chloride, with a temperature of 90°C, and 6 *m* nitrate (with a NO_3/Cl ratio of 1.00).

Figure 6-50. Model Results for Crevice Corrosion Susceptibility of the Waste Package Outer Barrier as a Function of pH for 6 *m* Nitrate

6.4.4.6.5 Localized Corrosion Susceptibility versus Nitrate-Ion Concentration for 90°C and 6 Molal Chloride at Various pH Values

Figure 6-51 shows the prediction intervals for the *unconstrained* long-term corrosion potential and crevice repassivation potential models at 90°C, 6 *m* chloride-ion concentration, and a pH of 7. The two sets of curves are almost parallel. The –2 standard deviation prediction interval for the crevice repassivation potential and the +2 standard deviation prediction interval for the long-term corrosion potential cross at a nitrate-ion concentration of about 2.5 *m*. For these exposure conditions, Figure 6-51 indicates that crevice corrosion initiation is slightly more probable at higher nitrate concentrations. Overall, given the very small amount of overlap between the prediction intervals, crevice corrosion initiation is not likely. As shown in Figure 6-52, for a 6 *m* chloride-ion solution at a pH of 4 at 90°C, the mean long-term corrosion potential and crevice repassivation potential curves cross at a nitrate-ion concentration of about 3.8 *m*. A comparison of Figures 6-51 and 6-52 indicates that, while increases in nitrate-ion concentration at pH 7 (Figure 6-51) increase the likelihood of crevice corrosion initiation, at pH 4 (Figure 6-52) increases in nitrate-ion concentrations decrease the likelihood of crevice corrosion initiation.

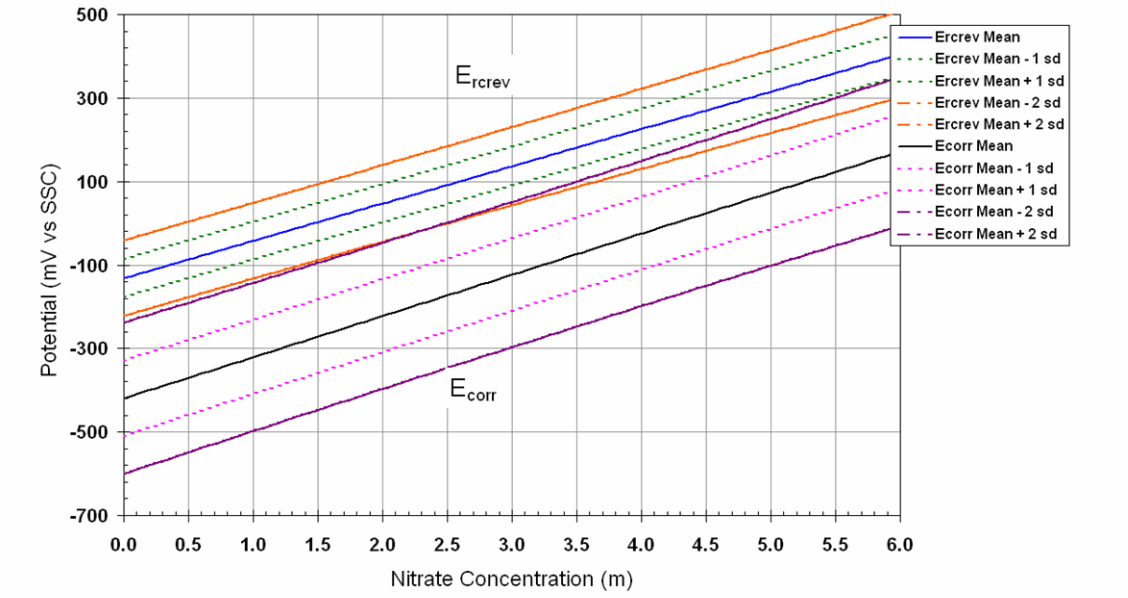

Output DTN: MO0612WPOUTERB.000, file: *dEvsNO3_T90Cl6pH7.xls*.

NOTE: Figure shows E_{rcrev} and E_{corr} versus nitrate concentration for 6 *m* chloride, with a pH of 7 and a temperature of 90°C.

Figure 6-51. Model Results for Crevice Corrosion Susceptibility of the Waste Package Outer Barrier as a Function of Nitrate Concentration for a pH of 7

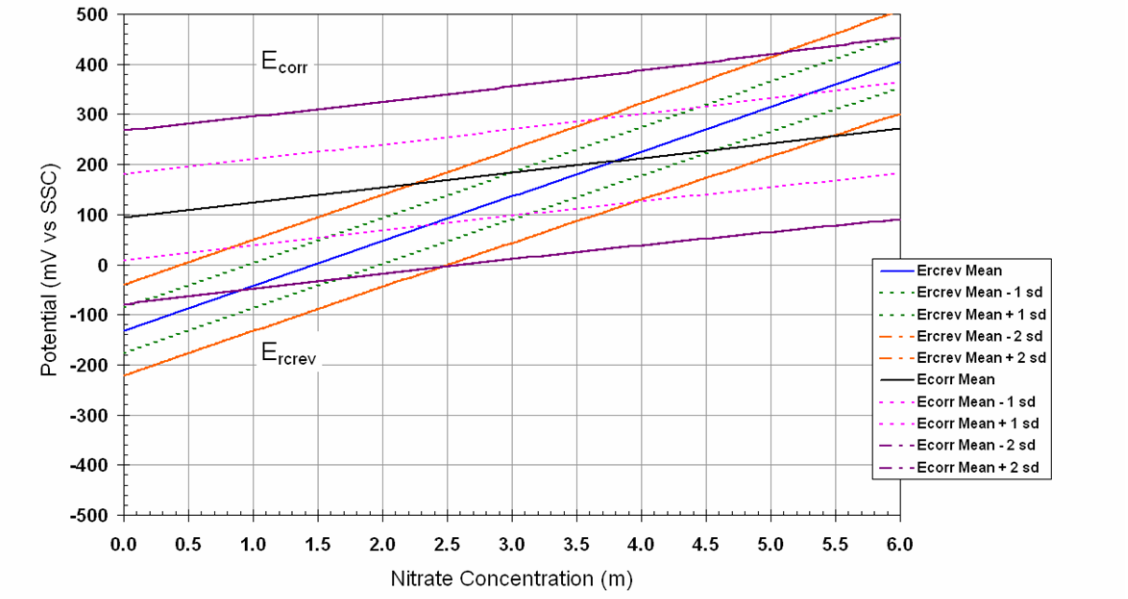

Output DTN: MO0612WPOUTERB.000, file: *dEvsNO3_T90Cl6pH4.xls*.

NOTE: Figure shows E_{rcrev} and E_{corr} versus nitrate concentration for 6 *m* chloride, with a pH of 4 and a temperature of 90°C.

Figure 6-52. Model Results for Crevice Corrosion Susceptibility of the Waste Package Outer Barrier as a Function of Nitrate Concentration for a pH of 4

6.4.4.6.6 Implementation of the Waste Package Outer Barrier Localized Corrosion Initiation Model

As discussed in the previous sections, the crevice repassivation potential model was constructed using data from pure chloride solutions and mixed chloride and nitrate solutions, including some data at high nitrate (up to 10 *m*) and chloride (up to 20 *m*) concentrations and high temperatures (up to 120°C). However, the long-term corrosion potential model was constructed using data from relatively dilute (in terms of chloride- and nitrate-ion content) mixed ionic solutions (e.g., SAW and SCW), chloride solutions (up to about 13 *m*), and mixed chloride and nitrate solutions (up to about 13 *m* chloride ions and up to about 10 *m* nitrate ions). The maximum temperature for any data point used in construction of the long-term corrosion potential model was 120°C.

The WPOB crevice corrosion initiation model was used to evaluate the crevice corrosion initiation behavior of the Alloy 22 WPOB. The Alloy 22 WPOB contains solution-heat-treated welds and base metal that have had the solution-heat-treated film removed, as well as low-plasticity burnished closure weld regions (e.g., SNL 2007 [DIRS 179394], Section 4.1.2). The area of the Alloy 22 WPOB that is contacted by seepage is potentially subject to localized corrosion. Localized corrosion of the WPOB is considered to initiate when the open-circuit corrosion potential (E_{corr}) is equal to or greater than a critical potential (the crevice repassivation potential (E_{rcrev}) in the current model), that is, ΔE ($=E_{rcrev} - E_{corr}$) ≤ 0. If the exposure temperature is greater than or equal to 20°C and less than or equal to 120°C then the WPOB crevice corrosion initiation model is implemented by evaluating the empirical correlations for the long-term corrosion potential (E_{corr}) and crevice repassivation potential (E_{rcrev}) (Sections 6.4.4.3 and 6.4.4.5) in accordance with the following implementation rules:

1) If the nitrate ion-to-chloride ion ratio in the environment exceeds 1, then evaluate E_{rcrev} and E_{corr} at a nitrate ion-to-chloride ion ratio of 1. If the molality of chloride ion is less than 0.0005 *m*, the nitrate ion-to-chloride ion ratio should be evaluated with a chloride-ion concentration of 0.0005 *m*.

2) If the molality of chloride ion in the environment exceeds 20 *m*, then evaluate E_{rcrev} and E_{corr} at a chloride-ion molality of 20 *m*. If the molality of chloride ion is less than 0.0005 *m*, then evaluate E_{rcrev} and E_{corr} at a chloride-ion molality of 0.0005 *m*.

3) If the pH in the environment exceeds 10, then evaluate E_{corr} at a *pH* of 10. If the pH in the environment is less than 1.9, then initiate localized corrosion.

If crevice corrosion is determined to initiate, then crevice corrosion occurs at a constant rate throughout the simulation period regardless of changes in the bulk chemical exposure environment. This is a conservative modeling assumption (Assumption 5.4, Section 5) and is used because the crevice corrosion model does not account for the possibility of crevice corrosion repassivation or stifling.

The values of the crevice repassivation potential are *constrained* to be within the range defined by the ±2 standard deviation prediction interval of the *unconstrained* crevice repassivation potential model. That is, the ±2 standard deviation prediction intervals of the *unconstrained*

crevice repassivation potential relationship (Equation 6-35 adjusted by Equation 6-38) are used as bounds on the value that the crevice repassivation potential may have. Thus, if the calculated *unconstrained* crevice repassivation potential exceeds the +2 standard deviation prediction bound of the *unconstrained* crevice repassivation potential model, the crevice repassivation potential value of the +2 standard deviation prediction bound of the *unconstrained* crevice repassivation potential model should be used as the value of the crevice repassivation potential for the given exposure conditions. Similarly, if the calculated *unconstrained* crevice repassivation potential does not exceed the −2 standard deviation prediction bound of the *unconstrained* crevice repassivation potential model, the crevice repassivation potential value of the −2 standard deviation prediction bound of the *unconstrained* crevice repassivation potential model should be used as the value of the crevice repassivation potential for the given exposure conditions.

Similarly, the values of the long term corrosion potential are *constrained* to be within the range defined by the ±2 standard deviation prediction interval of the *unconstrained* long term corrosion potential model. That is, the ±2 standard deviation prediction interval of the *unconstrained* long term corrosion potential relationship (Equation 6-39 adjusted by Equation 6-41) are used as bounds on the value that the long term corrosion potential may have. Thus, if the calculated *unconstrained* long term corrosion potential exceeds the +2 standard deviation prediction bound of the *unconstrained* long term corrosion potential model, the long term corrosion potential value of the +2 standard deviation prediction bound of the *unconstrained* long term corrosion potential model should be used as the value of the long term corrosion potential for the given exposure conditions. Similarly, if the calculated *unconstrained* long term corrosion potential does not exceed the −2 standard deviation prediction bound of the *unconstrained* long term corrosion potential model, the long term corrosion potential value of the −2 standard deviation prediction bound of the *unconstrained* long term corrosion potential should be used as the value of the long term corrosion potential for the given exposure conditions.

The chemical limits specified are conservative. Limiting the nitrate ion-to-chloride ion ratio used in evaluation of the model to 1 is conservative because, at a given temperature and chloride-ion concentration, E_{rcrev} increases markedly with nitrate-ion concentration, while E_{corr} is less sensitive than E_{rcrev} to nitrate-ion concentration at lower pH values where crevice corrosion is more likely to initiate (e.g., Figure 6-52). Limiting the nitrate ion-to-chloride ion ratio to 1 limits the beneficial effect of nitrate concentration in the crevice corrosion initiation model. Both E_{rcrev} and E_{corr} generally decrease with increasing chloride-ion concentration, at a given nitrate-ion concentration, temperature, and pH (only for E_{corr}). Without the use of a limiting chloride concentration, here chosen to be 20 *m* (consistent with the highest chloride-ion concentration at which E_{rcrev} data was obtained), the value of ΔE ($=E_{rcrev} - E_{corr}$) is greater than is obtained with the use of a limiting chloride concentration. This is illustrated in Appendix X. Therefore, limiting the chloride-ion concentration to 20 *m* is conservative for determination of crevice corrosion initiation.

The functional forms for E_{corr} (Equation 6-39) and E_{rcrev} (Equation 6-35) contain nitrate ion-to-chloride-ion ratio terms that could increase to what may be unrealistically high values for use in evaluation of crevice corrosion initiation at low (less than 0.0005 *m*) chloride-ion concentrations. Also, it is necessary to impose a lower limit (0.0005 *m*) to the chloride-ion concentration, because the functional forms for E_{corr} and E_{rcrev} involve a logarithm of chloride-ion concentration that is undefined (approaches $-\infty$) at zero chloride-ion concentration. E_{corr} decreases with

increasing pH at constant temperature and nitrate- and chloride-ion concentrations (e.g., Figure 6-50). It is conservative to use an upper limit on pH of 10 (consistent with the highest pH at which E_{corr} data were obtained), because E_{corr} is restricted from decreasing further at higher pH values. Also, it is conservative to initiate localized corrosion at the lower limiting pH of 1.9 (consistent with the lowest pH at which E_{corr} data were obtained). The lowest pH value at which E_{rcrev} data was obtained was about 3.2; however, the E_{corr} data (Appendix VIII, SAW cells) shows that the passive film is stable at these low pH values. The model validation activities undertaken in Section 7.2.4 add further confidence in the validity of these implementation criteria.

6.4.4.7 Localized Corrosion Penetration Rate Model

If the long-term corrosion potential of the WPOB exceeds the critical potential, crevice corrosion is predicted to initiate and penetration of the barrier by localized corrosion is modeled. Very little data exists for localized corrosion penetration rates under repository-relevant exposure conditions. A reasonable lower bound for the localized corrosion propagation rate of Alloy 22 would be its average corrosion rate in a highly aggressive 10% ferric chloride crevice corrosion test solution. According to Haynes International (1997 [DIRS 100897], p. 8), the average corrosion rate of Alloy 22 in a 10% ferric chloride solution (i.e., about 2.1 *m* [Cl^-]) at 75°C is 0.5 mils/yr or 12.7 μm/yr. Because the occluded chemistry in a propagating crevice is expected to have a high chloride-ion concentration and hydrolyzed metal ions (including Fe^{3+}), the Alloy 22 corrosion rate of 12.7 μm/yr measured in a $FeCl_3$ solution containing about 2.1 *m* chloride ions at 75°C is a suitable analogue crevice solution for estimating metal dissolution. The presence in the solution of Fe^{3+}, an oxidant, could have further enhanced the corrosion rate of Alloy 22, yet this corrosion rate is considered the lower bound because the pH in a propagating crevice may be lower than that in the $FeCl_3$ solution.

A reasonable upper bound for the localized corrosion penetration rates of Alloy 22 would be a corrosion rate obtained in a concentrated HCl solution at an elevated temperature (e.g., 75°C). The rationale for this is that a concentrated hydrochloric acid solution will have a high concentration of chloride ions, which are known to be very effective anions in causing crevice corrosion initiation on metals and alloys. Further, the pH of a concentrated hydrochloric acid solution is expected to be very low because of the high concentration of H^+ in it. A solution having a high chloride concentration and low pH at an elevated temperature (e.g., 75°C) can be as corrosive as the critical crevice solution, which is generally considered responsible for causing the dissolution of the passive film on the creviced metal. Alloy 22 corrosion rates of 5 and 50 mils/yr (i.e., 127 μm/yr and 1,270 μm/yr) (Haynes International 1997 [DIRS 100896], p. 12) were obtained by exposing Alloy 22 specimens to such a highly corrosive solution (i.e., a solution having low pH, high chloride concentration, and high temperature). Of these two corrosion rates of Alloy 22 obtained in this environment, the higher corrosion rate of 50 mils/yr (i.e., 1,270 μm/yr) is conservatively used in this report as the upper bound for Alloy 22 crevice corrosion penetration rate.

Although some other higher corrosion rates are shown in the cited reference, the chosen rates are considered high enough to adequately represent the localized corrosion penetration rate of Alloy 22 for modeling purposes. A 25-mm-thick Alloy 22 barrier would be penetrated in 20 to 2,000 years using the upper and lower bound values of the penetration rate. Therefore, these

rates are considered sufficient for their intended use. It is possible that the "true" localized corrosion penetration rates in local areas could be higher than those normally observed during uniform dissolution. However, the literature data discussed above were obtained from short-term tests conducted by exposing Alloy 22 specimens to highly corrosive solutions (e.g., hot concentrated HCl). Since the localized corrosion penetration rate generally decreases with increasing time (Section 6.4.4.8.2), initial uniform dissolution rates of Alloy 22 obtained in a very aggressive solution, such as concentrated HCl at an elevated temperature of 75°C, could be at least as high as the average crevice corrosion penetration rate on Alloy 22. Therefore, the above rates are appropriate for use in the long-term localized corrosion degradation analysis of Alloy 22.

Based on these data, as shown in Table 6-15, the localized corrosion penetration rates for the WPOB are modeled in a range from 12.7 to 1,270 μm/yr with the median value of 127 μm/yr. A log-uniform distribution between the bounds was chosen for the localized corrosion penetration rate. The rationale for this selection is that the penetration rate values from the literature span three orders of magnitude, and the percentiles provided are consistent with a log-uniform distribution. This statistical distribution is recommended for use in situations where the upper and lower bounds of the distribution are known and the upper bound value is greater than the lower bound value by multiple orders of magnitude, but a low state of knowledge exists about how the parameter value (e.g., penetration rate) varies between these bounds (Mishra 2003 [DIRS 163603], Section 2.3). This distribution is based on data that bound those extreme penetration rates found in the literature and that are a highly conservative representation of localized corrosion rates of Alloy 22 for the exposure conditions expected in the postclosure repository. The entire variance in the penetration rate is attributed to uncertainty.

Table 6-15. Distribution of Localized Corrosion Rates for Alloy 22

Percentile	Localized Corrosion Rate (μm/yr)
0th	12.7
50th	127.0
100th	1,270.0

Output DTN: MO0703PAGENCOR.001, file: *LC_Propagation.pdf*.

6.4.4.8 Alternative Conceptual Models for Localized Corrosion

ACMs are based on modeling assumptions and simplifications different from those employed in the model. An important reason for considering ACMs is to help build confidence that changes in modeling assumptions or simplifications will not change conclusions regarding subsystem and total system performance. Conceptual model uncertainty results from limited experimental data and a lack of available information to corroborate or refute plausible alternative interpretations of the subsystem and the processes occurring within the subsystem. This section discusses the ACMs for the localized corrosion models of the WPOB.

6.4.4.8.1 Temperature-Based Localized Corrosion Initiation Criterion

Localized corrosion of the WPOB is modeled with two model components: an initiation model and a propagation model. Localized corrosion of the WPOB occurs when the open-circuit corrosion potential (E_{corr}) is equal to or greater than a critical potential (the crevice repassivation

potential (E_{rcrev}) in this report), that is, ΔE ($=E_{rcrev} - E_{corr}$) ≤ 0. This conceptual model of localized corrosion initiation is recognized by the corrosion community (e.g., Dunn et al. 2005 [DIRS 178451] and Beavers et al. 2002 [DIRS 158781], Section 8.3). The ΔE criterion was developed on the basis of information found throughout the corrosion science literature (Böhni 2000 [DIRS 164137], Section B; Dunn et al. 2000 [DIRS 164495]; Dunn et al. 2003 [DIRS 164138]; Frankel 1998 [DIRS 162216]; Frankel 2002 [DIRS 164140]; Frankel and Kelly 2002 [DIRS 164141]). Exposure conditions in the repository will evolve with time, making it necessary to know E_{corr} and E_{rcrev} as a function of key environmental parameters.

An alternative parameter that can be used to determine susceptibility to localized corrosion is temperature. The evolution of waste package temperature with time can be calculated with reasonable certainty and used in conjunction with a critical temperature for the initiation of localized corrosion (pitting/crevice corrosion) to determine when localized corrosion may occur.

The use of critical temperatures for localized corrosion is well documented (Frankel 1998 [DIRS 162216]), and values of critical pitting temperature and critical crevice corrosion temperature have been measured for a series of alloys, including Alloy 22, in relatively pure concentrated chloride solutions (i.e., high salinity, Cl^- = 24,300 μg/g (approximately 0.69 *m*), and a high Cl^--to-SO_4^{2-} ratio) (Haynes International 1997 [DIRS 100897], p. 9; McGuire et al. 1998 [DIRS 152193], Section 5.1.2). Under these corrosive conditions, the critical crevice corrosion temperature for Alloy 22 was measured to be 102°C, and for Alloy 276 to be 80°C. The critical pitting temperature for Alloy 22 was greater than 150°C, and that for Alloy 276 was 150°C. However, the test conditions are not directly relevant to the potential environments on the waste package surface. Additionally, critical temperature predictions are generally based on extrapolation of short-term behavior.

The critical temperature-based model is not recommended for use because no data relevant to repository environments are currently available to support the development of a critical temperature model. Additionally, a critical temperature-based model for localized corrosion initiation would be based on measurements in a specific environment and would not take into account the variations in the amount of corrosion-inhibiting anions such as nitrate and sulfate present in the groundwater at the repository.

6.4.4.8.2 Time-Dependent Growth Law for Localized Corrosion

The model developed in this report uses the assumption that, when localized corrosion of the WPOB occurs, it propagates at a constant (time-independent) rate (Assumption 5.4, Section 5). This assumption is highly conservative because it is known that the localized corrosion rate of many alloys can decrease with time (CRWMS M&O 1998 [DIRS 100349], Table 3-2; Hunkeler and Boehni 1983 [DIRS 162221]; McGuire et al. 1998 [DIRS 152193], Section 5.2.8; EPRI 2002 [DIRS 158069], Section 5.3.1; Frankel 1998 [DIRS 162216]; Newman and Franz 1984 [DIRS 162250]). A study by the CNWRA (He and Dunn 2006 [DIRS 176645]) showed that the crevice corrosion propagation rate of Alloy 22 can also decrease with time in a similar manner.

An ACM for the localized corrosion penetration is a time-dependent growth-law model. A growth-law model can be developed based on a combination of electrochemical and corrosion exposure measurements. A simple pitting model based on hemispherical pit growth yields a

penetration rate law given in Equation 6-42 (CRWMS M&O 1998 [DIRS 100349], Table 3-2; Hunkeler and Boehni 1983 [DIRS 162221]; McGuire et al. 1998 [DIRS 152193], Section 5.2.8):

$$D = k \cdot t^n \quad \text{(Eq. 6-42)}$$

where D is the depth of penetration, t is time, and k is a growth constant. The growth constant depends on the properties of the material, particularly its susceptibility to anodic dissolution in the acidic environment prevailing in a propagating localized corrosion site. The time exponent, n, would be about 0.5 for pit growth that is both diffusion-controlled (i.e., the rate determined by diffusion of metal ions out of the pit) and ohmically controlled (i.e., the rate determined by the ohmic potential drop that develops in the electrolyte in the pit) (McGuire et al. 1998 [DIRS 152193], Section 5.2.8). The above model was used in a separate analysis for the repository by EPRI (2002 [DIRS 158069], Section 5.3.1).

This pit penetration law has been discussed by Frankel (1998 [DIRS 162216]) in terms of a pit growth current density (i) proportional to the inverse square root of time (i.e., $i \propto t^{-1/2}$) in potentiostatic electrochemical experiments. Hunkeler and Boehni (1983 [DIRS 162221]) have shown that this growth law is obeyed for both the pitting and crevice corrosion of stainless steels. Newman and Franz (1984 [DIRS 162250]) have also observed a similar relationship for pitting of stainless steel.

When trying to adapt such a law for repository-type applications, two main problems arise: (1) insufficient penetration-rate data are available, especially for relatively new materials such as Alloy 22, to determine values of k and n; and (2) the factors that control the form of this apparently simple growth law are complex and, at best, only qualitatively understood. In order to determine values of k and n, it is necessary to employ short-term experiments in which the pit growth process is accelerated electrochemically. In these experiments, those features of the propagation process that enhance growth (the development of critical chemistry; the evolution of pit geometry) are dominant. However, it is necessary to predict penetration behavior after long periods of exposure, when those factors that limit growth (potential drop, loss of critical chemistry, evolution of metallurgical factors, polarization of cathodic processes) are more important.

The literature data available for less corrosion-resistant materials than Alloy 22 (e.g., carbon steel and stainless steel) (Hunkeler and Boehni 1983 [DIRS 162221]; Marsh et al. 1991 [DIRS 162234]; Mughabghab and Sullivan 1989 [DIRS 162235]; Sharland et al. 1991 [DIRS 162238]; Ishikawa et al. 1991 [DIRS 162222]) clearly show that a penetration growth law of the form of Equation 6-42 is appropriate, and that a value of n = 0.5, the theoretically predicted value, is justifiable. A key point with these materials is that they would be expected to undergo rapid propagation. Providing propagation is not stifled by the accumulation of corrosion product deposits or slow cathodic kinetics, it would be limited by diffusive or ohmic effects, leading to a value of n approaching 0.5.

By contrast, for highly corrosion-resistant materials such as Alloy 22 designed to resist localized corrosion, metallurgical features will be more important in determining the value of n. One example of such a metallurgical influence that is pertinent to the case of Alloy 22 is the ability of molybdenum to decrease the pitting current densities in stainless steels, possibly by reducing the

active dissolution rate within the pit (Frankel 1998 [DIRS 162216]; Newman 1985 [DIRS 162251]). This prevents the maintenance of the critical pit or crevice chemistry required to sustain propagation, leading to repassivation. Again, the *n* value in the growth law in Equation 6-42 would effectively tend to zero. This is supported by the observations of Kehler and Scully (2005 [DIRS 177529]), who showed that the depth of crevice penetration for Alloy 22 electrochemically driven in extremely saline solutions (containing 5 *M* LiCl, 0.26 *M* Na_2SO_4, 0.24 *M* $NaNO_3$ and 0.20 *M* HCl) of pH 2.75 at temperatures ranging from 60°C to 85°C was less than 100 μm. The adoption of such a value considers that metallurgical features, such as the influence of molybdenum on pit/crevice propagation, will suppress penetration.

Investigators at the CNWRA initiated crevice corrosion on Alloy 22 specimens by adding 2×10^{-4} *M* $CuCl_2$ solution to 5 *M* NaCl solution at 95°C. They observed that crevice corrosion penetration rates on Alloy 22 decreased significantly with time due to stifling and arrest (He and Dunn 2006 [DIRS 176645]). They found the lowest value of the time exponent (i.e., *n* in Equation 6-42) to be 0.233. The deepest penetration observed in these experiments was 310 μm in 70 days. The maximum penetration on Alloy 22 specimens in 10,000 years by crevice corrosion in 5 *M* NaCl solutions containing 2×10^{-4} *M* $CuCl_2$ at 95°C was calculated to be 5.3 mm (He and Dunn 2006 [DIRS 176645], Figure 11). This means a maximum of about 20% of a 25-mm-thick Alloy 22 container could be penetrated in 10,000 years by crevice corrosion in a chloride-containing acidic solution without nitrate at 95°C.

Localized corrosion rate data are needed to obtain a value for *k*. The only presently available source of crevice corrosion rate data is that published by Haynes International (1997 [DIRS 100897]) and summarized in Table 22 of Gdowski (1991 [DIRS 100859]). These data were recorded in 10 wt % $FeCl_3$ (i.e., under extremely aggressive oxidizing conditions).

The localized corrosion growth-law model of the form of Equation 6-42 is not used in the TSPA because of lack of data relative to the values of the model parameters, *n* and *k*, for Alloy 22 for the exposure conditions relevant to the repository. The base-case model (i.e., the time-independent constant penetration rate model) is much more conservative than the growth-law model. The model should bound the penetration rate range for localized corrosion of the WPOB when it occurs.

6.4.4.8.3 Estimation of the Minimum Waste Package Surface Area Subject to Crevice Corrosion

In the localized corrosion model developed in this report, the area of the Alloy 22 WPOB that is contacted by seepage is potentially subject to localized corrosion. In this section, an alternative conceptual model is developed to estimate of the minimum waste package area subject to crevice corrosion processes. The maximum available area for localized corrosion is the area of the waste package wetted by seepage. The minimum waste package creviced surface area is determined based on the waste package-to-emplacement pallet contact area. Considering the geometry of physical contact between the waste package and the emplacement pallet (i.e., the waste package support material), as represented by the schematic in Figure 6-53, the minimum area which may undergo crevice corrosion can be estimated as discussed below.

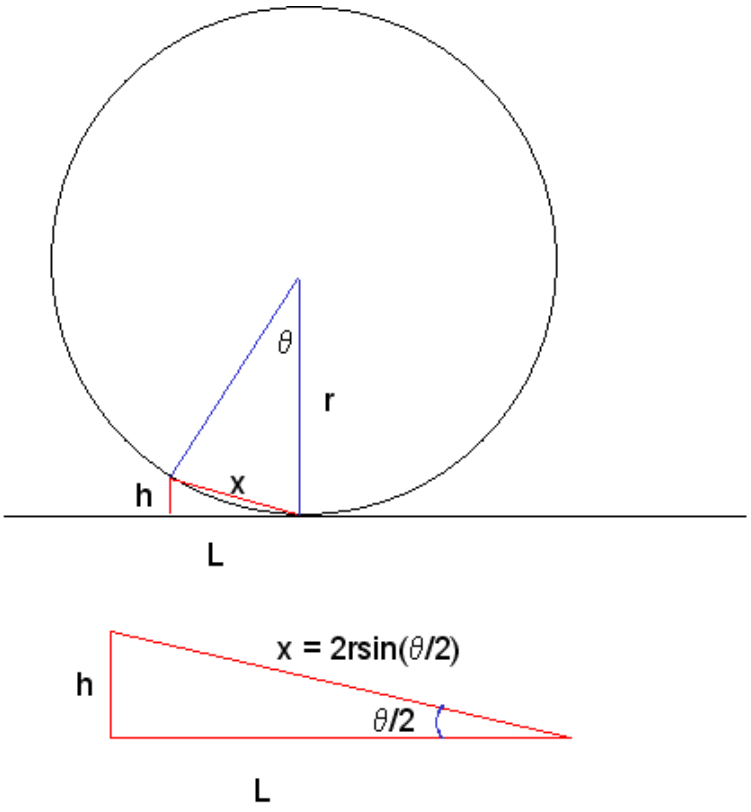

Output DTN: MO0612WPOUTERB.000, file: *PalletArea.pdf*.

Figure 6-53. Schematic of Waste Package-to-Pallet Contact

From Figure 6-53, $\sin(\theta/2) = x/(2r) = h/x$, where x is the length of the minimum waste package-to-pallet contact area and r is the waste package radius; thus, $x = \sqrt{2hr}$. In this analysis, h is considered the maximum crevice-mouth dimension where crevice corrosion could occur. According to *Analysis of Dust Deliquescence for FEP Screening* (SNL 2007 [DIRS 181267], Section 6.4.3.2), in order to compete with dust layers for brine, a waste package crevice would have to have a crevice-mouth dimension of about 1 µm. Based on analyses presented in *Analysis of Dust Deliquescence for FEP Screening* (SNL 2007 [DIRS 181267], Section 6.4.3.2; DTN: LB0503DUSTPCAP.001 [DIRS 173259], file: *Capil_Bundle.xls*), 10 µm is a conservative value for this parameter. The conservatism arises from the fact that h = 10 µm will correspond to a much greater calculated value of the minimum waste package creviced surface area (i.e., waste package-to-pallet contact area) than that corresponding to h = 1 µm. As the pallet on which the waste package is emplaced in the repository is composed of two pedestals each with two contact areas having a width of w, the total minimum waste package-pallet contact area (A) can be calculated from the equation, $A = 8wx$. Using w = 542.9 mm (SNL 2007 [DIRS 179354], Table 4-3), h = 10 µm and $r = \frac{1{,}962.8}{2}$ mm, where 1,962.8 mm is the diameter of the TAD-canister waste package configuration of 5,850.1 mm in length (SNL 2007 [DIRS 179394], Table 4-2), the calculated minimum waste package-pallet contact area is 1.924×10^4 mm^2. Therefore, the minimum creviced area is about 0.05% of the total waste package surface area of 36.074 m^2 for the TAD canister-bearing waste package configuration.

The lower and upper bound values of the creviced area should be distributed uniformly between 0.05% and the percentage of the waste package surface area wetted by seepage, if both values are in the same order of magnitude. The choice of a uniform distribution is appropriate because this statistical distribution is recommended (Mishra 2003 [DIRS 163603], Section 2.3) when the upper and lower bounds of the distribution are known reasonably well but only a low state of knowledge exists about how the values (i.e., the minimum area subject to crevice corrosion) vary between these two bounds. However, if the maximum wetted area is one order of magnitude (or more) greater than the minimum value (i.e., 0.05%), then a log-uniform distribution will be used (Mishra 2003 [DIRS 163603], Section 2.3). Consistent with the aforementioned low state of knowledge, the variation in the waste package minimum area subject to crevice corrosion is considered solely due to uncertainty.

6.4.5 Microbially Influenced Corrosion

MIC of a susceptible material (e.g., a metal or alloy) may be defined as enhanced corrosion of that material due to the metabolic activities of microorganisms. Some microorganisms can affect the corrosion behavior of a metal (or an alloy) by acting directly on its surface or by generating metabolic products that are aggressive to a metal. Most often MIC occurs due to an increase in the rate(s) of anodic or cathodic reaction(s) on the metal or alloy via indirect chemical effects of metabolic products of microorganisms on the surrounding aqueous environment. For example, some aerobic bacteria may produce sulfuric acid by oxidizing reduced forms of sulfur (e.g., elemental sulfur, sulfide, sulfite and thiosulfate) and thereby increase the corrosivity of the environment. Certain fungi can increase the acidity, and hence corrosivity, of an environment by transforming organic matter into organic acids (Fontana 1986 [DIRS 100890], Section 8-10). Bacterial isolates from Yucca Mountain have been reported to be capable of iron oxidation, acid production, sulfate reduction, and slime generation (Lian et al. 1999 [DIRS 110238]).

Evaluation of Potential Impacts of Microbial Activities on Drift Chemistry (BSC 2004 [DIRS 169991], Section 7.1) categorizes microorganisms into one of two broad groups based on different nutritional requirements:

- *Heterotrophs*, which use organic carbon compounds as their carbon and energy source
- *Autotrophs*, which derive their metabolic energy from the oxidation of inorganic compounds and cell carbon from CO_2.

The development of both groups of microorganisms will likely be limited within the in-drift environment at Yucca Mountain. The organic carbon supply in the repository will be extremely low, as Yucca Mountain groundwater contains only a trace concentration of organic carbon. The scarcity of organic carbon in the repository will be an important limiting factor in the growth of heterotrophs. Similarly, autotrophic microbial growth will be limited by the lack of available inorganic electron donors in the oxic repository environment (BSC 2004 [DIRS 169991], Section 7.1).

6.4.5.1 Impact of Relative Humidity on Microbially Influenced Corrosion

Most microbes can thrive only when the relative humidity is above 90%, although some microbes can be active at a relative humidity as low as 75% (BSC 2004 [DIRS 169991], Section 7.1). *Evaluation of Potential Impacts of Microbial Activities on Drift Chemistry* (BSC 2004 [DIRS 169991], Section 7.1) recommends the use of 90% relative humidity as the threshold above which microbial activity will affect the degradation of the WPOB (i.e., the MIC relative humidity threshold); however, the observation of microbial activity at relative humidities as low as 75% suggests that an appropriate uncertainty treatment for this parameter would be to adopt the use of a uniform distribution between 75% relative humidity and 90% relative humidity. This choice of MIC relative humidity threshold distribution is conservative because other factors such as limited nutrient supplies will also constrain microbial activity (BSC 2004 [DIRS 169991], Section 7.1). A uniform distribution has been chosen for the MIC relative humidity threshold because this statistical distribution is recommended when the upper and lower bounds of the distribution are reasonably well known, as discussed above, but only a low state of knowledge exists about how the MIC relative humidity threshold varies between these bounds (Mishra 2003 [DIRS 163603], Section 2.3). Consistent with the aforementioned low state of knowledge, the variation in the MIC relative humidity threshold is considered solely due to uncertainty.

6.4.5.2 Electrochemical Evaluation of Microbially Influenced Corrosion in the Presence of Yucca Mountain Bacteria

There are no standard tests designed specifically to investigate the susceptibility of an engineering alloy to MIC (Stoecker 1987 [DIRS 162243]). One commonly used method to evaluate the effect of MIC is to test the alloy of interest in the field using the same variables as for the intended application. However, testing in the laboratory with live organisms can provide more control of environmental variables, and sterile controls can be incorporated to better assess MIC-specific effects (Horn and Jones 2002 [DIRS 162220]). The latter approach (i.e., laboratory testing) was used to evaluate the effects of microbiological processes on general corrosion of the WPOB.

Lian et al. (1999 [DIRS 110238]) measured the polarization resistance of Alloy 22 in the presence and absence of Yucca Mountain bacteria. Other researchers have reported isolating over 1,100 discrete strains of bacteria from springs near the Yucca Mountain site (Yang et. al. 2004 [DIRS 178563], Section 3.2). In the study by Lian et al. (1999 [DIRS 110238]), a series of 12 strains of Yucca Mountain bacteria, including acid and slime producers, sulfate reducers, and iron-oxidizers were cultured from material taken from the Yucca Mountain site. The growth medium consisted of 100× concentrated simulated J-13 well water, augmented with 0.5% glucose and 0.75% protease peptone (Lian et al. 1999 [DIRS 110238]). All measured current was conservatively considered to result from metal oxidation, and the obtained polarization resistance was converted to a corrosion rate (Table 6-16). These results indicate that the presence of Yucca Mountain bacteria may enhance the general corrosion rate of Alloy 22 if the bacteria are provided sufficient nutrients and appropriate exposure conditions.

Electrochemical tests were performed to obtain corrosion rates for welded Alloy 22 coupons exposed to 100× J-13 well water plus 0.1% glucose at ambient temperature

(DTN: LL040402912251.085 [DIRS 170222]). The testing was carried out in both Yucca Mountain microorganism-inoculated and sterile environments following ASTM G 59-97 (1998 [DIRS 163907]), *Standard Test Method for Conducting Potentiodynamic Polarization Resistance Measurements.* Again, the interfacial reaction was conservatively considered to be entirely due to metal oxidation. The tests were run for periods ranging from 70 days to 125 days at room temperature. This testing is conservative because the test environment contained 0.1% glucose as an additional nutrient for the bacteria, and there is no glucose supply in the Yucca Mountain repository. The results (Figure 6-54) show that the corrosion rates obtained for welded coupons in nonsterile environments are only slightly higher than those in sterile environments and are consistent with the corrosion enhancement observed in the mill-annealed coupon data (see Table 6-16). The YMP data further show that the corrosion rates for welded coupons are essentially the same as those for mill-annealed coupons.

Table 6-16. Alterations in Corrosion Rates of Mill-Annealed Alloy 22 Associated with Microbial Degradation at Room Temperature

Tested Sample Initial Condition	Average Corrosion Rate (μm/yr)
Alloy 22 + Yucca Mountain Microbes	0.022
Sterile Alloy 22	0.011

Source: DTN: LL991203505924.094 [DIRS 138343], SEP table S99502_001.

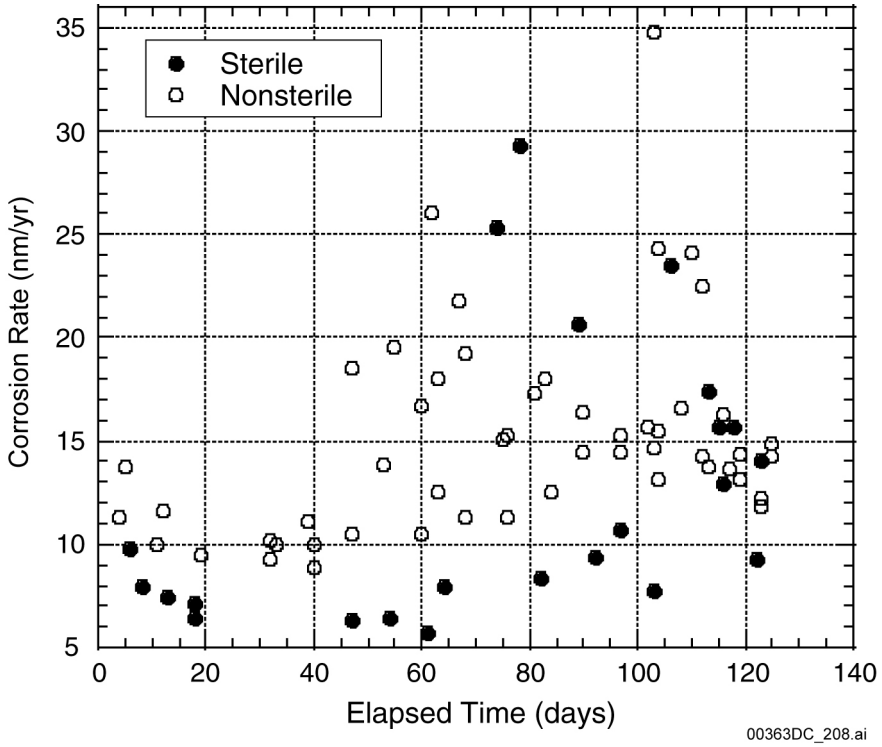

Source: DTN: LL040402912251.085 [DIRS 170222].

Figure 6-54. Corrosion Rates Determined by Polarization Resistance Testing of Welded Alloy 22 Coupons

MIC testing was also performed by incubating Alloy 22 coupons with sterile or unsterilized Yucca Mountain rock in simulated concentrated (10×) groundwater (i.e., J-13 well water) with 0.1% glucose for almost five years (Martin et al. 2004 [DIRS 175394]; DTN: LL040303612251.078 [DIRS 170221]). The vessels were held at either 22°C or 30°C. SEM micrographs of unexposed, sterile control, and nonsterile samples exposed at 22°C are shown in Figure 6-55.

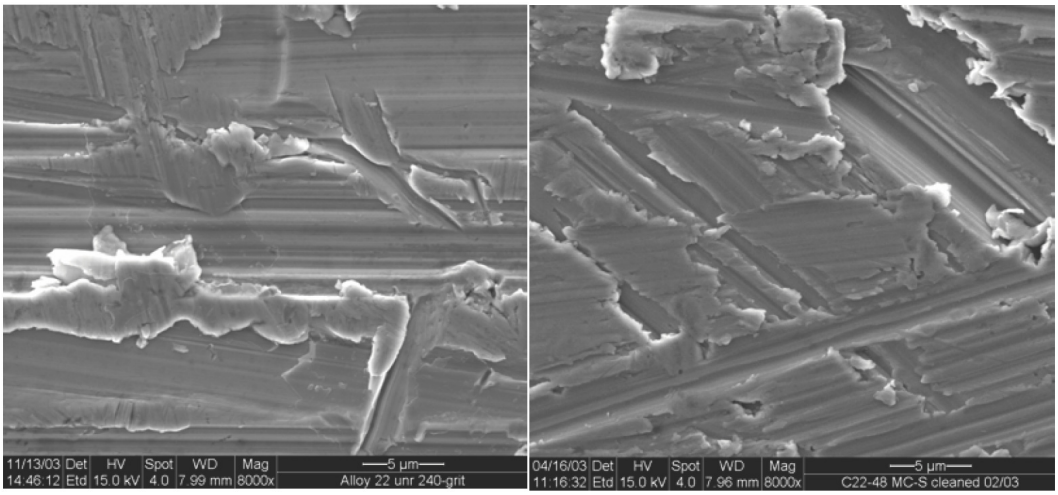

Source: Reproduced from Martin et al. 2004 [DIRS 175394], Figure 7.

NOTE: Coupons were (a) unincubated/non-reacted, (b) exposed for 43 months in a sterile microcosm, and (c) exposed for 57 months in a nonsterile microcosm.

Figure 6-55. Comparison of Scanning Electron Microscopy–Imaged Alloy 22 Coupons (8,000× magnification)

Coupons incubated in the non-sterile microcosm reactors developed micropits, primarily along the ridges formed by polishing, while coupons incubated in sterile microcosms and those that

were not reacted in microcosms showed no evidence of micropit formation. The mouth of the typical micropit was less than one micron in diameter. Coupons analyzed prior to cleaning contained a micropit density similar to those that were cleaned. Micropits in coupons exposed at 22°C were filled with deposited or precipitated minerals, while those formed at 30°C appeared to be empty. Polishing marks were still evident on both sterile and nonsterile sample surfaces even after about five years of exposure. Atomic force microscopy and SEM analyses indicate that the overall surface roughness of the nonsterile coupons decreased as a function of exposure time, even as microscale roughness increased due to the micropits (Martin et al. 2004 [DIRS 175394]). The depth of the micropits was not characterized.

6.4.5.3 Incorporation of the Impact of Microbially Influenced Corrosion on the Corrosion of the Waste Package Outer Barrier

As illustrated in Section 6.4.5.2, MIC resulting from strains of bacteria taken from the Yucca Mountain site resulted in a reduction in the microscopic surface roughness of exposed Alloy 22 samples, as well as formation of a uniform distribution of micropits across the metal surface. For both types of degradation, the damage is confined to the surface of the Alloy 22 sample (i.e., no deep-penetrating attack has been observed to date). As such, the impact of MIC on Alloy 22 is represented by an amplification factor applied directly to the abiotic general corrosion rate.

Based on the results in Table 6-16, an MIC general corrosion enhancement factor, f_{MIC}, is calculated as the ratio of the general corrosion rates (microbes to sterile). The value of f_{MIC} for Alloy 22 in sterile media is 1 ($f_{MIC} = 1$), whereas the value of f_{MIC} for Alloy 22 in inoculated media is 2 ($f_{MIC} = 2$). The effect of MIC is then described by Equation 6-43:

$$CR_{MIC} = CR_{st} \cdot f_{MIC} \quad \text{(Eq. 6-43)}$$

where CR_{MIC} is the general corrosion rate in the presence of microorganisms, CR_{st} is the general corrosion rate of the alloy in the absence of microorganisms, and f_{MIC} is the MIC general corrosion enhancement factor.

Although it has been reported that a spatial heterogeneity in the distribution of microbial communities in the repository is likely (Yang et al. 2004 [DIRS 178563], Section 4.1.3), no data are currently available regarding the composition of the bacterial community over the changing environmental conditions anticipated during repository evolution. This issue has been addressed in the current Alloy 22 degradation model by determining overall corrosion rates under a standardized set of conditions, in the presence and absence of a defined set of characterized Yucca Mountain bacteria.

Since soil is naturally heterogeneous, the availability of chemical species that can be used as substrates and/or nutrients by the microorganisms is expected to vary spatially in the repository. Further, the nuclear wastes contained in various waste packages will differ in radioactive decay rate. As a result, the WPOB surface temperature will exhibit spatial variation. The spatial variation of temperature and soil water content together, in turn, will cause spatial variation of the quantity of aqueous solutions contacting the WPOB surface. Moreover, moderate wettability of Alloy 22 by water will also lead to the formation of patchy water film on the WPOB surface. Thus, the fundamental factors controlling microbial cell growth, such as water, nutrient supplies,

and temperature, will vary spatially within the repository. Consequently, the concentration of microbial cells will vary spatially within the repository, as will the effect of microbial activity on corrosion of the WPOB. Therefore, the MIC general corrosion enhancement factor for Alloy 22, f_{MIC}, is expected to vary spatially in the repository.

Based on experimental results obtained using YMP bacteria, as mentioned above, the MIC general corrosion enhancement factor for Alloy 22 (i.e., f_{MIC}) is chosen to have values uniformly distributed between 1 and 2, and the variance of this distribution is attributed to variability of the corrosion rate among various areas or patches on the Alloy 22 comprising the WPOB surface. A uniform distribution has been chosen for the MIC enhancement factor for Alloy 22, because this statistical distribution is recommended for use in situations where the upper and lower bounds of the distribution are reasonably well known, as discussed above, but only a low state of knowledge exists about how the MIC general corrosion enhancement factor varies between these bounds (Mishra 2003 [DIRS 163603], Section 2.3).

6.4.6 Fabrication Effects on the Corrosion Susceptibility of Alloy 22

6.4.6.1 Effects of Thermal Aging on the Corrosion Behavior of Alloy 22

The WPOB base metal and all fabrication welds (not including the welds for the closure lid) are to be fully solution-annealed before the waste packages are loaded with waste (SNL 2007 [DIRS 179394], Section 4.1.2). Analyses documented in *Aging and Phase Stability of Waste Package Outer Barrier* (BSC 2004 [DIRS 171924], Section 8) demonstrate that repository thermal hydrologic exposure conditions will not significantly impact the performance of Alloy 22 base metal and welded material in the repository. At equilibrium, Alloy 22, at its nominal compositions and at low temperatures, should exhibit, besides the face-centered cubic matrix, a long-range order of Ni_2Cr-type, complex Frank–Kasper phases (e.g., the P phase), carbides and silicides. The kinetics of long-range order formation at relatively low temperatures does not favor formation of ordered phases of the Ni_2Cr-type, since the phase formation kinetics are primarily driven by diffusion. Alloys homogenized (or annealed) at high temperatures and quenched at relevant repository conditions should not display any deleterious phases (BSC 2004 [DIRS 171924], Section 8). Extrapolation of computationally derived time/temperature/transformation curves to lower temperatures, which bound repository time/temperature profiles, indicates that forming the P- or oP6-ordered phases from the face-centered-cubic solid solution will not be a concern (BSC 2004 [DIRS 171924], Section 8). Minor compositional changes in Alloy 22 are also expected to have little or no effect on the rate of precipitation (BSC 2004 [DIRS 171924], Section 8). The quantities of carbide and σ phases tended to be low in the Alloy 22 specimens examined. Therefore, the formation of these phases is not likely to significantly impact the overall performance of the WPOB (BSC 2004 [DIRS 171924], Section 8). The average precipitation area fraction of as-welded Alloy 22 specimens was determined to be 0.16% (DTN: LL030103612251.006 [DIRS 162012], file: *Haynes_Weld_Area_Fraction.xls*).

Nonthermal stress-mitigation processes, currently planned for the outer lid closure weld, may introduce cold work into the material. Angeliu (2001 [DIRS 165442]) observed that unmitigated Stainless Steel Type 316NG weldments could contain up to 20% cold work due to weld shrinkage and differential thermal expansion. Therefore, it is reasonable to consider that welded

Alloy 22 specimens also have up to 20% cold work. Given that the phase instability analysis included welded Alloy 22 samples, the effects of moderate amounts of cold work have been accounted for in the analysis as well.

Project data show that the corrosion properties of weldments that had been thermally aged for 173 hours at 700°C are comparable to those of unaged welds. In order to analyze the effect of thermal aging on the corrosion of Alloy 22, three metallurgical conditions of Alloy 22 were studied at the LTCTF, using the MCA samples: mill-annealed, as-welded, and as-welded plus thermally aged (at 700°C for 173 hours). The samples were tested in 5 *M* $CaCl_2$ and 5 *M* $CaCl_2$ + 0.5 *M* $Ca(NO_3)_2$ solutions with the test temperatures up to 120°C. As described in Appendix I, after being immersed in the test solution in an open-circuit condition for 24 hours, the polarization resistance of the samples was measured.

Comparison of the calculated corrosion rates of the mill-annealed, as-welded, and as-welded plus thermally aged samples is shown in Figure 6-56 for 5 *M* $CaCl_2$ solutions and Figure 6-57 for 5 *M* $CaCl_2$ + 0.5 *M* $Ca(NO_3)_2$ solutions. As discussed earlier (Sections 4.1.1.4 and 6.4.3.4), corrosion rates from polarization resistance measurements are only for comparative analysis of the effect of thermal aging on corrosion rates; the tests are not intended to be used to obtain absolute values of the corrosion rate. The absolute values of the general corrosion rates of Alloy 22 are determined from weight-loss measurements, as discussed in Section 6.4.3.4. The mill-annealed MCA samples in 5 *M* $CaCl_2$ solutions at differing temperatures were considered the baseline condition for analysis. The baseline condition rates were compared with those of the as-welded and as-welded plus thermally aged MCA samples tested in the same electrolyte solution condition. The comparison shown in Figure 6-56 clearly demonstrates that there is no significant enhancement of the corrosion rate attributable to welding or thermal aging of the welded samples for the tested conditions.

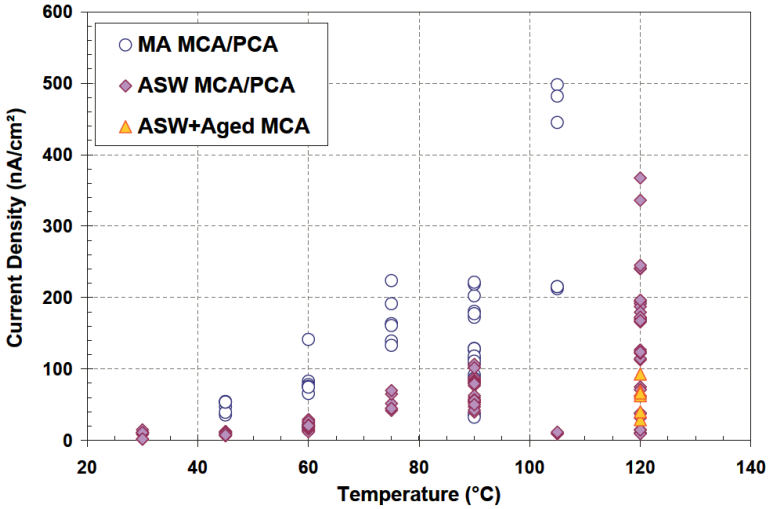

Source: DTN: LL060900812251.180 [DIRS 178409], file: *176PRFit.xls*.

Output DTN: MO0612WPOUTERB.000, file: *Aging.xls*.

Figure 6-56. Comparison of Corrosion Rates from Polarization Resistance Measurements of Mill-Annealed, As-Welded, and As-Welded Plus Aged Alloy 22 Multiple Crevice Assembly and Prism Crevice Assembly Samples in 5 *M* $CaCl_2$ Brines at Varying Temperatures

A similar comparison was made for the corrosion rates measured in 5 *M* $CaCl_2$ + 0.5 *M* $Ca(NO_3)_2$ solutions, as shown in Figure 6-57. As for the 5 *M* $CaCl_2$ solution case, the mill-annealed MCA samples at differing temperatures were considered the baseline condition. The comparison in Figure 6-57 again clearly shows no significant enhancement of the corrosion rate due to welding or thermal aging of the welded samples.

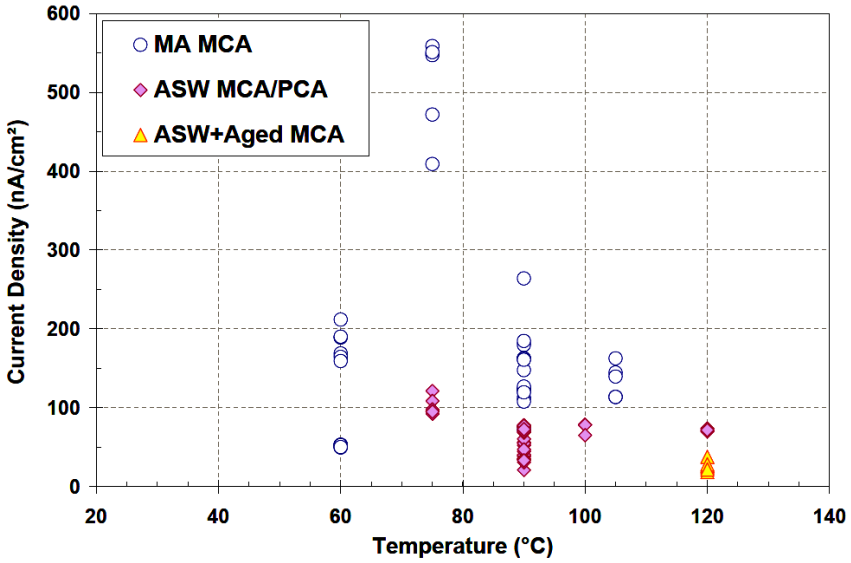

Source: DTN: LL060900812251.180 [DIRS 178409], file: *PRFit189.xls*.

Output DTN: MO0612WPOUTERB.000, file: *Aging.xls*.

Figure 6-57. Comparison of Corrosion Rates from Polarization Resistance Measurements of Mill-Annealed, As-Welded, and As-Welded Plus Aged Alloy 22 Multiple Crevice Assembly and Prism Crevice Assembly Samples in 5 *M* $CaCl_2$ + 0.5 *M* $Ca(NO_3)_2$ Brines at Varying Temperatures

Results reported in the published literature are consistent with the analyses shown in Figure 6-56 and Figure 6-57. Comparisons of the anodic passive current densities of as-welded Alloy 22 samples to those of base metal samples have shown no significant effect of the presence of welds on the passive current density, obtained by polarization resistance, of the alloy (Brossia et al. 2001 [DIRS 159836], Section 3.2.1.3, Figure 3-13). Rebak et al. (2002 [DIRS 162237]) investigated the effects of high-temperature aging on the corrosion resistance of Alloy 22 in concentrated multi-ionic solutions (e.g., SCW and SAW), concentrated oxidizing acid solutions (e.g., 50% sulfuric acid + 42 g/L ferric sulfate solutions), and hot reducing acid solutions (e.g., boiling 2.5% hydrochloric acid solution). The test specimens were prepared from Alloy 22 aged for a variety of times (up to 3,000 hours) at temperatures between 482°C and 760°C. These investigators found that precipitation of secondary phases at grain boundaries (due to the aging treatments) was detrimental to the corrosion resistance of Alloy 22 in aggressive acidic solutions but did not significantly affect the corrosion resistance in concentrated multi-ionic solutions, which are more relevant to the exposure conditions expected in the Yucca Mountain repository (Rebak et al. 2002 [DIRS 162237]).

Based on the above analysis and insignificant aging and phase instability processes under the thermal conditions expected in the repository (BSC 2004 [DIRS 171924], Section 8), the

corrosion performance of the WPOB is not expected to be affected by the aging and phase instability in the repository. Hence, the effects of thermal aging and phase instability of the WPOB were not included in the models developed in this report.

Topologically close-packed (TCP) secondary phases that form during aging at high temperatures could reduce corrosion resistance of Alloy 22. However, these phases are not significantly enriched or depleted of chromium (CNWRA 2004 [DIRS 166948], Section 4.3.4, Table 3-2). Since the passive dissolution rate of Alloy 22 is dependent on chromium, and formation of these TCP phases during thermal aging (or welding) does not produce chromium-depleted regions, the general corrosion rate of Alloy 22 is not expected to increase significantly due to thermal aging (or welding).

Although thermal aging does not significantly increase the general corrosion rate of Alloy 22 under repository relevant aqueous conditions, it could increase the localized corrosion susceptibility of the alloy by increasing the corrosion potential (i.e., E_{corr}) of this material. An increase in E_{corr} could result from the redistribution of molybdenum during thermal aging (or welding) of Alloy 22. The TCP phases, which form preferentially at grain boundaries during the aging of Alloy 22 at higher temperatures, are rich in molybdenum (CNWRA 2004 [DIRS 166948], Section 4.3.4). Due to high concentration of molybdenum in the TCP phases, slight molybdenum depletion is expected in the adjacent matrix (CNWRA 2004 [DIRS 166948], Table 3-2). This, in turn, could potentially lead to the formation of galvanic cells with molybdenum-rich areas acting as cathodes and molybdenum-depleted areas acting as anodes. Therefore, thermal aging (or welding) could increase the susceptibility of Alloy 22 to intergranular corrosion, a form of localized corrosion (CNWRA 2004 [DIRS 166948], Section 4.3.4). Thus, the CNWRA observation of intergranular corrosion of heat treated Alloy 22 is not unexpected.

Due to the impact which TCP phases have on alloy composition near grain boundaries, the CNWRA observation of intergranular corrosion of heat-treated Alloy 22 (in agreement with Rebak et al. (2002 [DIRS 162237])) is not unexpected. The latter investigators studied the corrosion behavior of welded and thermally aged Alloy 22 in 2.5% boiling HCl (boiling point approximately 101°C) and observed intergranular corrosion. The susceptibility of Alloy 22 to intergranular corrosion in this environment was observed to increase with an increase in aging time and temperature (Rebak et al. 2002 [DIRS 162237]). However, it should be noted that both CNWRA data (CNWRA 2004 [DIRS 166948], Section 4.3.4) and YMP data (Rebak et al. 2002 [DIRS 162237]) used Alloy 22 thermally treated at temperatures of 870°C and 482°C to 760°C, respectively. Such high temperatures are unattainable at any time in the Yucca Mountain repository because the waste package surface temperature will not exceed 482°C (Figure 6-2 and Figure 6-3) and deleterious phase formation requires much longer aging times at lower temperatures (BSC 2004 [DIRS 171924], Section 6.6.4). This makes the thermal aging test results of both research groups irrelevant to the Yucca Mountain repository. Based on the same argument, the observed E_{corr} and E_{rcrev} values for heat-treated and annealed specimens (which have not had the solution-annealed film removed) in the LTCTF are also not considered repository-relevant. Therefore, the E_{corr} and E_{rcrev} values for the heat-treated and annealed specimens have been excluded during the development of current localized corrosion model for Alloy 22.

6.4.6.2 Fabrication Effects on the Crevice Corrosion Susceptibility of Alloy 22

This section deals with the analysis of the available data to study the effects of fabrication processes on the anodic behavior and crevice repassivation potential (i.e., E_{rcrev}) of Alloy 22. CPP was used to study the anodic behavior and obtain crevice repassivation potentials of Alloy 22. Experiments were performed in three representative aqueous solutions, e.g., (1) 1 *M* NaCl at 90°C, (2) 6 *m* NaCl + 0.9 *m* KNO_3 at 80°C and 100°C, and (3) 5 *M* $CaCl_2$ at 90°C to study the effects of: (1) surface stress mitigation and (2) mockup fabrication on the repassivation potential of Alloy 22. Data collected under these experimental conditions were used in developing the localized corrosion initiation model described in Section 6.4.4.

According to Hayes et al. (2004 [DIRS 178246]), the anodic dissolution rate of nonwelded and welded Alloy 22 specimens was not significantly different in 1 *M* NaCl at 90°C in acidic, neutral, and alkaline pHs. The comparable susceptibility of the weld metal and base metal to localized corrosion was demonstrated by Day et al. (2006 [DIRS 178252]) in SCW and 1 *M* NaCl for both gas tungsten arc welding (GTAW) and reduced-pressure electron beam weldments. A negligible effect of welding on the crevice repassivation potential was also observed by the CNWRA investigators (Brossia et al. 2001 [DIRS 159836], Section 3.2.2, Figure 3-19). However, at a high chloride concentration (e.g., 5 *M* $CaCl_2$), the repassivation potential of Alloy 22 is observed to decrease with an increase in temperature (up to 90°C) (Evans et al. 2005 [DIRS 178247]). The decreasing trend is more pronounced for as-welded specimens than for the mill-annealed specimens. Stress mitigation by low-plasticity burnishing (LPB) and laser-shock peening (LSP) could reduce crevice corrosion susceptibility of Alloy 22 by increasing its repassivation potential. The stress mitigation effects are discussed below in terms of the observed crossover potentials in CPP curves obtained in three representative aqueous solutions. The results of these comparisons are discussed in more detail in the following sections.

6.4.6.2.1 Crevice Repassivation Potential—Effect of Stress Mitigation

As part of the fabrication of the waste container, a stress-mitigation treatment will be applied to the final Alloy 22 WPOB closure weld. The objective of this surface treatment is to eliminate surface tensile stresses that may be detrimental to the initiation and propagation of stress corrosion cracking. From the point of view of localized corrosion resistance, it was important to determine if any stress-mitigation surface treatment considered for use on the waste package affected the resistance of Alloy 22 to localized corrosion. Two Alloy 22 plates, each 1-in-thick and approximately 16-in-long and 6-in-wide, were welded lengthwise using the GTAW process and 0.045-in-thick Alloy 22 wire for filler metal.

Two surface treatments were studied—LPB and LSP. LPB is a process by which a smooth, hard ball is rolled over the surface of the metal to be burnished imparting compressive deformation. The treatment in the studied Alloy 22 welded plates was performed in two steps using balls of two different sizes, the larger one with an effective surface area (i.e., the area in contact with the work piece) of about 0.0154 in^2 (9.94 mm^2) and the smaller one with an effective surface area of about 0.00067 in^2 (0.43 mm^2). In the first step, the larger ball was rolled at a pressure of 780 ksi to create compressive stresses to a larger depth. In the second step, the smaller ball was rolled at a pressure of 821 ksi to increase the level of compressive stresses near the surface.

LSP is a process by which a laser beam is pulsed upon a metallic surface producing a planar shockwave that travels though the work piece and plastically deforms a surface layer of material resulting in compressive stresses. The laser beam is generally applied to the work piece though a transparent overlay and an absorbent coating. A plasma forms under the overlay, increasing the pressure and therefore the compressive stresses on the treated part. The LSP treatment was performed by applying laser pulses with an energy value of 14 Joules and duration of 25 nanoseconds. Each spot dimension was approximately 2.5 mm^2.

The susceptibility of specimens that had been treated with LPB or LSP to localized corrosion was assessed using the CPP technique based on the American Society for Testing and Materials standard (ASTM G61-86 1987 [DIRS 127897]) in de-aerated solutions. The potential scan was started 100 mV below the open circuit potential at a set scan rate of 0.167 mV/s. The scan direction was reversed when the current density reached 5 mA/cm^2 in the forward scan. Depending on the range of applied potentials, each CPP test could last between one and three hours. From the polarization curve, the value of repassivation potential was obtained.

The relative resistance of Alloy 22 to localized corrosion between the nonmitigated and the mitigated surfaces was assessed by comparing the values of crevice repassivation potential (E_{rcrev}). This comparison was carried out in 1 *M* NaCl at 90°C and 6 *m* NaCl + 0.9 *m* KNO_3 at 80°C and 100°C. Appendix IX lists the crevice repassivation potentials of the unmitigated specimens used for the comparison (i.e., only unmitigated specimens which had undergone localized corrosion were used to compare to the measured repassivation potentials from the mitigated specimens). All measured crevice repassivation potentials for stress-mitigated specimens were used for these comparisons (regardless of whether the initiation of localized corrosion could be verified or not) due to the limited amount of data available for stress-mitigated specimens. However, it may be noted that no specimen for which localized corrosion initiation could not be verified was used in the development of the current crevice corrosion initiation model.

Figure 6-58 and Figure 6-59 show the average crevice repassivation potential (E_{rcrev}) for Alloy 22 as a function of type of tested material in 1 *M* NaCl at 90°C and 6 *m* NaCl + 0.9 *m* KNO_3 at 100°C. Figure 6-58 and Figure 6-59 show that the repassivation potential in both solutions was practically the same for both the surface stress-mitigated materials (LPB PCA and LSP PCA) and for the non-mitigated material (as-welded PCA) (DTN: LL040902712251.119 [DIRS 173720], file: *Reduced Data Ahmet Yilmaz WBL 11Feb05.xls*). Figure 6-58 and Figure 6-59 also show that repassivation potentials for both surface-stress-mitigated materials are comparable to those of the nonmitigated specimens (as-welded MCA and mill-annealed MCA). The same findings were reported previously (Fix et al. 2005 [DIRS 173721]). That is, surface treatments, such as LPB, do not decrease the resistance of Alloy 22 to crevice corrosion in either pure-chloride solutions or chloride-plus-nitrate solutions.

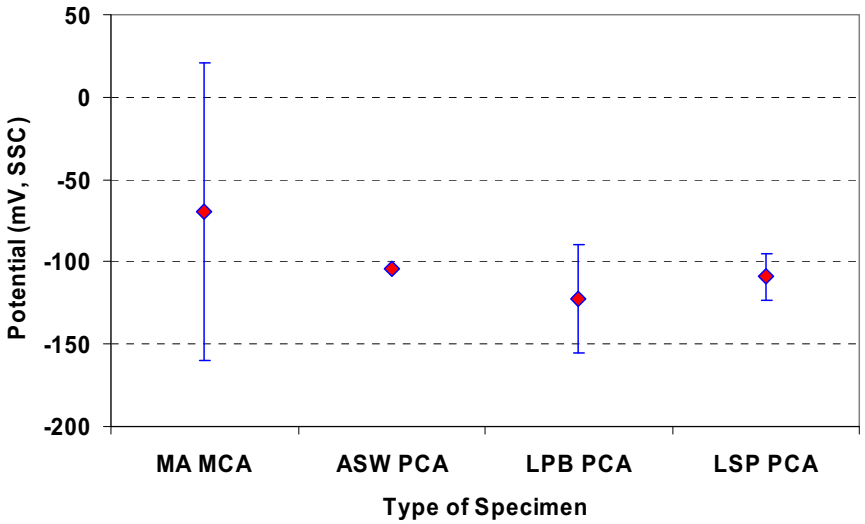

Sources: DTNs: LL060803712251.170 [DIRS 179387], file: *Rep Pot N06022 vs Temp NaCl RBR 07Oct06.xls*; LL040902712251.119 [DIRS 173720], file: *Reduced Data Ahmet Yilmaz WBL 11Feb05.xls*.

Output DTN: MO0612WPOUTERB.000, file: *Stress Mitigation.xls*.

NOTES: Error bars are 2 standard deviations.

MA = mill-annealed, ASW = as-welded, MCA = multiple crevice assembly, PCA = prism crevice assembly, LPB = low-plasticity burnishing, LSP = laser-shock peening.

Figure 6-58. Effect of Surface Stress Mitigation on the Repassivation Potential for Alloy 22 in 1 *M* NaCl at 90°C

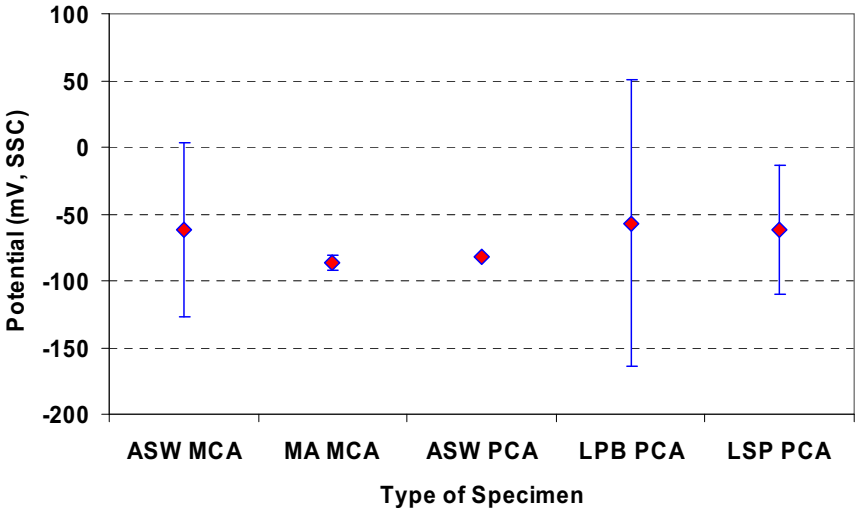

Sources: DTNs: LL060603812251.164 [DIRS 178269], file *Rep Pot N06022 vs Temp NaCl + KNO3 60-100C RBR 07Aug06.xls*; LL040902712251.119 [DIRS 173720], file: *Reduced Data Ahmet Yilmaz WBL 11Feb05.xls*.

Output DTN: MO0612WPOUTERB.000, file: *Stress Mitigation.xls*.

NOTES: Error bars are 2 standard deviations.

MA = mill-annealed, ASW = as-welded, MCA = multiple crevice assembly, PCA = prism crevice assembly, LPB = low-plasticity burnishing, LSP = laser-shock peening.

Figure 6-59. Effect of Surface Stress Mitigation on the Repassivation Potential for Alloy 22 in 6 *m* NaCl + 0.9 *m* KNO_3 at 100°C

6.4.6.2.2 Crevice Repassivation Potential – Mockup Fabrication

A full-diameter, quarter-length mockup container was fabricated in order to assess the properties of materials which had undergone the fabrication process planned for the full-sized waste packages (Gordon 2002 [DIRS 165793]). The anodic behavior and crevice repassivation potential (E_{rcrev}) for specimens from the mock-up container were evaluated in several repository-relevant environments (DTN: LL050302312251.129 [DIRS 173921]). These specimens were fabricated from samples taken from the longitudinal weld seam of the mockup containers.

The susceptibility of these specimens to localized corrosion was assessed using the CPP technique based on the ASTM standard (ASTM G61-86 1987 [DIRS 127897]) in deaerated solutions. The potential scan was started 100 mV below the open circuit potential at a set scan rate of 0.167 mV/s. The scan direction was reversed when the current density reached 5 mA/cm^2 in the forward scan. Depending on the range of applied potentials, each CPP test could last between one and three hours. From the polarization curve, the value of repassivation potential was obtained.

Appendix IX lists the crevice repassivation potentials of the unmitigated specimens used for the comparison (i.e., only specimens which had undergone localized corrosion were used to compare to the measured repassivation potentials from the mockup specimens). All measured crevice repassivation potentials for mockup specimens were used for these comparisons (regardless of whether the initiation of localized corrosion could be verified) due to the limited amount of data available for mockup specimens. Only data obtained from specimens on which localized corrosion was observed were used in the development of the crevice corrosion initiation model. Figure 6-60, Figure 6-61, and Figure 6-62 show the repassivation potentials for Alloy 22 in 1 *M* NaCl at 90°C, 6 *m* NaCl + 0.9 *m* KNO_3 at 100°C, and 5 *M* $CaCl_2$ at 90°C, respectively. The repassivation potential for the specimens prepared from the mockup container are the same as or more positive than the repassivation potentials determined from specimens prepared from laboratory plates. Because E_{corr} must exceed E_{rcrev} in order for localized corrosion to initiate, an increase in E_{rcrev} decreases the likelihood of initiating localized corrosion.

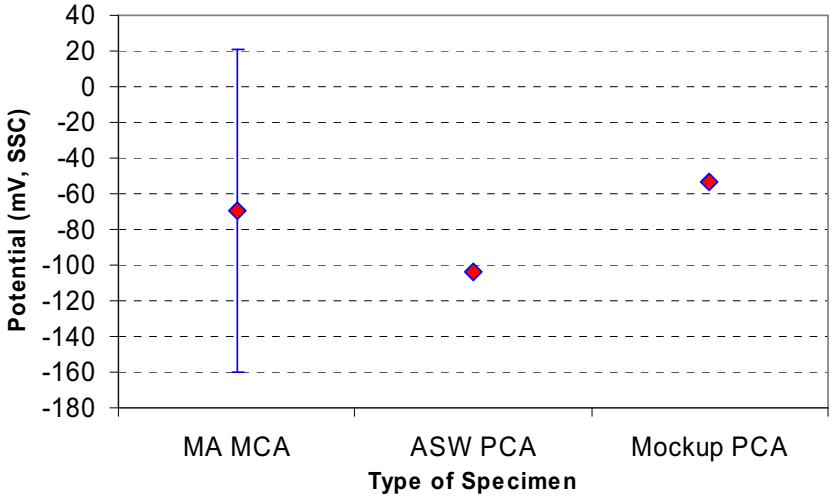

Sources: DTNs: LL060803712251.170 [DIRS 179387], file: *Rep Pot N06022 vs Temp NaCl RBR 07Oct06.xls*; LL040902712251.119 [DIRS 173720], file: *Reduced Data Ahmet Yilmaz WBL 11Feb05.xls*; LL050302312251.129 [DIRS 173921], file: *Mockup Developed RBR 21May05.xls*.

Output DTN: MO0612WPOUTERB.000, file: *Mockup.xls*.

NOTES: Error bars are 2 standard deviations.

MA = mill-annealed, ASW = as-welded, MCA = multiple crevice assembly, PCA = prism crevice assembly.

Figure 6-60. Repassivation Potentials for Alloy 22 Specimens Fabricated from a Mockup Container in 1 *M* NaCl at 90°C

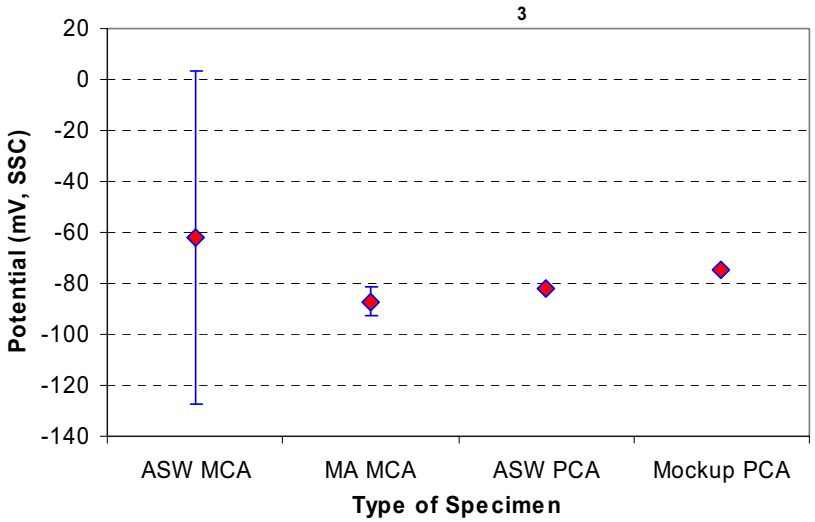

Sources: DTNs: LL060603812251.164 [DIRS 178269], file *Rep Pot N06022 vs Temp NaCl + KNO3 60-100C RBR 07Aug06.xls*; LL040902712251.119 [DIRS 173720], file: *Reduced Data Ahmet Yilmaz WBL 11Feb05.xls*; LL050302312251.129 [DIRS 173921], file: *Mockup Developed RBR 21May05.xls.*

Output DTN: MO0612WPOUTERB.000, file: *Mockup.xls*.

NOTES: Error bars are 2 standard deviations.

MA = mill-annealed, ASW = as-welded, MCA = multiple crevice assembly, PCA = prism crevice assembly.

Figure 6-61. Repassivation Potentials for Alloy 22 Specimens Fabricated from a Mockup Container in 6 *m* NaCl + 0.9 *m* KNO_3 at 100°C

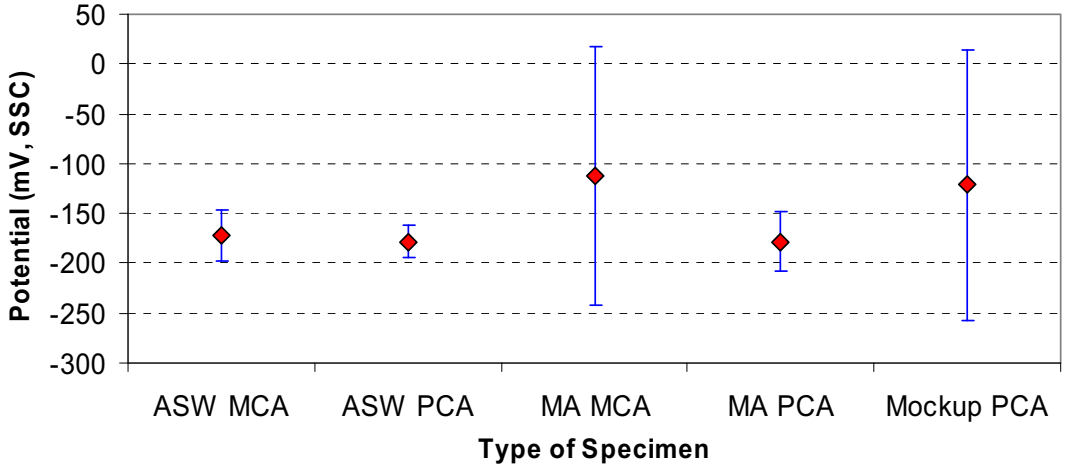

Sources: DTNs: LL060700312251.166 [DIRS 179385], file: *Rep Pot N06022 vs Temp 5M CaCl2 RBR 19Dec06.xls*; LL050302312251.129 [DIRS 173921], file: *Mockup Developed RBR 21May05.xls*.

Output DTN: MO0612WPOUTERB.000, file: *Mockup.xls*.

NOTES: Error bars are 2 standard deviations.

MA = mill-annealed, ASW = as-welded, MCA = multiple crevice assembly, PCA = prism crevice assembly.

Figure 6-62. Repassivation Potentials for Alloy 22 Specimens Fabricated from a Mockup Container in 5 *M* $CaCl_2$ at 90°C

7. VALIDATION

Models described in this report will adequately predict general and localized corrosion processes of the waste package outer barrier (WPOB) under the exposure conditions expected in the repository for the period of geologic stability. This long time of application makes it impossible to validate these models by comparing predicted values from the model to experimental observations for the whole range of time (ASTM C 1174-97 1998 [DIRS 105725], Sections 19.3 and 20.4). However, by justifying the input parameter values used and comparing these parameters and model predictions to available peer-reviewed and qualified Yucca Mountain Project (YMP) data, these models have been validated. As stated in SCI-PRO-002, *Planning for Science Activities*, and the technical work plan (TWP) (SNL 2007 [DIRS 178849], Section 2.3.1), the required level of confidence (i.e., the level of validation) for the models developed in this report is the highest, which is Level II according to SCI-PRO-002. As discussed below, the required level of confidence in the WPOB general and localized corrosion models has been obtained by building confidence in the methods used to develop the models and corroborating the model output values and alternate conceptual models with those available in the peer reviewed scientific literature.

7.1 CONFIDENCE BUILDING DURING MODEL DEVELOPMENT TO ESTABLISH SCIENTIFIC BASIS AND ACCURACY FOR INTENDED USE

The inputs to the general and localized corrosion models for the WPOB have all been obtained from controlled sources (Table 4-1, Section 4.1.1), and discussion about selection of input and design parameters and their adequacy for the model's intended use is provided in Sections 4.1.1 and 6 (as appropriate). Model assumptions have been described in Section 5 and rationale is provided there as to why they are appropriate for the model's intended use. Detailed discussion about model concepts can be found throughout Section 8 and particularly in Section 6.3. Initial and boundary conditions are described in Sections 1.2, 6, and 8, where the waste package degradation models and ranges of application are discussed. Sections 6.4.3 and 6.4.4 provide discussion of various model results (i.e., those of convergence runs). Discussion about nonconvergence runs is not applicable to this report because none were encountered. Uncertainties associated with the WPOB's capabilities are summarized in Sections 8.1, 8.2, and 8.3. More detailed discussions of the impact of uncertainties in the model results developed in this report are found in Sections 6.4.3, 6.4.4, and 6.4.5.

Section 6.4.3 discusses the development of the general corrosion model, including the effects of data uncertainties on the model. Uncertainties in the data used for the general corrosion model analysis (five-year weight-loss measurements and short-term polarization resistance measurements) were characterized, quantified, and propagated through the general corrosion model abstraction (Section 6.4.3). Section 6.4.4 discusses the effects of data uncertainties on the localized corrosion model developed in this report. Uncertainties in the data used for the localized corrosion model analysis (crevice repassivation potentials and long-term steady-state corrosion potentials) were characterized, quantified, and propagated through the localized corrosion model abstraction (Section 6.4.4). A conservative bounding approach, based on the literature data for Alloy 22 in highly corrosive environments, was used to capture the uncertainty in the localized corrosion rate of Alloy 22 (Section 6.4.4). Section 6.4.5 discusses the effects of data uncertainties on the microbially influenced corrosion (MIC) model developed in this report.

7.2 POSTDEVELOPMENT ACTIVITIES FOR CONFIDENCE BUILDING IN MODELS BY DEMONSTRATING ACCURACY OF THE MODELS FOR THEIR INTENDED USE

Postdevelopment model validation activities, documented in the TWP (SNL 2007 [DIRS 178849], Section 2.3.1), are undertaken to ensure the required level of confidence in these models for their stated purposes has been achieved. These activities are:

Activity One: Show that the propagation rates for the waste package are reasonable and consistent with rates determined by alternative techniques or alternative models for the conditions expected in the repository. This activity will be considered successful if trends in the model predictions are matched by trends seen in the data.

Activity Two: Show that the modeled propagation rates of general corrosion and localized corrosion of the waste package are reasonable and consistent with rates from literature data and/or natural analogues and/or industrial analogues of relevant corrosion resistant alloys for the conditions expected in the repository. This activity will be considered successful if the modeled propagation rates are greater than or within one order of magnitude of the corroborating data.

Activity Three: The response of the correlations of E_{corr} and $E_{critical}$ are to be demonstrated to be reasonable and consistent with literature data on relevant corrosion-resistant alloys and available analogues for the conditions expected in the repository. This activity will be considered successful if the corroborating data for the localized corrosion initiation model components fall within the three-standard deviations of the median for the relevant localized corrosion model component.

Activity Four: Demonstrate that the response of the correlations for E_{corr} and $E_{critical}$ of the waste package is consistent with other alternative models for localized corrosion initiation for the conditions expected in the repository. This activity will be considered successful if the corroborating data for the localized corrosion initiation model components fall within three standard deviations of the median for the relevant localized corrosion model component.

These validation activities are performed to fulfill the model validation requirements of SCI-PRO-006, *Models* (Section 6.3.2). In relation to the activities, it should be noted that the activities have been reworded for clarity. The rewording is not considered significant enough to constitute a deviation from the TWP (SNL 2007 [DIRS 178849]). For Activities Three and Four, both of the localized corrosion initiation model components are constrained to fall within the ±2 standard deviation prediction intervals of their respective unconstrained models (Sections 6.4.4.3.1 and 6.4.4.5) (i.e., Activities Three and Four will increase model confidence if the corroborating data for the localized corrosion initiation model components fall within the ±2 standard deviation prediction intervals of their respective unconstrained models). The use of ±2 standard deviations is a deviation from the TWP (SNL 2007 [DIRS 178849]). This deviation is acceptable because the ±2 standard deviation prediction interval is narrower than the ±3 standard

deviation prediction interval. A detailed description of the validation of the WPOB general and localized corrosion models follows.

7.2.1 General Corrosion Model of the Waste Package Outer Barrier

Validation of the general corrosion model of the WPOB requires meeting the criteria stated in Activities One and Two.

Activity One: Show that the propagation rates for the waste package are reasonable and consistent with rates determined by alternative techniques or alternative models for the conditions expected in the repository. This activity will be considered successful if trends in the model predictions are matched by trends seen in the data.

Activity Two: Show that the modeled propagation rates of general corrosion and localized corrosion of the waste package are reasonable and consistent with rates from literature data and/or natural analogues and/or industrial analogues of relevant corrosion resistant alloys for the conditions expected in the repository. This activity will be considered successful if the modeled propagation rates are greater than or within one order of magnitude of the corroborating data.

As described in Section 6.4.3.4, the general corrosion model for the WPOB is based on the temperature dependence of the corrosion process, represented by an apparent activation energy using the natural logarithmic form of a modified Arrhenius relation. The model is expressed as Equation 7-1 (Section 6.4.3.4, Equation 6-28):

$$\ln(R_T) = \ln(R_o) + C_1\left(\frac{1}{T_0} - \frac{1}{T}\right) \qquad \text{(Eq. 7-1)}$$

where R_T is the temperature-dependent general corrosion rate in nm/yr, T is the temperature in Kelvin, T_0 is equal to 333.15 K, and R_o and C_1 are constants. The temperature-dependence term (C_1) was obtained from short-term polarization resistance data for Alloy 22 specimens tested for a range of sample configurations, metallurgical conditions, and exposure conditions. Section 6.4.3.4 provides details of the model derivation and parameter evaluation. A normally distributed temperature-dependence term with a mean of 4,905 K and a standard deviation of 1,413 K was chosen. The apparent activation energy was estimated to be 40.78 ± 11.75 kJ/mol. The general corrosion rate distribution (R_o) derived from the weight-loss data of the five-year crevice specimens was fit to a Weibull distribution, and the uncertainty associated with the fitting procedure was evaluated, leading to low, medium, and high estimates for this distribution and its parameters (Table 6-7 and Figure 6-23). This distribution is considered to represent the distribution of long-term general corrosion rates of the WPOB at 60°C.

The validation of the general corrosion model consists of two parts: evaluation of the adequacy and accuracy of the apparent activation energy value (or the temperature-dependence term, C_1) of the model and evaluation of the adequacy and accuracy of the general corrosion rates predicted by the model. As discussed below, the evaluation was performed by comparing the

aforementioned model properties with literature data for Alloy 22 (or other corrosion-resistant alloys similar to Alloy 22) measured in repository-relevant environmental conditions.

Temperature dependence of the passive corrosion rate of Alloy 22 was also reported by other investigators. Based on passive current densities of Alloy 22 measured at 60°C, 80°C, and 95°C in 5 *M* LiCl solutions with small amounts of $[SO_4^-]$ and $[NO_3^-]$ added (Scully et al. 2001 [DIRS 154513], Table 4, Section II.1), an apparent activation energy range from 20 to 50 kJ/mol was estimated. An apparent activation energy of 32 kJ/mol was found from the measured passive current densities of Alloy 22 polarized at 350 mV versus a silver/silver chloride reference electrode (using 0.1 *M* KCl (i.e., 288 mV versus the normal hydrogen electrode)) in a solution of 1 *M* NaCl and 0.1 *M* H_2SO_4 (Lloyd et al. 2003 [DIRS 167921]). Electric Power Research Institute (EPRI 2002 [DIRS 158069], Section 5.3.2) estimated an apparent activation energy of 19 kJ/mol for Alloy C-4 based on corrosion rates determined from weight-loss measurements of the alloy measured over a period of three to five years at temperatures in the range of 90°C to 200°C in saturated Mg^{2+}-dominated brines (Smailos et al. 1987 [DIRS 159774]). The report by EPRI (2002 [DIRS 158069], Section 5.3.2) initially questioned the use of a temperature dependence for modeling general corrosion rate of Alloy 22 in light of experiments conducted by the Center for Nuclear Waste Regulatory Analyses (CNWRA) (Dunn et al. 1999 [DIRS 154481], Section 3.1), which showed little or no temperature dependence in 4 *M* NaCl solutions, and the lack of a significant temperature dependence in the YMP's weight-loss experiments. EPRI did, however, use an activation energy of 19 kJ/mol in modeling the Alloy 22 general corrosion rate (EPRI 2002 [DIRS 158069], Section 5.3.2). Also, the EPRI report (2002 [DIRS 158069], Section 5.3.2) mentioned that the data used to develop the temperature dependence in modeling the Alloy 22 general corrosion rate (Smailos et al. 1987 [DIRS 159774]) were based on weight-loss measurements from specimens that had undergone localized corrosion during testing. Further, it should be noted that subsequent experiments conducted in 4 *M* NaCl solutions in autoclaves by the CNWRA investigators (Dunn et al. 2005 [DIRS 178104], Section 3.2) generated a temperature dependence of 33.6 kJ/mol for Alloy 22 general corrosion rate in the temperature range of approximately 40°C to 175°C.

Hua and Gordon (2004 [DIRS 171013]) conducted weight-loss experiments on mill-annealed and as-welded Alloy 22 specimens at exposure temperatures from 60°C to 105°C for a total of eight weeks in a BSW solution with a room temperature pH of about 12. No significant difference was found between the apparent activation energies of the as-welded and mill-annealed materials. After four weeks of exposure, the apparent activation energy for the combined data set was 19.3 kJ/mol and increased to 25.3 kJ/mol after eight weeks of exposure.

Researchers at the CNWRA have studied the effect of temperature on the passive corrosion of Alloy 22 (Pensado et al. 2002 [DIRS 166944], Section 4.3). They reported a mean apparent activation energy of 44.7 kJ/mol with a standard deviation of 5.5 kJ/mol, based on potentiostatic anodic current measurements of smooth cylindrical specimens polarized at 100 mV_{SCE} in de-aerated 0.028 *M* NaCl solutions. In another study (Dunn et al. 2004 [DIRS 171452]), CNWRA researchers reported an apparent activation energy of 46.3 kJ/mol for the temperature dependence of Alloy 22 general corrosion in 0.028 *M* NaCl over the temperature range between 25°C and 95°C, and an apparent activation energy of 49.6 kJ/mol in a 35% $MgCl_2$ solution for the temperature range between 40°C and 120°C.

As mentioned above, the apparent activation energy of Alloy 22 determined in this report is 40.78 ± 11.75 kJ/mol (±1 standard deviation). Variation in the apparent activation energy is truncated between −3 standard deviations (666 K corresponding to an apparent activation energy of 5.54 kJ/mol) and +2 standard deviations (7,731 K corresponding to an apparent activation energy of 64.28 kJ/mol). This range is inclusive of the apparent activation energy of Alloy 22 determined by Hua and Gordon (2004 [DIRS 171013]) and several other values of this parameter reported in the literature (Scully et al. 2001 [DIRS 154513], Table 4, Section 1.4; Lloyd et al. 2003 [DIRS 167921]; EPRI 2002 [DIRS 158069], Section 5.3.2; Pensado et al. 2002 [DIRS 166944], Section 4.3). This comparison validates the adequacy and accuracy of the temperature-dependence term (i.e., C_1) used in the temperature-dependent general corrosion model for the WPOB.

Because of the extremely low corrosion rates of Alloy 22, there are few data for Alloy 22 in the scientific literature that could be used to evaluate the general corrosion model. However, similar passive corrosion behavior has also been observed for Ni-Cr-Mo corrosion-resistant alloys. For example, Alloy C (UNS N06455) specimens exposed for 44 years to a marine environment at North Carolina's Kure Beach (i.e., with salt air and alternate wetting and drying, as well as the presence of surface deposits) (Baker 1988 [DIRS 154510], p. 134 and Table 6) indicate that passivity was maintained over this long exposure period as evidenced by the observation of a mirror-like surface finish after surface deposits were removed. Examination of specimens from this alloy after more than 50 years of exposure indicates that the samples continued to maintain a mirror-like finish indicative of passive behavior (McCright 1998 [DIRS 114637], Figure ES-1). Under these same conditions, the less corrosion-resistant Alloy 600 exhibited a corrosion rate equal to 8 nm/yr after 36 years of exposure. This long-term corrosion rate is consistent with the model prediction, as discussed below.

An apparent activation energy of 40.78 ± 11.75 kJ/mol (±1 standard deviation) corresponds to C_1 = 4,905 K with a standard deviation of 1,413 K. The 50th, 95th, and 99.99th percentile rates predicted by the general corrosion model at 25°C, using the medium level of uncertainty for the 60°C general corrosion rate distribution (b = 8.134 nm/yr, c = 1.476, from Table 6-7) and the medium temperature dependence (C_1 = 4,905 K), are 1.13 nm/yr, 3.04 nm/yr, and 6.50 nm/yr, respectively (Figure 6-26, 25°C model result CDF). Using the low level of uncertainty for the 60°C general corrosion rate distribution (b = 6.628 nm/yr, c = 1.380, from Table 6-7) and the low temperature dependence (C_1 = 666 K), the 50th, 95th, and 99.99th percentile rates predicted by the model at 25°C are 4.02, 11.6, and 26.2 nm/yr, respectively (output DTN: MO0612WPOUTERB.000, file: *BaseCase GC CDFs2.xls*). Therefore, the model predicts Alloy 22 general corrosion behavior consistent with that of other corrosion-resistant Ni-Cr-Mo alloys (e.g., Alloy C and Alloy 600). This observation indicates that the Alloy 22 general corrosion model is reasonable and provides confidence that the Alloy 22 general corrosion model is adequate for its intended use.

The model validation for intermediate and elevated temperature conditions was performed by comparing the model results to the recently reported weight-loss measurements of mill-annealed and as-welded Alloy 22 multiple crevice assembly (MCA) specimens after exposure to the basic saturated water (BSW) solutions at temperatures from 60°C to 105°C over a period of eight weeks (Hua et al. 2002 [DIRS 160670]). From the eight-week weight-loss measurements, an average general corrosion rate of 75 nm/yr at 60°C and 300 nm/yr at 105°C were reported for the Alloy 22 MCA specimens. The model results for the 50th, 95th, and 99.99th percentile rates at

60°C for the medium uncertainty level are 6.35, 17.1, and 36.6 nm/yr, respectively. At 105°C, using the median temperature dependence (C_1 = 4,905 K), the model-calculated 50th, 95th, and 99.99th percentile rates are 36.6, 98.6, and 211 nm/yr, respectively. It appears that the model-predicted general corrosion rates are lower using the medium uncertainty and median temperature dependence than those obtained by Hua et al. (2002 [DIRS 160670]). However, it should be noted that the general corrosion rate of Alloy 22 is expected to decrease with increasing exposure time (Figure 7-1). Considering the shorter-term nature (i.e., eight weeks) of the data obtained by Hua et al. (2002 [DIRS 160670]) compared to the five-year data used in the model development, the model results are in good agreement with the trends observed in Alloy 22 general corrosion rate data for this repository-relevant exposure environment.

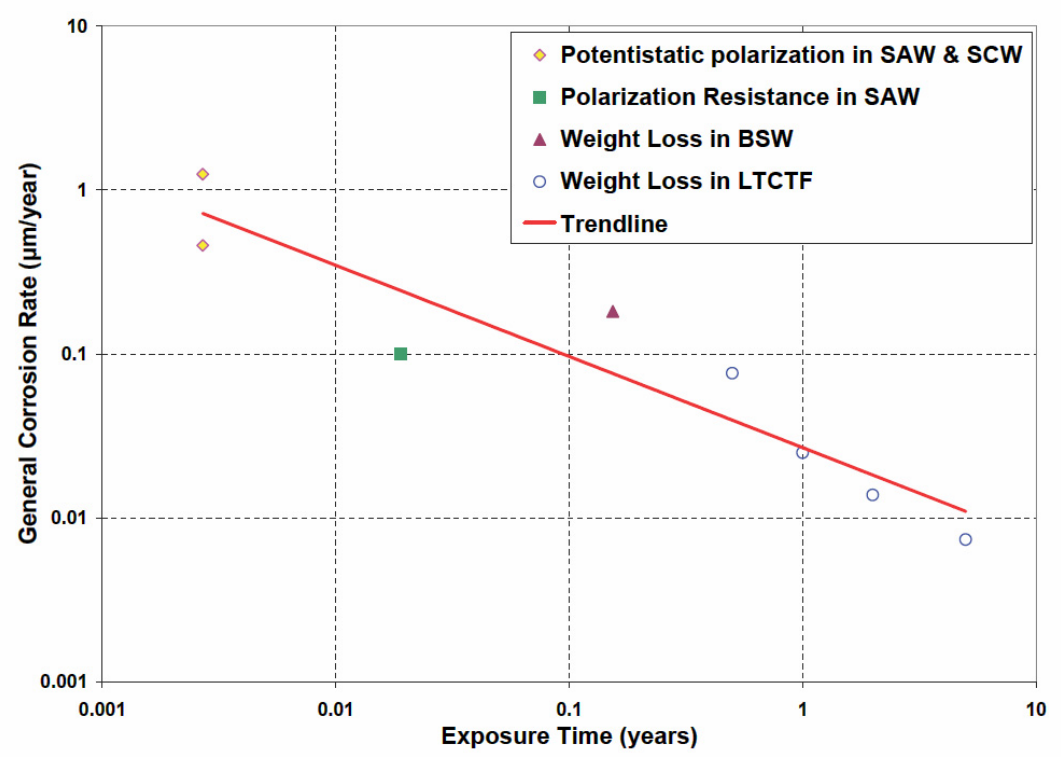

Source: Table 7-1.

NOTE: Basic saturated water; LTCTF = Long-Term Corrosion Test Facility; SAW = simulated acidified water; SCW = simulated concentrated water.

Figure 7-1. Decrease of the Mean General Corrosion Rate of Alloy 22 with Time at 90°C

As discussed below, the model predictions for high-temperature chloride-containing brines also bound the general corrosion-rate data gathered from the open literature for welded Alloy C-4 samples tested at 150°C in NaCl-rich brines (Smailos 1993 [DIRS 168164], Table IV). According to these researchers, the samples corroded uniformly under the test conditions, with mean general corrosion rates of 70 and 60 nm/yr observed for 12- and 18-month test periods, respectively. The reported general corrosion rates are the average values of five samples. For the same NaCl-rich brines containing 6×10^{-4} M Na_2S, the reported mean general corrosion rates of the surface-welded alloy were 510 and 120 nm/yr for 12- and 18-month test periods, respectively. An additional six months of exposure resulted in a decrease in the corrosion rate of

Alloy C-4 from 510 to 120 nm/yr. According to this trend, the corrosion rates of Alloy C-4 are expected to be significantly lower than 120 nm/yr after five years of exposure. The model-predicted 50th, 95th and 99.99th percentile rates at 150°C for the medium level of uncertainty for the 60°C general corrosion rate distribution (b = 8.134 nm/yr, c = 1.476 nm/yr, from Table 6-7) and the mean apparent activation energy (40.78 kJ/mol) are 145 nm/yr, 392 nm/yr, and 839 nm/yr, respectively (Figure 6-26, 150°C model result CDF). These values are considerably higher than those expected (i.e., less than 120 nm/yr) for Alloy C-4 in the five-year time frame. Thus, the Alloy 22 general corrosion rate model predictions are reasonable estimates of the general corrosion rate of Alloy 22 at elevated temperatures (e.g., 150°C) and are sufficiently accurate for their intended use.

Using the low level of uncertainty for the 60°C general corrosion rate distribution (b = 6.628 nm/yr, c = 1.380¸ from Table 6-7) and the highest temperature dependence (C_1 = 7,731 K), the model results for the 50th, 95th, and 99.99th percentile rates at 25°C are 0.33, 0.96, and 2.17 nm/yr, respectively (Figure 6-27 25°C model result CDF). The 200°C model results for the low level of uncertainty for the 60°C general corrosion rate distribution (b = 6.628 nm/yr, c = 1.380, rom Table 6-7) and the highest temperature dependence (C_1 = 7,731 K) are 4,880, 14,100, and 31,800 nm/yr, respectively (output DTN: MO0612WPOUTERB.000, file: *BaseCase GC CDFs2.xls*). The model results for general corrosion rates at 200°C are extremely high. This suggests that the model results for general corrosion rates of Alloy 22 beyond 150°C may be highly conservative. However, one should note that researchers from the CNWRA have reported Alloy 22 general corrosion rates between 0.95 to 9.4 μm/yr (950 to 9,400 nm/yr) for specimens immersed in nitrate-rich chloride-containing brines at temperatures between 150°C to 180°C (Yang 2006 [DIRS 178411], Section 3.2.3).

The general corrosion rate is temperature dependent, and, for a given temperature, it is assumed to be constant (i.e., time-independent) (Assumption 5.2, Section 5). Therefore, for a given temperature, the depth of penetration or thinning of the WPOB by general corrosion is equal to the general corrosion rate at that temperature, multiplied by the time duration that the waste package surface is at that temperature. However, the general corrosion rates of metals and alloys tend to decrease with time. The dependence of the general corrosion rate of Alloy 22 on the exposure time is shown in Figure 7-1 for the mean general corrosion rates of Alloy 22 at 90°C, measured with different test techniques (potentiostatic polarization, polarization resistance, and weight-loss measurements) for exposure times up to five years. Given the differences between the techniques used to determine corrosion rates presented in the figure, some variation about the central trend line is to be expected. A trend-line was drawn for better visualization of the data trend. The data shown in the figure are summarized in Table 7-1.

Table 7-1. Summary of Mean General Corrosion Rates of Alloy 22 at 90°C versus Exposure Time

Exposure Time (years)	Exposure Time (days)	Mean Rate (μm/yr)	Sources
0.0027	1	0.460	Lian et al. 2002 [DIRS 164856], Table 3, potentiostatic polarization technique at 100 mV versus SSC applied potential in SAW, 90°C, N_2 purge.
0.0027	1	1.250	Lian et al. 2002 [DIRS 164856], Table 3, potentiostatic polarization technique at 100 mV versus SSC applied potential in SCW, 90°C, N_2 purge.
0.019	7	0.100	Evans and Rebak 2002 [DIRS 164857], Figure 2, polarization resistance technique, after one week in open-circuit potential in SAW, 90°C, air purge.
0.154	56	0.182	Hua and Gordon 2004 [DIRS 171013] calculated from regression fit for 56-day weight-loss in BSW, CR (MPY) = 31.3*exp(-25300/RT).
0.50	183	0.076	LL990610605924.079 [DIRS 104994] s99359_032 DATA REPORT (weight-loss) and s99359_031 DATA REPORT (crevice)
1.00	365	0.025	LL990610605924.079 [DIRS 104994] s99359_005 DATA REPORT (crevice data) and s99359_006 DATA REPORT (weight-loss data)
2.00	730	0.014	LL000112205924.112 [DIRS 141284] S00041_005 DATA REPORT (Combined crevice and weight-loss data)
5.00	1,825	0.007	Section 6.4.3.3, Table 6-6

Validation DTN: MO0706WPOBVALR.000, file: *Figure 7-1.xls*.

NOTE: BSW = basic saturated water; CR = corrosion rate; MPY = mills per year; SAW = simulated acidified water; SCW = simulated concentrated water; SSC = saturated silver chloride electrode.

The exposure time ranges from one day to more than five years of exposure at the Long-Term Corrosion Test Facility (LTCTF). The five-year general corrosion rate is the mean of the weight-loss measurements of 58 crevice samples from the LTCTF (Table 6-6 and Section 6.4.3.4). The mean general corrosion rate of the crevice samples after five-year exposure at the LTCTF was about 0.007 μm/yr. It is noted that the corrosion rates measured by short-term electrochemical techniques provide corroboration of the rates from the weight-loss method. The trend of decreasing general corrosion rate with time is consistent with the expected corrosion behavior of passive alloys such as Alloy 22 under repository-relevant aqueous conditions.

Given that the corrosion rate of Alloy 22 decreases with time, an alternative methodology to assess the Alloy 22 general corrosion rate would be to evaluate the weight change, ΔW_o, of a specimen after a nonzero exposure time of t_o (thus, ΔW_o = (initial weight) – (weight at t_o)) and the weight change, ΔW_1, of the same specimen after an exposure time of $t_1 > t_o$ (so that ΔW_1 = (initial weight) – (weight at t_1)). The effective corrosion rate could be given by $(\Delta W_1 - \Delta W_o)/(t_1 - t_o)$. Based on Figure 7-1, this effective corrosion rate would be expected to be less (perhaps much less) than a corrosion rate determined with a t_o value of zero (as was done in developing the distribution used for the Alloy 22 general corrosion model developed in this report).

Obviously, the process of descaling a specimen in order to obtain a weight-loss measurement precludes the use of that specimen for further weight-loss evaluation; however, a distribution could potentially be developed based on the difference between the weight-loss distributions at two exposure times t_1 and t_o. What is clear, given the apparent decrease in Alloy 22 general corrosion rate shown in Figure 7-1, is that the approach taken in this report (using $t_o = 0$) is conservative relative to the alternative methodology. The current conservative approach using a constant (time-independent) general corrosion rate at a given temperature in the waste package degradation analysis provides additional confidence in the general corrosion model.

A comparison of the rates obtained from the temperature-dependent Alloy 22 general corrosion model with the rates from alternative techniques from the scientific literature shows that Activities One and Two have been met. In addition, the conservative approach used in calculating the penetration depth by general corrosion over time provides additional confidence that the model, and the modeling approach, is adequate for its intended use.

7.2.2 Long-Term Corrosion Potential Model of the Waste Package Outer Barrier

Validation of the long-term corrosion potential model of the WPOB requires meeting the criterion stated in Activity Three.

Activity Three: The response of the correlations of E_{corr} and $E_{critical}$ are to be demonstrated to be reasonable and consistent with literature data on relevant corrosion resistant alloys and available analogues for the conditions expected in the repository. This activity will increase model confidence if the corroborating data for the localized corrosion initiation model components fall within the three-standard deviations of the median for the relevant localized corrosion model component.

In this section, results obtained from the Alloy 22 long-term corrosion potential model are corroborated with data acquired by the YMP not previously used to develop or calibrate the model. Also, the results obtained from the Alloy 22 long-term corrosion potential model are corroborated by relevant information published in refereed journals or literature that was not used to develop or calibrate the model.

The long-term corrosion potential model developed to analyze the localized corrosion behavior of the WPOB under the conditions expected in the repository is expressed as follows (Section 6.4.4.5, Equation 6-39):

$$E_{corr} = c_o + c_1 T + c_2 pH + c_3 \frac{[NO_3^-]}{[Cl^-]} + c_4 T \frac{[NO_3^-]}{[Cl^-]} + c_5 pH \frac{[NO_3^-]}{[Cl^-]} + c_6 pH \ln[Cl^-] + \varepsilon_{corr} \quad \text{(Eq. 7-2)}$$

where E_{corr} is the long-term corrosion potential in mV versus SSC, T is the temperature (°C), $[Cl^-]$ is the chloride-ion concentration in molality, $[NO_3^-]$ is the molal nitrate-ion concentration, and c_o, c_1, c_2, c_3, c_4, c_5, and c_6 are coefficients of the model parameters. The error term, ε_{corr}, is a term representing data variance not explained by the fitting procedure. The estimated regression coefficients and their uncertainty (±1 standard deviation) are: c_0 = 1,051.219 ± 119.774, c_1 = −3.024 ± 0.977, c_2 = −155.976 ± 11.495, c_3 = −1,352.040 ± 252.224, c_4 = 10.875 ± 1.890, c_5 = 137.856 ± 23.158, and c_6 = −8.498 ± 0.801. The units of the coefficients are such that the units of E_{corr} are mV versus SSC. The standard deviation of the error term was determined to be 85.265 mV versus SSC. This model is used to estimate the long-term steady-state open-circuit corrosion potential of Alloy 22 for a range of exposure conditions related to the repository. The model is not intended to predict short-term corrosion potential because the corrosion potential of Alloy 22 evolves with time under the conditions relevant to the repository.

Few data exist for the steady-state corrosion potential of Alloy 22 for under repository-relevant conditions that can be used to evaluate the corrosion potential model. The Nuclear Energy Research Initiative, a study sponsored by the U.S. Department of Energy (DOE), published measurements of the open-circuit corrosion potential of Alloy 22 under air-saturated conditions in a saturated NaCl solution at 80°C for a period of 200 days (Jayaweera et al. 2003 [DIRS 162225], pp. 9-18 to 9-22, Figure 9.13). The chloride-ion concentration of the solution was about 6.2 *m*, and a pH of 3 (measured by a homemade "pH stat") was maintained by HCl additions (Jayaweera et al. 2003 [DIRS 162225], p. 9-2). The measured corrosion potential at the end of the testing (200 days) ranged from about 160 to 250 mV versus the standard hydrogen electrode (SHE). At 25°C (77°F), the SSC scale is more noble than the SHE scale by 199 mV (Sawyer and Roberts 1974 [DIRS 162259], pp. 39 to 45, Table 2-4). Therefore, the range of 160 to 250 mV versus SHE corresponds to a range of –39 to 51 mV versus SSC.

For these exposure conditions, using a pH of 3 as input, the mean value of the corrosion potential from the long-term corrosion potential model is 295 mV versus SSC, and the upper and lower bounding values are 476 and 114 mV versus SSC, respectively (Appendix XI and Table 7-2). The upper and lower bounding values are based on the ±2 standard deviation prediction interval values for the *unconstrained* long-term corrosion potential model. Although the lower-bound of the predicted long-term corrosion potential (114 mV versus SSC) is higher than the value in Jayaweera et al. (2003 [DIRS 162225], Figure 9-13) by about 63 mV, the model prediction is considered a reasonably good match, considering that the investigators indicated that their corrosion potential had likely not reached steady state during testing. After about four months of testing, the investigators also observed fluctuations in the measured corrosion potential (evident in Jayaweera et al. 2003 [DIRS 162225], Figure 9.13), which were attributed to pit initiation. The pits formed under these exposure conditions were found to be few in number, very shallow, and within the noise level of the laser confocal microscopic elevation diagrams obtained (Jayaweera et al. 2003 [DIRS 162225], p. 9-20). In spite of the observation of pitting, it is clear from the results of this investigation (Jayaweera et al. 2003 [DIRS 162225], Figure 9.13) that the corrosion potential was trending toward values between 160 to 250 mV versus SHE before (and after) pitting initiated, justifying the use of these data for corroboration of the long-term corrosion potential model. In addition, the long-term corrosion potential model conservatively overestimates the corrosion potentials obtained by Jayaweera et al. (2003 [DIRS 162225], Figure 9.13). This is conservative because, for a given exposure condition, the overestimates of the long-term corrosion potential could result in predictions of crevice corrosion initiation under conditions in which it would not be observed.

General Electric Global Research Center measured long-term corrosion potential (after about 915 days) of Alloy 22 compact tension specimens at 110°C in an aerated BSW solution composed of 10.6 g Na_2CO_3 (anhydrous), 9.7 g KCl, 8.8 g NaCl, 0.2 g NaF, 13.6 g $NaNO_3$, 1.4 g Na_2SO_4 (anhydrous), and 4.1 g $Na_2SiO_3 \cdot 9H_2O$ dissolved in 55.3 g H_2O (Andresen et al. 2003 [DIRS 170360], Table 1-4; pp. 66 and 78). Note that these data are independent of the data from Andresen et al. (2003 [DIRS 170360]) used as direct input in Table 4-2. Therefore, these data are appropriate for use in validation activities. The long-term corrosion potential was found to be between 100 and 110 mV versus SHE. This corresponds to a range of –99 to –89 mV versus SSC. The solution is calculated to have 5.08 *m* chloride ions and 2.89 *m* nitrate ions (Appendix XI and Table 7-2). DTN: LL060904312251.186 [DIRS 178283], file: *AtmCO2GetEQData.xls*, contains Pitzer pH values for a BSW solution used in long-term

corrosion potential cell 19, which is 4.62 *m* chloride ions and 2.82 *m* nitrate ions. The Pitzer pH for the cell 19 solution is 8.58 at 110°C. The long-term corrosion potentials predicted by the model using 4.62 *m* chloride ions, 2.82 *m* nitrate ions, and a pH of 8.58 at 110°C is –104 mV versus SSC (mean), 70 mV versus SSC (upper bound), and −279 mV versus SSC (lower bound) (Appendix XI and Table 7-2). Using the calculated 5.08 *m* chloride-ion and 2.89 *m* nitrate-ion concentrations (Appendix XI and Table 7-2), these values change to –154 mV versus SSC (mean), 20 mV versus SSC (upper bound), and −328 mV versus SSC (lower bound). The long-term corrosion potentials predicted by the model are consistent with these measured values, providing confidence in the accuracy of the long-term corrosion potential model.

Table 7-2. Summary of Model Validation Analysis for the Long-Term Corrosion Potential Model

Test Condition, and Data Source	Measured E_{corr} (mV_{SHE})	Measured E_{corr} (mV_{SSC})[a]	Environmental Condition Inputs to Model Calculation	E_{corr} Model	
				Mean (mV_{SSC})	Bounds (mV_{SSC})
Alloy 22 in 6.2 *m* NaCl, 80°C, nominal pH of 3 (Jayaweera et al. 2003 [DIRS 162225], pp. 9-18 to 9-22, Figure 9.13)	160 to 250	−39 to 51	6.2 *m* Cl, 80°C, pH 3	295	114 (Lower) 476 (Upper)
Alloy 22 in basic saturated water at 110°C, (Andresen et al. 2003 [DIRS 170360], Table 1-4; pp. 66 and 78)	100 to 110	−99 to −89	4.62 *m* Cl, 2.82 *m* NO_3, 110°C, pH 8.58	−104	−279 (Lower) 70 (Upper)
Alloy 22 in basic saturated water at 110°C, (Andresen et al. 2003 [DIRS 170360], Table 1-4; pp. 66 and 78)	100 to 110	−99 to −89	5.08 *m* Cl, 2.89 *m* NO_3, 110°C, pH 8.58	−154	−328 (Lower) 20 (Upper)

[a] These values are converted from the SHE reference electrode scale (against which the experimental measurements were made) to the SSC reference electrode scale. At 25°C the SSC reference electrode is 199 mV more noble than the SHE (Sawyer and Roberts 1974 [DIRS 162259], pp. 39 to 45, Table 2 4).

Validation DTN: MO0706WPOBVALR.000, file: *Ecrit_EcorrValid3.xmcd contains the calculated Ecorr values*.

Based on these analyses, the long-term corrosion potential model results compare well with literature and YMP data not used for development of the model. Thus, the long-term corrosion potential model is considered adequate for its intended use.

One additional long-term corrosion potential is available from the literature. Dunn et al. (2003 [DIRS 164138], Figure 7) measured the corrosion potential of an Alloy 22 crevice corrosion test specimen exposed to an air-saturated 4 *M* NaCl solution. The specimen was periodically removed and examined for signs of localized corrosion. During more than 750 days of testing, no localized corrosion was observed (Dunn et al. 2003 [DIRS 164138], p. 5). Over the last 200 days of testing, the corrosion potential reached a maximum value near −130 mV_{SCE}. At 25°C the SSC reference electrode is 199 mV more noble than the SHE (Sawyer and Roberts 1974 [DIRS 162259], pp. 39 to 45, Table 2-4), and the saturated calomel electrode (SCE) reference electrode is 241 mV more noble than the SHE (ASTM G 3-89 1989 [DIRS 138911]). Therefore, the SCE scale potentials are converted to the SSC scale potentials by adding 42 mV. Thus, −130 mV_{SCE} is equivalent to −88 mV versus SSC. In case 13 of DTN: LL060904312251.186 [DIRS 178283], file: *AtmCO2GetEQData.xls*, a 4 *M* (4.4 *m*) NaCl solution was determined to have a Pitzer pH of 5.55 at 95°C. For these exposure conditions, the

mean value of the predicted long-term corrosion potential is –172 mV versus SSC, and the upper and lower bound values are 2 mV and -345 mV versus SSC, respectively (Appendix XI). These values are consistent with the measured long-term corrosion potential values. However, the 4 *M* NaCl solution used in these experiments may have also contained 1.24 *mM* $NaHCO_3$, 0.20 *mM* Na_2SO_4, 0.16 *mM* $NaNO_3$, and 0.10 *mM* NaF (Dunn et al. 2003 [DIRS 164138]). It is possible that these minor additions had little effect on pH and/or that the solutions equilibrated with the laboratory air over the course of the over 750-day experimental period.

Because of the uncertainty caused by these possible additions, these data are not being used for model validation, although they are worthy of discussion, because the experiment that produced them is one of few long-term corrosion potential experiments available in the open literature for comparison to the long-term corrosion potential model. The effect of possible changes of ±0.5 pH units is considered. If the pH is 5.05, the mean value of the predicted long-term corrosion potential is −87 mV versus SSC, and the upper and lower bound values are 85 mV and −260 mV versus SSC, respectively (Appendix XI). If the pH is 6.05, the mean value of the corrosion potential from the long-term corrosion potential model is −256 mV versus SSC, and the upper and lower bound values are −81 mV and −431 mV versus SSC, respectively (Appendix XI).

A comparison of the long-term corrosion potential obtained from the long-term corrosion potential model with the long-term corrosion potential data of Alloy 22 measured independently has shown that the criterion of Activity Three relating to the long-term corrosion potential model has been met.

7.2.3 Critical Potential Model of the Waste Package Outer Barrier

As with validation of the long-term corrosion potential model of the WPOB, validation of the critical potential model of the WPOB requires meeting the criterion for Activity Three.

Activity Three: The response of the correlations of E_{corr} and $E_{critical}$ are to be demonstrated to be reasonable and consistent with literature data on relevant corrosion resistant alloys and available analogues for the conditions expected in the repository. This activity will increase model confidence if the corroborating data for the localized corrosion initiation model components fall within the three-standard deviations of the median for the relevant localized corrosion model component.

In this section, results obtained from the crevice repassivation potential model are corroborated with data acquired from the laboratory not previously used to develop or calibrate the model. In addition, the model results are corroborated with other model results obtained from implementation of other independent mathematical models developed for similar or comparable intended use/purpose.

$E_{critical}$ can be defined as a threshold potential above which the current density or corrosion rate of Alloy 22 increases significantly above the general corrosion rate of the passive metal. As a conservative measure, the localized corrosion model uses the crevice repassivation potential

(E_{rcrev}) as the critical potential for the localized corrosion initiation analysis. The crevice repassivation potential (E_{rcrev}) is expressed in Equation 7-3 (Section 6.4.4.3 and Equation 6-35):

$$E_{rcrev} = a_o + a_1 T + a_2 \ln\left[Cl^-\right] + a_3 \frac{\left[NO_3^-\right]}{\left[Cl^-\right]} + a_4 T \cdot \left[Cl^-\right] + \varepsilon_{rcrev} \qquad \text{(Eq. 7-3)}$$

where E_{rcrev} is the crevice repassivation potential (mV versus SSC), a_o, a_1, a_2, a_3,and a_4 are coefficients of the model parameters, T is the temperature (°C), $[Cl^-]$ is the molal chloride-ion concentration, $[NO_3^-]$ is the molal nitrate-ion concentration, and ε_{rcrev}, is the error term. The mean values of the coefficients of the model parameters and their ±1 standard deviation values from the fitting were determined to be: a_o = 190.242 ± 18.373, $a_1 = -3.008 \pm 0.225$, $a_2 = -46.800 \pm 3.126$, $a_3 = 535.625 \pm 26.140$, and $a_4 = 0.061 \pm 0.010$. The units of the coefficients are such that the units of E_{rcrev} are mV versus SSC. The error term has a normal distribution with a mean of zero and a standard deviation of 45.055 mV versus SSC.

There are limited data in the scientific literature for the crevice repassivation potential of Alloy 22 for exposure conditions relevant to the repository. For the literature data that may be applicable, it can be difficult to use those data to evaluate the crevice repassivation potential model because they were obtained using different criteria and/or measurement approaches (Section 6.4.4.1).

The experimentally determined crevice repassivation potentials for two specimens, DEA3130 (from DTN: LL060803712251.170 [DIRS 179387], file: *Rep Pot N06022 vs Temp NaCl RBR 07Oct06.xls*) and KE0416 (from DTN: LL060603812251.164 [DIRS 178269], file: *Rep Pot N06022 vs Temp NaCl + KNO3 60-100C RBR 07Aug06.xls*) were not used in development of the crevice repassivation potential model and are used for model validation. A measured crevice repassivation potential for specimen DEA3130 of –67 mV versus SSC was obtained in 1 *M* NaCl solution at 90°C, and a measured crevice repassivation potential for specimen KE0416 of –77 mV versus SSC was obtained in 6 *m* NaCl + 0.9 *m* KNO_3 solution at 100°C (Table 7-3). As can be seen from Table 7-3, the predicted values from the crevice repassivation potential model are sufficiently accurate with respect to the measured data. The upper and lower bounding values are based on the ±2 standard deviation prediction interval values for the *unconstrained* crevice repassivation potential model (Section 6.4.4.3.1).

Table 7-3. Comparison of Measured Data to Data from Crevice Repassivation Potential Model

Exposure Environment and Data Source	Measured E_{rcrev} (mV_{SSC})	Environmental Condition Inputs to Model Calculation	E_{rcrev} Model	
			Mean (mV_{SSC})	Bounds (mV_{SSC})
1 *M* NaCl at 90°C DTN: LL060803712251.170 [DIRS 179387], file: *Rep Pot N06022 vs Temp NaCl RBR 07Oct06.xls*, worksheet "DEA3130"	−67	1.02 *m* Cl, 0 *m* NO_3, pH 6.16, 90°C	−76	15 (Upper) −167 (Lower)

Table 7-3. Comparison of Measured Comparison to Data from Crevice Repassivation Potential Model (Continued)

Exposure Environment and Data Source	Measured E_{rcrev} (mV_{SSC})	Environmental Condition Inputs to Model Calculation	E_{rcrev} Model	
			Mean (mV_{SSC})	Bounds (mV_{SSC})
6 *m* NaCl + 0.9 *m* KNO_3 at 100°C DTN: LL060603812251.164 [DIRS 178269], file: *Rep Pot N06022 vs Temp NaCl + KNO3 60-100C RBR 07Aug06.xls*, worksheet "KE0416"	−77	6 *m* Cl, 0.9 *m* NO_3, pH 5.81, 100°C	−77	13 (Upper) −168 (Lower)

Sources: pH and molalities are listed in output DTN: MO0612WPOUTERB.000, file: *ErcrevRawData3.xls,* and were calculated based on DTN: LL090604312251.186, file: *NoCO1GetEQData.xls.*

Validation DTN: MO0706WPOBVALR.000, file: *Ecrit_EcorrValid3.xmcd*, contains the calculated E_{rcrev} values.

Investigators at the CNWRA have published a crevice repassivation model (Dunn et al. 2005 [DIRS 178451]) for Alloy 22. For alloys in the mill-annealed condition, this model is given by Equation 7-4:

$$E_{rCNWRA} = 1300 - 13.1T + (-362.7 + 2.3T)\log\left[Cl^-\right] + 800\frac{\min\left(\frac{\left[NO_3^-\right]}{\left[Cl^-\right]}, 0.1\right)}{0.1} + 42 \quad \text{(Eq. 7-4)}$$

where T is temperature in °C and a factor of 42 has been added to convert from the SCE potential scale to the SSC potential scale. At 25°C the SSC reference electrode is 199 mV more noble than the SHE (Sawyer and Roberts 1974 [DIRS 162259], pp. 39 to 45, Table 2-4) and the SCE reference electrode is 241 mV more noble than the SHE (ASTM G 3-89 1989 [DIRS 138911]). Therefore, the SCE scale potentials are converted to the SSC scale potentials by adding 42 mV.

In Equation 7-4, the ion concentrations are molar, while in Equation 7-3, the ion concentrations are molal. Also Equation 7-4 has been written in a form where nitrate ions are the only inhibiting ions considered. Comparison of the models is shown in Table 7-4 and Appendix XI. For the examples shown in Table 7-4, data for the crevice repassivation potential model are consistent with or underestimate the data for the crevice repassivation potential model published by the CNWRA (Dunn et al. 2005 [DIRS 178451]). Table 7-4 contains comparisons of the two models over a fairly broad range of chloride-ion and nitrate-ion concentrations.

Comparisons over the full range of chloride and nitrate compositions are significantly hampered by the different concentration scales used in the two models. Appendix XI contains three-dimensional graphs of both model results versus chloride-ion and nitrate-ion concentration in molality. These graphs are produced assuming that molar ion concentrations are equivalent to molal ion concentrations in evaluating the CNWRA crevice repassivation potential model, which (as demonstrated in Table 7-4) is not a very good assumption. Nonetheless, the comparison

shows that, while the crevice repassivation potential model developed in this report predicts lower crevice repassivation potential values over a majority of repository relevant chloride- and nitrate-ion molal values, the CNWRA crevice repassivation potential model may predict lower crevice repassivation potential values at high temperatures (greater than approximately 100°C) and at very low nitrate-ion concentrations (less than approximately 0.1 *m*). Additionally, at very high nitrate-ion molalities, which are not likely seepage compositions, the crevice repassivation potential model developed in this report may predict higher crevice repassivation potential values than does the CNRWA crevice repassivation potential model.

Table 7-4. Alternate Model Comparison to Crevice Repassivation Potential Model

Exposure Environment	[Cl] molal	[NO_3] molal	pH	E_{rCNWRA} (mV_{SSC})	E_{rcrev} Model	
					Mean (mV_{SSC})	Bounds (mV_{SSC})
1 *M* NaCl at 80°C	1.02	0	6.25	294	−46	44 (Upper) −137 (Lower)
4 *M* NaCl at 120°C	4.4	0	5.75	−282	−208	−116 (Upper) −300 (Lower)
5 *M* $CaCl_2$ at 105°C	11.99	0	4.00	−155	−165	−174 (Upper) −256 (Lower)
5 *M* $CaCl_2$ + 0.05 *M* $Ca(NO_3)_2$ at 120°C	11.70	0.12	3.96	−237	−195	−103 (Upper) −286 (Lower)
5 *M* $CaCl_2$ + 0.5 *M* $Ca(NO_3)_2$ at 105°C	12.59	1.26	3.15	645	−110	−19 (Upper) −201 (Lower)
1 *M* $CaCl_2$ + 1 *M* $Ca(NO_3)_2$ at 120°C	2.62	2.58	5.82	544	331	434 (Upper) 228 (Lower)

Sources: pH and chloride- and nitrate-ion molalities are from DTN: LL060904312251.186 [DIRS 178283], file: *NoCO2GetEQData.xls.*

Validation DTN: MO0706WPOBVALR.000, file: *Ecrit_EcorrValid3.xmcd* contains the calculated E_{rcrev} values.

A comparison of the crevice repassivation potentials obtained from the crevice repassivation potential model with the crevice repassivation potential data of Alloy 22 measured independently has shown that the validation criterion for Activity Three relating to the crevice repassivation model has been met. The comparisons to the CNWRA crevice repassivation potential model add further confidence that the YMP crevice repassivation potential model is adequate for its intended use.

7.2.4 Crevice Corrosion Initiation Model of the Waste Package Outer Barrier

The discussion in this section considers the correlations for E_{rcrev} and E_{corr} (or more accurately their difference, $\Delta E = E_{rcrev} - E_{corr}$) and compares the predicted results with experimental data/observations and the ACM discussed in Section 6.4.4.8.1. These discussions provide validation documentation for criteria related to Activities Three and Four.

Activity Three: The response of the correlations of E_{corr} and $E_{critical}$ are to be demonstrated to be reasonable and consistent with literature data on relevant corrosion resistant alloys and available analogues for the conditions expected in the repository. This activity will increase model confidence if the corroborating data for the localized corrosion initiation model components fall within the

three-standard deviations of the median for the relevant localized corrosion model component.

Activity Four: Demonstrate that the response of the correlations for E_{corr} and $E_{critical}$ of the waste package are consistent with other alternative models for localized corrosion initiation for the conditions expected in the repository. This activity will increase model confidence if the corroborating data for the localized corrosion initiation model components fall within the three-standard deviations of the median for the relevant localized corrosion model component.

Additional model validation was performed by comparing the model predictions for localized corrosion susceptibility with relevant observations. As discussed in Section 6.4.3 for the WPOB general corrosion model analysis, Alloy 22 creviced specimens were tested for over five years in three different solutions (SDW, SCW, and SAW) in the LTCTF. None of the creviced specimens suffered localized corrosion attack after being tested for this period. These observations are used to develop further confidence in the localized corrosion initiation model as a whole (i.e., crevice repassivation potential model (E_{rcrev}) compared to the long-term corrosion potential model (E_{corr})). If $\Delta E = E_{rcrev} - E_{corr}$ is negative, then crevice corrosion initiation is predicted to occur. The analysis results are summarized in Table 7-5. As indicated by the results in the table, the model predicts no localized corrosion occurrence for the exposure conditions of the five-year LTCTF crevice samples exposed to SDW and SCW at 90°C. The model predicts crevice corrosion will initiate for most specimens exposed to the acidic SAW solution at 90°C. It is possible that localized corrosion will initiate in the SAW solution later; however, the localized corrosion model may be conservative in this respect. These results show that the crevice corrosion initiation model adequately predicts the crevice corrosion susceptibility of Alloy 22 and is conservative in some cases.

Table 7-5. Comparison of Model Prediction for Loc alized Corrosion Susceptibility with Experimental Observations of Alloy 22 Crevice Samples Tested for Over Five Years in the Long-Term Corrosion Testing Facility

Long-Term Immersion Test Results					Model Results		
Exposure Environment	**Crevice Corrosion Observation**	**pH**	**[Cl] molal**	**[NO_3] molal**	**Mean ΔE (mV vs. SSC)**	**Lower Bound ΔE (mV vs. SSC)**	**Upper Bound ΔE (mV vs. SSC)**
SDW, 90°C	No	9.41	3.30×10^{-3}	9.73×10^{-4}	304	18	590
SCW, 90°C	No	10.04	0.21	0.12	373	101	646
SAW, 90°C	No	2.72	0.77	0.37	−168	−435	98

Sources: pH and chloride- and nitrate-ion molalities are from DTN: LL060904312251.186 [DIRS 178283], file: *AtmCO2GetEQData,xls*, "Case 9" for SDW, Case 2oc for SCW, and Case 1oc for SAW.

Validation DTN: MO0706WPOBVALR.000, file: *Ecrit_EcorrValid3.xmcd* contains the calculated ΔE values.

NOTES: SDW = simulated dilute water, SCW = simulated concentrated water, SAW = simulated acidified water, SSC = saturated silver chloride electrode.

To build further confidence in the long-term corrosion potential and crevice repassivation potential models, a summary of observations from the long-term corrosion potential experiments was produced (Table 7-6). Table 7-6 contains the solution chemistry, immersion time, cell

number, the number of creviced geometry specimens exposed, the number of creviced specimens observed to undergo crevice corrosion (column labeled "CC"), the number of rod geometry specimens exposed, the number of rod geometry specimens observed to undergo pitting corrosion (column labeled "PC"), and the mean and the bounding values of $\Delta E = E_{rcrev} - E_{corr}$. If ΔE is negative, then crevice corrosion initiation is predicted to occur.

Table 7-6. Summary of Long-Term Corrosion Test Cell Data

Solution	Immersion Days	Cell #	T(°C)	Creviced Geometry	CC	Rod Geometry	PC	Modeled ΔE		
								Lower Bound	Mean	Upper Bound
5 *m* $CaCl_2$ + 5 *m* $Ca(NO_3)_2$	723	33	120	4	0	2	0	−398	−116	166
5 *m* $CaCl_2$ + 5 *m* $Ca(NO_3)_2$	729	32	100	4	0	2	0	−184	93	370
3.5 *m* NaCl + 0.175 *m* KNO_3 + 0.7 *m* $MgSO_4$	735	31	80	4	2	2	0	−227	38	303
1 *M* NaCl + 0.15 *M* KNO_3	741	30	90	4	0	2	0	−202	62	325
1 *M* NaCl + 0.15 *M* KNO_3	749	29	75	4	0	2	0	−185	80	344
5 *M* $CaCl_2$	650	28	90	4	4	2	0	−466	−201	63
3.5 *m* NaCl + 0.175 *m* KNO_3	252	25	100	4	0	0	0	−225	39	304
3.5 *m* NaCl + 0.525 *m* KNO_3	256	24	100	4	0	0	0	−223	41	305
6 *m* NaCl + 0.9 *m* KNO_3	265	23	100	4	2	0	0	−236	28	291
6 *m* NaCl + 0.3 *m* KNO_3	280	22	100	4	0	0	0	−239	26	290
5 *M* $CaCl_2$ + 0.5 *M* $Ca(NO_3)_2$	463	21	90	6	6	6	0	−597	−332	-66
5 *M* $CaCl_2$	497	20	120	6	6	6	0	−462	−191	79
BSW	256	19	105	0	0	8	0	15	284	554
4 *M* NaCl	328	18	90	0	0	6	0	−233	31	295
SAW w/o Silicate	375	17	90	0	0	6	0	−485	−216	52
SCW	394	16	90	0	0	6	0	124	394	665
5 *M* $CaCl_2$ + 0.5 *M* $Ca(NO_3)_2$	693	15	90	0	0	6	1	−597	−332	−66
5 *M* $CaCl_2$ + 0.05 *M* $Ca(NO_3)_2$	704	14	90	0	0	6	1	−458	−194	70
1 *M* $CaCl_2$ + 1 *M* $Ca(NO_3)_2$	622	13	90	0	0	6	0	−93	186	465
4.5 years LTCTF SAW	834	10	90	0	0	8	0	−435	−168	98
SAW	876	9	90	0	0	8	0	−587	−322	−57
SAW - LTCTF Vessel 26	846	7-2	25	0	0	3	0	−178	106	390
SDW - LTCTF Vessel 30	1,089	6	90	0	0	2	0	18	304	590
SDW - LTCTF Vessel 29	1,089	5	60	0	0	2	0	107	393	678
BSW	729	4	105	1	0	1	0	15	284	554
SCW - LTCTF Vessel 28	1,089	3	90	0	0	2	0	101	373	646
SAW - LTCTF Vessel 26	1,102	2	90	0	0	2	0	−435	−168	98
SAW - LTCTF Vessel 25	1,089	1	60	0	0	2	0	−312	−42	228

Table 7-6. Summary of Long-Term Corrosion Test Cell Data (Continued)

Solution	Immersion Days	Cell #	T(°C)	Creviced Geometry	CC	Rod Geometry	PC	Modeled ΔE		
								Lower Bound	Mean	Upper Bound
Data below is from cells not used for long-term corrosion potential model development										
1 *m* NaCl + 0.05 *m* KNO_3	223	27	100	4	0	0	0	−218	47	312
1 *m* NaCl + 0.15 *m* KNO_3	230	26	100	4	0	0	0	−217	47	312
5 *M* $CaCl_2$	894	8	120	0	0	5	5	−462	−191	79
SCW - LTCTF Vessel 27	218	7-1	60	0	0	2	0	281	559	837

Source: DTN: LL060900512251.177 [DIRS 178271], file: *Summary Ecorr Cells 1-36 29Sep06.xls*.

Output DTN: MO0703PAGENCOR.001, file: *Ecrit_EcorrValid_Cells3a.xmcd*.

NOTES: Variations in solution composition (e.g., between the SAW solution compositions in Cells, 2, 9, 10, and 17) can lead to variations in the calculated ΔE values. Details of the cell solution compositions can be found in Output DTN: MO0703PAGENCOR.001, file: *EcorrRawData3.xls*.

CC = crevice corrosion, LTCTF = Long-Term Corrosion Test Facility, PC = pitting corrosion, SAW = simulated acidified water, SCW = simulated concentrated water, SDW = simulated dilute water.

Examination of Table 7-6 reveals that the crevice corrosion initiation model is consistent with or conservative relative to the long-term corrosion test results. For example, Cells 32 and 33 contain 5 *m* $CaCl_2$ + 5 *m* $Ca(NO_3)_2$ at 100°C and 120°C, respectively. Each cell contained four creviced geometry specimens and two rod (boldly exposed) specimens. No localized corrosion (neither crevice nor pitting) was initiated during about 730 days of exposure. Using the results obtained for ΔE, the crevice corrosion initiation model predicts that crevice corrosion should have initiated for over 50% of specimens at 120°C (the mean ΔE is negative) and for less than 50% of the specimens exposed at 100°C. Neither crevice corrosion nor pitting corrosion was observed, indicating that the crevice corrosion initiation model is conservative (or crevice corrosion could initiate for longer exposure times).

For 5 *M* $CaCl_2$ + 0.5 *M* $Ca(NO_3)_2$ at 90°C (cells 15 and 21), crevice corrosion was observed on six out of six creviced geometry specimens, and pitting corrosion was observed on one out of 12 rods. The crevice corrosion initiation model predicts that crevice corrosion should initiate for virtually all creviced specimens in agreement with these observations. The crevice corrosion initiation model is conservative with respect to the observations in SAW (cells 1, 2, 7-2, 9, and 17). In this solution, no localized corrosion was observed (although only rod specimens were exposed); however, the crevice corrosion initiation model indicates that crevice corrosion initiation is very likely. The crevice corrosion initiation model is consistent with experimental observations obtained in BSW, SDW, and SCW solutions (Cells 3, 4, 5, 6, 7-1, 16, and 19) in that crevice corrosion initiation was not observed for specimens exposed to these media and the predicted crevice repassivation potentials are positive (i.e., no crevice corrosion initiation is predicted) for these exposure conditions. The comparisons in Table 7-6 indicate that the crevice corrosion initiation model is consistent with or conservative relative to the long-term corrosion test results, and sufficiently accurate for its intended use in total system performance assessment (TSPA).

This favorable comparison between the crevice corrosion initiation model ($\Delta E = E_{rcrev} - E_{corr}$) and the long-term corrosion potential test observations also adds confidence in the use of the crevice corrosion initiation model implementation criteria discussed in Section 6.4.4.6.6.

Section 6.4.4.8.1 documents the use of temperature as an alternative parameter to determine susceptibility to localized corrosion. Values of critical pitting temperature and critical crevice corrosion temperature have been measured for Alloy 22, in relatively pure concentrated chloride solutions (i.e., high salinity, $[Cl^-]$ = 24,300 μg/g, and a high $[Cl^-]$ to $[SO_4^{2-}]$ ratio) (Haynes International 1997 [DIRS 100897], p. 9; McGuire et al. 1998 [DIRS 152193], Section 5.1.2). Under these highly corrosive conditions, the critical crevice corrosion temperature for Alloy 22 was measured to be 102°C. Since this critical temperature has been evaluated only in a limited set of environments, it would not be expected to be applicable to a wider range of environments. Therefore, the use of a critical temperature-based model is not advisable. Also, the crevice corrosion initiation model developed in this report utilizes long-term corrosion potential data while testing of the critical crevice corrosion temperature used a 100-hr exposure period. Furthermore, several of the graphs in Section 6.4.4.6 (e.g., Figure 6-43, Figure 6-44, Figure 6-45, and Figure 6-46) indicate that the crevice corrosion initiation model predicts the possibility for crevice corrosion initiation at temperatures below 102°C for some exposure conditions. This observation gives further confidence in the crevice corrosion initiation model.

The model validation documented in this section has shown that the criterion for Activity Four has been met and provides additional confidence that Activity Three has been met. Therefore, the crevice corrosion initiation model of the WPOB is adequate for its intended use.

7.2.5 Localized Corrosion Penetration Model of the Waste Package Outer Barrier

Validation of the localized corrosion penetration rate model of the WPOB requires meeting the validation criterion for Activities One and Two.

Activity One: Show that the propagation rates for the waste package are reasonable and consistent with rates determined by alternative techniques or alternative models for the conditions expected in the repository. This activity will be considered successful if trends in the model predictions are matched by trends seen in the data.

Activity Two: Show that the modeled propagation rates of general corrosion and localized corrosion of the waste package are reasonable and consistent with rates from literature data and/or natural analogues and/or industrial analogues of relevant corrosion resistant alloys for the conditions expected in the repository. This activity will be considered successful if the modeled propagation rates must be greater than or within one order of magnitude of the corroborating data.

Due to the outstanding corrosion resistance of Alloy 22, very little data exist for such localized corrosion under the conditions expected in the repository. The literature data for localized corrosion of relevant alloys that were considered for the current localized penetration rate model (Section 6.4.4.7) were obtained in extremely corrosive conditions. Those extreme penetration rates found in the literature were used to bound the localized corrosion rates of Alloy 22 under repository conditions.

In the development of the localized corrosion penetration model, it was noted that the Alloy 22 average corrosion rate in a highly aggressive 10% ferric chloride crevice corrosion test solution was about 12.7 μm/yr. The average corrosion rate of Alloy C-276 and Alloy C-4 (Ni-Cr-Mo

alloys similar to Alloy 22) in the same test solution were 1.4 mils/yr (35.6 μm/yr) and 20 mils/yr (508 μm/yr), respectively (Haynes International 1997 [DIRS 100897], p. 8). These values fall within the range of rates used for the Alloy 22 localized corrosion penetration model; in addition, they illustrate that Alloy 22 is more corrosion resistant than these alloys. In a solution composed of 7 volume % H_2SO_4, 3 volume % HCl, 1 wt % $FeCl_3$, and 1 wt % $CuCl_2$, a penetration rate of 610 μm/yr measured by weight-loss was observed for Alloy C-276 at 102°C (Gdowski 1991 [DIRS 100859], Table 23). This value also falls within the range of rates used for the Alloy 22 localized corrosion penetration model. The purpose of adding oxidants such as $Fe^{3+}$and Cu^{2+} in the solutions used in these short term corrosion tests (Gdowski 1991 [DIRS 100859], Table 23; Haynes International 1997 [DIRS 100897], p. 8) was to increase the corrosivity of the exposure environment. Although this environment could be relevant to some applications of Alloy 22, the composition of the crevice solution in the repository could be different. While anions such as chloride and sulfate are expected to be present in the repository crevice solution and some Fe^{3+}can also be present due to dissolution of iron from Alloy 22, Cu^{2+} is not expected to be present in the crevice solution because Alloy 22 does not contain copper.

Smailos (1993 [DIRS 168164]) tested Alloy C-4 in two aggressive $MgCl_2$-based brines (Brines 1 and 2) and one NaCl-based brine (Brine 3) at 150°C for up to 18 months. It was found that localized corrosion (pitting) was observed in Brines 1 and 2 (the $MgCl_2$-based brines) but not in Brine 3 (the NaCl-based brine). Maximum pit depths between 300 and 900 μm were observed in Brines 1 and 2 after 18 months of testing (Smailos 1993 [DIRS 168164], Table III). These values correspond to pit penetration rates of between 200 and 600 μm/yr. These values fall within the range of rates used for the Alloy 22 localized corrosion penetration model. Pitting was not observed in Brine 1 at 12 months, and the maximum pit depth reported at 18 months was 300 μm, which, assuming all pit growth occurred in six months, corresponds to a pit growth rate of 600 μm/yr. Also, after 18 months of testing, pitting was not observed in Brine 3 (the NaCl-based brine), which is likely to be more representative of repository conditions than $MgCl_2$-based brines, although pitting might have initiated if the testing period had been longer. At 25°C, the pH of Brine 1 was reported to be 4.6, the pH of Brine 2 was reported to be 4.1, and the pH of Brine 3 was reported to be 6.5 (Smailos 1993 [DIRS 168164], Table II). This difference in pH values between the brines may explain differences in their ability to initiate localized corrosion. CNWRA investigators reported the maximum crevice corrosion penetration rate of 13 mm/yr (i.e., 1,300 μm/yr) for creviced Alloy 22 in a 5 *M* NaCl solution at 95°C containing 2×10^{-4} *M* $CuCl_2$ (He and Dunn 2005 [DIRS 178453], Section 3.3). This value is corroborative of the upper bound value of the crevice corrosion penetration rate of 1,270 μm/yr for Alloy 22 (Section 6.4.4.7).

In addition, the localized corrosion penetration model assumes that, when it occurs, localized corrosion of the WPOB propagates at a (time-independent) constant rate (Assumption 5.4, Section 5). This assumption is highly conservative because it is known that the localized corrosion rate decreases with time, and this is particularly more likely under the discontinuous and tortuous thin water film conditions expected on the waste package surface in the postclosure repository. Section 6.4.4.8.2 provides further discussion on the above issues.

Based on the above discussion, the range of propagation rates used in the localized corrosion model of WPOB is reasonable and consistent with the literature data on relevant corrosion-resistant alloys for the conditions expected in the repository. Thus, the validation criteria for

Activities One and Two have been met. Therefore, the localized corrosion penetration model of the WPOB is adequate for its intended use.

7.3 SUMMARY OF MODEL VALIDATION

In light of the discussion, it is concluded that the general and localized corrosion models for the WPOB and their output are corroborated by those reported in the scientific literature. Results of the validation activities performed for building confidence in the models demonstrate they have a strong and defensible scientific basis. Criteria used to evaluate whether the required level of confidence was achieved were met, and the model results are valid for their intended use.

INTENTIONALLY LEFT BLANK

8. CONCLUSIONS

8.1 MODEL SUMMARY

This report documents the analyses and models for general and localized corrosion of the waste package outer barrier (WPOB). The technical product outputs of this report are contained in output DTNs: MO0703PAGENCOR.001 and MO0612WPOUTERB.000. Analyses related to validation of the models developed in this report are contained in validation DTN: MO0706WPOBVALR.000. The purpose of the general and localized corrosion models is to predict degradation of the Alloy 22 WPOB by general and localized corrosion processes under the expected repository environmental conditions over the repository performance period. The general and localized corrosion models account for aqueous general corrosion, microbially influenced corrosion (MIC), crevice corrosion initiation, and crevice corrosion growth. A model overview is graphically presented in Figure 8-1.

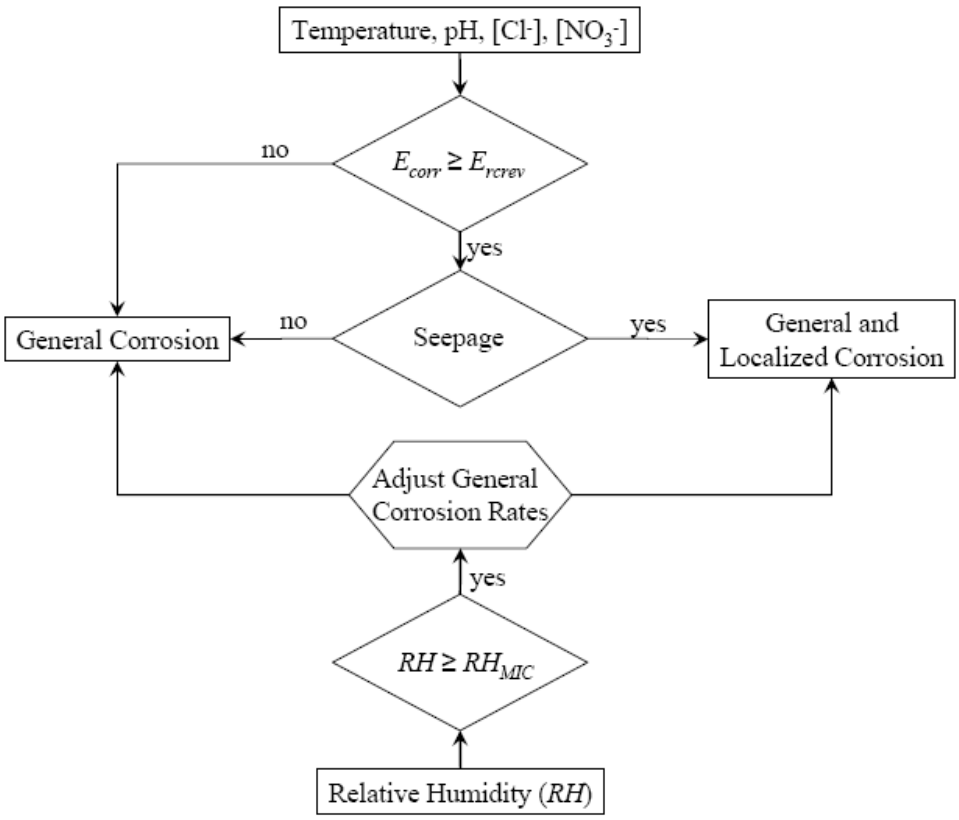

Figure 8-1. Schematic Representation of General Corrosion and Localized Corrosion Model of the Waste Package Outer Barrier

Dry oxidation is not a performance-limiting process of the WPOB under the exposure conditions expected in the repository and is not considered for the waste package performance analysis (Section 6.4.2). Aging and phase instability of Alloy 22 is not expected to significantly impact the WPOB corrosion performance under the thermal conditions expected in the repository; therefore, this process is not considered in the waste package performance analysis (Section 6.4.6).

The extremely low general corrosion rates and excellent resistance to localized corrosion of the WPOB in the repository depend on the long-term stability of the passive film under repository exposure conditions. The passivity of Alloy 22 was evaluated by examining the oxide layers formed in a mixed-salt environment at 95°C (Section 6.4.1.2). The surface analysis data indicated that the oxide layers responsible for passivity of Alloy 22 consist of chromium oxide (Cr_2O_3) containing nickel. The collected data indicated that the passive film on Alloy 22 is very protective and stable.

The general corrosion rate of the WPOB is a function of temperature, expressed with an apparent activation energy using a modified Arrhenius relation (Section 6.4.3.4). As a bounding and conservative analysis, for a constant waste package surface temperature of 150ºC, and using the medium level of uncertainty for the 60°C general corrosion rate distribution (b = 8.134 nm/yr, c = 1.476 nm/yr, from Table 6-7) and the medium temperature dependence (C_1 = 4,905 K), the median general corrosion rate is about 145 nm/yr. For example, using these values, the depth of general corrosion penetration in 10,000 years is about 1.45 mm, or about 6% of the total thickness of the WPOB (25.4 mm). This analysis demonstrates that the waste package performance in the repository is not limited by general corrosion during the first 10,000 years after repository closure.

The WPOB is subject to MIC when the relative humidity at the waste package surface is equal to or greater than a relative humidity threshold uniformly distributed between 75% and 90% relative humidity (Section 6.4.5). The MIC effect is represented by an enhancement to the abiotic general corrosion rate of the WPOB, which is uniformly distributed between 1 and 2 (Section 6.4.5).

Localized corrosion of the WPOB is modeled with a crevice corrosion initiation model and a propagation model (Section 6.4.4). In the crevice corrosion initiation model, crevice corrosion of the WPOB initiates when the long-term corrosion potential (E_{corr}) is equal to or greater than the crevice repassivation potential (E_{rcrev}), that is, ΔE (= $E_{rcrev} - E_{corr}$) ≤ 0. The WPOB is resistant to crevice corrosion initiation if the solution contacting the waste package has a neutral to alkaline pH and contains significant concentrations of inhibitive ions such as nitrate. The WPOB is potentially susceptible to crevice corrosion if an acidic chloride-containing solution with relatively low concentrations of inhibitive ions contacts the waste package while it is at elevated temperatures. However, once the waste package cools and the solutions contacting the waste package become less concentrated and less aggressive, localized corrosion is not expected to initiate.

Additional details of the model summary are given in the following sections.

8.2 WASTE PACKAGE OUTER BARRIER GENERAL CORROSION MODEL OUTPUTS

The general corrosion model for the WPOB (Section 6.4.3.4) is based on a temperature dependence of the general corrosion process, represented by an apparent activation energy using a modified Arrhenius relation. The model is expressed in Equation 8-1 (Section 6.4.3.4, Equation 6-28):

$$\ln(R_T) = \ln(R_o) + C_1\left(\frac{1}{T_0} - \frac{1}{T}\right) \quad \text{(Eq. 8-1)}$$

where R_T is the temperature-dependent general corrosion rate in nm/yr, T is absolute temperature in Kelvin, T_0 = 333.15 K (60°C), and R_o and C_1 are constants. The temperature-dependence term (C_1) was obtained from short-term polarization resistance data for Alloy 22 specimens tested for a range of sample configurations, metallurgical conditions, and exposure conditions. The temperature-dependence term is normally distributed with a mean of 4,905 K and a standard deviation of 1,413 K. The apparent activation energy was estimated to be 40.78 ± 11.75 kJ/mol. R_o is a Weibull distribution (with parameters given in Table 6-7) that was fit to the general corrosion rate distribution derived from weight-loss data of the five-year exposed crevice specimens. The five-year data were considered to represent the distribution of long-term general corrosion rates of the WPOB at T_0 = 333.15 K (60°C). In TSPA, the low, medium, and high general corrosion rate distribution parameters should be randomly selected in such a way that the low and high general corrosion rate distributions are each used for 5% of realizations and the medium general corrosion rate distribution is used for the remaining 90% of realizations.

The entire variance in R_o represents variability in the general corrosion process. The general corrosion rate variability is applied among the individual waste packages and among individual areas on the surface of a waste package. The entire variance in the temperature-dependence term (C_1) is due to uncertainty, and the uncertainty is truncated at −3 and +2 standard deviations.

The general corrosion model developed in this report (Section 6.4.3.4) was developed using data from both mixed ionic environments and simple salt solutions, including highly concentrated chloride brines and chloride brines containing nitrate ions. In Section 7.2, the general corrosion model is validated against data obtained at temperatures as high as 180°C. Therefore, the general corrosion model should be applicable over all repository exposure environments.

The general corrosion model is applied to all environmental conditions in the repository and is based on corrosion measurements in the presence of an aqueous electrolyte. The WPOB is considered subject to MIC when the relative humidity at the WPOB surface is equal to or greater than a relative humidity threshold uniformly distributed between 75% and 90% relative humidity (Section 6.4.5). This is a conservative approach because MIC occurs when a source of moisture (e.g., relative humidity) and supporting nutrients are simultaneously available to a microbial community. The effect of MIC on general corrosion of the WPOB is represented by an enhancement factor applied to the general corrosion rate determined from Equation 8-1. The MIC enhancement factor is uniformly distributed between 1 and 2, and the entire variance of the distribution is due to variability.

The technical product outputs of the general corrosion model analysis are documented in the output DTN: MO0703PAGENCOR.001 and summarized in Table 8-1.

Table 8-1. Summary of General Corrosion Model Output for Waste Package Outer Barrier

Parameter Name	Parameter Definition/Description	Parameter Type	Parameter Value and Uncertainty/Variability	Parameter Source
lnR_o TSPA model file names are *WDlnR_ESC_L_cdf* *WDlnR_ESC_M_cdf* *WDlnR_ESC_H_cdf*	Cumulative distribution function for the natural logarithm of the general corrosion rate for Alloy 22 (R_o) R_o is the general corrosion rate of Alloy 22 at 60°C. Variance in R_o represents spatial variability in the general corrosion process. (Section 6.4.3.4)	Stochastic	Three sets of values corresponding to low, medium, and high levels of uncertainties in GC_shape and GC_scale parameters	Source: Developed by TSPA from GC_Scale and GC_Shape parameters.
GC_scale	Scale parameter for Weibull distribution (b) (Section 6.4.3.4)	Stochastic	6.628 (low): 5% of realizations 8.134 (medium): 90% of realizations 9.774 (high): 5% of realizations Different values are uncertainty. Overall distribution is spatial variability Table 6-7	DTN: MO0703PAGENCOR.001 file: *BaseCase GC CDFs.xls*.
GC_shape	Shape parameter for Weibull distribution (c) (Section 6.4.3.4)	Stochastic	1.380 (low): 5% of realizations 1.476 (medium): 90% of realizations 1.578 (high): 5% of realizations Different values are uncertainty. Overall distribution is spatial variability Table 6-7	DTN: MO0703PAGENCOR.001 file: *BaseCase GC CDFs.xls*.
C1_GenCorr_A22_a	Parameter for the temperature dependence of general corrosion rate (C_1) (Section 6.4.3.4)	Stochastic	Truncated (at –3 and +2 standard deviations) normal distribution. Mean: 4,905 K, standard deviation: 1,413 K. Uncertainty	DTN: MO0703PAGENCOR.001 file: *BaseCase GC CDFs.xls*.
MIC_A22_a	MIC general corrosion enhancement factor (Section 6.4.5)	Stochastic	Uniform distribution between 1 and 2 Spatial variability	DTN: MO0703PAGENCOR.001 file: *MIC Summary.pdf*.
MIC_RHThresh_a	Relative humidity threshold for MIC (Section 6.4.5)	Stochastic	Uniform distribution between 75% to 90% Uncertainty	DTN: MO0703PAGENCOR.001 file: *MIC Summary.pdf*.

8.3 WASTE PACKAGE OUTER BARRIER LOCALIZED CORROSION MODEL OUTPUTS

Localized corrosion of the WPOB is modeled with two model components: an initiation model and a propagation model (Section 6.4.4).

8.3.1 Waste Package Outer Barrier Localized Corrosion Initiation Outputs

Localized corrosion of the WPOB initiates when the long-term corrosion potential (E_{corr}) is equal to or greater than a critical potential ($E_{critical}$), that is, ΔE ($= E_{critical} - E_{corr}$) ≤ 0. As a conservative measure, the localized corrosion initiation model uses the crevice repassivation potential (E_{rcrev}) as the critical potential. The crevice repassivation potential model (E_{rcrev}) is expressed in Equation 8-2 (Section 6.4.4.3, Equation 6-35):

$$E_{rcrev} = a_o + a_1 T + a_2 \ln\left[Cl^-\right] + a_3 \frac{\left[NO_3^-\right]}{\left[Cl^-\right]} + a_4 T \cdot \left[Cl^-\right] + \varepsilon_{rcrev} \qquad \text{(Eq. 8-2)}$$

where E_{rcrev} is the crevice repassivation potential (mV versus SSC) in the absence of inhibiting nitrate ions, a_o, a_1, a_2, a_3, and a_4 are constants, T is the temperature (°C), and $[Cl^-]$ is the molal chloride-ion concentration. The error term, ε_{rcrev}, represents data variance not explained by the fitting procedure. The potentials are in mV versus SSC. The mean values of the model coefficients and their uncertainty (±1 standard deviation) were determined to be: a_o = 190.242 ± 18.373, $a_1 = -3.008 \pm 0.225$, $a_2 = -46.800 \pm 3.126$, $a_3 = 535.625 \pm 26.140$, and $a_4 = 0.061 \pm 0.010$. The units of the coefficients are such that the units of E_{rcrev} are mV versus SSC. The variance of the model coefficients is calculated via a covariance matrix (Equation 8-3), and the entire variance is due to uncertainty. The model coefficients are sampled from a multivariate normal distribution with the above-mentioned mean values consistent with the covariance matrix given in Equation 8-3 (Section 6.4.4.3, Equation 6-37).

$$r\Sigma = \begin{pmatrix} 3.376\text{E+002} & -3.909\text{E+000} & -9.310\text{E+000} & 8.236\text{E+001} & 3.559\text{E-002} \\ -3.909\text{E+000} & 5.077\text{E-002} & 9.271\text{E-002} & -1.202\text{E+000} & -8.308\text{E-004} \\ -9.310\text{E+000} & 9.271\text{E-002} & 9.770\text{E+000} & 1.930\text{E+000} & -2.048\text{E-002} \\ 8.236\text{E+001} & -1.202\text{E+000} & 1.930\text{E+000} & 6.833\text{E+002} & -2.790\text{E-002} \\ 3.559\text{E-002} & -8.308\text{E-004} & -2.048\text{E-002} & -2.790\text{E-002} & 1.011\text{E-004} \end{pmatrix} \qquad \text{(Eq. 8-3)}$$

The error term, ε_{rcrev}, represents data variance not explained by the fitting procedure and has a normal distribution with a mean of zero mV versus SSC and a standard deviation (s_{rcrev}) of 45.055 mV versus SSC. Variance in the error term, ε_{rcrev}, is attributed to uncertainty.

The prediction intervals for the *unconstrained* crevice repassivation potential model are calculated by adding to the median estimate (i.e., the expected value of E_{rcrev} obtained by using the mean values of the model coefficients from Equation 8-2) an adjustment based on the standard deviation of the error term (s_{rcrev}), the covariance matrix of the model coefficients (Equation 8-3), and the values of the exposure parameters for the data point being evaluated.

The adjustment factor is written in matrix form as Equation 8-4:

$$\pm z\sqrt{\left[1 \quad T \quad \ln\left[Cl^-\right] \quad \frac{[NO_3^-]}{[Cl^-]} \quad T\cdot\ln\left[Cl^-\right]\right] r\Sigma \left[1 \quad T \quad \ln\left[Cl^-\right] \quad \frac{[NO_3^-]}{[Cl^-]} \quad T\cdot\ln\left[Cl^-\right]\right]^T + s_{rcrev}^2} \quad \text{(Eq. 8-4)}$$

where z would be the number of standard deviations at which the adjustment factor is to be evaluated. The values of the crevice repassivation potential are *constrained* to be within the range defined by the ±2 standard deviation (i.e., $z = \pm 2$) prediction interval of the *unconstrained* crevice repassivation potential model. That is, the ±2 standard deviation prediction intervals of the *unconstrained* crevice repassivation potential relationship (Equation 8-2 adjusted by Equation 8-4) are used as bounds on the value that the crevice repassivation potential may have. Thus, if the calculated *unconstrained* crevice repassivation potential exceeds the +2 standard deviation prediction bound of the *unconstrained* crevice repassivation potential model, the crevice repassivation potential value of the +2 standard deviation prediction bound of the *unconstrained* crevice repassivation potential model should be used as the value of the crevice repassivation potential for the given exposure conditions. Similarly, if the calculated *unconstrained* crevice repassivation potential does not exceed the −2 standard deviation prediction bound of the *unconstrained* crevice repassivation potential model, the crevice repassivation potential value of the −2 standard deviation prediction bound of the *unconstrained* crevice repassivation potential model should be used as the value of the crevice repassivation potential for the given exposure conditions.

The long-term corrosion potential model (E_{corr}) for the WPOB is expressed in Equation 8-5 (Section 6.4.4.5, Equation 6-39):

$$E_{corr} = c_o + c_1 T + c_2\, pH + c_3 \frac{[NO_3^-]}{[Cl^-]} + c_4 T \frac{[NO_3^-]}{[Cl^-]} + c_5\, pH \frac{[NO_3^-]}{[Cl^-]} + c_6\, pH \ln[Cl^-] + \varepsilon_{corr} \quad \text{(Eq. 8-5)}$$

where T is the temperature (°C), $[Cl^-]$ is the chloride-ion concentration in molality (m, moles/kg water), $[NO_3^-]$ is the molal nitrate-ion concentration, and c_o, c_1, c_2, c_3, c_4, c_5, and c_6 are coefficients of the model parameters. The mean values of the model coefficients and their uncertainty (±1 standard deviation) are: $c_0 = 1{,}051.219 \pm 119.774$, $c_1 = -3.024 \pm 0.977$, $c_2 = -155.976 \pm 11.495$, $c_3 = -1{,}352.040 \pm 252.224$, $c_4 = 10.875 \pm 1.890$, $c_5 = 137.856 \pm 23.158$, and $c_6 = -8.498 \pm 0.801$. The variance of the model coefficients is calculated via a covariance matrix (Equation 8-5), and the entire variance is due to uncertainty. The model coefficients are sampled from a multivariate normal distribution with the above-mentioned mean values consistent with the covariance matrix given in Equation 8-5.

$$r\Sigma 2 = \begin{pmatrix} 1.435E+004 & -1.031E+002 & -9.152E+002 & -2.762E+004 & 1.802E+002 & 1.884E+003 & -1.660E+001 \\ -1.031E+002 & 9.539E-001 & 2.770E+000 & 1.846E+002 & -1.519E+000 & -6.817E+000 & -7.543E-002 \\ -9.152E+002 & 2.770E+000 & 1.321E+002 & 1.971E+003 & -6.909E+000 & -2.515E+002 & 4.409E+000 \\ -2.762E+004 & 1.846E+002 & 1.971E+003 & 6.362E+004 & -4.223E+002 & -4.107E+003 & 5.959E+001 \\ 1.802E+002 & -1.519E+000 & -6.909E+000 & -4.223E+002 & 3.573E+000 & 1.337E+001 & -2.622E-001 \\ 1.884E+003 & -6.817E+000 & -2.515E+002 & -4.107E+003 & 1.337E+001 & 5.363E+002 & -6.697E+000 \\ -1.660E+001 & -7.543E-002 & 4.409E+000 & 5.959E+001 & -2.622E-001 & -6.697E+000 & 6.418E-001 \end{pmatrix} \quad \text{(Eq. 8-6)}$$

The error term, ε_{corr}, represents data variance not explained by the fitting procedure and has a normal distribution with a mean of zero mV versus SSC and a standard deviation of 85.265 mV versus SSC. Variance in the error term, ε_{corr}, is attributed to uncertainty.

The prediction intervals are calculated by adding to the median estimate (E_{corr} from Equation 8-5) an adjustment based on the standard deviation of the error term (s_{corr}), the covariance matrix (Equation 8-6) and the values of the exposure parameters for the data point being evaluated. The adjustment factor is written in matrix form as Equation 8-7:

$$\pm z\sqrt{\left[1 \quad T \quad pH \quad \frac{[NO_3^-]}{[Cl^-]} \quad T\cdot\frac{[NO_3^-]}{[Cl^-]} \quad pH\frac{[NO_3^-]}{[Cl^-]} \quad pH\ln[Cl^-]\right] r\Sigma 2 \left[1 \quad T \quad pH \quad \frac{[NO_3^-]}{[Cl^-]} \quad T\cdot\frac{[NO_3^-]}{[Cl^-]} \quad pH\frac{[NO_3^-]}{[Cl^-]} \quad pH\ln[Cl^-]\right]^T + s_{corr}^2} \quad \text{(Eq. 8-7)}$$

where z would be the number of standard deviations at which the adjustment factor is to be evaluated. The values of the long-term corrosion potential are *constrained* to be within the range defined by the ±2 standard deviation (i.e., $z = \pm 2$) prediction interval of the *unconstrained* long-term corrosion potential model. That is, the ±2 standard deviation prediction interval of the *unconstrained* long-term corrosion potential relationship (Equation 8-5 adjusted by Equation 8-7) are used as bounds on the value that the long-term corrosion potential may have. That is, if the calculated *unconstrained* long-term corrosion potential exceeds the +2 standard deviation prediction bound of the *unconstrained* long-term corrosion potential model, the long-term corrosion potential value of the +2 standard deviation prediction bound of the *unconstrained* long-term corrosion potential model should be used as the value of the long-term corrosion potential for the given exposure conditions. Similarly, if the calculated *unconstrained* long-term corrosion potential does not exceed the −2 standard deviation prediction bound of the *unconstrained* long-term corrosion potential model, the long-term corrosion potential value of the −2 standard deviation prediction bound of the *unconstrained* long-term corrosion potential should be used as the value of the long-term corrosion potential for the given exposure conditions.

The empirical correlations used in the WPOB crevice corrosion initiation model for the long-term corrosion potential (E_{corr}) and crevice repassivation potential (E_{rcrev}) are expressed as functions of temperature, *pH* (for E_{corr} only), chloride-ion concentration, and nitrate-ion concentration (Sections 6.4.4.3 and 6.4.4.5). Based on the range of environmental conditions in which the input data were obtained (Appendices VIII and IX) and the model validation activities (Sections 7.2.2 and 7.2.3), the application of the WPOB crevice corrosion initiation model can be summarized as follows.

The WPOB crevice corrosion initiation model is used to evaluate the crevice corrosion initiation behavior of the Alloy 22 WPOB. The Alloy 22 WPOB contains solution-heat-treated welds and

base metal that have had the solution-heat-treated film removed, as well as low-plasticity burnished closure weld regions (e.g., SNL 2007 [DIRS 179394], Section 4.1.2). The area of the Alloy 22 WPOB that is contacted by seepage is potentially subject to localized corrosion. Localized corrosion of the WPOB is considered to initiate when the open-circuit corrosion potential (E_{corr}) is equal to or greater than a critical potential (the crevice repassivation potential (E_{rcrev}) in the current model), that is, ΔE ($=E_{rcrev} - E_{corr}$) ≤ 0. If the exposure temperature is greater than or equal to 20°C and less than or equal to 120°C, then the WPOB crevice corrosion initiation model is implemented by evaluating the long-term corrosion potential (E_{corr}) and crevice repassivation potential (E_{rcrev}) (Sections 6.4.4.3 and 6.4.4.5) in accordance with the following implementation rules:

1) If the nitrate ion-to-chloride ion ratio in the environment exceeds 1, then evaluate E_{rcrev} and E_{corr} at a nitrate ion-to-chloride ion ratio of 1. If the molality of chloride ion is less than 0.0005 *m*, the nitrate ion-to-chloride ion ratio should be evaluated with a chloride-ion concentration of 0.0005 *m*.

2) If the molality of chloride ion in the environment exceeds 20 *m*, then evaluate E_{rcrev} and E_{corr} at a chloride-ion molality of 20 *m*. If the molality of chloride ion is less than 0.0005 *m*, then evaluate E_{rcrev} and E_{corr} at a chloride-ion molality of 0.0005 *m*.

3) If the *pH* in the environment exceeds 10, then evaluate E_{corr} at a *pH* of 10. If the *pH* in the environment is less than 1.9, then initiate localized corrosion.

If crevice corrosion is determined to initiate, then crevice corrosion occurs at a constant rate throughout the simulation period regardless of changes in the bulk chemical exposure environment. This is a conservative modeling assumption (Assumption 5.4, Section 5) and is used because the crevice corrosion model does not account for the possibility of crevice corrosion repassivation or stifling. Nitrate ions inhibit localized corrosion initiation (Section 6.4.4.3). In addition, carbonate and sulfate ions may have an inhibitive effect on localized corrosion. Therefore, because only nitrate ions are accounted for in the model, the results for solutions with significant amounts of other potentially inhibitive ions in addition to nitrate ions are conservative. The model results for the beneficial effects of the inhibitive ions combined with alkaline pH conditions of the typical carbonate-containing waters in the repository are consistent with the experimental observations on the immunity of Alloy 22 to localized corrosion in those waters (Section 7.2.3).

The entire variance of the crevice corrosion initiation model (i.e., the crevice repassivation potential model and the corrosion potential model) is due to uncertainty. Variability in the crevice repassivation potential and long-term corrosion potential among the waste packages to be modeled is represented with the temporally and spatially varying waste package temperature and water chemistry contacting the waste packages. These results are summarized in Table 8-2.

The chemical exposure conditions on the waste package surface can be affected by the process of salt-separation (SNL 2007 [DIRS 177412], Section 6.15.1.3). If the relative humidity on a waste package undergoing seepage falls below a threshold relative humidity value (determined by lookup tables supplied to TSPA by *Engineered Barrier System: Physical and Chemical Environment* (SNL 2007 [DIRS 177412], Section 6.15.1.3)), chloride salts (halite or sylvite) will

precipitate. Once a chloride salt has precipitated, the remaining brine, or some fraction of it, can advect off of the waste package, or at least away from the precipitated salts, and hence be physically separated from the precipitated salts. Because the brine is chemically different from the bulk brine-salt geochemical system, brine-salt separation changes the bulk composition of the system represented by the precipitated salts and whatever brine is retained by them. In general, because the removed brine is nitrate-rich relative to the bulk system (chloride salts have precipitated), the remaining salt-brine system is more chloride-rich. As the relative humidity in the drift begins to rise (i.e., as the temperature decreases), the chloride-rich brine residue absorbs water and TSPA must assume a chloride-rich brine will form. This chloride-rich brine may be aggressive enough to initiate localized corrosion. The effects of salt separation on localized corrosion are not outputs of this report and are included here for completeness. Salt separation is analyzed in *Engineered Barrier System: Physical and Chemical Environment* (SNL 2007 [DIRS 177412], Section 6.15.1.3).

Table 8-2. Summary of Localized Corrosion Model Output for Waste Package Outer Barrier

Parameter Name	Parameter Definition/Description	Parameter Type	Parameter Value and Uncertainty/Variability	Parameter Source DTN
LC_a0 LC_a1 LC_a2 LC_a3 LC_a4	Coefficients of crevice repassivation potential model Equation 8-2 (a_o, a_1, a_2, a_3, a_4)	Stochastic	Mean LC_a0 = 190.242 Mean LC_a1 = -3.008 Mean LC_a2 = -46.800 Mean LC_a3 = 535.625 Mean LC_a4 = 0.061 Covariance matrix given in Equation 8-3 Uncertainty	DTN: MO0703PAGENCOR.001 file: *LC_Initiation.pdf*.
LC_eps_rcrev_a	Error term of crevice repassivation potential model Equation 8-2 (ε_{rcrev})	Stochastic	Normal distribution with a mean of zero mV versus SSC and a standard deviation of 45.055 mV versus SSC Uncertainty	DTN: MO0703PAGENCOR.001 file: *LC_Initiation.pdf*.
LC_c0 LC_c1 LC_c2 LC_c3 LC_c4 LC_c5 LC_c6	Coefficients of long-term corrosion potential model, Equation 8-5 (c_o, c_1, c_2, c_3, c_4, c_5, c_6)	Stochastic	Mean LC_c0 = 1051.219 Mean LC_c1 = -3.024 Mean LC_c2 = -155.976 Mean LC_c3 = -1352.040 Mean LC_c4 = 10.875 Mean LC_c5 = 137.856 Mean LC_c6 = -8.498 Covariance matrix given in Equation 8-6 Uncertainty	DTN: MO0703PAGENCOR.001 file: *LC_Initiation.pdf*.
LC_eps_corr_a	Error term of long-term corrosion potential model Equation 8-5 (ε_{corr})	Stochastic	Normal distribution with a mean of zero mV versus SSC and a standard deviation of 85.265 mV versus SSC Uncertainty	DTN: MO0703PAGENCOR.001 file: *LC_Initiation.pdf*.
LC_WP_Frac_Area_a	Percentage of surface area affected by crevice corrosion	Stochastic	Percentage of waste package area wetted by seepage Uncertainty	DTN: MO0703PAGENCOR.001 file: *LC_Initiation.pdf*.

The crevice corrosion initiation model is used exclusively for evaluating the long-term localized corrosion susceptibility of the WPOB and is not intended for short-term transient behavior.

The technical product outputs of the crevice corrosion initiation model analysis are documented in the output DTN: MO0703PAGENCOR.001 and summarized in Table 8-2.

8.3.2 Localized Corrosion Propagation Model Outputs

The localized corrosion penetration model assumes that localized corrosion, when it occurs, propagates at a constant (time-independent) rate (Assumption 5.4, Section 5). This is a highly conservative assumption because it is known that the localized corrosion rate decreases with time (Section 6.4.4.8.2). Also, in general, localized corrosion tends to arrest shortly after initiation.

The literature data for localized corrosion of relevant alloys that were considered for the current localized penetration rate model are for extremely corrosive conditions not expected in the repository. Those extreme penetration rates found in the literature were used to bound localized corrosion rates of Alloy 22 under repository conditions.

The technical product outputs of the crevice corrosion propagation model analysis are documented in the output DTN: MO0703PAGENCOR.001 and summarized in Table 8-3.

Table 8-3. Summary of Localized Corrosion Propa gation Model Output for Waste Package Outer Barrier

Parameter Name	Parameter Definition/Description	Parameter Type	Parameter Value and Uncertainty/Variability	Parameter Source DTN
LC_Rate_a	Crevice corrosion propagation rate	Stochastic	0 percentile = 12.7 µm/yr 50th percentile = 127 µm/yr 100th percentile = 1,270 µm/yr Log-uniform distribution Uncertainty (Table 6-15)	DTN: MO0703PAGENCOR.001 file: *LC_Propagation.pdf*.

8.4 YUCCA MOUNTAIN REVIEW PLAN ACCEPTANCE CRITERIA

Yucca Mountain Review Plan, Final Report (YMRP) (NRC 2003 [DIRS 163274]) contains acceptance criteria intended to establish the basis for the review of the material contained in the license application. As this report serves, in part, as the basis for the license application, it is important to show how the information contained herein addresses each of the applicable YMRP acceptance criteria.

The YMRP (NRC 2003 [DIRS 163274]) acceptance criteria applicable to this report are identified in *Technical Work Plan for Postclosure Engineered Barrier Degradation Modeling* (SNL 2007 [DIRS 178849], Table 3-1). For each applicable criterion, the criterion is quoted in italics, followed by pointers to where within the report the information addressing the criterion can be found. In some cases, the criterion is only partially addressed in this report. A demonstration of full compliance requires a review of multiple reports.

8.4.1 System Description and Demonstration of Multiple Barriers

Acceptance criteria governing the description and capabilities of the Engineered Barrier System (EBS) are found in Section 2.2.1.1.3 of the YMRP (NRC 2003 [DIRS 163274]). The system that this model report addresses is the EBS, and the specific feature that this report addresses is the waste package outer barrier (WPOB).

Acceptance Criterion 1 – Identification of Barriers is Adequate

> *Barriers relied on to achieve compliance with 10 CFR 63.113(b), as demonstrated in the total system performance assessment, are adequately identified, and are clearly linked to their capability. The barriers identified include at least one from the engineered system and one from the natural system.*

This model report addresses the EBS, and the specific feature of the EBS that this report addresses is the WPOB. The WPOB functions are addressed throughout this report and more specifically in Sections 1.3 and 6.3. This report does not address natural systems.

Acceptance Criterion 2 – Description of Barrier Capability is Acceptable

> *The capability of the identified barriers to prevent or substantially reduce the rate of movement of water or radionuclides from the Yucca Mountain repository to the accessible environment, or prevent the release or substantially reduce the release rate of radionuclides from the waste is adequately identified and described:*
>
> *(1) The information on the time period over which each barrier performs its intended function, including any changes during the compliance period, is provided.*
>
> *(2) The uncertainty associated with barrier capabilities is adequately described.*
>
> *(3) The described capabilities are consistent with the results from the total system performance assessment.*
>
> *(4) The described capabilities are consistent with the definition of a barrier at 10 CFR 63.2.*

The WPOB contributes to waste isolation by keeping water away from the waste for its lifetime and, when breached, by reducing the contact of water with the waste and radionuclide release rate from the waste. The WPOB functions are addressed throughout this report and more specifically in Sections 1.3 and 6.3. The models to describe these capabilities are summarized in Sections 8.1, 8.2, and 8.3. Uncertainties associated with the WPOB capabilities are also summarized in Sections 8.1, 8.2, and 8.3. The WPOB degradation models and their associated uncertainties are consistent with the models used in TSPA. The EBS meets the definition of a barrier in 10 CFR 63.2 [DIRS 180319].

Acceptance Criterion 3 – Technical Basis for Barrier Capability Is Adequately Presented

The technical bases are consistent with the technical basis for the performance assessment. The technical basis for assertions of barrier capability is commensurate with the importance of each barrier's capability and the associated uncertainties.

The technical basis for the barrier capability is documented in Sections 6.4.2, 6.4.3, 6.4.4, 6.4.5, and 6.4.6. Section 6.4.3 documents the technical basis for the general corrosion model, Section 6.4.4 for the localized corrosion model, and Section 6.4.5 for the MIC model. Section 6.4.2 documents the technical basis for the conclusion that the degradation of the WPOB by dry oxidation is negligible under the repository thermal conditions and, therefore, is not included in the WPOB degradation analysis. Section 6.4.6 documents the technical basis for the conclusion that aging and phase instability of Alloy 22 will not significantly affect the corrosion performance of the WPOB in the repository and, therefore, is not included in the WPOB degradation analysis. The technical bases are consistent with the corresponding technical bases in performance assessment because the WPOB degradation models are used as input to TSPA.

8.4.2 Degradation of Engineered Barriers

Acceptance criteria governing the processes associated with the degradation of the EBS and in particular the WPOB are presented in Section 2.2.1.3.1.3 of the YMRP (NRC 2003 [DIRS 163274]) and discussed here.

Acceptance Criterion 1 – System Description and Model Integration are Adequate

(*1) TSPA adequately incorporates important design features, physical phenomena and couplings and uses consistent assumptions throughout the degradation of engineered barriers abstraction process.*

(2) Abstraction uses assumptions, technical bases, data and models that are appropriate and consistent with [those used] in other related abstractions.

(3) The descriptions of the engineered barriers, design features, degradation processes, physical phenomena, and couplings that may affect the degradation of the engineered barriers are adequate.

(4) Initial and boundary conditions are propagated consistently throughout the abstraction process.

(5) Sufficient technical basis for the inclusion [and exclusion] of FEPs are provided;

(6) Adequate technical bases are provided, for selecting the design criteria, that mitigate any potential impact of in-package criticality on repository performance, including considering all features, events, and processes that may increase the reactivity of the system inside the waste package.

(7) Guidance in NUREG 1297 and NUREG 1298 [re: Expert Elicitation] are followed.

The physical phenomena (factors including design features, environmental factors, and their coupling) are described in Section 6.3 as part of the conceptual model discussion for general and localized corrosion of the WPOB. The models developed in this report are adequately incorporated into TSPA. Integration of the model components for WPOB corrosion degradation analysis (e.g., general corrosion, MIC, crevice repassivation potential, corrosion potential, and localized corrosion penetration) is also described in Section 6.3. Throughout this report, the analyses use assumptions, technical bases, input data, and models that appropriately reflect the design of the WPOB and the humid air and groundwater media that may come in contact with the WPOB. Assumptions used in this report are addressed in Section 5. The data, technical bases, and models are addressed in Sections 4.1 and 6. This information is used in a manner that is consistent with other abstractions of processes associated with the degradation of the WPOB. Initial and boundary conditions are propagated consistently throughout the abstraction process as described in Sections 1.2, 6, and 8, where the WPOB degradation model and ranges of application are discussed.

The features, events, and processes (FEPs) treated in this report are identified in Section 6.2. Sufficient technical bases for the inclusion of FEPs (Table 6-1) are provided in Section 6.3, as part of the conceptual model discussion for general and localized corrosion of the WPOB, and Sections 6.4.3, 6.4.4, and 6.4.5. Section 6.4.3 documents the technical basis for inclusion of general corrosion, Section 6.4.4 for inclusion of localized corrosion, and Section 6.4.5 for inclusion of MIC.

Those sections of the acceptance criterion that relate to the selection of design criteria are not applicable to this report because design criteria are not selected in this report. Those sections of the acceptance criterion that relate to the use of expert elicitation are not applicable to this report because expert elicitation was not used in this report.

Acceptance Criterion 2 – Data Are Sufficient for Model Justification

(1) Parameters used to evaluate the degradation of EBS are adequately justified and describes how the data were used, interpreted, and appropriately synthesized into the parameters.

(2) Sufficient data have been collected to establish initial and boundary conditions.

(3) Data on the degradation of the engineered barriers are based on laboratory measurements, site-specific field measurements, industrial and/or natural analogs and tests designed to replicate anticipated conditions. As appropriate, sensitivity or uncertainty analyses are provided and are shown to be adequate to determine the possible need for additional data.

(4) Degradation models for the applicable processes are adequate.

Section 4.1.1 documents the input data and their use in the model analysis. The appendices to this report and the output DTNs: MO0703PAGENCOR.001 and MO0612WPOUTERB.000 document the numerical values of the data used in the model development and analysis. The input data and parameters used to evaluate the performance of the WPOB were obtained from controlled sources and were adequately justified for their intended use (Section 4.1.1). Section 4.1.1, the appendices and output DTNs: MO0703PAGENCOR.001 and MO0612WPOUTERB.000 show that sufficient data have been collected to establish initial and boundary conditions for the models developed in this report. The data used were based on laboratory measurements under testing conditions designed to represent anticipated repository exposure conditions. Degradation models for the processes relevant to degradation of the WPOB were given appropriate consideration (Section 6) and were found to be adequate for their intended use (Section 7).

Acceptance Criterion 3 – Data Uncertainty is Characterized and Propagated through the Model Abstraction

> *(1) Models use parameter values, assumed ranges, probability distributions and/or bounding assumptions that are technically defensible, reasonably account for uncertainties and variabilities, and do not result in under-representation of the risk estimate.*
>
> *(2) Appropriate parameters, based on techniques that may include laboratory experiments, field measurements, industrial analogs and process-level modeling studies conducted under conditions relevant to the range of environmental conditions within the waste package emplacement drifts are used.*
>
> *(3) Assumed range of values and probability distributions for parameters used in conceptual and process-level models are not likely to underestimate the actual degradation and failure of engineered barriers.*
>
> *(4) Appropriate methods were used for nondestructive examination of fabricated engineered barriers to assess the type, size, and location of fabrication defects that may lead to premature failure as a result of rapidly initiated engineered barrier degradation. Specify and justify the allowable distribution of fabrication defects in the engineered barriers, and assess the effects of defects that cannot be detected on the performance of the engineered barriers.*
>
> *(5) Where sufficient data do not exist, the definition of parameter values and conceptual models is based on appropriate use of other sources, such as expert elicitation.*

Each of the models developed in this report uses parameter values, assumed ranges, probability distributions, or technically defensible bounding assumptions that reasonably account for uncertainties and variabilities and do not result in under-representation of the risk estimate. The various models developed in this report use data and parameters developed based on laboratory experiments (Section 4.1.1, the appendices, and output DTNs: MO0703PAGENCOR.001 and MO0612WPOUTERB.000) or bounding assumptions, or both, that are technically defensible

and reasonably account for uncertainties and variabilities. The effects of data uncertainties on the parameter ranges and uncertainty distributions in the models developed in this report are discussed in Sections 6.4.3, 6.4.4, and 6.4.5.

Section 6.4.3 discusses the effects of data uncertainties on the general corrosion model developed in this report. Uncertainties in the data used for the general corrosion model analysis (five-year weight-loss measurements and short-term polarization resistance measurements) were characterized and quantified, and propagated through the general corrosion model abstraction (Section 6.4.3). The treatment of general corrosion in this report is not likely to under-represent the risk estimate from general corrosion. For example, the general corrosion model uses (at a given temperature) a constant rate of uniform penetration (Assumption 5.2, Section 5) based on laboratory weight-loss measurements from samples with creviced geometries exposed for five years in repository relevant solutions. This assumption is conservative because the general corrosion rate of Alloy 22 decreases with time (Figure 7-1). Therefore, it is not likely that the general corrosion model developed in this report will under-represent the risk estimate from general corrosion.

Section 6.4.4 discusses the effects of data uncertainties on the localized corrosion model developed in this report. Uncertainties in the data used for the localized corrosion model analysis (crevice repassivation potentials and long-term steady-state corrosion potentials) were characterized and quantified, and propagated through the localized corrosion model abstraction (Section 6.4.4). A conservative bounding approach, based on the literature data for Alloy 22 in highly corrosive environments, was used to capture the uncertainty in the localized corrosion rate of Alloy 22 (Section 6.4.4). The treatment of localized corrosion in this report is not likely to under-represent the risk estimate from localized corrosion. For example, the localized corrosion model developed in this report uses a localized corrosion initiation criterion based on crevice corrosion (Assumption 5.3, Section 5). This treatment is conservative because initiation thresholds (in terms of exposure parameters such as temperature and solution chemistry) for crevice corrosion are lower than for pitting (another type of localized corrosion attacking boldly exposed surfaces). Furthermore, the localized corrosion model uses a localized corrosion rate, which is a time-independent constant rate (Assumption 5.4, Section 5). Lastly, crevice corrosion tends to be stifled as the geometric conditions supporting crevice corrosion degrade as corrosion progresses. The model takes no credit for this effect. Therefore, it is not likely that the localized corrosion model developed in this report will under-represent the risk estimate from localized corrosion.

Section 6.4.5 discusses the effects of data uncertainties on the MIC model developed in this report. The treatment of MIC in this report is not likely to under-represent the risk estimate from MIC. The MIC relative humidity initiation threshold is a reasonable representation of the conditions necessary for microbes to be active in the repository environment. Relevant data were analyzed to determine the effects of microbial action on corrosion rates. Given that the effect of MIC is a multiplier on the general corrosion rate (discussed above as a conservative representation), the treatment of MIC in this report is unlikely to under-represent the risk estimate from MIC.

Those sections of the acceptance criterion that relate to nondestructive examination of fabricated engineered barriers are not applicable to this report because no analyses of nondestructive

examination of fabricated engineered barriers were analyzed in this report. Those sections of the acceptance criterion that relate to the use of other sources, such as expert elicitation, are not applicable to this report because no other sources were used in the creation of this report.

Acceptance Criterion 4 – Model Uncertainty is Characterized and Propagated Through the Model Abstraction

> *(1) Alternative modeling approaches of features, events, and processes are considered and are consistent with available data and current scientific understanding and the results and limitations are appropriately considered in the abstraction.*
>
> *(2) Consideration of conceptual model uncertainty is consistent with available site characterization data, laboratory experiments,…and the treatment of uncertainty does not result in under-representation of the risk estimate.*
>
> *(3) Alternative modeling approaches, consistent with available data and current scientific understanding, are used and the modeling results are evaluated using tests and analyses that are sensitive to the processes modeled.*

The uncertainties in the general corrosion and localized corrosion models are addressed through the qualitative assessment of ACMs (Sections 6.4.3.5 and 6.4.4.8), which were consistent with available data and current scientific understanding. Although these alternative models are not used in TSPA, they are used, where applicable, for model validation in Section 7. Consideration of uncertainties of the models developed in this report is an integral part of the model development and validation. Conceptual model uncertainty is consistent with the information that has been developed through laboratory experiments (Section 4.1.1 and the appendices). As discussed in Acceptance Criterion 3, the treatment of uncertainty is unlikely to result in under-representation of the risk estimates.

Acceptance Criterion 5 – Model Abstraction Output Is Supported By Objective Comparisons

> *(1) Models implemented in this total system performance assessment abstraction provide results consistent with output from detailed process-level models and or empirical observations (laboratory and field testing, and/or natural analogs).*
>
> *(2) Numerical corrosion models used to calculate the lifetimes of the engineered barriers are adequate representations, considering the associated uncertainties in the expected long-term behaviors, the range of conditions (including residual stresses), and the variability in engineered barrier fabrication processes (including welding).*
>
> *(3) Evidence is sufficient to show that models will not underestimate the actual degradation and failure of engineered barriers.*

(4) Mathematical degradation models are based on the same environmental parameters, material factors, assumptions and approximations shown to be appropriate for closely analogous applications.

(5) Accepted and well documented procedures are used to construct and test the numerical models that simulate the EBS chemical environment and degradation of engineered barriers.

(6) Sensitivity analyses or bounding analyses are provided to support the abstraction of degradation of engineered barriers that cover ranges consistent with the site data, field or laboratory experiments and tests, and industrial analogs.

The results of WPOB degradation models developed in this report are implemented in the TSPA as specified in this report; therefore the TSPA model results are consistent with output from this report. The models developed in this report were compared with laboratory data used to develop the models in Section 6. The models developed in this report were compared with laboratory and/or literature data not used in model development in Section 7. As discussed in Acceptance Criterion 3, there is sufficient evidence that the models developed in this report will not underestimate the actual degradation and failure of engineered barriers. The mathematical models developed in this report were based on data collected using materials (Alloy 22) and exposure environments relevant to those expected in the repository. The models developed in this report were constructed following the accepted and well-documented scientific methodology outlined in SCI-PRO-006, *Models*.

INTENTIONALLY LEFT BLANK

9. INPUTS AND REFERENCES

9.1 DOCUMENTS CITED

163034 Agarwal, D.C. 2000. "Nickel and Nickel Alloys." Chapter 45 of *Uhlig's Corrosion Handbook*. 2nd Edition. Revie, R.W., ed. New York, New York: John Wiley & Sons. TIC: 248360.

163903 Akashi, M.; Nakayama, G.; and Fukuda, T. 1998. "Initiation Criteria for Crevice Corrosion of Titanium Alloys Used for HLW Disposal Overpack." *Corrosion in Advanced Materials and Systems, Proceedings of Corrosion/98 Research Topical Symposium*. Paper No. 158. Houston, Texas: NACE International. TIC: 254584.

170360 Andresen, P.L.; Kim, Y.J.; Emigh, P.W.; Catlin, G.M.; and Martiniano, P.J. 2003. *GE GRC Final Report*. BSC PO 2450-100-PO-10508. Las Vegas, Nevada: Bechtel SAIC Company. ACC: MOL.20040520.0076.

165442 Angeliu, T.M. 2001. "Microstructural Characterization of L-Grade Stainless Steels Relative to the IGSCC Behavior in BWR Environments." *Corrosion/2001 56th Annual Conference & Exposition, March 11-16, 2001, Houston, Texas, USA*. Paper No. 01121. Houston, Texas: NACE International. TIC: 254941.

133378 ASM International. 1987. *Corrosion* . Volume 13 of *ASM Handbook*. Formerly 9th Edition, Metals Handbook. Materials Park, Ohio: ASM International. TIC: 240704.

154510 Baker, E.A. 1988. "Long-Term Corrosion Behavior of Materials in the Marine Atmosphere." *Degradation of Metals in the Atmosphere, Proceedings of the Symposium on Corrosion of Metals, Philadelphia, Pennsylvania, 12-13 May 1986*. Dean, S.W. and Lee, T.S., eds. ASTM STP 965. Pages 125-144. Philadelphia, Pennsylvania: American Society for Testing and Materials. TIC: 224019.

158781 Beavers, J.A.; Devine, T.M., Jr.; Frankel, G.S.; Jones, R.H.; Kelly, R.G.; Latanision, R.M.; and Payer, J.H. 2002. *Final Report, Waste Package Materials Performance Peer Review Panel, February 28, 2002*. Las Vegas, Nevada: Waste Package Materials Performance Peer Review Panel. ACC: MOL.20020614.0035.

164137 Böhni, H. 2000. "Localized Corrosion of Passive Metals." Chapter 10 of *Uhlig's Corrosion Handbook*. Revie, R.W., ed. 2nd Edition. New York, New York: John Wiley & Sons. TIC: 248360.

159836 Brossia, C.S.; Browning, L.; Dunn, D.S.; Moghissi, O.C.; Pensado, O.; and Yang, L. 2001. *Effect of Environment on the Corrosion of Waste Package and Drip Shield Materials*. CNWRA 2001-003. San Antonio, Texas: Center for Nuclear Waste Regulatory Analyses. TIC: 252324.

169131 BSC (Bechtel SAIC Company) 2004. *Abstraction of Drift Seepage.* MDL-NBS-HS-000019 REV 01. Las Vegas, Nevada: Bechtel SAIC Company. ACC: DOC.20041103.0003.

171924 BSC 2004. *Aging and Phase Stability of Waste Package Outer Barrier.* ANL-EBS-MD-000002 REV 02. Las Vegas, Nevada: Bechtel SAIC Company. ACC: DOC.20041005.0003.

169991 BSC 2004. *Evaluation of Potential Impacts of Microbial Activities on Drift Chemistry.* ANL-EBS-MD-000038 REV 01. Las Vegas, Nevada: Bechtel SAIC Company. ACC: DOC.20041118.0005; DOC.20050505.0001; DOC.20050609.0001.

175539 BSC 2005. *Q-List*. 000-30R-MGR0-00500-000-003. Las Vegas, Nevada: Bechtel SAIC Company. ACC: ENG.20050929.0008.

165441 Chen, H.-L.; Evans, K.J.; Hackel, L.A.; Rankin, J.E.; Yamamoto, R.M.; Demma, A.G.; Dewald, A.T.; Lee, M.J.; and Hill, M.R. 2002. *Mitigation of Tensile Weld Stresses in Alloy 22 Using Laser Peening*. UCRL-ID-151055. Livermore, California: Lawrence Livermore National Laboratory. ACC: MOL.20030911.0252.

100349 CRWMS M&O (Civilian Radioactive Waste Management System Management and Operating Contractor) 1998. *Waste Package Degradation Expert Elicitation Project*. Rev. 1. Las Vegas, Nevada: CRWMS M&O. ACC: MOL.19980727.0002.

160320 D'Agostino, R.B. and Stephens, M.A., eds. 1986. *Goodness-Of-Fit Techniques*. Statistics, Textbooks and Monographs Volume 68. New York, New York: Marcel Dekker. TIC: 253256.

178252 Day, S.D.; Wong, F.M.; Gordon, S.R.; Wong, L.L.; and Rebak, R.B. 2006. "Electrochemical Testing of Gas Tungsten Arc Welded and Reduced Pressure Electron Beam Welded Alloy 22." *Proceeding of ASME PVP 2006 and ICPVT-11 Conference, July 23-27, 2006, Vancouver, British Columbia, Canada.* Pages 1-11. New York, New York: American Society of Mechanical Engineers. TIC: 258646.

182051 DOE (U.S. Department of Energy) 2007. *Quality Assurance Requirements and Description.* DOE/RW-0333P, Rev. 19. Washington, D. C.: U.S. Department of Energy, Office of Civilian Radioactive Waste Management. ACC: DOC.20070717.0006.

118716 Draper, N.R. and Smith, H. 1981. *Applied Regression Analysis*. 2nd Edition. New York, New York: John Wiley & Sons. TIC: 231231.

140067 Drever, J.I. 1997. *The Geochemistry of Natural Waters, Surface and Groundwater Environments*. 3rd Edition. Upper Saddle River, New Jersey: Prentice Hall. TIC: 246732.

162213 Dunn, D.S. and Brossia, C.S. 2002. "Assessment of Passive and Localized Corrosion Processes for Alloy 22 as a High-Level Nuclear Waste Container Material." *Corrosion/2002, 57th Annual Conference & Exposition, April 7-11, 2002, Denver, Colorado*. Paper No. 02548. Houston, Texas: NACE International. TIC: 254579.

164495 Dunn, D.S.; Cragnolino, G.A.; and Sridhar, N. 2000. "An Electrochemical Approach to Predicting Long-Term Localized Corrosion of Corrosion-Resistant High-Level Waste Container Materials." *Corrosion*, *56*, (1), 90-104. Houston, Texas: National Association of Corrosion Engineers. TIC: 254836.

171452 Dunn, D.S.; Cragnolino, G.A.; Pan, Y.M.; and Tang, L.T. 2004. "Effect of Fabrication Processes on Alloy 22 Corrosion Resistance." *Corrosion/2004, 59th Annual Conference & Exposition, March 28-April 1, 2004, New Orleans*. Paper No. 04698. Houston, Texas: NACE International. TIC: 255943.

166948 Dunn, D.S.; Daruwalla, D.; and Pan, Y.-M. 2003. *Effect of Fabrication Processes on Material Stability—Characterization and Corrosion*. CNWRA 2004-01. San Antonio, Texas: Center for Nuclear Waste Regulatory Analyses. TIC: 255881.

154481 Dunn, D.S.; Pan, Y-M.; and Cragnolino, G.A. 1999. *Effects of Environmental Factors on the Aqueous Corrosion of High-Level Radioactive Waste Containers—Experimental Results and Models.* CNWRA 99-004. San Antonio, Texas: Center for Nuclear Waste Regulatory Analyses. TIC: 246615.

178451 Dunn, D.S.; Pensado, O.; and Cragnolino, G.A. 2005. "Performance Assessment of Alloy 22 as a Waste Package Outer Barrier." *Corrosion/2005, 60th Annual Conference & Exposition, 1945-2005, April 3-7, 2005, George R. Brown Convention Center, Houston, Texas.* Paper No. 05588. Houston, Texas: NACE International. TIC: 257165.

178104 Dunn, D.S.; Pensado, O.; Pan, Y.-M; Pabalan, R.T.; Yang, L.; He, X.; and Chiang, K.T. 2005. *Passive and Localized Corrosion of Alloy 22 - Modeling and Experiments.* CNWRA 2005-02. San Antonio, Texas: Center for Nuclear Waste Regulatory Analyses. ACC: LLR.20070305.0002.

164138 Dunn, D.S.; Yang, L.; Pan, Y.-M.; and Cragnolino, G.A. 2003. "Localized Corrosion Susceptibility of Alloy 22." *Corrosion/2003, 58th Annual Conference & Exposition, March 16-20, 2003, San Diego, California*. Paper No. 03697. Houston, Texas: NACE International. TIC: 254387.

103967 Efron, B. and Gong, G. 1983. "A Leisurely Look at the Bootstrap, the Jackknife, and Cross-Validation." *The American Statistician, 37*, (1), 36-48. Washington, D.C.: American Statistical Association. TIC: 245820.

158069 EPRI (Electric Power Research Institute) 2002. *Evaluation of the Proposed High-Level Radioactive Waste Repository at Yucca Mountain Using Total System Performance Assessment, Phase 6*. EPRI TR-1003031. Palo Alto, California: Electric Power Research Institute. TIC: 252239.

117697 Estill, J.C. 1998. "Long-Term Corrosion Studies." Section 2.2 of *Engineered Materials Characterization Report*. McCright, R.D., ed. UCRL-ID-119564 Volume 3 Rev.1.1. Livermore, California: Lawrence Livermore National Laboratory. ACC: MOL.19981222.0137.

163849 Estill, J.C.; Hust, G.A.; and Rebak, R.B. 2003. "Long Term Corrosion Potential Behavior of Alloy 22." *Corrosion/2003, 58th Annual Conference & Exposition, March 16-20, 2003, San Diego, California*. Paper No. 03688. Houston, Texas: NACE International. TIC: 254387.

164857 Evans, K.J. and Rebak, R.B. 2002. "Passivity of Alloy 22 in Concentrated Electrolytes Effect of Temperature and Solution Composition." *Corrosion Science, A Retrospective and Current Status in Honor of Robert P. Frankenthal, Proceedings of the International Symposium*. Frankel, G.S.; Isaacs, H.S.; Scully, J.R.; and Sinclair, J.D., eds. Proceedings Volume 2002-13. Pages 344-354. Pennington, New Jersey: Electrochemical Society. TIC: 254801.

178247 Evans, K. J.; Yilmaz, A.; Day, S. D.; Wong, L. L.; Estill, J. C.; and Rebak, R. B. 2005. "Using Electrochemical Methods to Determine Alloy 22's Crevice Corrosion Repassivation Potential." *Journal of Metals*, pp. 56 - 61. Livermore, California: Lawrence Livermore National Laboratory. ACC: MOL.20070104.0001.

112115 Evans, M.; Hastings, N.; and Peacock, B. 1993. *Statistical Distributions*. 2nd Edition. New York, New York: John Wiley & Sons. TIC: 246114.

179983 Fix, D.V.; Estill, J.C.; and Rebak, R.B. 2005. "Effect of Small Variation in the Composition of Plates and Weld Filler Wires on the General Corrosion Rate of Ni-Cr-Mo Alloys." *Transportation, Storage and Disposal of Radioactive Materials, 2005, Presented at the 2005 ASME Pressure Vessels and Piping Conference, Denver, Colorado, July 17-21, 2005.* New York, New York: American Society of Mechanical Engineers. TIC: 257583.

173721 Fix, D.V.; Yilmaz, A.; Wong, L.L.; Estill, J.C.; and Rebak, R.B. 2005. "Effect of Surface Stress Mitigation on the Corrosion Behavior of Alloy 22." *Corrosion/2005, 60th Annual Conference & Exposition, 1945-2005, April 3-7, 2005, George R. Brown Convention Center, Houston, Texas.* Paper No. 05606. Houston, Texas: NACE International. TIC: 257165.

100890 Fontana, M.G. 1986. *Corrosion Engineering*. 3rd Edition. New York, New York: McGraw-Hill. TIC: 240700.

164140 Frankel, G.S. 2002. "Localized Corrosion Phenomenology and Controlling Parameters." Section 6 of *Waste Package Materials Performance Peer Review, A Compilation of Special Topic Reports*. Wong, F.M.G. and Payer, J.H., eds. Las Vegas, Nevada: Waste Package Materials Performance Peer Review Panel. ACC: MOL.20020731.0138.

162216 Frankel, G.S. 1998. "Pitting Corrosion of Metals, A Review of the Critical Factors." *Journal of the Electrochemical Society*, *145*, (6), 2186-2198. Pennington, New Jersey: Electrochemical Society. TIC: 254587.

164141 Frankel, G.S. and Kelly, R.G. 2002. "Passivity-Induced Ennoblement." Section 11 of *Waste Package Materials Performance Peer Review, A Compilation of Special Topic Reports*. Wong, F.M.G. and Payer, J.H., eds. Las Vegas, Nevada: Waste Package Materials Performance Peer Review Panel. ACC: MOL.20020731.0138.

100859 Gdowski, G.E. 1991. *Survey of Degradation Modes of Four Nickel-Chromium-Molybdenum Alloys*. UCRL-ID-108330. Livermore, California: Lawrence Livermore National Laboratory. ACC: NNA.19910521.0010.

165793 Gordon, G.M. 2002. "F.N. Speller Award Lecture: Corrosion Considerations Related to Permanent Disposal of High-Level Radioactive Waste." *Corrosion, 58,* (10), 811-825. Houston, Texas: NACE International. TIC: 256497.

100893 Gruss, K.A.; Cragnolino, G.A.; Dunn, D.S.; and Sridhar, N. 1998. "Repassivation Potential for Localized Corrosion of Alloys 625 and C22 in Simulated Repository Environments." *Proceedings of Corrosion 98, March 22-27, 1998, San Diego, California*. Pages 149/1 to 149/15. Houston, Texas: NACE International. TIC: 237149.

100814 Harrar, J.E.; Carley, J.F.; Isherwood, W.F.; and Raber, E. 1990. *Report of the Committee to Review the Use of J-13 Well Water in Nevada Nuclear Waste Storage Investigations*. UCID-21867. Livermore, California: Lawrence Livermore National Laboratory. ACC: NNA.19910131.0274.

178246 Hayes, J.R.; Szmodiz, A.W.; Anderson, K.L.; and Orme, C.A. 2004. "Effect of the Environment and Alloy Compositions on the Electrochemical Behavior of Ni-Cr-Mo Alloys." *Corrosion/2004, 59th Annual Conference & Exposition, March 28-April 1, 2004, New Orleans.* Paper No. 04697. Houston, Texas: NACE International. TIC: 255943.

100896 Haynes International. 1997. *Hastelloy C-22 Alloy* . Kokomo, Indiana: Haynes International. TIC: 238121.

100897 Haynes International. 1997. *Hastelloy Alloy C-276*. Haynes International Product Brochure. Kokomo, Indiana: Haynes International. TIC: 238832.

178453 He, X. and Dunn, D.S. 2005. *Crevice Corrosion Penetration Rates of Alloy 22 in Chloride-Containing Waters-Progress Report.* CNWRA 2006-001. San Antonio, Texas: Center for Nuclear Waste Regulatory Analyses. ACC: MOL.20061127.0161.

176645 He, X. and Dunn, D.S. 2006. "Crevice Corrosion Penetration Rates of Alloy 22 in Chloride-Containing Waters." *Corrosion 2006, 61st Annual Conference & Exposition, San Diego Convention Center, March 12-16, 2006.* Paper No. 06618. Houston, Texas: NACE International. TIC: 258178.

162220 Horn, J. and Jones, D. 2002. "Microbiologically Influenced Corrosion: Perspectives and Approaches." *Manual of Environmental Microbiology*. 2nd Edition. Hurst, C.J., ed. Pages 1072-1083. Washington, D.C.: ASM Press. TIC: 254738.

171013 Hua, F. and Gordon, G. 2004. "Corrosion Behavior of Alloy 22 and Ti Grade 7 in a Nuclear Waste Repository Environment." *Corrosion, 60,* (8), 764-777. Houston, Texas: NACE International. TIC: 256354.

160670 Hua, F.; Sarver, J.; Jevec, J.; and Gordon, G. 2002. "General Corrosion Studies of Candidate Container Materials in Environments Relevant to Nuclear Waste Repository." *Corrosion/2002, 57th Annual Conference & Exposition, April 7-11, 2002, Denver, Colorado*. Paper No. 02530. Houston, Texas: NACE International. TIC: 252067.

162221 Hunkeler, F. and Boehni, H. 1983. "Pit Growth Measurements on Stainless Steels." *Passivity of Metals and Semiconductors, Proceedings of the Fifth International Symposium on Passivity, Bombannes, France, May 30-June 3, 1983*. Froment, M., ed. Pages 655-660. New York, New York: Elsevier. TIC: 236283.

173814 Ilevbare, G.O. 2005. "The Effect of Sulfate Anions on the Crevice Breakdown and Repassivation Potentials of Alloy 22 in 4M NaCl." *Corrosion/2005, 60th Annual Conference & Exposition, 1945-2005, April 3-7, 2005, George R. Brown Convention Center, Houston, Texas.* Paper No. 05611. Houston, Texas: NACE International. TIC: 257165.

162222 Ishikawa, H.; Honda, A.; and Sasaki, N. 1994. "Long Life Prediction of Carbon Steel Overpacks for Geological Isolation of High-Level Radioactive Waste." *Life Prediction of Corrodible Structures*. Parkins, R.N., ed. Volume 1. Pages 454-483. Houston, Texas: NACE International. TIC: 254834.

164087 Jain, V.; Dunn, D.; Sridhar, N.; and Yang, L. 2003. "Effect of Measurement Methods and Solution Chemistry on the Evaluation of the Localized Corrosion of Candidate High-Level Waste Container Materials." *Corrosion/2003, 58th Annual Conference & Exposition, March 16-20, 2003, San Diego, California*. Paper No. 03690. Houston, Texas: NACE International. TIC: 254387.

162225 Jayaweera, P.; Priyantha, N.; Macdonald, D.D.; Engelhard, G.; and Davydov, A. 2003. *Deterministic Prediction of Localized Corrosion Damage to Alloy C-22 HLNW Canisters*. SRI Project 10333. Menlo Park, California: SRI International. TIC: 253900.

169906 Jones, D.A. 1992. *Principles and Prevention of Corrosion*. 1st Edition. New York, New York: Macmillan. TIC: 242631.

155193 Kain, R.M. 1987. "Evaluation of Crevice Corrosion." In *Corrosion*, Volume 13, Pages 303-310 of *ASM Handbook*. Formerly 9th Edition, Metals Handbook. Materials Park, Ohio: ASM International. TIC: 240704.

162230 Kehler, B.A.; Ilevbare, G.O.; and Scully, J.R. 1999. "Comparison of the Crevice Corrosion Resistance of Alloys 625 and C22." *Passivity and Localized Corrosion, An International Symposium in Honor of Professor Norio Sato*. Seo, M.; MacDougall, B.; Takahashi, H.; and Kelly, R.G., eds. *99-27*, 644-654. Pennington, New Jersey: Electrochemical Society. TIC: 254581.

162231 Kehler, B.A.; Ilevbare, G.O.; and Scully, J.R. 2001. "Crevice Corrosion Stabilization and Repassivation Behavior of Alloy 625 and Alloy 22." *Corrosion*, *57*, (12), 1042-1065. Houston, Texas: NACE International. TIC: 254305.

177529 Kehler, B.A. and Scully, J.R. 2005. "Role of Metastable Pitting in Crevices on Crevice Corrosion Stabilization in Alloys 625 and 22." *Corrosion, 61,* (7), 665-684. Houston, Texas: NACE International. TIC: 258548.

100051 Langmuir, D. 1997. *Aqueous Environmental Geochemistry*. Upper Saddle River, New Jersey: Prentice Hall. TIC: 237107.

164856 Lian, T.; Estill, J.C.; Hust, G.A.; Fix, D.V.; and Rebak, R.B. 2002. "Passive Corrosion Behavior of Alloy 22 in Multi-Ionic Aqueous Environments." *Transportation, Storage, and Disposal of Radioactive Materials –2002– Presented at the 2002 ASME Pressure Vessels and Piping Conference, Vancouver, British Columbia, Canada, August 5-9, 2002*. Hafner, R.S.; Farmer, J.C.; Hensel, S.J.; Lake, W.H., Jr.; and Smith, A.C., eds. PVP-Vol. 449. Pages 67-74. New York, New York: American Society of Mechanical Engineers. TIC: 254800.

110238 Lian, T.; Martin, S.; Jones, D.; Rivera, A.; and Horn, J. 1999. "Corrosion of Candidate Container Materials by Yucca Mountain Bacteria." *Corrosion 99, 54th Annual Conference and Expo, San Antonio, Texas, April 25-30, 1999*. Paper No. 476. Houston, Texas: NACE International. TIC: 245833.

131202 Lide, D.R., ed. 1991. *CRC Handbook of Chemistry and Physics*. 72nd Edition. Boca Raton, Florida: CRC Press. TIC: 3595.

167921 Lloyd, A.C.; Shoesmith, D.W.; McIntyre, N.S.; and Noël, J.J. 2003. "Effects of Temperature and Potential on the Passive Corrosion Properties of Alloys C22 and C276." *Journal of the Electrochemical Society*, *150*, (4), B120-B130. New York, New York: Electrochemical Society. TIC: 255963.

154718 Lorang, G.; Jallerat, N.; Vu Quang, K.; and Langeron, J.-P. 1990. "AES Depth Profiling of Passive Overlayers Formed on Nickel Alloys." *Surface and Interface Analysis*, *16*, 325-330. Chichester, England: John Wiley & Sons. TIC: 249830.

154720 Macdonald, D.D. 1992. "The Point Defect Model for the Passive State." *Journal of the Electrochemical Society*, *139*, (12), 3434-3449. Manchester, New Hampshire: Electrochemical Society. TIC: 249804.

154721 Macdonald, D.D. 1999. "Passivity–The Key to Our Metals-Based Civilization." *Pure and Applied Chemistry*, *71*, (6), 951-978. Oxford, England: Blackwell Science. TIC: 249795.

154738 Marcus, P. and Maurice, V. 2000. "Passivity of Metals and Alloys." Chapter 3 of *Corrosion and Environmental Degradation*. Schütze, M., ed. Volume I. Materials Science and Technology Volume 19. New York, New York: Wiley-VCH. TIC: 249831.

162234 Marsh, G.P.; Taylor, K.J.; and Harker, A.H. 1991. *The Kinetics of Pitting Corrosion of Carbon Steel Applied to Evaluating Containers for Nuclear Waste Disposal*. SKB TR-91-62. Stockholm, Sweden: Svensk Kärnbränsleförsörjning AB. TIC: 206582.

175394 Martin, S.; Horn, J.; and Carrillo, C. 2004. "Micron-Scale MIC of Alloy 22 After Long Term Incubation in Saturated Nuclear Waste Repository Microcosms." *Corrosion/2004, 59th Annual Conference & Exposition, March 28-April 1, 2004, New Orleans.* Paper No. 04596. Houston, Texas: NACE International. TIC: 255943.

114637 McCright, R.D. 1998. *Corrosion Data and Modeling, Update for Viability Assessment*. Volume 3 of *Engineered Materials Characterization Report*. UCRL-ID-119564, Rev. 1.1. Livermore, California: Lawrence Livermore National Laboratory. ACC: MOL.19980806.0177.

152193 McGuire, R.; Vlasity, J.; Kessler, J.; Long, A.; Childs, S.; Ross, B.; Schwartz, F.; Shoesmith, D.; Kolar, M.; Apted, M.; Zhou, W.; Sudicky, E.; Smith, G.; Kozak, M.; Salter, P.; Klos, R.; Venter, A.; Stenhouse, M.; Watkins, B.; and Little, R. 1998. *Alternative Approaches to Assessing the Performance and Suitability of Yucca Mountain for Spent Fuel Disposal*. EPRI TR-108732. Palo Alto, California: Electric Power Research Institute. TIC: 248813.

163603 Mishra, S. 2002. *Assigning Probability Distributions to Input Parameters of Performance Assessment Models.* SKB TR-02-11. Stockholm, Sweden: Svensk Kärnbränsleförsörjning A.B. TIC: 252794.

162235 Mughabghab, S.F. and Sullivan, T.M. 1989. "Evaluation of the Pitting Corrosion of Carbon Steels and Other Ferrous Metals in Soil Systems." *Waste Management*, *9*, (4), 239-251. Elmsford, New York: Pergamon Press. TIC: 254591.

162251 Newman, R.C. 1985. "The Dissolution and Passivation Kinetics of Stainless Alloys Containing Molybdenum—I. Coulometric Studies of Fe–Cr and Fe–Cr–Mo Alloys." *Corrosion Science*, *25*, (5), 331-339. New York, New York: Elsevier. TIC: 254590.

162250 Newman, R.C. and Franz, E.M. 1984. "Growth and Repassivation of Single Corrosion Pits in Stainless Steel." *Corrosion*, *40*, (7), 325-330. Houston, Texas: National Association of Corrosion Engineers. TIC: 254580.

163274 NRC (U.S. Nuclear Regulatory Commission) 2003. *Yucca Mountain Review Plan, Final Report*. NUREG-1804, Rev. 2. Washington, D.C.: U.S. Nuclear Regulatory Commission, Office of Nuclear Material Safety and Safeguards. TIC: 254568.

167863 Oldfield, J.W. and Sutton, W.H. 1980. "New Technique for Predicting the Performance of Stainless Steels in Sea Water and Other Chloride-Containing Environments." *British Corrosion Journal, 15,* (1), 31-34. London, England: Institute of Materials. TIC: 255666.

162236 Papoulis, A. 1965. *Probability, Random Variables, and Stochastic Processes*. New York, New York: McGraw-Hill. TIC: 254701.

166944 Pensado, O.; Dunn, D.S.; Cragnolino, G.A.; and Jain, V. 2002. *Passive Dissolution of Container Materials—Modeling and Experiments*. CNWRA 2003-01. San Antonio, Texas: Center for Nuclear Waste Regulatory Analyses. TIC: 254056.

174186 Rebak, R.B. 2005. "Factors Affecting the Crevice Corrosion Susceptibility of Alloy 22." *Corrosion/2005, 60th Annual Conference & Exposition, 1945-2005, April 3-7, 2005, George R. Brown Convention Center, Houston, Texas.* Paper No. 05610. Houston, Texas: NACE International. TIC: 257165.

162237 Rebak, R.B.; Edgecumbe Summers, T.S.; Lian, T.; Carranza, R.M.; Dillman, J.R.; Corbin, T.; and Crook, P. 2002. "Effect of Thermal Aging on the Corrosion Behavior of Wrought and Welded Alloy 22." *Corrosion/2002, 57th Annual Conference & Exposition, April 7-11, 2002, Denver, Colorado*. Paper No. 02542. Houston, Texas: NACE International. TIC: 254582.

159370 Revie, R.W., ed. 2000. *Uhlig's Corrosion Handbook*. 2nd Edition. New York, New York: John Wiley & Sons. TIC: 248360.

110056 Sargent-Welch Scientific Company 1979. *Periodic Table of the Elements.* Catalog Number S-18806. Skokie, Illinois: Sargent-Welch Scientific Company. TIC: 245069.

162259 Sawyer, D.T. and Roberts, J.L., Jr. 1974. "II. Reference Electrodes." *Experimental Electrochemistry for Chemists*. Pages 34-60. New York, New York: John Wiley & Sons. TIC: 254739.

110246 Scully, J.R.; Hudson, J.L.; Lunt, T.; Ilevbare, G.; and Kehler, B. 1999. *Localized Corrosion Initiation and Transition to Stabilization in Alloys 625 and C-22*. Charlottesville, Virginia: University of Virginia. TIC: 246630.

154513 Scully, J.R.; Ilevbare, G.; and Marks, C. 2001. *Passivity and Passive Corrosion of Alloys 625 and 22*. SEAS Report No. UVA/527653/MSE01/103. Charlottesville, Virginia: University of Virginia, School of Engineering & Applied Science. TIC: 248056.

162238 Sharland, S.M.; Naish, C.C.; Taylor, K.J.; and Marsh, G.P. 1994. "An Experimental and Modelling Study of the Localized Corrosion of Carbon Steel Overpacks for the Geological Disposal of Radioactive Waste." *Life Prediction of Corrodible Structures*. Parkins, R.N., ed. Volume 1. Pages 402-418. Houston, Texas: NACE International. TIC: 254835.

168164 Smailos, E. 1993. "Corrosion of High-Level Waste Packaging Materials in Disposal Relevant Brines." *Nuclear Technology*, *104*, 343-350. La Grange Park, Illinois: American Nuclear Society. TIC: 249836.

159774 Smailos, E. and Köster, R. 1987. "Corrosion Studies on Selected Packaging Materials for Disposal of High Level Wastes." *Materials Reliability in the Back End of the Nuclear Fuel Cycle, Proceedings of a Technical Committee Meeting, Vienna, 2-5 September 1986*. IAEA TECHDOC-421, 7-24. Vienna, Austria: International Atomic Energy Agency. TIC: 252877.

181267 SNL (Sandia National Laboratories) 2007. *Analysis of Dust Deliquescence for FEP Screening.* ANL-EBS-MD-000074 REV 01 AD 01. Las Vegas, Nevada: Sandia National Laboratories.

177430 SNL 2007. *Dike/Drift Interactions.* MDL-MGR-GS-000005 REV 02. Las Vegas, Nevada: Sandia National Laboratories.

177412 SNL 2007. *Engineered Barrier System: Physical and Chemical Environment*. ANL-EBS-MD-000033 REV 06. Las Vegas, Nevada: Sandia National Laboratories.

181383 SNL 2007. *Multiscale Thermohydrologic Model*. ANL-EBS-MD-000049 REV 03 AD01. Las Vegas, Nevada: Sandia National Laboratories.

177417 SNL 2007. *Stress Corrosion Cracking of Waste Package Outer Barrier and Drip Shield Materials*. ANL-EBS-MD-000005 REV 03. Las Vegas, Nevada: Sandia National Laboratories. ACC: DOC.20070530.0012.

178849 SNL 2007. *Technical Work Plan for Postclosure Engineered Barrier Degradation Modeling.* TWP-EBS-MD-000020 REV 00. Las Vegas, Nevada: Sandia National Laboratories. ACC: DOC.20070216.0001.

179567 SNL 2007. *Total System Performance Assessment Data Input Package for Requirements Analysis for DOE SNF/HLW and Navy SNF Waste Package Overpack Physical Attributes Basis for Performance Assessment.* TDR-TDIP-ES-000009 REV 00. Las Vegas, Nevada: Sandia National Laboratories.

179354 SNL 2007. *Total System Performance Assessment Data Input Package for Requirements Analysis for EBS In-Drift Configuration.* TDR-TDIP-ES-000010 REV 00. Las Vegas, Nevada: Sandia National Laboratories.

179394 SNL 2007. *Total System Performance Assessment Data Input Package for Requirements Analysis for TAD Canister and Related Waste Package Overpack Physical Attributes Basis for Performance Assessment.* TDR-TDIP-ES-000006 REV 00. Las Vegas, Nevada: Sandia National Laboratories.

105941 Stedinger, J.R.; Vogel, R.M.; and Foufoula-Georgiou, E. 1993. "Frequency Analysis of Extreme Events." Chapter 18 of *Handbook of Hydrology*. Maidment, D.R., ed. New York, New York: McGraw-Hill. TIC: 236568.

162243 Stoecker, J.G., II. 1987. "Evaluation of Microbiological Corrosion." In *Corrosion*, Volume 13, Pages 314-315 of *Metals Handbook*. 9th Edition. Metals Park, Ohio: ASM International. TIC: 209807.

162260 Taylor, B.N. and Kuyatt, C.E. 1994. *Guidelines for Evaluating and Expressing the Uncertainty of NIST Measurement Results*. NIST Technical Note 1297. 1994 Edition. Gaithersburg, Maryland: National Institute of Standards and Technology, Physics Laboratory. TIC: 254588.

154741 Urquidi, M. and Macdonald, D.D. 1985. "Solute-Vacancy Interaction Model and the Effect of Minor Alloying Elements on the Initiation of Pitting Corrosion." *Journal of the Electrochemical Society*, *132*, (3), 555-558. New York, New York: Electrochemical Society. TIC: 249843.

159088 Venables, W.N. and Ripley, B.D. 2001. *Modern Applied Statistics with S-PLUS.* 3rd Edition. New York, New York: Springer-Verlag. TIC: 252781.

114895 Welsch, G.; Smialek, J.L.; Doychak, J.; Waldman, J.; and Jacobson, N.S. 1996. "High Temperature Oxidation and Properties." Chapter 2 of *Oxidation and Corrosion of Intermetallic Alloys*. Welsch, G. and Desai, P.D., eds. West Lafayette, Indiana: Purdue University. TIC: 245280.

174800 Wong, L.L.; Lian, T.; Fix, D.V.; Sutton, M.; and Rebak, R.B. 2004. "Surface Analysis of Alloy 22 Coupons Exposed for Five Years to Concentrated Ground Waters." *Corrosion/2004, 59th Annual Conference & Exposition, March 28 - April 1, 2004, New Orleans.* Paper No. 04701. Houston, Texas: NACE International. TIC: 255943.

178563 Yang, L.; Birnbaum, S.; and Cragnolino, G.A. 2004. *Microbially Influenced Corrosion Studies of Engineered Barrier System Materials*. CNWRA 2005-01. San Antonio, Texas: Center for Nuclear Waste Regulatory Analyses. ACC: MOL.20070303.0228.

178411 Yang, L. 2006. *Corrosion of Alloy 22 in Concentrated Nitrate and Chloride Salt Environments at Elevated Temperatures-Progress Report.* CNWRA 2006-02. San Antonio, Texas: Center for Nuclear Waste Regulatory Analyses. ACC: MOL.20061025.0031.

154743 Zhang, L. and Macdonald, D.D. 1998. "Segregation of Alloying Elements in Passive Systems—I. XPS Studies on the Ni–W System." *Electrochimica Acta*, *43*, (18), 2661-2671. New York, New York: Pergamon Press. TIC: 249845.

154742 Zhang, L. and Macdonald, D.D. 1998. "Segregation of Alloying Elements in Passive Systems—II. Numerical Simulation." *Electrochimica Acta*, *43*, (18), 2673-2685. New York, New York: Pergamon Press. TIC: 249846.

9.2 CODES, STANDARDS, REGULATIONS, AND PROCEDURES

180319 10 CFR 63. 2007. Energy: Disposal of High-Level Radioactive Wastes in a Geologic Repository at Yucca Mountain, Nevada. Internet Accessible.

147465 ASTM B 575-99a. 1999. *Standard Specification for Low-Carbon Nickel-Molybdenum-Chromium, Low-Carbon Nickel-Chromium-Molybdenum, Low-Carbon Nickel-Chromium-Molybdenum-Copper, Low-Carbon Nickel-Chromium-Molybdenum-Tantalum, and Low-Carbon Nickel-Chromium-Molybdenum-Tungsten Alloy Plate, Sheet, and Strip.* West Conshohocken, Pennsylvania: American Society for Testing and Materials. TIC: 247534.

105725 ASTM C 1174-97. 1998. *Standard Practice for Prediction of the Long-Term Behavior of Materials, Including Waste Forms, Used in Engineered Barrier Systems (EBS) for Geological Disposal of High-Level Radioactive Waste*. West Conshohocken, Pennsylvania: American Society for Testing and Materials. TIC: 246015.

178286 ASTM C 1239-06A. 2006. *Standard Practice for Reporting Uniaxial Strength Data and Estimating Weibull Distribution Parameters for Advanced Ceramics.* West Conshohocken, Pennsylvania: American Society for Testing and Materials. TIC: 258790.

169968 ASTM E 178-02. 2002. *Standard Practice for Dealing with Outlying Observations* . West Conshohocken, Pennsylvania: American Society for Testing and Materials. TIC: 256164.

103515 ASTM G 1-90 (Reapproved 1999). 1999. *Standard Practice for Preparing, Cleaning, and Evaluating Corrosion Test Specimens*. West Conshohocken, Pennsylvania: American Society for Testing and Materials. TIC: 238771.

138911 ASTM G 3-89 (Reapproved 1999). 1989. *Standard Practice for Conventions Applicable to Electrochemical Measurements in Corrosion Testing*. West Conshohocken, Pennsylvania: American Society for Testing and Materials. TIC: 247076.

117479 ASTM G 5-94. 1994. *Standard Reference Test Method for Making Potentiostatic and Potentiodynamic Anodic Polarization Measurements*. Philadelphia, Pennsylvania: American Society for Testing and Materials. TIC: 231902.

154712 ASTM G 28-97. 1997. *Standard Test Methods of Detecting Susceptibility to Intergranular Corrosion in Wrought, Nickel-Rich, Chromium-Bearing Alloys.* West Conshohocken, Pennsylvania: American Society for Testing and Materials. TIC: 249897.

137688 ASTM G 30-94. 1994. *Standard Practice for Making and Using U-Bend Stress-Corrosion Test Specimens*. Philadelphia, Pennsylvania: American Society for Testing and Materials. TIC: 246890.

163907 ASTM G 59-97. 1998. *Standard Test Method for Conducting Potentiodynamic Polarization Resistance Measurements*. West Conshohocken, Pennsylvania: American Society for Testing and Materials. TIC: 249897.

127897 ASTM G 61-86 (Reapproved 1998). 1987. *Standard Test Method for Conducting Cyclic Potentiodynamic Polarization Measurements for Localized Corrosion Susceptibility of Iron-, Nickel-, or Cobalt-Based Alloys*. West Conshohocken, Pennsylvania: American Society for Testing and Materials. TIC: 246716.

163908 ASTM G 102-89 (Reapproved 1999). 1989. *Standard Practice for Calculation of Corrosion Rates and Related Information from Electrochemical Measurements*. West Conshohocken, Pennsylvania: American Society for Testing and Materials. TIC: 249897.

IM-PRO-002, *Control of the Electronic Management of Information*.

IM-PRO-003, *Software Management*.

SCI-PRO-002, *Planning for Science Activities.*

SCI-PRO-003, *Document Review*.

SCI-PRO-004, *Managing Technical Product Inputs*.

SCI-PRO-006, *Models.*

169585 TIP-CM-51 Rev. 0, Change Notice CM-51-0-4. *Long Term Corrosion Test Facility Specimen De-Scaling Procedure for Alloy 22, Alloy C4, Titanium Alloys, TiGr 7, TiGr 12, and TiGr 16 Specimens*. Livermore, California: Lawrence Livermore National Laboratory. ACC: MOL.20030927.0180.

9.3 SOURCE DATA, LISTED BY DATA TRACKING NUMBER

173259 LB0503DUSTPCAP.001. ECRB Dust Pore Diameter Distribution and Capillary Pressure Characteristic Curves. Submittal date: 3/25/2005.

141284 LL000112205924.112. Long Term Corrosion Test Facility Data. Submittal date: 01/25/2000.

162012 LL030103612251.006. Haynes Weld Data for Alloy 22 Transformation Kinetics and Arrhenius Plots. Submittal date: 01/21/2003.

163469 LL030406412251.045. Transmission Electron Microscopy (TEM) Images of Oxide Film on Air-Oxidized Alloy22 (UNS N06022) Samples Aged at 550C. Submittal date: 04/11/2003.

163712 LL030412512251.057. LTCTF Corrosion Rate Calculations for Five-year Exposed Alloy C22 Specimens Cleaned Under TIP-CM-51. Submittal date: 05/28/2003.

170221 LL040303612251.078. Microbiology Influenced Corrosion (MIC) Effects on Microcosm-Incubated Alloy 22. Submittal date: 03/29/2004.

170222 LL040402912251.085. Microbiologically Induced Corrosion (MIC) Linear Polarization Corrosion Rate of Alloy 22 Weldments for Sterile and Non-Sterile Coupons. Submittal date: 04/20/2004.

171362 LL040803112251.117. Target Compositions of Aqueous Solutions Used for Corrosion Testing. Submittal date: 08/14/2004.

173722 LL040806212251.118. Crevice Repassivation Potential (CRP) of Alloy 22 Determined by the Tsujikawa-Hisamatsu Electrochemical (THE) Method. Submittal date: 03/23/2005.

173720 LL040902712251.119. Corrosion Rate and Potential Parameter Data Taken From Cyclic Potentiodynamic Polarization (CPP) Curves for Laser Peened, Burnished, and As-Welded Alloy 22 Specimens. Submittal date: 02/15/2005.

173921 LL050302312251.129. Electrochemical Behavior of Alloy 22 Specimens Prepared from a Mockup Container. Submittal date: 05/24/2005.

178269 LL060603812251.164. Compilation of Crevice Repassivation Potentials for Alloy 22 in NaCl + KNO3 - Developed. Submittal date: 10/11/2006.

179385 LL060700312251.166. Compilation of Crevice Repassivation Potentials for Alloy 22 in 5 M CaCl2 - Developed. Submittal date: 12/19/2006.

179386 LL060801812251.168. Compilation of Crevice Repassivation Potentials for Alloy 22 in High Temperature High Nitrate Solutions - Developed. Submittal date: 01/16/2007.

179387 LL060803712251.170. Compilation of Crevice Repassivation Potentials for Alloy 22 in NaCl Solutions - Developed. Submittal date: 12/19/2006.

178271 LL060900512251.177. Long-Term Corrosion Potentials (Ecorr) of Alloy 22 in 37 Different Solutions - Developed. Submittal date: 11/01/2006.

178409 LL060900812251.180. Effect of Temperature on the Polarization Resistance of Alloy 22 - Developed. Submittal date: 11/06/2006.

178299 LL060901312251.181. Long-Term Open Circuit Potentials of Alloy 22 in Multi-Ionic Solutions (SAW, SDW, SCW and BSW) - 13 Cells - Acquired. Submittal date: 10/19/2006.

178300 LL060901412251.182. Long-Term Open Circuit Potentials of Alloy 22 in CaCl2 and Ca(NO3)2 Based Solutions - 7 Cells - Acquired. Submittal date: 10/21/2006.

178283 LL060904312251.186. Modeling of Pitzer pH for Selected Ecorr Test Solutions. Submittal date: 11/02/2006.

104994 LL990610605924.079. LTCTF Data for C-22, TIGR7, TIGR12 and TIGR16. Submittal date: 06/13/1999.

138343 LL991203505924.094. Approach and Supporting Data for MIC Modeling. Submittal date: 12/13/1999.

181613 MO0706SPAFEPLA.001. FY 2007 LA FEP List and Screening. Submittal date: 06/20/2007.

9.4 DEVELOPED DATA, LISTED BY DATA TRACKING NUMBER

MO0612WPOUTERB.000. Output from General and Localized Corrosion of Waste Package Outer Barrier Report 2006. Submittal date: 07/18/2007.

MO0703PAGENCOR.001. Output from General Corrosion and Localized Corrosion of Waste Package Outer Barrier 2007 Second Version. Submittal date: 07/18/2007.

MO0706WPOBVALR.000. Validation Files for General and Localized Corrosion of Waste Package Outer Barrier Report 2007. Submittal date: 06/27/2007.

INTENTIONALLY LEFT BLANK

APPENDIX I
SUMMARY OF THE ELECTROCHEMICAL CORROSION TEST PROCEDURES TO GENERATE INPUT DATA FOR ANALYSES AND MODELS IN THIS REPORT

APPENDIX I – SUMMARY OF THE ELECTROCHEMICAL CORROSION TEST PROCEDURES TO GENERATE INPUT DATA FOR ANALYSES AND MODELS IN THIS REPORT

This appendix summarizes the electrochemical corrosion tests that were employed to generate input data for the analyses and models of the Alloy 22 waste package outer barrier (WPOB) documented in this report. The typical sequence for electrochemical testing was as follows:

- The test specimen was ground and polished to eliminate residual effects of fabrication. The surface finishing of the test specimens corresponded to abrasive 600-grit paper. This grinding was done within one hour prior to immersing the test specimen in the electrolyte solution. The testing cell was as described in ASTM G 5-94 (1994 [DIRS 117479]).

- After immersion of the specimen in the electrolyte solution of interest, the free corrosion potential of the specimen was monitored for 24 hours. The value of the potential at the end of this 24-hr period was called the 24-hr corrosion potential. In a few cases, the corrosion potential was monitored for shorter times (one or two hours). The 24-hr corrosion potential was not used for evaluation of localized corrosion initiation. Long-term corrosion potentials were used for evaluation of localized corrosion initiation as described in Section 6.4.4.4.

- After this 24-hr period, at least three polarization resistance tests were carried out according to ASTM G 59-97 (1998 [DIRS 163907]). The polarization resistance data were used to determine the corrosion current density, which can be used to calculate the general corrosion rate (ASTM G 59-97 1998 [DIRS 163907]; ASTM G 102-89 1989 [DIRS 163908]).

- After the polarization resistance tests, one cyclic potentiodynamic polarization (CPP) test was carried out according to ASTM G 61-86 (1987 [DIRS 127897]). The cyclic polarization curve yielded the value of the critical potential for localized corrosion of the WPOB.

Details of the tests are provided in the corresponding scientific notebooks cited in the DTNs of the input data documented in Section 4.1.1.

I.1 DETERMINATION OF CORROSION RATES FROM POLARIZATION RESISTANCE TESTS

The polarization resistance test consists of determining an initial corrosion potential, then ramping the applied potential at a rate of 0.167 mV/s (0.6 V/hr) (consistent with ASTM G 59-97 1998 [DIRS 163907]) while recording the current. The initial corrosion potential was determined by recording the open-circuit potential (after a 24-hr stabilization period) for 10 seconds. The potential scan was started 20 mV below the initial corrosion potential and finished 20 mV above the initial corrosion potential. The resulting data consists of values of applied potential (E) and measured values of current (I). These data were then analyzed using

the Butler-Volmer equation modified for corrosion processes (Equation I-1) (Revie 2000 [DIRS 159370], p. 1,197):

$$i = i_{cor}\left\{\exp\left(\frac{2.303\left[E - E_{cor}\right]}{b_a}\right) - \exp\left(\frac{-2.303\left[E - E_{cor}\right]}{b_c}\right)\right\} \quad \text{Eq. I-1}$$

where i is the current density, E is the applied voltage, E_{cor} is the corrosion potential determined during the scan (at $i = 0$), i_{cor} is the corrosion current density, and b_a and b_c are the anodic and cathodic Tafel slopes, respectively. The applied potential versus measured current density (determined by dividing the measured current by the exposed specimen surface area) data was fit to Equation I-1, thereby determining $i_{cor,}$ b_a, and b_c. The corrosion rate can be calculated from the corrosion current density by ASTM G 59-97 (1998 [DIRS 163907], p. 1), as shown in Equation I-2:

$$CR = K_1\left(\frac{EW}{\rho}\right)i_{cor} \quad \text{Eq. I-2}$$

where $K_1 = 3.272 \times 10^3$ (nm g)/(μA cm yr) (ASTM G 102-89 1989 [DIRS 163908], Table 2). This value of K_1 allows for conversion of corrosion current density in μA/cm² with equivalent weight (EW; dimensionless; see also ASTM G 102-89 1989 [DIRS 163908], p. 1) and mass density (ρ) in g/cm^3 (to get the corrosion rate in nm/yr).

The calculation performed in the current report was done considering the following.

- The exposed area of the specimens: For multiple crevice assembly (MCA) samples, the area changed according to the length of the immersed specimen in the electrolyte solution. The exposed area of samples with other geometries (e.g., prism, rod and disc) also varies from sample to sample.

- The equivalent weight, EW, for Alloy 22 (N06022): This value was calculated considering that the alloy dissolves stoichiometrically, and that it depended on the valence for the dissolved elements. The value used, $EW = 23.28$, was taken from Table 1 of ASTM G 102-89 (1989 [DIRS 163908]), third oxidation state.

- The density, ρ, of Alloy 22 (N06022): The value used was 8.69 g/cm³ (Haynes International 1997 [DIRS 100896], p. 13).

I.2 DETERMINATION OF THE CRITICAL POTENTIAL OR REPASSIVATION POTENTIAL FROM THE CYCLIC POLARIZATION TESTS

In the cyclic polarization tests, the specimen was polarized at a constant scan rate, while the applied current was recorded. The potential scan rate was 0.167 mV/s or 0.6 V/hr, starting at a potential of 150 mV below the 24-hr corrosion potential and continuing until the current density reached a value of 5 mA/cm² (ASTM G 61-86 1987 [DIRS 127897]). At this point the scan rate was reversed, and the test was terminated at the original E_{corr} or before. The scan may also have

been terminated manually after the reversing curve intersects the forward curve. Illustrations of the specimen geometries used are shown in the following figures.

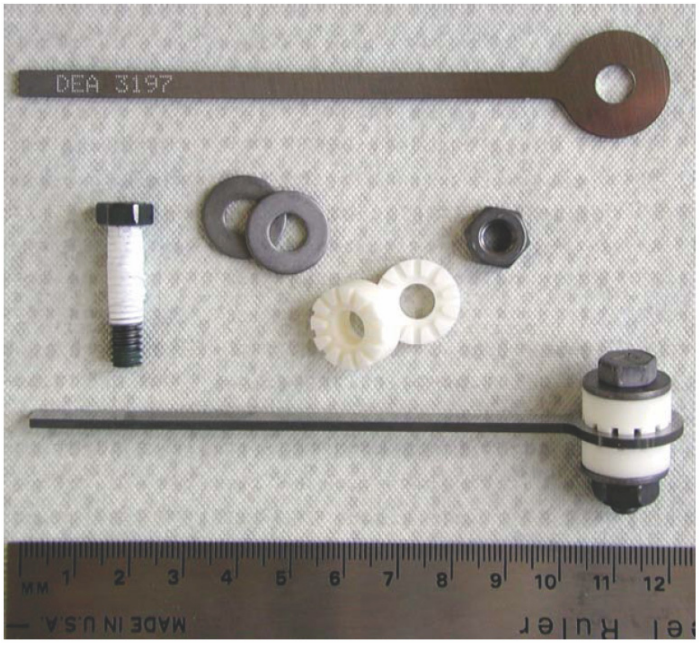

Source: Ilevabre 2005 [DIRS 173814], Figure 1.

NOTE : Applied torque = 70 in-lb.

Figure I-1. Illustration of Multiple Crevice Assembly (MCA) Specimen Showing the Teflon-Wrapped Bolts, Washers, Nut and Ceramic Crevice Formers

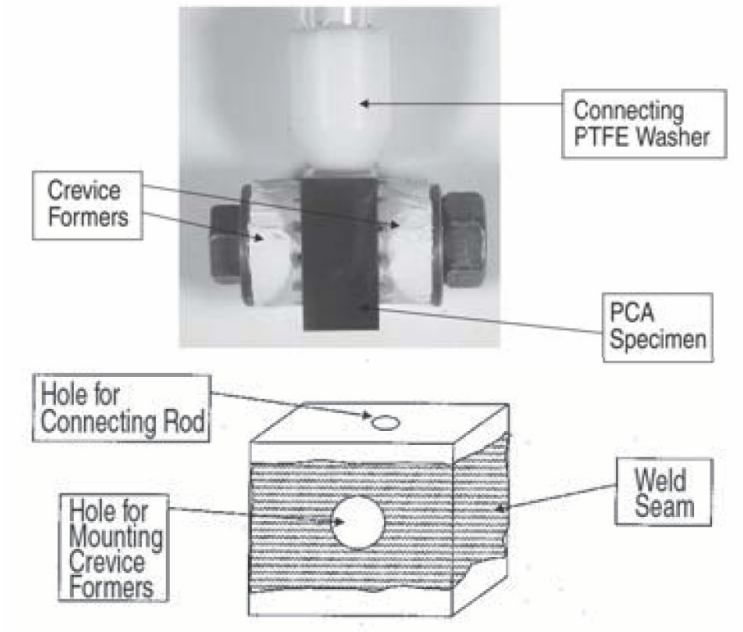

Source: Evans et al. 2005 [DIRS 178247].

Figure I-2. Illustration of Prism Crevice Assembly (PCA) Specimen Showing the Bolts, Washers, Nut and Teflon-Wrapped Ceramic Crevice Formers

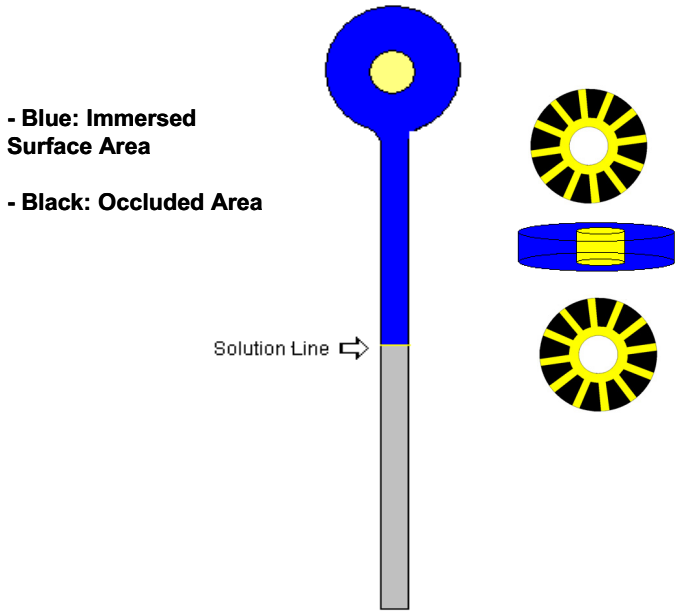

Source: Not applicable – Schematic.

Figure I-3. Schematic Showing the Exposed Surface Area of a Multiple Crevice Assembly Sample during Electrochemical Testing

APPENDIX II
GENERAL CORROSION RATES OF ALLOY 22 CREVICE SAMPLES BASED ON WEIGHT-LOSS MEASUREMENTS AFTER FIVE-YEAR EXPOSURE IN THE LONG-TERM CORROSION TEST FACILITY

APPENDIX II – GENERAL CORROSION RATES OF ALLOY 22 CREVICE SAMPLES BASED ON WEIGHT-LOSS MEASUREMENTS AFTER FIVE-YEAR EXPOSURE IN THE LONG-TERM CORROSION TEST FACILITY

Sample ID	Length (in)	Width (in)	Thickness (in)	Initial Weight (g)	Sample Condition[a]	Exposure Environment	Final Weight (g)	Weight-Loss (g)	Exposed Time (hours)	Surface Area (cm^2)	Corrosion Rate (nm/yr)[b]
DCA 019	2.0120	2.0120	0.1145	64.6723	MA Crevice	SAW Vapor Phase 60°C	64.6698	0.0025	46296	57.917	9.40
DCA 020	2.0155	2.0150	0.1175	66.3190	MA Crevice	SAW Vapor Phase 60°C	66.3168	0.0022	46296	58.270	8.22
DCA 021	2.0105	2.0125	0.1165	65.4770	MA Crevice	SAW Vapor Phase 60°C	65.4747	0.0023	46296	58.006	8.63
DCA 022	2.0135	2.0135	0.1175	65.8096	MA Crevice	SAW Aqueous Phase 60°C	65.8079	0.0017	46296	58.174	6.36
DCA 023	2.0135	2.0115	0.1165	65.5176	MA Crevice	SAW Aqueous Phase 60°C	65.5150	0.0026	46296	58.061	9.75
DCA 024	2.0125	2.0110	0.1165	64.9706	MA Crevice	SAW Aqueous Phase 60°C	64.9646	0.0060	46296	58.019	22.52
DCA 049	2.0175	2.0120	0.1180	66.0889	MA Crevice	SAW Vapor Phase 90°C	66.0857	0.0032	45960	58.272	12.04
DCA 050	2.0170	2.0160	0.1175	66.1281	MA Crevice	SAW Vapor Phase 90°C	66.1235	0.0046	45960	58.339	17.29
DCA 051	2.0160	2.0155	0.1205	67.2585	MA Crevice	SAW Vapor Phase 90°C	67.2543	0.0042	45960	58.473	15.75
DCA 052	2.0135	2.0090	0.1015	57.4226	MA Crevice	SAW Aqueous Phase 90°C	57.4211	0.0015	45960	57.119	5.76
DCA 053	2.0140	2.0140	0.1160	65.4009	MA Crevice	SAW Aqueous Phase 90°C	65.3987	0.0022	45960	58.114	8.30
DCA 054	2.0160	2.0140	0.1170	65.8061	MA Crevice	SAW Aqueous Phase 90°C	65.8044	0.0017	45960	58.227	6.40
DCA 079	2.0135	2.0120	0.1160	65.3198	MA Crevice	SCW Vapor Phase 60°C	65.3190	0.0008	45456	58.045	3.06
DCA 080	2.0160	2.0155	0.1000	57.5590	MA Crevice	SCW Vapor Phase 60°C	57.5582	0.0008	45456	57.277	3.10
DCA 081	2.0155	2.0155	0.1160	65.5190	MA Crevice	SCW Vapor Phase 60°C	65.5179	0.0011	45456	58.196	4.19
DCA 082	2.0160	2.0145	0.1170	65.7599	MA Crevice	SCW Aqueous Phase 60°C	65.7574	0.0025	45456	58.241	9.52
DCA 083	2.0190	2.0145	0.1160	65.2679	MA Crevice	SCW Aqueous Phase 60°C	65.2660	0.0019	45456	58.265	7.23
DCA 084	2.0150	2.0100	0.1030	59.6044	MA Crevice	SCW Aqueous Phase 60°C	59.6006	0.0038	45456	57.274	14.71
DCA 109	2.0110	2.0155	0.1160	65.2077	MA Crevice	SCW Vapor Phase 90°C	65.2062	0.0015	44832	58.073	5.81
DCA 110	2.0130	2.0145	0.1165	65.2979	MA Crevice	SCW Vapor Phase 90°C	65.2949	0.0030	44832	58.129	11.60
DCA 111	2.0165	2.0165	0.1190	66.6259	MA Crevice	SCW Vapor Phase 90°C	66.6244	0.0015	44832	58.427	5.77
DCA 112	2.0150	2.0115	0.1120	63.2332	MA Crevice	SCW Aqueous Phase 90°C	63.2324	0.0008	44832	57.840	3.11
DCA 113	2.0105	2.0150	0.1065	60.1129	MA Crevice	SCW Aqueous Phase 90°C	60.1102	0.0027	44832	57.492	10.56
DCA 114	2.0175	2.0125	0.1080	60.9881	MA Crevice	SCW Aqueous Phase 90°C	60.9853	0.0028	44832	57.702	10.91
DCA 139	2.0170	2.0105	0.1110	62.0138	MA Crevice	SDW Vapor Phase 60°C	62.0126	0.0012	44448	57.809	4.71

Sample ID	Length (in)	Width (in)	Thickness (in)	Initial Weight (g)	Sample Condition[a]	Exposure Environment	Final Weight (g)	Weight-Loss (g)	Exposed Time (hours)	Surface Area (cm^2)	Corrosion Rate (nm/yr)[b]
DCA 140	2.0140	2.0120	0.1100	61.6079	MA Crevice	SDW Vapor Phase 60°C	61.6070	0.0009	44448	57.709	3.54
DCA 141	2.0180	2.0160	0.1110	62.3601	MA Crevice	SDW Vapor Phase 60°C	62.3594	0.0007	44448	57.987	2.74
DCA 142	2.0150	2.0115	0.1120	62.7895	MA Crevice	SDW Aqueous Phase 60°C	62.7879	0.0016	44448	57.840	6.27
DCA 143	2.0120	2.0120	0.1115	62.4663	MA Crevice	SDW Aqueous Phase 60°C	62.4648	0.0015	44448	57.742	5.89
DCA 144	2.0100	2.0125	0.1100	61.4272	MA Crevice	SDW Aqueous Phase 60°C	61.4251	0.0021	44448	57.614	8.27
DCA 175	2.0170	2.0120	0.0900	49.9140	MA Crevice	SDW Vapor Phase 90°C	49.9138	0.0002	43488	56.625	0.82
DCA 176	2.0075	2.0090	0.1045	58.6401	MA Crevice	SDW Vapor Phase 90°C	58.6399	0.0002	43488	57.130	0.81
DCA 177	2.0125	2.0100	0.1100	61.7156	MA Crevice	SDW Vapor Phase 90°C	61.7040	0.0116	43488	57.614	46.67[c]
DCA 178	2.0145	2.0120	0.1140	63.9838	MA Crevice	SDW Aqueous Phase 90°C	63.9817	0.0021	43488	57.956	8.40
DCA 179	2.0125	2.0100	0.1075	60.3046	MA Crevice	SDW Aqueous Phase 90°C	60.3033	0.0013	43488	57.468	5.24
DCA 180	2.0135	2.0065	0.1020	57.4820	MA Crevice	SDW Aqueous Phase 90°C	57.4807	0.0013	43488	57.079	5.28
DCB 019	2.0010	1.9975	0.0810	45.0056	ASW Crevice	SAW Vapor Phase 60°C	45.0030	0.0026	46296	55.279	10.24
DCB 020	1.9945	2.0010	0.1035	55.5235	ASW Crevice	SAW Vapor Phase 60°C	55.5217	0.0018	46296	56.501	6.94
DCB 022	2.0030	2.0000	0.0900	49.1369	ASW Crevice	SAW Aqueous Phase 60°C	49.1354	0.0015	46296	55.921	5.84
DCB 023	2.0050	2.0110	0.1010	56.3136	ASW Crevice	SAW Aqueous Phase 60°C	56.3118	0.0018	46296	56.912	6.89
DCB 049	2.0045	2.0070	0.0865	46.3703	ASW Crevice	SAW Vapor Phase 90°C	46.3662	0.0041	45960	55.948	16.07
DCB 050	2.0050	2.0115	0.0840	44.8726	ASW Crevice	SAW Vapor Phase 90°C	44.8689	0.0037	45960	55.937	14.51
DCB 052	2.0040	2.0040	0.0925	50.3147	ASW Crevice	SAW Aqueous Phase 90°C	50.3136	0.0011	45960	56.202	4.29
DCB 053	2.0000	2.0065	0.0830	45.6403	ASW Crevice	SAW Aqueous Phase 90°C	45.6388	0.0015	45960	55.610	5.92
DCB 079	2.0010	2.0030	0.0835	45.7966	ASW Crevice	SCW Vapor Phase 60°C	45.7961	0.0005	45456	55.572	2.00
DCB 080	2.0130	2.0000	0.0920	52.2193	ASW Crevice	SCW Vapor Phase 60°C	52.2173	0.0020	45456	56.307	7.88
DCB 082	2.0010	1.9990	0.0840	46.2660	ASW Crevice	SCW Aqueous Phase 60°C	46.2611	0.0049	45456	55.493	19.58
DCB 083	1.9970	1.9965	0.0855	48.1762	ASW Crevice	SCW Aqueous Phase 60°C	48.1728	0.0034	45456	55.405	13.61
DCB 109	2.0060	2.0150	0.1040	57.7242	ASW Crevice	SCW Vapor Phase 90°C	57.7231	0.0011	44832	57.223	4.32
DCB 110	1.9940	1.9990	0.0950	51.1169	ASW Crevice	SCW Vapor Phase 90°C	51.1164	0.0005	44832	55.941	2.01
DCB 112	2.0105	2.0095	0.1035	56.9739	ASW Crevice	SCW Aqueous Phase 90°C	56.9716	0.0023	44832	57.167	9.05
DCB 113	2.0055	2.0040	0.0870	48.0842	ASW Crevice	SCW Aqueous Phase 90°C	48.0815	0.0027	44832	55.923	10.86
DCB 139	1.9805	1.9860	0.1045	56.1890	ASW Crevice	SDW Vapor Phase 60°C	56.1890	0.0000	44448	55.775	0.00[d]

Sample ID	Length (in)	Width (in)	Thickness (in)	Initial Weight (g)	Sample Condition[a]	Exposure Environment	Final Weight (g)	Weight-Loss (g)	Exposed Time (hours)	Surface Area (cm^2)	Corrosion Rate (nm/yr)[b]
DCB 140	1.9965	1.9975	0.0920	48.7987	ASW Crevice	SDW Vapor Phase 60°C	48.7980	0.0007	44448	55.795	2.85
DCB 142	2.0015	2.0025	0.0900	49.2450	ASW Crevice	SDW Aqueous Phase 60°C	49.2445	0.0005	44448	55.949	2.03
DCB 143	1.9985	1.9985	0.0900	49.7742	ASW Crevice	SDW Aqueous Phase 60°C	49.7728	0.0014	44448	55.760	5.69
DCB 175	1.9990	2.0060	0.1090	59.1477	ASW Crevice	SDW Vapor Phase 90°C	59.1476	0.0001	43488	57.077	0.41
DCB 176	2.0050	2.0030	0.0825	45.3890	ASW Crevice	SDW Vapor Phase 90°C	45.3885	0.0005	43488	55.621	2.08
DCB 178	2.0015	2.0035	0.0865	47.7164	ASW Crevice	SDW Aqueous Phase 90°C	47.7161	0.0003	43488	55.772	1.25
DCB 179	2.0040	2.0120	0.0845	47.0565	ASW Crevice	SDW Aqueous Phase 90°C	47.0564	0.0001	43488	55.953	0.41

[a] MA = mill-annealed, ASW = as-welded.
[b] The input data from DTN: LL030412512251.057 [DIRS 163712], file: *C22 5 Year Coupon Corrosion Rates 4-14-03.xls*, are the initial and final weight measurements, sample dimensions, and exposure conditions and time. The sample surface areas and corrosion rates were calculated in this report (Output DTN: MO0612WPOUTERB.000, file: *Alloy22_5yr_CreviceAnalysis.xls*). The calculated corrosion rates in this table are slightly different from those in DTN: LL030412512251.057 [DIRS 163712], file: *C22 5 Year Coupon Corrosion Rates 4-14-03.xls*, due to differences in the number of significant digits used. The final weight is the average of three weighings after the final cleaning to remove observable surface deposits.
[c] Outlier, not included in the analysis.
[d] Zero value not included in the analysis.

Source: DTN: LL030412512251.057 [DIRS 163712], file: *C22 5 Year Coupon Corrosion Rates 4-14-03.xls*.

Output DTN: MO0612WPOUTERB.000, file: *Alloy22_5yr_CreviceAnalysis.xls.*

INTENTIONALLY LEFT BLANK

APPENDIX III
GENERAL CORROSION RATE OF ALLOY 22 WEIGHT-LOSS SAMPLES BASED ON THE WEIGHT-LOSS MEASUREMENT AFTER FIVE-YEAR EXPOSURE IN THE LONG-TERM CORROSION TEST FACILITY

APPENDIX III – GENERAL CORROSION RATE OF ALLOY 22 WEIGHT-LOSS SAMPLES BASED ON THE WEIGHT-LOSS MEASUREMENT AFTER FIVE-YEAR EXPOSURE IN THE LONG-TERM CORROSION TEST FACILITY

Sample ID	Length (in)	Width (in)	Thickness (in)	Initial Weight (g)	Sample Condition	Exposure Environment	Final Weight (g)	Weight Loss (g)	Exposed Time (hours)	Surface Area (cm^2)	Corrosion Rate (nm/yr)[a]
DWA 019	2.0135	1.0100	0.1120	30.3252	MA WL	SAW Vapor Phase 60°C	30.3246	0.0006	46296	30.3317	4.31
DWA 020	2.0135	1.0085	0.1130	30.9953	MA WL	SAW Vapor Phase 60°C	30.9950	0.0003	46296	30.3359	2.15
DWA 021	2.0145	1.0095	0.1140	31.0549	MA WL	SAW Vapor Phase 60°C	31.0544	0.0005	46296	30.4231	3.58
DWA 022	2.0120	1.0115	0.1140	31.0362	MA WL	SAW Aqueous Phase 60°C	31.0361	0.0001	46296	30.4417	0.72
DWA 023	2.0110	1.0095	0.1125	30.2366	MA WL	SAW Aqueous Phase 60°C	30.2361	0.0005	46296	30.3044	3.59
DWA 024	2.0095	1.0085	0.0945	25.6040	MA WL	SAW Aqueous Phase 60°C	25.6035	0.0005	46296	29.4406	3.70
DWA 034	2.0145	1.0105	0.1125	30.5218	MA WL	SAW Waterline 60°C[b]	30.5213	0.0005	46296	30.3826	3.58
DWA 039	2.0155	1.0120	0.1145	31.2482	MA WL	SAW Waterline 90°C[b]	31.2476	0.0006	45960	30.5290	4.31
DWA 059	2.0100	1.0110	0.1130	30.5308	MA WL	SAW Vapor Phase 90°C	30.5304	0.0004	45960	30.3537	2.89
DWA 060	2.0135	1.0095	0.1130	30.9395	MA WL	SAW Vapor Phase 90°C	30.9391	0.0004	45960	30.3633	2.89
DWA 061	2.0170	1.0120	0.1105	29.9892	MA WL	SAW Vapor Phase 90°C	29.9891	0.0001	45960	30.3692	0.72
DWA 062	2.0120	1.0090	0.1120	30.0884	MA WL	SAW Aqueous Phase 90°C	30.0882	0.0002	45960	30.2826	1.45
DWA 063	2.0145	1.0100	0.1145	31.0229	MA WL	SAW Aqueous Phase 90°C	31.0225	0.0004	45960	30.4595	2.88
DWA 064	2.0080	1.0100	0.1150	30.5525	MA WL	SAW Aqueous Phase 90°C	30.5521	0.0004	45960	30.3879	2.89
DWA 089	2.0145	1.0120	0.1160	31.0278	MA WL	SCW Vapor Phase 60°C	31.0280	−0.0002	45456	30.5825	−1.45[c]
DWA 090	2.0175	1.0105	0.1145	30.7848	MA WL	SCW Vapor Phase 60°C	30.7848	0.0000	45456	30.5168	0.00[c]
DWA 091	2.0150	1.0070	0.1160	30.8690	MA WL	SCW Vapor Phase 60°C	30.8687	0.0003	45456	30.4523	2.18
DWA 092	2.0100	1.0095	0.1065	29.9109	MA WL	SCW Aqueous Phase 60°C	29.9106	0.0003	45456	30.0183	2.22
DWA 093	2.0090	1.0095	0.1100	29.7822	MA WL	SCW Aqueous Phase 60°C	29.7820	0.0002	45456	30.1623	1.47
DWA 094	2.0155	1.0115	0.1165	30.8081	MA WL	SCW Aqueous Phase 60°C	30.8077	0.0004	45456	30.6060	2.90
DWA 104	2.0140	1.0100	0.1120	30.6273	MA WL	SCW Waterline 60°C[b]	30.6270	0.0003	45456	30.3389	2.19
DWA 109	2.0160	1.0110	0.1100	30.0620	MA WL	SCW Waterline 90°C[b]	30.0620	0.0000	45984	30.3046	0.00[c]
DWA 129	2.0155	1.0090	0.1005	27.1346	MA WL	SCW Vapor Phase 90°C	27.1343	0.0003	44832	29.8117	2.26
DWA 130	2.0105	1.0125	0.1160	31.3506	MA WL	SCW Vapor Phase 90°C	31.3501	0.0005	44832	30.5380	3.68
DWA 131	2.0190	1.0115	0.1130	30.7217	MA WL	SCW Vapor Phase 90°C	30.7215	0.0002	44832	30.4980	1.47

Sample ID	Length (in)	Width (in)	Thickness (in)	Initial Weight (g)	Sample Condition	Exposure Environment	Final Weight (g)	Weight Loss (g)	Exposed Time (hours)	Surface Area (cm^2)	Corrosion Rate (nm/yr)[a]
DWA 132	2.0135	1.0095	0.1090	29.0636	MA WL	SCW Aqueous Phase 90°C	29.0623	0.0013	44832	30.1820	9.68
DWA 133	2.0160	1.0100	0.1115	30.2796	MA WL	SCW Aqueous Phase 90°C	30.2786	0.0010	44832	30.3452	7.41
DWA 134	2.0155	1.0100	0.1150	30.8393	MA WL	SCW Aqueous Phase 90°C	30.8385	0.0008	44832	30.4967	5.90
DWA 147	2.0135	1.0090	0.1155	31.2833	MA WL	SDW Vapor Phase 60°C	31.2833	0.0000	44448	30.4629	0.00[c]
DWA 148	2.0130	1.0100	0.1050	28.2562	MA WL	SDW Aqueous Phase 60°C	28.2561	0.0001	44448	30.0071	0.76
DWA 154	2.0185	1.0100	0.1140	30.7483	MA WL	SDW Waterline 60°C[b]	30.7479	0.0004	44448	30.4949	2.97
DWA 167	2.0010	1.0030	0.1255	33.5921	MA WL	SDW Waterline 90°C[b]	33.5918	0.0003	43488	30.5685	2.27
DWA 174	2.0015	1.0025	0.1250	33.6543	MA WL	SDW Vapor Phase 90°C	33.6542	0.0001	43488	30.5395	0.76
DWA 175	2.0020	0.9960	0.1245	33.2710	MA WL	SDW Aqueous Phase 90°C	33.2710	0.0000	43488	30.3459	0.00[c]
DWB 019	2.0000	1.0055	0.1005	27.1924	ASW WL	SAW Vapor Phase 60°C	27.1922	0.0002	46296	29.4949	1.48
DWB 020	1.9990	1.0030	0.1000	27.0152	ASW WL	SAW Vapor Phase 60°C	27.0152	0.0000	46296	29.3904	0.00[c]
DWB 021	1.9995	1.0050	0.1000	27.2070	ASW WL	SAW Vapor Phase 60°C	27.2070	0.0000	46296	29.4517	0.00[c]
DWB 022	1.9995	1.0035	0.0980	26.6246	ASW WL	SAW Aqueous Phase 60°C	26.6241	0.0005	46296	29.3209	3.71
DWB 023	2.0045	1.0070	0.0940	25.5992	ASW WL	SAW Aqueous Phase 60°C	25.5990	0.0002	46296	29.3062	1.49
DWB 024	1.9920	1.0010	0.1045	28.0650	ASW WL	SAW Aqueous Phase 60°C	28.0645	0.0005	46296	29.4390	3.70
DWB 059	1.9990	1.0060	0.1095	29.6327	ASW WL	SAW Vapor Phase 90°C	29.6327	0.0000	45960	29.9001	0.00[c]
DWB 060	2.0020	1.0065	0.1120	30.1549	ASW WL	SAW Vapor Phase 90°C	30.1548	0.0001	45960	30.0697	0.73
DWB 061	1.9960	1.0065	0.1075	28.9565	ASW WL	SAW Vapor Phase 90°C	28.9563	0.0002	45960	29.7803	1.47
DWB 062	2.0000	1.0050	0.1080	29.1079	ASW WL	SAW Aqueous Phase 90°C	29.1073	0.0006	45960	29.8196	4.41
DWB 063	1.9985	1.0050	0.1075	29.0647	ASW WL	SAW Aqueous Phase 90°C	29.0646	0.0001	45960	29.7755	0.74
DWB 064	1.9955	1.0025	0.1105	29.2528	ASW WL	SAW Aqueous Phase 90°C	29.2526	0.0002	45960	29.7996	1.47
DWB 089	2.0000	1.0045	0.1130	30.0101	ASW WL	SCW Vapor Phase 60°C	30.0100	0.0001	45456	30.0314	0.74
DWB 090	2.0015	1.0045	0.0995	27.0584	ASW WL	SCW Vapor Phase 60°C	27.0583	0.0001	45456	29.4441	0.75
DWB 091	1.9950	1.0020	0.0980	26.6267	ASW WL	SCW Vapor Phase 60°C	26.6267	0.0000	45456	29.2164	0.00[c]
DWB 092	1.9970	1.0005	0.0960	26.1388	ASW WL	SCW Aqueous Phase 60°C	26.1385	0.0003	45456	29.1143	2.29
DWB 093	1.9950	1.0050	0.1090	29.3467	ASW WL	SCW Aqueous Phase 60°C	29.3462	0.0005	45456	29.7928	3.72
DWB 094	1.9910	0.9995	0.1075	28.8795	ASW WL	SCW Aqueous Phase 60°C	28.8786	0.0009	45456	29.5189	6.76
DWB 129	1.9780	1.0055	0.1075	29.1972	ASW WL	SCW Vapor Phase 90°C	29.1971	0.0001	44832	29.4947	0.76

Sample ID	Length (in)	Width (in)	Thickness (in)	Initial Weight (g)	Sample Condition	Exposure Environment	Final Weight (g)	Weight Loss (g)	Exposed Time (hours)	Surface Area (cm^2)	Corrosion Rate (nm/yr)[a]
DWB 130	1.9955	1.0020	0.1065	28.6787	ASW WL	SCW Vapor Phase 90°C	28.6784	0.0003	44832	29.6060	2.28
DWB 131	2.0040	1.0050	0.1070	29.2996	ASW WL	SCW Vapor Phase 90°C	29.2993	0.0003	44832	29.8319	2.26
DWB 132	2.0000	1.0025	0.1065	28.7651	ASW WL	SCW Aqueous Phase 90°C	28.7637	0.0014	44832	29.6840	10.60
DWB 133	2.0000	1.0015	0.1105	29.7020	ASW WL	SCW Aqueous Phase 90°C	29.7005	0.0015	44832	29.8370	11.30
DWB 134	1.9960	1.0040	0.1075	29.2460	ASW WL	SCW Aqueous Phase 90°C	29.2444	0.0016	44832	29.7125	12.11
DWB 147	1.9955	1.0025	0.1060	28.6604	ASW WL	SDW Vapor Phase 60°C	28.6603	0.0001	44448	29.5971	0.77
DWB 148	1.9955	1.0045	0.1085	29.4282	ASW WL	SDW Aqueous Phase 60°C	29.4280	0.0002	44448	29.7639	1.52
DWB 174	1.9960	0.9960	0.1180	30.5213	ASW WL	SDW Vapor Phase 90°C	30.5210	0.0003	43488	29.9671	2.32
DWB 175	2.0000	0.9995	0.1110	28.4575	ASW WL	SDW Aqueous Phase 90°C	28.4573	0.0002	43488	29.8051	1.56

[a] The input data from DTN: LL030412512251.057 [DIRS 163712], file: *C22 5 Year Coupon Corrosion Rates 4-14-03.xls*, are the initial and final weight measurements, sample dimensions, and exposure conditions and time. The sample surface areas and corrosion rates were calculated in this report (Output DTN: MO0612WPOUTERB.000, file: *Alloy22_5yr_WLAnalysis.xls*). The calculated corrosion rates in this table are slightly different from those in DTN: LL030412512251.057 [DIRS 163712], file: *C22 5 Year Coupon Corrosion Rates 4-14-03.xls*, due to differences in the number of significant digits used. The final weight is the average of three weighings after the final cleaning to remove observable surface deposits.

[b] The waterline data are treated as the aqueous-phase data in the analysis.

[c] Negative or zero rate not included in the analysis.

Source: DTN: LL030412512251.057 [DIRS 163712], file: *C22 5 Year Coupon Corrosion Rates 4-14-03.xls*.

Output DTN: MO0612WPOUTERB.000, file: *Alloy22_5yr_WLAnalysis.xls*.

NOTE: MA = mill-annealed, ASW = as-welded, WL = weight-loss.

INTENTIONALLY LEFT BLANK

APPENDIX IV
COMPARISION OF DISTRIBUTIONS FIT TO THE WEIGHT-LOSS DATA FROM CREVICE SAMPLES

APPENDIX IV – COMPARISION OF DISTRIBUTIONS FIT TO THE WEIGHT-LOSS DATA FROM CREVICE SAMPLES

This worksheet compares how well several distributions fit the five year creviced specimen data. The worksheet then evaluates several fitting methods for the Weibull distribution and concludes the maximum likelihood estimators (MLEs) provide a good parametric description of the data for interpolation and extrapolation of rates for further analyses.The Weibull MLEs are fit to the data for further analyses.

Read in creviced specimen five year weight-loss corrosion rates in nm/yr.

data :=

GC-data.txt data := sort(data) Read data and sort it

$n := \text{length}(data)$ $n = 58$

$i := 1..n$

Use approximate Median Rank plotting positions (Stedinger et al. 1993 [DIRS 105941], Table 18.3.1).

$$pp_i := \frac{i - 0.3175}{n - 2\cdot(0.3175) + 1}$$

Consideration of several distributions:

The Uniform, Normal, Log-Normal, Gamma, and Weibull distributions are considered by examination of probability plots (D'Agostino and Stephens 1986 [DIRS 160320], Chap. 2 and 11). The distribution values are plotted on a scale such that if the distribution is appropriate the data will graph as a straight line.
A linear fit line is added to the graphs for reference.

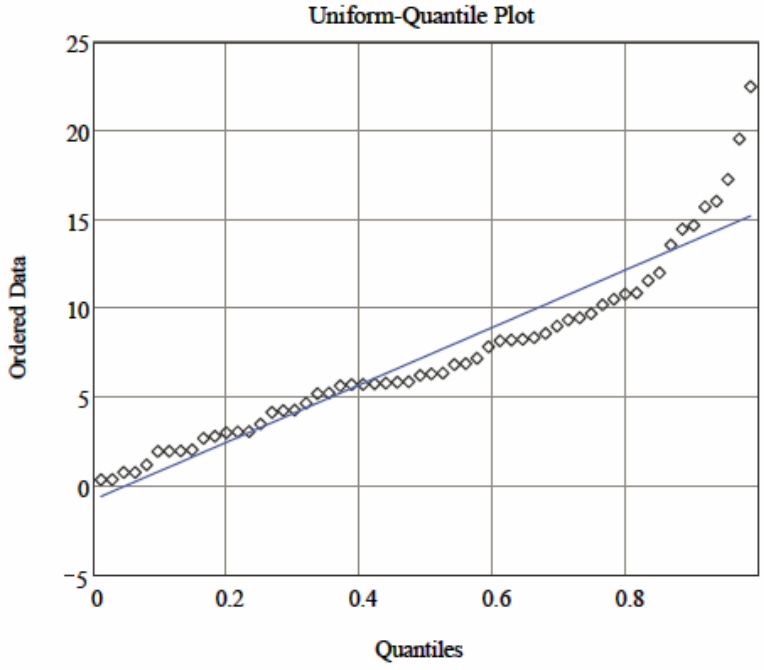

Conclude Uniform distribution is not a good fit

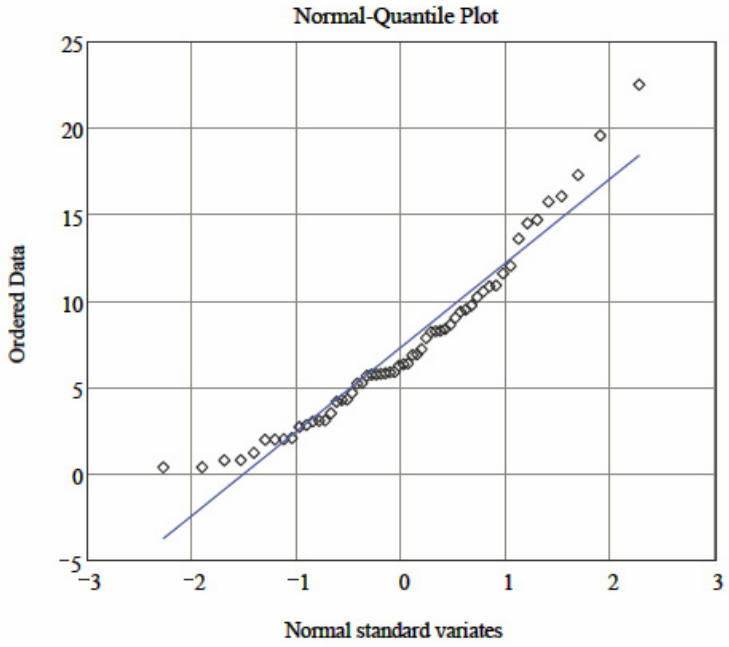

Conclude Normal distribution is not a good fit

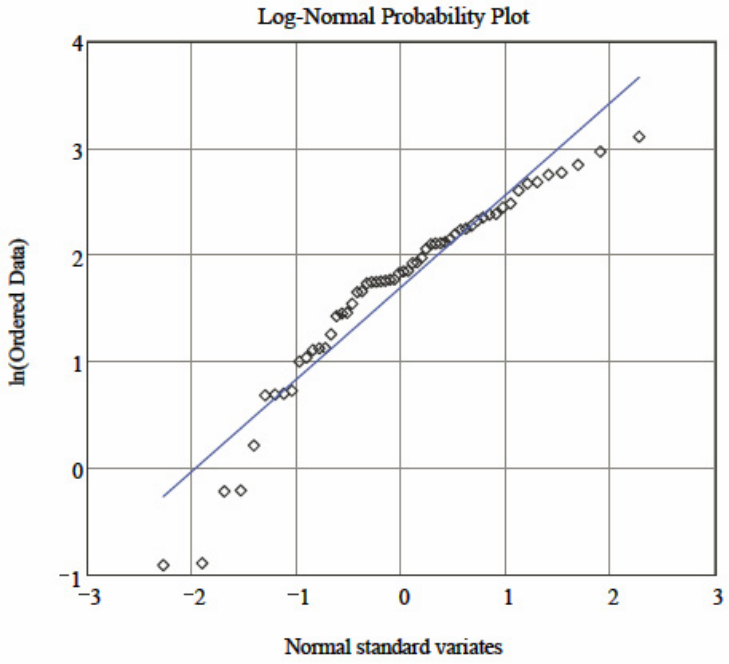

Conclude Log-Normal distribution is not a good fit

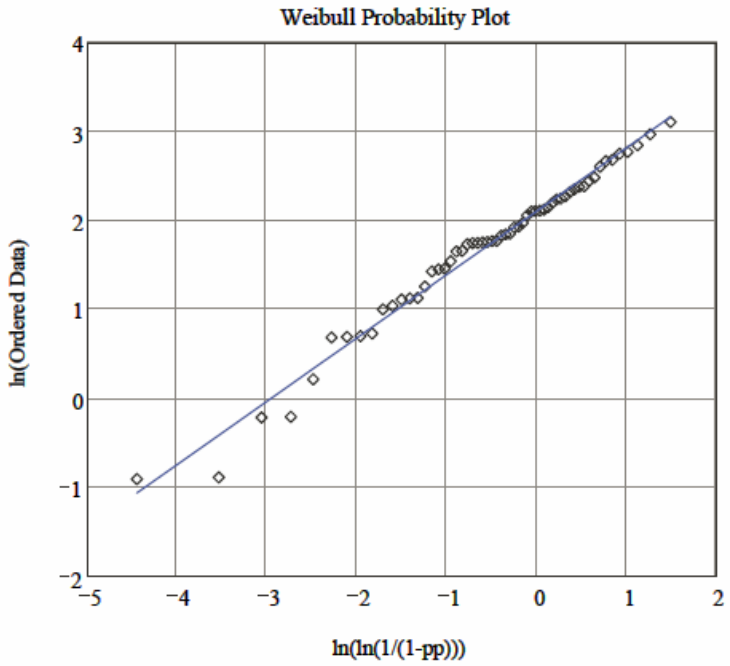

Conclude Weibull distribution is a good fit

Gamma Distribution

As the Gamma distribution does not have an analytical form suitable to form a probability plot, first maximum likelihood estimators (MLEs) are calculated and then a Quantile-Quantile plot is made using them. MLEs are given as equations to be solved iteratively (Evans et al. 1993 [DIRS 112115], Section 18.2).

Provide initial guess for solver. $c := 1.4$

Given

$$\ln(c) - \mathrm{Psi}(c) = \ln\left[\frac{\mathrm{mean}(data)}{\left(\prod_{i=1}^{n} data_i\right)^{\frac{1}{n}}}\right]$$

$c_G := \mathrm{Find}(c)$ $\quad c_G = 1.880$

$b_G := \frac{\mathrm{mean}(data)}{c_G}$ $\quad b_G = 3.913$

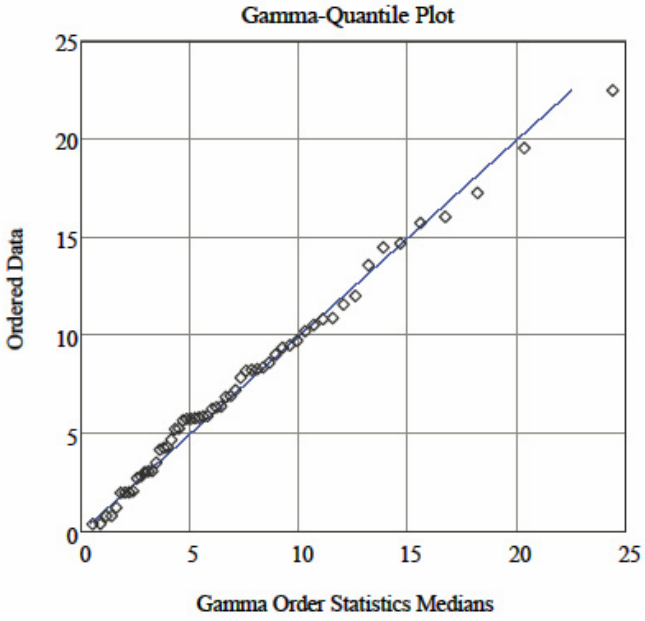

Calculate R-squared value for gamma distribution

$$1 - \frac{\sum\left(\text{data} - b_G \cdot \text{qgamma}\left(\text{pp}, c_G\right)\right)^2}{\sum\left(\text{data} - \text{mean}(\text{data})\right)^2} = 0.989$$

Conclude gamma distribution is a good fit but Weibull is preferable, as will be seen below.

Evaluation of Weibull distribution fit

Maximum Likelihood Estimation of Weibull Parameters

MLEs given as equations to be solved iteratively (Algebraic rearrangement of equations in Evans et al. 1993 [DIRS 112115], Section 41.3).

$$\text{TOL} := 10^{-8}$$

$$f(c) := \frac{\sum_{i=1}^{n}\left[\left(\text{data}_i\right)^c \cdot \ln\left(\text{data}_i\right)\right]}{\sum_{i=1}^{n}\left[\left(\text{data}_i\right)^c\right]} - \frac{\sum_{i=1}^{n}\left(\ln\left(\text{data}_i\right)\right)}{n} - \frac{1}{c}$$

$$\text{Find\_b}(c) := \left[\frac{\sum_{i=1}^{n}\left[\left(\text{data}_i\right)^c\right]}{n}\right]^{\frac{1}{c}}$$

$c_{ML} := \text{root}(f(c), c)$

$b_{ML} := \text{Find\_b}(c_{ML})$

$c_{ML} := 0.977 \cdot c_{ML}$ For a sample size of 58, the unbiasing factor for the shape estimator is 0.977 (ASTM C 1239 - 06A 2006 [DIRS 178286], Table 1).

$c_{ML} = 1.476$

$b_{ML} = 8.141$

Parameter Estimation by Nonlinear Regression using plotting positions.

Decrease tolerance from default (0.001) in order to converge to a solution.

$CTOL := 0.07$

$b := 8.0$

Given

$$pp = 1 - \exp\left[-\left(\frac{data}{b}\right)^{c}\right]$$

$$\begin{pmatrix} c1 \\ b1 \end{pmatrix} := \text{Find}(c, b)$$

$c1 = 1.562$

$b1 = 8.207$

Parameter Estimation by Least Squares using plotting positions

D'Agostino and Stephens (1986 [DIRS 160320], Chapter 11).

$c2 := \text{slope}(\ln(data), \ln(-\ln(1 - pp)))$

$$b2 := \exp\left(\frac{-\text{intercept}(\ln(data), \ln(-\ln(1 - pp)))}{c2}\right)$$

$c2 = 1.380$

$b2 = 8.291$

$$c3 := \frac{1}{\text{slope}(\ln(-\ln(1 - pp)), \ln(data))}$$

$b3 := \exp(\text{intercept}(\ln(-\ln(1 - pp)), \ln(data)))$

$c3 = 1.403$

$b3 = 8.234$

Calculate Goodness of Fit values for estimates

Weibull distribution functions (D'Agostino and Stephens 1986 [DIRS 160320], Section 4.11) for the Cumulative Distribution Function (CDF), pW, and inverse-CDF, qW.

$$pW(x,b,c) := 1 - \exp\left[-\left(\frac{x}{b}\right)^{c}\right]$$

$$qW(p,b,c) := b\cdot(-\ln(1-p))^{\frac{1}{c}}$$

R-square goodness of fit measure for Weibull Distribution (values closest to one better).

$$R2(p,b,c) := 1 - \frac{\sum (data - qW(p,b,c))^2}{\sum (data - mean(data))^2}$$

$R2(pp,b1,c1) = 0.992$

$R2(pp,b2,c2) = 0.984$

$R2(pp,b3,c3) = 0.989$

$R2\left(pp,b_{ML},c_{ML}\right) = 0.995$

Anderson-Darling goodness of fit measure for Weibull Distribution (lower value better).

$$AD(n,w) := \left(1 + \frac{0.2}{\sqrt{n}}\right)\cdot\left[-n - \frac{1}{n}\cdot\sum_{j=1}^{n}\left[(2\cdot j - 1)\cdot\left(\ln\left(w_j\right) + \ln\left(1 - w_{n-j+1}\right)\right)\right]\right]$$

$AD(n,pW(data,b1,c1)) = 0.239$

$AD(n,pW(data,b2,c2)) = 0.335$

$AD(n,pW(data,b3,c3)) = 0.296$

$AD\left(n,pW\left(data,b_{ML},c_{ML}\right)\right) = 0.234$

MLEs had highest R-squared and lowest Anderson-Darling measure.
Conclude MLEs provide best fit to data.
Overall conclusion: Weibull distribution (with MLEs) provide a good parametric description of the data for interpolation and extrapolation of rates for further analyses.

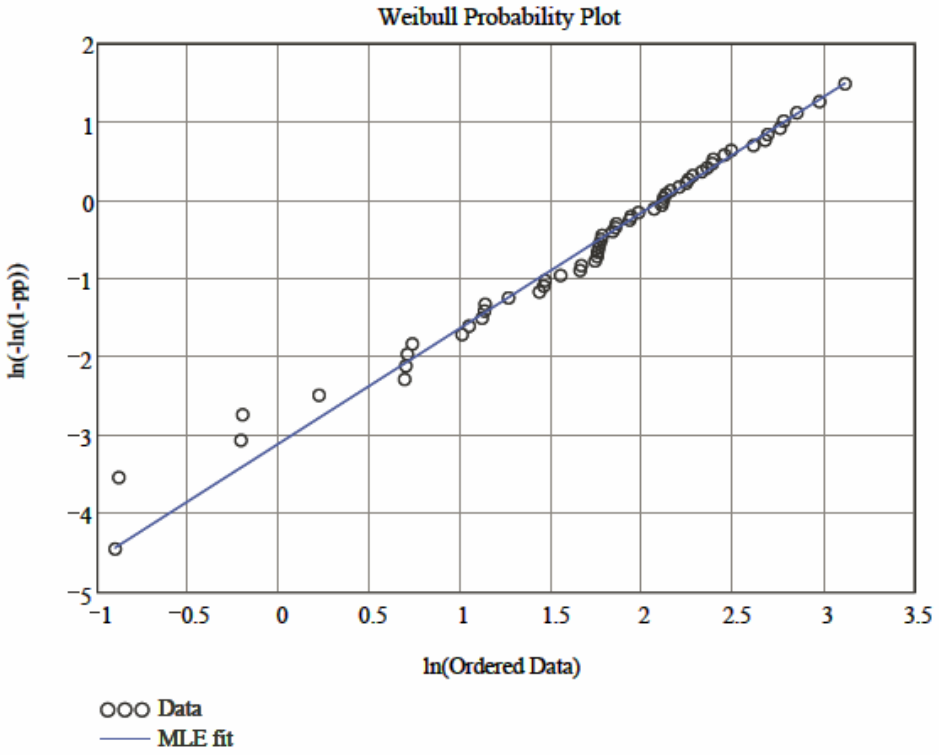
Weibull Probability Plot
ln(-ln(1-pp))
ln(Ordered Data)
Data
MLE fit

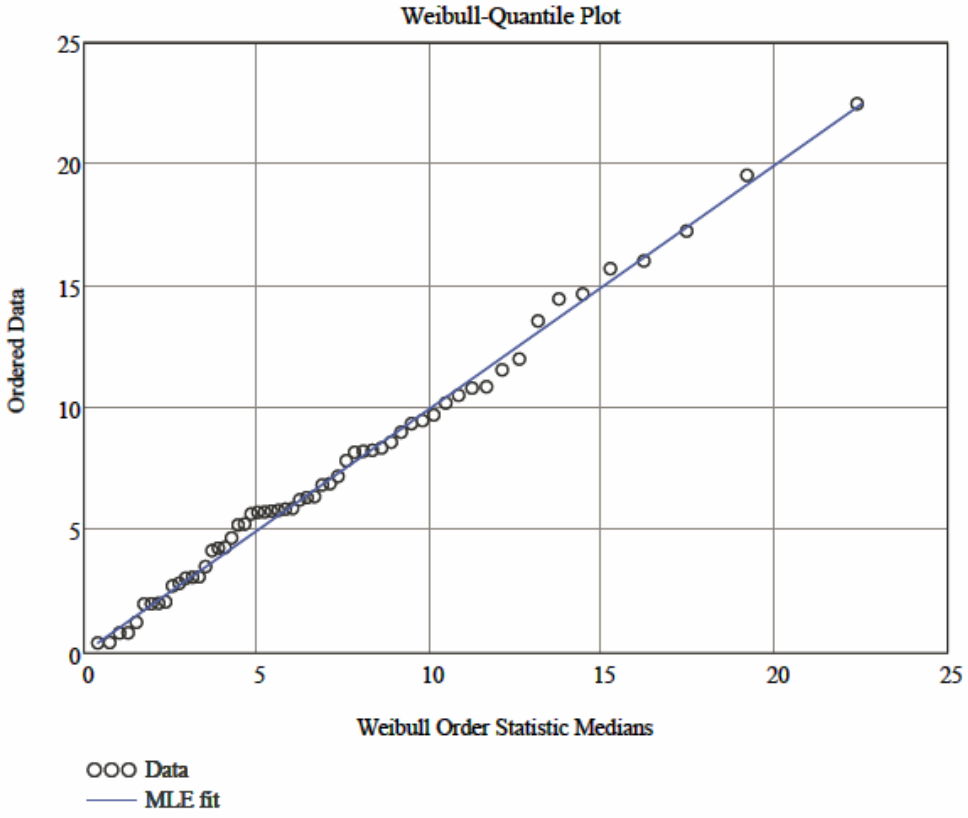
Weibull-Quantile Plot
Ordered Data
Weibull Order Statistic Medians
Data
MLE fit

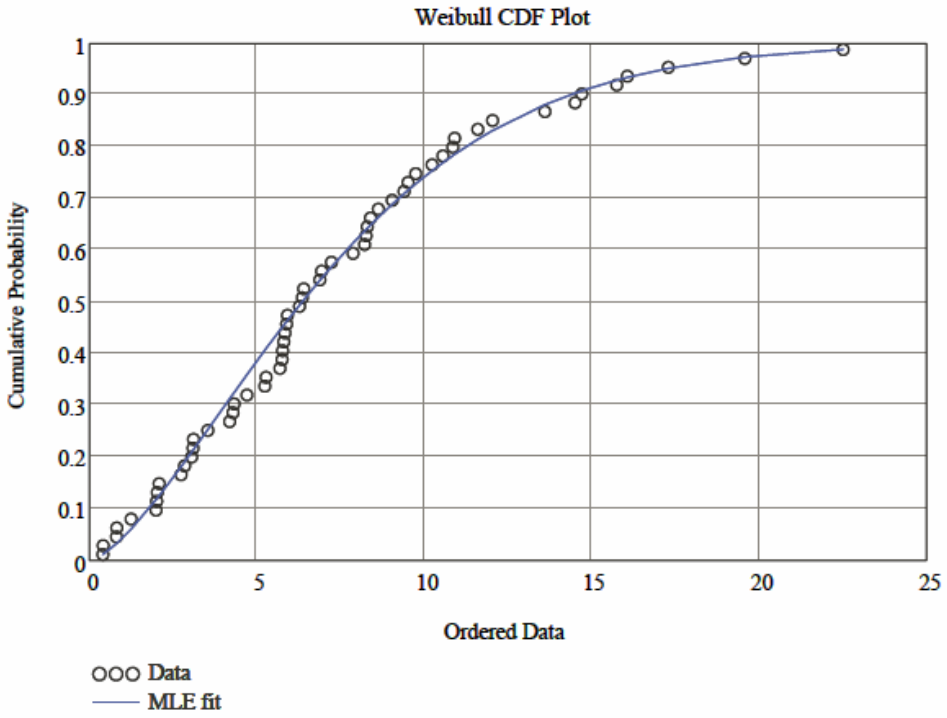
Weibull CDF Plot
Cumulative Probability
0
0.1
0.2
0.3
0.4
0.5
0.6
0.7
0.8
0.9
1
0
5
10
15
20
25
Ordered Data
Data
MLE fit

APPENDIX V
EVALUATION OF UNCERTAINTY DUE TO FITTING CREVICE SPECIMEN DATA TO A WEIBULL DISTRIBUTION

APPENDIX V – EVALUATION OF UNCERTAINTY DUE TO FITTING CREVICE SPECIMEN DATA TO A WEIBULL DISTRIBUTION

Weibull Uncertainty Specification

This spreadsheet determines the uncertainty specification for maximum likelyhood estimators for the Weibull distribultion, for a sample size of fifty-eight. The uncertainty is estimated by monte carlo simulation to create an empirical distribution of the joint distribution of the scale, b, and shape, c, parameters. This distribution is then partitioned into a low (lowest 5%), median (middle 90%), and high (highest 5%) characterization. This is performed by partitioning the major axis from a principal components analysis.

$TOL := 1 \times 10^{-8}$

$ORIGIN := 1$

$Seed(1129344008) = 1.000$

$b := 8.141$ Maximum likelihood estimate (MLE) estimate of scale parameter

$c := 1.476$ MLE of shape parameter (corrected for bias)

$n := 58$ Sample Size

$KK := 100000$ Number of monte carlo realizations is KK.

$kk := 1..KK$ Loop over all KK realizations

$i := 1..n$ Loop over sample size, n

$W_{i,kk} := b \cdot (-\ln(rnd(1)))^{\frac{1}{c}}$ KK sets of n Weibull samples

Solve the maximum likelihood equations for c and b.

$$Fc(c,kk) := \frac{\sum_{i=1}^{n} \left[\left(W_{i,kk}\right)^{c} \cdot \ln\left(W_{i,kk}\right) \right]}{\sum_{i=1}^{n} \left[\left(W_{i,kk}\right)^{c} \right]} - \frac{\sum_{i=1}^{n} \left(\ln\left(W_{i,kk}\right) \right)}{n} - \frac{1}{c}$$

$cg := 1$ Guess for c

$c\_mc_{kk} := root(Fc(cg,kk), cg)$ Find c-values

$$b\_mc_{kk} := \left[\frac{\sum_{i=1}^{n} \left(W_{i,kk}\right)^{c\_mc_{kk}}}{n} \right]^{\frac{1}{c\_mc_{kk}}}$$ Find b-values

Apply bias correction. For a sample size of 58, the unbiasing factor is 0.977 (ASTM C 1239-06A 2006 [DIRS 178286], Table 1).

$c\_mc_{kk} := (0.977) \cdot c\_mc_{kk}$

Estimate covariance matrix and calculate eigen vectors.

$$Cov := \begin{pmatrix} cvar(b\_mc, b\_mc) & cvar(b\_mc, c\_mc) \\ cvar(c\_mc, b\_mc) & cvar(c\_mc, c\_mc) \end{pmatrix} \cdot \frac{KK}{KK - 1}$$

$$FV := eigenvecs(Cov)$$

Center estimate vectors and then rotate along principle components.

$$C^{\langle 1 \rangle} := b\_mc - mean(b\_mc)$$

$$C^{\langle 2 \rangle} := c\_mc - mean(c\_mc)$$

$$E := C \cdot FV$$

Partition the estimate vectors into low, median, and high groups along major axis.

$$\alpha := 0.10$$

$$D1 := submatrix\left(csort(E, 1), 1, round\left(KK \cdot \frac{\alpha}{2}\right), 1, 2\right)$$ Lowest 5% of values stored to D1

$$D2 := submatrix\left[csort(E, 1), round\left(KK \cdot \frac{\alpha}{2}\right), round\left[KK \cdot \left(1 - \frac{\alpha}{2}\right)\right], 1, 2\right]$$ Middle 90% of values stored to D2

$$D3 := submatrix\left[csort(E, 1), round\left[KK \cdot \left(1 - \frac{\alpha}{2}\right)\right], KK, 1, 2\right]$$ Highest 5% of values stored to D3

Calculate means of the partitioned groups.

$$G1 := \begin{pmatrix} mean\left(D1^{\langle 1 \rangle}\right) & mean\left(D1^{\langle 2 \rangle}\right) \\ mean\left(D2^{\langle 1 \rangle}\right) & mean\left(D2^{\langle 2 \rangle}\right) \\ mean\left(D3^{\langle 1 \rangle}\right) & mean\left(D3^{\langle 2 \rangle}\right) \end{pmatrix}$$

Rotate mean values for partion groups back to original coordinates adding in means.

$$mn(i, j) := (j = 0) \cdot mean(b\_mc) + (j = 1) \cdot mean(c\_mc)$$

$$Ha := G1 \cdot FV^{T} + matrix(rows(G1), 2, mn)$$

Results of Analysis

$b = 8.141$ $mean(b\_mc) = 8.140$

$c = 1.476$ $mean(c\_mc) = 1.477$

Average of all Monte Carlo b-values very close to original b-value.
Average of all Monte Carlo c-values very close to original c-value.

$$Ha = \begin{pmatrix} 6.628 & 1.380 \\ 8.134 & 1.476 \\ 9.774 & 1.578 \end{pmatrix}$$

Column 1 contains b-value and column 2 c-values for the 3 levels of uncertainty

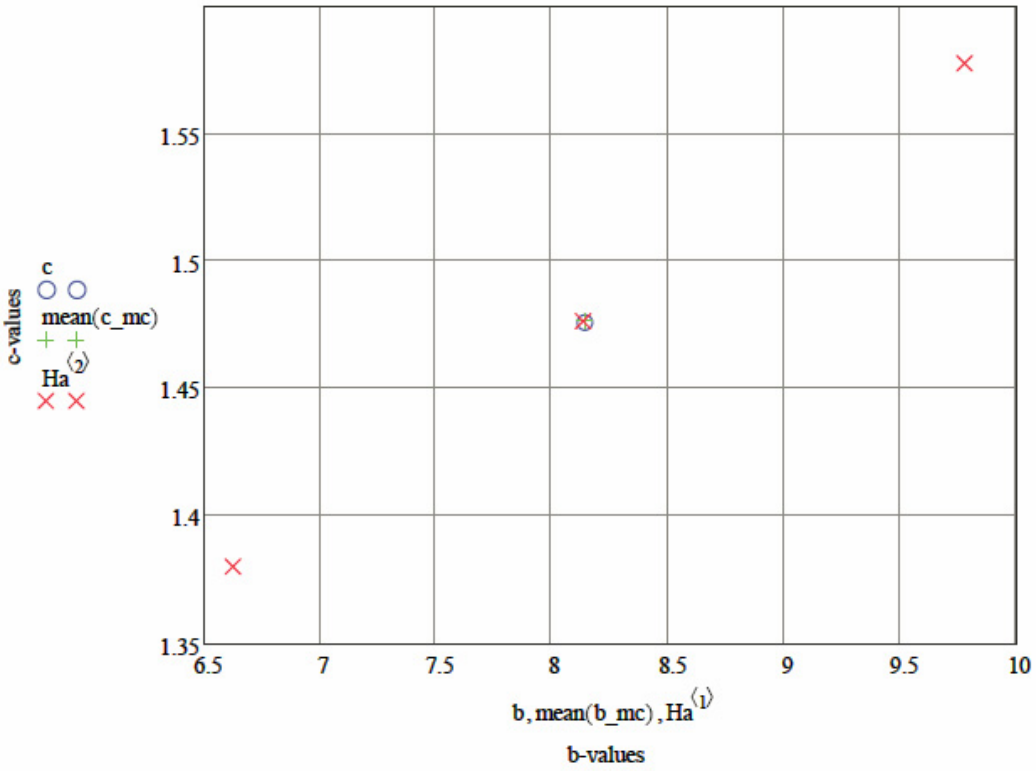
c
mean(c_mc)
Ha⟨2⟩
c-values
1.55
1.5
1.45
1.4
1.35
6.5
7
7.5
8
8.5
9
9.5
10
b, mean(b_mc), Ha⟨1⟩
b-values

INTENTIONALLY LEFT BLANK

APPENDIX VI
ALTERNATE CONCEPTUAL MODEL FOR GENERAL CORROSION

APPENDIX VI – ALTERNATE CONCEPTUAL MODEL FOR GENERAL CORROSION

data :=
...\GC_WLdata.txt

ORIGIN := 1

n := length(data) n = 53

i := 1 .. n

Evaluation of Weibull distribution fit
Maximum Likelihood Estimation of Weibull Parameters

MLEs given as equations to be solved iteratively (Algebraic rearrangement of equations in Evans et al. 1993 [DIRS 112115], Section 41.3). A bias correction factor on the shape estimator is not used.

TOL := 10^{-8} c := 1.3

$$f(c) := \frac{\sum_{i=1}^{n}\left[\left(data_i\right)^{c}\cdot\ln\left(data_i\right)\right]}{\sum_{i=1}^{n}\left[\left(data_i\right)^{c}\right]} - \frac{\sum_{i=1}^{n}\left(\ln\left(data_i\right)\right)}{n} - \frac{1}{c}$$

$$Find\_b(c) := \left[\frac{\sum_{i=1}^{n}\left[\left(data_i\right)^{c}\right]}{n}\right]^{\frac{1}{c}}$$

$c_{ML} := root(f(c), c)$ $c_{ML} = 1.318$

$b_{ML} := Find\_b(c_{ML})$ $b_{ML} = 3.447$

Use approximate Median Rank plotting positions (Stedinger et al. 1993 [DIRS 105941], Table 18.3.1).

$$pp_i := \frac{i - 0.3175}{n - 2\cdot(0.3175) + 1}$$

Weibull distribution functions (D'Agostino and Stephens 1986 [DIRS 160320], Section 4.11) for the Cumulative Distribution Function (CDF), pW, and inverse- CDF, qW.

$$pW(x,b,c) := 1 - \exp\left[-\left(\frac{x}{b}\right)^c\right]$$

$$qW(p,b,c) := b\cdot(-\ln(1-p))^{\frac{1}{c}}$$

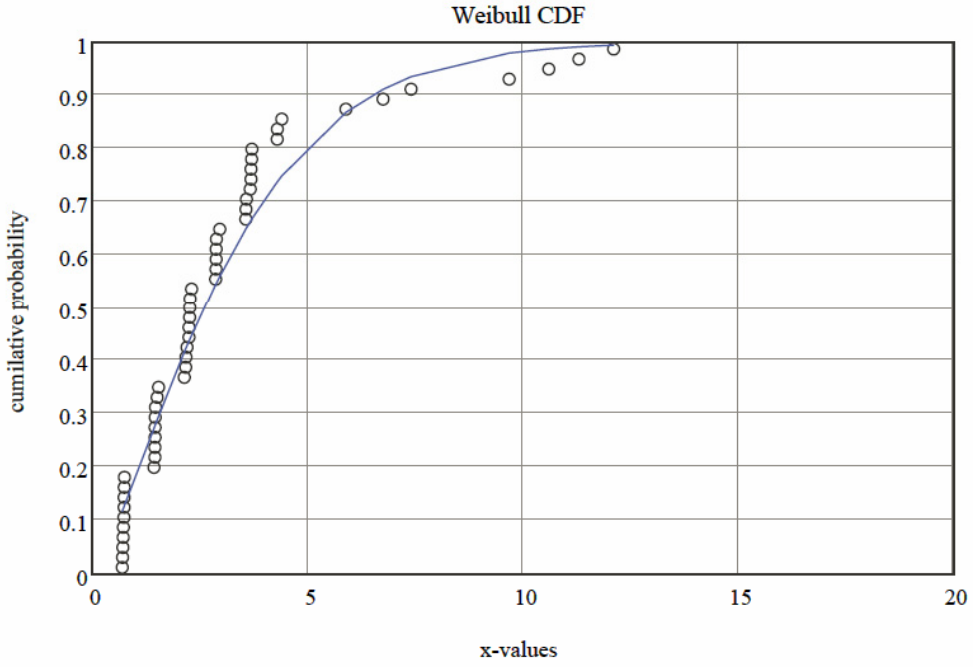

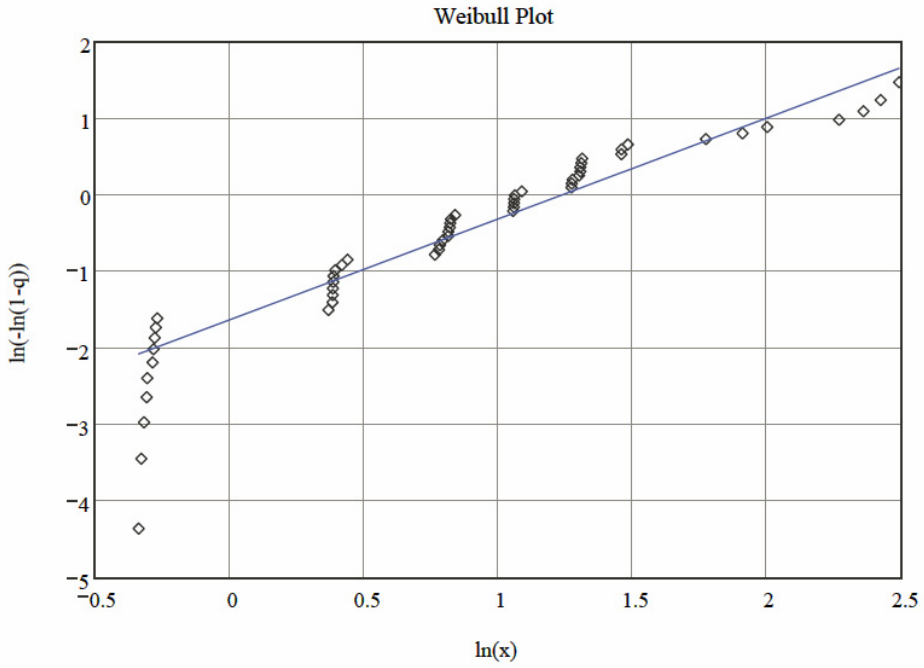
Weibull Plot
ln(-ln(1-q))
ln(x)
2
1
0
−1
−2
−3
−4
−5
−0.5
0
0.5
1
1.5
2
2.5

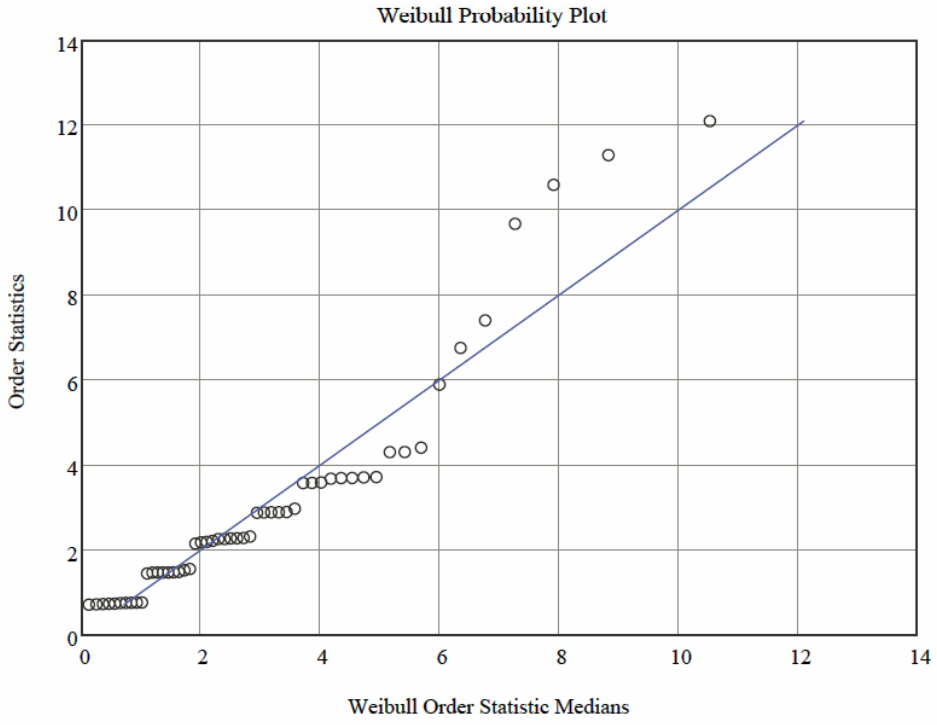
Weibull Probability Plot
Order Statistics
Weibull Order Statistic Medians
14
12
10
8
6
4
2
0
0
2
4
6
8
10
12
14

INTENTIONALLY LEFT BLANK

APPENDIX VII
CORROSION RATE OF ALLOY 22 AS A FUNCTION OF TEMPERATURE

APPENDIX VII – CORROSION RATE OF ALLOY 22 AS A FUNCTION OF TEMPERATURE

This appendix provides details of the development of the temperature-dependence portion of the Alloy 22 general corrosion model (Section 6.4.3.4). The polarization resistance data for solution set F (DTN: LL060900812251.180 [DIRS 178409], file: *175 PRFitv2.xls*) was used for this purpose. As discussed in Section 6.4.3.4 and Table 6-8, solution set F contains nine solutions composed of three chloride-ion concentration levels and three nitrate-to-chloride ion ratios at each chloride-ion concentration level. These data were fit to Equation VII-1 to estimate the apparent activation energy, E_a, which characterizes the temperature dependence of Alloy 22 general corrosion:

$$\ln(R_T) = \ln(R_o) + E_a\left[\frac{1}{R \cdot T_0} - \frac{1}{R \cdot T}\right] \qquad \text{(Eq. VII-1)}$$

where T_0 = 333.15 K (60°C) and R is the universal gas constant (8.314 J/mol K) (Lide 1991 [DIRS 131202], inside rear cover).

In a plot of logarithmic reaction rates versus adjusted inverse temperature, x (see below), the slope is thus expected to be E_a. The transformed variables y and x were used in the model fitting according to Equation VII-2, such that:

$$\begin{aligned} y &= \ln(R_T) = \beta_0 + \beta_1 x \\ x &= \left[\frac{1}{R \cdot T_0} - \frac{1}{R \cdot T}\right] \\ \beta_0 &= \ln(R_o), \quad \beta_1 = E_a \end{aligned} \qquad \text{(Eq. VII-2)}$$

where x is the adjusted inverse temperature. The fitting is accomplished in S-PLUS 2000 Professional Release 2, using commands entered at the command line. A listing of the commands entered to accomplish the fitting is provided in file: *dataF-fit.txt* in output DTN: MO0612WPOUTERB.000. Also included in output DTN: MO0612WPOUTERB.000 is file: *Output_dataF-fit.txt*, which includes the commands entered and the S-PLUS responses (in essence an echo of the input and output session in S-PLUS). A listing of the first part of *Output_dataF-fit.txt* is provided below:

```
> # obtain data
> dataF.df <- read.table(file = "dataF.txt", header=TRUE, sep="\t", na.strings="NA")
>
> # create Temperature and rate linear variables
> X <- (1000/8.314)*(1/333.15 - 1/(dataF.df$T.C + 273.15))
> Y <- log((0.003272)*(23.28/8.69)*dataF.df$i.cor)
> dataF.df <- data.frame(Y, X, dataF.df)
>
> # fit OLS model
> mF.OLS <- lm(formula = Y ~ X, data = dataF.df, na.action = na.exclude)
>
> # create graph
> trellis.device(pdf.graph, file="GSD2.pdf", color=T, background.color=64)

> xyplot(Y ~ X | Soln, data = dataF.df, main="Lot-F Solutions", aspect = 1,
+  panel = function(x,y) {
```

```
+    panel.grid(h=-1,v=-1)
+    panel.xyplot(x,y, col = 1)
+    panel.loess( x,y,     lty = 4, col = 8, span=1)
+    panel.lmline(x,y,     lty = 3, col = 6)
+    panel.abline( mF.OLS, lty = 1, col = 1)
+  },
+  xlab = "x, adjusted inverse temperature [mol/kJ]",
+  ylab = "y, ln(rate) ln[m/yr]",
+  layout = c(3, 3),
+  key = list(text  = list(c("LOESS-fit", "OLS-fit","population OLS"), cex=rep(.85,3)),
+    lines = list(lty= c(4,3,1), col=c(8,6,1)),
+    border=1, transparent=F , space="top")
+ )
> dev.off()
 null device
           1
>
```

The statements following the S-PLUS command line prompt, >, are user entries entered at the command line during a S-PLUS session. The "+" character indicates a continuation of an S-PLUS user entry. The lines not preceded by the prompt of "+" character are S-Plus outputs.

The expression for x (`X <- (1000/8.314)*(1/333.15 - 1/(dataF.df$T.C + 273.15))`) makes use of the value of R, the universal gas constant (8.314 J/mol K) (Lide 1991 [DIRS 131202], inside rear cover), and converts the temperature to Kelvin from Celsius.

The expression for y (`Y <- log((0.003272)*(23.28/8.69)*dataF.df$i.cor)`) is basically a restatement of Equation I-2 in logarithmic form with current density given in nA/cm^2 and corrosion rates in μm/yr (i.e., the conversion factor K_1 in Equation I-2 is six orders of magnitude smaller here, because different units of current density and corrosion rate are being used).

At this point, S-PLUS produces the graph shown in Figure 6-24 (output DTN: MO0612WPOUTERB.000, file: *GSD2.pdf*). The ordinary-least-squares (OLS) model corresponding to the simple linear regression of the estimated logarithmic corrosion rates (y) on the adjusted inverse temperature (x) is given as Equation VII-3:

$$y_{ij} = (\beta_0) + (\beta_1) x_{ij} + \varepsilon_{ij}, \quad \varepsilon_{ij} \sim N(0, \sigma^2) \qquad \text{(Eq. VII-3)}$$

Where β_0 and β_1 are, respectively, the fixed effects for the intercept and the slope, and the ε_{ij} are the independent and identically distributed random error effects.

To account for the heterogeneity in the intercepts and slopes, a linear mixed-effects (LME) model was fit (Venables and Ripley 2001 [DIRS 159088], Section 6.11). The LME model corresponding to the simple linear regression of the estimated logarithmic corrosion rates (y) for the jth sample within the ith solution group on the adjusted inverse temperature (x) is given as Equation VII-4:

$$y_{ij} = (\beta_0 + b_{0i}) + (\beta_1 + b_{1i}) x_{ij} + \varepsilon_{ij},$$
$$b_i = \begin{bmatrix} b_{0i} \\ b_{1i} \end{bmatrix} \sim N\left(0, \Sigma = \begin{bmatrix} \tau_0^2 & \tau_{01} \\ \tau_{01} & \tau_1^2 \end{bmatrix}\right), \quad \varepsilon_{ij} \sim N(0, \sigma^2) \qquad \text{(Eq. VII-4)}$$

where β_0 and β_1 are, respectively, the fixed effects for the intercept and the slope; the b_i is a random-effects vector, assumed to be independent for different solutions; and the ε_{ij} is the independent and identically distributed within-group random error effect, considered independent of the other random effects. From Equation VII-4, it can be seen that the value of β_1 will be the mean apparent activation energy and the value of τ_1 will be the standard deviation of the apparent activation energy.

The LME model mentioned above is fit in S-PLUS using the built-in LME function. The statements that accomplish this fit are reproduced from the second part of *Output_dataF-fit.txt* (Output DTN: MO0612WPOUTERB.000) and are provided below:

```
> # fit mixed-effects model
> model2 <- lme(Y~1+X, random=~1+X|Soln, data=dataF.df, method="ML", na.action = na.exclude)
> summary(model2)
Linear mixed-effects model fit by maximum likelihood
 Data: dataF.df
       AIC      BIC    logLik
  981.1853 1004.826 -484.5926

Random effects:
 Formula:  ~ 1 + X | Soln
 Structure: General positive-definite
                StdDev   Corr
(Intercept)  0.2181264 (Inter
          X 11.7504430 -0.011
   Residual  0.8384550

Fixed effects: Y ~ 1 + X
               Value Std.Error  DF   t-value p-value
(Intercept)  -2.68760  0.105784 370 -25.40645  <.0001
          X  40.77755  4.777778 370   8.53483  <.0001
 Correlation:
  (Intr)
X -0.334

Standardized Within-Group Residuals:
      Min         Q1        Med        Q3      Max
 -3.37215 -0.5257155 0.09103175 0.6721034 2.964984

Number of Observations: 380
Number of Groups: 9
>
> # create graph of model2 results
> cbind(ranef(model2)[1] + fixef(model2)[1],ranef(model2)[2] + fixef(model2)[2])
   (Intercept)        X
F1   -2.525236 58.05575
F2   -2.563318 45.22027
F3   -2.715840 47.57846
F4   -2.610021 50.62530
F5   -2.659588 35.85623
F6   -2.751231 28.45819
F7   -2.503667 26.00269
F8   -2.823777 43.23865
F9   -3.035705 31.96239
> ranef.df <- data.frame(cbind(ranef(model2)[1] + fixef(model2)[1],
+    ranef(model2)[2] + fixef(model2)[2]))
> ranef.df <- data.frame(row.names(ranef.df), ranef.df)
> names(ranef.df) <- c('Soln','int','slope')
> dataF2.df <- merge(dataF.df, ranef.df)
>
> trellis.device(pdf.graph, file="GSD3.pdf", color=T, background.color=64)


> xyplot(Y ~ X | Soln, data = dataF2.df, main="Lot-F Solutions", aspect = 1,
+  panel = function(x,y, subscripts) {
+    panel.grid(h=-1,v=-1)
```

```
+    panel.xyplot(x,y, col = 1)
+    panel.abline( c(fixef(model2)[1], fixef(model2)[2]), lty=4, col = 8)
+    panel.abline( c(dataF2.df$int[subscripts][1],dataF2.df$slope[subscripts][2]),lty=3,col=6)
+  },
+  subscripts=T,
+  xlab = "x, adjusted inverse temperature [mol/kJ]",
+  ylab = "y, ln(rate) ln[m/yr]",
+  layout = c(3, 3),
+  key = list(text  = list(c("model2-population","model2-Random"), cex=rep(.85,2)),
+    lines = list(lty= c(4,3), col=c(8,6)),
+    border=1, transparent=F , space="top")
+ )
> dev.off()
 null device
           1
>
```

At this point S-PLUS produces the graph shown in Figure 6-25. It should be noted that the individual slopes for each solution in solution set F are included in this listing and are reproduced in Table 6-10.

Lastly, the apparent activation energies were calculated by OLS for solutions contained in DTN: LL060900812251.180 [DIRS 178409], files: *176PRFit.xls*, *179PRFit.xls*, and *187PRFit.xls,* which were not used to determine temperature-dependence of Alloy 22 general corrosion. The calculations were accomplished using the commands contained in *data2-fit.txt* (Output DTN: MO0612WPOUTERB.000). Also included in that output DTN is the file, *Output_data2-fit.txt*, which includes the commands entered and the S-PLUS responses. A listing of *Output_data2-fit.txt* is provided below:

```
> # obtain data
> dataG.df <- read.table(file = "dataG.txt", header=TRUE, sep="\t", na.strings="NA")
> dataK.df <- read.table(file = "dataK.txt", header=TRUE, sep="\t", na.strings="NA")
> dataL.df <- read.table(file = "dataL.txt", header=TRUE, sep="\t", na.strings="NA")
>
> dataGKL.df <- rbind(dataG.df, dataK.df, dataL.df)
>
> # create Temperature and rate linear variables
> X <- (1000/8.314)*(1/333.15 - 1/(dataGKL.df$T.C + 273.15))
> Y <- log((0.003272)*(23.28/8.69)*dataGKL.df$i.cor)
> dataGKL.df <- data.frame(Y, X, dataGKL.df)
>
> tapply(dataGKL.df$Y, dataGKL.df$Soln, length)     # counts in each group
 G1 G2 G3 K1  L1 L2
 68 51 53 23 149 76
>
> # create graph
> trellis.device(pdf.graph, file="GSD4.pdf", color=T, background.color=64)

> xyplot(Y ~ X | Soln, data = dataGKL.df, main="Other Solutions", aspect = 1,
+    panel = function(x,y) {
+    panel.grid(h=-1,v=-1)
+    panel.xyplot(x,y, col = 1)
+    panel.loess( x,y,     lty = 4, col = 8, span=1)
+    panel.lmline(x,y,     lty = 3, col = 6)
+  },
+  xlab = "x, adjusted inverse temperature [mol/kJ]",
+  ylab = "y, ln(rate) ln[m/yr]",
+  layout = c(3,2),
+  key = list(text  = list(c("LOESS-fit", "OLS-fit"), cex=rep(.85,2)),
+     lines = list(lty= c(4,3), col=c(8,6)),
+     border=1, transparent=F , space="top")
+ )
> dev.off()
 null device
           1
```

```
> # fit linear model in each group to graph intervals
> mGKL.lis <- lmList(Y ~ X | Soln, data = dataGKL.df, na.action = na.include)
> coef(mGKL.lis)
   (Intercept)          X
G1  -1.1834650   7.692254
G2  -1.9741995  51.028597
G3  -2.4931316  45.842090
K1  -3.8302796  35.603032
L1  -1.3557871  28.072785
L2   0.2986552 -15.132388
>
>
```

Individual slopes for each solution are included in this listing and are reproduced in Table 6-9. These commands also produce a graph showing the general corrosion rate data from each solution along with a smooth line estimate (LOESS-fit) and an OLS fit within each group (Figure VII-1). This graph can be compared to Figure 6-24 for solution set F.

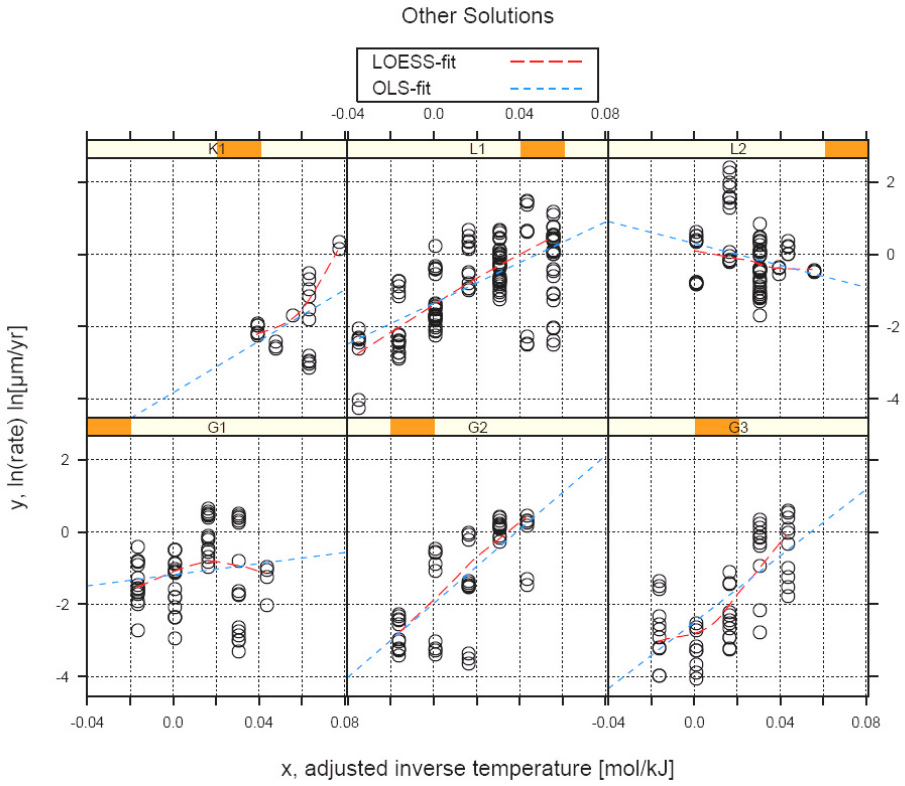

Source: DTN: LL060900812251.180 [DIRS 178409], files: *176PRFit.xls, 179PRFit.xls, and 187PRFit.xls.*

Output DTN: *MO0612WPOUTERB.000, file: GSD4.pdf.*

Figure VII-1. Corrosion Rates in Each Solution with a Smooth-Line Estimate (LOESS-fit) and an Ordinary-Least-Squares Fit Within Each Group

The general corrosion temperature-dependence slope values are asserted to follow a normal (Gaussian) distribution. This is validated qualitatively by observing the slope values graphically on a quantile-normal plot where they appear linear. A quantitative evaluation is applied in a Shapiro-Wilk goodness-of-fit test. The p-value calculated is consistent with the normal distribution as shown below.

Normal Distribution Hypothesis Test for Slope Estimates

The slope values are asserted to follow a Normal (Gaussian) distribution. This is validated qualitatively by observing the slope values graphically on a Quantile-Normal plot where they appear linear. A quantitative evaluation is applied in a Shapiro-Wilk Goodness-of-Fit test. The p-value calculated is consistent with the Normal distribution.

$ORIGIN := 1$

Number of data points: $N_d := 9$

estimated slope values from nine solutions:

$b := (58.05575 \quad 45.22027 \quad 47.57846 \quad 50.6253 \quad 35.85623 \quad 28.45819 \quad 26.00269 \quad 43.23865 \quad 31.96239)^T$

Null Hypothesis: Slopes are from a Normal distribution

$ii := 1 .. N_d$

$p_{ii} := \dfrac{ii - \frac{3}{8}}{N_d + 1 - 2 \cdot \frac{3}{8}}$ Blom plotting positions (Stedinger et al. 1993 [DIRS 105941], Table 18.3.1)

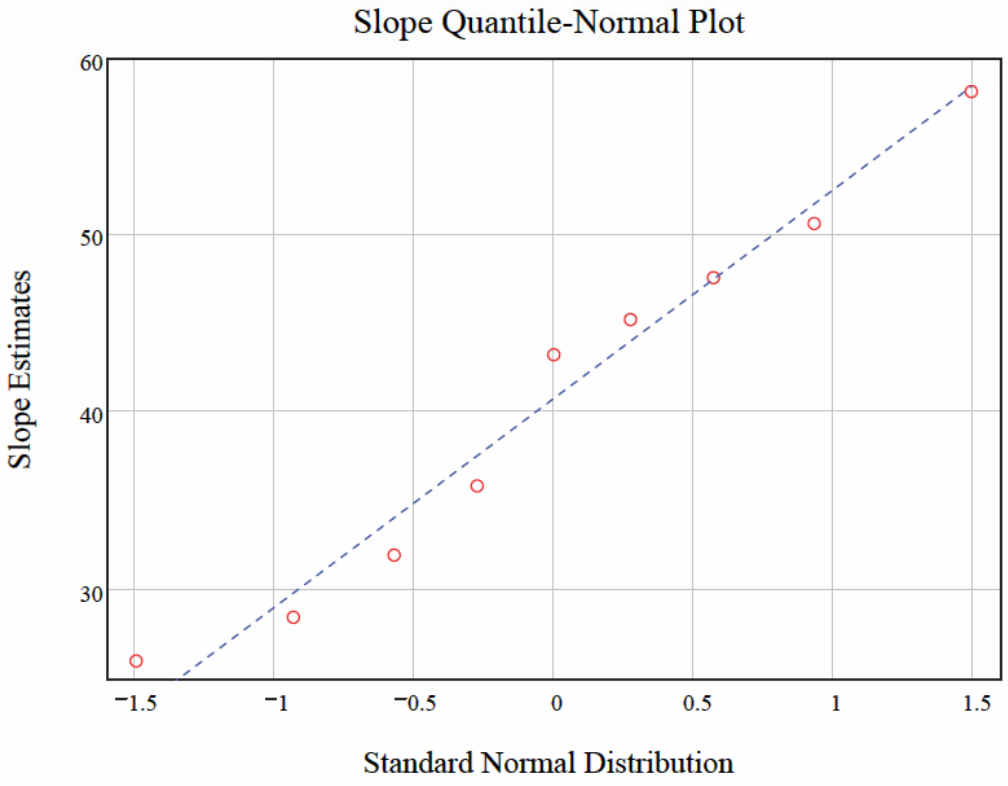

Shapiro-Wilk Goodness of Fit Statistic for Normality

coefficients for a (D'Agostino and Stephens 1986 [DIRS 160320], Table 5.4)

$$a := (0.5888 \quad 0.3244 \quad 0.1976 \quad 0.0947)^T$$

$$b := \text{sort}(b)$$

$$W_{sw} := \frac{\left[\sum_{i=1}^{\text{length}(a)} \left[a_i \cdot \left(b_{N_d - i + 1} - b_i\right)\right]\right]^2}{\sum_{i=1}^{N_d} \left[\left(b_i - \text{mean}(b)\right)^2\right]}$$

$$W_{sw} = 0.96$$

p-value by table interpolation (D'Agostino and Stephens 1986 [DIRS 160320], Table 5.5)

$$0.5 + \left(\frac{W_{sw} - 0.935}{0.972 - 0.935}\right) \cdot (0.9 - 0.5) = 0.8$$

Accept the null hypothesis that the slopes are from the specified normal distribution.
The p-value is the probability that the test statistic will take a value at least as extreme as that actually observed (Pr[W_{sw} < Observed]). Small p-values (e.g., less than 0.05) suggest evidence against the null hypothesis, indicating that the data set is unlikely to have been drawn from the specified distribution. Large p-values indicate the data set is consistent with the null hypothesis.

In addition, the temperature-dependence of Alloy 22 general corrosion rates of weight-loss samples immersed in the SCW solution for five-years was investigated as discussed in Section 6.4.3.4). For coupons immersed in SCW at 60°C (note that one coupon was at the water-line and is considered to be immersed for this analysis), seven Alloy 22 general corrosion rates were calculated (output DTN: MO0612WPOUTERB.000, file: *Alloy22_5yr_WLAnalysis.xls*). Let this group of values be called b60. For coupons immersed in SCW at 90°C six Alloy 22 general corrosion rates were calculated (output DTN: MO0612WPOUTERB.000, file: *Alloy22_5yr_WLAnalysis.xls*). Let this group of values be called b90. The temperature-dependence of these general corrosion rates was calculated (to determine C_1) by a regression fit of these data to Equation 6-25 and uncertainty in this estimator was determined utilizing the bootstrap technique (Efron and Gong 1983 [DIRS 103967]).

One-hundred thousand bootstrap estimates of the temperature-dependence of Alloy 22 general corrosion rates were generated. The first step in the analysis was to sample 100,000 sets of seven values (general corrosion rates) from b60 and 100,000 sets of six values from b90. b60 and b90 were treated as discrete populations (i.e., no interpolation between values occurred) from which the sampling was done with replacement (i.e., the same corrosion rate value could be sampled more than once). The first bootstrap estimate of the Alloy 22 general corrosion temperature-dependence was generated by fitting Equation 6-25 by linear regression to the first set of seven values sampled from b60 with the first set of six values sampled from b90. The second bootstrap estimate of the Alloy 22 general corrosion temperature-dependence was generated by fitting Equation 6-25 by linear regression to the second set of seven values sampled from b60 with the second set of six values sampled from b90, and so on until all 100,000

estimates of the Alloy 22 general corrosion temperature-dependence were obtained. The 100,000 bootstrap estimates of C_1 define an empirical distribution for the uncertainty in this parameter. The details of this analysis are presented below.

Bootstrap of Temperature Dependent Mean Rates to Determine an Activation Energy Distribution for Uncertainty

Set origin for indexing $ORIGIN := 1$

Unit conversion $kJ := 1000J$

Gas Constant from Lide 1991 ([DIRS 131202], inside rear cover)

$$R := 8.314\frac{J}{mol \cdot K}$$

Data from Alloy22_5yr_WLAnalysis.xls

SCW Aqueous Phase 60°C, seven samples

$$r60 := \begin{pmatrix} 2.22 \\ 1.47 \\ 2.90 \\ 2.29 \\ 3.72 \\ 6.76 \\ 2.19 \end{pmatrix} \text{nm/yr} \qquad \begin{pmatrix} \text{"DWA 092"} \\ \text{"DWA 093"} \\ \text{"DWA 094"} \\ \text{"DWB 092"} \\ \text{"DWB 093"} \\ \text{"DWB 094"} \\ \text{"DWA 104"} \end{pmatrix}$$

SCW Aqueous Phase 90°C, six samples

$$r90 := \begin{pmatrix} 9.68 \\ 7.41 \\ 5.90 \\ 10.60 \\ 11.30 \\ 12.11 \end{pmatrix} \text{nm/yr} \qquad \begin{pmatrix} \text{"DWA 132"} \\ \text{"DWA 133"} \\ \text{"DWA 134"} \\ \text{"DWB 132"} \\ \text{"DWB 133"} \\ \text{"DWB 134"} \end{pmatrix}$$

$$X60 := \frac{-1}{(273.15 + 60.0)K} \qquad X90 := \frac{-1}{(273.15 + 90.0)K}$$

Inverse temperature variables

$$vx := stack\left[\begin{pmatrix} X60 \\ X60 \\ X60 \\ X60 \\ X60 \\ X60 \\ X60 \end{pmatrix}, \begin{pmatrix} X90 \\ X90 \\ X90 \\ X90 \\ X90 \\ X90 \end{pmatrix}\right]$$

Assemble into vectors

$$vy := stack(\ln(r60), \ln(r90))$$

Activation Energy from regression estimation.

$$\text{slope}(vx, vy) = 4876\,\text{K} \qquad \text{slope}(vx, vy)\cdot R = 40.54\,\frac{\text{kJ}}{\text{mol}}$$

Activation Energy based on regression of bootstrap samples

Number of bootstrap estimates

$$B := 10^5$$

$$b := 1..B$$

$$b60_b := \begin{pmatrix} r60_{\text{floor}(\text{rnd}(7)+1)} \\ r60_{\text{floor}(\text{rnd}(7)+1)} \\ r60_{\text{floor}(\text{rnd}(7)+1)} \\ r60_{\text{floor}(\text{rnd}(7)+1)} \\ r60_{\text{floor}(\text{rnd}(7)+1)} \\ r60_{\text{floor}(\text{rnd}(7)+1)} \\ r60_{\text{floor}(\text{rnd}(7)+1)} \end{pmatrix} \qquad b90_b := \begin{pmatrix} r90_{\text{floor}(\text{rnd}(6)+1)} \\ r90_{\text{floor}(\text{rnd}(6)+1)} \\ r90_{\text{floor}(\text{rnd}(6)+1)} \\ r90_{\text{floor}(\text{rnd}(6)+1)} \\ r90_{\text{floor}(\text{rnd}(6)+1)} \\ r90_{\text{floor}(\text{rnd}(6)+1)} \end{pmatrix}$$

$$by_b := \text{stack}\left(\ln\left(b60_b\right), \ln\left(b90_b\right)\right)$$

Bootstrap estimates of Activation Energy

$$C1_b := \text{slope}\left(vx, by_b\right)$$

Estimated cumulative probability values for order statistics

$$cp_b := \frac{b-1}{B-1}$$

$$C1s := \text{sort}(C1)$$

$$CI95 := \text{augment}(\text{linterp}(cp, C1s, 0.05), \text{linterp}(cp, C1s, 0.95))$$ 95% Confidence Interval

Distribution summary values

$$\text{mean}(C1) = 4872\ \text{K} \qquad \text{mean}(C1)\cdot R = 40.51\,\frac{\text{kJ}}{\text{mol}}$$

$$\text{median}(C1) = 4901\ \text{K} \qquad \text{median}(C1)\cdot R = 40.75\,\frac{\text{kJ}}{\text{mol}}$$

$$CI95 = (3499 \quad 6147)\ \text{K} \qquad CI95\cdot R = (29.09 \quad 51.10)\,\frac{\text{kJ}}{\text{mol}}$$ 95% Confidence Interval

$$\min(C1) = 682\ \text{K} \qquad \min(C1)\cdot R = 5.67\,\frac{\text{kJ}}{\text{mol}}$$

$$\max(C1) = 7811\ \text{K} \qquad \max(C1)\cdot R = 64.94\,\frac{\text{kJ}}{\text{mol}}$$

201 point CDF Table creation

$nT := 201 \quad i := 1..nT \quad cpr_i := \frac{i-1}{nT-1}$

$C1\_v := linterp(cp, C1s, cpr)$

$CDF\_Table := stack\left[(nT \;\; 2), augment\left(\frac{C1\_v}{K}, cpr\right)\right]$

$WRITEPRN("WDC1GC.cdf") := CDF\_Table$

Graphic comparision of bootstrap and apparent activation energy distribution from polarization resistance data (normal distribution with a mean of 4905 K (40.78 kJ/mol) and standard deviation of 1413 K (11.75 kJ/mol))

$k := 2..B-1$

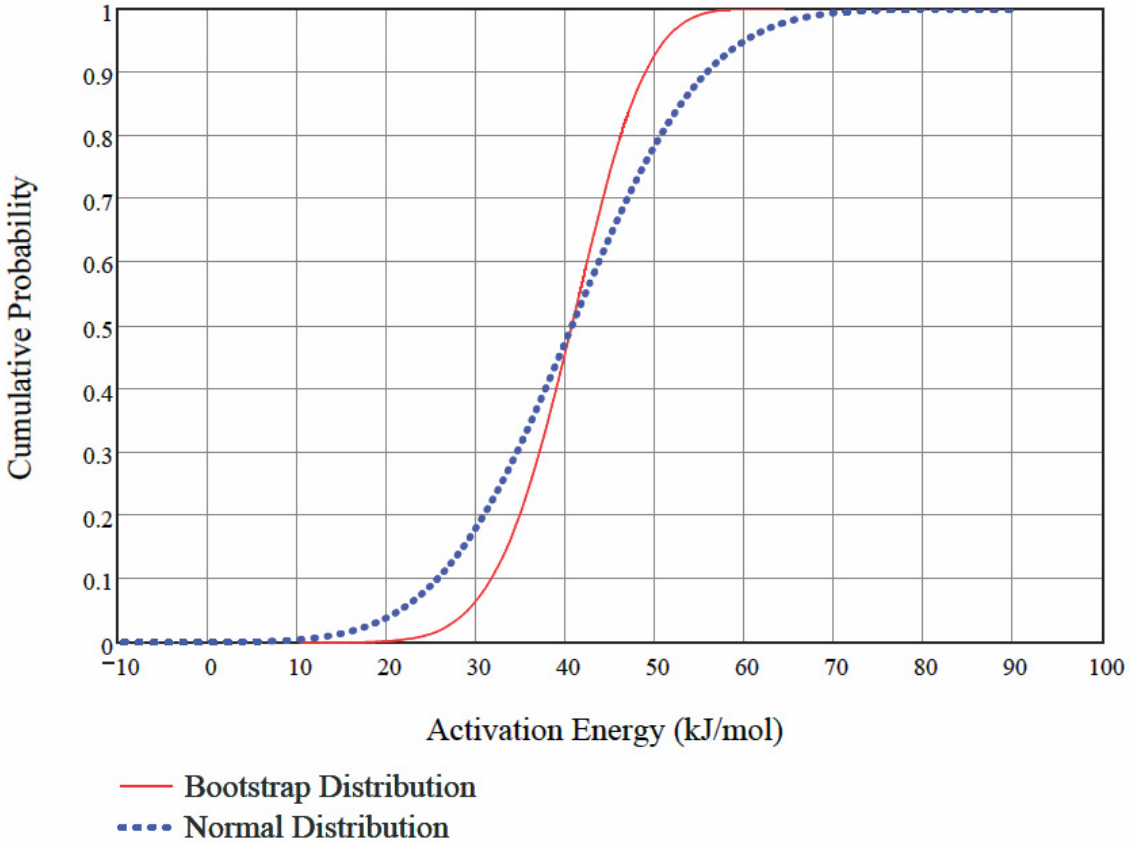

Calculate -3 and +2 standard deviation values for apparent activation energy normal distribution with a mean of 4905 K (40.78 kJ/mol) and standard deviation of 1413 K (11.75 kJ/mol)

$qnorm(cnorm(-3), 4905, 1413) \cdot K = 666.00\ K$ $\qquad$ $qnorm(cnorm(-3), 4905, 1413) \cdot R \cdot K = 5.54 \frac{kJ}{mol}$

$qnorm(cnorm(2), 4905, 1413) \cdot K = 7731.00\ K$ $\qquad$ $qnorm(cnorm(2), 4905, 1413) \cdot R \cdot K = 64.28 \frac{kJ}{mol}$

APPENDIX VIII
LONG-TERM STEADY-STATE CORROSION POTENTIAL MEASUREMENTS OF ALLOY 22 SAMPLES USED IN THE CORROSION POTENTIAL MODEL AND ANALYSIS

APPENDIX VIII – LONG-TERM STEADY-STATE CORROSION POTENTIAL MEASUREMENTS OF ALLOY 22 SAMPLES USED IN THE CORROSION POTENTIAL MODEL AND ANALYSIS

Cell	Specimen ID	Specimen Type [a]	Material Condition [a]	Solution [a]	T (°C)	Calculated Pitzer pH [b]	[Cl] (*m*) [b]	[NO_3] (*m*) [b]	NO_3/Cl [b]	Ecorr mV_{SSC}	Immersion Days
33	KE0260	PCA	ASW	5 *m* $CaCl_2$ + 5 *m* $Ca(NO_3)_2$	120	5.17	10.00	10.00	1.00	482	723
33	KE0261	PCA	ASW	5 *m* $CaCl_2$ + 5 *m* $Ca(NO_3)_2$	120	5.17	10.00	10.00	1.00	483	723
33	KE0262	PCA	ASW	5 *m* $CaCl_2$ + 5 *m* $Ca(NO_3)_2$	120	5.17	10.00	10.00	1.00	483	723
33	KE0263	PCA	ASW	5 *m* $CaCl_2$ + 5 *m* $Ca(NO_3)_2$	120	5.17	10.00	10.00	1.00	483	723
33	JE2074	Rod	ASW	5 *m* $CaCl_2$ + 5 *m* $Ca(NO_3)_2$	120	5.17	10.00	10.00	1.00	447	723
33	JE2075	Rod	ASW	5 *m* $CaCl_2$ + 5 *m* $Ca(NO_3)_2$	120	5.17	10.00	10.00	1.00	453	723
32	KE0256	PCA	ASW	5 *m* $CaCl_2$ + 5 *m* $Ca(NO_3)_2$	100	5.28	10.00	10.00	1.00	263	729
32	KE0257	PCA	ASW	5 *m* $CaCl_2$ + 5 *m* $Ca(NO_3)_2$	100	5.28	10.00	10.00	1.00	244	729
32	KE0258	PCA	ASW	5 *m* $CaCl_2$ + 5 *m* $Ca(NO_3)_2$	100	5.28	10.00	10.00	1.00	234	729
32	KE0259	PCA	ASW	5 *m* $CaCl_2$ + 5 *m* $Ca(NO_3)_2$	100	5.28	10.00	10.00	1.00	215	729
32	JE2072	Rod	ASW	5 *m* $CaCl_2$ + 5 *m* $Ca(NO_3)_2$	100	5.28	10.00	10.00	1.00	173	729
32	JE2073	Rod	ASW	5 *m* $CaCl_2$ + 5 *m* $Ca(NO_3)_2$	100	5.28	10.00	10.00	1.00	190	729
31	KE0252	PCA	ASW	3.5 *m* NaCl + 0.175 *m* KNO_3 + 0.7 *m* $MgSO_4$	80	5.56	3.50	0.175	0.05	31	735
31	KE0255	PCA	ASW	3.5 *m* NaCl + 0.175 *m* KNO_3 + 0.7 *m* $MgSO_4$	80	5.56	3.50	0.175	0.05	27	735
31	JE2070	Rod	ASW	3.5 *m* NaCl + 0.175 *m* KNO_3 + 0.7 *m* $MgSO_4$	80	5.56	3.50	0.175	0.05	38	735
31	JE2071	Rod	ASW	3.5 *m* NaCl + 0.175 *m* KNO_3 + 0.7 *m* $MgSO_4$	80	5.56	3.50	0.175	0.05	2	735
30	KE0251	PCA	ASW	1 *M* NaCl + 0.15 *M* KNO_3	90	5.76	1.00	0.15	0.15	−114	741
30	KE0250	PCA	ASW	1 *M* NaCl + 0.15 *M* KNO_3	90	5.76	1.00	0.15	0.15	−119	741
30	KE0249	PCA	ASW	1 *M* NaCl + 0.15 *M* KNO_3	90	5.76	1.00	0.15	0.15	−63	741
30	KE0248	PCA	ASW	1 *M* NaCl + 0.15 *M* KNO_3	90	5.76	1.00	0.15	0.15	−120	741
30	JE2068	Rod	ASW	1 *M* NaCl + 0.15 *M* KNO_3	90	5.76	1.00	0.15	0.15	−40	741

Cell	Specimen ID	Specimen Type [a]	Material Condition [a]	Solution [a]	T (°C)	Calculated Pitzer pH [b]	[Cl] (*m*) [b]	[NO_3] (*m*) [b]	NO_3/Cl [b]	Ecorr mV_{SSC}	Immersion Days
30	JE2069	Rod	ASW	1 *M* NaCl + 0.15 *M* KNO_3	90	5.76	1.00	0.15	0.15	−35	741
29	KE0149	PCA	ASW	1 *M* NaCl + 0.15 *M* KNO_3	75	5.72	1.00	0.15	0.15	−82	749
29	KE0150	PCA	ASW	1 *M* NaCl + 0.15 *M* KNO_3	75	5.72	1.00	0.15	0.15	−114	749
29	KE0246	PCA	ASW	1 *M* NaCl + 0.15 *M* KNO_3	75	5.72	1.00	0.15	0.15	−119	749
29	KE0247	PCA	ASW	1 *M* NaCl + 0.15 *M* KNO_3	75	5.72	1.00	0.15	0.15	−112	749
29	JE2066	Rod	ASW	1 *M* NaCl + 0.15 *M* KNO_3	75	5.72	1.00	0.15	0.15	−110	749
29	JE2067	Rod	ASW	1 *M* NaCl + 0.15 *M* KNO_3	75	5.72	1.00	0.15	0.15	−108	749
28	JE2064	Rod	ASW	5 *M* $CaCl_2$	90	4.00	11.99	0.00	0.00	−30	650
28	JE2065	Rod	ASW	5 *M* $CaCl_2$	90	4.00	11.99	0.00	0.00	−4	650
25	KE0133	PCA	ASW	3.5 *m* NaCl + 0.175 *m* KNO_3	100	5.61	3.50	0.175	0.18	−131	252
25	KE0134	PCA	ASW	3.5 *m* NaCl + 0.175 *m* KNO_3	100	5.61	3.50	0.175	0.18	−154	252
25	KE0135	PCA	ASW	3.5 *m* NaCl + 0.175 *m* KNO_3	100	5.61	3.50	0.175	0.18	−137	252
25	KE0136	PCA	ASW	3.5 *m* NaCl + 0.175 *m* KNO_3	100	5.61	3.50	0.175	0.18	−123	252
24	KE0129	PCA	ASW	3.5 *m* NaCl + 0.175 *m* KNO_3	100	5.60	3.50	0.525	0.15	−152	256
24	KE0130	PCA	ASW	3.5 *m* NaCl + 0.175 *m* KNO_3	100	5.60	3.50	0.525	0.15	−153	256
24	KE0131	PCA	ASW	3.5 *m* NaCl + 0.175 *m* KNO_3	100	5.60	3.50	0.525	0.15	−155	256
24	KE0132	PCA	ASW	3.5 *m* NaCl + 0.175 *m* KNO_3	100	5.60	3.50	0.525	0.15	−154	256
23	KE0125	PCA	ASW	6 *m* NaCl + 0.9 *m* KNO_3	100	5.41	6.00	0.90	0.15	−83	265
23	KE0126	PCA	ASW	6 *m* NaCl + 0.9 *m* KNO_3	100	5.41	6.00	0.90	0.15	−72	265
22	KE0121	PCA	ASW	6 *m* NaCl + 0.3 *m* KNO_3	100	5.43	6.00	0.30	0.05	−129	280
22	KE0122	PCA	ASW	6 *m* NaCl + 0.3 *m* KNO_3	100	5.43	6.00	0.30	0.05	−140	280
22	KE0123	PCA	ASW	6 *m* NaCl + 0.3 *m* KNO_3	100	5.43	6.00	0.30	0.05	−123	280
22	KE0124	PCA	ASW	6 *m* NaCl + 0.3 *m* KNO_3	100	5.43	6.00	0.30	0.05	−130	280
21	DEA2827	Rod	MA	5 *M* $CaCl_2$ + 0.5 *M* $Ca(NO_3)_2$	90	2.97	12.59	1.26	0.10	482	463
21	DEA2828	Rod	MA	5 *M* $CaCl_2$ + 0.5 *M* $Ca(NO_3)_2$	90	2.97	12.59	1.26	0.10	482	463

Cell	Specimen ID	Specimen Type [a]	Material Condition [a]	Solution [a]	T (°C)	Calculated Pitzer pH [b]	[Cl] (*m*) [b]	[NO_3] (*m*) [b]	NO_3/Cl [b]	Ecorr mV_{SSC}	Immersion Days
21	DEA2829	Rod	MA	5 *M* $CaCl_2$ + 0.5 *M* $Ca(NO_3)_2$	90	2.97	12.59	1.26	0.10	481	463
21	JE2055	Rod	ASW	5 *M* $CaCl_2$ + 0.5 *M* $Ca(NO_3)_2$	90	2.97	12.59	1.26	0.10	82	463
21	JE2056	Rod	ASW	5 *M* $CaCl_2$ + 0.5 *M* $Ca(NO_3)_2$	90	2.97	12.59	1.26	0.10	47	463
21	JE2063	Rod	ASW	5 *M* $CaCl_2$ + 0.5 *M* $Ca(NO_3)_2$	90	2.97	12.59	1.26	0.10	28	463
20	DEA2824	Rod	MA	5 *M* $CaCl_2$	120	3.93	11.99	0.00	0.00	−164	497
20	DEA2825	Rod	MA	5 *M* $CaCl_2$	120	3.93	11.99	0.00	0.00	−56	497
20	DEA2826	Rod	MA	5 *M* $CaCl_2$	120	3.93	11.99	0.00	0.00	−39	497
20	JE2052	Rod	ASW	5 *M* $CaCl_2$	120	3.93	11.99	0.00	0.00	22	497
20	JE2053	Rod	ASW	5 *M* $CaCl_2$	120	3.93	11.99	0.00	0.00	166	497
20	JE2054	Rod	ASW	5 *M* $CaCl_2$	120	3.93	11.99	0.00	0.00	−19	497
19	DEA2822	Rod	MA	BSW	105	8.61	4.62	2.82	0.61	−97	256
19	DEA2823	Rod	MA	BSW	105	8.61	4.62	2.82	0.61	−124	256
19	DEA2820	Rod Halar Coated	MA	BSW	105	8.61	4.62	2.82	0.61	−231	256
19	DEA2821	Rod Halar Coated	MA	BSW	105	8.61	4.62	2.82	0.61	−198	256
19	JE2050	Rod	ASW	BSW	105	8.61	4.62	2.82	0.61	−211	256
19	JE2051	Rod	ASW	BSW	105	8.61	4.62	2.82	0.61	−208	256
19	JE2048	Rod Halar Coated	ASW	BSW	105	8.61	4.62	2.82	0.61	−252	256
19	JE2049	Rod Halar Coated	ASW	BSW	105	8.61	4.62	2.82	0.61	−214	256
18	DEA2816	Rod	MA	4 *M* NaCl	90	5.55	4.40	0.00	0.00	−170	328
18	DEA2817	Rod	MA	4 *M* NaCl	90	5.55	4.40	0.00	0.00	−165	328
18	DEA2818	Rod	MA	4 *M* NaCl	90	5.55	4.40	0.00	0.00	−175	328
18	JE2045	Rod	ASW	4 *M* NaCl	90	5.55	4.40	0.00	0.00	−133	328
18	JE2046	Rod	ASW	4 *M* NaCl	90	5.55	4.40	0.00	0.00	−84	328
18	JE2047	Rod	ASW	4 *M* NaCl	90	5.55	4.40	0.00	0.00	−83	328
17	DEA2813	Rod	MA	SAW - w/out Silicate	90	1.93	0.76	0.39	0.52	389	375[c]

Cell	Specimen ID	Specimen Type [a]	Material Condition [a]	Solution [a]	T (°C)	Calculated Pitzer pH [b]	[Cl] (*m*) [b]	[NO_3] (*m*) [b]	NO_3/Cl [b]	Ecorr mV_{SSC}	Immersion Days
17	DEA2814	Rod	MA	SAW - w/out Silicate	90	1.93	0.76	0.39	0.52	389	375[c]
17	DEA2815	Rod	MA	SAW - w/out Silicate	90	1.93	0.76	0.39	0.52	387	375[c]
17	JE2042	Rod	ASW	SAW - w/out Silicate	90	1.93	0.76	0.39	0.52	395	375[c]
17	JE2043	Rod	ASW	SAW - w/out Silicate	90	1.93	0.76	0.39	0.52	394	375[c]
17	JE2044	Rod	ASW	SAW - w/out Silicate	90	1.93	0.76	0.39	0.52	394	375[c]
16	DEA2810	Rod	MA	SCW	90	9.98	0.21	0.11	0.52	−191	394[c]
16	DEA2811	Rod	MA	SCW	90	9.98	0.21	0.11	0.52	−173	394[c]
16	DEA2812	Rod	MA	SCW	90	9.98	0.21	0.11	0.52	−160	394[c]
16	JE2039	Rod	ASW	SCW	90	9.98	0.21	0.11	0.52	−133	394[c]
16	JE2040	Rod	ASW	SCW	90	9.98	0.21	0.11	0.52	−207	394[c]
16	JE2041	Rod	ASW	SCW	90	9.98	0.21	0.11	0.52	−163	394[c]
15	DEA2806	Rod	MA	5 *M* $CaCl_2$ + 0.5 *M* $Ca(NO_3)_2$	90	2.97	12.59	1.26	0.10	188	693
15	DEA2808	Rod	MA	5 *M* $CaCl_2$ + 0.5 *M* $Ca(NO_3)_2$	90	2.97	12.59	1.26	0.10	75	693
15	DEA2809	Rod	MA	5 *M* $CaCl_2$ + 0.5 *M* $Ca(NO_3)_2$	90	2.97	12.59	1.26	0.10	113	693
15	JE2037	Rod	ASW	5 *M* $CaCl_2$ + 0.5 *M* $Ca(NO_3)_2$	90	2.97	12.59	1.26	0.10	232	558
15	JE2038	Rod	ASW	5 *M* $CaCl_2$ + 0.5 *M* $Ca(NO_3)_2$	90	2.97	12.59	1.26	0.10	275	558
14	DEA2801	Rod	MA	5 *M* $CaCl_2$ + 0.05 *M* $Ca(NO_3)_2$	90	4.03	11.70	0.12	0.01	253	704
14	DEA2803	Rod	MA	5 *M* $CaCl_2$ + 0.05 *M* $Ca(NO_3)_2$	90	4.03	11.70	0.12	0.01	57	704
14	DEA2804	Rod	MA	5 *M* $CaCl_2$ + 0.05 *M* $Ca(NO_3)_2$	90	4.03	11.70	0.12	0.01	92	704
14	JE2035	Rod	ASW	5 *M* $CaCl_2$ + 0.05 *M* $Ca(NO_3)_2$	90	4.03	11.70	0.12	0.01	176	561
14	JE2036	Rod	ASW	5 *M* $CaCl_2$ + 0.05 *M* $Ca(NO_3)_2$	90	4.03	11.70	0.12	0.01	214	561
13	DEA3087	Rod	MA	1 *M* $CaCl_2$ + 1 *M* $Ca(NO_3)_2$	90	6.39	2.62	2.58	0.99	321	622
13	DEA3088	Rod	MA	1 *M* $CaCl_2$ + 1 *M* $Ca(NO_3)_2$	90	6.39	2.62	2.58	0.99	324	622
13	DEA3089	Rod	MA	1 *M* $CaCl_2$ + 1 *M* $Ca(NO_3)_2$	90	6.39	2.62	2.58	0.99	321	622
13	DEA3090	Rod	MA	1 *M* $CaCl_2$ + 1 *M* $Ca(NO_3)_2$	90	6.39	2.62	2.58	0.99	316	622

Cell	Specimen ID	Specimen Type [a]	Material Condition [a]	Solution [a]	T (°C)	Calculated Pitzer pH [b]	[Cl] (*m*) [b]	[NO_3] (*m*) [b]	NO_3/Cl [b]	Ecorr mV_{SSC}	Immersion Days
13	JE2033	Rod	ASW	1 *M* $CaCl_2$ + 1 *M* $Ca(NO_3)_2$	90	6.39	2.62	2.58	0.99	360	457
13	JE2034	Rod	ASW	1 *M* $CaCl_2$ + 1 *M* $Ca(NO_3)_2$	90	6.39	2.62	2.58	0.99	341	457
10	DEA2850	Rod	MA	4.5 years LTCTF SAW	90	2.72	0.77	0.37	0.49	387	834
10	DEA2851	Rod	MA	4.5 years LTCTF SAW	90	2.72	0.77	0.37	0.49	381	834
10	DEA2852	Rod	MA	4.5 years LTCTF SAW	90	2.72	0.77	0.37	0.49	374	834
10	DEA2854	Rod	MA	4.5 years LTCTF SAW	90	2.72	0.77	0.37	0.49	382	834
10	DEA2855	Rod	MA	4.5 years LTCTF SAW	90	2.72	0.77	0.37	0.49	384	834
10	DEA2856	Rod	MA	4.5 years LTCTF SAW	90	2.72	0.77	0.37	0.49	373	834
10	DEA2857	Rod	MA	4.5 years LTCTF SAW	90	2.72	0.77	0.37	0.49	377	834
10	DEA2858	Rod	MA	4.5 years LTCTF SAW	90	2.72	0.77	0.37	0.49	382	834
9	DEA2797	Rod	MA	SAW	90	2.38	1.39	0.40	0.29	400	876
9	DEA2853	Rod	MA	SAW	90	2.38	1.39	0.40	0.29	400	876
9	DEA2881	Rod	MA	SAW	90	2.38	1.39	0.40	0.29	397	876
9	DEA2928	Rod	MA	SAW	90	2.38	1.39	0.40	0.29	399	876
9	DEA2940	Rod	MA	SAW	90	2.38	1.39	0.40	0.29	388	525
9	DEA3010	Rod	MA	SAW	90	2.38	1.39	0.40	0.29	389	525
9	DEA3014	Rod	MA	SAW	90	2.38	1.39	0.40	0.29	385	525
9	DEA3082	Rod	MA	SAW	90	2.38	1.39	0.40	0.29	387	525
7-2	DEA2802	Rod	MA	SAW - LTCTF Origin Vessel 26	25	2.02	0.77	0.37	0.49	266	846
7-2	DEA2807	Rod	MA	SAW - LTCTF Origin Vessel 26	25	2.02	0.77	0.37	0.49	254	846
7-2	DEA2859	Rod	MA	SAW - LTCTF Origin Vessel 26	25	2.02	0.77	0.37	0.49	238	846
6	DUB132	Prev tested U-bend	ASW	SDW - LTCTF Origin Vessel 30	90	9.41	3.30×10^{-3}	9.73×10^{-4}	0.29	101	1,089
6	DUB162	Untested U-bend	ASW	SDW - LTCTF Origin Vessel 30	90	9.41	3.30×10^{-3}	9.73×10^{-4}	0.29	110	1,089
5	DUB128	Prev tested U-bend	ASW	SDW - LTCTF Origin Vessel 29	60	9.30	3.30×10^{-3}	9.73×10^{-4}	0.29	55	1,089
5	DUB160	Untested U-bend	ASW	SDW - LTCTF Origin Vessel 29	60	9.30	3.30×10^{-3}	9.73×10^{-4}	0.29	32	1,089

Cell	Specimen ID	Specimen Type [a]	Material Condition [a]	Solution [a]	T (°C)	Calculated Pitzer pH [b]	[Cl] (*m*) [b]	[NO_3] (*m*) [b]	NO_3/Cl [b]	Ecorr mV_{SSC}	Immersion Days
4	ARC22 U-20A & ARC22 U-20B	Prev tested U-bend	MA	BSW	105	8.61	4.62	2.82	0.61	62	729
4	DUB163	Untested U-bend	ASW	BSW	105	8.61	4.62	2.82	0.61	5	729
3	DUB112	Prev tested U-bend	ASW	SCW - LTCTF Origin Vessel 28	90	10.04	0.21	0.12	0.56	−24	1,089
3	DUB161	Untested U-bend	ASW	SCW - LTCTF Origin Vessel 28	90	10.04	0.21	0.12	0.56	−61	1,089
2	DUB052	Prev tested U-bend	ASW	SAW - LTCTF Origin Vessel 26	90	2.72	0.77	0.37	0.49	290	1,102 [d]
2	DUB159	Untested U-bend	ASW	SAW - LTCTF Origin Vessel 26	90	2.72	0.77	0.37	0.49	372	1,102 [d]
1	DUB028	Prev tested U-bend	ASW	SAW - LTCTF Origin Vessel 25	60	2.39	0.77	0.37	0.49	374	1,089
1	DUB157	Untested U-bend	ASW	SAW - LTCTF Origin Vessel 25	60	2.39	0.77	0.37	0.49	406	1,089

[a] MA = mill-annealed, non-welded specimen; PCA = prism crevice assembly; ASW = as-welded; SCW = simulated concentrated water; SAW = simulated acidified water; SDW = simulated dilute water; BSW = basic saturated water; LTCTF = Long-Term Corrosion Test Facility

[b] Pitzer pH values and molalities (if solution concentration was expressed in molarity) are from DTN: LL060904312251.186 [DIRS 178283], file: *AtmCO2GetEQData.xls*. Pitzer pH and molalities were extracted electronically (from worksheets copied from DTN: LL060904312251.186 [DIRS 178283], file: *AtmCO2GetEQData.xls*) using the "VLOOKUP" Excel command. The nitrate ion-to-chloride ion ratio is supplied here for completeness. These results are displayed with two decimal places except cells 5 and 6, which contained the very dilute SDW solution and cells 24, 25, and 31 where the molality of nitrate ions was known to three decimal places.

[c] There is a gap in data collection in the last 30 days. The average was calculated with the data of 30 consecutive days before this gap. Also Cell 17 contains "SAW w/o Si" according to DTN: LL060901312251.181 [DIRS 178299], file: *s06121_001_001.pdf*.

[d] After 9/25/2003 1:45:45 PM (day 894) there was a sudden decrease of potentials. Data after day 894 are considered corrupted. The average long-term corrosion potential was calculated from the starting time of day 864 to the final time of day 894.

Sources: DTN: LL06090051 2251.177 [DIRS 178271], file: *Summary Ecorr Cells 1-36 29Sep06.xls* except as discussed in note b).

NOTES: No long-term corrosion potential data obtained above 120°C or for exposure times less than 250 days were used. DTN: LL060901312251.181 [DIRS 178299], file: *s06121_001_001.pdf* indicates that specimens labeled DUB are ASW single U-bends and ARC22 U-20A & ARC22 U-20B is a non-welded double U-bend (Cells 1-6).

APPENDIX IX
ALLOY 22 CREVICE REPASSIVATION POTENTIAL DATA USED IN THE CREVICE REPASSIVATION POTENTIAL MODEL

APPENDIX IX – ALLOY 22 CREVICE REPASSIVATION POTENTIAL DATA USED IN THE CREVICE REPASSIVATION POTENTIAL MODEL

Source DTN	Specimen ID	Sample Type	Material Condition	Electrolyte	Type of LC	Temperature (°C)	Calculated Pitzer pH	[Cl] molal	[NO_3] molal	NO_3/Cl molal ratio	E_{rcrev} (mV vs. SSC)
LL060803712251.170 [DIRS 179387]	KE0614	PCA	ASW	0.0005 *M* NaCl	CC	60	6.51	5×10^{-4}	0.00	0.00	339
LL060803712251.170 [DIRS 179387]	KE0117	PCA	ASW	0.0005 *M* NaCl	CC	90	6.21	5×10^{-4}	0.00	0.00	214
LL060803712251.170 [DIRS 179387]	KE0618	PCA	ASW	0.005 *M* NaCl	CC	60	6.51	5.8×10^{-3}	0.00	0.00	359
LL060803712251.170 [DIRS 179387]	KE0617	PCA	ASW	0.05 *M* NaCl	CC	60	6.51	0.05	0.00	0.00	161
LL060803712251.170 [DIRS 179387]	KE0610	PCA	ASW	0.5 *M* NaCl	CC	60	6.45	0.51	0.00	0.00	61
LL060803712251.170 [DIRS 179387]	JE3321	MCA	MA	1 *M* NaCl	CC	60	6.45	1.02	0.00	0.00	84
LL060803712251.170 [DIRS 179387]	JE3322	MCA	MA	1 *M* NaCl	CC	60	6.45	1.02	0.00	0.00	28
LL060803712251.170 [DIRS 179387]	DEA3129	MCA	MA	1 *M* NaCl	CC	90	6.16	1.02	0.00	0.00	−24
LL060803712251.170 [DIRS 179387]	JE3324	MCA	MA	1 *M* NaCl	CC	90	6.16	1.02	0.00	0.00	−126
LL060803712251.170 [DIRS 179387]	JE3328	MCA	MA	1 *M* NaCl	CC	90	6.16	1.02	0.00	0.00	−109
LL060803712251.170 [DIRS 179387]	DEA3262	MCA	MA	1 *M* NaCl	CC	90	6.16	1.02	0.00	0.00	−42
LL040902712251.119 [DIRS 173720]	W6	PCA	ASW	1 *M* NaCl	CC	90	6.16	1.02	0.00	0.00	−104
LL040902712251.119 [DIRS 173720]	B3	PCA	ASW − LPB	1 *M* NaCl	CC	90	6.16	1.02	0.00	0.00	−134
LL040902712251.119 [DIRS 173720]	P5	PCA	ASW − LSP	1 *M* NaCl	CC	90	6.16	1.02	0.00	0.00	−114

Source DTN	Specimen ID	Sample Type	Material Condition	Electrolyte	Type of LC	Temperature (°C)	Calculated Pitzer pH	[Cl] molal	[NO_3] molal	NO_3/Cl molal ratio	E_{rcrev} (mV vs. SSC)
LL060803712251.170 [DIRS 179387]	DEA3263	MCA	MA	1 *M* NaCl	CC	90	6.16	1.02	0.00	0.00	−45
LL050302312251.129 [DIRS 173921]	AY009	PCA	ASW − Mockup	1 *M* NaCl	CC	90	6.16	1.02	0.00	0.00	−54
LL050302312251.129 [DIRS 173921]	AY010	PCA	ASW − Mockup	1 *M* NaCl	CC	90	6.16	1.02	0.00	0.00	−52
LL060803712251.170 [DIRS 179387]	DEA3267	MCA	MA	1.25 *M* NaCl	LC	60	6.44	1.29	0.00	0.00	48
LL060803712251.170 [DIRS 179387]	DEA3268	MCA	MA	1.25 *M* NaCl	LC	60	6.44	1.29	0.00	0.00	23
LL060803712251.170 [DIRS 179387]	DEA3271	MCA	MA	1.25 *M* NaCl	CC	90	6.14	1.29	0.00	0.00	−33
LL060803712251.170 [DIRS 179387]	DEA3269	MCA	MA	1.25 *M* NaCl	CC	90	6.14	1.29	0.00	0.00	−65
LL060803712251.170 [DIRS 179387]	KE0612	PCA	ASW	4 *M* NaCl	CC	60	6.25	4.40	0.00	0.00	−52
LL060803712251.170 [DIRS 179387]	DEA3296	MCA	MA	4 *M* NaCl	CC	60	6.25	4.40	0.00	0.00	−116
LL060803712251.170 [DIRS 179387]	DEA3297	MCA	MA	4 *M* NaCl	CC	60	6.25	4.40	0.00	0.00	−107
LL060803712251.170 [DIRS 179387]	DEA3298	MCA	MA	4 *M* NaCl	CC-II	60	6.25	4.40	0.00	0.00	−50
LL060803712251.170 [DIRS 179387]	DEA3299	MCA	MA	4 *M* NaCl	CC-II	60	6.25	4.40	0.00	0.00	−69
LL060803712251.170 [DIRS 179387]	DEA3304	MCA	MA	4 *M* NaCl	CC	75	6.10	4.40	0.00	0.00	−140
LL060803712251.170 [DIRS 179387]	DEA3305	MCA	MA	4 *M* NaCl	CC	75	6.10	4.40	0.00	0.00	−140
LL060803712251.170 [DIRS 179387]	DEA3307	MCA	MA	4 *M* NaCl	CC	75	6.10	4.40	0.00	0.00	−157
LL060803712251.170 [DIRS 179387]	KE0710	PCA	MA	4 *M* NaCl	CC	75	6.10	4.40	0.00	0.00	−118

Source DTN	Specimen ID	Sample Type	Material Condition	Electrolyte	Type of LC	Temperature (°C)	Calculated Pitzer pH	[Cl] molal	[NO_3] molal	NO_3/Cl molal ratio	E_{rcrev} (mV vs. SSC)
LL060803712251.170 [DIRS 179387]	DEA3306	MCA	MA	4 *M* NaCl	CC-II	75	6.10	4.40	0.00	0.00	−148
LL060803712251.170 [DIRS 179387]	DEA3300	MCA	MA	4 *M* NaCl	CC	90	5.97	4.40	0.00	0.00	−161
LL060803712251.170 [DIRS 179387]	DEA3301	MCA	MA	4 *M* NaCl	CC	90	5.97	4.40	0.00	0.00	−168
LL060803712251.170 [DIRS 179387]	DEA3302	MCA	MA	4 *M* NaCl	CC	90	5.97	4.40	0.00	0.00	−160
LL060803712251.170 [DIRS 179387]	DEA3303	MCA	MA	4 *M* NaCl	CC	90	5.97	4.40	0.00	0.00	−165
LL060803712251.170 [DIRS 179387]	DEA3312	MCA	MA	4 *M* NaCl	CC	105	5.85	4.40	0.00	0.00	−157
LL060803712251.170 [DIRS 179387]	DEA3313	MCA	MA	4 *M* NaCl	CC	105	5.85	4.40	0.00	0.00	−168
LL060803712251.170 [DIRS 179387]	DEA3314	MCA	MA	4 *M* NaCl	CC	105	5.85	4.40	0.00	0.00	−119
LL060803712251.170 [DIRS 179387]	DEA3315	MCA	MA	4 *M* NaCl	CC	105	5.85	4.40	0.00	0.00	−142
LL060801812251.168 [DIRS 179386]	KE0571	PCA	ASW	3 *m* KCl + 3 *m* NaCl + 3 *m* KNO_3 + 3 *m* $NaNO_3$ (+ 0.0001 *m* HCl)	CC-II	110	3.19	6.00	6.00	1.00	330
LL060801812251.168 [DIRS 179386]	KE0575	PCA	ASW	3 *m* KCl + 3 *m* NaCl + 3 *m* KNO_3 + 3 *m* $NaNO_3$ (+ 0.0001 *m* HCl)	CC-II	110	3.19	6.00	6.00	1.00	413
LL060801812251.168 [DIRS 179386]	KE0588	PCA	ASW	4 *m* $CaCl_2$	CC	110	4.41	8.00	0.00	0.00	−243
LL060801812251.168 [DIRS 179386]	KE0689	PCA	ASW	4 *m* KCl + 4 *m* NaCl	CC	110	5.76	8.00	0.00	0.00	−223
LL060801812251.168 [DIRS 179386]	KE0691	PCA	ASW	4 *m* KCl + 4 *m* NaCl	CC	110	5.76	8.00	0.00	0.00	−210
LL060801812251.168 [DIRS 179386]	KE0688B	PCA	ASW	4 *m* KCl + 4 *m* NaCl + 0.4 *m* KNO_3 + 0.4 *m* $NaNO_3$	CC	90	5.89	8.00	0.80	0.10	−82

Source DTN	Specimen ID	Sample Type	Material Condition	Electrolyte	Type of LC	Temperature (°C)	Calculated Pitzer pH	[Cl] molal	[NO_3] molal	NO_3/Cl molal ratio	E_{rcrev} (mV vs. SSC)
LL060801812251.168 [DIRS 179386]	KE0579	PCA	ASW	4 *m* KCl + 4 *m* NaCl + 0.4 *m* KNO_3 + 0.4 *m* $NaNO_3$	CC	90	5.89	8.00	0.80	0.10	−80
LL060801812251.168 [DIRS 179386]	KE0687	PCA	ASW	4 *m* KCl + 4 *m* NaCl + 0.4 *m* KNO_3 + 0.4 *m* $NaNO_3$	CC	110	5.76	8.00	0.80	0.10	−50
LL060801812251.168 [DIRS 179386]	KE0692	PCA	ASW	4 *m* KCl + 4 *m* NaCl + 0.4 *m* KNO_3 + 0.4 *m* $NaNO_3$	CC	110	5.76	8.00	0.80	0.10	−103
LL060801812251.168 [DIRS 179386]	KE0573	PCA	ASW	4 *m* KCl + 4 *m* NaCl + 0.4 *m* KNO_3 + 0.4 *m* $NaNO_3$ (+ 0.0001 *m* HCl)	CC	110	3.36	8.00	0.80	0.10	−106
LL060801812251.168 [DIRS 179386]	KE0589	PCA	ASW	4 *m* KCl + 4 *m* NaCl + 0.8 *m* KNO3 + 0.8 *m* NaNO3	CC	110	5.76	8.00	1.60	0.20	−44
LL060801812251.168 [DIRS 179386]	KE0572	PCA	ASW	4 *m* KCl + 4 *m* NaCl + 2 *m* KNO_3 + 2 *m* $NaNO_3$ (+ 0.0001 *m* HCl)	CC-II	110	3.09	8.00	4.00	0.50	446
LL060700312251.166 [DIRS 179385]	JE1647	MCA	ASW	5 *M* $CaCl_2$	CC	30	4.55	11.99	0.00	0.00	−57
LL060700312251.166 [DIRS 179385]	KE0381	PCA	ASW	5 *M* $CaCl_2$	CC	60	4.20	11.99	0.00	0.00	−65
LL060700312251.166 [DIRS 179385]	KE0380	PCA	ASW	5 *M* $CaCl_2$	CC	60	4.20	11.99	0.00	0.00	−64
LL060700312251.166 [DIRS 179385]	JE0114	MCA	ASW	5 *M* $CaCl_2$	CC-II	45	4.36	11.99	0.00	0.00	24
LL060700312251.166 [DIRS 179385]	JE0112	MCA	ASW	5 *M* $CaCl_2$	CC-II	60	4.20	11.99	0.00	0.00	−88
LL060700312251.166 [DIRS 179385]	JE0113	MCA	ASW	5 *M* $CaCl_2$	CC-II	60	4.20	11.99	0.00	0.00	−48
LL060700312251.166 [DIRS 179385]	JE0111	MCA	ASW	5 *M* $CaCl_2$	CC-II	60	4.20	11.99	0.00	0.00	−47
LL060700312251.166 [DIRS 179385]	DEA3295	MCA	MA	5 *M* $CaCl_2$	CC-II	60	4.20	11.99	0.00	0.00	18
LL060700312251.166 [DIRS 179385]	DEA3294	MCA	MA	5 *M* $CaCl_2$	CC-II	60	4.20	11.99	0.00	0.00	22

Source DTN	Specimen ID	Sample Type	Material Condition	Electrolyte	Type of LC	Temperature (°C)	Calculated Pitzer pH	[Cl] molal	[NO_3] molal	NO_3/Cl molal ratio	E_{rcrev} (mV vs. SSC)
LL060700312251.166 [DIRS 179385]	DEA3226	MCA	MA	5 *M* $CaCl_2$	LC	60	4.20	11.99	0.00	0.00	−27
LL060700312251.166 [DIRS 179385]	DEA3224	MCA	MA	5 *M* $CaCl_2$	LC	60	4.20	11.99	0.00	0.00	−2
LL060700312251.166 [DIRS 179385]	DEA3225	MCA	MA	5 *M* $CaCl_2$	LC	60	4.20	11.99	0.00	0.00	29
LL060700312251.166 [DIRS 179385]	DEA3228	MCA	MA	5 *M* $CaCl_2$	LC	75	4.08	11.99	0.00	0.00	−147
LL060700312251.166 [DIRS 179385]	DEA3233	MCA	MA	5 *M* $CaCl_2$	LC	75	4.08	11.99	0.00	0.00	−138
LL060700312251.166 [DIRS 179385]	KE0383	PCA	ASW	5 *M* $CaCl_2$	LC	75	4.08	11.99	0.00	0.00	−138
LL060700312251.166 [DIRS 179385]	KE0382	PCA	ASW	5 *M* $CaCl_2$	LC	75	4.08	11.99	0.00	0.00	−137
LL060700312251.166 [DIRS 179385]	DEA3278	MCA	MA	5 *M* $CaCl_2$	LC	75	4.08	11.99	0.00	0.00	−128
LL060700312251.166 [DIRS 179385]	JE0040	MCA	ASW	5 *M* $CaCl_2$	LC	75	4.08	11.99	0.00	0.00	−126
LL060700312251.166 [DIRS 179385]	JE0042	MCA	ASW	5 *M* $CaCl_2$	LC	75	4.08	11.99	0.00	0.00	−125
LL060700312251.166 [DIRS 179385]	DEA3281	MCA	MA	5 *M* $CaCl_2$	LC	75	4.08	11.99	0.00	0.00	−121
LL060700312251.166 [DIRS 179385]	DEA3238	MCA	MA	5 *M* $CaCl_2$	LC	75	4.08	11.99	0.00	0.00	−119
LL060700312251.166 [DIRS 179385]	JE0041	MCA	ASW	5 *M* $CaCl_2$	LC	75	4.08	11.99	0.00	0.00	−117
LL060700312251.166 [DIRS 179385]	DEA3221	MCA	MA	5 *M* $CaCl_2$	LC	75	4.08	11.99	0.00	0.00	−115
LL060700312251.166 [DIRS 179385]	DEA3220	MCA	MA	5 *M* $CaCl_2$	LC	75	4.08	11.99	0.00	0.00	−97
LL060700312251.166 [DIRS 179385]	DEA3279	MCA	MA	5 *M* $CaCl_2$	LC	75	4.08	11.99	0.00	0.00	−93

Source DTN	Specimen ID	Sample Type	Material Condition	Electrolyte	Type of LC	Temperature (°C)	Calculated Pitzer pH	[Cl] molal	[NO_3] molal	NO_3/Cl molal ratio	E_{rcrev} (mV vs. SSC)
LL060700312251.166 [DIRS 179385]	DEA3222	MCA	MA	5 *M* $CaCl_2$	LC	75	4.08	11.99	0.00	0.00	−88
LL060700312251.166 [DIRS 179385]	DEA3223	MCA	MA	5 *M* $CaCl_2$	LC	75	4.08	11.99	0.00	0.00	−77
LL060700312251.166 [DIRS 179385]	DEA3260	MCA	MA	5 *M* $CaCl_2$	LC	75	4.08	11.99	0.00	0.00	−19
LL060700312251.166 [DIRS 179385]	DEA3280	MCA	MA	5 *M* $CaCl_2$	LC	75	4.08	11.99	0.00	0.00	−8
LL060700312251.166 [DIRS 179385]	DEA3261	MCA	MA	5 *M* $CaCl_2$	LC	75	4.08	11.99	0.00	0.00	42
LL060700312251.166 [DIRS 179385]	JE0037	MCA	ASW	5 *M* $CaCl_2$	LC	90	4.00	11.99	0.00	0.00	−189
LL060700312251.166 [DIRS 179385]	KE0701	PCA	MA	5 *M* $CaCl_2$	LC	90	4.00	11.99	0.00	0.00	−189
LL060700312251.166 [DIRS 179385]	KE0373	PCA	ASW	5 *M* $CaCl_2$	LC	90	4.00	11.99	0.00	0.00	−184
LL060700312251.166 [DIRS 179385]	DEA3216	MCA	MA	5 *M* $CaCl_2$	LC	90	4.00	11.99	0.00	0.00	−183
LL060700312251.166 [DIRS 179385]	DEA3376	MCA	MA	5 *M* $CaCl_2$	LC	90	4.00	11.99	0.00	0.00	−183
LL060700312251.166 [DIRS 179385]	JE0039	MCA	ASW	5 *M* $CaCl_2$	LC	90	4.00	11.99	0.00	0.00	−175
LL060700312251.166 [DIRS 179385]	KE0374	PCA	ASW	5 *M* $CaCl_2$	LC	90	4.00	11.99	0.00	0.00	−172
LL060700312251.166 [DIRS 179385]	KE0702	PCA	MA	5 *M* $CaCl_2$	LC	90	4.00	11.99	0.00	0.00	−168
LL060700312251.166 [DIRS 179385]	JE1635	MCA	ASW	5 *M* $CaCl_2$	LC	90	4.00	11.99	0.00	0.00	−164
LL060700312251.166 [DIRS 179385]	JE0038	MCA	ASW	5 *M* $CaCl_2$	LC	90	4.00	11.99	0.00	0.00	−161
LL060700312251.166 [DIRS 179385]	DEA3219	MCA	MA	5 *M* $CaCl_2$	LC	90	4.00	11.99	0.00	0.00	−143

Source DTN	Specimen ID	Sample Type	Material Condition	Electrolyte	Type of LC	Temperature (°C)	Calculated Pitzer pH	[Cl] molal	[NO_3] molal	NO_3/Cl molal ratio	E_{rcrev} (mV vs. SSC)
LL060700312251.166 [DIRS 179385]	DEA3218	MCA	MA	5 *M* $CaCl_2$	LC	90	4.00	11.99	0.00	0.00	−133
LL060700312251.166 [DIRS 179385]	DEA3217	MCA	MA	5 *M* $CaCl_2$	LC	90	4.00	11.99	0.00	0.00	−129
LL060700312251.166 [DIRS 179385]	DEA3176	MCA	MA	5 *M* $CaCl_2$	LC	90	4.00	11.99	0.00	0.00	−85
LL060700312251.166 [DIRS 179385]	DEA3388	MCA	MA	5 *M* $CaCl_2$	LC	90	4.00	11.99	0.00	0.00	−35
LL060700312251.166 [DIRS 179385]	DEA3177	MCA	MA	5 *M* $CaCl_2$	LC	90	4.00	11.99	0.00	0.00	−8
LL050302312251.129 [DIRS 173921]	AY007	PCA	ASW − Mockup	5 *M* $CaCl_2$	LC	90	4.00	11.99	0.00	0.00	−73
LL050302312251.129 [DIRS 173921]	AY008	PCA	ASW − Mockup	5 *M* $CaCl_2$	LC	90	4.00	11.99	0.00	0.00	−169
LL060700312251.166 [DIRS 179385]	DEA3167	MCA	MA	5 *M* $CaCl_2$	LC	105	3.95	11.99	0.00	0.00	−195
LL060700312251.166 [DIRS 179385]	DEA3168	MCA	MA	5 *M* $CaCl_2$	LC	105	3.95	11.99	0.00	0.00	−185
LL060700312251.166 [DIRS 179385]	DEA3235	MCA	MA	5 *M* $CaCl_2$	LC	120	3.93	11.99	0.00	0.00	−216
LL060700312251.166 [DIRS 179385]	DEA3237	MCA	MA	5 *M* $CaCl_2$	LC	120	3.93	11.99	0.00	0.00	−198
LL060700312251.166 [DIRS 179385]	KE0384	PCA	ASW	5 *M* $CaCl_2$	LC	120	3.93	11.99	0.00	0.00	−190
LL060700312251.166 [DIRS 179385]	KE0385	PCA	ASW	5 *M* $CaCl_2$	LC	120	3.93	11.99	0.00	0.00	−186
LL060700312251.166 [DIRS 179385]	JE0036	MCA	ASW	5 *M* $CaCl_2$	LC	120	3.93	11.99	0.00	0.00	−183
LL060700312251.166 [DIRS 179385]	JE0035	MCA	ASW	5 *M* $CaCl_2$	LC	120	3.93	11.99	0.00	0.00	−179
LL060700312251.166 [DIRS 179385]	DEA3236	MCA	MA	5 *M* $CaCl_2$	LC	120	3.93	11.99	0.00	0.00	−178

Source DTN	Specimen ID	Sample Type	Material Condition	Electrolyte	Type of LC	Temperature (°C)	Calculated Pitzer pH	[Cl] molal	[NO_3] molal	NO_3/Cl molal ratio	E_{rcrev} (mV vs. SSC)
LL060700312251.166 [DIRS 179385]	DEA3234	MCA	MA	5 *M* $CaCl_2$	LC	120	3.93	11.99	0.00	0.00	−164
LL060700312251.166 [DIRS 179385]	JE0034	MCA	ASW	5 *M* $CaCl_2$	LC	120	3.93	11.99	0.00	0.00	−161
LL060801812251.168 [DIRS 179386]	JE3463	MCA	ASW	10 *m* $CaCl_2$	LC	100	3.67	20.00	0.00	0.00	−197
LL060801812251.168 [DIRS 179386]	JE3464	MCA	ASW	10 *m* $CaCl_2$	LC	100	3.67	20.00	0.00	0.00	−183
LL060603812251.164 [DIRS 178269]	JE3209	MCA	ASW	1 *m* NaCl + 0.05 *m* KNO_3	CC-II	60	6.45	1.00	0.05	0.05	94
LL060603812251.164 [DIRS 178269]	JE3244	MCA	ASW	1 *m* NaCl + 0.05 *m* KNO3	CC	80	6.25	1.00	0.05	0.05	25
LL060603812251.164 [DIRS 178269]	JE3227	MCA	ASW	1 *m* NaCl + 0.05 *m* KNO_3	CC-II	80	6.25	1.00	0.05	0.05	−52
LL060603812251.164 [DIRS 178269]	JE3225	MCA	ASW	1 *m* NaCl + 0.05 *m* KNO_3	CC	100	6.08	1.00	0.05	0.05	−118
LL060603812251.164 [DIRS 178269]	JE3236	MCA	ASW	1 *m* NaCl + 0.05 *m* KNO_3	CC	100	6.08	1.00	0.05	0.05	−122
LL060603812251.164 [DIRS 178269]	KE0356	PCA	ASW	1 *m* NaCl + 0.05 *m* KNO_3	CC	100	6.08	1.00	0.05	0.05	−86
LL060603812251.164 [DIRS 178269]	KE0360	PCA	ASW	1 *m* NaCl + 0.05 *m* KNO_3	CC	100	6.08	1.00	0.05	0.05	−81
LL060603812251.164 [DIRS 178269]	KE0361	PCA	ASW	1 *m* NaCl + 0.05 *m* KNO_3	CC	100	6.08	1.00	0.05	0.05	−64
LL060603812251.164 [DIRS 178269]	KE0627	PCA	ASW	1 *m* NaCl + 0.15 *m* KNO_3	CC	80	6.25	1.00	0.15	0.15	68
LL060603812251.164 [DIRS 178269]	JE3237	MCA	ASW	1 *m* NaCl + 0.15 *m* KNO_3	CC-II	100	6.08	1.00	0.15	0.15	−65
LL060603812251.164 [DIRS 178269]	JE1771	MCA	ASW	3.5 *m* NaCl + 0.175 *m* KNO_3	CC-II	60	6.30	3.50	0.175	0.05	−6
LL060603812251.164 [DIRS 178269]	JE3204	MCA	ASW	3.5 *m* NaCl + 0.175 *m* KNO_3	CC-II	60	6.30	3.50	0.175	0.05	−73

Source DTN	Specimen ID	Sample Type	Material Condition	Electrolyte	Type of LC	Temperature (°C)	Calculated Pitzer pH	[Cl] molal	$[NO_3]$ molal	NO_3/Cl molal ratio	E_{crev} (mV vs. SSC)
LL060603812251.164 [DIRS 178269]	JE3232	MCA	ASW	3.5 *m* NaCl + 0.175 *m* KNO_3	CC	80	6.10	3.50	0.175	0.05	–77
LL060603812251.164 [DIRS 178269]	JE3234	MCA	ASW	3.5 *m* NaCl + 0.175 *m* KNO_3	CC	80	6.10	3.50	0.175	0.05	–85
LL060603812251.164 [DIRS 178269]	JE3221	MCA	ASW	3.5 *m* NaCl + 0.175 *m* KNO_3	CC	100	5.94	3.50	0.175	0.05	–132
LL060603812251.164 [DIRS 178269]	JE3239	MCA	ASW	3.5 *m* NaCl + 0.175 *m* KNO_3	CC	100	5.94	3.50	0.175	0.05	–104
LL060603812251.164 [DIRS 178269]	JE1773	MCA	ASW	3.5 *m* NaCl + 0.525 *m* KNO_3	CC	100	5.94	3.50	0.525	0.15	–85
LL060603812251.164 [DIRS 178269]	DEA3385	MCA	MA	3.5 *m* NaCl + 0.525 *m* KNO_3	CC	100	5.94	3.50	0.525	0.15	–88
LL060603812251.164 [DIRS 178269]	DEA3390	MCA	MA	3.5 *m* NaCl + 0.525 *m* KNO_3	CC	100	5.94	3.50	0.525	0.15	–3
LL060603812251.164 [DIRS 178269]	JE3242	MCA	ASW	3.5 *m* NaCl + 0.525 *m* KNO_3	CC-II	100	5.94	3.50	0.525	0.15	–96
LL060603812251.164 [DIRS 178269]	JE3210	MCA	ASW	6 *m* NaCl + 0.3 *m* KNO_3	CC-II	60	6.15	6.00	0.3	0.05	–18
LL060603812251.164 [DIRS 178269]	JE3313	MCA	MA	6 *m* NaCl + 0.3 *m* KNO_3	CC	80	5.96	6.00	0.3	0.05	–114
LL060603812251.164 [DIRS 178269]	JE3314	MCA	MA	6 *m* NaCl + 0.3 *m* KNO_3	CC	80	5.96	6.00	0.3	0.05	–107
LL060603812251.164 [DIRS 178269]	JE3217	MCA	ASW	6 *m* NaCl + 0.3 *m* KNO_3	CC-II	80	5.96	6.00	0.3	0.05	–95
LL060603812251.164 [DIRS 178269]	JE3228	MCA	ASW	6 *m* NaCl + 0.3 *m* KNO_3	CC-II	80	5.96	6.00	0.3	0.05	–97
LL060603812251.164 [DIRS 178269]	JE3201	MCA	ASW	6 *m* NaCl + 0.3 *m* KNO_3	CC	100	5.80	6.00	0.3	0.05	–88
LL060603812251.164 [DIRS 178269]	JE3223	MCA	ASW	6 *m* NaCl + 0.3 *m* KNO_3	CC	100	5.80	6.00	0.3	0.05	–120
LL060603812251.164 [DIRS 178269]	KE0358	PCA	ASW	6 *m* NaCl + 0.3 *m* KNO_3	CC	100	5.80	6.00	0.3	0.05	–93

Source DTN	Specimen ID	Sample Type	Material Condition	Electrolyte	Type of LC	Temperature (°C)	Calculated Pitzer pH	[Cl] molal	[NO_3] molal	NO_3/Cl molal ratio	E_{rcrev} (mV vs. SSC)
LL060603812251.164 [DIRS 178269]	KE0359	PCA	ASW	6 *m* NaCl + 0.3 *m* KNO_3	CC	100	5.80	6.00	0.3	0.05	−61
LL060603812251.164 [DIRS 178269]	JE3315	MCA	MA	6 *m* NaCl + 0.3 *m* KNO_3	CC	100	5.80	6.00	0.3	0.05	−88
LL060603812251.164 [DIRS 178269]	JE3316	MCA	MA	6 *m* NaCl + 0.3 *m* KNO_3	CC	100	5.80	6.00	0.3	0.05	−79
LL060603812251.164 [DIRS 178269]	JE3317	MCA	MA	6 *m* NaCl + 0.9 *m* KNO_3	CC	80	5.97	6.00	0.90	0.15	−52
LL060603812251.164 [DIRS 178269]	JE3318	MCA	MA	6 *m* NaCl + 0.9 *m* KNO_3	CC	80	5.97	6.00	0.90	0.15	−27
LL060603812251.164 [DIRS 178269]	JE3203	MCA	ASW	6 *m* NaCl + 0.9 *m* KNO_3	CC-II	80	5.97	6.00	0.90	0.15	26
LL060603812251.164 [DIRS 178269]	JE3319	MCA	MA	6 *m* NaCl + 0.9 *m* KNO_3	CC	100	5.81	6.00	0.90	0.15	−85
LL060603812251.164 [DIRS 178269]	JE3320	MCA	MA	6 *m* NaCl + 0.9 *m* KNO_3	CC	100	5.81	6.00	0.90	0.15	−89
LL060603812251.164 [DIRS 178269]	JE3215	MCA	ASW	6 *m* NaCl + 0.9 *m* KNO_3	CC-II	100	5.81	6.00	0.90	0.15	−85
LL060603812251.164 [DIRS 178269]	JE3240	MCA	ASW	6 *m* NaCl + 0.9 *m* KNO_3	CC-II	100	5.81	6.00	0.90	0.15	−39
LL050302312251.129 [DIRS 173921]	AY005	PCA	ASW − Mockup	6 *m* NaCl + 0.9 *m* KNO_3	CC	100	5.81	6.00	0.90	0.15	−75
LL050302312251.129 [DIRS 173921]	AY006	PCA	ASW − Mockup	6 *m* NaCl + 0.9 *m* KNO_3	CC	100	5.81	6.00	0.90	0.15	−74
LL060801812251.168 [DIRS 179386]	JE3284	MCA	ASW	10 *m* $CaCl_2$ + 0.5 *m* $Ca(NO_3)_2$	LC	100	3.89	20.00	1.00	0.05	−41
LL060801812251.168 [DIRS 179386]	JE3270	MCA	ASW	10 *m* $CaCl_2$ + 0.5 *m* $Ca(NO_3)_2$	LC	100	3.89	20.00	1.00	0.05	−39
LL060801812251.168 [DIRS 179386]	JE3285	MCA	ASW	10 *m* $CaCl_2$ + 1.5 *m* $Ca(NO_3)_2$	LC	100	4.38	20.00	3.00	0.15	18
LL060801812251.168 [DIRS 179386]	KE0369	PCA	ASW	10 *m* $CaCl_2$ + 5 *m* $Ca(NO_3)_2$	LC	100	5.39	20.00	10.00	0.50	76

Source DTN	Specimen ID	Sample Type	Material Condition	Electrolyte	Type of LC	Temperature (°C)	Calculated Pitzer pH	[Cl] molal	[NO_3] molal	NO_3/Cl molal ratio	E_{rcrev} (mV vs. SSC)
LL060801812251.168 [DIRS 179386]	KE0371	PCA	ASW	10 *m* $CaCl_2$ + 5 *m* $Ca(NO_3)_2$	LC	100	5.39	20.00	10.00	0.50	83
LL060801812251.168 [DIRS 179386]	KE0370	PCA	ASW	10 *m* $CaCl_2$ + 5 *m* $Ca(NO_3)_2$	LC	100	5.39	20.00	10.00	0.50	87
LL060801812251.168 [DIRS 179386]	JE3286	MCA	ASW	10 *m* $CaCl_2$ + 5 *m* $Ca(NO_3)_2$	LC	100	5.39	20.00	10.00	0.50	105
LL060801812251.168 [DIRS 179386]	KE0372	PCA	ASW	10 *m* $CaCl_2$ + 5 *m* $Ca(NO_3)_2$	LC	100	5.39	20.00	10.00	0.50	179

Sources: DTNs: LL060904312 251.186 [DIRS 178283], file: *NoCO2GetEQData.xls* (calculated Pitzer pH and chloride- and nitrate-ion concentration values); LL060904312251.186 [DIRS 178283] file: *NoCO2GetEQData.xls* (Pitzer pH values and molalities (if solution concentration was expressed in molarity)). Pitzer pH and molalities were extracted electronically (from worksheets copied from DTN: LL060904312251.186 [DIRS 178283], *file: NoCO2GetEQData.xls*) using the "VLOOKUP" Excel command.
All other columns are from DTNs: LL040902712251.119 [DIRS 173720], file: *Reduced Data Ahmet Yilmaz WBL 11Feb05.xls*; LL050302312251.129 [DIRS 173921], file: *Mockup Developed RBR 21May05.xls*; LL060603812251.164 [DIRS 178269], file: *Rep Pot N06022 vs Temp NaCl + KNO3 60-100C RBR 07Aug06.xls*; LL060700312251.166 [DIRS 179385], file: *Rep Pot N06022 vs Temp 5M CaCl2 RBR 19Dec06.xls*; LL060801812251.168 [DIRS 179386], file: *Rep Pot N06022 High Temp High NO3 RBR.xls*; LL060803712251.170 [DIRS 179387], file: *Rep Pot N06022 vs Temp NaCl RBR 07Oct06.xls* as noted in column 1.

NOTES: Samples W6, B3, and P5 were verified to have crevice corrosion in DTN: LL040902712251.119 [DIRS 173720], file: *05606 Rebak.pdf.*
DTN: LL050302312251.129 [DIRS 173921], file: *Mockup Developed RBR 21May05.xls*, indicates that specimens were prepared from mockup containers using hockey pucks removed from the longitudinal weld. Therefore, specimens AY005, AY006, AY007, AY008, AY009, and AY010 are ASW. Specimen KE0572 (shaded line on fourth page of table) was not used in the final version of the crevice repassivation potential model, as it was determined to be an outlier.

ASW = as-welded, CC = crevice corrosion, CC-II = crevice corrosion type II, LC = localized corrosion, MA = mill-annealed, MCA = multiple crevice assembly, PCA = prism crevice assembly.

INTENTIONALLY LEFT BLANK

APPENDIX X
MATHCAD WORKSHEETS FOR REGRESSION ANALYSIS OF THE CORROSION POTENTIAL MODEL AND CREVICE REPASSIVATION POTENTIAL MODEL AND FOR LOCALIZED CORROSION SUSCEPTIBILITY ANALYSES

APPENDIX X – MATHCAD WORKSHEETS FOR REGRESSION ANALYSIS OF THE CORROSION POTENTIAL MODEL AND CREVICE REPASSIVATION POTENTIAL MODEL AND FOR LOCALIZED CORROSION SUSCEPTIBILITY ANALYSES

This worksheet fits the crevice repassivation potential data to the following functional form:

$$E_{rcrev} = a_o + a_1 T + a_2 \ln\left[Cl^-\right] + a_3 \frac{\left[NO_3^-\right]}{\left[Cl^-\right]} + a_4 T \cdot \left[Cl^-\right] + \varepsilon_{rcrev}$$

Dat :=

ErcrevData3.txt Read in the data

Dat =

	Specimen ID	Temp (°C)	pH	[Cl] (m)	[NO_3] (m)	NO_3/Cl	E_{rcrev} (mV SSC)
	0	1	2	3	4	5	6
0	"KE0614"	60.00	6.51	$5.00 \cdot 10^{-4}$	0.00	0.00	339.00
1	"KE0117"	90.00	6.21	$5.00 \cdot 10^{-4}$	0.00	0.00	214.00
2	"KE0618"	60.00	6.51	$5.80 \cdot 10^{-3}$	0.00	0.00	359.00
3	"KE0617"	60.00	6.51	0.05	0.00	0.00	161.00
4	"KE0610"	60.00	6.45	0.51	0.00	0.00	61.00
5	"JE3321"	60.00	6.45	1.02	0.00	0.00	84.00
6	"JE3322"	60.00	6.45	1.02	0.00	0.00	28.00
7	"DEA3129"	90.00	6.16	1.02	0.00	0.00	-24.00
8	"JE3324"	90.00	6.16	1.02	0.00	0.00	-126.00
9	"JE3328"	90.00	6.16	1.02	0.00	0.00	-109.00
10	"DEA3262"	90.00	6.16	1.02	0.00	0.00	-42.00
11	"W6"	90.00	6.16	1.02	0.00	0.00	-104.00
12	"B3"	90.00	6.16	1.02	0.00	0.00	-134.00
13	"P5"	90.00	6.16	1.02	0.00	0.00	-114.00
14	"DEA3263"	90.00	6.16	1.02	0.00	0.00	-45.00
15	"AY009"	90.00	6.16	1.02	0.00	0.00	-54.00

$Y := Dat^{\langle 6 \rangle}$ E_{rcrev}

$X^{\langle 0 \rangle} := \overrightarrow{\left(\frac{Dat^{\langle 1 \rangle}}{Dat^{\langle 1 \rangle}}\right)}$ Dummy column of 1's - used to get constant in model

$X^{\langle 1 \rangle} := Dat^{\langle 1 \rangle}$ T °C

$X^{\langle 2 \rangle} := \ln\left(Dat^{\langle 3 \rangle}\right)$ ln(Cl)

$X^{\langle 3 \rangle} := \frac{Dat^{\langle 4 \rangle}}{Dat^{\langle 3 \rangle}}$ NO_3/Cl Ratio

$X^{\langle 4 \rangle} := \overrightarrow{\left(Dat^{\langle 1 \rangle} \cdot Dat^{\langle 3 \rangle}\right)}$ T x Cl

Regression Coefficients

$b := \left(X^T \cdot X\right)^{-1} \cdot X^T \cdot Y$ $\quad b^T = (183.686 \;\; -2.919 \;\; -46.109 \;\; 580.849 \;\; 0.057)$

$SStot := \sum (Y - mean(Y))^2$ $\quad SStot = 2.095 \times 10^6$ Sum of Squares total

$SSres := \sum (Y - X \cdot b)^2$ $\quad SSres = 4.353 \times 10^5$ Sum of Squares residual

$SSreg := \sum (X \cdot b - mean(Y))^2$ $\quad SSreg = 1.660 \times 10^6$ Sum of Squares regression or "Explained SS"

$Rsq := 1 - \frac{SSres}{SStot}$ $\quad Rsq = 0.792$ Coefficient of determination

Evaluate the standard deviation and variance of the error term ε_{rcrev}

$N := length(Y)$ $\quad K := cols(X)$

$s_{rcrev} := \sqrt{\frac{SSres}{N - K}}$ $\quad s_{rcrev} = 52.993$ $\quad s_{rcrev}^2 = 2.808 \times 10^3$

Covariance of coefficients

$\Sigma := s_{rcrev}^2 \cdot \left(X^T \cdot X\right)^{-1}$

$$\Sigma = \begin{pmatrix} 4.660E{+}002 & -5.394E{+}000 & -1.278E{+}001 & 1.207E{+}002 & 4.865E{-}002 \\ -5.394E{+}000 & 7.005E{-}002 & 1.268E{-}001 & -1.756E{+}000 & -1.141E{-}003 \\ -1.278E{+}001 & 1.268E{-}001 & 1.350E{+}001 & 1.955E{+}000 & -2.827E{-}002 \\ 1.207E{+}002 & -1.756E{+}000 & 1.955E{+}000 & 8.984E{+}002 & -3.456E{-}002 \\ 4.865E{-}002 & -1.141E{-}003 & -2.827E{-}002 & -3.456E{-}002 & 1.395E{-}004 \end{pmatrix}$$

$b^T = (183.686 \;\; -2.919 \;\; -46.109 \;\; 580.849 \;\; 0.057)$ Coefficients

$\sqrt{diag(\Sigma)}^T = (21.587 \;\; 0.265 \;\; 3.675 \;\; 29.974 \;\; 0.012)$ Standard deviations of coefficients

Function to evaluate median values and prediction intervals.
z corresponds to how many standard deviations at which to evaluate the prediction interval.

$$Ercrev0(T, pH, Cl, NO3, z) := \left| \begin{array}{l} R2 \leftarrow \min\left(1, \frac{NO3}{\max(Cl, 0.0005)}\right) \\ Cl \leftarrow \max(0.0005, \min(Cl, 20)) \\ Xc \leftarrow [1 \;\; T \;\; \ln(Cl) \;\; R2 \;\; T \cdot (Cl)] \\ Xc \cdot b + z \cdot \sqrt{Xc \cdot \Sigma \cdot (Xc)^T + s_{rcrev}^2} \end{array} \right.$$

Comparison of Model Predictions to Input Data

$out0^{\langle 0 \rangle} := \overrightarrow{Ercrev0\left(Dat^{\langle 1 \rangle}, Dat^{\langle 2 \rangle}, Dat^{\langle 3 \rangle}, Dat^{\langle 4 \rangle}, 0\right)}$ Median

$out0^{\langle 1 \rangle} := \overrightarrow{Ercrev0\left(Dat^{\langle 1 \rangle}, Dat^{\langle 2 \rangle}, Dat^{\langle 3 \rangle}, Dat^{\langle 4 \rangle}, -2\right)}$

$out0^{\langle 2 \rangle} := \overrightarrow{Ercrev0\left(Dat^{\langle 1 \rangle}, Dat^{\langle 2 \rangle}, Dat^{\langle 3 \rangle}, Dat^{\langle 4 \rangle}, 2\right)}$ ±2 SD prediction intervals

$out0^{\langle 3 \rangle} := Dat^{\langle 6 \rangle}$ Raw data

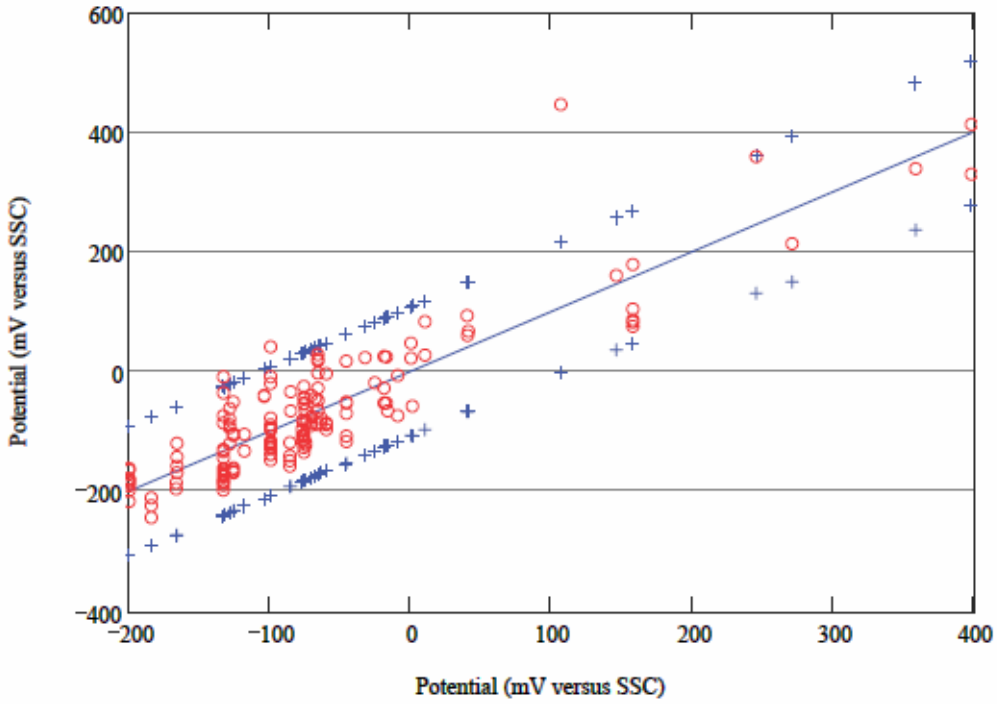

$$\left(Dat^{T}\right)^{\langle 50 \rangle} = \begin{pmatrix} \text{"KE0572"} \\ 110.000 \\ 3.090 \\ 8.000 \\ 4.000 \\ 0.500 \\ 446.000 \end{pmatrix}$$

$Ercrev0\left(Dat_{50,1}, Dat_{50,2}, Dat_{50,3}, Dat_{50,4}, 0\right) = 108$

$Ercrev0\left(Dat_{50,1}, Dat_{50,2}, Dat_{50,3}, Dat_{50,4}, -3\right) = -57$

$Ercrev0\left(Dat_{50,1}, Dat_{50,2}, Dat_{50,3}, Dat_{50,4}, 3\right) = 272$

Doing the same analysis removing the underestimated data point (KE0572) lying outside the previous prediction interval:

Dat1 := ErcrevData3m1.txt Read in the data

Dat1 =

	Specimen ID	Temp (°C)	pH	[Cl] (m)	[NO_3] (m)	NO_3/Cl	E_{rcrev} (mV SSC)
	0	1	2	3	4	5	6
0	"KE0614"	60.00	6.51	$5.00 \cdot 10^{-4}$	0.00	0.00	339.00
1	"KE0117"	90.00	6.21	$5.00 \cdot 10^{-4}$	0.00	0.00	214.00
2	"KE0618"	60.00	6.51	$5.80 \cdot 10^{-3}$	0.00	0.00	359.00
3	"KE0617"	60.00	6.51	0.05	0.00	0.00	161.00
4	"KE0610"	60.00	6.45	0.51	0.00	0.00	61.00
5	"JE3321"	60.00	6.45	1.02	0.00	0.00	84.00
6	"JE3322"	60.00	6.45	1.02	0.00	0.00	28.00
7	"DEA3129"	90.00	6.16	1.02	0.00	0.00	-24.00
8	"JE3324"	90.00	6.16	1.02	0.00	0.00	-126.00
9	"JE3328"	90.00	6.16	1.02	0.00	0.00	-109.00
10	"DEA3262"	90.00	6.16	1.02	0.00	0.00	-42.00
11	"W6"	90.00	6.16	1.02	0.00	0.00	-104.00
12	"B3"	90.00	6.16	1.02	0.00	0.00	-134.00
13	"P5"	90.00	6.16	1.02	0.00	0.00	-114.00
14	"DEA3263"	90.00	6.16	1.02	0.00	0.00	-45.00
15	"AY009"	90.00	6.16	1.02	0.00	0.00	-54.00

$rY := Dat1^{\langle 6 \rangle}$ E_{rcrev}

$rX^{\langle 0 \rangle} := \left(\frac{\overrightarrow{Dat1^{\langle 1 \rangle}}}{Dat1^{\langle 1 \rangle}}\right)$ Dummy column of 1's - used to get constant in model

$rX^{\langle 1 \rangle} := Dat1^{\langle 1 \rangle}$ T °C

$rX^{\langle 2 \rangle} := \ln\left(Dat1^{\langle 3 \rangle}\right)$ ln(Cl)

$rX^{\langle 3 \rangle} := \frac{Dat1^{\langle 4 \rangle}}{Dat1^{\langle 3 \rangle}}$ NO_3/Cl Ratio

$rX^{\langle 4 \rangle} := \overrightarrow{\left(Dat1^{\langle 1 \rangle} \cdot Dat1^{\langle 3 \rangle}\right)}$ T x Cl

Regression Coefficients

$rb := \left(rX^{T} \cdot rX\right)^{-1} \cdot rX^{T} \cdot rY \qquad rb^{T} = (190.242 \quad -3.008 \quad -46.800 \quad 535.625 \quad 0.061)$

$SStot := \sum (rY - mean(rY))^{2} \qquad SStot = 1.828 \times 10^{6}$ Sum of Squares total

$SSres := \sum (rY - rX \cdot rb)^{2} \qquad SSres = 3.126 \times 10^{5}$ Sum of Squares residual

$SSreg := \sum (rX \cdot rb - mean(rY))^{2} \qquad SSreg = 1.515 \times 10^{6}$ Sum of Squares regression or "Explained SS"

$Rsq := 1 - \frac{SSres}{SStot} \qquad Rsq = 0.829$ Coefficient of determination

Evaluate the standard deviation and variance of the error term ε_{rcrev}

$N := length(rY) \qquad K := cols(rX)$

$s_{rcrev} := \sqrt{\frac{SSres}{N - K}} \qquad s_{rcrev} = 45.055 \qquad s_{rcrev}^{2} =$

Covariance of coefficients

$r\Sigma := s_{rcrev}^{2} \cdot \left(rX^{T} \cdot rX\right)^{-1}$

$$r\Sigma = \begin{pmatrix} 3.376E{+}002 & -3.909E{+}000 & -9.310E{+}000 & 8.236E{+}001 & 3.559E{-}002 \\ -3.909E{+}000 & 5.077E{-}002 & 9.271E{-}002 & -1.202E{+}000 & -8.308E{-}004 \\ -9.310E{+}000 & 9.271E{-}002 & 9.770E{+}000 & 1.930E{+}000 & -2.048E{-}002 \\ 8.236E{+}001 & -1.202E{+}000 & 1.930E{+}000 & 6.833E{+}002 & -2.790E{-}002 \\ 3.559E{-}002 & -8.308E{-}004 & -2.048E{-}002 & -2.790E{-}002 & 1.011E{-}004 \end{pmatrix}$$

$rb^{T} = (190.242 \quad -3.008 \quad -46.800 \quad 535.625 \quad 0.061)$ Coefficients

$\sqrt{diag(r\Sigma)}^{T} = (18.373 \quad 0.225 \quad 3.126 \quad 26.140 \quad 0.010)$ Standard deviations of coefficients

Function to evaluate median values and prediction intervals.
z corresponds to how many standard deviations at which to evaluate the prediction interval.

$$Ercrev(T, pH, Cl, NO3, z) := \left| \begin{array}{l} R2 \leftarrow \min\left(1, \frac{NO3}{\max(Cl, 0.0005)}\right) \\ Cl \leftarrow \max(0.0005, \min(Cl, 20)) \\ Xc \leftarrow [1 \quad T \quad \ln(Cl) \quad R2 \quad T \cdot (Cl)] \\ Xc \cdot rb + z \cdot \sqrt{Xc \cdot r\Sigma \cdot (Xc)^{T} + s_{rcrev}^{2}} \end{array} \right.$$

Although E_{rcrev} does not depend on pH, pH was left in the argument list to more easily facillitate comparisions between E_{corr} and E_{rcrev} (i.e., each function has the same argument list

Comparison of Model Predictions to Input Data

$out1^{\langle 0 \rangle} := \overrightarrow{Ercrev\left(Dat1^{\langle 1 \rangle}, Dat1^{\langle 2 \rangle}, Dat1^{\langle 3 \rangle}, Dat1^{\langle 4 \rangle}, 0\right)}$ Median

$out1^{\langle 1 \rangle} := \overrightarrow{Ercrev\left(Dat1^{\langle 1 \rangle}, Dat1^{\langle 2 \rangle}, Dat1^{\langle 3 \rangle}, Dat1^{\langle 4 \rangle}, -2\right)}$ ±2 SD prediction intervals

$out1^{\langle 2 \rangle} := \overrightarrow{Ercrev\left(Dat1^{\langle 1 \rangle}, Dat1^{\langle 2 \rangle}, Dat1^{\langle 3 \rangle}, Dat1^{\langle 4 \rangle}, 2\right)}$

$out1^{\langle 3 \rangle} := Dat1^{\langle 6 \rangle}$ Raw data

WRITEPRN("PErcrev_vs_Data.txt") := out1 Output to text file

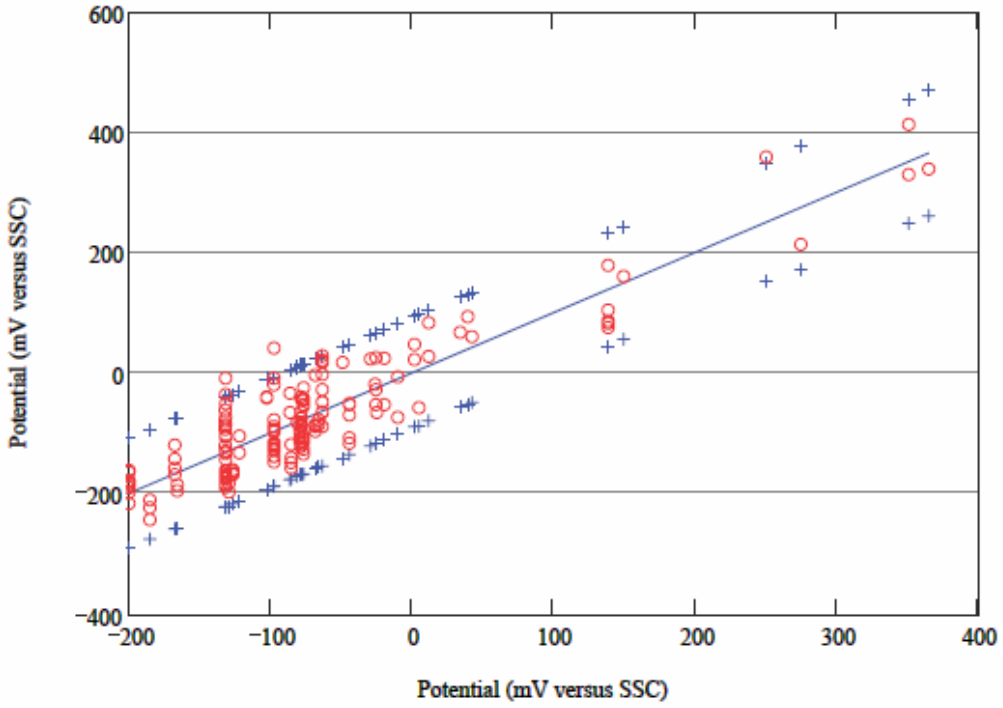

This worksheet fits the long-term corrosion potential data to the following functional form:

$$E_{corr} = c_o + c_1 T + c_2 pH + c_3 \frac{[NO_3^-]}{[Cl^-]} + c_4 T \frac{[NO_3^-]}{[Cl^-]} + c_5 pH \frac{[NO_3^-]}{[Cl^-]} + c_6 pH \ln[Cl^-] + \varepsilon_{corr}$$

Dat2 := EcorrData3.txt Read in the data

Dat2 =

	Specimen ID	Temp (°C)	pH	[Cl] (m)	[NO_3] (m)	NO_3/Cl	E_{corr} (mV SSC)
	0	1	2	3	4	5	6
0	"KE0260"	120.00	5.17	10.00	10.00	1.00	482.00
1	"KE0261"	120.00	5.17	10.00	10.00	1.00	483.00
2	"KE0262"	120.00	5.17	10.00	10.00	1.00	483.00
3	"KE0263"	120.00	5.17	10.00	10.00	1.00	483.00
4	"JE2074"	120.00	5.17	10.00	10.00	1.00	447.00
5	"JE2075"	120.00	5.17	10.00	10.00	1.00	453.00
6	"KE0256"	100.00	5.28	10.00	10.00	1.00	263.00
7	"KE0257"	100.00	5.28	10.00	10.00	1.00	244.00
8	"KE0258"	100.00	5.28	10.00	10.00	1.00	234.00
9	"KE0259"	100.00	5.28	10.00	10.00	1.00	215.00
10	"JE2072"	100.00	5.28	10.00	10.00	1.00	173.00
11	"JE2073"	100.00	5.28	10.00	10.00	1.00	190.00
12	"KE0252"	80.00	5.56	3.50	0.18	0.05	31.00
13	"KE0255"	80.00	5.56	3.50	0.18	0.05	27.00
14	"JE2070"	80.00	5.56	3.50	0.18	0.05	38.00
15	"JE2071"	80.00	5.56	3.50	0.18	0.05	2.00

$rY2 := Dat2^{\langle 6 \rangle}$ E_{corr}

$rX2^{\langle 0 \rangle} := \overrightarrow{\left(\frac{Dat2^{\langle 1 \rangle}}{Dat2^{\langle 1 \rangle}}\right)}$ Dummy column of 1's - used to get constant in model

$rX2^{\langle 1 \rangle} := Dat2^{\langle 1 \rangle}$ T °C

$rX2^{\langle 2 \rangle} := Dat2^{\langle 2 \rangle}$ pH

$rX2^{\langle 3 \rangle} := \frac{Dat2^{\langle 4 \rangle}}{Dat2^{\langle 3 \rangle}}$ NO_3/Cl Ratio

$rX2^{\langle 4 \rangle} := \overrightarrow{\left(Dat2^{\langle 1 \rangle} \cdot rX2^{\langle 3 \rangle}\right)}$ T x Ratio

$rX2^{\langle 5 \rangle} := \overrightarrow{\left(Dat2^{\langle 2 \rangle} \cdot rX2^{\langle 3 \rangle}\right)}$ pH x Ratio

$rX2^{\langle 6 \rangle} := \overrightarrow{\left(Dat2^{\langle 2 \rangle} \cdot \ln\left(Dat2^{\langle 3 \rangle}\right)\right)}$ pH x ln[Cl]

Regression Coefficients

$rb2 := \left(rX2^{T} \cdot rX2\right)^{-1} \cdot rX2^{T} \cdot rY2$ $rb2^{T} = (1051.219 \ -3.024 \ -155.976 \ -1352.040 \ 10.875 \ 137.856 \ -8.498)$

$SStot := \sum (rY2 - mean(rY2))^{2}$ $SStot = 6.909 \times 10^{6}$ Sum of Squares total

$SSres := \sum (rY2 - rX2 \cdot rb2)^{2}$ $SSres = 8.870 \times 10^{5}$ Sum of Squares residual

$SSreg := \sum (rX2 \cdot rb2 - mean(rY2))^{2}$ $SSreg = 6.022 \times 10^{6}$ Sum of Squares regression or "Explained SS"

$Rsq := 1 - \frac{SSres}{SStot}$ $Rsq = 0.872$ Coefficient of determination

Evaluate the standard deviation and variance of the error term ε_{corr}

$N := length(rY2)$ $K := cols(rX2)$

$s_{corr} := \sqrt{\frac{SSres}{N - K}}$ $s_{corr} = 85.265$ $s_{corr}^{2} = 7270.141$

Covariance of coefficients

$r\Sigma 2 := s_{corr}^{2} \cdot \left(rX2^{T} \cdot rX2\right)^{-1}$

$$r\Sigma 2 = \begin{pmatrix} 1.435E+004 & -1.031E+002 & -9.152E+002 & -2.762E+004 & 1.802E+002 & 1.884E+003 & -1.660E+001 \\ -1.031E+002 & 9.539E-001 & 2.770E+000 & 1.846E+002 & -1.519E+000 & -6.817E+000 & -7.543E-002 \\ -9.152E+002 & 2.770E+000 & 1.321E+002 & 1.971E+003 & -6.909E+000 & -2.515E+002 & 4.409E+000 \\ -2.762E+004 & 1.846E+002 & 1.971E+003 & 6.362E+004 & -4.223E+002 & -4.107E+003 & 5.959E+001 \\ 1.802E+002 & -1.519E+000 & -6.909E+000 & -4.223E+002 & 3.573E+000 & 1.337E+001 & -2.622E-001 \\ 1.884E+003 & -6.817E+000 & -2.515E+002 & -4.107E+003 & 1.337E+001 & 5.363E+002 & -6.697E+000 \\ -1.660E+001 & -7.543E-002 & 4.409E+000 & 5.959E+001 & -2.622E-001 & -6.697E+000 & 6.418E-001 \end{pmatrix}$$

$rb2^{T} = (1051.219 \ -3.024 \ -155.976 \ -1352.040 \ 10.875 \ 137.856 \ -8.498)$ Coefficients

$\sqrt{diag(r\Sigma 2)}^{T} = (119.774 \ 0.977 \ 11.495 \ 252.224 \ 1.890 \ 23.158 \ 0.801)$ Standard deviations of coefficients

Function to evaluate median values and prediction intervals.
z corresponds to how many standard deviations at which to evaluate the prediction interval.

$$Ecorr(T, pH, Cl, NO3, z) := \left| \begin{array}{l} R2 \leftarrow \min\left(1, \frac{NO3}{\max(Cl, 0.0005)}\right) \\ pH \leftarrow \min(pH, 10) \\ Cl \leftarrow \max(0.0005, \min(Cl, 20)) \\ Xc \leftarrow (1 \ \ T \ \ pH \ \ R2 \ \ T \cdot R2 \ \ pH \cdot R2 \ \ pH \cdot \ln(Cl)) \\ Xc \cdot rb2 + z \cdot \sqrt{Xc \cdot r\Sigma 2 \cdot (Xc)^{T} + s_{corr}^{2}} \end{array} \right.$$

Comparison of Model Predictions to Input Data

$\overrightarrow{out2^{\langle 0\rangle} := Econ\left(Dat2^{\langle 1\rangle}, Dat2^{\langle 2\rangle}, Dat2^{\langle 3\rangle}, Dat2^{\langle 4\rangle}, 0\right)}$ Median values

$\overrightarrow{out2^{\langle 1\rangle} := Econ\left(Dat2^{\langle 1\rangle}, Dat2^{\langle 2\rangle}, Dat2^{\langle 3\rangle}, Dat2^{\langle 4\rangle}, -2\right)}$

$\overrightarrow{out2^{\langle 2\rangle} := Econ\left(Dat2^{\langle 1\rangle}, Dat2^{\langle 2\rangle}, Dat2^{\langle 3\rangle}, Dat2^{\langle 4\rangle}, 2\right)}$ ±2 SD prediction intervals

$out2^{\langle 3\rangle} := Dat2^{\langle 6\rangle}$ Long-term corrosion potential data

WRITEPRN("PEcorr_vs_Data.txt") := out2 Output to text file

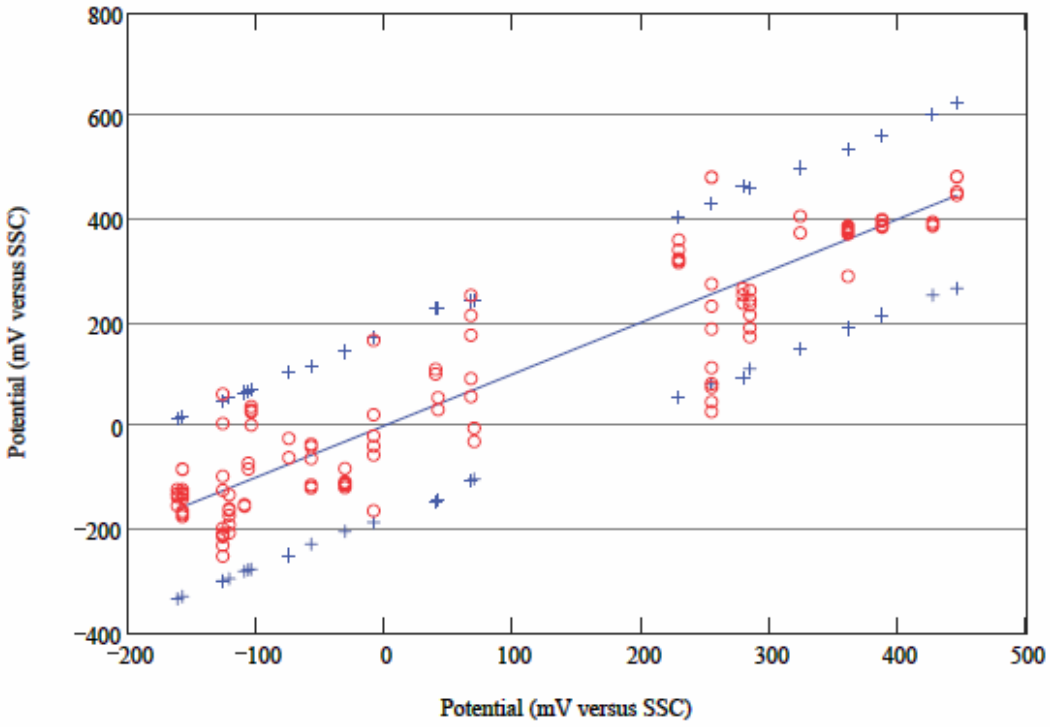

$Np := 100$ Number of points at which to evaluate is Np+1 (indexing starts at zero)

$nn := 0..Np$ Range variable takes integer values between zero and Np

E_{rcrev} and E_{corr} vs. Temperature at the following [Cl], [NO3], and pH

$Cl := 6$ $NO3 := 1.8$ $pH := 7$ $\frac{NO3}{Cl} = 0.300$

$Temp_{nn} := 30 + \frac{120 - 30}{Np} \cdot nn$ $out^{\langle 0 \rangle} := Temp$

$out^{\langle 1 \rangle} := \overrightarrow{Ercrev(Temp, pH, Cl, NO3, 0)}$ $out^{\langle 6 \rangle} := \overrightarrow{Ecorr(Temp, pH, Cl, NO3, 0)}$

$out^{\langle 2 \rangle} := \overrightarrow{Ercrev(Temp, pH, Cl, NO3, -1)}$ $out^{\langle 7 \rangle} := \overrightarrow{Ecorr(Temp, pH, Cl, NO3, -1)}$

$out^{\langle 3 \rangle} := \overrightarrow{Ercrev(Temp, pH, Cl, NO3, 1)}$ $out^{\langle 8 \rangle} := \overrightarrow{Ecorr(Temp, pH, Cl, NO3, 1)}$

$out^{\langle 4 \rangle} := \overrightarrow{Ercrev(Temp, pH, Cl, NO3, -2)}$ $out^{\langle 9 \rangle} := \overrightarrow{Ecorr(Temp, pH, Cl, NO3, -2)}$

$out^{\langle 5 \rangle} := \overrightarrow{Ercrev(Temp, pH, Cl, NO3, 2)}$ $out^{\langle 10 \rangle} := \overrightarrow{Ecorr(Temp, pH, Cl, NO3, 2)}$

$WRITEPRN("dEvsT\_pH7Cl6N1p8.txt") := out$ Write to file

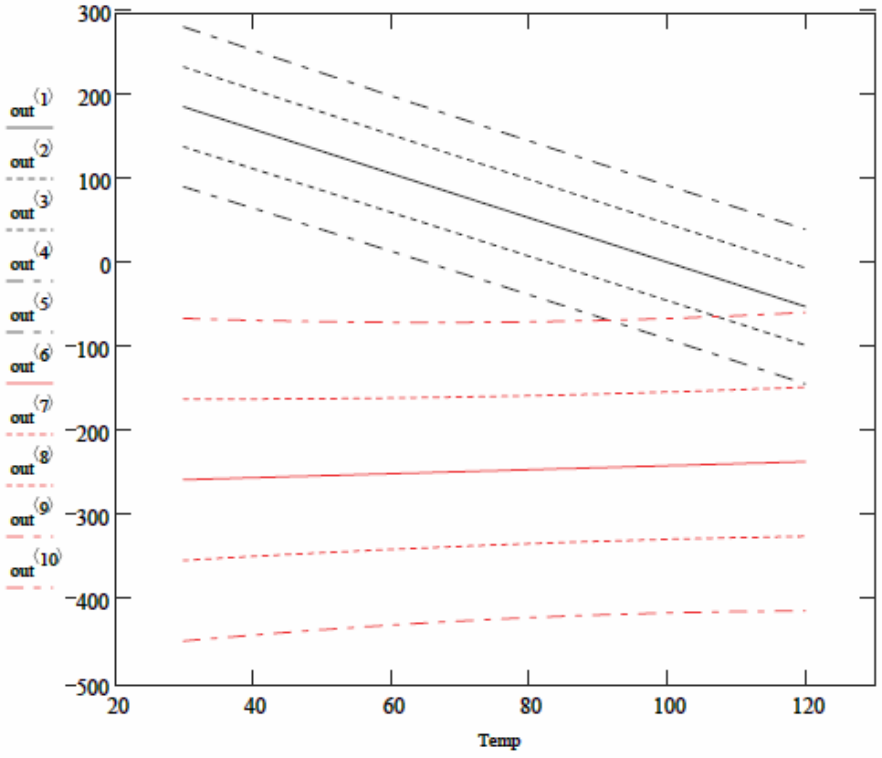

E_{rcrev} and E_{corr} vs. Temperature at the following [Cl], [NO3], and pH

$Cl := 6 \quad NO3 := 1.8 \quad pH := 5$

$Temp_{nn} := 30 + \frac{120 - 30}{Np} \cdot nn \qquad out^{\langle 0 \rangle} := Temp$

$out^{\langle 1 \rangle} := \overrightarrow{Ercrev(Temp, pH, Cl, NO3, 0)} \qquad out^{\langle 6 \rangle} := \overrightarrow{Ecorr(Temp, pH, Cl, NO3, 0)}$

$out^{\langle 2 \rangle} := \overrightarrow{Ercrev(Temp, pH, Cl, NO3, -1)} \qquad out^{\langle 7 \rangle} := \overrightarrow{Ecorr(Temp, pH, Cl, NO3, -1)}$

$out^{\langle 3 \rangle} := \overrightarrow{Ercrev(Temp, pH, Cl, NO3, 1)} \qquad out^{\langle 8 \rangle} := \overrightarrow{Ecorr(Temp, pH, Cl, NO3, 1)}$

$out^{\langle 4 \rangle} := \overrightarrow{Ercrev(Temp, pH, Cl, NO3, -2)} \qquad out^{\langle 9 \rangle} := \overrightarrow{Ecorr(Temp, pH, Cl, NO3, -2)}$

$out^{\langle 5 \rangle} := \overrightarrow{Ercrev(Temp, pH, Cl, NO3, 2)} \qquad out^{\langle 10 \rangle} := \overrightarrow{Ecorr(Temp, pH, Cl, NO3, 2)}$

$WRITEPRN("dEvsT\_pH5Cl6N1p8.txt") := out$ Write to file

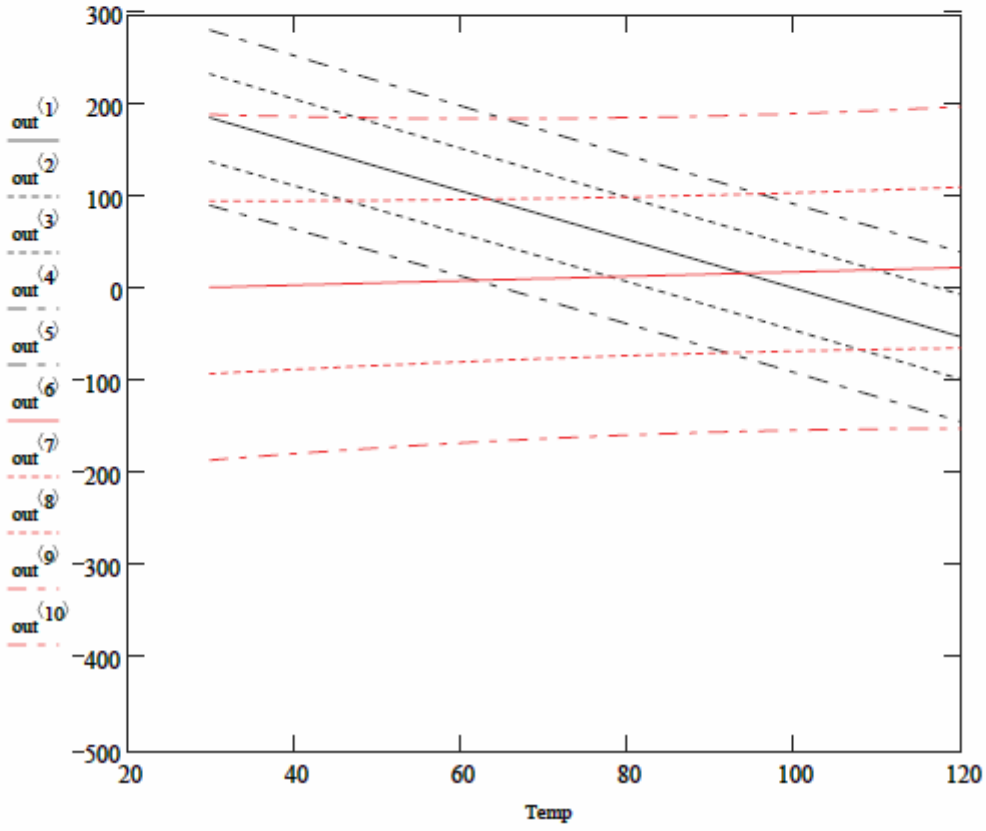

E_{rcrev} and E_{corr} vs. Temperature at the following [Cl], [NO3], and pH

$Cl := 6 \quad NO3 := 1.8 \quad pH := 4$

$$Temp_{nn} := 30 + \frac{120 - 30}{Np} \cdot nn \qquad out^{\langle 0 \rangle} := Temp$$

$out^{\langle 1 \rangle} := \overrightarrow{Ercrev(Temp, pH, Cl, NO3, 0)}$ $\quad out^{\langle 6 \rangle} := \overrightarrow{Ecorr(Temp, pH, Cl, NO3, 0)}$

$out^{\langle 2 \rangle} := \overrightarrow{Ercrev(Temp, pH, Cl, NO3, -1)}$ $\quad out^{\langle 7 \rangle} := \overrightarrow{Ecorr(Temp, pH, Cl, NO3, -1)}$

$out^{\langle 3 \rangle} := \overrightarrow{Ercrev(Temp, pH, Cl, NO3, 1)}$ $\quad out^{\langle 8 \rangle} := \overrightarrow{Ecorr(Temp, pH, Cl, NO3, 1)}$

$out^{\langle 4 \rangle} := \overrightarrow{Ercrev(Temp, pH, Cl, NO3, -2)}$ $\quad out^{\langle 9 \rangle} := \overrightarrow{Ecorr(Temp, pH, Cl, NO3, -2)}$

$out^{\langle 5 \rangle} := \overrightarrow{Ercrev(Temp, pH, Cl, NO3, 2)}$ $\quad out^{\langle 10 \rangle} := \overrightarrow{Ecorr(Temp, pH, Cl, NO3, 2)}$

$WRITEPRN("dEvsT\_pH4Cl6N1p8.txt") := out$ Write to file

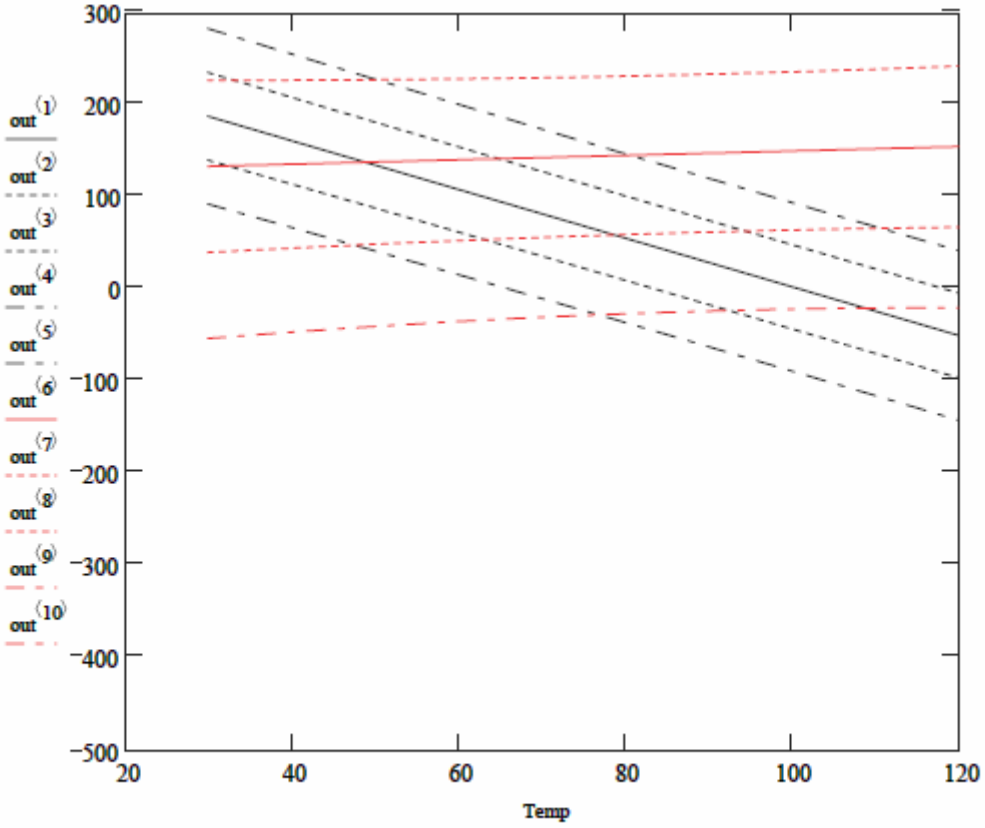

E_{rcrev} and E_{corr} vs. Temperature at the following [Cl], [NO3], and pH

$Cl := 6 \quad NO3 := 3 \quad pH := 4 \qquad \frac{NO3}{Cl} = 0.500$

$Temp_{nn} := 30 + \frac{120 - 30}{Np} \cdot nn \qquad out^{\langle 0 \rangle} := Temp$

$out^{\langle 1 \rangle} := \overrightarrow{Ercrev(Temp, pH, Cl, NO3, 0)} \qquad out^{\langle 6 \rangle} := \overrightarrow{Ecorr(Temp, pH, Cl, NO3, 0)}$

$out^{\langle 2 \rangle} := \overrightarrow{Ercrev(Temp, pH, Cl, NO3, -1)} \qquad out^{\langle 7 \rangle} := \overrightarrow{Ecorr(Temp, pH, Cl, NO3, -1)}$

$out^{\langle 3 \rangle} := \overrightarrow{Ercrev(Temp, pH, Cl, NO3, 1)} \qquad out^{\langle 8 \rangle} := \overrightarrow{Ecorr(Temp, pH, Cl, NO3, 1)}$

$out^{\langle 4 \rangle} := \overrightarrow{Ercrev(Temp, pH, Cl, NO3, -2)} \qquad out^{\langle 9 \rangle} := \overrightarrow{Ecorr(Temp, pH, Cl, NO3, -2)}$

$out^{\langle 5 \rangle} := \overrightarrow{Ercrev(Temp, pH, Cl, NO3, 2)} \qquad out^{\langle 10 \rangle} := \overrightarrow{Ecorr(Temp, pH, Cl, NO3, 2)}$

$WRITEPRN("dEvsT\_pH4Cl6N3.txt") := out$ Write to file

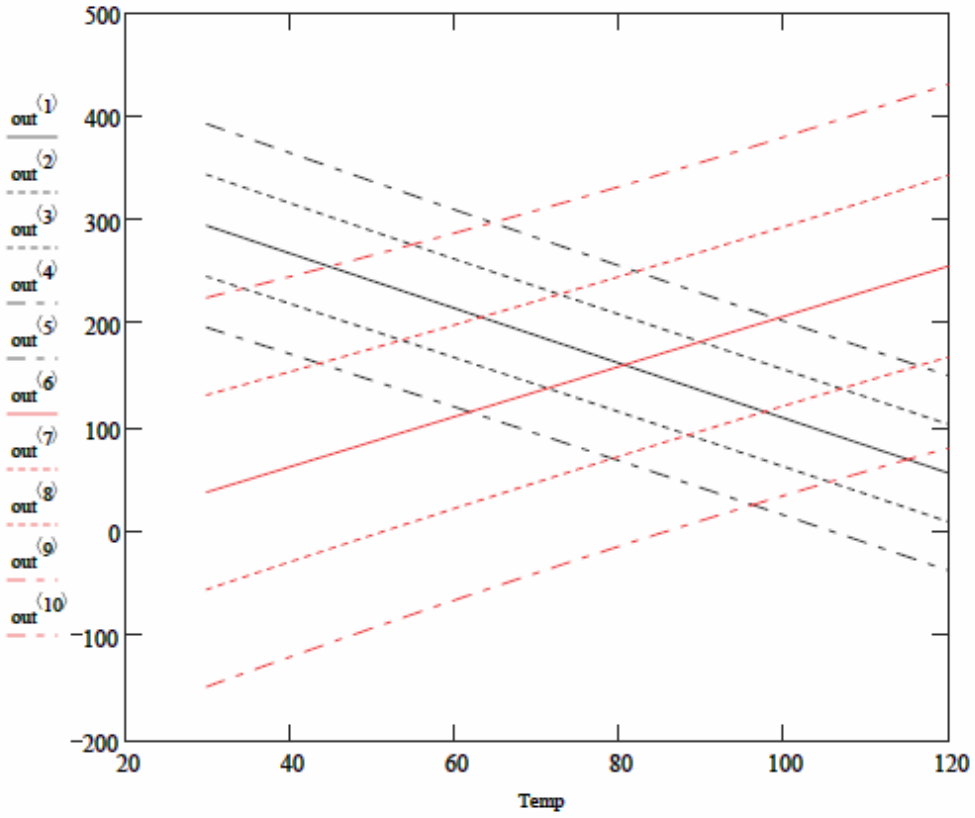

E_{rcrev} and E_{corr} vs. Temperature at the following [Cl], [NO3], and pH

$Cl := 6 \quad NO3 := 6 \quad pH := 4 \qquad \frac{NO3}{Cl} = 1.000$

$Temp_{nn} := 30 + \frac{120 - 30}{Np} \cdot nn \qquad out^{\langle 0 \rangle} := Temp$

$out^{\langle 1 \rangle} := \overrightarrow{Ercrev(Temp, pH, Cl, NO3, 0)} \qquad out^{\langle 6 \rangle} := \overrightarrow{Ecorr(Temp, pH, Cl, NO3, 0)}$

$out^{\langle 2 \rangle} := \overrightarrow{Ercrev(Temp, pH, Cl, NO3, -1)} \qquad out^{\langle 7 \rangle} := \overrightarrow{Ecorr(Temp, pH, Cl, NO3, -1)}$

$out^{\langle 3 \rangle} := \overrightarrow{Ercrev(Temp, pH, Cl, NO3, 1)} \qquad out^{\langle 8 \rangle} := \overrightarrow{Ecorr(Temp, pH, Cl, NO3, 1)}$

$out^{\langle 4 \rangle} := \overrightarrow{Ercrev(Temp, pH, Cl, NO3, -2)} \qquad out^{\langle 9 \rangle} := \overrightarrow{Ecorr(Temp, pH, Cl, NO3, -2)}$

$out^{\langle 5 \rangle} := \overrightarrow{Ercrev(Temp, pH, Cl, NO3, 2)} \qquad out^{\langle 10 \rangle} := \overrightarrow{Ecorr(Temp, pH, Cl, NO3, 2)}$

$WRITEPRN("dEvsT\_pH4Cl6N6.txt") := out$ Write to file

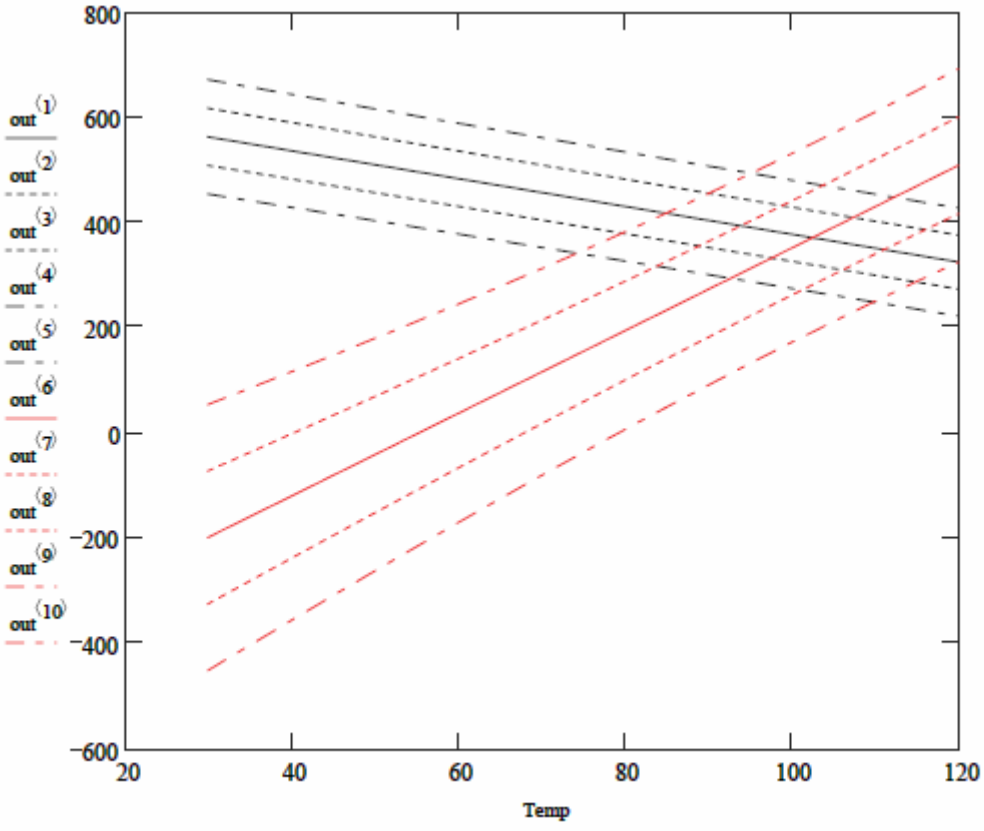

E_{rcrev} and E_{corr} vs. Chloride at the following T, [NO3], and pH

Temp := 90 NO3 := 3 pH := 7

$$Cl_{nn} := \frac{25}{Np} \cdot nn \qquad out^{\langle 0 \rangle} := Cl$$

$$out^{\langle 1 \rangle} := \overrightarrow{Ercrev(Temp, pH, Cl, NO3, 0)} \qquad out^{\langle 6 \rangle} := \overrightarrow{Ecorr(Temp, pH, Cl, NO3, 0)}$$

$$out^{\langle 2 \rangle} := \overrightarrow{Ercrev(Temp, pH, Cl, NO3, -1)} \qquad out^{\langle 7 \rangle} := \overrightarrow{Ecorr(Temp, pH, Cl, NO3, -1)}$$

$$out^{\langle 3 \rangle} := \overrightarrow{Ercrev(Temp, pH, Cl, NO3, 1)} \qquad out^{\langle 8 \rangle} := \overrightarrow{Ecorr(Temp, pH, Cl, NO3, 1)}$$

$$out^{\langle 4 \rangle} := \overrightarrow{Ercrev(Temp, pH, Cl, NO3, -2)} \qquad out^{\langle 9 \rangle} := \overrightarrow{Ecorr(Temp, pH, Cl, NO3, -2)}$$

$$out^{\langle 5 \rangle} := \overrightarrow{Ercrev(Temp, pH, Cl, NO3, 2)} \qquad out^{\langle 10 \rangle} := \overrightarrow{Ecorr(Temp, pH, Cl, NO3, 2)}$$

WRITEPRN("dEvsCl_T90pH7N3.txt") := out Write to file

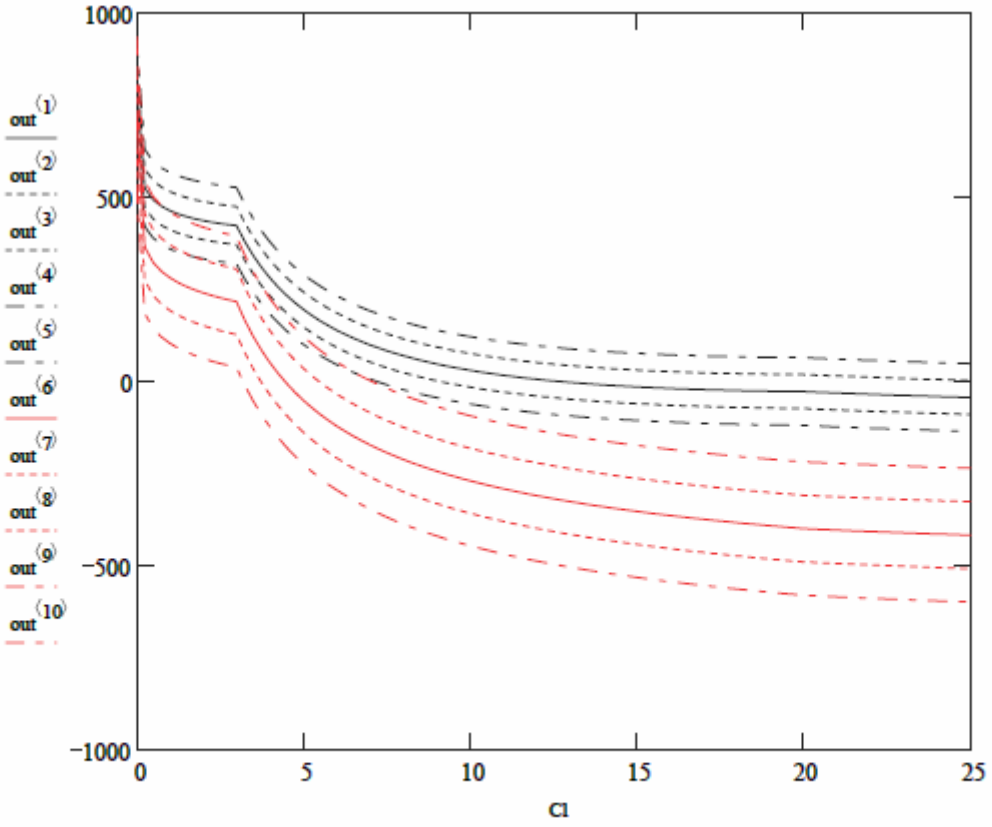

E_{rcrev} and E_{corr} vs. Chloride at the following T, [NO3], and pH

$Temp := 90 \quad NO3 := 3 \quad pH := 4$

$Cl_{nn} := \frac{25}{Np} \cdot nn$ $\quad out^{\langle 0 \rangle} := Cl$

$out^{\langle 1 \rangle} := \overrightarrow{Ercrev(Temp, pH, Cl, NO3, 0)}$ $\quad out^{\langle 6 \rangle} := \overrightarrow{Ecorr(Temp, pH, Cl, NO3, 0)}$

$out^{\langle 2 \rangle} := \overrightarrow{Ercrev(Temp, pH, Cl, NO3, -1)}$ $\quad out^{\langle 7 \rangle} := \overrightarrow{Ecorr(Temp, pH, Cl, NO3, -1)}$

$out^{\langle 3 \rangle} := \overrightarrow{Ercrev(Temp, pH, Cl, NO3, 1)}$ $\quad out^{\langle 8 \rangle} := \overrightarrow{Ecorr(Temp, pH, Cl, NO3, 1)}$

$out^{\langle 4 \rangle} := \overrightarrow{Ercrev(Temp, pH, Cl, NO3, -2)}$ $\quad out^{\langle 9 \rangle} := \overrightarrow{Ecorr(Temp, pH, Cl, NO3, -2)}$

$out^{\langle 5 \rangle} := \overrightarrow{Ercrev(Temp, pH, Cl, NO3, 2)}$ $\quad out^{\langle 10 \rangle} := \overrightarrow{Ecorr(Temp, pH, Cl, NO3, 2)}$

WRITEPRN("dEvsCl_T90pH4N3.txt") := out Write to file

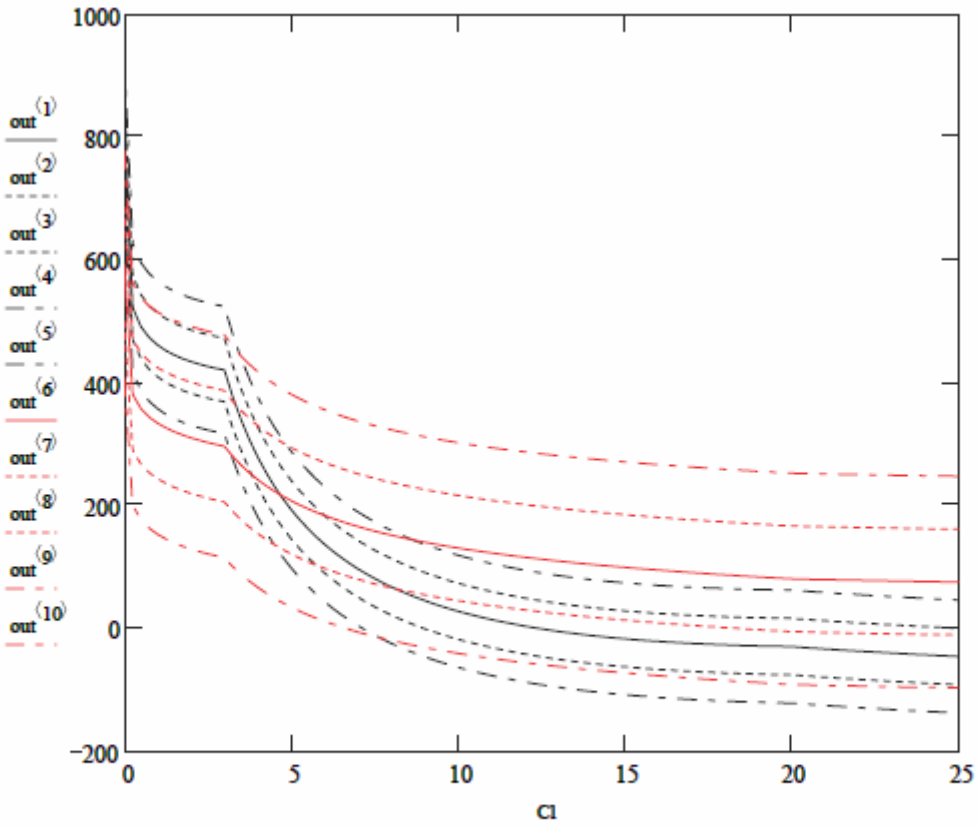

E_{rcrev} and E_{corr} vs. pH at the following T, [Cl], and [NO3]

$Temp := 90$ $Cl := 6$ $NO3 := 3$

$pH_{nn} := 2 + \frac{8-2}{Np} \cdot nn$ $out^{\langle 0 \rangle} := pH$

$out^{\langle 1 \rangle} := Ercrev(Temp, pH, Cl, NO3, 0)$ $out^{\langle 6 \rangle} := Ecorr(Temp, pH, Cl, NO3, 0)$

$out^{\langle 2 \rangle} := Ercrev(Temp, pH, Cl, NO3, -1)$ $out^{\langle 7 \rangle} := Ecorr(Temp, pH, Cl, NO3, -1)$

$out^{\langle 3 \rangle} := Ercrev(Temp, pH, Cl, NO3, 1)$ $out^{\langle 8 \rangle} := Ecorr(Temp, pH, Cl, NO3, 1)$

$out^{\langle 4 \rangle} := Ercrev(Temp, pH, Cl, NO3, -2)$ $out^{\langle 9 \rangle} := Ecorr(Temp, pH, Cl, NO3, -2)$

$out^{\langle 5 \rangle} := Ercrev(Temp, pH, Cl, NO3, 2)$ $out^{\langle 10 \rangle} := Ecorr(Temp, pH, Cl, NO3, 2)$

$WRITEPRN("dEvspH\_T90Cl6N3.txt") := out$ Write to file

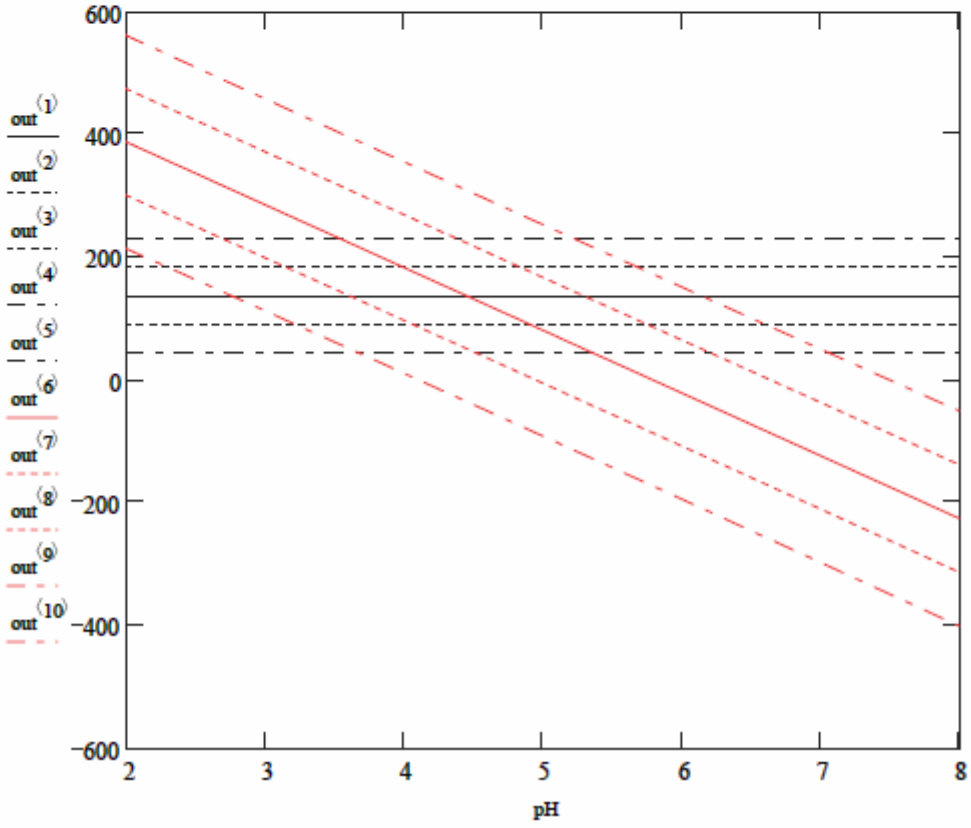

E_{rcrev} and E_{corr} vs. pH at the following T, [Cl], and [NO3]

Temp := 90 Cl := 6 NO3 := 6

$pH_{nn} := 2 + \frac{8-2}{Np} \cdot nn$ $out^{\langle 0 \rangle} := pH$

$out^{\langle 1 \rangle} := \overrightarrow{Ercrev(Temp, pH, Cl, NO3, 0)}$ $out^{\langle 6 \rangle} := \overrightarrow{Ecorr(Temp, pH, Cl, NO3, 0)}$

$out^{\langle 2 \rangle} := \overrightarrow{Ercrev(Temp, pH, Cl, NO3, -1)}$ $out^{\langle 7 \rangle} := \overrightarrow{Ecorr(Temp, pH, Cl, NO3, -1)}$

$out^{\langle 3 \rangle} := \overrightarrow{Ercrev(Temp, pH, Cl, NO3, 1)}$ $out^{\langle 8 \rangle} := \overrightarrow{Ecorr(Temp, pH, Cl, NO3, 1)}$

$out^{\langle 4 \rangle} := \overrightarrow{Ercrev(Temp, pH, Cl, NO3, -2)}$ $out^{\langle 9 \rangle} := \overrightarrow{Ecorr(Temp, pH, Cl, NO3, -2)}$

$out^{\langle 5 \rangle} := \overrightarrow{Ercrev(Temp, pH, Cl, NO3, 2)}$ $out^{\langle 10 \rangle} := \overrightarrow{Ecorr(Temp, pH, Cl, NO3, 2)}$

WRITEPRN("dEvspH_T90Cl6N6.txt") := out Write to file

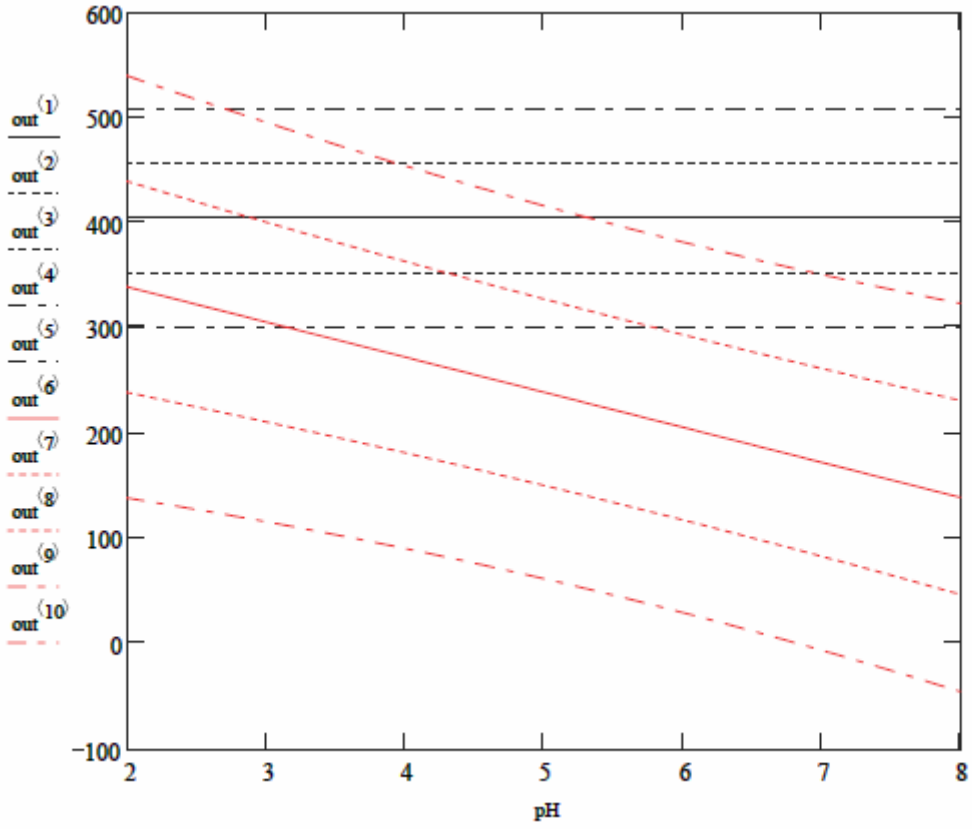

E_{rcrev} and E_{corr} vs. NO3 at the following T, [Cl], and pH

$Temp := 90 \qquad Cl := 6 \qquad pH := 7$

$NO3_{nn} := \frac{6}{Np} \cdot nn \qquad out^{\langle 0 \rangle} := NO3$

$out^{\langle 1 \rangle} := \overrightarrow{Ercrev(Temp, pH, Cl, NO3, 0)} \qquad out^{\langle 6 \rangle} := \overrightarrow{Ecorr(Temp, pH, Cl, NO3, 0)}$

$out^{\langle 2 \rangle} := \overrightarrow{Ercrev(Temp, pH, Cl, NO3, -1)} \qquad out^{\langle 7 \rangle} := \overrightarrow{Ecorr(Temp, pH, Cl, NO3, -1)}$

$out^{\langle 3 \rangle} := \overrightarrow{Ercrev(Temp, pH, Cl, NO3, 1)} \qquad out^{\langle 8 \rangle} := \overrightarrow{Ecorr(Temp, pH, Cl, NO3, 1)}$

$out^{\langle 4 \rangle} := \overrightarrow{Ercrev(Temp, pH, Cl, NO3, -2)} \qquad out^{\langle 9 \rangle} := \overrightarrow{Ecorr(Temp, pH, Cl, NO3, -2)}$

$out^{\langle 5 \rangle} := \overrightarrow{Ercrev(Temp, pH, Cl, NO3, 2)} \qquad out^{\langle 10 \rangle} := \overrightarrow{Ecorr(Temp, pH, Cl, NO3, 2)}$

$WRITEPRN("dEvsNO3\_T90Cl6pH7.txt") := out$ Write to file

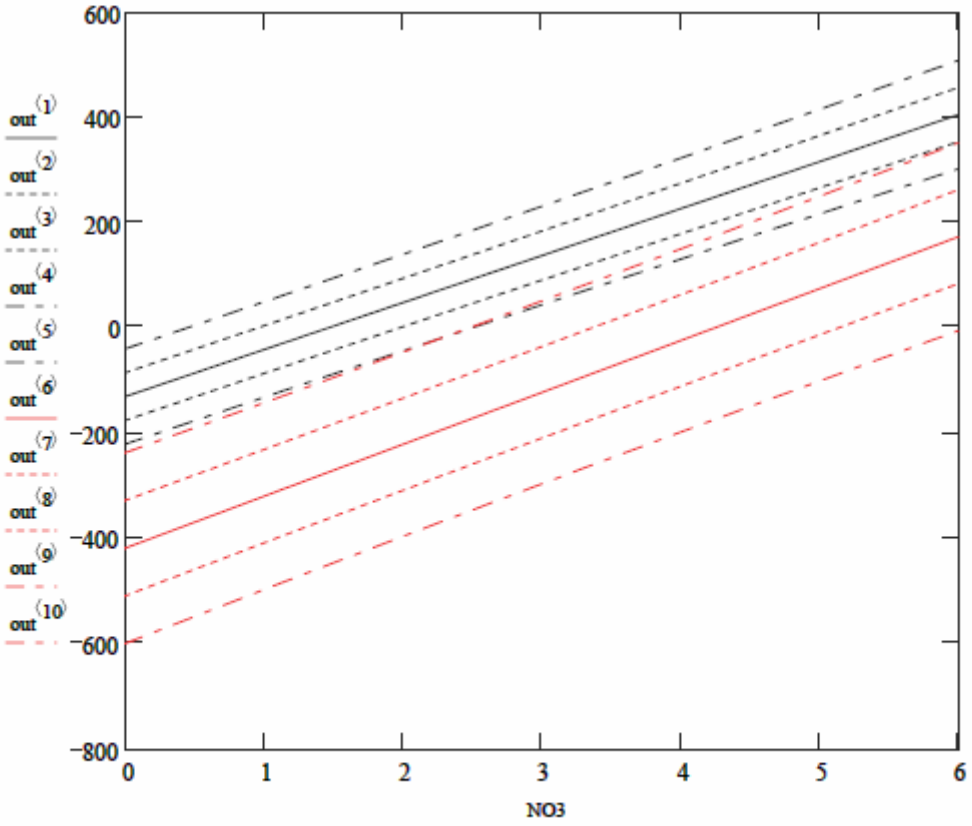

E_{rcrev} and E_{corr} vs. NO3 at the following T, [Cl], and pH

$Temp := 90 \qquad Cl := 6 \qquad pH := 4$

$$NO3_{nn} := \frac{6}{Np} \cdot nn \qquad out^{\langle 0 \rangle} := NO3$$

$$out^{\langle 1 \rangle} := \overrightarrow{Ercrev(Temp, pH, Cl, NO3, 0)} \qquad out^{\langle 6 \rangle} := \overrightarrow{Ecorr(Temp, pH, Cl, NO3, 0)}$$

$$out^{\langle 2 \rangle} := \overrightarrow{Ercrev(Temp, pH, Cl, NO3, -1)} \qquad out^{\langle 7 \rangle} := \overrightarrow{Ecorr(Temp, pH, Cl, NO3, -1)}$$

$$out^{\langle 3 \rangle} := \overrightarrow{Ercrev(Temp, pH, Cl, NO3, 1)} \qquad out^{\langle 8 \rangle} := \overrightarrow{Ecorr(Temp, pH, Cl, NO3, 1)}$$

$$out^{\langle 4 \rangle} := \overrightarrow{Ercrev(Temp, pH, Cl, NO3, -2)} \qquad out^{\langle 9 \rangle} := \overrightarrow{Ecorr(Temp, pH, Cl, NO3, -2)}$$

$$out^{\langle 5 \rangle} := \overrightarrow{Ercrev(Temp, pH, Cl, NO3, 2)} \qquad out^{\langle 10 \rangle} := \overrightarrow{Ecorr(Temp, pH, Cl, NO3, 2)}$$

$WRITEPRN("dEvsNO3\_T90Cl6pH4.txt") := out$ Write to file

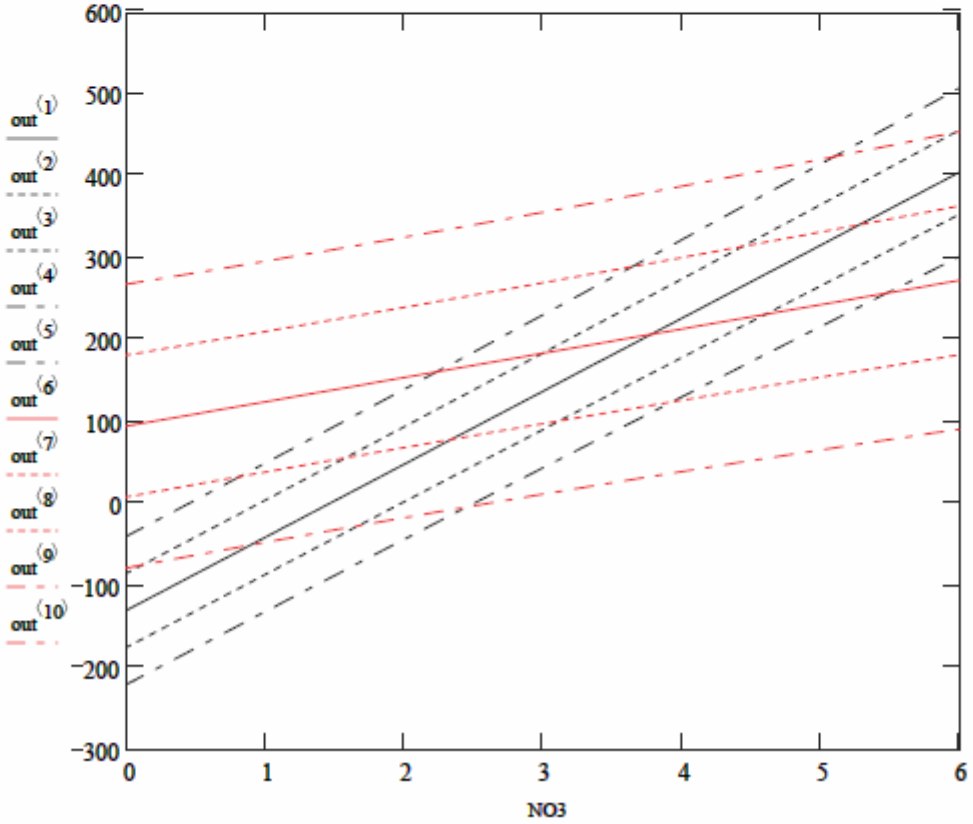

delE is the function describing ΔE = Ercrev - Ecorr. delE1 is constructed with a limiting chloride ion concentration of 20 molal (see the use min(Cl,20) used in the construction of Ecorr and Ercrev functions) and delE2 has no upper limiting chloride ion concentration. Comparision of delE1 and delE2 allows for evaluation of the use of a limiting chloride ion concentration on crevice corrosion initiation behavior of the crevice corrosion initiation model.

$$\mathbf{delE1}(T, pH, Cl, NO3, z) := \mathrm{Ercrev}(T, pH, Cl, NO3, -z) - \mathrm{Ecorr}(T, pH, Cl, NO3, z)$$

$$\mathbf{ErcrevU}(T, pH, Cl, NO3, z) := \left| \begin{array}{l} R2 \leftarrow \min\left(1, \dfrac{NO3}{\max(Cl, 0.0005)}\right) \\ Cl \leftarrow \max(0.0005, Cl) \\ Xc \leftarrow [1 \quad T \quad \ln(Cl) \quad R2 \quad T \cdot (Cl)] \\ Xc \cdot rb + z \cdot \sqrt{Xc \cdot r\Sigma \cdot (Xc)^T + s_{rcrev}^2} \end{array} \right.$$

$$\mathbf{EcorrU}(T, pH, Cl, NO3, z) := \left| \begin{array}{l} R2 \leftarrow \min\left(1, \dfrac{NO3}{\max(Cl, 0.0005)}\right) \\ pH \leftarrow \min(pH, 10) \\ Cl \leftarrow \max(0.0005, Cl) \\ Xc \leftarrow (1 \quad T \quad pH \quad R2 \quad T \cdot R2 \quad pH \cdot R2 \quad pH \cdot \ln(Cl)) \\ Xc \cdot rb2 + z \cdot \sqrt{Xc \cdot r\Sigma 2 \cdot (Xc)^T + s_{corr}^2} \end{array} \right.$$

$$\mathbf{delE2}(T, pH, Cl, NO3, z) := \mathrm{ErcrevU}(T, pH, Cl, NO3, -z) - \mathrm{EcorrU}(T, pH, Cl, NO3, z)$$

ΔE vs Cl and NO_3

$Nm := 100$ $np := 0..Nm$ $nt := 0..Nm$

$NO3_{nt,np} := \frac{10}{Nm} \cdot nt$ $Cl_{nt,np} := \frac{40}{Nm} \cdot np$

$TT := 120$ $ppH := 4$

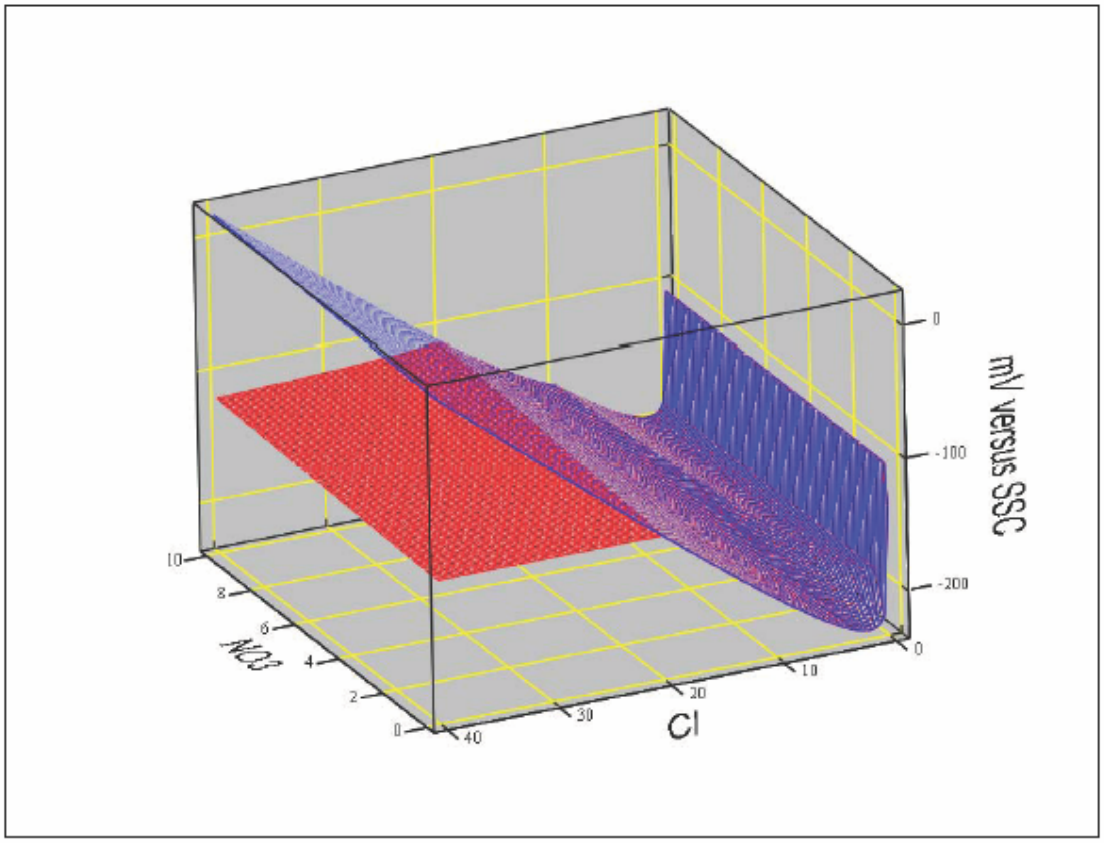

$\left(NO3, Cl, \overrightarrow{delE1(TT, ppH, Cl, NO3, 0)}\right), \left(NO3, Cl, \overrightarrow{delE2(TT, ppH, Cl, NO3, 0)}\right)$

Red Blue

Above 20 molal chloride ion concentration, delE2 exceeds delE1 indicating that it is conservative to use the functional form with a limiting chloride ion concentration (delE1)

TT := 60 ppH := 4

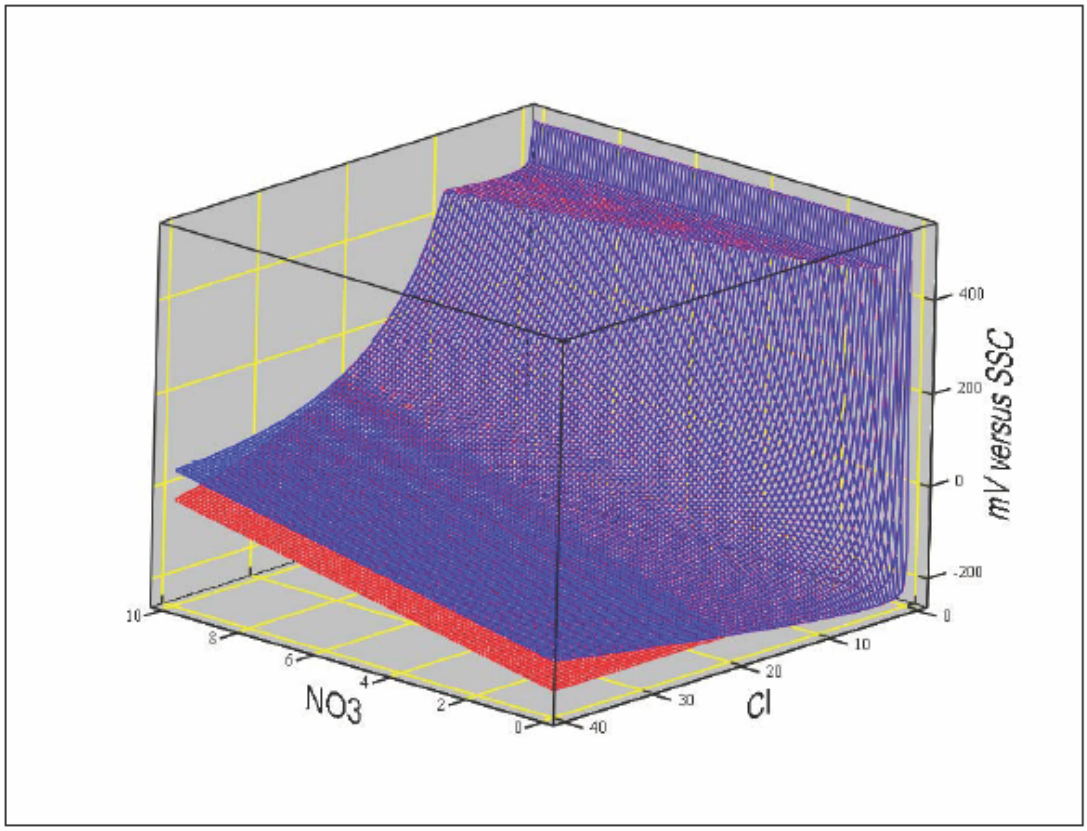

$\left(NO3, Cl, \overrightarrow{delE1(TT, ppH, Cl, NO3, 0)}\right), \left(NO3, Cl, \overrightarrow{delE2(TT, ppH, Cl, NO3, 0)}\right)$

Red Blue

Above 20 molal chloride ion concentration, delE2 exceeds delE1 indicating that it is conservative to use the functional form with a limiting chloride ion concentration (delE1)

TT := 120 ppH := 7

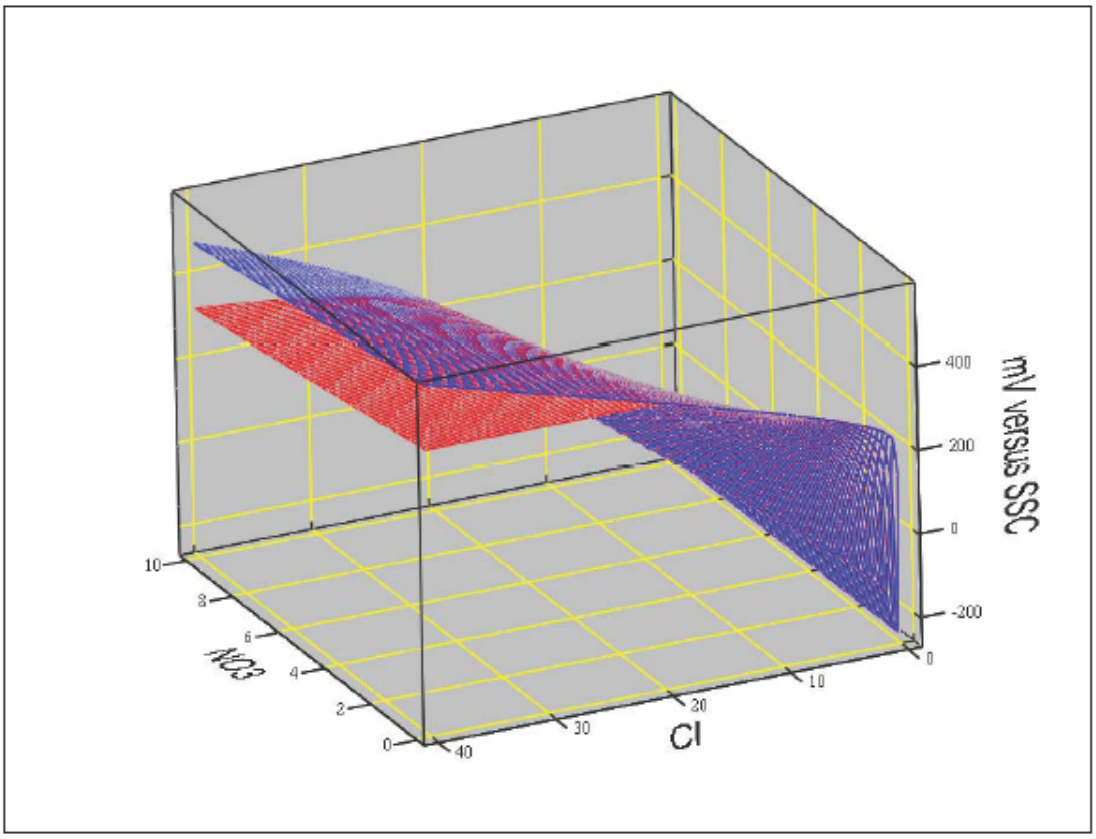

$\left(NO3, Cl, \overrightarrow{delE1(TT, ppH, Cl, NO3, 0)}\right), \left(NO3, Cl, \overrightarrow{delE2(TT, ppH, Cl, NO3, 0)}\right)$

Red Blue

Above 20 molal chloride ion concentration, delE2 exceeds delE1 indicating that it is conservative to use the functional form with a limiting chloride ion concentration (delE1)

TT := 60 ppH := 7

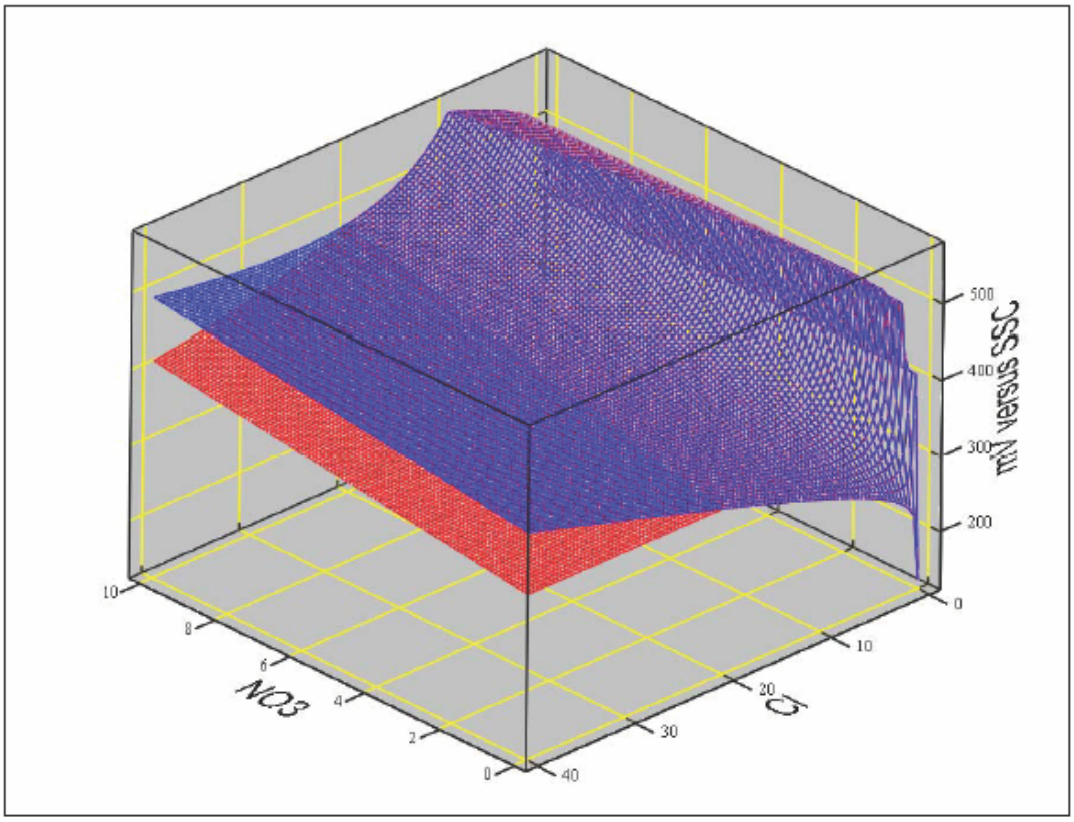

$\left(\overrightarrow{NO3, Cl, delE1(TT, ppH, Cl, NO3, 0)}\right), \left(\overrightarrow{NO3, Cl, delE2(TT, ppH, Cl, NO3, 0)}\right)$

Red Blue

Above 20 molal chloride ion concentration, delE2 exceeds delE1 indicating that it is conservative to use the functional form with a limiting chloride ion concentration (delE1)

INTENTIONALLY LEFT BLANK

APPENDIX XI
MATHCAD WORKSHEETS USED FOR MODEL VALIDATION

APPENDIX XI – MATHCAD WORKSHEETS USED FOR MODEL VALIDATION

This worksheet fits the crevice repassivation potential data to the following functional form:

$$E_{rcrev} = a_o + a_1 T + a_2 \ln[Cl^-] + a_3 \frac{[NO_3^-]}{[Cl^-]} + a_4 T \cdot [Cl^-] + \varepsilon_{rcrev}$$

Dat :=
ErcrevData3m1.txt Read in the data

Dat =

	Specimen ID	Temp (°C)	pH	[Cl] (m)	[NO_3] (m)	NO_3/Cl	E_{rcrev} (mV SSC)
	0	1	2	3	4	5	6
0	"KE0614"	60.00	6.51	$5.00 \cdot 10^{-4}$	0.00	0.00	339.00
1	"KE0117"	90.00	6.21	$5.00 \cdot 10^{-4}$	0.00	0.00	214.00
2	"KE0618"	60.00	6.51	$5.80 \cdot 10^{-3}$	0.00	0.00	359.00
3	"KE0617"	60.00	6.51	0.05	0.00	0.00	161.00
4	"KE0610"	60.00	6.45	0.51	0.00	0.00	61.00
5	"JE3321"	60.00	6.45	1.02	0.00	0.00	84.00
6	"JE3322"	60.00	6.45	1.02	0.00	0.00	28.00
7	"DEA3129"	90.00	6.16	1.02	0.00	0.00	-24.00
8	"JE3324"	90.00	6.16	1.02	0.00	0.00	-126.00
9	"JE3328"	90.00	6.16	1.02	0.00	0.00	-109.00
10	"DEA3262"	90.00	6.16	1.02	0.00	0.00	-42.00
11	"W6"	90.00	6.16	1.02	0.00	0.00	-104.00
12	"B3"	90.00	6.16	1.02	0.00	0.00	-134.00
13	"P5"	90.00	6.16	1.02	0.00	0.00	-114.00
14	"DEA3263"	90.00	6.16	1.02	0.00	0.00	-45.00
15	"AY009"	90.00	6.16	1.02	0.00	0.00	-54.00

$rY := Dat^{\langle 6 \rangle}$ E_{rcrev}

$rX^{\langle 0 \rangle} := \overrightarrow{\left(\frac{Dat^{\langle 1 \rangle}}{Dat^{\langle 1 \rangle}}\right)}$ Dummy column of 1's - used to get constant in model

$rX^{\langle 1 \rangle} := Dat^{\langle 1 \rangle}$ T °C

$rX^{\langle 2 \rangle} := \ln\left(Dat^{\langle 3 \rangle}\right)$ ln(Cl)

$rX^{\langle 3 \rangle} := \frac{Dat^{\langle 4 \rangle}}{Dat^{\langle 3 \rangle}}$ NO_3/Cl Ratio

$rX^{\langle 4 \rangle} := \overrightarrow{\left(Dat^{\langle 1 \rangle} \cdot Dat^{\langle 3 \rangle}\right)}$ T x Cl

Regression Coefficients

$$rb := \left(rX^{T} \cdot rX\right)^{-1} \cdot rX^{T} \cdot rY \qquad rb^{T} = (190.242 \quad -3.008 \quad -46.800 \quad 535.625 \quad 0.061)$$

$$SStot := \sum (rY - mean(rY))^{2} \qquad SStot = 1.828 \times 10^{6}$$ Sum of Squares total

$$SSres := \sum (rY - rX \cdot rb)^{2} \qquad SSres = 3.126 \times 10^{5}$$ Sum of Squares residual

$$SSreg := \sum (rX \cdot rb - mean(rY))^{2} \qquad SSreg = 1.515 \times 10^{6}$$ Sum of Squares regression or "Explained SS"

$$Rsq := 1 - \frac{SSres}{SStot} \qquad Rsq = 0.829$$ Coefficient of determination

Evaluate the standard deviation and variance of the error term ε_{rcrev}

$$N := length(rY) \qquad K := cols(rX)$$

$$s_{rcrev} := \sqrt{\frac{SSres}{N - K}} \qquad s_{rcrev} = 45.055 \qquad s_{rcrev}^{2} = 2.030 \times 10^{3}$$

Covariance of coefficients

$$r\Sigma := s_{rcrev}^{2} \cdot \left(rX^{T} \cdot rX\right)^{-1}$$

$$r\Sigma = \begin{pmatrix} 3.376E{+}002 & -3.909E{+}000 & -9.310E{+}000 & 8.236E{+}001 & 3.559E{-}002 \\ -3.909E{+}000 & 5.077E{-}002 & 9.271E{-}002 & -1.202E{+}000 & -8.308E{-}004 \\ -9.310E{+}000 & 9.271E{-}002 & 9.770E{+}000 & 1.930E{+}000 & -2.048E{-}002 \\ 8.236E{+}001 & -1.202E{+}000 & 1.930E{+}000 & 6.833E{+}002 & -2.790E{-}002 \\ 3.559E{-}002 & -8.308E{-}004 & -2.048E{-}002 & -2.790E{-}002 & 1.011E{-}004 \end{pmatrix}$$

$$rb^{T} = (190.242 \quad -3.008 \quad -46.800 \quad 535.625 \quad 0.061)$$ Coefficients

$$\sqrt{diag(r\Sigma)}^{T} = (18.373 \quad 0.225 \quad 3.126 \quad 26.140 \quad 0.010)$$ Standard deviations of coefficients

Function to evaluate median values and prediction intervals.
z corresponds to how many standard deviations at which to evaluate the prediction interval.

$$Ercrev(T, pH, Cl, NO3, z) := \left| \begin{array}{l} R2 \leftarrow \min\left(1, \frac{NO3}{\max(Cl, 0.0005)}\right) \\ Cl \leftarrow \max(0.0005, \min(Cl, 20)) \\ Xc \leftarrow [1 \quad T \quad \ln(Cl) \quad R2 \quad T \cdot (Cl)] \\ Xc \cdot rb + z \cdot \sqrt{Xc \cdot r\Sigma \cdot (Xc)^{T} + s_{rcrev}^{2}} \end{array} \right.$$

Although E_{rcrev} does not depend on pH, pH was left in the argument list to more easily facillitate comparisions between E_{corr} and E_{rcrev} (i.e., each function has the same argument list

This worksheet fits the long-term corrosion potential data to the following functional form:

$$E_{corr} = c_o + c_1 T + c_2 pH + c_3 \frac{[NO_3^-]}{[Cl^-]} + c_4 T \frac{[NO_3^-]}{[Cl^-]} + c_5 pH \frac{[NO_3^-]}{[Cl^-]} + c_6 pH \ln[Cl^-] + \varepsilon_{corr}$$

Dat2 := EcorrData3.txt Read in the data

Dat2 =

	Specimen ID	Temp (°C)	pH	[Cl] (m)	[NO_3] (m)	NO_3/Cl	E_{corr} (mV SSC)
	0	1	2	3	4	5	6
0	"KE0260"	120.00	5.17	10.00	10.00	1.00	482.00
1	"KE0261"	120.00	5.17	10.00	10.00	1.00	483.00
2	"KE0262"	120.00	5.17	10.00	10.00	1.00	483.00
3	"KE0263"	120.00	5.17	10.00	10.00	1.00	483.00
4	"JE2074"	120.00	5.17	10.00	10.00	1.00	447.00
5	"JE2075"	120.00	5.17	10.00	10.00	1.00	453.00
6	"KE0256"	100.00	5.28	10.00	10.00	1.00	263.00
7	"KE0257"	100.00	5.28	10.00	10.00	1.00	244.00
8	"KE0258"	100.00	5.28	10.00	10.00	1.00	234.00
9	"KE0259"	100.00	5.28	10.00	10.00	1.00	215.00
10	"JE2072"	100.00	5.28	10.00	10.00	1.00	173.00
11	"JE2073"	100.00	5.28	10.00	10.00	1.00	190.00
12	"KE0252"	80.00	5.56	3.50	0.18	0.05	31.00
13	"KE0255"	80.00	5.56	3.50	0.18	0.05	27.00
14	"JE2070"	80.00	5.56	3.50	0.18	0.05	38.00
15	"JE2071"	80.00	5.56	3.50	0.18	0.05	2.00

$rY2 := Dat2^{\langle 6 \rangle}$ E_{corr}

$rX2^{\langle 0 \rangle} := \overrightarrow{\left(\frac{Dat2^{\langle 1 \rangle}}{Dat2^{\langle 1 \rangle}}\right)}$ Dummy column of 1's - used to get constant in model

$rX2^{\langle 1 \rangle} := Dat2^{\langle 1 \rangle}$ T °C

$rX2^{\langle 2 \rangle} := Dat2^{\langle 2 \rangle}$ pH

$rX2^{\langle 3 \rangle} := \frac{Dat2^{\langle 4 \rangle}}{Dat2^{\langle 3 \rangle}}$ NO_3/Cl Ratio

$rX2^{\langle 4 \rangle} := \overrightarrow{\left(Dat2^{\langle 1 \rangle} \cdot rX2^{\langle 3 \rangle}\right)}$ T x Ratio

$rX2^{\langle 5 \rangle} := \overrightarrow{\left(Dat2^{\langle 2 \rangle} \cdot rX2^{\langle 3 \rangle}\right)}$ pH x Ratio

$rX2^{\langle 6 \rangle} := \overrightarrow{\left(Dat2^{\langle 2 \rangle} \cdot \ln\left(Dat2^{\langle 3 \rangle}\right)\right)}$ pH x ln[Cl]

Regression Coefficients

$$rb2 := \left(rX2^{T} \cdot rX2\right)^{-1} \cdot rX2^{T} \cdot rY2 \quad rb2^{T} = (1051.219 \;\; -3.024 \;\; -155.976 \;\; -1352.040 \;\; 10.875 \;\; 137.856 \;\; -8.498)$$

$SStot := \sum (rY2 - mean(rY2))^2$ $\quad SStot = 6.909 \times 10^6$ Sum of Squares total

$SSres := \sum (rY2 - rX2 \cdot rb2)^2$ $\quad SSres = 8.870 \times 10^5$ Sum of Squares residual

$SSreg := \sum (rX2 \cdot rb2 - mean(rY2))^2$ $\quad SSreg = 6.022 \times 10^6$ Sum of Squares regression or "Explained SS"

$Rsq := 1 - \frac{SSres}{SStot}$ $\quad Rsq = 0.872$ Coefficient of determination

Evaluate the standard deviation and variance of the error term ε_{corr}

$N := length(rY2)$ $\quad K := cols(rX2)$

$s_{corr} := \sqrt{\frac{SSres}{N - K}}$ $\quad s_{corr} = 85.265$ $\quad s_{corr}^{2} = 7.270 \times 10^3$

Covariance of coefficients

$$r\Sigma 2 := s_{corr}^{2} \cdot \left(rX2^{T} \cdot rX2\right)^{-1}$$

$$r\Sigma 2 = \begin{pmatrix} 1.435E{+}004 & -1.031E{+}002 & -9.152E{+}002 & -2.762E{+}004 & 1.802E{+}002 & 1.884E{+}003 & -1.660E{+}001 \\ -1.031E{+}002 & 9.539E{-}001 & 2.770E{+}000 & 1.846E{+}002 & -1.519E{+}000 & -6.817E{+}000 & -7.543E{-}002 \\ -9.152E{+}002 & 2.770E{+}000 & 1.321E{+}002 & 1.971E{+}003 & -6.909E{+}000 & -2.515E{+}002 & 4.409E{+}000 \\ -2.762E{+}004 & 1.846E{+}002 & 1.971E{+}003 & 6.362E{+}004 & -4.223E{+}002 & -4.107E{+}003 & 5.959E{+}001 \\ 1.802E{+}002 & -1.519E{+}000 & -6.909E{+}000 & -4.223E{+}002 & 3.573E{+}000 & 1.337E{+}001 & -2.622E{-}001 \\ 1.884E{+}003 & -6.817E{+}000 & -2.515E{+}002 & -4.107E{+}003 & 1.337E{+}001 & 5.363E{+}002 & -6.697E{+}000 \\ -1.660E{+}001 & -7.543E{-}002 & 4.409E{+}000 & 5.959E{+}001 & -2.622E{-}001 & -6.697E{+}000 & 6.418E{-}001 \end{pmatrix}$$

$rb2^{T} = (1051.219 \;\; -3.024 \;\; -155.976 \;\; -1352.040 \;\; 10.875 \;\; 137.856 \;\; -8.498)$ Coefficients

$\sqrt{diag(r\Sigma 2)}^{T} = (119.774 \;\; 0.977 \;\; 11.495 \;\; 252.224 \;\; 1.890 \;\; 23.158 \;\; 0.801)$ Standard deviations of coefficients

Function to evaluate median values and prediction intervals.
z corresponds to how many standard deviations at which to evaluate the prediction interval.

$$Ecorr(T, pH, Cl, NO3, z) := \left| \begin{array}{l} R2 \leftarrow \min\left(1, \frac{NO3}{\max(Cl, 0.0005)}\right) \\ pH \leftarrow \min(pH, 10) \\ Cl \leftarrow \max(0.0005, \min(Cl, 20)) \\ Xc \leftarrow (1 \;\; T \;\; pH \;\; R2 \;\; T{\cdot}R2 \;\; pH{\cdot}R2 \;\; pH{\cdot}\ln(Cl)) \\ Xc \cdot rb2 + z \cdot \sqrt{Xc \cdot r\Sigma 2 \cdot (Xc)^{T} + s_{corr}^{2}} \end{array} \right.$$

Long term corrosion potential model

Jayaweera et al. 2003 [DIRS 162225] - 80°C NaCl, nominal pH 3:

$$Ecorr\left[80, 3, 6.2, 0, \begin{pmatrix} -2 \\ 0 \\ 2 \end{pmatrix}\right] = \begin{pmatrix} 114 \\ 295 \\ 476 \end{pmatrix}$$ mV versus SSC

Jayaweera et al. measured -39 to 51 mV SSC

Andresen et al. 2003 [DIRS170360], Table 1-4; p. 66 and 78

Case 3 from DTN: LL060904312251.186 [DIRS 178283] is BSW solution and was determined to have a Pitzer pH of 8.58 at 110°C

$$Ecorr\left[110, 8.58, 4.62, 2.82, \begin{pmatrix} -2 \\ 0 \\ 2 \end{pmatrix}\right] = \begin{pmatrix} -279 \\ -104 \\ 70 \end{pmatrix}$$ mV versus SSC

Andresen et al. measured between -99 mV and -88 mV versus SSC

Determine molalities of chloride and nitrate ions:

$mwK := 39.10$ $mwCl := 35.45$

$mwNa := 22.99$ $mwNO3 := 14.01 + 3 \cdot 16$

Atomic weights from Sargent-Welch Scientific Company 1979 [DIRS 110056]

$$\frac{\frac{9.7}{mwK + mwCl} + \frac{8.8}{mwNa + mwCl}}{\frac{55.3}{1000}} = 5.08 \qquad \frac{\frac{13.6}{mwNa+mwNO3}}{\frac{55.3}{1000}} = 2.89$$

Using the molalities calculated from the solution composition:

$$Ecorr\left[110, 8.58, 5.08, 2.89, \begin{pmatrix} -2 \\ 0 \\ 2 \end{pmatrix}\right] = \begin{pmatrix} -328 \\ -154 \\ 20 \end{pmatrix}$$ mV versus SSC

Dunn [DIRS 164138] measured about -130 mV versus SCE (-88 mV versus SSC) in 4 M NaCl at 95°C

Case 13 from DTN: LL060904312251.186 [DIRS 178283] is 4 Molar (4.4 molal) NaCl solution and was determined to have a Pitzer pH of 5.55 at 95°C

$$\text{Ecorr}\left[95, 5.55, 4.4, 0, \begin{pmatrix} -2 \\ 0 \\ 2 \end{pmatrix}\right] = \begin{pmatrix} -345 \\ -172 \\ 2 \end{pmatrix} \text{ mV SSC}$$

$$\text{Ecorr}\left[95, 5.05, 4.4, 0, \begin{pmatrix} -2 \\ 0 \\ 2 \end{pmatrix}\right] = \begin{pmatrix} -260 \\ -87 \\ 85 \end{pmatrix} \text{ mV SSC}$$

$$\text{Ecorr}\left[95, 6.05, 4.4, 0, \begin{pmatrix} -2 \\ 0 \\ 2 \end{pmatrix}\right] = \begin{pmatrix} -431 \\ -256 \\ -81 \end{pmatrix} \text{ mV SSC}$$

Crevice repassivation potential model

The experimentally-determined crevice repassivation potentials for two specimens, DEA3130 (from DTN: LL060803712251.170 [DIRS179387], file: Rep Pot N06022 vs Temp NaCl RBR 07Oct06.xls) and KE0416 (from DTN: LL060603812251.164 [DIRS 178269], file: Rep Pot N06022 vs Temp NaCl + KNO3 60-100C RBR 07Aug06.xls) were not used in development of the crevice repassivation potential model and will be used for model validation. A measured crevice repassivation potential for specimen DEA3130 of -67 mV versus SSC was obtained in 1 M NaCl solution at 90°C and a measured crevice repassivation potential for specimen KE0416 of -77 mV versus SSC was obtained in 6 *m* NaCl + 0.9 *m* KNO_3 solution at 100°C

$$\text{Ercrev}\left[90, 6.16, 1.02, 0, \begin{pmatrix} -2 \\ 0 \\ 2 \end{pmatrix}\right] = \begin{pmatrix} -167 \\ -76 \\ 15 \end{pmatrix}$$

$$\text{Ercrev}\left[100, 5.81, 6, 0.9, \begin{pmatrix} -2 \\ 0 \\ 2 \end{pmatrix}\right] = \begin{pmatrix} -168 \\ -77 \\ 13 \end{pmatrix}$$

Repassivation model from the CNWRA (Dunn et al. 2005 [DIRS178451])

$$\mathrm{ErCNWRA}(T, Cl, NO3) := 1300 - 13.1 \cdot T + (-362.7 + 2.3 \cdot T) \cdot \log(Cl) + 800 \cdot \frac{\min\left(\frac{NO3}{Cl}, 0.1\right)}{0.1} + 42$$

pH and chloride and nitrate ion molalities are from DTN: LL060904312251.186 [DIRS178283]

1 M NaCl at 80°C

$$\mathrm{Ercrev}\left[80, 6.25, 1.02, 0, \begin{pmatrix} -2 \\ 0 \\ 2 \end{pmatrix}\right] = \begin{pmatrix} -137 \\ -46 \\ 44 \end{pmatrix} \qquad \mathrm{ErCNWRA}(80, 1, 0) = 294$$

4 M NaCl at 120°C

$$\mathrm{Ercrev}\left[120, 5.75, 4.40, 0, \begin{pmatrix} -2 \\ 0 \\ 2 \end{pmatrix}\right] = \begin{pmatrix} -300 \\ -208 \\ -116 \end{pmatrix} \qquad \mathrm{ErCNWRA}(120, 4, 0) = -282$$

5 M $CaCl_2$ at 105°C

$$\mathrm{Ercrev}\left[105, 4, 11.99, 0, \begin{pmatrix} -2 \\ 0 \\ 2 \end{pmatrix}\right] = \begin{pmatrix} -256 \\ -165 \\ -74 \end{pmatrix} \qquad \mathrm{ErCNWRA}(105, 10, 0) = -155$$

5 M $CaCl_2$ + 0.05 M $Ca(NO_3)_2$ at 120°C

$$\mathrm{Ercrev}\left[120, 3.96, 11.70, 0.12, \begin{pmatrix} -2 \\ 0 \\ 2 \end{pmatrix}\right] = \begin{pmatrix} -286 \\ -195 \\ -103 \end{pmatrix} \qquad \mathrm{ErCNWRA}(120, 10, 0.1) = -237$$

5 M $CaCl_2$ + 0.5 M $Ca(NO_3)_2$ at 105°C

$$\mathrm{Ercrev}\left[105, 3.15, 12.59, 1.26, \begin{pmatrix} -2 \\ 0 \\ 2 \end{pmatrix}\right] = \begin{pmatrix} -201 \\ -110 \\ -19 \end{pmatrix} \qquad \mathrm{ErCNWRA}(105, 10, 1) = 645$$

1 M $CaCl_2$ + 1 M $Ca(NO_3)_2$ at 120°C

$$\mathrm{Ercrev}\left[120, 5.82, 2.62, 2.58, \begin{pmatrix} -2 \\ 0 \\ 2 \end{pmatrix}\right] = \begin{pmatrix} 228 \\ 331 \\ 434 \end{pmatrix} \qquad \mathrm{ErCNWRA}(120, 2, 2) = 544$$

Ercrev - ErCNWRA vs Cl and NO_3

$Nm := 100$

$np := 0..Nm \quad nt := 0..Nm$ $\quad lc := 0.0005 \quad delE(T, pH, Cl, NO3, z)$

$NO3_{nt,np} := \frac{10}{Nm} \cdot nt$ $\quad Cl_{nt,np} := lc + \frac{20 - lc}{Nm} \cdot np$

$zero_{nt,np} := 0$ $\quad TT := 100$

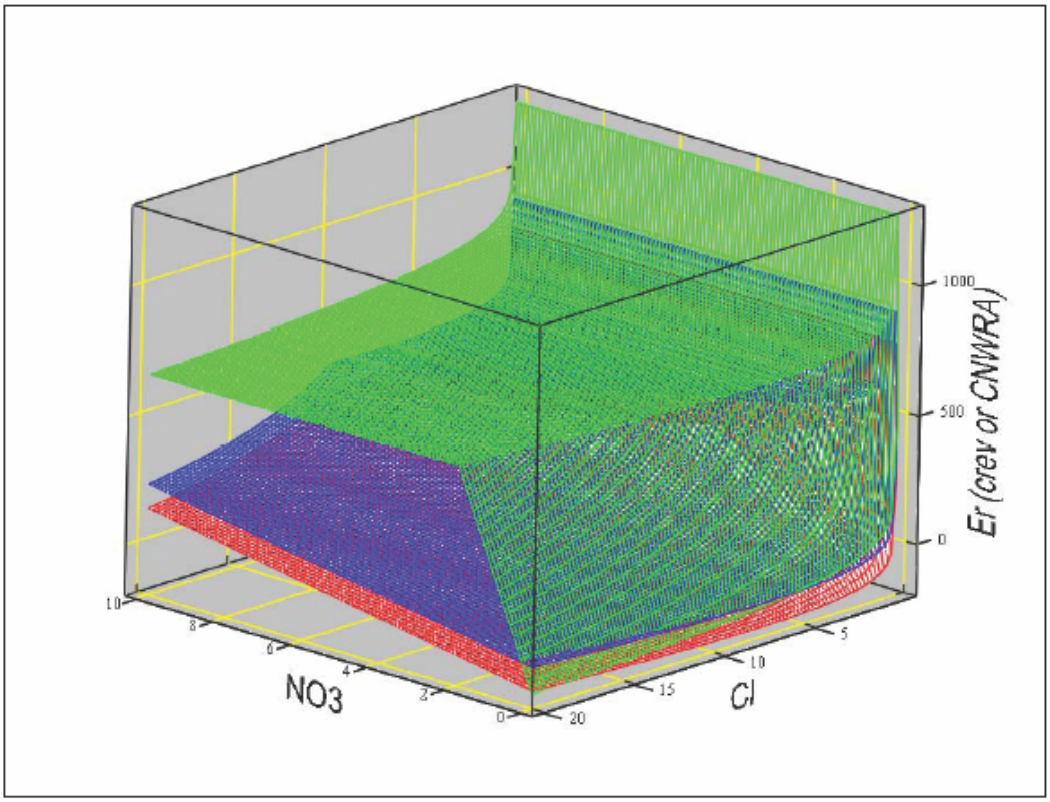

$\left(NO3, Cl, \overrightarrow{Ercrev(TT, 7, Cl, NO3, 0)}\right), \left(NO3, Cl, \overrightarrow{Ercrev(TT, 7, Cl, NO3, 2)}\right), \left(NO3, Cl, \overrightarrow{ErCNWRA(TT, Cl, NO3)}\right)$

Red Blue Green

Ercrev - ErCNWRA vs Cl and NO_3

$Nm := 100$

$np := 0..Nm \quad nt := 0..Nm$ $\quad lc := 0.0005$

$NO3_{nt,np} := \frac{10}{Nm} \cdot nt$ $\quad Cl_{nt,np} := lc + \frac{20 - lc}{Nm} \cdot np$

$zero_{nt,np} := 0$ $\quad TT := 80$

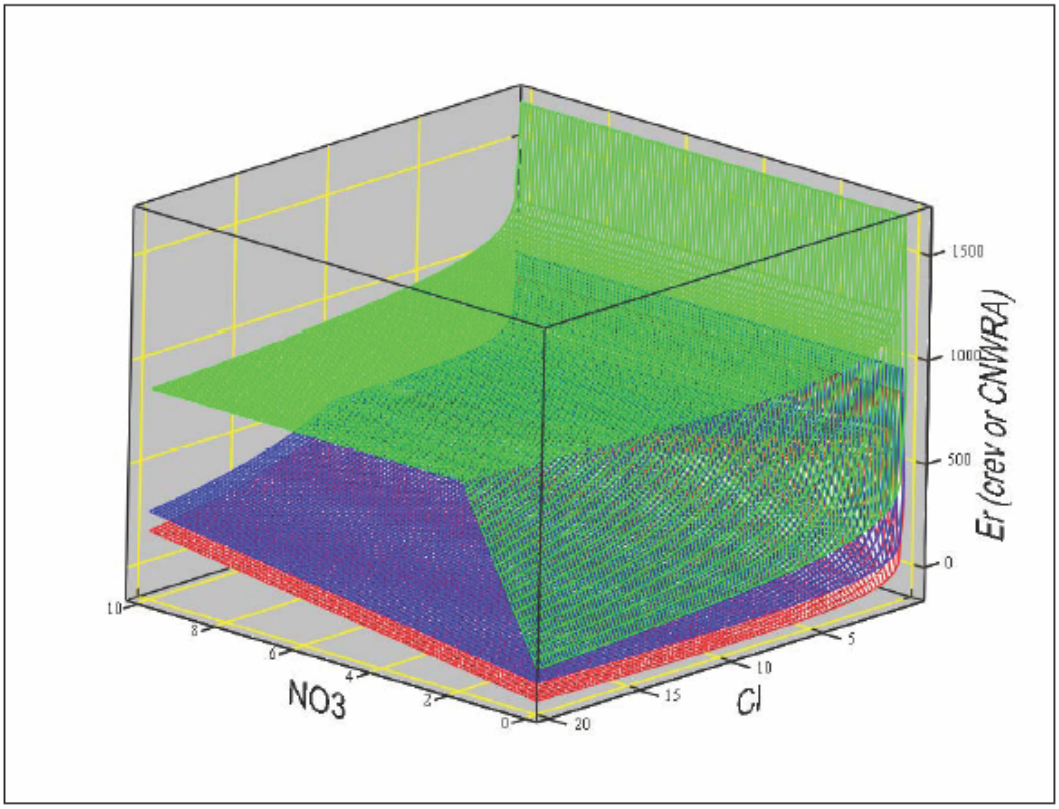

$\left(\overrightarrow{NO3, Cl, Ercrev(TT, 7, Cl, NO3, 0)}\right), \left(\overrightarrow{NO3, Cl, Ercrev(TT, 7, Cl, NO3, 2)}\right), \left(\overrightarrow{NO3, Cl, ErCNWRA(TT, Cl, NO3)}\right)$

Red Blue Green

E_{rcrev} versus E_{corr} comparision

Evaluate the $\Delta E = E_{rcrev} - E_{corr}$. Note that Ercrev is evaluated at z and Ecorr is evaluated at -z standard deviations. That is at z = 2, one obtains the upper bound of ΔE and at z = -2 one obtains the lower bound ΔE.

$$\mathbf{delE}(T,pH,Cl,NO3,z) := \mathrm{Ercrev}(T,pH,Cl,NO3,z) - \mathrm{Ecorr}(T,pH,Cl,NO3,-z)$$

pH and chloride and nitrate ion molalities are from DTN: LL060904312251.186 [DIRS178283], AtmCO2GetEQData.xls, Case 9 for SDW, Case 2oc for SCW, and Case 1oc for SAW.

SDW at 90°C

$$\mathbf{delE}\left[90,9.41,0.0033,0.000973,\begin{pmatrix}-2\\0\\2\end{pmatrix}\right] = \begin{pmatrix}18\\304\\590\end{pmatrix}$$

Crevice corrosion not expected - No crevice corrosion observed

SCW at 90°C

$$\mathbf{delE}\left[90,10.04,0.21,0.12,\begin{pmatrix}-2\\0\\2\end{pmatrix}\right] = \begin{pmatrix}101\\373\\646\end{pmatrix}$$

Crevice corrosion not expected - No crevice corrosion observed

SAW at 90°C

$$\mathbf{delE}\left[90,2.72,0.77,0.37,\begin{pmatrix}-2\\0\\2\end{pmatrix}\right] = \begin{pmatrix}-435\\-168\\98\end{pmatrix}$$

Crevice corrosion expected - No crevice corrosion observed

Evaluate the $\Delta E = E_{rcrev} - E_{corr}$ for each long term corrosion potential cell

$\mathbf{DatC} :=$ EcorrData_Cells.txt

Read in cell number, temperature, and solution compositions

$$\mathbf{DatC}^{\langle 5\rangle} := \overrightarrow{\mathbf{delE}\left(\mathbf{DatC}^{\langle 1\rangle},\mathbf{DatC}^{\langle 2\rangle},\mathbf{DatC}^{\langle 3\rangle},\mathbf{DatC}^{\langle 4\rangle},-2\right)}$$

$$\mathbf{DatC}^{\langle 6\rangle} := \overrightarrow{\mathbf{delE}\left(\mathbf{DatC}^{\langle 1\rangle},\mathbf{DatC}^{\langle 2\rangle},\mathbf{DatC}^{\langle 3\rangle},\mathbf{DatC}^{\langle 4\rangle},0\right)}$$

$$\mathbf{DatC}^{\langle 7\rangle} := \overrightarrow{\mathbf{delE}\left(\mathbf{DatC}^{\langle 1\rangle},\mathbf{DatC}^{\langle 2\rangle},\mathbf{DatC}^{\langle 3\rangle},\mathbf{DatC}^{\langle 4\rangle},2\right)}$$

Append mean and ±2 standard deviation prediction bounds for ΔE

DatC =

	Cell Number	T °C	pH	[Cl] m	NO_3 m	ΔE Lower Bound	ΔE Mean	ΔE Upper Bound
	0	1	2	3	4	5	6	7
0	33.00	120.00	5.17	10.00	10.00	-397.85	-115.94	165.98
1	32.00	100.00	5.28	10.00	10.00	-183.67	93.16	369.99
2	31.00	80.00	5.56	3.50	0.18	-227.15	37.77	302.69
3	30.00	90.00	5.76	1.00	0.15	-201.63	61.62	324.88
4	29.00	75.00	5.72	1.00	0.15	-185.21	79.52	344.25
5	28.00	90.00	4.00	11.99	0.00	-465.51	-201.50	62.51
6	25.00	100.00	5.61	3.50	0.18	-225.04	39.48	303.99
7	24.00	100.00	5.60	3.50	0.53	-223.26	40.70	304.66
8	23.00	100.00	5.41	6.00	0.90	-235.86	27.80	291.47
9	22.00	100.00	5.43	6.00	0.30	-238.51	25.65	289.81
10	21.00	90.00	2.97	12.59	1.26	-596.95	-331.66	-66.36
11	20.00	120.00	3.93	11.99	0.00	-461.67	-191.43	78.82
12	19.00	105.00	8.61	4.62	2.82	15.03	284.40	553.77
13	18.00	90.00	5.55	4.40	0.00	-233.19	30.87	294.94
14	17.00	90.00	1.93	0.76	0.39	-484.54	-216.08	52.38
15	16.00	90.00	9.98	0.21	0.11	124.10	394.40	664.69
16	15.00	90.00	2.97	12.59	1.26	-596.95	-331.66	-66.36
17	14.00	90.00	4.03	11.70	0.12	-457.63	-193.85	69.93
18	13.00	90.00	6.39	2.62	2.58	-92.66	186.40	465.46
19	10.00	90.00	2.72	0.77	0.37	-435.00	-168.27	98.46
20	9.00	90.00	2.38	1.39	0.40	-587.37	-322.27	-57.17
21	72.00	25.00	2.02	0.77	0.37	-177.97	106.03	390.03
22	6.00	90.00	9.41	3.30·10-3	9.73·10-4	18.27	304.24	590.20
23	5.00	60.00	9.30	3.30·10-3	9.73·10-4	107.35	392.60	677.84
24	4.00	105.00	8.61	4.62	2.82	15.03	284.40	553.77
25	3.00	90.00	10.04	0.21	0.12	101.28	373.44	645.61
26	2.00	90.00	2.72	0.77	0.37	-435.00	-168.27	98.46
27	1.00	60.00	2.39	0.77	0.37	-312.40	-42.28	227.85
28	27.00	100.00	5.77	1.00	0.05	-217.82	46.96	311.74
29	26.00	100.00	5.77	1.00	0.15	-216.78	47.43	311.64
30	8.00	120.00	3.93	11.99	0.00	-461.67	-191.43	78.82
31	71.00	60.00	10.03	0.21	0.12	280.76	559.00	837.25

Note that Cells 7-1 and 7-2 have been renamed 71 and 72 for this exercise

DatC =

	Cell Number	T °C	pH	[Cl] m	NO_3 m	-2 ΔE	Mean Prediction	+2 Interval
	0	1	2	3	4	5	6	7
0	33.00	120.00	5.17	10.00	10.00	-322.76	-115.94	90.89
1	32.00	100.00	5.28	10.00	10.00	-109.14	93.16	295.46
2	31.00	80.00	5.56	3.50	0.18	-158.67	37.77	234.21
3	30.00	90.00	5.76	1.00	0.15	-133.14	61.62	256.39
4	29.00	75.00	5.72	1.00	0.15	-116.55	79.52	275.59
5	28.00	90.00	4.00	11.99	0.00	-397.13	-201.50	-5.86
6	25.00	100.00	5.61	3.50	0.18	-156.48	39.48	235.44
7	24.00	100.00	5.60	3.50	0.53	-154.72	40.70	236.12
8	23.00	100.00	5.41	6.00	0.90	-167.46	27.80	223.07
9	22.00	100.00	5.43	6.00	0.30	-170.09	25.65	221.39
10	21.00	90.00	2.97	12.59	1.26	-528.44	-331.66	-134.87
11	20.00	120.00	3.93	11.99	0.00	-392.09	-191.43	9.23
12	19.00	105.00	8.61	4.62	2.82	85.88	284.40	482.92
13	18.00	90.00	5.55	4.40	0.00	-164.80	30.87	226.55
14	17.00	90.00	1.93	0.76	0.39	-414.13	-216.08	-18.03
15	16.00	90.00	9.98	0.21	0.11	195.03	394.40	593.76
16	15.00	90.00	2.97	12.59	1.26	-528.44	-331.66	-134.87
17	14.00	90.00	4.03	11.70	0.12	-389.30	-193.85	1.60
18	13.00	90.00	6.39	2.62	2.58	-17.51	186.40	390.31
19	10.00	90.00	2.72	0.77	0.37	-364.97	-168.27	28.43
20	9.00	90.00	2.38	1.39	0.40	-518.39	-322.27	-126.15
21	72.00	25.00	2.02	0.77	0.37	-104.08	106.03	316.14
22	6.00	90.00	9.41	$3.30 \cdot 10^{-3}$	$9.73 \cdot 10^{-4}$	92.62	304.24	515.86
23	5.00	60.00	9.30	$3.30 \cdot 10^{-3}$	$9.73 \cdot 10^{-4}$	182.10	392.60	603.09
24	4.00	105.00	8.61	4.62	2.82	85.88	284.40	482.92
25	3.00	90.00	10.04	0.21	0.12	172.71	373.44	574.18
26	2.00	90.00	2.72	0.77	0.37	-364.97	-168.27	28.43
27	1.00	60.00	2.39	0.77	0.37	-241.57	-42.28	157.02
28	27.00	100.00	5.77	1.00	0.05	-149.09	46.96	243.01
29	26.00	100.00	5.77	1.00	0.15	-148.06	47.43	242.93
30	8.00	120.00	3.93	11.99	0.00	-392.09	-191.43	9.23
31	71.00	60.00	10.03	0.21	0.12	353.40	559.00	764.61

Note that Cells 7-1 and 7-2 have been renamed 71 and 72 for this exercise